



**HAL**  
open science

# Search for organic compounds with MTBSTFA/DMF derivatization and TMAH thermochemolysis on Mars

Yuanyuan He

► **To cite this version:**

Yuanyuan He. Search for organic compounds with MTBSTFA/DMF derivatization and TMAH thermochemolysis on Mars. Chemical and Process Engineering. Université Paris-Saclay, 2021. English. NNT : 2021UPAST003 . tel-03228713

**HAL Id: tel-03228713**

**<https://theses.hal.science/tel-03228713v1>**

Submitted on 18 May 2021

**HAL** is a multi-disciplinary open access archive for the deposit and dissemination of scientific research documents, whether they are published or not. The documents may come from teaching and research institutions in France or abroad, or from public or private research centers.

L'archive ouverte pluridisciplinaire **HAL**, est destinée au dépôt et à la diffusion de documents scientifiques de niveau recherche, publiés ou non, émanant des établissements d'enseignement et de recherche français ou étrangers, des laboratoires publics ou privés.

# Search for organic compounds with MTBSTFA/DMF derivatization and TMAH thermochemolysis on Mars

**Thèse de doctorat de l'université Paris-Saclay**

École doctorale n° 579 : sciences mécaniques et énergétiques,  
matériaux et géosciences (SMEMAG)

Spécialité de doctorat : Génie des procédés

Unité de recherche : Université Paris-Saclay, CentraleSupélec, Laboratoire de  
Génie des Procédés et Matériaux, 91190, Gif-sur-Yvette, France.

Référent : CentraleSupélec

**Thèse présentée et soutenue à Gif-Sur-Yvette, le 21  
Janvier, 2021. Par**

**Yuanyuan HE**

## Composition du Jury

<b>Filipa Lopes</b> Professeur, CentraleSupélec (Université Paris-Saclay)	Présidente
<b>Laurent Remusat</b> DR, HDR, IMPMC (UPMC – MNHN)	Rapporteur & Examineur
<b>Grégoire Danger</b> MCF, HDR, PIMS (Université Aix-Marseille)	Rapporteur & Examineur
<b>Cornelia Meinert</b> DR, HDR, ICN (Université Nice)	Examinatrice
<b>Katell Quénéa</b> MCF, HDR, METIS (UPMC)	Examinatrice
<b>Cyril Szopa</b> Professeur, LATMOS (UVSQ)	Examineur
<b>Arnaud Buch</b> HDR, MCF, CentraleSupélec (Université Paris-saclay)	Directeur de thèse



## **Acknowledgements**

I would first and foremost like to thank my Ph.D. adviser Dr. Arnaud BUCH. This work would certainly not have been possible without his incredible guidance and support throughout the last 3 years. He always helps me in times when I meet obstacles in experiments and life; he guides me when I feel lost in research; he gives me enough freedom to do the research that I'm interested in, which exercised my ability to think and do research independently. He told me many times that he trusted me completely, which motivates me to keep innovating and pursuing excellent results. He always summons my will whenever I feel like giving up. His positive and optimistic attitude influences me, he always says "we don't care", which encouraged me to be brave and not care about others' opinions and perspectives. He is very kind, he once helped me provide a housing guarantee when I first came to France; he encourages me to do a postdoc in another lab to learn new things and grow stronger in my career. I would also like to thank Dr. Pin Lv for his help provided during my Ph.D. application and study.

I would like to thank Dr. Cyril SZOPA and Dr. Caroline FRESSINET from Laboratoire atmosphères, milieux, observations spatiales (LATMOS). They always give me great supports when I put forward novel ideas. They help me buy various samples and bacterial samples, which help me to turn my ideas into reality. Thanks to the whole SAM and MOMA team, especially Dr. Melissa GUZMAN and Dr. Amy J. Williams, they helped me a lot in revising the papers. Thanks to Dr. Tony Z. JIA from Earth-Life Science Institute and Dr. Jihua HAO from Rutgers University and other collaborators for their inspiration for the research and their suggestions on the experimental samples.

The entire Laboratoire Génie des Procédés et Matériaux (LGPM) lab has also been incredibly supportive and helpful in all my research endeavors, and I am very grateful and very happy to have been a part of this team. I would like to thank all the members of the lab with whom I have directly collaborated and who helped me to do my experiments. Especially, I would like to thank Vincent BUTIN, who always helped on time, and he helps me to transport and install the gas cylinders, helped me to measure the concentration of perchlorate, etc. Dr. Andrea FANESI helps me cultivating bacteria, and we have also had many great scientific discussions and came up with some unique experimental ideas together. I could not complete the bacterial experiments without his help. Jamila EL BEKRI helps to detect the concentration of water in



my sample; she is very kind and helps me whenever I come to her for help. Thanks to Corinne ROUSSEL and H  l  ne SANTIGNY, they clean up our laboratory so that I have a clean experimental environment. They are very nice, warm heart and like grandmas. Thanks Mathilde CHARTERS for ordering the gas cylinders whenever I need them. Thanks, Sebastien GAUTHIER, for connecting the liquid nitrogen with CryoMill, Thierry MARTIN for filling the bottom of liquid nitrogen. Thanks to Magali DUPUY for helping me solve the problem whenever my computer or printer encounters a problem; Thanks to the secretary team Elisabeth LOBO and Sandra Anchier JULIEN, Corinne Morvan (from Latmos) help me book the tickets for the business trips to Le teich, Orl  an, and Seattle.

Especially, I would like to thank Dr. Manasa PERIYAPATTANA, who is one of my colleges and my friends, who keeps me accompany during my whole Ph.D. life. We are from different countries, but we have a similar experience of growing up and similar temper and personalities, which makes us such good friends. We share our stories and encourage each other when we meet problems both in research and in life. We explore the culture and interesting things in Paris, she helps me open my mind and let me learn to think in a western or international way rather only in the traditional Chinese way, which makes me respect different thoughts and behaviors rather judge people casually. She pushed me to do sports at the very beginning and I fall love with doing sports later, which helps me to build a healthy body and release the pressure and anxiety during my Ph. D. life.

I would also like to thank to my Chinese friends, thanks Wangshu CHEN, Minhao YANG, Li GONG, Hanlu ZHANG, and Wenbiao JIANG for helping me when I had a “bed bugs” emergency and have to move from one place to another. Thanks to my friends Hainan LIU, Xianwu JIANG, Xiaoxia ZHANG, Daogui TANG, Yong TIAN, Chaohe HU, Kangyi XU, Shuoliang DING, Yan GAO, Sufang LI, et.al, we had a great time together. Thank you all for helping me overcomes difficulties in my Ph.D. life.

I would not have the chance to achieve my Ph.D. diplomas without Prof. Fan Li, who is my master advisor and changed my life completely. She is not only a supervisor in my scientific research career, but she also teaches us in accordance with our aptitude. She encourages us to develop in an all-round way. For example, she demands us to have a short speech when we have dinner together; she organizes English corners to improve our oral English. I used to be a host and performer at the New Year party and Graduation party, which helps me to be confident when I give a public speech in front of people. I had a great time during those 3 years. She is

also the advisor in my life. She broadens our horizons by telling us different stories, which aroused my curiosity and yearning for life studying abroad. She also supports me in pursuing my dream, no matter how difficult it is. She told me, there will be more solutions than problems or obstacles in life, we have to be strong, perseverant, confident, and be well prepared even for a small opportunity, etc. Her optimism and enthusiasm for life also affects me deeply. She is one of my role models, who inspired me to be a professor like her in the future, and guide as many as students to achieve their dreams. Thanks to all the friends in the Fan family; we had a wonderful time together.

Furthermore, I would like to thank for the finance from China Scholarship Council (CSC) and the teachers who work in the Service de l'éducation Ambassade de la République Populaire de Chine en République Française. Thanks to the CSC scholarship help me achieve my dream of study in France.

Last but not the least, I would like to thank my family-my parents, my sisters, and brothers, my grandparents, my uncles and aunts, who have been supportive through my life and have stuck with me in the good times and in the bad.

I am so grateful to people who have helped me in my life.

Finally, I would like to thank you, the reader, for taking the time to read this dissertation. I hope you can acquire what you want from this dissertation, and I hope it could be fruitful to you and can bring you inspiration in both life and scientific research.

## General preamble

The work described in this thesis manuscript was carried out at the laboratory LGPM (Laboratoire de Génie des Procédés et Matériaux), belonging to CentraleSupélec (Université Paris-Saclay).

The manuscript is based on four publications, which make up chapters 1, 2, 3 and 4, with some additional unpublished information also included. The contents of the publications were unchanged except for the section, figure, table and equation numbers and the corresponding references to these in the text (the numbering was adapted to follow the manuscript format). The publications are listed as below:

1. He Y, Buch A, Szopa C, et al. The search for organic compounds with TMAH thermochemolysis: from Earth analyses to space exploration experiments [J]. *TrAC Trends in Analytical Chemistry*, 2020: 115896.
2. He Y, Buch A, Morisson M, et al. Application of TMAH thermochemolysis to the detection of nucleobases: Application to the MOMA and SAM space experiment [J]. *Talanta*, 2019, 204: 802-811.
3. He Y, Buch A, Szopa C, et al. Influence of calcium perchlorate on the search for organics on Mars with TMAH thermochemolysis [J]. *Astrobiology*, 2020 accepted.
4. He Y, Buch A, Szopa C, et al. Influence of calcium perchlorate on the derivatization of MTBSTFA/DMF [J]. Under review.

This work was also presented at four international conferences, as below:

1. AbSciCon 2019, Seattle, USA. He Y, Buch A, Morisson M, et al. Optimization of the *in situ* detection of Nucleobase on MOMA and SAM experiments[C]//2019 Astrobiology Science Conference. AGU, 2019.
2. EANA conference 2019, Orléan, France. He Y, Buch A, Szopa C, et al. Influence of calcium perchlorate on the search for organics on Mars with TMAH thermochemolysis.
3. EANA conference 2020, Virtual. He Y, Buch A, Szopa C, et al. The detection of DNA/RNA with TMAH thermochemolysis on SAM.

4. Astrobiology Australasia meeting 2020, Virtual. He Y, Buch A, Szopa C, et al. Search for life biosignatures on Mars: the detection of DNA/RNA with TMAH thermochemolysis on SAM.

## Résumé en français

Dans son plus jeune âge Mars, planète tellurique, avec une atmosphère, un climat, et une géologie diverse et complexe comme la Terre. La mission Mars Science Laboratory a prouvé qu'elle a été habitable durant le premier milliard d'année. Si elle a abrité une quelconque forme de vie alors il pourrait y avoir des molécules organiques préservées en subsurface. D'autre part des organiques exogènes provenant par exemple de micrométéorites et des particules de poussière interplanétaire pendant la période amazonienne de l'histoire de Mars peuvent également être présent en surface et subsurface. Toutefois, les radiations et oxydation de surface peuvent altérer les potentiels composés organiques présent en surface martienne. C'est pourquoi Curiosity et la mission MSL s'intéressent plus particulièrement à la subsurface martienne car les argiles comme les phyllosilicates, les carbonates et les sulfates pourraient permettre la préservation de ces composés organiques. Par ailleurs, des composés tels que des acides aminés, des acides carboxyliques, des nucléobases qui sont essentiels à la vie ont été détectés dans les météorites. Or ces météorites pourraient être des sources exogènes de composés organiques. Par conséquent, il pourrait être possible d'avoir ces composés organiques essentiels sur Mars pour soutenir la vie. C'est pourquoi ce travail est principalement basé sur la recherche de matière organique sur Mars, qui est l'un des principaux objectifs de l'expérience SAM (Sample Analysis at Mars) à bord du rover Curiosity de la NASA. La recherche de composés organiques sur Mars pourrait aider à comprendre l'origine de la vie sur Terre.

Depuis 1975, Plusieurs missions ont été menées pour rechercher des traces de vie sur Mars, en particulier les atterrisseurs Viking, le rover Curiosity (2012), Persévérance (2021, atterrissage le 18 février 2021) et ExoMars (qui sera lancé en 2022). Ces missions ont fourni et fourniront des informations substantielles sur Mars, par exemple sur l'atmosphère martienne et la composition du sol martien. Parmi ces rovers, seuls les atterrisseurs Viking, le rover Curiosity et ExoMars disposent d'un laboratoire de chimie. Ils ont été conçus pour rechercher des traces de vie en analysant les composés organiques du sol martien. Les instruments Mars Organic Molecule Analyzer (MOMA) et Sample Analysis at Mars (SAM) respectivement à bord des rovers Exomars 2022 et Mars Science Laboratory, sont quant à eux capables de détecter la présence de matières organique jusqu'au ppb et pour MOMA de différencier les matières organiques potentiellement biogènes des matières abiotiques. Pour identifier les matières organiques, ces instruments utilisent la pyrolyse-chromatographie en phase gazeuse couplée à la spectrométrie de masse (Pyr-GC/MS), la dérivatisation avec un mélange de N-tert-butyldiméthylsilyl-N-méthyltrifluoroacétamide (MTBSTFA) et de N,N-diméthylformamide (DMF) et la thermochimie avec le réactif hydroxyde de tétraméthylammonium (TMAH) (25 % dans le méthanol).

Grace à l'instrument SAM, les premières molécules organiques endogène ont pu être mise en évidence. Parmi ces dernières des composés thiophéniques, aromatiques et aliphatiques libérés à haute

température (500 à 820 °C) ont été détectées [51]. Ces composés ont pu être préservés dans des mudstones lacustres à la base de la formation de Murray, vieille de 3,5 milliards d'années, à Phahrump Hills. La présence de thiophène démontre que de la matière organique ayant subi une sulfuration a pu être préservée sur Mars. Les thiophènes sont généralement présents sur Terre dans le kérogène, le charbon et le pétrole brut, ainsi que dans les stromatolites et les microfossiles.

En plus des composés soufrés des composés chlorés ont également été détectés sur Mars. Le chlorométhane (environ 15 ppb) et le dichlorométhane (environ 2-40 ppb) ont d'abord été détectés par les atterrisseurs jumeaux Viking 1975/76 (VL-1 et VL-2). Cependant, les composés chlorés signalés à l'époque, notamment le chlorométhane et le dichlorométhane, ont tout d'abord été attribués à une contamination terrestre résultant de l'utilisation de solvants chlorés ou de la réaction entre du méthanol et du HCl [53]. La première détection *in situ* de composés de perchlorate ou d'oxychlorure par Mars Phoenix Lander en 2008 [54] pourrait cependant offrir une explication alternative à la présence de chlorométhane et de dichlorométhane dans les ensembles de données GC/MS de Viking [55]. En effet, depuis 2012, plusieurs autres composés chlorés ont été détectés par SAM à bord du rover Curiosity. Glavin et al [56] ont rapporté la détection par SAM de chlorométhane, de dichlorométhane, de trichlorométhane et de chlorométhylpropène. Cependant, ces composés chlorés ont été attribués à la réaction de l'oxychlorure/perchlorate martien avec le carbone organique du MTBSTFA. Le chlorobenzène a d'abord été attribué aux réactions du chlore martien libéré par le perchlorate avec le benzène ou le toluène terrestre dérivé de l'oxyde de 2,6-diphénylphénylène (Tenax®) provenant du piège à hydrocarbures de SAM [56]. Par la suite, Curiosity a détecté certains composés chlorés, tels que le 1,2-dichloroéthane, le 1,2-dichloropropane, le 1,2-dichlorobutane, le trichlorométhylpropane et le chlorobenzène, avec des quantités maximales de ~150 à 300 ppbw [57], le dichlorobenzène de ~0,5 à 17 ppbw [58], etc.

Avec la détection de composés chlorés sur Mars, le MTBSTFA/DMF, est considéré comme la source de carbone possible de certaines substances organiques qui ont été détectées sur Mars. Par conséquent, les sous-produits de la dégradation des réactifs avec et sans perchlorates doivent être listés de façon exhaustive et considérés comme des données de référence. En plus du MTBSTFA, le TMAH est également utilisé pour rechercher des composés organiques pouvant être des bioindicateurs et des biosignatures sur Mars ses produits de décompositions doivent également être identifiés.

Nous avons d'abord évalué les effets de la température de pyrolyse et du mode de chauffage sur la dégradation du MTBSTFA, du DMF et d'un mélange MTBSTFA/DMF (4:1). Nous avons également évalué l'effet du perchlorate de calcium sur la dégradation du MTBSTFA et du DMF. Nous avons rapporté les produits de pyrolyse de MTBSTFA/DMF aux différentes températures de 210, 300, 600 et 850 °C, à la fois en absence et en présence de perchlorate de calcium. Tous les produits de MTBSTFA et DMF produits dans ces différentes expériences ont été identifiés afin de former une base de données

pour soutenir l'interprétation des données obtenues par les instruments spatiaux SAM et MOMA. Les résultats démontrent que le mélange MTBSTFA/DMF peut être utilisé efficacement à une température inférieure à 300 °C pendant la flash pyrolyse, ce qui donne lieu à relativement peu de sous-produits. Le TFMA, le MSW et le BSW sont les principaux produits, formés après le craquage de la liaison N-Si du groupe fonctionnel de dérivation TBDMS pendant le processus de pyrolyse. Beaucoup d'autres composés contenant du fluor ont été formés lorsque la température de pyrolyse atteint 850 °C, ce qui démontre que la rupture de la liaison F-C nécessite de hautes températures. Diverses aromatiques ont été formés, comme le benzène, le toluène, le naphthalène, le fluoranthène et le pyrène. Le chlorométhane et le chloro-tert-butylméthylsilane ont également été détectés. De plus, par rapport au nombre de produits de la flash pyrolyse du MTBSTFA/DMF, moins de produits du MTBSTFA/DMF ont été détectés lors de la pyrolyse en rampe de type SAM (35°C/min) quelle que soit la température maximale. Nous concluons donc que le MTBSTFA/DMF peut être utilisé avec une vitesse de chauffage lente avec une température finale allant jusqu'à 850 °C. La présence de perchlorate de calcium n'a pas d'effet évident sur la pyrolyse en rampe en présence de MTBSTFA/DMF. Enfin, nous notons que ce travail confirme que les matières organiques indigènes des échantillons martiens, contenant également des espèces de perchlorate, pourraient être l'une des sources de carbone possibles des composés chlorobenzènes, en accord avec la conclusion de Freissinet et al. (2015).

En plus du MTBSTFA/DMF, la dégradation du TMAH avec et sans la présence de perchlorate de calcium lors de la flash pyrolyse et de la pyrolyse en rampe à 600 °C a été étudiée. Certains composés chlorés ont été détectés pendant la pyrolyse du TMAH avec >10 % en poids de perchlorate de calcium, notamment le chlorométhane, le chlorure de tétraméthylammonium, le 5-chloro-2-pyridinol, le 5-chloro-1-méthylimidazole et le 4,5-dichloro-1-méthyl-imidazole. Bien que l'intensité du pic de ces composés chlorés soit plus de 1000 fois inférieure à celle des produits principaux, ils sont des potentiels candidats pour les sous-produits chlorés du TMAH. Toutefois, le TMAH a montré une faible réactivité avec les substances contenant du chlore. Nous notons que le perchlorate de calcium n'affecte pas la dégradation du TMAH à une température de pyrolyse en rampe de type SAM de 600 °C lorsque les concentrations de perchlorate de calcium sont inférieures à 10 % en poids. Bien que le TMA et l'éther diméthylque soient les principaux sous-produits de la pyrolyse du TMAH, certains nouveaux sous-produits sont formés lorsque les concentrations de perchlorate de calcium sont supérieures à 10 % en poids. Le DMF est formé en raison de l'oxydation du groupe méthyle par l'O<sub>2</sub> libéré lors de la décomposition du perchlorate de calcium et suivi par la formation de cyanamide et d'acétonitrile par la voie de cyanation des amines. Le TMTAC est formé par la trimérisation du DMF, qui est un intermédiaire crucial pour la formation d'autres sous-produits azotés du TMAH. L'urée est formée par la réaction de Ritter et la réaction de Manich, et le réarrangement de Steven et l'élimination de Hofmann sont impliqués dans la formation de divers intermédiaires et ylides. Cependant, dans nos conditions expérimentales, le perchlorate de calcium n'a pas affecté la récupération des acides gras par

thermochromolyse au TMAH, même lorsque le volume d'acides gras était faible. Ces éléments de preuve démontrent que le TMAH est un bon réactif de thermochimie à haute température (600 °C) pour la méthylation et la détection de substances organiques sur Mars avec les instruments SAM et MOMA.

Après avoir testé l'influence du perchlorate de calcium sur l'application du réactif de thermochromolyse TMAH, nous avons étudié l'application de la thermochromolyse TMAH sur la détection des nucléobases. Sept types de nucléobases ont été étudiés ici : l'adénine, la thymine, l'uracile, la cytosine, la guanine, la xanthine et l'hypoxanthine. Les produits de thermochimie TMAH de sept standards de nucléobases et de mélanges pyrolysés à différentes températures ont été analysés individuellement par Pyr-GC/MS. Les dérivations de toutes les nucléobases à la température optimale de pyrolyse, ainsi que la limite de détection (LOD) et la limite de quantification (LOQ) des nucléobases ont été déterminées. En outre, les mécanismes de thermochromolyse de toutes les nucléobases dans le TMAH ont été analysés. Ces données sont les premières du genre, permettant de déterminer s'il serait possible de détecter toutes ou certaines des bases azotées étudiées avec sur les expériences SAM et MOMA. Toutefois, il convient de noter que sur Mars, les nucléobases sont contenues dans une matrice solide dont il faudra les extraire.

Nous concluons que la thermochimolyse TMAH permet la méthylation et la détection des sept nucléobases étudiées ici. La température optimale pour la thermochimolyse des nucléobases dans les conditions SAM et MOMA est de 600°C. La triméthyl-adénine, la 1,3-diméthyl-thymine, le 1,3-diméthyl-uracile, la triméthyl-cytosine, la 1, 3, 7-triméthyl-xanthine (caféine) et la diméthyl-hypoxanthine étaient les principaux produits méthylés de l'adénine, de la thymine, de l'uracile, de la cytosine, de la guanine, de la xanthine et de l'hypoxanthine, respectivement, car ce sont les formes les plus stables de chaque nucléobase en phase gazeuse ou sous forme aqueuse. En outre, il n'y a pas eu d'interaction entre ces nucléobases lorsqu'elles ont été pyrolysées dans un mélange, ce qui permet de détecter différentes nucléobases dans des échantillons naturels. D'après les valeurs de LOD et LOQ pour chaque nucléobase, l'adénine, la thymine et l'uracile sont plus faciles à détecter, puisqu'ils peuvent être détectés à environ 0,15 nmol. Il est possible, bien que plus difficile, de détecter la guanine, la cytosine et l'hypoxanthine (LOD=0,40, 0,55 et 0,75 nmol, respectivement). Cependant, la matrice complexe doit être prétraitée avec le processus d'extraction afin de détecter les nucléobases sur Mars, la LOD peut être plus élevée que la valeur de notre étude.

En un mot, il serait possible de détecter les nucléobases si les échantillons sont frais et si leur contenu est supérieur à la limite de détection des instrument spatialisés.

Puisque la thermochimie au TMAH peut être appliquée pour analyser efficacement les bases nucléiques, l'application de cette technique à la détection des acides nucléiques a également été étudiée. En effet, l'acide désoxyribonucléique (ADN), en tant que support d'information, stocke l'information qui définit l'organisme dans des ordres uniques de quatre bases (A, T, C, G) situées dans de minuscules



molécules, et cette façon de stocker l'information a continué pendant trois milliards d'années. Certaines études ont suggéré que l'ADN peut être placé dans les régions extrêmement froides de la Terre ou même sur Mars pour un stockage de plusieurs millénaires [144]. L'ARN a probablement constitué la base de la première forme de vie terrestre. Il est composé de séquences de quatre nucléotides différents, ces derniers pouvant être formés par une source de réaction. Les polymères d'ARN ont dû apparaître très rapidement après le dépôt des météorites (moins de quelques années), et la synthèse des nucléotides et leur polymérisation en ARN se sont produites en un ou quelques cycles d'humidité et de sécheresse seulement [145]. Même les acides nucléiques artificiels peuvent exister dans un grand nombre d'alternatives chimiques. Le rôle de l'ARN dans l'origine de la vie est bien établi, et la façon dont l'ARN a émergé sur la Terre primitive est l'une des premières étapes de la compréhension de l'origine de la vie [678]. Il est donc essentiel d'étudier l'efficacité de la détection de l'ADN ou de l'ARN et de leurs fragments. Les nucléobases, les nucléosides et les nucléotides sont les composants de l'ADN et de l'ARN. Les nucléobases sont les éléments constitutifs les plus importants de l'ADN et de l'ARN ; les nucléosides sont constitués de nucléobases et de ribose. Les nucléotides et les nucléotriphosphates sont des molécules organiques constituées d'un nucléoside et d'un phosphate. Comme leurs structures sont différentes même si elles présentent certaines similitudes, leurs comportements pourraient être différents lors de la thermochimie avec le TMAH. C'est pourquoi, dans ce chapitre, les nucléosides, les nucléotides et les nucléotides triphosphates de l'ADN et de l'ARN ont été analysés par thermochromolyse au TMAH, afin d'évaluer l'efficacité et le potentiel du TMAH sur l'analyse d'échantillons réels d'ADN ou d'ARN. Enfin, la thermochimie TMAH a été appliquée pour analyser le poly A, qui est la queue de l'ARN et joue un rôle important dans la protection de la molécule d'ARN.

Les produits des nucléosides, nucléotides et nucléotides phosphates avec la thermochimie au TMAH ont été étudiés en flash pyrolyse et en pyrolyse avec rampe de température de type SAM. Nous en avons conclu que les nucléobases méthylées sont les principaux composés des nucléosides, nucléotides et nucléotides triphosphate lors de leur thermochémiolyse au TMAH. La température optimale pour la détection des nucléobases méthylées, des nucléosides et des dérivés du ribose tels que le furfuryl méthyl éther est de 200 °C ; 300 °C est la température optimale pour la détection du méthyl phosphate. Cependant, une température plus élevée peut être nécessaire pour la détection des nucléosides, des nucléotides et des nucléotides triphosphate en raison de la forte adsorption des matières organiques sur la matrice solide. Nos résultats ont permis de montrer que les nucléobases méthylées pouvaient être détectées même à une température élevée de 600 °C. Par conséquent, les nucléosides, les nucléotides et les nucléotides triphosphate pourraient encore être détectés s'ils étaient contenus dans les échantillons de sol martien. La structure des bases nucléiques d'origine influence la détection des composés caractéristiques. Par exemple, l'abondance des nucléosides méthylés issus de la méthylation des nucléosides et des nucléotides est différente. L'intensité des nucléosides méthylés issus de la thermochimie des nucléosides avec le TMAH est plus élevée que celle des nucléotides thermochimisés

avec le TMAH. Bien que 200 °C soit la température optimale pour la détection des nucléobases méthylées, pour le poly A, l'abondance d'adénine méthylée est la plus élevée à 400 °C. Ceci démontre que l'efficacité de la thermochimolyse à la TMAH dépend de la dégradation des fragments d'ADN. Par conséquent, la température de la thermochimolyse de la TMAH affecte l'efficacité de la détection des fragments d'ADN. Ainsi, s'il y a de la vie sur Mars, et notamment la présence de bactéries, les conditions expérimentales de détection de la vie devront être optimisées.

Pour tester l'efficacité du TMAH sur l'application de l'analyse des composés organiques ou des nucléobases des cellules, les composés organiques des cellules d'E.coli ont été étudiés en premier lieu. De nombreux esters méthyliques d'acides gras ont été détectés lors de la flash pyrolyse de E.coli avec le TMAH, les acides gras comprennent le vanillate de méthyle, l'ester méthylique de l'acide dodécanoïque, l'ester méthylique de l'acide tétradécanoïque, le myristoléate de méthyle, le palmitoléate de méthyle. En outre, l'ester méthylique de l'acide (Z)-9-octadécénoïque, l'ester méthylique de l'acide octadécanoïque, l'ester méthylique de l'acide cis-10-nonadécénoïque ont également été détectés. En plus des acides gras, des nucléobases ont également été trouvées à partir d'E.coli lors de la thermochimie au TMAH.

L'un des principaux objectifs de SAM est de faire l'inventaire des composés organiques sur Mars en analysant les composés organiques du sol martien. Étant donné l'environnement difficile de Mars, les problèmes de préservation de la vie sont d'énormes défis pour la vie. Cependant, nous pensons que les micro-organismes pourraient éventuellement survivre dans des conditions extrêmes. En outre, certaines bactéries telles que les cyanobactéries ont été détectées dans l'échantillon du désert d'Atacama, qui est un analogue martien sur Terre. On ne peut exclure la possibilité qu'il y ait des bactéries vivantes sur Mars. S'il y a des bactéries sur Mars, l'application de la thermochimie TMAH à la détection des bactéries pourrait être essentielle. Par conséquent, l'application de la thermochimie TMAH à la détection de composés organiques provenant de cyanobactéries (*Chroococcidiopsis cubana*), d'actinobactéries (*Rubrobacter radiotolerans*) qui ont été détectées dans l'échantillon d'Atacama, et d'archées halophiles (*Halobacterium salinarum*) pourraient éventuellement survivre dans un environnement extrême a été étudiée avec la thermochimie TMAH. Les principaux produits de ces vies réelles avec la thermochémolyse TMAH ont été étudiés, et la température de thermochémolyse a été optimisée.

Pour tester l'efficacité du TMAH sur l'application de l'analyse des composés organiques ou des nucléobases des cellules, les composés organiques des cellules d'E.coli ont été étudiés en premier lieu. De nombreux esters méthyliques d'acides gras ont été détectés lors de la flash pyrolyse de E.coli avec le TMAH, les acides gras comprennent le vanillate de méthyle, l'ester méthylique de l'acide dodécanoïque, l'ester méthylique de l'acide tétradécanoïque, le myristoléate de méthyle, le palmitoléate de méthyle. En outre, l'ester méthylique de l'acide (Z)-9-octadécénoïque, l'ester méthylique de l'acide octadécanoïque, l'ester méthylique de l'acide cis-10-nonadécénoïque ont également été détectés. En plus des acides gras, des nucléobases ont également été détectées à partir d'E.coli.

Les composés organiques varient selon les espèces. Les principaux composés des échantillons de cyanobactéries et d'actinobactéries sont les acides gras et les alcools, variant de C11~C19, ils sont les composés organiques les plus détectables. C'est le cas des composés tels que l'acide 9-hexadécénoïque, l'acide hexadécanoïque, l'acide octadécanoïque, l'acide 9,12-octadécadiénoïque. Le glucopyranoside est également l'un des composés organiques les plus importants. Par exemple, l'éther tétraméthyle du L(-)-Fucose, le  $\alpha$ -D-méthyl 2,3,4,6-tétra-O-méthyl-galactopyranoside,  $\alpha$ -D-méthyl 2,3,4,6-tétra-O-phényl-glucopyranoside,  $\alpha$ -D-méthyl 2,3,4,6-tétra-O-glucopyranoside. D'autre part, des dérivés de la lignine ont été détectés dans cette étude. Le 1,2,4-triméthoxy-benzène au temps de rétention de 19,69 min est l'unité guaiacyl ; PCA (unités p-coumarate) ont été détectés, y compris l'ester méthylique de l'acide p-méthoxy-cinamique, 1-(4-méthoxyphényl)-4-méthyl-1-penten-3-one, etc. Les produits de dégradation de la chlorophylle ont été détectés. Le phytol et ses dérivés ont été trouvés dans les chromatogrammes. L'acétate de phytol et le phytol ont pu être dégradés à partir de la chlorophylle dans les cyanobactéries.

Pour tester l'efficacité du TMAH sur l'application de l'analyse des composés organiques ou des nucléobases des cellules, les composés organiques des cellules d'E.coli ont été étudiés en premier lieu. De nombreux esters méthyliques d'acides gras ont été détectés lors de la pyrolyse flash de E.coli avec le TMAH, les acides gras comprennent le vanillate de méthyle, l'ester méthylique de l'acide dodécanoïque, l'ester méthylique de l'acide tétradécanoïque, le myristoléate de méthyle, le palmitoléate de méthyle. En outre, l'ester méthylique de l'acide (Z)-9-octadécénoïque, l'ester méthylique de l'acide octadécanoïque, l'ester méthylique de l'acide cis-10-nonadécénoïque ont également été détectés. En plus des acides gras, des nucléobases ont également été trouvées à partir d'E.coli avec la thermochimie au TMAH.

Pour les cellules de *Rubrobacter radiotolerans*, les acides gras, le glucopyranoside, et les produits des pigments sont les principaux produits. Les acides gras comprennent l'acétate de lauryl, l'acétate de 1-hexadécanol, l'ester méthylique de l'acide heptadécanoïque, l'ester méthylique de l'acide octadécanoïque, le nonadécanoate de méthyle, l'ester méthylique de l'acide eicosanoïque, l'acide tétradécanedioïque, l'ester méthylique de l'acide (Z)-13-docosénoïque. Certains alcanols ont également été détectés, comme le 1-nonadécanol, le 1-octadécanol, le 1-hexadécanol, le 1-docosanol. Ces longues chaînes contenant des acides gras et des alcanols pourraient être les produits de la dégradation des membranes cellulaires de *Rubrobacter radiotolerans*. Carreto [686] a également étudié la composition en acides gras de *Rubrobacter radiotolerans* avec GC/MS combiné avec la triméthylsilylation par bis-(triméthylsilyl)-trifluoroacétamide, l'acide 12-méthylhexadécanoïque (12-méthyl-16:0) et l'acide 14-méthyl-octadécanoïque (14-méthyl-18:0) ont été déterminés comme les principaux acides gras. Les sucres ou les composés contenant du sucre représentent une grande partie des produits de *Rubrobacter radiotolerans*. Parmi ces dérivés glucopyranosides, l'abondance du phényl 2,3,4,6-tétra-O-méthyl- $\alpha$ -D-glucopyranoside est la plus élevée. En outre, la bactériorubérine et la monoanhydrobactériorubérine sont

les deux principaux pigments caroténoïdes qui ont été détectés chez *Rubrobacter radiotolerans*.

Pour les Archaea halophiles, les dérivés de l'adénine et le squalène sont les plus faciles à trouver et sont les plus abondants par rapport aux autres composés organiques de *Halobacterium salinarum*. L'adénine pourrait provenir de la dégradation de l'ATP, qui est une molécule liée à la transformation de l'énergie pour maintenir la viabilité des cellules. Le squalène, un isoprénoïde à 30 carbones, est le principal composant de la fraction non polaire, connu principalement pour son association avec la bactériorhodopsine. Les acides gras sont d'autres composés importants trouvés chez *Halobacterium salinarum*. Les membranes des extrémophiles constituent la première ligne de défense contre les agressions environnementales. La partie lipidique polaire de la membrane de *Halobacterium salinarum* est principalement composée de phospholipides et de glycolipides à base d'archéol, un lipide diéther de glycérol contenant des chaînes phytanyles dérivées d'isoprénoïdes.

Le glucopyranoside est l'un des composés cibles les plus importants des trois bactéries extrémophiles utilisées ici. Cependant, son abondance est différente dans chaque échantillon. L'abondance du glucopyranoside-dérivé est la plus faible chez *Halobacterium salinarum*, la plus élevée chez *Cyanobacterium*. L'abondance du phényl glucopyranoside est la plus élevée chez *Rubrobacter radiotolerans*. Les caroténoïdes sont les principaux pigments chez *Rubrobacter radiotolerans* et *Halobacterium salinarum*. Le squalène est leur composé majoritaire dans le cas d'une présence de caroténoïdes. D'après les résultats, nous pouvons conclure que 200 °C pourrait être suffisant pour la décomposition des membranes cellulaires, bien qu'une température plus élevée puisse favoriser la détection de certains composés organiques plus réfractaires. De nombreux composés organiques ont été détectés à partir de ces échantillons de vie naturelle ; cependant, d'autres expériences sont nécessaires pour identifier tous les composés organiques. Il s'agit d'une nouvelle méthode et d'un nouveau projet pour étudier les composés caractéristiques des échantillons naturels.

Le désert d'Atacama est un ancien désert hyperaride tempéré, qui s'étend sur près de 1000 km le long de la côte Pacifique de l'Amérique du Sud, de 30 °S à 20 °S. Son extrême aridité peut être attribuée à l'inversion constante de température provoquée par le courant de Humboldt, frais et orienté vers le nord, et à la présence du fort anticyclone du Pacifique [67,68]. C'est l'un des plus importants analogues martiens sur Terre, et c'est un point chaud pour les extrémophiles et les microorganismes extrémotolérants où les limites chimiques et physiques de la vie peuvent être étudiées [76]. Il est donc essentiel d'étudier les composés organiques de l'échantillon d'Atacama par thermochimie TMAH, afin d'optimiser les conditions expérimentales pour l'analyse in-situ de l'échantillon martien. Dans ce chapitre, les composés organiques de l'échantillon du désert d'Atacama (AT05-177 et AT05-22) ont été analysés avec et sans thermochimie au TMAH, et à différents taux de chauffage, avec trois types de programmes, dont la flash pyrolyse, la rampe de type MOMA et la pyrolyse en rampe de type SAM.

# Contents

Acknowledgements .....	1
General preamble .....	4
Résumé en français .....	6
Contents.....	14
List of figures .....	20
List of tables .....	29
List of abbreviations and acronyms.....	31
Chapter 1. Introduction.....	36
1.1 The background of the study.....	36
1.1.1 The habitability of Mars .....	37
1.1.1.1 The Red planet-Mars .....	37
1.1.1.2 Why go to Mars? .....	38
1.1.2 Mars missions – the search for traces of life with <i>in-situ</i> analysis .....	39
1.1.2.1 Viking landers .....	40
1.1.2.2 Curiosity- SAM .....	41
1.1.2.3 ExoMars-MOMA .....	43
1.2 The detection of organic and inorganic compounds on Mars .....	44
1.2.1 Organic compounds.....	44
1.2.2 Oxychlorides on Mars .....	46
1.3 Possible life bioindices on Mars .....	47
1.3.1 Organic compounds from Atacama Desert .....	47
1.3.2 The possible bacteria on Mars.....	48
1.3.2.1 Halotolerant bacteria .....	49
1.3.2.2 Cyanobacteria.....	51
1.3.3 The organics in Bacteria.....	53
1.3.3.1 Lipids.....	53
1.3.3.2 Amino acids.....	54
1.3.3.3 Nucleic acids .....	54
1.3.3.4 Polysaccharides .....	56
1.3.3.5 Pigments .....	57
1.3.3.6 Proteins.....	61
1.3.4 Important organic compounds for life.....	61
1.4 The search for organic compounds with TMAH thermochemolysis: From Earth analyses to space exploration experiments .....	62

Abstract: .....	62
Keywords: .....	62
1.4.1 Introduction .....	63
1.4.1.1 What is thermochemolysis?.....	63
1.4.1.2 Factors influencing thermochemolysis.....	65
1.4.1.3 Set-ups for thermochemolysis and complementary technologies .....	70
1.4.2 Applications.....	73
1.4.2.1 Lignin and plants .....	73
1.4.2.2 Coal .....	77
1.4.2.3 Lacquer and heritage .....	81
1.4.2.4 Soil .....	87
1.4.2.5 Polymers.....	90
1.4.2.6 Thermochemolysis for space exploration.....	92
1.4.2.7 Others .....	97
1.4.3 Quantitative analysis .....	98
1.4.4 The reactional mechanisms involved in TMAH thermochemolysis .....	102
1.4.4.1 The mechanism of TMAH thermochemolysis .....	102
1.4.4.2 The mechanism of TMAH degradation.....	102
1.4.5 Conclusions and future trends .....	104
1.5 Conclusions .....	105
1.5.1 Thesis scope, objectives and hypotheses.....	105
1.5.2 Thesis outline .....	106
Chapter 2. Influence of pyrolysis and calcium perchlorate on the search for organic compounds using derivatization with MTBSTFA/DMF.....	108
2.1 Introduction .....	108
2.2 Experimental .....	111
2.2.1 Chemical products.....	111
2.2.2 Pyrolysis experiments.....	112
2.2.3 Analysis of pyrolysis products .....	113
2.3 Results .....	113
2.3.1 MTBSTFA and DMF flash pyrolysis at different temperatures.....	113
2.3.1.1 DMF flash pyrolysis at different temperatures.....	113
2.3.1.2 MTBSTFA flash pyrolysis at different temperatures .....	115
2.3.1.3 MTBSTFA/DMF flash pyrolysis at different temperatures .....	121
2.3.2 MTBSTFA/DMF flash pyrolysis with Ca(ClO <sub>4</sub> ) <sub>2</sub> at different temperatures.....	122
2.3.3 MTBSTFA/DMF and calcium perchlorate pyrolysis with SAM-like ramp.....	124

2.3.4 Flash pyrolysis at 850 °C of Murchison meteorite and calcium perchlorate.....	126
2.4 Discussion .....	128
2.4.1 The mechanism of MTBSTFA/DMF degradation at different temperatures .....	128
2.4.2 The mechanism of MTBSTFA/DMF pyrolysis in the presence of calcium perchlorate....	131
2.4.3 Consequences on the origin of chlorine bearing organic molecules detected from the pyrolysis of Martian rock samples with the SAM experiment .....	138
2.4.3.1 The formation of organic compounds from the pyrolysis of the Murchison meteorite	138
2.4.3.2 The formation of Cl-containing compounds from the pyrolysis of the Murchison meteorite.....	139
2.5 Conclusion.....	140
Chapter 3. Influence of calcium perchlorate on the search for organics on Mars with TMAH thermochemolysis.....	142
3.1 Introduction .....	142
3.2. Experimental design.....	146
3.2.1 Samples and chemical products.....	146
3.2.2 Pyrolysis experiments.....	148
3.2.3 GC/MS analysis.....	149
3.3 Results and discussion.....	149
3.3.1 Flash pyrolysis of TMAH at 600 °C.....	149
3.3.1.1 Products of TMAH treated with flash pyrolysis at 600 °C.....	149
3.3.1.2 Effect of Ca(ClO <sub>4</sub> ) <sub>2</sub> on flash pyrolysis of TMAH .....	153
3.3.2 The pyrolysis of TMAH under SAM experimental conditions .....	164
3.3.2.1 Products of TMAH pyrolysis under SAM experiment conditions .....	164
3.3.2.2 The effect of calcium perchlorate on TMAH under SAM-like pyrolysis experimental conditions .....	166
3.3.3 Mechanism of reaction of perchlorate with TMAH during the pyrolysis .....	168
3.3.4 Fatty acid recovery with TMAH thermochemolysis in the presence of calcium perchlorate .....	179
3.4 Conclusions .....	181
Chapter 4. Application of TMAH thermochemolysis to the detection of the nucleobases: application to the MOMA and SAM space experiment. ....	184
4.1 Introduction .....	184
4.2 Experiments.....	186
4.2.1 Materials and methods.....	186
4.2.2 Pyrolysis-GC/MS and methods .....	187
4.2.3 Quantification of all nucleobases .....	187
4.3 Results and Discussion.....	188

4.3.1 Optimization of the thermochemolysis for nucleobases.....	188
4.3.1.1 Adenine .....	188
4.3.1.2 Thymine and Uracil.....	191
4.3.1.3 Cytosine.....	192
4.3.1.4 Guanine .....	194
4.3.1.5 Xanthine .....	197
4.3.1.6 Hypoxanthine .....	197
4.3.2 Thermochemolysis patterns.....	198
4.3.3 Analysis of the mixture of nucleobases.....	204
4.3.4 Quantification study of nucleobases.....	206
4.4 Conclusion.....	208
Chapter 5. Application of TMAH thermochemolysis to the detection of nucleic acids: application to the MOMA and SAM space experiment.....	210
5.1 Experiment conditions.....	211
5.1.1 Samples .....	211
5.1.2 Py-GC/MS and methods.....	214
5.2 TMAH thermochemolysis of nucleosides .....	214
5.2.1 TMAH thermochemolysis for nucleosides.....	214
5.2.2 Optimization of thermochemolysis for nucleosides .....	218
5.2.3 Analysis of the mixture of nucleosides at different temperatures .....	222
5.2.4 SAM-like ramp pyrolysis .....	223
5.3 TMAH thermochemolysis of nucleotides .....	227
5.3.1 TMAH thermochemolysis for nucleotides .....	227
5.3.2 Optimization of thermochemolysis for nucleotides.....	230
5.3.3 Analysis of the mixture of nucleosides at different temperatures .....	234
5.3.4 SAM-like ramp pyrolysis .....	235
5.4 TMAH thermochemolysis of nucleotides triphosphate.....	237
5.4.1 Flash pyrolysis.....	237
5.4.2 SAM-like ramp pyrolysis .....	242
5.5 TMAH thermochemolysis of poly A.....	243
5.5.1 Flash pyrolysis.....	244
5.5.2 SAM-ramp like pyrolysis .....	246
5.6 Thermochemolysis patterns.....	249
5.7 Conclusions .....	250
Chapter 6. Application of TMAH thermochemolysis to the detection of bacteria: application to the MOMA and SAM space experiment.....	252



6.1 Experimental .....	252
6.1.1 Cultures .....	252
6.1.1.1 E.coli culture .....	252
6.1.1.2 Chroococcidiopsis cubana culture .....	253
6.1.1.3 Rubrobacter radiotolerans culture .....	253
6.1.1.4 Halobacterium salinarum culture .....	253
6.1.2 Separation of cells .....	253
6.1.3 Py-GC/MS .....	254
6.2 Organic compounds from <i>E.coli</i> with TMAH thermochemolysis .....	254
6.2.1 Flash pyrolysis.....	254
6.2.1.1 Organic compounds from E.coli with TMAH thermochemolysis.....	255
6.2.1.2 The distribution of organic compounds from E.coli.....	257
6.2.2 SAM-like ramp pyrolysis .....	260
6.3 TMAH thermochemolysis of cyanobacteria .....	260
6.3.1 Organics from cyanobacteria.....	260
6.3.2 Optimal temperature for the detection of organic compounds .....	266
6.4 TMAH thermochemolysis of Anctinobacteria .....	267
6.4.1 Organics from <i>Rubrobacter radiotolerans</i> .....	267
6.4.2 Optimal temperature for the detection of organic compounds .....	280
6.5 TMAH thermochemolysis of halophilic bacteria .....	283
6.6 Conclusions .....	294
Chapter 7. Application of TMAH thermochemolysis on the analysis of Atacama sample.....	296
7.1 Experimental conditions.....	296
7.1.1 Sample preparation.....	296
7.1.2 Extraction of Atacama sample.....	297
7.1.3 Pyrolysis and GC/MS .....	298
7.2 Organic compounds of Atacama sample.....	299
7.2.1 Pyrolysis-GC/MS .....	299
7.2.2 Atacama sample with TMAH thermochemolysis .....	304
7.3 Conclusions .....	305
Chapter 8. Conclusions and perspectives .....	307
8.1 General conclusion.....	307
8.2 Future work .....	309
Reference:.....	311
Appendix .....	388
Résumer (French).....	404



## List of figures

**Figure 1-1** The facts of Mars, from NASA website.

**Figure 1-2** The Viking landers and the sample analysis instruments.

**Figure 1-3** The Curiosity rover and SAM instruments, adapted from [1].

**Figure 1-4** The three SAM instruments the Quadrupole Mass Spectrometer (QMS), the Gas Chromatograph (GC), and the Tunable Laser Spectrometer (TLS) on SAM, from [2].

**Figure 1-5** The ExoMars and MOMA instruments.

**Figure 1-6** Chain of sample processing and analysis, cited from [3].

**Figure 1-7** Structural formulas of carotenoids.

**Figure 1-8** The structures of lignin that react with TMAH thermochemolysis, adapted from [4–8]. (A)  $\beta$ -O-4' alkyl-aryl ethers; (A')  $\gamma$ -acylated  $\beta$ -O-4' alkyl-aryl ethers ; (B) phenylcoumarans; (C) resinols; (C') tetrahydrofuran structures formed by  $\beta$ - $\beta$  coupling of monolignols acylated at the  $\gamma$ -carbon; (D) dibenzodioxocins; (D') spirodienone structures formed by  $\beta$ -1' coupling; (E) C $\alpha$ -oxidized  $\beta$ -O-4' structures; (I) cinnamyl alcohol end-groups; (I')  $\gamma$ -acylated cinnamyl alcohol end-groups; (J) cinnamyl aldehyde end-groups; (PCA) *p*-coumarate units; (FA) ferulates; (H) *p*-hydroxyphenyl units; (G) guaiacyl units; (S) syringyl units; (S') oxidized syringyl units bearing a carbonyl (R, lignin side-chain) or carboxyl (R, hydroxyl group) group at C $\alpha$ .

**Figure 1-9** The structure of bituminous structure, adapted from [9].

**Figure 1-10** TMAH thermochemolysis with different organic compounds.

**Figure 1-11** The structures of polymers that react with TMAH during thermochemolysis, adapted from [10–21].

**Figure 1-12** Sample Monitoring System (SMS) and close up of the SAM oven. Adapted from [22].

**Figure 1-13** Tapping station with its oven (left) and derivatization capsule (right).

**Figure 1-14** The structure of nucleobases and fatty acids, adapted from [22,23].

**Figure 1-15** The mechanism of TMAH thermochemolysis, adapted from [24–26].

**Figure 1-16** the Outline of this thesis.

**Figure 2-1** Example of fatty acids and amino acids derivatized by MTBSTFA.

**Figure 2-2** Chromatograms (TIC) of the compounds detected after DMF pyrolysis at different temperatures. Peak attributions: 1: Dimehtylamine; 2: Ethanolamine; 3: N, N, N', N'-

tetramethyl-methanedi-amine; 4: Dimethylamino-acetonitrile; 5: Hexahydro-1,3,5-trimethyl-1,3,5-triazine; 6: Hydracrylonitrile; 7: Benzene.

**Figure 2-3** Chromatogram (TIC) of MTBSTFA flash pyrolysis at different temperatures. GC conditions can be seen in section 2.3 analysis of pyrolysis products. Peak attributions: 1: tert-butyl-dimethylsilyl-fluorosilane; 2: N-methyltrifluoroacetamide (TFMA); 3: tert-butyl-dimethylsilyl-MSW; 4: N-Methyl-N-trimethylsilyl-trifluoroacetamide (MSTFA); 5: BSW; 6: Tris(trimethylsilyl)borate; 7: 3-methyl-3H-cyclonona[def]biphenylene.

**Figure 2-4** Chromatograms of MTBSTFA/DMF (4:1) pyrolyzed at different temperatures compared with those obtained with MTBSTFA only under the same conditions (as Section 2.3 analysis of pyrolysis products).

**Figure 2-5** Chromatograms of MTBSTFA/DMF (4:1) pyrolysis with and without calcium perchlorate at 210 °C.

**Figure 2-6** Influence of calcium perchlorate on the abundance of main products of MTBSTFA/DMF flash pyrolysis at 210 °C.

**Figure 2-7** Chromatograms (TIC) of MTBSTFA/DMF (4:1) mixture pyrolyzed at different temperatures. Peak attributions 1: CO<sub>2</sub>; 2: TBDMS-F; 3: DMF; 4: TFMA; 5: MSW; 6: MSTFA; 7: Ethyl isopropyl(dimethyl)silyl ether; 8: BSW; 9: Bis(tert-butyl-dimethylsilyl)amine; 10: tert-butyl-dimethylsilyl isocyanate; 11: Tris(trimethylsilyl)borate; 12: tert-butyl(methoxy)dimethylsilyl; IS: Naphthalene-d<sub>8</sub>(Internal standard).

**Figure 2-8** Influence of the amount of calcium perchlorate on the main chemical products observed when MTBSTFA/DMF (4 :1) pyrolyzing at SAM-like ramp of 300 °C.

**Figure 2-9:** Chromatogram of flash pyrolysis at 850 °C of the Murchison meteorite.

**Figure 2-10:** Chromatogram of flash pyrolysis of Murchison and carbon-free Murchison with calcium perchlorate (Chloro-bearing benzene and their isomers).

**Figure 2-11** Distribution of the byproducts detected from MTBSTFA flash pyrolysis at different temperatures.

**Figure 2-12** Possible reaction pathways of MTBSTFA pyrolyzed at different temperatures.

**Figure 2-13** Abundance of CO<sub>2</sub> from MTBSTFA/DMF pyrolysis with Ca (ClO<sub>4</sub>)<sub>2</sub> at different conditions.

**Figure 2-14** Chlorinated compounds detected from the pyrolysis of MTBSTFA/DMF with calcium perchlorate.

**Figure 2-15** Chromatograms of MTBSTFA/DMF (4:1) stepped pyrolysis with 15wt% of ClO<sub>4</sub><sup>-</sup> at different temperatures. Peak 1: tert-Butyl-dimethylsilyl-MSW; 2: tert-butyl-dimethyl-fluorosilane; 3: TFMA; 4: N-Methyl-N-(trimethylsilyl)trifluoroacetamide; 5: BSW; 6:

Tris(trimethylsilyl)borate; 7: DMF; 8: trimethylamine; 9: N,N-dimethyltrifluoroacetamide; 10: Carbon dioxide.

**Figure 2-16** Distribution of CO<sub>2</sub> and CH<sub>3</sub>Cl of MTBSTFA/DMF (4:1) step pyrolysis with 15wt.% of ClO<sub>4</sub><sup>-</sup> at different temperatures.

**Figure 3-1** Thermal decomposition of alkyltrimethylammonium deuteroxide[27]. Case 1: R<sup>1</sup>, R<sup>2</sup>, and R<sup>3</sup> =H; Case 2: R<sup>1</sup>=CH<sub>3</sub>, R<sup>2</sup> and R<sup>3</sup>=H; Case 3: R<sup>2</sup>=H, R<sup>1</sup>and R<sup>3</sup>=CH<sub>3</sub>; Case 4: R<sup>1</sup>, R<sup>2</sup>, and R<sup>3</sup>=CH<sub>3</sub>. TS=Transition State.

**Figure 3-2** The calibration curve of H<sub>2</sub>O detection.

**Figure 3-3** The chromatogram of TMAH flash pyrolysis at 600 °C. Peak 1: CO<sub>2</sub> ; Peak 2: 3-Aminobutanoic acid ; Peak 3: Dimethyl ether ; Peak 4 : Trimethylamine ; Peak 5 : Dimethoxy-methane ; Peak 6: N- methyl-ethylamine ; Peak 7: Urea ; Peak 8, 9: N,N-dimethyl-ethylamine; Peak 10: Betaine; Peak 11: 1, 2-dimethoxy-ethane.

**Figure 3-4** The mechanism of TMAH degradation via flash pyrolysis.

**Figure 3-5** Chromatograms of TMAH pyrolysis with Ca (ClO<sub>4</sub>)<sub>2</sub> in different abundance at 600 °C. (Peak 1: dimethyl ether; 2: 2-methoxyethoxy-ethene; 3: N,N-dimethyl-methylamine; 4: Tetramethylammonium acetate?; 5: 1-methylaziridine; 6: N,N-dimethyl-ethylamine; 7,8 : N,N,N',N'-tetramethyl-methanediamine; 9: dimethylamino-acetonitrile; 10: dimethyl-cyanamide; 11: N-methyl-N-(2-hydroxyethyl)carbamic acid, methyl ester; 12: N,N-dimethyl-formamide; 13: propenal dimethylhydrazone; 14: 1-methyl-3-pipridinol; 15: N,N-dimethylacetamide; 16: hexahydro-1,3,5-trimethyl-1,3,5-triazine; 17: N-methyl-N-(2-hydroxyethyl)carbamic acid, methyl ether; 18: benzoic acid, methyl ester; 19: N,N,4-trimethyl-benzenemethanamine; 20: hexadecanoic acid, methyl ester(plalmitic acid, methyl ester); 21: octadecanoic acid; methyl ester ( Stearic acid, methyl ester); 22: 2-butenedioic acid(Z)-diethyl ester( Maleic acid diethyl ester).

**Figure 3-6** Effect of perchlorate on the main products of TMAH pyrolysis at 600 °C(A<sub>i</sub>/A<sub>s</sub> represents the peak area of the internal standard divided by the peak area of the target compounds).

**Figure 3-7** Chromatography of TMAH pyrolysis at SAM ramp. Peak 1: CO<sub>2</sub> ; peak 2,4 : Dimethyl ether; peak 3: Ethanedioic acid; peak 5: Trimethylamine; peak 6: N,N-dimethyl-Ethylamine; peak 7: N,N'-dimethyl-Ethylenediamine; peak 8: 2-propanamine; peak 9: Diethylamine; peak 10: 2,2-dimethoxy-ethanamine.

**Figure 3-8** Chromatograms of TMAH pyrolysis with Ca(ClO<sub>4</sub>)<sub>2</sub> at SAM ramp. Peak 1: N,N-dimethyl-ethylamine; peak 2 and 4 : N,N,N',N'-tetramethyl-methanediamine; peak 3: Dimethylamino-acetonitrile; peak 5: DMF; peak 6: N-ethyl-acetamide; peak 7: TMTAC.

**Figure 3-9** The effect of  $\text{Ca}(\text{ClO}_4)_2$  on the pyrolysis products of TMAH at a heating rate of  $35\text{ }^\circ\text{C}\cdot\text{min}^{-1}$  from 50 to  $600\text{ }^\circ\text{C}$ .

**Figure 3-10** The chromatography of TMAH with 20 wt.%  $\text{ClO}_4^-$ , TMAH, and  $\text{Ca}(\text{ClO}_4)_2$  pyrolysis at 400 to  $500\text{ }^\circ\text{C}$  at a heating rate of  $35\text{ }^\circ\text{C}\cdot\text{min}^{-1}$ .

**Figure 3-11** Chromatograms of TMAH pyrolysis (a heating rate of  $35\text{ }^\circ\text{C}\cdot\text{min}^{-1}$ ) with 20 wt. % calcium perchlorate at different temperatures ( Peak1:  $\text{CO}_2$ ); 2: chloromethane; 3 and 5: TMA; 4: N,N-dimethyl-ethylamine; 5, 6: N,N,N',N'-tetramethyl-methanediamine; 7: 1-Methyl-pyrrole; 8: Dimethylamino-acetonitrile; 9: Dimethyl-cyanamide; 10: N,N-dimethylformamide; 11: TMTAC; 12: Dimethyl ether.)

**Figure 3-12** The chromatography of DMF flash pyrolysis at  $600\text{ }^\circ\text{C}$ .

**Figure 3-13** The plausible mechanism of TMAH degradation with the presence of calcium perchlorate at  $600\text{ }^\circ\text{C}$ .

**Figure 3-14** The effect of calcium perchlorate on the recovery of fatty acids by TMAH thermochemolysis.

**Figure 3-15** The recovery of fatty acids with TMAH thermochemolysis on Mars-like conditions. The concentration of perchlorate is the ratio of perchlorate to organics (300 ppb of fatty acids).

**Figure 4-1** Chromatograms of adenine thermochemolysis in TMAH performed at different temperature (A:  $600^\circ\text{C}$ ,  $500^\circ\text{C}$ , and  $400^\circ\text{C}$ .) and different amount (B: (a) 0.125 nmol (b) 0.25 nmol (c) 2.5 nmol). Chromatogram A: Peak 1: 3-methyl-3H-purin-6-amine; Peak 2: N, 9-dimethyl-9H-purin-6-amine; Peak 3: N, N, 9-trimethyl-9H-purin-6-amine; Peak 4: N, N, 3-trimethyl-3H-purin-6-amine; Peak 5: dimethyl adenine; Peak 6,7,8,9: trimethyl adenine. Note the break in the intensity scale to show the height of peak 3; Chromatogram B: Peak 1: 3-methyl-adenine; Peak 2: N, 9-dimethyl-adenine; Peak 3: N, N, 9-trimethyl adenine; Peak 4: N, N, 3-trimethyl-adenine; Peak 5: dimethyl adenine; Peak 6,7,8,9: trimethyl adenine. Note the break in the intensity scale to show the height of peak 3 in the 2.5 nmol chromatogram.

**Figure 4-2** Mass spectra of adenine methylated through thermochemolysis. (a-e) 162 m/z corresponds to the molecular ion of dimethyladenine and (b-e) 177 m/z corresponds to the molecular ion of trimethylated adenine.

**Figure 4-3** Chromatograms of thymine (0.26 nmol) and uracil (0.26 nmol) thermochemolysis in TMAH at different temperatures.

**Figure 4-4** Chromatograms of cytosine (15 nmol) thermochemolysis in TMAH thermochemolysis at different temperatures (1: 4-amino-2-methoxy-pyrimidine; 2: dimethyl

cytosine; 3: trimethyl-cytosine; 4: N, N, N'-trimethyl-cytosine; 5: trimethyl-cytosine; 6: siloxane).

**Figure 4-5** Mass spectra of methylated cytosine. 139  $m/z$  corresponds to the molecular ion of the dimethylated cytosine and 153  $m/z$  corresponds to the molecular ion of the trimethylated cytosine.

**Figure 4-6** Chromatograms of guanine (11 nmol) thermochemolysis in TMAH at 600 °C, 500 °C, and 400 °C. (1: caffeine; 2: dimethyl-guanine; 3 and 5: trimethylguanine; 4, 6, 7, 8: tetramethylguanine; 9: trimethylguanine).

**Figure 4-7** Mass spectrum of methylated guanine. 179  $m/z$  corresponds to the molecular ion of dimethyl guanine, 193  $m/z$  corresponds to the molecular ion of trimethylated guanine, and 207  $m/z$  corresponds to the molecular ion of tetramethylated guanine.

**Figure 4-8** Chromatograms of xanthine (0.22 nmol) and hypoxanthine (1.2 nmol) thermochemolysis in TMAH at different temperatures.

**Figure 4-9** The TMAH thermochemolysis schemes of seven nucleobases.

**Figure 4-10** Chromatograms of seven nucleobases mixtures dissolved in TMAH thermochemolysis at 600°C. Peak 1: 1, 3-dimethyl-uracil ; Peak 2 : 1, 3-dimethyl-thymine; Peak 3 : N, N, N'-trimethyl-cytosine; Peak 4 : N, N, 9-trimethyl-adenine; Peak 5 : 1, 3, 7-trimethyl-xanthine (caffeine); Peak 6 : 1,7-dimethyl-hypoxanthine; Peak 7: methyl ester hexadecanoic acid; Peak 8 : trimethyl-guanine; Peak 9 : trimethyl-adenine Peak X: Siloxane.

**Figure 4-11** Calibration curves for the seven nucleobases.

**Figure 5-1** The structures of nucleobases, nucleosides, nucleotides, and nucleotides triphosphate.

**Figure 5-2** The chromatogram of nucleosides with TMAH thermochemolysis at flash pyrolysis of 200 °C.

**Figure 5-3** Mass spectrum of the organic compounds from nucleosides with TMAH thermochemolysis.

**Figure 5-4** The chromatograms of nucleosides with TMAH thermochemolysis at different flash pyrolysis temperatures.

**Figure 5-5** Distribution of thermochemolysis products of nucleosides in TMAH at different temperatures ( $A_i/A_{IS}$  is the ratio of area of organics and the area of internal standard).

**Figure 5-6** The abundance of methyl fufuryl obtained from nucleosides with TMAH at different temperatures ( $A_i/A_{IS}$  is the ratio of area of organics and the area of internal standard).

**Figure 5-7** Chromatograms of nucleosides (10 nmol each) after TMAH thermochemolysis at different temperatures. Peak 1 : Furfuryl methyl ether; Peak 2 : 2'-deoxy-Cytidine?; peak 3 : 3-

methyl-1,2-cyclopentanedione?; peak 4 : 1,3-dimethyl-uracil ; peak 5 : 1,3-dimethyl-thymine; peak 6: N,N,9-trimethyl-adenine; peak 7,9 : 1,7-dimethyl-hypoxanthine; peak 8: N,N,3-trimethyl-adenine; peak 10: 2'-deoxy-3-methyl-3',5'-di-O-methyl-Uridine; peak 11: 2'-deoxy-N,O,O-trimethyl-thymidine ; peak 12 : 2'-deoxy-N,O,O,O- tetramethyl-Adenosine.

**Figure 5-8** The pyrolysis products of nucleosides at SAM-like ramp pyrolysis.

**Figure 5-9** The chromatogram of the mixtures of nucleosides at SAM-like ramp pyrolysis. Peak 1: Furfuryl methyl ether; 2: 1,3-dimethyl-uracil; 3: 1,3-dimethyl- thymine; 4: trimethyl-cytosine; 5: N,N,9-Trimethyl-adenine; 6,8: 1,7-dimethyl-hypoxanthine; 7: N,N,3-Trimethyl-adenine; 9: 2'-Deoxy-3-methyl-3',5'-di-O-methyl-Uridine; 10: 2'-Deoxy-3-methyl-3',5'-di-O-methyl-Uridine; 11: 2'-deoxy-N,N,O,O-tetramethyl-adenosine; 12: 2'-deoxy-N,N,O,O-tetramethyl-Cytidine.

**Figure 5-10** The abundance of each nucleoside detected by Py-GC/MS at SAM-like ramp pyrolysis with TMAH thermochemolysis.

**Figure 5-11** The chromatography of nucleotides with TMAH thermochemolysis at flash 200 °C.

**Figure 5-12** Chromatograms of nucleotides with TMAH thermochemolysis at different flash temperatures.

**Figure 5-13** The abundance of methyl phosphate from 4mix of nucleotides monphosphate with TMAH thermochemolysis at different temperatures.

**Figure 5-14** The mass spectrum of methylated phosphate.

**Figure 5-15** Distribution of thermochemolysis products of nucleotides in TMAH at different temperatures ( $A_i/A_{IS}$  is the ratio of area of organics and the area of internal standard).

**Figure 5-16** Chromatograms of nucleotides (10 nmol) thermochemolysis in TMAH at different temperatures. Peak 1 : Methyl phosphate ; peak 2 :1,3-dimethyl-uracil ; peak 3 : 1,3-dimethyl-thymine; peak 4: N,N,9-trimethyl-adenine; peak 5: Hexadecanoic acid, methyl ester; peak6: N,N,3-trimethyl-adenine; peak 7: Octadecanoic acid, methyl ester; peak 8: 2'-deoxy-N,O,O-trimethyl-thymidine(trimethyl-dT) ; peak 9: 2'-deoxy-N,O,O,O- tetramethyl-Adenosine(tetramethyl-dA).

**Figure 5-17** Chromatograms of nucleotides (10 nmol) thermochemolysis in TMAH at SAM-like ramp pyrolysis.

**Figure 5-18** Chromatograms of the mixtures of nucleotides (10 nmol) thermochemolysis in TMAH at SAM-like ramp pyrolysis.

**Figure 5-19** Chromatograms of nucleotides with TMAH thermochemolysis at different flash temperatures.



**Figure 5-20** The abundance of methyl phosphate from 5mix of nucleotides triphosphate with TMAH thermochemolysis at different temperatures.

**Figure 5-21** Distribution of thermochemolysis products of nucleotides triphosphate in TMAH at different temperatures ( $A_i/A_{IS}$  is the ratio of area of organics and the area of internal standard).

**Figure 5-22** The mixtures of nucleotides triphosphate with TMAH thermochemolysis at different temperatures. Peak 1: 1,3-dimethyl-uracil; 2: 1,3-dimethyl-thymine; 3: N,N,9-trimethyl-adenine; 4: N,N,3-trimethyl-adenine; 5: Tetramethyl-guanine.

**Figure 5-23** The pyrolysis products of nucleotides triphosphate with TMAH at SAM-like ramp pyrolysis.

**Figure 5-24** Chromatograms of mixtures of nucleotides triphosphate thermochemolysis in TMAH at SAM-like ramp pyrolysis. Peak 1: 1-chlorocyclohexene; 2: Furfuryl methyl ether; 3: methyl phosphate; 4: 1,3-dimethyl-uracil; 5: 1,3-dimethyl-thymine; 6: N,N,9-Trimethyl-adenine; 7: trimethyl-cytosine; 8: N,N,3-Trimethyl-adenine; 9,10::tetramethyl-guanine.

**Figure 5-25** The structures of Poly A.

**Figure 5-26** Chromatograms of PolyA (5.15 nmol) thermochemolysis in TMAH at different temperatures.

**Figure 5-27** Distribution of thermochemolysis products of Poly A in TMAH at different temperatures ( $A_i/A_{IS}$  is the ratio of area of organics and the area of internal standard).

**Figure 5-28** Chromatogram of Poly A (5.15 nmol) thermochemolysis in TMAH at SAM-like ramp pyrolysis. Peak 1: methyl phosphate; 2: N,N,9-Trimethyl-9H-Purin-6-amine or N,N,9-Trimethyl-adenine; 3: Hexadecanoic acid, methyl ester; 4: N,N,3-Trimethyl-3H-Purine-6-amine N,N,9-Trimethyl-adenine; 5: Methyl stearate; 6: 2'-deoxy-N,N,O-tetramethyl-adenosine.

**Figure 5-29** The relative intensity of methyl phosphate from poly A with TMAH thermochemolysis at different conditions.

**Figure 5-30** the plausible mechanism of poly A with TMAH thermochemolysis.

**Figure 5-31** The thermal stability of nucleosides, nucleotides, nucleotides triphosphate and their plausible pathway with TMAH thermochemolysis at different temperatures.

**Figure 6-1** The samples of *Chroococcidiopsis cubana*(C.C.), *Rubrobacter radiotolerans*(R.R.), and *Halobacterium salinarum*(H.S).

**Figure 6-2** The chromatograms of *E.coli* with TMAH thermochemolysis at different flash pyrolysis temperatures. Peak 1: Furfuryl methyl ether; 2: Methyl phosphate; 3: Methyl vanillate; 4: Dodecanoic acid, methyl ester; 5: Tetradecanoic acid, methyl ester; 6: Methyl myristoleate; 7: Methyl palmitoleate; 8: Hexadecanoic acid, methyl ester; 9: cis-10-Heptadecenoic acid,

methyl ester; 10: 9-Octadecenoic acid(Z)-,methyl ester; 11: Octadecanoic acid, methyl ester; 12: cis-10-Nonadecenoic acid, methyl ester; 13: N,N-dimethyl-Adenosine.

**Figure 6-3** The nucleobases detected from *E.coli* with TMAH thermochemolysis at flash 300 °C.

**Figure 6-4** the distribution of fatty acids from *E.coli* with TMAH thermochemolysis at different temperatures (200 °C to 600 °C).

**Figure 6-5** The abundance of methyl phosphate detected from *E.coli* with TMAH thermochemolysis at different temperatures (200 °C to 600 °C).

**Figure 6-6** The abundance of methyl furfuryl detected from *E.coli* with TMAH thermochemolysis at different temperatures (200 °C to 600 °C).

**Figure 6-7** Chromatograms of *E.coli* with TMAH thermochemolysis at SAM-like ramp pyrolysis.

**Figure 6-8** The chromatograms of *chroococcidiopsis cubana* with TMAH thermochemolysis at different flash pyrolysis temperatures. Peak 1: p-methoxy-cinnamic acid, methyl ester; 2: Heptadecane; 3: N,N,9-trimethyl-Adenine; 4: Methyl palmitoleate; 5: Palmitic acid, methyl ester ; 6,15: GlcA-DG, permethylated; 7: 2(3H)-Furanone,5-heptyldihydro-; 8: Phytol; 9: Octadecanoic acid, emthyl ester; 10: Linoleic acid, methyl ester; 11: Glucopyranoside, phenyl 2,3,4,6-tetra-O-methyl, A-d-; 12: Manmopyranoside,methyk 2,3,4,6-tetra-O-methyl, a-D-; 13,14: Glucopyranoside, methyl 2,3,4,6-tetra-O-methyl-,a-D-.

**Figure 6-9** the distribution of organic compounds from *chroococcidiopsis cubana* with TMAH thermochemolysis at different flash pyrolysis temperatures.

**Figure 6-10** The chromatograms of *Rubrobacter radiotolerans* with TMAH thermochemolysis at different flash pyrolysis temperatures. Peak 1: N,N,9-trimethyl-adenine; 2: Cyclohexane, 1R-acetamido-4-cis-acetoxy-5,6Zcisepoxy-2-cis,3trans-dimethoxy-3: a-D-Glucopyranoside, phenyl 2,3,4,6-tetra-O-methyl-; 4: 1-Nonadecanol; 5: Methyl 3-methoxy-2-[(2,3,4,6-tetra-O-methylhexopyranosyl)oxy]propanoate; 6: Heptadecanoic acid, methyl ester; 7:1-Docosanol; 8: 1-Hexadecanol; 9: Methyl nonadecanoate; 10: a-D-Glucopyranoside,2,3,4,6-tetra-O-methyl-a-glucopyranosyl 2,3,4,6-tetra-O-methyl-; 11: a-D-Glucopyranoside, phenyl 2,3,4,6-tetra-O-methyl-; 12:Triethylene glycol monododecyl ether; 13: 1,5-Anhydro-2,3,4,6-tetra-O-methyl-D-mannitol; 14: 1,2,3,4-Tetramethylmannose; 15: 2-hydroxy-tetradecanoic acid; 16: Squalene.

**Figure 6-11** The distribution of long-chain bearing fatty acids and alkanes from *Rubrobacter radiotolerans* with TMAH thermochemolysis at different flash pyrolysis temperatures. RT=25.61 min: n-tridecanol; 27.30 min: 1-Hexadecanol; 27.92 min: 1-Docosene; 28.86 min:

1-Octadecanol; 29.34 min: 1-Hexadecanol; 29.46 min: 1-Nonadecene; 29.94 min: 1-Docosanol; 30.29 min: Methyl nonadecanoate; 33.14 min: Chimilether; 35.07 min: Squalene.

**Figure 6-12** The abundance of adenine, cytidine and glucopyranoside from *Rubrobacter radiotolerans* with TMAH thermochemolysis at different flash pyrolysis temperatures.

**Figure 6-13** The chromatograms of *halobacterium salinarum* with TMAH thermochemolysis at different flash pyrolysis temperatures.

**Figure 6-14** The distribution of main organics from *halobacterium salinarum* with TMAH thermochemolysis at different flash pyrolysis temperatures.

**Figure 7-1** Cryogenic Mixer Mill CryoMill, Retsch, Germany.

**Figure 7-2** the extraction device of Atacama sample. 1: Serpentine condenser; 2: Condensate pipe; 3: Extraction tube and round-bottomed flask; 4: Iron stand; 5: Electric heating mantle.

**Figure 7-3** The chromatograms of AT 05-177 and AT 02-22 with TMAH thermochemolysis at flash pyrolysis, MOMA-like ramp pyrolysis, and SAM-like ramp pyrolysis.

**Figure 7-4** The chromatograms of AT05- 177 sample without and with TMAH thermochemolysis at flash pyrolysis, MOMA-like ramp, and SAM-like ramp pyrolysis.

**Figure 7-5** The chromatograms of AT02-22 sample without and with TMAH thermochemolysis at flash pyrolysis, MOMA-like ramp, and SAM-like ramp pyrolysis.

## List of tables

**Table 1-1** Thermochemolysis reagents have been used in the detection of organic compounds.

**Table 1-2** Combined analyses methods with TMAH-thermochemolysis.

**Table 1-3** The organic compounds detected in ancient samples with TMAH-Py-GC/MS in previous studies.

**Table 1-4** The organic compounds detected in soil samples with TMAH-Py-GC/MS in previous studies.

**Table 1-5** Quantification using Py-GC/MS with the external calibration curves.

**Table 1-6** Quantification using internal standards.

**Table 2-1:** Products detected from DMF flash pyrolysis at 210, 300, 600, 850 °C.

**Table 2-2:** The main products of MTBSTFA flash pyrolysis at different temperatures.

**Table 2-3:** The chlorinated compounds have been detected in previous SAM and MOMA studies.

**Table 3-1** The pyrolysis products of TMAH flash pyrolysis at 600 °C, refers to Figure 3-3.

**Table 3-2** The products of TMAH flash pyrolysis with calcium perchlorate over 10 wt.% at 600 °C, refers to Figure 3-5.

**Table 3-3** the distribution of the pyrolysis products of TMAH with 10 wt. % of perchlorate during the flash pyrolysis at 600 °C.

**Table 3-4** The products of TMAH pyrolysis at 600 °C at a heating rate of 35°C .min<sup>-1</sup> from 50°C to 600 °C, refers to Figure 3-7.

**Table 3-5** The step pyrolysis products of TMAH with 20 wt. % calcium perchlorate at a heating rate of 35 °C.min<sup>-1</sup>.

**Table 3-6** The pyrolysis products of DMF flash pyrolysis at 600 °C.

**Table 4-1** Detailed information of nucleobases used in this study.

**Table 4-2** The thermochemolysis products detected from different nucleobases.

**Table 4-3** The characteristic peaks of the seven nucleobases in TMAH.

**Table 4-4** The methylated components detected from pyrolysis of the nucleobases mixture.

**Table 4-5** LOD and LOQ values and the standard curves of each nucleobase.

**Table 5-1** Detailed information of samples used in this study.

**Table 5-2** The compounds of nucleosides and nucleotides with TMAH thermochemolysis at 200 °C.

**Table 5-3** The target compounds of nucleosides with TMAH thermochemolysis.

**Table 5-4** The main products of nucleotides with TMAH thermochemolysis at flash 200 °C

**Table 5-5** The main compounds detected from Poly A with TMAH thermochemolysis at flash pyrolysis.

**Table 6-1** The organic compounds from Cyanobacteria with TMAH thermochemolysis at 200 °C.

**Table 6-2** The organic compounds from Anctinobacterium with TMAH thermochemolysis.

**Table 6-3** The organic compounds from *halobacterium salinarum* with TMAH thermochemolysis.

**Table 7-1** Organic compounds detected from AT 05-177 sample flash pyrolysis at 600 °C.

**Table 7-2** Organic compounds detected from AT 02-22 sample flash pyrolysis at 600 °C.

## List of abbreviations and acronyms

AD	Dimethyl adipate
A/P ratio	A ratio of azeleic acid to palmitic acid methyl esters
AT	Atacama Desert
BA	Butylene adipate
BD	Butanediol dimethyl ether
BM	Butanediol monomethyl ether
BS	Butylene succinate
BSTFA	N, O-bis-(trimethylsilyl)trifluoroacetamide
BSW	1,3-bis (1, 1-dimethylethyl)-1,1,3,3-tetramethyldisiloxane or bi-silylated water
<i>C.C.</i>	<i>Chroococidiopsis cubana</i>
dA	Deoxyadenosine
dAMP	Nucleotides include 2'-deoxyadenosine 5'-monophosphate
dATP	Nucleotides triphosphates include deoxyadenosine triphosphate
dC	2'-Deoxycytidine
dCMP	2'-Deoxycytidine 5'-monophosphate
dCTP	Deoxycytosine triphosphate
dG	Deoxyguanosine
dGMP	2'-Deoxyguanosine 5'- monophosphate sodium salt hydrate
dGTP	Deoxyguanosine triphosphate
2D-HSQC-NMR	Heteronuclear single quantum coherence spectroscopy
dI	Deoxyinosine
dIMP	2'-Deoxyinosine 5'-monophosphate sodium salt
dITP	Deoxyinosine triphosphate
DKPs	Piperazine-2,5-diones
DMF	N,N-Dimethylformamide
DMF-DMA	N,N-Dimethylformamide dimethyl acetal
DNA	Deoxyribonucleic acid
dNMPs	Deoxynucleotides
2D NMR	Two-dimensional nuclear magnetic resonance
DSC	Differential Scanning Calorimetry
dT	Thymidine
dTMP	Thymidine 5'-monophosphate disodium, salt hydrate
DTMS	Direct temperature resolved mass spectrometry
dTTP	Deoxythymine triphosphate

dU	2'-Deoxyuridine
dUMP	2'-Deoxyuridine 5'-monophosphatedisodium salt
dUTP	Deoxyuridine triphosphate
<i>E.coli</i>	<i>Escherichia coli</i>
EDTA	Ethylenediaminetetraacetic acid
EGA	Evolved Gas Analysis
EtOAc	Ethyl acetate
FAMEs	Fatty acid methyl esters
FTIR	Fourier transform infrared spectroscopy
FTIR-ATR	Fourier transform infrared spectroscopy attenuated total reflectance
G	Guaiacyl units
GC/MS	Gas chromatography mass spectrometry
H	<i>p</i> -Hydroxyphenyl units
HCl/MeCN	Hydrogen chloride /acetonitrile
HF	Hydrogen fluoride
HILIC-UHPLC-TQ-MS/MS	Triple-quadrupole tandem mass spectrometry
<sup>1</sup> H NMR	Hydrogen nuclear magnetic resonance
HPLC	High performance liquid chromatography
<i>H.S.</i>	<i>Halobacterium salinarum</i>
ICP-MS	Inductively coupled plasma mass spectrometry
ICP-QQQ	Triple-quadrupole inductively coupled plasma-mass spectrometry
IOM	Acid-insoluble molecular
LC-MS	Liquid chromatography-mass spectrometry
LDI	Laser desorption / ionization
L/F	Litter/fermentation layer
LHA	Leonardite humic acids
LM	Light microscopy
LPS	Lipopolysaccharides
LOD	Limit of detection
LOQ	Limit of quantification
LOS	Lipooligosaccharides
MAAs	Mycosporine-like amino acids
MALDI-TOF MS	Matrix Assisted Laser Desorption Ionization-Time of flight-mass spectrometry
MCL	Milled-cork lignins
MFT	Microfade testing electron paramagnetic resonance spectroscopy

MMRS	Mars Micro-beam Raman Spectrometer
MOMA	Mars Organic Molecule Analyzer
MSL	Mars Science Laboratory
MSTFA	N-methyl-N-trimethylsilyltrifluoroacetamide
MSW	Tert-butyldimethylsilanol or monosilylated water
MTB	<i>Mycobacterium tuberculosis complex</i>
MTBSTFA	N-methyl-N-tert-butyldimethylsilyl- trifluoroacetamide
NASA	National Aeronautics and Space Administration
N(CH <sub>3</sub> ) <sub>4</sub> <sup>+</sup>	Tetramethylammonium
NHA	Nitrohumic acids
NIST	National institute of standards and technology
NMR	Nuclear magnetic resonance spectroscopy
NTM	Non-tuberculous mycobacteria
OD600	Optical density at a wavelength of 600 nm
OM	Optical microscopy
PA6	Polyamide 6
PAHs	Poly aromatic hydrocarbons
PBSA	Poly (butylene succinate- <i>co</i> -butylene adipate)
PC	Polycarbonate
PCA	p-Coumarate units
PCB	Polychlorinated biphenyl
PDA	Photodiode array
PDIM	Phthiocerol dimycocerosate
PE	Polyethylene
PET	Polyethylene terephthalate
PG	Phosphatidylglycerol
PGP-Me	Phosphatidylglycerophosphate methyl ester
<i>p</i> -HBA	<i>p</i> -Hydroxybenzoic acid
PHB	Polyhydroxybutyrate
P(3HB- <i>co</i> -3HHx)	Poly (3-hydroxybutyrate- <i>co</i> -3-hydroxyhexanoate)
PMMA	Poly(methyl methacrylate)poly(alkyl methacrylate),
POC	Particulate organic carbon
Poly A	Ployadenylic acid
PP	Polypropylene
ppb(m/w)	Parts per billion by mass or weight
PS	Polystyrene



P/S ratios	Ratios of palmitic to stearic acid methyl esters
PVC	Polyvinyl chloride
Py-GC-ITMS	Pyrolysis GC ion trap mass spectrometry
Pyr-GC/MS	Pyrolysis-Gas Chromatography coupled to Mass Spectrometry
QMS	Quadrupole Mass Spectrometer
RH	Relative humidity
RNA	Ribonucleic acid
RR	Roots plus rhizomes
<i>R.R.</i>	<i>Rubrobacter radiotolerans</i>
RT	Retention time
S	Syringyl units
SAM	Sample Analysis at Mars
SD	Dimethyl succinate
SEM	Scanning electron microscope
SEM–EDX	Scanning electron microscopy–energy dispersive X-ray spectroscopy
SH	Posidonia australis sheaths
SMS	Sample Monitoring System
SOM	Soil organic matter
SOM	Solvent-soluble
SSL	Split/SplitLess
TAAH	Tetraalkylammonium hydroxides
TBAH	Tetrabutylammonium hydroxide
TBDMS	Tert-butyldimethylsilane
TBDMS-Cl	Chloro-tertbutyldimethylsilane
TBDMS-F	Tert-butyldimethylfluorosilane
TBSA	Tuberculostearic acid
TEAH	Tetraethylammonium hydroxide
TEM	Transmission electron microscopy
TFMA	N-methyl-2,2,2-trifluoroacetamide; N-methyltrifluoroacetamide
TFTMAH	m-(Trifluoromethyl)phenyltrimethylammonium hydroxide
TG	Thermal gravimetry
TGA-MS	Thermogravimetric analyzer –mass spectrometry
THM	Thermally assisted hydrolysis and methylation
TID	Total ionizing dose
TMA	Trimethylamine
TMAAc	Tetramethylammonium acetate

TMAH	Tetramethylammonium hydroxide
TMAH-Py-GC/MS	TMAH thermochemolysis combined with Pyrolysis-gas chromatography and mass spectrometry
TMCS	Trimethylchlorosilane
TMPAH	Phenyltrimethylammonium hydroxide
TMSH	Trimethylsulfonium hydroxide
TMSI	Trimethylsilylimidazole
TMTAC	Hexahydro-1,3,5-trimethyl-1,3,5-triazine
UASB	Up-flow anaerobic sludge blanket
UV	Ultraviolet
WCL	Wet chemistry laboratory
XRD	X-ray diffraction
XRF	Fluorescence spectrometry
XPS	X-ray photoelectron spectroscopy
YPG medium	Yeast, peptone and glucose medium

# Chapter 1. Introduction

## 1.1 The background of the study

This work is mainly based on the search for organic material on Mars, which is one of the main goals of the Sample Analysis at Mars (SAM) experiment [2] aboard the NASA Curiosity rover. Searching for organic compounds on Mars could develop the understanding of the origin of life on Earth. There are three main theories about the origin of life on Earth. One is the theory proposed by Haldane and Oparin: they thought that life could originate from inorganic matters, which could spontaneously generate organic matters. Haldane and Oparin speculated that living matter evolved from self-replication, but non-living molecules could explain the origin of life on Earth. Therefore, another two hypotheses for the origin of life were proposed. One is that organic molecules that support life come from space. The detection of organic compounds such as nucleobases and amino acids could prove this theory. The third main origin theory suggests that Earth's primordial organic materials were first generated in deep-sea fumaroles-hydrothermal vents. Each of these three main theories for the origin of life are not mutually exclusive. Life could have occurred in different ways and could be combining with the delivery of extraterrestrial compounds. In order to identify if there is extraterrestrial life, we have to search for biosignatures or the biomarkers that relate to life directly at extraterrestrial locations. Therefore, some missions have been designed to search for biosignatures in space, including missions to Mars, Venus, and Saturn, and to Saturn's largest satellite, Titan, as well as to cometary destinations, etc. Among these planets, Mars is the most plausible candidate planet that possibly allows life to survive since there is evidence showing that Mars had a similar environment around 3.8 Gy ago to that of the Earth when terrestrial life first started. However, Mars cooled more quickly, leading to a possible extinction of life, or a dormant and buried life on Mars. Hence, many efforts have been made to explore biosignatures on Mars, including the Viking missions (1976), Spirit and Opportunity (2004), the Mars Express mission (2003) [28], Phoenix spacecraft (2008), Curiosity rover (2012), and the latest Perseverance rover (2020). Among these missions, one of the most important ways to detect biosignatures is the GC/MS system.

In 1976, the first *in situ* landing mission to Mars, the Viking mission, aimed at finding extraterrestrial life using a GC/MS system. In recent missions, more advanced analytical methods and systems have been applied. Pyrolysis-GC/MS was carried out by SAM, and wet

chemistry has been applied to analyze possible organic compounds on Mars. Derivatization reagents, MTBSTFA/DMF and TMAH, are carried by SAM to detect refractory organics on Mars possibly linked with traces of life. Those organic compounds could be fatty acids, amino acids, nucleobases etc. To guide the space experiments and to explain the results collected by rovers on Mars, lab experiments need to be done, including optimizing the experimental conditions and understanding the byproducts of reagents. Therefore, this thesis is focused on the optimization of experimental conditions and providing the corresponding data reference for the interpretation of data from SAM. In addition, previous work on the application of derivatization reagents and related work has been reviewed.

### 1.1.1 The habitability of Mars

#### 1.1.1.1 The Red planet-Mars

Mars is the 4<sup>th</sup> planet from the Sun and is an arid, rocky, cold, and apparently lifeless world. It has some similarities and differences compared with the Earth. There are two moons of Mars, Phobos (13.8 miles) and Deimos (7.8 miles). The size of Mars (4220 miles in diameter) is smaller than Earth (7926 miles in diameter). The average distance of Mars from the Sun is about  $1.42 \times 10^8$  miles. A year on Mars is almost twice as long as a year on Earth; there are 687 Earth days on Mars. The volume of Mars is one-sixth the volume of the Earth, and Mars has about one tenth of the mass of the Earth. The gravity of Mars is about 62.5% less than that on Earth.

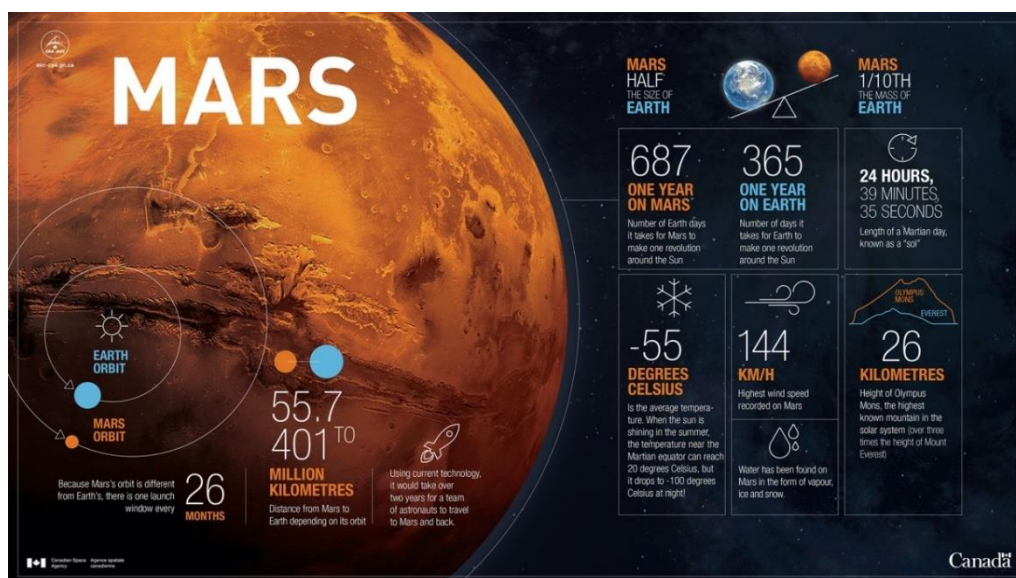


Figure 1-1 The facts of Mars, from NASA website.

The environment of Mars is also different from that of the Earth. On Mars, the temperature is very low and varies from -140 °C to 30 °C; the average temperature is about -63 °C. The atmosphere of Mars contains 96% carbon dioxide, < 2% argon, < 2% nitrogen, and < 1% other gases. On the surface of Mars, there are a lot of rocks composed of minerals such as olivine, pyroxene, amphiboles, carbonates, sulfates, silica, phyllosilicates, phosphates, feldspar, and iron oxides (hematite). Based on similar landforms on Earth and Mars, some places on Earth have been considered as Martian analogues. Samples from Iceland (with more iron), Antarctica (with a cold and dry environment), the Atacama Desert in Chile (very dry and similar rocks to Mars), Arizona (basaltic volcanism) and Hawaii (large basaltic shield volcanoes) are some examples of Martian analogue samples.

#### ***1.1.1.2 Why go to Mars?***

For us, Mars is one of the most accessible places in the Solar System. Exploring Mars could provide the opportunity to possibly answer the question of the origin and the evolution of life, and it could someday be a destination for the survival of humankind.

Mars has been considered as a terrestrial planet with an atmosphere and climate, and has diverse and complex geology like Earth. It would have been habitable for life in the past and the climate on Mars appears to have changed over its history. From -4.56 Gy to -4.1 billion years ago, it was the pre-Noachian period on Mars. During the pre-Noachian period, Mars was formed and differentiated, and the Martian Crust formed [29,30]. However, there would not be traces remaining. Liquid water would have existed during the Noachian and Hesperian periods on Mars, though it was lost during the Amazonian period. Those three periods are the three major geological periods in Martian history: 1) The Noachian (-4.1 to 3.7 billion years ago). During the Noachian period, there would have possibly been the presence of perennial liquid water at the Martian surface. There is evidence for an ancient ocean on Mars because of the global distribution of deltas and valleys [31]; 2) The Hesperian (-3.7 to 3.0 billion years ago). During the Hesperian period, liquid flow at the surface become rarer and the climate conditions changed, the temperature decreased, and the atmosphere become thinner. There were still volcanic activities [32]; 3) The Amazonian (-3.0 billion years ago to today). The planet gradually became a cryosphere via the loss of water [33]. Glacial and/or wind hydrological processes were the main activates. In this period, the most friable rocks were turned into grains and dusts [34].

In addition, Mars is impacted by UV radiation from the Sun. This radiation could promote photochemistry in the atmosphere at the surface of Mars. The formation of a magnetic field (during the first billion of <4.5 Ga) [35] on Mars could protect the surface from energy sources such as energetic particles and galactic cosmic rays [36]. As we know that Mars had geophysical activity related to volcanism [37], the gradient of geothermal flow is a possible energy source. In addition, there would have been hydrothermal events serving as a type of energy source. These energy sources could have promoted the formation and development of life on primitive Mars.

There could be organic molecules at the surface of Mars, deposited by exogenous sources such as micrometeorites and interplanetary dust particles, which were particularly bombarding the surface of Mars during the Amazonian period of Mars's history. Organic compounds could also be formed by abiotic photosynthesis or electrochemical reduction of CO<sub>2</sub> [38]. It could also be possible that organic compounds are from biotic sources present in the subsurface of Mars. Organic compounds on Mars could be destroyed by ultraviolet radiation and by oxidation processes at the surface of Mars, although clays such as phyllosilicates, carbonates, and sulfates could serve as preservers for those organic compounds. Additionally, organic compounds such as amino acids, carboxylic acids, and nucleobases that are essential for life have been detected in meteorites, such as the Murchison meteorite [39–42]. Meteorites could be an exogenous source of organic compounds. Therefore, it is possible that these essential organic compounds are present on Mars and could have supported the formation of life.

Therefore, liquid water, an energy source, and organic compounds essential for life would have been present across geologic timescales in Mars's past. Mars would have been a habitable planet in the past. Therefore, searching for the traces of life could be an important way to study the origin and the development of life.

### **1.1.2 Mars missions – the search for traces of life with *in-situ* analysis**

*In-situ* analysis is one of the most important methods to detect traces of life on Mars. There have been several missions focused on the search for traces of life on Mars, including the Viking landers, the MERs, Spirit and Opportunity (2004), the Mars Express mission (2003), the Phoenix mission (2010), the Curiosity rover (2012), Perseverance (2021, landing February 18, 2021), and ExoMars (will be launched in 2022). Those missions have provided and will provide substantial information about Mars, *e.g.* the Martian atmosphere and the composition

of the Martian soil. Among these rovers, only the Viking landers, the Curiosity rover and ExoMars have a chemistry lab. They were designed to search for traces of life by analyzing organic compounds in the Martian soil. Therefore, the instruments and the exploration have been reviewed in this section.

### ***1.1.2.1 Viking landers***

The Viking mission was the first *in situ* landed mission to Mars aimed at finding extraterrestrial life. Two twin landers were successfully placed on the surface of Mars in 1976. The Viking 1 lander, launched on August 20, 1975, touched down on the surface of western *Chryse Planitia* at 22.697 deg N latitude and 48.222 deg W longitude on July 20, 1976. The Viking 2 lander was launched on September 9, 1975 and touched down on September 3, 1976. Viking 2 landed about 200 km west of the crater Mie in *Utopia Planitia* at 48.269 deg N latitude and 225.990 deg W longitude. Both of the two landers were designed to achieve the following goals: 1) to study the biological and chemical composition (organic and inorganic), meteorology, seismology, magnetic properties, appearance, and physical properties of the Martian surface and atmosphere; 2) to search for Earth-like life; 3) to measure for heterotrophic metabolism.

For achieving these goals, the landers carried the Pyrolytic Release Experiment (PR) and a GC/MS instrument (Figure 1-2). Before the sample was sent to the PR experiment, it passed through a sample preparation system. The Martian sample was sieved to obtain a particle size smaller than 300  $\mu\text{m}$ . The Martian samples were heated in the pyrolyzer from 50 to 500  $^{\circ}\text{C}$ . The PR experiment includes an oven to heat the Martian samples that had been exposed to radioactively tagged  $\text{CO}_2/\text{CO}$  in the presence of sunlight to measure either photosynthetic or chemosynthetic fixation of  $\text{CO}_2$  or  $\text{CO}$  into organic compounds. Volatiles could be formed during the PR experiments; they were then carried by a carrier helium flow and sent to the GC for separation and the MS for the detection of organic compounds. That was the first time a GC system was used for a space exploration application. The GC was 9×9×6 cm, connected to an injection system, which could facilitate an injection of a sample volume of up to 100  $\mu\text{L}$ . The GC column was heated at a heating rate of 8  $^{\circ}\text{C min}^{-1}$  from 50  $^{\circ}\text{C}$  (held for 10 min) to 200  $^{\circ}\text{C}$ , and held for 1 hour at 200  $^{\circ}\text{C}$ . The carrier gas was helium, and the flow rate was 2  $\text{mL min}^{-1}$ . The mass detection range of the MS was 12 to 215 Da [43].

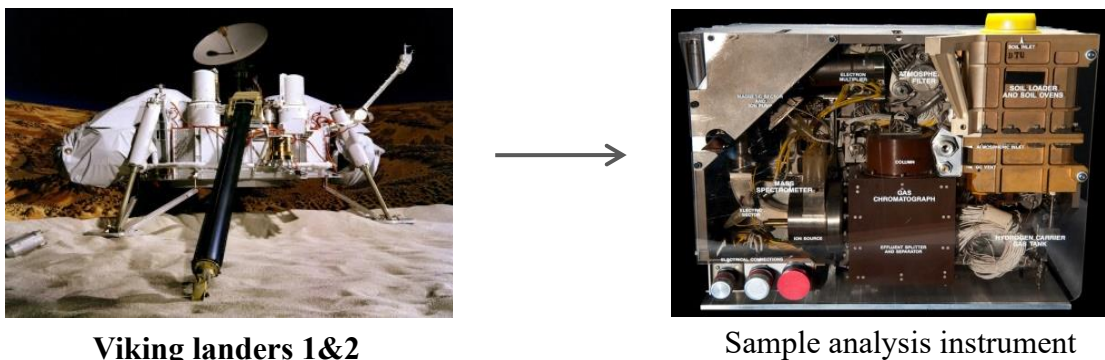


Figure 1-2 The Viking landers and the sample analysis instruments.

### 1.1.2.2 Curiosity- SAM

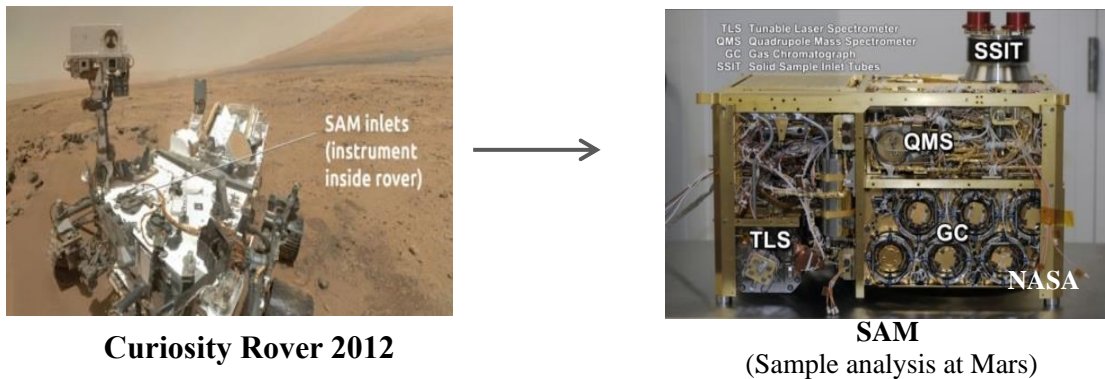
NASA's Mars Science Laboratory (MSL) was launched from Cape Canaveral Air Force Station, Florida, in November 26, 2011. The Mars Curiosity rover landed successfully at Gale Crater, at 4.6 degrees on south latitude, 137.4 degrees east longitude, on August 6, 2012. The Curiosity Rover is a big rover (about 3 meters or 10 feet), weighing 899 kilograms (1982 pounds). It has been designed to explore the habitability of Mars in the past and present, through the exploration and assessment of a local region on the surface of Mars as a potential habitat for life.

There are scientific instruments and a sample acquisition, processing, and distribution system onboard the Curiosity rover. Acquired Martian samples of rocks, soil, and atmosphere are analyzed by the analytical instruments. The Sample Analysis at Mars (SAM) experiment (Figure 1-3) was designed to analyze the molecular and elemental chemistry relevant to life. SAM can analyze organic compounds, the chemical state of light elements other than carbon, and isotopic tracers of planetary change [1]. SAM contains a Quadrupole Mass Spectrometer (QMS), a GC, and a Tunable Laser Spectrometer (TLS) (Figure 1-4). The QMS is the second detector, after a TCD detector (Thermal Conductivity Detector) for the GC with a mass range of 2-523 Dalton. The GC and GC/MS systems analyze volatiles released from the solid samples (rocks or soils). Those volatiles released by Martian samples are carried by a helium carrier gas and sent to the GC for separation. The TLS analyzes precise isotope ratios for carbon and oxygen in CO<sub>2</sub>.

Besides the analytical system, the sample preparation system still plays an important role for the analysis of organic compounds on Mars. The *in-situ* derivatization and pyrolysis methods are essential for the detection of organic compounds in Martian samples. To prepare the Martian samples, the solid phase materials such as soil or rocks are sampled by sieving them



( $\leq 150 \mu\text{m}$ ) and transporting them to one of 74 SMS sample cups. Those samples are sent to the EGA experiment. The oven is heated up to its final temperature ( $950 \text{ }^\circ\text{C}$  to  $1100 \text{ }^\circ\text{C}$ ) at a heating rate of  $35 \text{ }^\circ\text{C}/\text{min}$ . All the volatiles released by EGA are collected by SAM hydrocarbon traps for later GC/MS analysis.



**Curiosity Rover 2012**

**SAM**  
(Sample analysis at Mars)

Figure 1-3 The Curiosity rover and SAM instrument, adapted from [1].

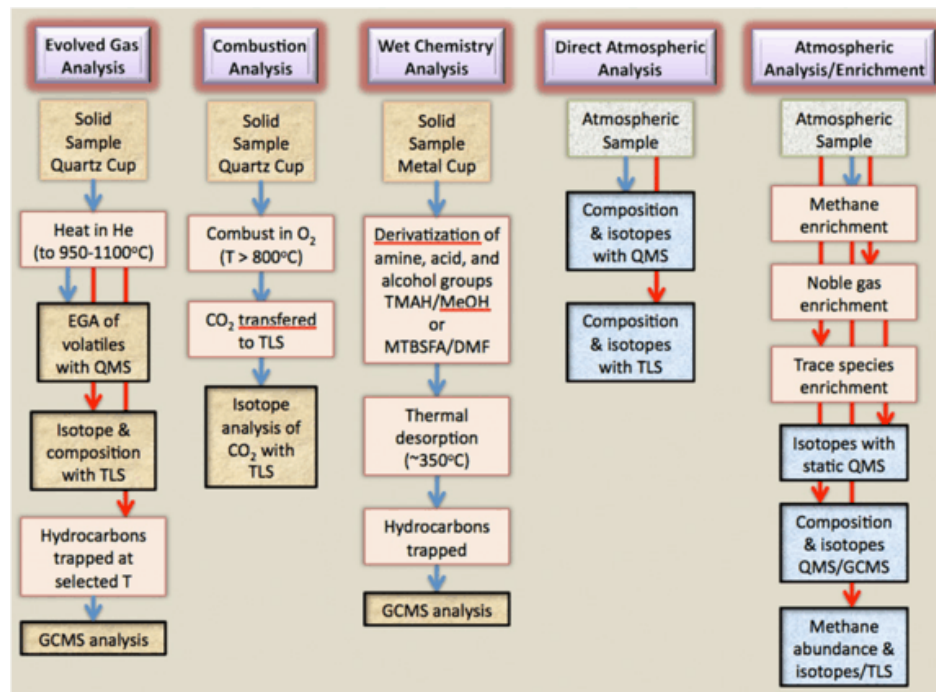


Figure 1-4 The three SAM instruments are the Quadrupole Mass Spectrometer (QMS), the Gas Chromatograph (GC), and the Tunable Laser Spectrometer (TLS) on SAM, from [2].

In addition, organic compounds in solid samples can be analyzed by GC/MS aided by wet chemistry. The SAM instrument is able to perform a lower temperature ( $75\text{--}300 \text{ }^\circ\text{C}$ ) wet chemical processing step prior to GCMS analysis. The application of derivatization reagents,

such as MTBSTFA/DMF and TMAH, can transform targeted organic compounds into species that are sufficiently volatile and amenable to separation by GC columns in order to enable their detection by GC/MS [44]. MTBSTFA/DMF is a type of reagent used for the silylation of organics; TMAH can be applied for the methylation of labile organic compounds at high temperature such as 600 °C. Those organic compounds could be amino acids, fatty acids, and carboxylic acids, etc. The use of wet chemistry can improve the volatility and reduce the polarity of targeted organic compounds, which improves the probability of detection of these compounds. Because TMAH thermochemolysis is the main method that was studied in this thesis, the application of TMAH thermochemolysis is reviewed in the next section.

### 1.1.2.3 ExoMars-MOMA

The Mars Organic Molecule Analyzer (MOMA) instrument will be onboard the ESA/Roscosmos ExoMars rover (to launch in 2022). ExoMars will be able to analyze the organic compounds of the Martian sample drilling from 2m below the Martian surface. The main goal of ExoMars is to search for traces of life in the past or present life on Mars. This goal could be divided into several sub-goals, *e.g.*, 1) search for molecular biosignatures; 2) Search for evidence of active processes (geochemical, biologic, or exogenous); 3) Understand the geologic context. To achieve these goals, MOMA has been designed with four analytical objectives. It would be able to detect and characterize organic molecular species in solid samples with high sensitivity, analyze the organic compounds at a wide range of weight, analyze the chiral organics, and study the inorganic geochemical components of the organic analyses. The ExoMars and MOMA instruments are shown in Figure 1-5.

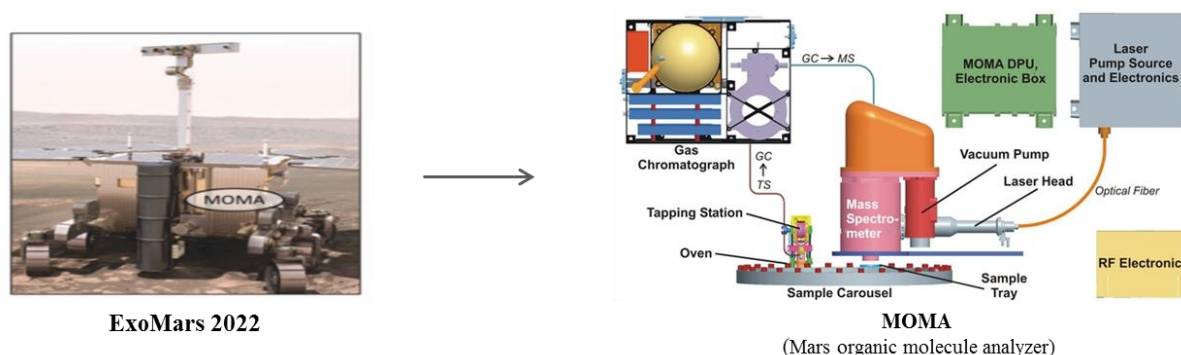


Figure 1-5 The ExoMars and MOMA instruments.

To analyze organic compounds in volatile at a wide range of weight, pyrolysis-GC/MS and combined with wet chemical method will also be applied on MOMA. For non-volatile

organics, the LDMS will be applied to produce gas-phase ions by high-intensity laser pulses, the products in gas phase will be analyzed by MS, with a common linear ion trap MS (ITMS) for detection and identification of molecular ions. Figure 1-6 is the chain of sample processing and analysis. First, the sample in the subsurface of Mars will be collected by drilling and ground into powder, then it will be delivered into the refillable sample tray and the oven, and be treated by laser or heated by oven and chemical alteration (derivatization and thermochemolysis), respectively. The mixtures of these products formed during this process will be sent to aperture valve and GC. At last, MS or TCD and MS will be applied to detect the mass fragments of organic compounds. All the detailed information of these instruments have been explained in the review article of Goesmann et.al [3].

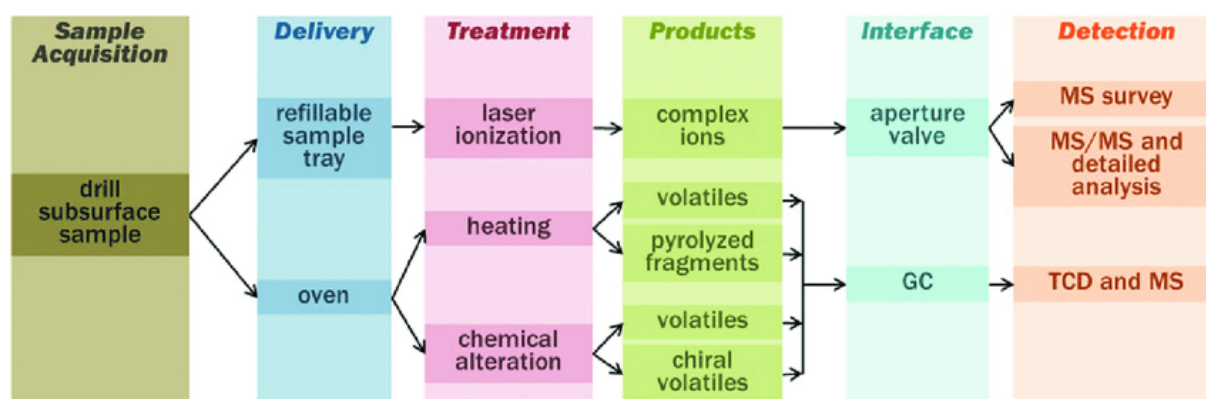


Figure 1-6 Chain of sample processing and analysis, cited from [3].

## 1.2 The detection of organic and inorganic compounds on Mars

### 1.2.1 Organic compounds

Organic compounds are widespread throughout the solar system, and the access to its primitive form is achieved by analyzing extraterrestrial samples from comets, asteroids, meteorites and dust particles. They have been studied in the last few decades. Organic compounds can be divided into solvent-soluble (SOM) and acid-insoluble (IOM), which is obtained after demineralization. The SOM content of meteorites showed a high molecular diversity with ten thousands of different molecular compositions [45], such as carboxylic acids, amino acids, purines, sugars and sugar-related compounds, hydrocarbons, alcohols, amines, etc. The IOM is a type of macromolecular organic solid which accounts for more than half of total organic carbon, and their intact molecular structure is still unknown because of its complex configuration [46]. In addition, the origin of the organic containing materials is not certain. This

is mainly because that alteration may have occurred in the organic containing parent body, such as thermal metamorphism, aqueous alteration, impact shock and brecciation (fragments of older rock fused together) may have influenced the chemical composition of chondrites [47–49].

During the detection of organic compounds on Mars, plumes or patches of methane in the Martian atmosphere that vary over monthly time scales have been detected by the tunable laser spectrometer (TLS) of the Sample Analysis on Mars instrument suite on Curiosity at Gale crater [50]. Compared with the background level of the atmospheric methane of mean value  $0.69 \pm 0.25$  ppbv (95% confidence interval, CI), the elevated levels of methane of  $7.2 \pm 2.1$  ppbv (95% CI) demonstrated that Mars is episodically producing methane from an additional unknown source.

Some organic matters including thiophenic, aromatic, and aliphatic compounds released at high temperatures (500 to 820 °C) were detected by SAM [51]. These organic matters were preserved in lacustrine mudstones at the base of ~3.5-billion-year-old Murray formation at Phahrup Hills, Gale crater, Mars. Thiophene is one of the important organic matters that have been detected on Mars, demonstrating that sulfurization aided organic matter could have been preserved on Mars. Thiophenes are typically occurring on Earth in kerogen, coal and crude oil as well as in stromatolites and microfossils. Their results showed that the abundance of thiophenes and sulfur-bearing minerals showed a close correlation [52], however, the origin of thiophene derivatives is controversial, and there is no evidence that it is of biotic origin.

In addition, chlorine-bearing compounds are important organic compounds that have been detected on Mars. The detection of chloromethane (about 15ppb) and dichloromethane (about 2-40 ppb) were detected by the twin 1976 Viking landers (VL-1 and VL-2) firstly. However, the chlorine-bearing compounds that have been reported at that time, including chloromethane and dichloromethane were attributed to either terrestrial contamination resulting from the use of chlorinated cleaning solvents, or from the reaction of absorbed traces of methanol and HCl [53]. The first *in situ* detection of perchlorate or oxychloride compounds by 2008 Mars Phoenix Lander [54], however, could offer an alternative explanation for the presence of chloromethane and dichloromethane in the Viking GC/MS data sets [55]. Since 2012, several other chloride compounds have been detected by SAM aboard the Curiosity rover. Glavin et al. [56] reported that chloromethane, dichloromethane, trichloromethane, and a chloromethylpropene, were detected by SAM. However, these chlorine-bearing compounds were attributed to the reaction of Martian chloride with terrestrial organic carbon of MTBSTFA. Chlorobenzene was firstly attributed to the reactions of Martian chlorine released from perchlorate with the terrestrial benzene or toluene derived from 2,6-diphenylphenylene oxide

(Tenax) coming from the SAM hydrocarbon trap [56]. Later, the Curiosity detected some chloride-bearing compounds, such as 1,2-dichloroethane, 1,2-dichloropropane, 1,2-dichlorobutane, trichloromethylpropane, and chlorobenzene at the highest amount of ~150 to 300 ppbw [57], dichlorobenzene of ~0.5 to 17 ppbw [58], etc. Guzman et al. [59] reanalyzed the Viking GCMS data sets and searched for chlorobenzene signals, they found that the presence of chlorobenzene was considered in the light of possible sources of organic carbon that possibly indigenous from the martian sample and instrument contaminations. For example, the degradation products of the Tenax®, a polymer-based chemical trap on Curiosity Rover, could react with perchlorate forming chloride-bearing aromatic compounds. The abundance of chlorinated compounds depend on the quantity of calcium perchlorate, the type of Tenax® and the desorption temperature [60]. As the detection of chlorine-bearing compounds on Mars proved that the chlorobenzene detected from Cumberland was from martian origin [57]. However, the precursors that could react with chlorine-bearing compounds forming chlorobenzene are still not clear. Therefore, some studies were focused on the possible precursors of chlorobenzene and other chlorine-bearing compounds. Because there was leaks of MTBSTFA/DMF [56], it could possibly be one of the precursor of chlorobenzene. Therefore, more studies need to be done to determine the precursors of chlorobenzene that has been detected on Mars.

### 1.2.2 Oxychlorides on Mars

NASA's 2008 Phoenix Mars lander and its wet chemistry laboratory (WCL) was the first experiment on Mars which detected ~0.4-0.6 wt.%  $\text{ClO}_4^-$  ions in the Martian soil [54]. Later, chlorine bearing compounds were detected by the Sample Analysis at Mars (SAM) instrument, one of ten instruments on the Mars Science Laboratory (MSL) Curiosity rover, such as hydrogen chloride gas, chloromethane, dichloromethane, chlorobenzene [61], and isomers of dichlorobenzene [62]. From these results, a reinterpretation of the data obtained with the GCMS experiment onboard the 1976 Viking landers suggest that perchlorates and/or chlorates were also present in the samples analyzed by these experiments [59,63]. Further, analysis of the Rocknest wind ripple with the SAM instrument and a comparison with results obtained from laboratory measurements indicates that calcium perchlorate is a better candidate for the perchlorate species than Fe-, Mg-, Ca-, Na- and K-perchlorates [64,65]. These chlorine-bearing hydrocarbons have been attributed to the reaction of oxychlorine related species with organic compounds during the pyrolysis of the samples analyzed with SAM [57,62].

The detection of widespread perchlorates and likely chlorates on Mars has led to several studies related to the potential effect of perchlorates on the detection of organic compounds with various instruments. Perchlorate is a strong oxidizing agent because oxygen can be released from the decomposition of perchlorates and could be the main cause of the degradation of organic compounds. On the other hand, the chlorine could form chlorine-bearing organic compounds. There are two main possible carbon and chlorine sources, one is the terrestrial carbon source on Mars; the other one is the non-terrestrial sources such as contaminants from the sample handling chain and the reagent has leaked into the system [56,57,66]. As MTBSTFA/DMF is one of the derivatization reagents that have been applied in SAM and will be applied in MOMA *in-situ* analysis of Martian samples, it is essential to study the possible chlorinated compounds formed during the pyrolysis of MTBSTFA/DMF in the presence of calcium perchlorate.

### **1.3 Possible life bioindices on Mars**

#### **1.3.1 Organic compounds from Atacama Desert**

Atacama Desert (Chile) is an ancient temperate hyperarid desert, which runs nearly 1000 km along the Pacific coast of South America from 30 °S to 20 °S. Its extreme aridity can be attributed to the constant temperature inversion caused by the cool, north- flowing Humboldt Current and the presence of the strong Pacific anticyclone [67,68]. The mean temperature of this region is about 14-16°C with an increase in precipitation along the North-to-South latitude gradient [69]. Atacama Desert has been treated as one of the most important and interesting Martian analogues on Earth. Therefore, many studies have been done to have a well understanding of Atacama Desert samples, and to have a further understanding on Mars.

Some researchers studied the igneous minerals, carbonates, sulfates and carbonaceous materials were unambiguously identified by Mars Micro-beam Raman Spectrometer (MMRS) in the Atacama Desert (Chile) [70]. The interaction of gas atmosphere with fossilization process was studied. Viennet [71] studied the influence of CO<sub>2</sub> vs. N<sub>2</sub>/O<sub>2</sub> on the fossilization process using an emblematic biomolecule (RNA) and clay minerals, at 200 °C for 7 days. Their results demonstrated that the gas phase impacts the chemical structural of the residual N-rich organic compounds trapped within the interlayer spaces of Mg-smectites. It's mainly aliphatic-rich under CO<sub>2</sub> atmosphere, whereas, the heterocycles, mainly piperidine or pyrrolidine are the predominant products from the atmosphere of N<sub>2</sub>/O<sub>2</sub>.

The organic compounds and microbiomes of Martian soil have been studied. Amine biomarkers were detected through compositional analysis of soil samples and the detection of amino acids from ancient terrestrial life in the most arid Yungay region of the Atacama desert [72]. Aerts [73] studied the organic compounds and the microorganism communities of Atacama Desert, which include wet and dry, and intermediate to high elevation salt flat. Several amino acids extracted from salt crusts and sediments were detected by using liquid chromatography and multidimensional gas chromatography mass spectrometry. These amino acids include *L-asp*, *L-glu*, *D-glu*, *L-Iso-Leu*. et al. Proteinogenic amino acids are the most abundant types and enantiomeric ratio of L-amino acids and D-amino acids indicates biotic origin of these molecules, meaning L-amino acids have higher abundances than their D- amino acids counterparts. In addition, DNA has been extracted from soil samples and determined the composition of microbial communities. Halophilic archaeal family *Halobacteriaceae* (Phylum Euryarchaeota) dominates the dataset making up 39% of the total number of sequences reads. *Haloparvum*, *Natronomonas*, *Halorubrum*, *Halomicrobium*, and *Haloarcula* are some of the most dominant genera from halophilic archaeal. Amino acids and organic carbon and nitrogen found with the Atacama soils match the microbial observations in that they generally correlate with the presence of pronounced life. Salts, such as halite and gypsum, which dominate these salts, have strong preservation potential for biomarkers shown on Mars.

The organic compounds in the Martian subsurface have also been studied. Laura [74] simulated a robotic drilling mission searching for signs of life in the Martian subsurface in the Río Tinto basin (Southwestern Spain), by using a 1m-class planetary prototype drill mounted on a full-scale mockup of NASA's Phoenix and InSight lander platforms. The organic compounds from soil samples such as lipids were analyzed by GC/MS combined with lipid extraction. The distribution of bacteria was studied by DNA extraction, polymerase chain reaction amplification, and DNA sequencing. Their results demonstrating that subsurface biosignatures spanning a wide range of compositional nature, preservation potential, and taxonomic specificity can be recovered from an iron-rich Mars analog site. Non-volatile such as polycarboxylic acids could be in the subsurface of Atacama, though they could be oxidized completely at the top surface of Atacama [75]. This means that it's possible to find life biomarkers under the surface of Atacama Desert because the ground could protect the organic compounds from oxidizing or radiation.

### **1.3.2 The possible bacteria on Mars**

Atacama is a hotpot for extremophiles and extremotolerant microorganisms where the chemical and physical limits for life may be studied [76]. Only extreme organisms which are capable of surviving at very low temperatures and water shortage on Earth, could present hypothetical habitants of Mars [77]. What is “extreme”? Perhaps extreme is the eye of beholder [78]. An organism thrives in an extreme environment more than one extreme called extremophile. The definition of extreme conditions is based on the evolutionary perspective, meaning the earliest environment for life defines what is “extreme”; and the physical definition of “extreme”, such as temperature, radiation, pressure, desiccation, salinity, pH, oxygen, and other extreme conditions. This definition is congruent with the colloquial definition, with exceptions [78]. Various microorganisms, including phototrophic [79] and heterotrophic bacteria, archaea and fungi, were identified in halite crusts of the Atacama Desert. Among these bacteria, the microbial communities are generally dominated by members of the Halobacteriales (e.g. *Halococcus*, *Halorhabdus*, *Haloterrigena*, *Natrinema*), Bacteroidetes (e.g. *Salini-bacter*) and Cyanobacteria (e.g. *Halothece*) [80]. Therefore, some extremophile microorganisms that could be possible survived on Mars will be reviewed in the following subsections.

### ***1.3.2.1 Halotolerant bacteria***

A candidate form of life that could possibly exist in Martian brine is the family of halophile bacteria, such as *halobacterium halobium* [81,82]. Halobacteria is a form of extremophilic Archaea; they could adapt to survive in saturated salt solutions, and they are able to revive in the presence of water after being desiccated into a crust of solid salt. In addition to being adapted to high salt, the halophilic archaeon *halobacterium halobium*, also shows a strong resistance to desiccation, high pressure, UV radiation, and IR [83,84]. Halophilic Archaea could be long-term survived in ancient halite and the preservation of DNA within fluid inclusions for periods of tens of thousands of years [85]. They also could be able to travel hundreds or even thousands of miles in the form of dry, windblown dust and salt and by this means colonize transient small pools [82]. Extremely halophilic archaea (haloarchaea) are of astrobiological interest since viable strains have been isolated from million years old salt deposits [86] and halite has been found in Martian meteorites and in surface pools [87]. Therefore, due to their ability to survive in extremes, they are often considered a model group of organisms to study responses to the harsh conditions associated with space [88]. Halophilic



Archaea has been proposed as a possible candidate for life on early Mars by Litchfield (1998) [89] and as a possible life form on present Mars by Landis [90] and Aerts [73].

With the detection of perchlorines on Mars, some research has been done to study the effect of perchlorate on the survival of *Halobacterium salinarum*. Perchlorate at a concentration of 0.2 M for up to 2 weeks did not affect the ability of a yeast extract-based medium to support growth of the archaeon *Halobacterium salinarum*. Halophilic microorganisms surprisingly well adapt to survival, and maybe even to life, under conditions prevailing on Mars, now or in the past [91]. Halotolerant yeast *Debaryomyces hansenii* was found to tolerant at most of 2.4 M NaClO<sub>4</sub> in liquid growth medium, which is the highest microbial perchlorate tolerance reported to date, more than twice as high as the record reported prior (for the bacterium *Planococcus halocryophilus*). This result demonstrated that it's plausible that Martian microbes, if they exist, could adapt to high perchlorate concentrations and also increase the likelihood of microbial life thriving in the Martian brines [92]. Hypersaline environments preserve biomolecules over geologically significant timescales; therefore, salt-bearing materials should be high-priority targets for the search for evidence of life on Mars [93]. Although the perchlorate are inhibitory for most microorganisms, the presence of Mg(ClO<sub>4</sub>)<sub>2</sub> and NaClO<sub>4</sub> on Mars would not inhibit the growth and the function of haloarchaea, such as *H. lacusprofundi*. Extreme halophiles may be tolerating higher concentrations of the perchlorate ions. For example, the amount of perchlorate tolerated by *H. lacusprofundi* and *Halobacterium* sp. NRC-1 is 30 times higher than that of methanobacteria [94]. Laboratory strain *Halobacterium salinarum* NRC-1 is one of the best-studied representative to date, and they are ideal candidates for space related studies [88]. Studies have investigated how this strain reacts to desiccation, shifts in osmotic pressure [84,95], heat [96], oxidative stress [97], ionizing radiation [98,99], oxygen limitation [97], and a broad range of different UV radiation regimes [100,101].

The main structure and its properties enable the halophilic Archaea to survive in harsh environment. For example, intracellular salts provide protection against ionizing radiation in *Halobacterium salinarum* NRC-1; High salt concentration could stabilize halophilic protein structures through solvation shells made up of hydrated salt ions [102]. This property is correlated with negatively charged protein surfaces; this is because of the enrichment in acidic amino acids and marginal hydrophobic amino acids, which favors repulsive interparticle forces to avoid aggregation in the high salt environment [103,104]. Most halophilic proteins display an obligatory requirement for high salt conditions in order to be active and stable [105]. Intracellular halides in *H. salinarum* could scavenge the reactive oxygen species, resulted in increased protection against nucleotide modification and carboxylation of protein residues

[106]. Manganese plays an important role in radiation resistance. The rich abundance of Mn, phosphate, amino acids, and peptides in *H. salinarum* provides a great level of enzyme protection against the deleterious effect of IR [83]. Association of Mn and trehalose was also essential for the extreme radiation resistance observed in *Rubrobacter* species [107]. In addition, the pigments inside of *Halobacterium salinarium* lend itself for use as a cosmetic colorant [108]. Bacterioruberin and monoanhydrobacterioruberin are the two main carotenoid pigments that have been detected from *Rubrobacter radiotolerans*[109]. *Rubrobacter radiotolerans* is also known to be highly extremely gamma radiation resistant [110].

### 1.3.2.2 Cyanobacteria

The Atacama Desert, the driest nonpolar desert in the world, is often referred to by astrobiologists as an analogue of Mars due to its environmental conditions. The association of cyanobacteria (*Chroococidiopsis sp.*) and bacteria belonging to Actinobacteria and Beta-Gammaproteobacteria and Firmicutes phyla were found inhabiting the near surface of salt (halite) deposits of the Salar Grande Basin, Atacama Desert (Chile) [111]. They are the example of life that has adapted to extreme environmental conditions caused by dryness, high irradiation, and metal concentrations. This suggests that the adaption of these micro communities is of importance in the investigation of life outside of Earth. Cockell et al. [112] found a sample of shocked gneiss containing a coherent band of cyanobacterial endolithic growth, from the Haughton impact crater in the Canadian Arctic. The organism inhabiting these rocks is the desiccation and radiation resistant cyanobacterium, *Chroococidiopsis sp.* The adaptability of *Chroococidiopsis sp.* to extreme environments was also demonstrated in the Martian analogue named the Mojave Desert. Therefore, *Chroococidiopsis sp.*, isolated from different rock types (talc, marble, quartz, white carbonate, and red-coated carbonate) was found to have shifted the photosynthetic pigment emissions, presumably as an adaptation to the rocks' different light transmission properties [113]. *Chroococidiopsis* is also probably the most desiccation-resistant cyanobacterium, the sole photosynthetic organism in extreme arid habitats. Its remarkable tolerance of environmental extremes makes *Chroococidiopsis* a prime candidate for use as a pioneer photosynthetic microorganism for terraforming of mars. It is noteworthy that under laboratory desiccation desert strains of *Chroococidiopsis* could survived several years of storage [114]. Charles et al. [115] reported that *Chroococidiopsis sp.* could survive under the high Martian UV flux if water and nutrient requirements for growth were met. After

8-hour exposure, equivalent to approximately 1 day on Mars, cell morphology was not changed, and DNA was still detectable by 4',6-diamidino-2-phenylindole staining.

Desiccation-, radiation-resistant desert strains of *Chroococcidiopsis* have been employed in several experiments to ground-based simulations of space and Martian conditions, in order to study the tendency of life as we know it, to investigate the possibility of detection of life biosignatures on Mars or other planets. The extreme conditions in space could damage DNA, which could lead to the chemical modification (alkylation or oxidation), cross-linking, base removal such as depurification, or damage by ionizing and non-ionizing radiation [116]. Because *Chroococcidiopsis* has the ability to repair and/or protect its genome under DNA-damaging conditions, such as extreme desiccation, ionizing radiation and UV-exposure, among desiccation-tolerant cyanobacteria it is the only one suitable to genetic manipulation [117].

Extracellular polysaccharides (EPS) are the most important compounds produced by cyanobacterial, contributing to its desiccation tolerance. The production of abundant polysaccharide-rich envelopes allows the high adaptability of *Chroococcidiopsis* to anhydrobiosis [118]. They provide both a repository for water and a matrix which stabilizes desiccation-related enzymes and molecules [119]. The productions of extracellular polysaccharides act in synergy with an accumulation of the disaccharide trehalose in the cytoplasm, which occurs in most anhydrobiotes upon desiccation. Trehalose could substitute water molecules and prevent the phase transition of cellular membranes and stabilizes dried proteins [120]. Trehalose appears to depress the phase transition temperature of the dry lipids after water has been removed and maintains them in the liquid crystalline state [121]. They could expand phospholipid monolayer films [116,122].

Biological lipids are among the most stable biomarkers over geological time scales and are easily analyzed. The alteration of lipid content of membranes in major importance in response to environmental stresses and maintenance of membrane integrity in anhydrobiotic organisms represents a Central mechanism of desiccation tolerance [121,123]. The characterization of *Chroococcidiopsis* EPS's lipidic component stability will give us a supplementary potential biosignatures for guiding future search for life missions [124]. As *Chroococcidiopsis* is able to resist up to 15 kGy of ionizing radiation in the active form, *Chroococcidiopsis* could potentially withstand a radiation environment equivalent to 200,000 years on the Martian surface. Its radiation resistance in the dormant desiccated state and at low temperatures could moreover be enhanced by the interplay of protection mechanism involved in both desiccation and radiation resistance [125–127].

### 1.3.3 The organics in Bacteria

To study the organic life biomarkers in space, the organic compounds in real bacteria sample is of primary importance. The major components of microbial biomass are protein, RNA, lipids, and glycogen. These four components have been reported to constitute 88% of the dry biomass, as the model gram-negative microbe *Escherichia coli* [128]. The relative abundance of the main compounds in *E.coli* is DNA (3.1% of dry weight), lipopolysaccharide (3.4%), peptidoglycan (2.5%), and intracellular metabolites, cofactors, and ions (3.5%), and the amounts of these components are expected to be relatively constant. If we take a look at molecules present in a bacterial cell, we find biopolymers (nucleic acids, polysaccharides), small organic molecules (lipids, saccharides, metabolites), and inorganic molecules. Over 50 % of the cell dry weight consists of proteins, which represents the phenotype of the organism and in spite of their high diversity. Lipids constitute approximately 50% of the weight of cellular membranes and 5–10% of the prokaryotic cell dry weight, but it means the highest number of molecules per cell [129]. There could be products derived from the organics in from microbial biomass. Zhu *et al* [130] studied the microbial biomass in subsea floor sediment by Py-GC/MS, benzyl nitrile (derived from DNA and protein), 2-furanmethanol (from DNA and peptidoglycan), indole (from peptidoglycan and protein), phenol (from DNA, peptidoglycan and protein) and pyrrole (from peptidoglycan) were determined as diagnostic fingerprints. Detection of microbial signals through the molecular fingerprints requires a cell density of at least  $10^6$  cells/g.

#### 1.3.3.1 Lipids

Lipids are the main components of cell walls. Fatty acids methyl esters have been detected in cells with derivatization of TMAH, such as C13-C18 FAMES [131–133]. Lipids in pathogens have been analyzed by Py-GC/MS combined with *in situ* thermal hydrolysis methylation of the whole bacteria, with a total analysis time less than 10 min/lipid profile. The lipids profiles of bacteria depend on growth factors such as the type of media, age of culture, and incubation temperature [134]. Lipopolysaccharides (LPS) and lipooligosaccharides (LOS) are components of the G<sup>-</sup>bacteria outer cell membrane and are responsible for the antigenic properties of bacterial cells. Lipid A of lipopolysaccharides is considered to be the most conserved part; oligosaccharidic core and O-antigen, which constitute conversely the most variable part and thus may be used as a specific biomarker [135]. In addition, the resilience of lipids from dead organic material in the saline sediments represented by samples from lakes

lends demonstrated that sulfates, in tandem with phyllosilicates and iron oxides, may be a viable target for preserved biomarkers on Mars [136].

### ***1.3.3.2 Amino acids***

Amino acids are the structural units that make up proteins, also important bioindices for life. Several amino acids have been detected in cell walls. For example, muramic acid occurs exclusively in bacterial cell walls, especially in the murein skeleton of Gram-positive species [137,138]. Galactosamine was also detected from cell walls, especially in peptidoglycan cell wall, but only the glucosamine that occurs in excess to muramic acid may be attributed to fungal sources [139]. Golecki [140] studied the composition of cell walls of the cyanobacterium *Anacystis nidulans*. Several organic compounds have been detected. Among this, in the insoluble electron dense layer, typical components include peptidoglycan diaminopimelic acid, muramic acid, glutamic acid, glucosamine and alanine in the molar ratio of 1.0 : 0.9 : 1.1 : 1.5 : 1.9. In addition, other amino acids (molar ratio from 0.05-0.36), mannosamine (molar ratio 0.54), and lipopolysaccharide components were detected in low concentration. Mycosporine-like amino acids (MAAs), scytonemin, ectoine, bacterioruberin, sphaerophorin, pannarin, and melanin have been isolated from UVR-resistant extremophiles. MAAs are characterized by a cyclohexenone or cyclohexenimine core conjugated with the nitrogen moiety of an amino acid, and are synthesized by the shikimic acid pathway via 3-dehydroquinic acid and 4-deoxygadusol, a known strong antioxidant [141,142]. MAAs could absorb UVR, which plays an essential role in photoabsorption [143]. Scytonemin, a kind of yellow to brown and lipid-soluble compound from cyanobacteria, also shows promise as a sunscreen. Scytonemin is a symmetrical indole-alkaloid consisting of fused heterocyclic units, connected via a carbon-carbon bond. In its structure, the complex ring structure and its conjugated double bonds make the compound particularly stable and allow for the absorption of UVR [142].

### ***1.3.3.3 Nucleic acids***

Deoxyribonucleic acid (DNA), as information carrier, stores the information that defines the organism in unique orders of four nucleobases (A, T, C, G) located in tiny molecules, and this way of storing information has continued for three billion years. Some studies have suggested that DNA can be placed in the extremely cold regions of the Earth or even on Mars

for millennium-long storage [144]. RNA probably formed the basis of first life, which is made up of sequences of four different nucleotides, the latter of which can be formed through reaction source. RNA polymers must have emerged very quickly after the deposition of meteorites (less than a few years), and the synthesis of nucleotides and their polymerization into RNA occurred in just one to a few wet-dry cycles [145].

Nucleosides, nucleotides, and nucleobases, a group of highly active compounds, are essential components of life; they constitute the building blocks of nucleic acids, RNA and DNA, and involved in the regulation and modulation of various physiological process in human body [146,147]. The structure of nucleobases, nucleosides, and nucleotides have been determined in previous studies [148–150], polynucleotides are composed of pentose sugar moieties linked by 3',5'-phosphodiester bonds forming a sugar-phosphate backbone. The furanose ring is centrally located in the sugar phosphate chains of nucleic acids [151].

Nucleic acids can be analyzed by HPLC, LC-MS-MS, GC/MS. ATP, ADP, AMP, adenine, adenosine, cAMP, ITP, IDP, IMP, hypoxanthine, inosine, cIMP, the guanine series, NAD, NADPH, xanthine, 3-methylxanthine were often characterized using high-performance liquid chromatography (HPLC) [152], in which peak height was used to quantify hypoxanthine, AMP, uric acid and ADP. Turner [153] characterized ribonucleotides and ribonucleosides by Py-GC decades ago where the sample was pyrolyzed at  $800 \pm 5^\circ\text{C}$ . The pyrolysis products include low-boiling products, such as CO, CO<sub>2</sub>, CH<sub>4</sub>, C<sub>2</sub>H<sub>4</sub>, etc., and the purine and pyrimidine structure contribute significantly to the formation of low molecular weight pyrolysis products. Py-GC was suggested as a means of characterizing fragments produced in the degradation of nucleic acids. GC/MS has long been used for identifying metabolites of biological fluid, however, this technique is limited by the volatility or the ability to form appropriate volatile derivatives of the molecules [154]. The determination of phosphorus is one of the most effective methods to quantify nucleotides, because DNA is composed of deoxynucleotides (dNMPs), which consist of deoxyribose, a base, and phosphate. The phosphorus measurements provides a highly accurate quantification of mass for both dNMPs and DNA [155]. Inductively coupled plasma mass spectrometry (ICP-MS) was used to quantify the DNA concentration by the phosphorus value, the detection limits of DNA sample obtained from ICP-MS were 3.1–26 ng/mL [155]. Stefan Neubauer [156] did the quantitative profiling of the nucleotides, nucleosides, and nucleobases in yeast extracts using LC-MS-MS, the limits of detection  $<1 \mu\text{mol L}^{-1}$  was obtained. Elemental species analysis method enabled determination of nucleotides by phosphorus detection [157]. The detection limit and absolute detection limit of phosphorus were 0.24  $\mu\text{g/L}$  and 0.012 pg, respectively. Guo [158] developed a rapid and

sensitive method to determine 20 nucleobases, nucleosides, and nucleotides in *Ziziphus* plants at trace levels by using hydrophilic interaction ultra-high performance liquid chromatography coupled with triple-quadrupole tandem mass spectrometry (HILIC–UHPLC–TQ-MS/MS). The LODs and LOQs were 0.11–3.12 ng mL<sup>-1</sup> and 0.29–12.48 ng mL<sup>-1</sup> for the 20 analytes, respectively. LC-MS-MS was applied to analyze nucleotides, nucleosides, and nucleobases, for the application to feed supplements [156], including cytosine, uracil, adenine, guanine, cytidine, uridine, adenosine, guanosine, inosine, 5'CMP, 5'UMP, 5'AMP, 3'AMP, 2'AMP, 5'GMP, 2'GMP and 3' GMP, and 5'IMP.

The analysis of DNA could help to determine the bacteria species contained in the Atacama Desert samples. DNA was extracted from different Atacama samples to determine the composition of microbial communities present within the soil samples, Microbial life was strongly represented in salars and halophilic organisms contributes to a large amount to the communities [73]. Amino acids and organic carbon and nitrogen found within the investigated soils match the microbial observations in that they generally correlate with the presence of pronounced life [73]. The low biomass was detected in Mars analogs such as high-elevation University Valley permafrost (10<sup>3</sup> cells/g) [159] and Lost Hammer Spring sediment (10<sup>5</sup> cells/g) [160], corresponding to ~0.01–1ng DNA based on an average bacterial genome size of ~2–5 Mbp and ~2.5–5 fg of DNA per genome.

In addition, the phosphate is one of the chemical nutrients thought to be essential for life and is also considered critical to reactions that may have led to life on Earth. Phosphate release rates during water-rock interactions on Mars that are as much as 45 times higher than on Earth, the phosphate concentrations of early wet Martian environments more than twice those of Earth, which suggested that available phosphate may have mitigated one of the hurdles to abiogenesis on Mars [161]. Phosphate possesses many contributes for biotic and prebiotic roles. Phosphate bond configuration and resulting net negative charge act to ionize and protect the macromolecule from hydrolysis, two qualities required for cell containment and the persistence of genetic material [162].

#### ***1.3.3.4 Polysaccharides***

The bacterial polysaccharides make up a group of polymers in which the structural variation is almost unlimited, and unusual sugars are often components of these polymers. These polysaccharides are generally composed of oligosaccharide repeating units, and structural studies should lead to a complete structure of the unit. In addition to the

polysaccharides proper, bacteria also produce other polymers containing mainly carbohydrates. The first type is comprised by lipopolysaccharides, which presents in the cell wall of gram-negative bacteria connecting with the specific polysaccharides. Peptidoglycans are one of the components of the bacterial cell wall, where polysaccharide chains are cross-linked via short peptide chains and form a two-dimensional network. A third type includes the teichoic acids in the bacterial cell walls. In these polymers, mono- or oligosaccharide residues are connected via phosphoric diester linkages [138].

During the biochemical analysis of Atacama samples, monosaccharides such as glucose, galactose, mannose, xylose, or glucuronic acid that usually are structural components of microbial extracellular and cell wall polysaccharides were detected [93]. Exopolysaccharides (EPS) are polysaccharides produced extracellularly by microorganisms and compose of simple sugars. The repeating units of these polysaccharides are very regular, branched or unbranched and interconnected by glycosidic linkages [163].

#### ***1.3.3.5 Pigments***

Biomolecules, especially photosynthetic pigments (chlorophyll and accessory pigments such as phycocyanin) and derivatives may be detectable beneath the oxidized zone in the near-subsurface profile of Mars [164]. Raman spectroscopy offers a promising tool for the detection of hopnanoids as long-lived bacterial cell wall products and the photosynthetic pigments as the most promising targets. In cyanobacteria, they contain photo protective and antioxidant molecules (e.g., carotenoids), ultraviolet screening compounds (e.g., scytonemin), photosynthetic pigments (e.g., chlorophyll a and phycobiliproteins), and their degradation products such as porphyrins, which have been classified as high priority targets for biomolecule detection [165]. In addition, pigments of different nature are widely used as biomarkers for the classification of microorganisms. Pigments include magnesium-containing chlorophylls and bacteriochlorophylls, phaeophytins and phycobiliproteins characteristic especially for cyanobacteria, retinal-containing pigments such as bacteriorhodopsin, halorhodopsin and proteorhodopsin, carotenoids, flexirubins and many others [166,167]. Especially carotenoids have a great structural variety, which represent a diversified group of chemicals with a polyene skeletal backbone. Carotenoids could participate in energy-harvesting complexes, UV protection and in the repair of cellular damage [168,169].



#### 1.3.3.5.1 Carotenoids

Carotenoids' pigment are promising targets to search for life on Mars due to their biogenic origin, they could be detected by Raman spectroscopy easily, especially with a 532 nm excitation because of the resonance effects. Therefore, Raman spectroscopy has been a classical instrument used to analyze carotenoids. And also, the desiccation can protect carotenoid Raman signatures in the desert cyanobacterium *Chroococcidiopsis sp.* For hydrated *Chroococcidiopsis sp.*, increasing gamma ray doses (from 0 to 113 kGy), the peaks of C=C, C-C, and CH<sub>3</sub> groups decreased significantly; however, for dried *Chroococcidiopsis sp.* cells, all the characteristic peaks are detectable after UV irradiation [170]. Most carotenoids of the *Halobacteriaceae* are colored brightly red-orange due to a high content of carotenoid pigments in their cell membrane. The reddish-pink color of saltern crystallizer brines is mainly caused by these archaeal carotenoids [167]. Therefore, the carotenoid-like signatures could be the possible biosignatures preserved for millions of years [170].

The specific carotenoids bacterioruberin and salinixanthin are excellent biomarkers for extremely halophilic heterotrophs. Bacterioruberin is an unusual C50 carotenoid constantly studied and analyzed by Raman spectroscopy [171,172], and present in some halophilic archaea and some actinobacteria belonging to the family *Rubro bacteraceae* [109]. Bacterioruberin is the main carotenoid component responsible for the color of the red Archaea of the family Halobacteriaceae. It has a distinct molecular structure in which it has a primary conjugated isoprenoid chain with a length of 13 C=C units without subsidiary conjugation arising from terminal groups, which contain four (or less) OH group functionalities [173]. However, salinixanthin from *Salinibacter ruber* the C40 conjugated chain with 13 double bonds and a fatty acid chain are linked to a  $\beta$ -D-glycoside [166,167,174]. Figure 1-7 shows the main structure of carotenoids.

Raman spectroscopy has been used as one of the most popular device instrumentations for analyzing the presence and the structure of carotenoids. It is able to analyze carotenoids in native samples from surface and subsurface colonization of rocks or sediments, thus trace pigment detection is sometimes possible using especially the excitation wavelengths 514.5 and 532 nm [175–177]. Marshall et al [175] detected carotenoids of members of the Halobacteriaceae by resonance Raman spectroscopy. Fendrihan et al. [178] tested the suitability of Raman spectroscopy for the detection of extremely halophilic Archaea embedded in halite in terrestrial and possibly extraterrestrial samples as well, a high abundance of carotenoids (bacterioruberin) were detected as well as peptide bonds and nucleic acids.

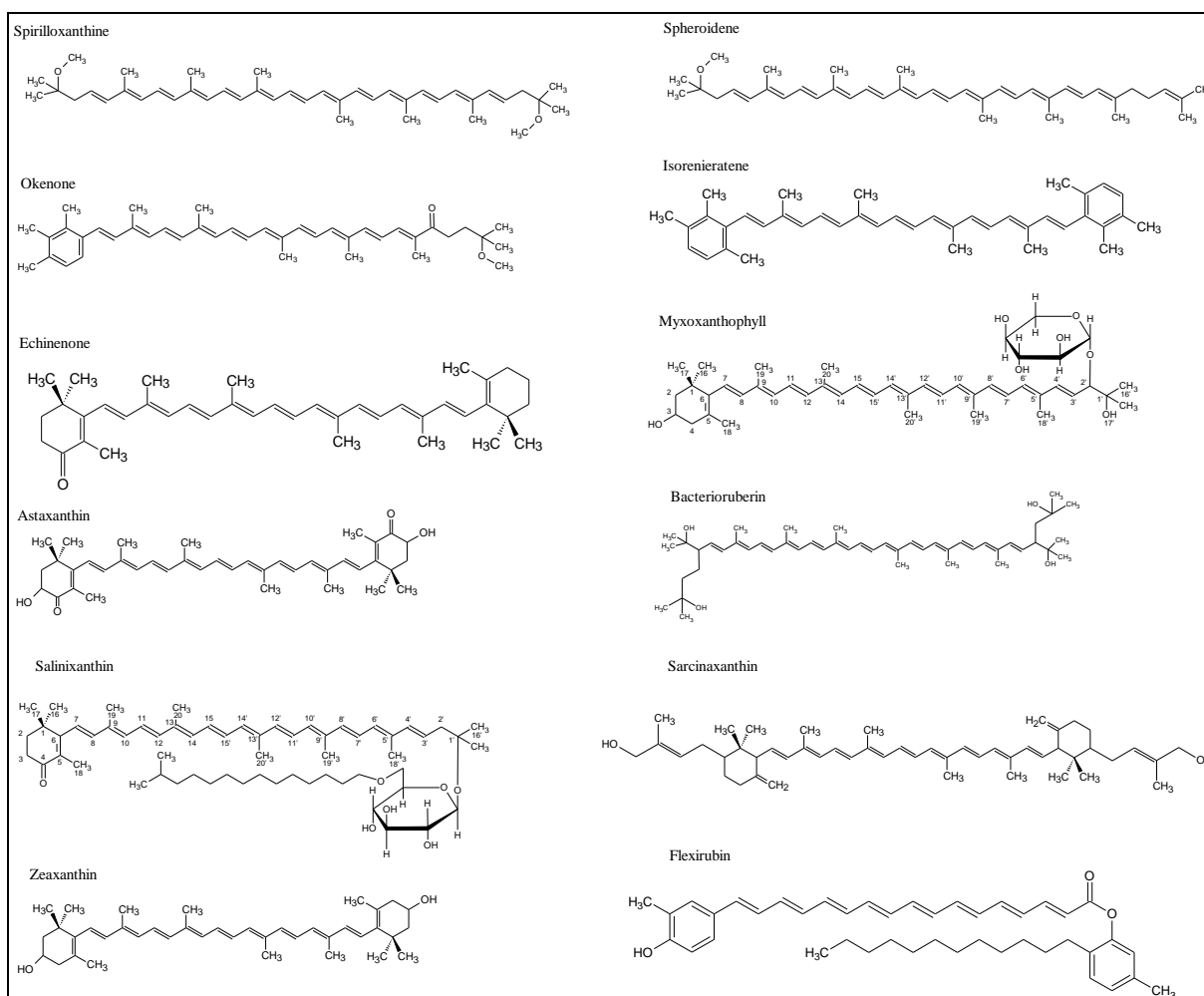


Figure 1-7 Structural formulas of carotenoids.

In addition, Carotenoids could be extracted from food and human samples with different extraction methods and solvents. Extraction methods include liquid-liquid [179–181], solid-liquid [182–184], supercritical-fluid extraction (SFE) [185], pressurized liquid extraction (PLE) [186–188], accelerated solvent extraction (ASE) [189,190], ultrasound-assisted extraction (UAE) and microwave-assisted extraction (MAE) [191–193], etc. Carotenoid identity can be confirmed by liquid chromatography coupled to mass spectrometry (LC-MS), comparing comparing the mass spectra with published fragment-ion abundances, or mass spectral libraries [194]. A range of LC-based techniques have been applied to analyze carotenoids, mainly coupled to a photodiode array (PDA) or UV-Vis detector [194]. Mass spectrometry is one of the most important methods for the detection and identification of carotenoids. MS instruments have been used to achieve high sensitivity in complex mixtures and to obtain molecular structure information on the basis of the molecular mass and fragmentation patterns. This demonstrated that MS system could be applied to determine the main structure of

carotenoids. GC/MS have been applied to analyze carotenoid and chlorophylls in leaves and bacteria [195,196], the carotenoid cleavage [197–201]. Their results demonstrated that GC/MS could be applied to analyze the fragments of carotenoids. However, few studies reported the application of GC/MS system on the detection of carotenoids.

It is not likely that the pigments such as bacterioruberin or carotenoids directly protect the DNA in terms of damage prevention, however, those pigments might aid in the recovery from UV damage by supplying energy indirectly to photo reactivating enzymes for the reversal of thymine dimers [169,202]. In addition, pigments are not the only possible biomarkers to indicate presence of halophilic and other microorganisms by using Raman spectroscopy [203]. Most halophilic and halotolerant microorganisms (but not including members of the *Halobacteriaceae* and *Salinibacter*) could accumulate high concentrations of different organic osmotic solutes, which could be excellent biomarkers [204].

#### 1.3.3.5.2 Chlorophyll

Chlorophyll fulfills the requirements from photosynthesis: the absorption of visible light, the photochemical capabilities, a rich supply of redox levels and chemical stability. The biosynthetic pathway of chlorophyll can be read as the evolutionary history of photosynthesis, which is the prerequisite of all life on earth [205]. In this process, porphyrins pigment is the base of chlorophyll. Chlorophyll c is a mixture of magnesium tetradehydro- and hexadehydrochlorophyllin a<sub>5</sub> monomethyl ester (Ia, Ib). Chlorophyll c is common in widely distributed plants including the most abundant organisms of the open seas, which means the marine diatoms, dinoflagellates, and brown algae. These organisms contain Chlorophyll c in addition to the predominant Chlorophyll a [206]. Chlorophyll was also detected from the colonies of cyanobacteria (*Gloeocapsa*, *Nostoc*) in gypsum and other evaporites in the High Arctic [207] and within halite from hyperarid areas of the Atacama Desert, Chile [208], by Raman system. Therefore, Chlorophyll could be one of the biomarkers for search life biosignatures on Mars. Since GC/MS system is one of the most important methods to detect the organic compounds, we found that GC/MS have been used to analyze chlorophyll and its degradation in previous study [209,210]. Therefore, SAM instruments could have the potential to analyze chlorophyll compounds by analyzing the products degraded from chlorophyll if they are presented in Martian soil.

### 1.3.3.6 Proteins

Some pigments are proteins. Bacteriorhodopsin, a retinal protein within the proteome of *Halobacterium*, is a photochemical material produced by halophiles. Its function was discovered in early 1970s within the cell membrane of *Halobacterium salinarum*. It serves as a light-driven proton pump and enables direct use of light energy to generate a proton gradient over the membrane that can be converted to ATP [163,211]. Halorhodopsin is the second retinal protein, also first discovered in *Halobacterium salinarum*. It has a quite similar structure to that of bacteriorhodopsin. However, this pigment can act as a chloride pump: excitation by light (absorption maximum 578 nm) drives transport of chloride ions from the medium into the cells [212]. Inward chloride transport is important for maintaining the proper ionic balance and is essential for cell growth. *Halobacterium salinarum* contains two more retinal-containing membrane proteins involving in light sensing for phototaxis. Sensory rhodopsin I is a green light receptor that responds to a color to which the cells are attracted. Sensory rhodopsin II, also termed photorhodopsin, is sensitive to blue light that acts as a repellent [167]. Photoactive yellow protein is another interesting photopigment used for light sensing in many halophilic anoxygenic phototrophic *Bacteria*. It was first observed in *Halorhodospira halophila* in 1985. This protein is a photoreceptor that mediates negative phototaxis to blue light [167]. Later it was identified as a 4-hydroxycubbamyl (p-coumaric acid) chromophore. It is covalently bound to Cys-69 of the protein via a thiol ester bond. [213].

### 1.3.4 Important organic compounds for life

From last section, we could conclude that important life biomarkers including lipids, amino acids, nucleic acids, saccharides, pigments such as chlorophyll and carotenoids, and proteins. This means that soluble organic matters, include sugar derivatives, amino acids, and nucleobases, could be potential metabolic reactants and genetic information recorders [214]. Carboxylic acids are the most abundant soluble compounds in Murchison, about 330 ppm [215] Phosphate is central to the origin of life [216–218]. Because it is a key component of nucleotides, phospholipids, and metabolites such as adenosine triphosphate used in cellular replication, compartmentalization, and energy transfer, respectively [219]. In addition, PAHs are invariably associated with highly altered fossils (e.g., fossil fuels and their combustion products) and thus are relatively unambiguous signatures of life [220]. PAHs are common in the interstellar medium, such as in Martian meteorite ALH84001 are biogenic [221].

As it has been described in the background, SAM and MOMA are designed for the detection of biomarkers that related for life or life activities. Pyrolysis-GC/MS combined with derivatization method has been applied to detect the possible organic compounds in Martian soil. MTBSTFA/DMF and TMAH are two derivatization reagents carried by SAM and will be used on MOMA. MTBSTFA/DMF have been applied to analyze the organic compounds on Mars since the launch of Curiosity rover [64,222,223], TMAH will be applied to study the organic compounds which could be the biomarkers or bioindicators for life on the surface or the subsurface of Mars. In addition, TMAH will be applied on Dragonfly (DraMS) and Europa Lander (Emily). Therefore, the applications of TMAH thermochemolysis on the detection of organic compounds need to be well understood. In the next Chapter, the application of TMAH thermochemolysis has been reviewed.

#### **1.4 The search for organic compounds with TMAH thermochemolysis: From Earth analyses to space exploration experiments**

**Abstract:**

Tetramethylammonium hydroxide (TMAH) is one of the most popular methylation reagents that have been increasingly used for the detection of organic compounds within a wide range of samples, such as soil, coal, lacquer, lignin, polymers and for *in situ* analysis of solid samples by space experiments. The analytical methods and instruments, experimental conditions, and the qualitative and quantitative analysis of organic compounds using TMAH thermochemolysis for the last 10 years were reviewed; additionally, the mechanism of TMAH thermochemolysis and TMAH degradation are overviewed herein. The objective of this paper is to give a broad view of the TMAH thermochemolysis analysis, to demonstrate how the technique can be used for the detection of organics on Mars and other planets, and to promote cooperation between different disciplines which may use thermochemolysis.

**Keywords:**

Tetramethylammonium hydroxide (TMAH); thermochemolysis; Pyrolysis-GC/MS; thermally assisted hydrolysis and methylation (THM); TMAH degradation; derivatization; quantitative analysis; internal standard; space experiment; SAM and MOMA.

## 1.4.1 Introduction

### 1.4.1.1 What is thermochemolysis?

The analysis of organic compounds is an essential way to detect and demonstrate if there are life signatures in space. Since the early 19<sup>th</sup> century, it has been hypothesized that there could be life-derived organic matter surviving in the martian soil and randomly distributed across the martian surface over geologic timescales [224]. Extraterrestrial matter and the potential for it to reach the surface of the Earth has been a topic of interest and debate for centuries. One of the oldest meteorites, which is still preserved today, fell from the sky on November 7<sup>th</sup>, 1492 and is still on display in the French region of Alsace. Since then, many meteorites have been found to contain soluble organic matter. Subsequent analyses explore how to distinguish a biotic from an abiotic origin for this organic matter [225]. Therefore, the analysis of organics plays a crucial role in the search for life beyond the Earth. Human beings continue to make efforts to explore the universe and search for other habitable planets, even within our own solar system. Today, the Mars Organic Molecule Analyzer (MOMA), an experiment onboard the 2022 ExoMars rover, will search for signs of past or present life on Mars by analyzing the potential organic content in samples collected from up to a two meter depth below the martian surface [3].

There are three main methods for analyzing complex and non-volatile organic compounds. Pyrolysis is a traditional method for analyzing the components of complex materials. Pyrolysis can be performed as slow pyrolysis, which requires a temperature ramp, and fast pyrolysis, in which the sample is heated at a different heating rate at relatively high temperatures in the absence of oxygen. The pyrolysis process, especially at high temperatures, can degrade the main chemical structures of the analyzed materials. Consequently, it is often very difficult to speculate about the initial chemical composition of unknown samples during the analysis of the pyrolysis products. For example, coal pyrolysis is the most traditional way to study the structure and composition of coal and the kinetic rates and mechanisms of coal pyrolysis [226]. Characterization of pyrolysis residues such as char [227] combined with gas releasing properties provide a valuable and comprehensive understanding of coal structure [228]. However, the pyrolysis process is always operated at temperatures higher than 200 °C and up to about 1800 °C [229,230], which can destroy the original structure of the sample and produce the char, tar and gas products that are released during coal pyrolysis. Pyrolysis is generally not a good way to conserve the main structure of samples.

Chemical derivatization is another analytical method which can keep intact the main chemical structure of substances by adding a derivatization reagent which reacts with the polar

and labile compounds at a relatively low temperature (below 200 °C). The derivatization reaction usually involves a substitution of a nonpolar functional group in place of a polar functional group, where the most common reactions are alkylation, acylation and silylation. Alkylation reagents reduce the polarity of the compounds by substituting labile hydrogens for an aliphatic or aliphatic–aromatic (e.g., benzyl) group. Silylation is the most prevalent derivatization technique, and common reagents are trimethylchlorosilane (TMCS), trimethylsilylimidazole (TMSI), N-methyl-trimethylsilyltrifluoroacetamide (MSTFA), N, O-bis-(trimethylsilyl)trifluoroacetamide (BSTFA) and N-(t-butyltrimethylsilyl)-N-methyltrifluoroacetamide (MTBSTFA). BSTFA and MTBSTFA are most frequently used, particularly when analyzing phenolic compounds, sterols and sugars [231,232]. Derivatization methods can be used to reduce the polarity of amino groups to improve their separation and detection by gas chromatography/mass spectrometry (GC/MS). Derivatization reactions of amines by GC were reviewed by Kataoka [233], with respect to reactivity, selectivity and sensitivity, for the application of environmental analysis related to human health. Common derivatization reactions for the GC analysis of amines were presented, including acylation, silylation, dinitrophenylation, permethylation, Schiff base formation, carbamate formation, sulphonamide formation and phosphonamide formation, and the derivatization reactions of different amines were reviewed, including primary amine, secondary amine, tertiary amine, ammonia, and nitrosamine. For volatile and polar compounds, MTBSTFA/DMF is one of the most popular silylation reagents. For the MTBSTFA derivatization reaction, silylation is always performed using mild experimental conditions at low temperatures between 75 °C to 300 °C [234], which can result in the replacement of the labile hydrogen atom in an -OH, -COOH, -SH, -NH, -CONH, -POH, -SOH group or enolizable carbonyl with a silyl group. This reduces the polarity of the analytes, increases their stability, and improves the GC behavior without damaging the main structure of the molecules. However, some refractory materials cannot be detected at low temperature; therefore, derivatization combined with a high temperature environment is needed to obtain important information of certain refractory materials.

Thermochemolysis, or thermally assisted hydrolysis and methylation (THM) in most cases [235], is a type of analytical pyrolysis for *in situ* characterization of complex samples with a wide range of materials [25]. This method can be tracked back to at least 56 years ago when a study investigated the analysis of fatty acids by GC in the presence of tetramethylammonium hydroxide (TMAH) [236]. The thermochemolysis method is a combination of the analytical techniques of pyrolysis and derivatization. Heat plays a key role in the thermochemolysis process, which facilitates the cleavage of the bonds between the main

structures at selected chemical bonds of analytes. The reorganization of the analytes' main part and the thermochemolysis functional groups produces the less polar, smaller molecular weight compounds, with higher stability and volatility, which are amenable to chromatographic analysis.

#### 1.4.1.2 Factors influencing thermochemolysis

##### 1.4.1.2.1 Thermochemolysis reagents

The reagent plays a key role in the thermochemolysis process. Therefore, thermochemolysis reagents that have been used for the characterization of organic compounds since 2010 have been reviewed, such as TMAH, trimethylsulfonium hydroxide (TMSH) [237,238], tetramethylammonium acetate (TMAAc) [10,239,240], *m*-(trifluoromethyl)phenyltrimethylammonium hydroxide (TFTMAH) [241], tetraalkylammonium hydroxides (TAAH) [242] et al. Table 1-1 lists some of the thermochemolysis reagents that have been used in the detection of organic compounds, mainly fatty acids. TMAH is a relatively strong thermochemolysis reagent with high efficiency in methylation, which is capable of methylating all available active hydrogens from various functional groups, including phenolic hydroxyl groups, carboxylic acids, amines etc. Compared with TMAH, TMSH is a competitive reagent with strong alkaline and heat-sensitive properties; however, TMSH requires lower temperature for its alkylation while TMAH can be used at a relatively high temperature up to 600 °C. Therefore, TMAH is one of the most popular thermochemolysis reagents. More than 90% of published thermochemolysis applications have used TMAH [25], therefore we mainly focus on the properties of TMAH thermochemolysis hereafter.

Table 1-1 Thermochemolysis reagents have been used in the detection of organic compounds.

Reagent	Sample	Functional groups	Publications
Tetraethylammonium hydroxide (TEAH); Tetrabutylammonium hydroxide (TBAH)	Wood sample	Fatty acid	[243]
Trimethylsulfonium hydroxide (TMSH)	Soils collected from three different ecosystems	Phospholipid fatty acids (PLFAs)	[244]
	Primary sludge; Water and articulate; Nexapa River basin samples	Thiol or polysulfidethiol	[245]
Tetraethylammonium acetate (TEAAc)	Lignite	Humic acids	[246]
Phenyltrimethylammonium hydroxide (TMPAH)	Milk	Fatty acids	[247]
<i>m</i> -(Trifluoromethyl) phenyltrimethylammonium hydroxide (TFTMAH)	Paint samples	Fatty acids	[241]



#### 1.4.1.2.2 TMAH thermochemolysis type (on-line and off-line)

There are mainly two types of thermochemolysis, off-line and on-line thermochemolysis. In the off-line case, the sample is mixed with a certain amount of TMAH inside some kind of sealed vessel and derivatized for a certain amount of time followed by an analysis by GC–MS. For example, Poerschmann [248] analyzed the organic compounds in the effluent from phytoremediation systems at the laboratory-scale using offline TMAH-assisted thermochemolysis GC/MS (TMAH-GC/MS). In this study, ~15 mg of lyophilized effluent samples was mixed with 2.5 mL of a 25% w/w freshly prepared TMAH solution in methanol (~40×excess TMAH by weight) inside glass ampoules. Next, the open glass ampoule was tightly closed and placed in a steel autoclave, constructed in-house, which allowed the thermochemolysis to take place at 240 °C for 180 min. Then the sample was analyzed by GC/MS. Carboxylic acids, phenols and the lignin-derived breakdown products were detected, which showed that TMAH thermochemolysis may serve to detect monomolecular organic compounds sorbed onto the root. Tadini [249] studied humic substances extracted from river sediments of northwestern São Paulo which had undergone different soil uses by off-line TMAH-GC–MS and solid state <sup>13</sup>C nuclear magnetic resonance (NMR) spectroscopy characterization. In this study, about 100 mg of dried composted organic biomasses was placed in a quartz boat and moistened with 1 mL of a TMAH (25% in methanol) solution. The sample was introduced into a Pyrex tubular reactor (50 cm × 3.5 cm i.d.) and heated at 400 °C for 30 min in a furnace (Barnstead Thermolyne 21100 furnace) after drying the mixture under a gentle stream of nitrogen for about 10 min. Organic compounds related to the humic acid in the structure were detected by off-line TMAH-GC/MS, including plant waxes, plant biopolyester and a large amount of fatty acid methyl ester. The characterization by NMR provided the carbon nuclei present in the structure, which inferred that the humic acids from an area characterized by sugar cane cultivation (41.9%) and a typical rural area (35.0%) showed the highest aromaticity percentage.

Compared with off-line thermochemolysis, on-line or *in-situ* thermochemolysis is a simpler process that involves mixing the sample with a certain amount of TMAH immediately before injection of the sample into the GC instrument. This process avoids laborious and time-consuming sample work-up steps and allows us to conduct the reaction efficiently only by mixing the specimen and reagents [250]. The on-line TMAH thermochemolysis technique is able to control the reaction temperature easily and reaction time with efficient transfer of volatiles to GC/MS analysis system. These advantages ensure the high efficiency of TMAH thermochemolysis. Therefore, on-line TMAH thermochemolysis has been widely used in the

characterization of a variety of natural and synthetic materials. It showed a good performance during the analysis of methylated lignin phenols and other from the rivers derived sediments [251], compounds of asphaltene biodegradation [252], lacquer compositions [253], model compounds guaiacyl palmitate and 2-nonyl palmitate [254], etc. For example, Mason [255] studied the molecular composition of grassland soil with adjacent unforested and afforested moorland ecosystems using on-line thermally assisted hydrolysis and methylation in the presence of both unlabelled and  $^{13}\text{C}$ -labelled TMAH. During the thermochemolysis experiment, an aqueous solution of TMAH and  $^{13}\text{C}$ -labelled TMAH (25%; w/w) were added into a quartz pyrolysis tube plugged with pre-extracted silica wool containing approximately 2 mg of sample immediately prior to thermal hydrolysis and methylation. The  $^{13}\text{C}$ -labelled TMAH thermochemolysis revealed the chemical composition of soil organic matter (SOM) and reflected the different vegetation inputs in each of the chemicals associated with a litter/fermentation (L/F) layer.

In addition, off-line thermochemolysis is able to detect more compounds, because of the longer retention time compared with online thermochemolysis, thus the recovery rate of off-line thermochemolysis is better than on-line thermochemolysis in some cases. However, the long reaction time such as 30 min could cause the rearrangements and decompositions of amino acids [250]. The off-line thermochemolysis requires several steps, including the solvent derivatization, extraction and the evaporation of the solvent. These processes are too technically complex to be fully automated for the *in situ* analysis in space missions, especially in the detection of organic compounds on Mars. Therefore, a simpler “on-line” thermochemolysis method has been implemented for SAM and MOMA [23], thanks to the advantage of being able to control the reaction temperature and reaction time with efficient transfer formed thermochemolyzates to GC/MS system.

#### 1.4.1.2.3 Sample pre-treatment methods

Direct thermochemolysis is the simplest way to derivative samples; it does not need any cumbersome sample pretreatment, only mixing the sample with derivatization reagent immediately followed by the analysis process. In our previous study, the nucleobases standard samples were characterized by TMAH direct thermochemolysis [23], without any pretreatment. Though without any tedious pretreatment, direct thermochemolysis could have a sufficient accuracy and efficiency. Baidurah’s team [12,13] compared the effect of direct thermochemolysis with conventional method with extraction pretreatment of bacterial samples. Through analyzing the yield of characteristic peaks of polymers from bacteria, direct

thermochemolysis showed a good performance as the conventional method with sample pretreatment process. However, in addition to the direct thermochemolysis, two pre-treatment processes prior to thermochemolysis could be used in the laboratory: extraction and mineralization, especially for solid matrix such as soils, kerogens, meteorites etc.

**Extraction:** Extraction is a separation process in which substances are separated from a solid or liquid matrix. This type of separation process mainly includes liquid-liquid extraction and solid-liquid extraction, and the solid-phase extraction. The first experimental application of solid-phase extraction started 50 years ago and is the most frequently used procedure for extraction of a wide range of organic analytes across many fields [256]; such as the extraction of fatty acids in bilayer oil paint models [257], of carbohydrates, lignin and lipids from peat bog or soil [2,258–260], of sputum specimen [261,262], of organic mercury species in petroleum [263], of the amino, carboxylic, and nucleic acids from martian analogue samples [264–266], of iodine from environmental samples [267,268], of trace elements from soil environmental matrices [269], of free small molecules from coal [270–272], of humic substances from lignocellulose waste [273], etc. Solid-phase extraction is faster and less labor intensive than the liquid-liquid extraction and only requires smaller volumes of reagents, generating less toxic waste and producing better analyte enrichment factors [274]; because of these advantages of the solid-phase extraction, it has been widely used for the analysis of soot from the combustion of fossil fuels and synthetic biofuels [275], drugs in waste water [276], etc.; isolate bisphenol A in urine [277], food analysis such as the extraction of ochratoxin A from red wines [278], botanic and marine applications, etc. For the *in situ* analysis of organic compounds that could possibly be detected in other surface environments such as that of Mars, solid-phase extraction is the optimal method for the characterization of that soil.

Recently, in order to comprehensively analyze the organics in solid samples such as soil, fossils [279], coal, and wood, some pre-treatments were used. Extraction has been one of the most popular pre-treatment techniques for solid sample analysis, which could include a sequential extraction of samples by different extraction solvents. For example, Allard [280] characterized the organic matter from a forest soil using sequential microwave assisted acid and TMAH hydrolysis at 190 °C. The solvent extraction included hydrogen chloride /acetonitrile (HCl/MeCN), H<sub>2</sub>O, and ethyl acetate (EtOAc) extraction. The different extracts were also derivatized by different reagents. Organic or aqueous extracts were analyzed by GC/MS; the residue was characterized by the solid state <sup>13</sup>C nuclear magnetic resonance (NMR) spectroscopy. Aromatic compounds are the main component of the organic extractions. Microwave-assisted acid hydrolysis provided information about hydrophilic constituents and

unaltered lignin-derived constituents of SOM. Microwave-assisted TMAH hydrolysis released predominantly aliphatic compounds from cutin and suberin.

**Demineralization:** Demineralization is a process in which different acids are used to remove the mineral that is tightly associated with organics in the solid matrix. For example, demineralization processes have been used to improve the efficiency of extraction and characterization of organic matter from soil/kerogen [281,282]. The solvent varies depending on the mineral that will be removed; normally water can remove the alkali and alkaline earth metals, while HCl and hydrogen fluoride (HF) can be used to remove the inherent minerals from coal [283]. HF media for demineralization treatment of soil samples were also used for organic analysis. This technique allows the demineralization of three kinds of agricultural soils followed by TMAH-GC/MS [284]. Results showed that the clay removal provided by HF pretreatment can improve the capacity of TMAH thermochemolysis. Doskočil [271] obtained a similar result when they studied the pyrolysis process of South Moravian lignite in its natural and treated forms, including extraction with chloroform, demineralization, and the remineralization or sorption of calcium ions on the demineralized lignite. TMAH thermochemolysis was also used to analyze the component of lignite. Results demonstrated that the highest yields of the aliphatic molecules were obtained in the case of demineralized lignite, which could be caused by the cracking of carboxylic groups between calcium bridges and functional groups during the demineralization process. Additionally, the Fourier transform infrared spectroscopy (FTIR) and TG-FTIR were also used to analyze the pyrolysis products in solid and gaseous states, respectively.

Extraction could increase the concentration of target compounds in a sample and improve the efficiency of sample analysis; therefore, when the organic compounds are in low abundance or the individual compounds need to be analyzed separately, the sequential extraction technique should be used; when the minerals in the sample could affect the detection of organic compounds, the demineralization process should be used to remove different minerals by using different reagents.

#### 1.4.1.2.4 Experimental conditions

Experimental conditions such as the temperature of thermochemolysis, the pH of the sample, and the amount of solvent influence the efficiency of TMAH thermochemolysis. The optimal temperature varies with the sample and the compounds that need to be derivatized. Decq [285] analyzed European lacquer and optimized the thermochemolysis temperature (350, 480, 550, 650 °C) of natural resins, including Sandarac, Mastic, Colophony, Manila copla, and

Congo copal. Results showed that 350 °C is the optimal thermochemolysis temperature for natural resins and that 550 °C is the second most optimal temperature. Polycommenic acid markers “b1” and “b4”, Pimaric acid, and the poly-ozic marker were used as the markers of Sandarac, Colophony, and Congo copal, respectively. For nucleobases, we found 600 °C is the optimal temperature for TMAH thermochemolysis combined with Pyrolysis-gas chromatography and mass spectrometry (TMAH-Py-GC/MS) [23]. The amount of TMAH could also influence the thermochemolysis result [23,286]. For example, TMAH concentration or pH values can cause the conversion of aliphatic model compounds [287], such as succinic, adipic, and azelaic acid, into diesters. At a sample pH of 7~8, the ester yield is the highest around 90%; however, at a higher pH value (>10), the methylation process can be negatively affected. TMAH is a strong thermochemolysis reagent which remains fully functional after exposure to a total ionizing dose (TID) up to 300 krad, with a post-exposure, GC/MS analysis showing no or few degradation products of the chemicals [234]. This result is very important for *in situ* space analyses where reagents can be exposed to high radiation doses. In addition, the minerals such as perchlorate and other oxyanion salts of soils and meteorites could possibly influence the type and numbers of organic compounds [288], though few researchers studied the influence of minerals on TMAH thermochemolysis. Therefore, plenty of experimental conditions of SAM and MOMA need to be studied in the future.

#### ***1.4.1.3 Set-ups for thermochemolysis and complementary technologies***

Py-GC/MS is the main device used for TMAH thermochemolysis, or namely reactive Pyrolysis-GC/MS [10,289–291], because the technique can provide precise information about the molecular formula and the structures of compounds. Commercial pyrolysis devices have been used in studies conducted over the past 10 years, such as a Curie-point [292–299], a CDS type pyrolyzer [300–303], a micro-furnace pyrolyzer [23,238,239,304–309], and a tubular oven [271,272,284,310–313]. Commercial GC/MS is used for the separation-detection of samples after thermochemolysis. The GC column plays a key role in the separation of volatiles, so different kinds of columns have been used, including fused silica capillary columns [292,297,310], HP-5 columns [301,314–318], Rtx-5Sil MS columns [284,294,311–313,319,320], and SLB 5MS capillary columns [304,305,321]. The type of column is the first and one of the most important steps to obtaining the optimal conditions in the analysis of organic compounds by using GC/MS. Selecting the column depends on four factors, including the stationary phase, the column inner diameter, the membrane thickness, and the column length,

with the stationary phase being the most important factor. Because TMAH is aggressive, the resistance of the stationary phase toward the TMAH is another factor that we have to take in account. SLB 5MS capillary columns with a 5% phenyl equivalent phase provide a boiling point elution order with a slight increase in selectivity, especially for aromatic compounds. The low bleed characteristics and durable nature make it the column of choice for any experiment in which a low bleed non-polar column is required. The Rtx-5Sil MS column, a low polar column, is appropriate for the analysis of amines, anesthesia analysis, Crossbond™, organochlorine pesticides, phenols, and phthalates. The HP-5 column has a wide range of applications since it is a high-performing non-polar column available in a variety of configurations, especially for active compounds including acidic and basic compounds.

Sawicka [322] investigated the removal of visually disturbing lead soap efflorescence with ethylenediaminetetraacetic acid (EDTA), and optimized conditions such as pH, concentration of EDTA solution and application. The result showed that it is feasible to thin the superficial material significantly. A combined method of ATR-FTIR and SEM-EDX analysis coupled to TMAH thermochemolysis were used. In this study, the TMAH was used as a kind of derivatized solvent and two kinds of internal standards (C<sub>13</sub> and C<sub>23</sub> fatty acids) were used. The lead stearate, lead palmitate and mineralized lead soap are the predominant components. Barden [323] studied a tadpole from the Oligocene Enspel Formation in Germany using the Py-GC/MS technique combined with TMAH thermal methylation of the fossil tadpole matrix, in addition to FTIR. Results showed that the organic remains of the tadpole are original and are not the result of external contamination. The Py-GC/MS analyses indicate the presence of bacterial biomarkers in the matrix but not the tadpole. SRS-XRF also has been used to analyze the levels of zinc. Table 1-2 lists all of the devices that have been used as a complementary method with TMAH thermochemolysis.

Table 1-2 Combined analyses methods with TMAH-thermochemolysis

Analysis	Instruments	Analysis goal	Publications
Thermal analysis	Pyrolysis-gas chromatography and mass spectrometry (Py-GC/MS) Thermogravimetric analyzer –mass spectrometry (TGA-MS)	Heat samples (flash pyrolysis or slow pyrolysis) and get volatiles, these volatiles were swept into GC and detected by MS Slow pyrolysis and fragments detection	[5,6,16,17,238,249,254,279,293,295,296,306,309,314,321,324–341] [271,273,342,343]
Separation	Gas chromatography (GC) High performance liquid chromatography (HPLC)	Separation of mixtures Separate, identify, and quantify each component in a mixture	[344,345] [337,346]
Chemical structures	liquid chromatography –mass spectrometry (LC-MS) Direct temperature resolved mass spectrometry (DTMS) Matrix Assisted Laser Desorption Ionization-Time of flight-mass spectrometry (MALDI-TOF MS) Inductively coupled plasma mass spectrometry (ICP-MS) 13C nuclear magnetic resonance (13C NMR) 2D nuclear magnetic resonance (2DNMR)  H nuclear magnetic resonance (H NMR) Raman spectroscopy  Fourier transform infrared spectroscopy (FTIR)	Separation of mixtures and organic compounds detection Chemical composition of a broad range of materials Sensitive detection of large, non-volatile, labile biomolecules  Binder characterization in artistic samples Chemical structure of C Characterize the structure of molecular components and functional groups in humic matter Chemical structure of H Identify molecules and study chemical bonding and intramolecular bonds Chemical functional groups	[332] [347–350] [351–353]  [305,354–370] [294,300,308,319,331,335,342,371–374] [375]  [376,377] [332,343,378,379]  [271,273,321,326,331,332,336,372,376–389]
Surface or crystal structures	Total organic carbon analysis (TOC) Fluorescence spectrometry (XRF)  X-ray diffraction (XRD)  X-ray photoelectron spectroscopy (XPS) Light microscopic (LM) Photography Transmission electron microscopy (TEM) Scanning electron microscope (SEM-EDX/EDS)  Fluorescence spectrum by 3DEEM spectrofluorometer Microfade testing electron paramagnetic resonance spectroscopy (MFT )	Total organic carbon content for soil analysis Mineral composition  Study the structure, composition, and physical properties of materials  Surface properties and chemical state of modified catalysts Examination of small objects Visible and ultraviolet-induced visible fluorescence images Image of the microstructure of sample Elemental analysis or chemical characterization of a sample  Direct quantification of Effluent Organic Matter (EfOM) fractions Direct lightfastness testing on objects or minute samples from objects	[364,390,391] [321,334,382,392]  [336,387,390]  [294,373,380,390] [332,347] [336] [380,387] [332,334,337,347,380,382,383,385,393,394]  [342] [395]

## 1.4.2 Applications

Since TMAH is one of the most popular thermochemolysis reagents [25], the studies about TMAH thermochemolysis have been reviewed for its application on the analyses of humic acids [273,306,312,327,396], humic-like substances [372,373,397,398], fatty acids [247,304,310,327], phenolic compounds [237,239,303,399], amino acids [286,400], aromatic and aliphatic compounds [254,401], and carbamates [402]. In addition, TMAH is not only a thermochemolysis reagent but is also used as an effective silicon etching solvent [403–405], for dissolution of *E. crypticus* [406], as a strong base catalyst for transesterification [407], as an extraction solvent for mercury [263,360,367,408,409], and Sulphur atom detection [238,410], as a dispersant [411], as a balance-fluid in the fabrication of functionalized-porosity layered-ceramics processes [412], as a digestion solvent for biological samples [413,414], for pH adjustment of solutions [415,416], and for extraction of different halogen elements in soils, such as fluorine [417], chloride [418,419], bromine [420,421], and iodine [359,364,422,423]. The detection of iodine can be useful for two main types of applications; the first, measurements of the concentration and distribution of iodine in soils [362,424,425], and the transference of iodine in different forms between soils and plants, [426–431] as well as foods, [357,432] have been combined with characterization by inductively coupled plasma mass spectrometry (ICP-MS). The second main application is to detect the concentration of iodine and related compounds in a contaminated environment [363,433–435]. For example, Yang [267] studied rapid iodine release from soil, sediments, and rock samples through mild TMAH extraction. The  $^{127}\text{I}$  concentration was analyzed by the triple-quadrupole inductively coupled plasma-mass spectrometry (ICP-QQQ) single MS mode and the  $^{129}\text{I}/^{127}\text{I}$  ratio was analyzed by the ICP-QQQ MS/MS mode. TMAH is also a major problem for wastewater [436], and could be degraded by biological treatment in an up-flow anaerobic sludge blanket (UASB), mainly the methanogens involved in methanogenic degradation of TMAH [436–438]. Hereafter we mainly focus on the application of TMAH thermochemolysis.

### 1.4.2.1 Lignin and plants

Lignin, the second most abundant terrestrial polymer on Earth after cellulose, and the only large-volume renewable feedstock composed of aromatics, is an essential raw materials for the polysaccharides, renewable source of fuels, functional polymers, materials, and aromatic chemicals such a phenol, vanillin, and ferulic acid [439,440]. Lignin is a complex



heterogeneous biopolymer mainly constructed out of three oxidative *p*-hydroxycinnamyl alcohol monolignols differing in their degree of methoxylation, such as *p*-coumaryl, coniferyl, and sinapyl alcohols. Each of them gives rise to a different type of lignin unit named *p*-hydroxyphenyl (H), guaiacyl (G) and syringyl (S) units, respectively [6]. Lignin is a highly aromatic cell-wall polymer typical of vascular plants that is of importance during the growth and development of the plant and for pathogen protection, meaning lignin provides structural support to woody and vascular plants and is believed to account for ca. 20% of the organic matter input to the biosphere [4,441]. On the other hand, lignocellulosic biomass is a sustainable source of organic carbon that is a valuable feedstock for the production of biofuels and materials [4]. Because of its availability and the variety of potential modifications offered by its chemical nature, lignin has long been attractive for many scientists. However, the recalcitrance of lignocelluloses associated with lignin is an obstacle for the utilization of lignin. Therefore, pretreatment and delignification is very important. There are two types of lignin depolymerization, chemical and biological delignification, which can be used to analyze degradation products of lignin as a way to characterize the depolymerization process. Examples include the analysis of lignin degradation products from white-rot basidiomycete fungi [302], brown rot fungi *Gloeophyllum trabeum* and *Postia placenta* [442], beetles [443], and termites [444].

Py-GC/MS and TMAH thermochemolysis is often used to analyze organic compounds released from the degradation of lignocellulosic biomass. The process of pyrolysis in the presence of TMAH avoids decarboxylation and releases intact methylated phenolic compounds [6]. Therefore, this method has been widely used for the analysis of the structure of lignin in various plants. For example, Kaal [445] analyzed the main compositions of plant organs of *P. oceanica* and the coarse organic matter from a mat core spanning 750 yrs using Py-GC/MS and TMAH (25% in water) combined with THM-GC/MS in order to improve our understanding of the molecular properties and their preservation during mat development. Results showed that constituents based on *p*-hydroxybenzoic acid (*p*-HBA) are the main component of leaf sheaths, roots and the outer parts of rhizomes. The inner rhizome and leaf blades are mainly composed of carbohydrates. Additionally, the changes in molecular composition of *Posidonia australis* sheaths (SH) and roots plus rhizomes (RR) along a sediment core were studied by using <sup>13</sup>C NMR, TMAH-Py-GC/MS [446]. Marques [5] studied the structure of lignin and suberin and ferulic acid in cork from *Quercus suber* L. The polymer structure in cork, corksap, and milled-cork lignins (MCL) was studied by TMAH-Py-GC/MS and heteronuclear single quantum coherence spectroscopy (2D-HSQC-NMR). Results showed that the suberin contained 94.4%

aliphatics and 3.2% phenolics with 90%  $\omega$ -hydroxyacids and  $\alpha,\omega$ -diacids. There is about 3% and 6% of ferulic acid in cork and cork lignin. The cork lignin is essentially a G-lignin with more than 96% G units, the structure of which is largely dominated by  $\beta$ -O-4' alkyl-aryl ether linkages.

Through the Py-GC/MS method combined with TMAH thermochemolysis, lignin is decomposed into different fragments. The main structures present in different plants are summarized in Figure 1-8. Based on these structures present in lignin, TMAH thermochemolysis could be used for the detection of byproducts coming from the degradation of lignin [6,302,447,448]. Lignin degradation can occur in leaves, needles, roots, the extracts from wood, sporollenin [260,328,449–452], and leaf and needle litter. Some of these byproducts, such as the phenolic compounds and fatty acids coming from lignin degradation [259,335,453–456], have been quantified by using  $^{13}\text{C}$ -labelled TMAH thermochemolysis [260,449,457]. For example, *in situ* TMAH-Py-GC/MS was used to study the lignocellulosic unlocking mechanism for carbohydrate hydrolysis in termites [444], which is able to characterize the product distribution between the control and the termite feces, and results indicated dehydroxylation and modification of selective inter-monomer side-chain linkages in the lignin in the termite feces. Later, the wood metabolites in each gut segment were tentatively analyzed using TMAH-Py-GC/MS [458], which showed a selectivity of  $\beta$ -O-4' linkages and subsequent methylation of all ring hydroxyls that were represented by the generation of abundant new pyrolyzates. This study helps to provide more information about the absolute structure change of lignin compared with a normal pyrolysis analysis. On the other hand, the stepwise lignin unlocking mechanism in termites was elucidated. The changes in lignin composition or structure could provide information to understand the reaction in nature; for example, the analysis of compositional changes of lignin in river samples could help to increase understanding of the responses of terrestrial vegetation in central Japan to global climate changes [299]. The study of lignin fractions isolated previously by sequential enzymatic hydrolyses using Py-GC/MS, with and without TMAH thermochemolysis, could help to well understand the behavior of the polymeric part of lignin exposed to fecal microbiota [329] and the molecular changes of corn stover lignin in the laccase system by comparing the methylated fractions of lignin [459].

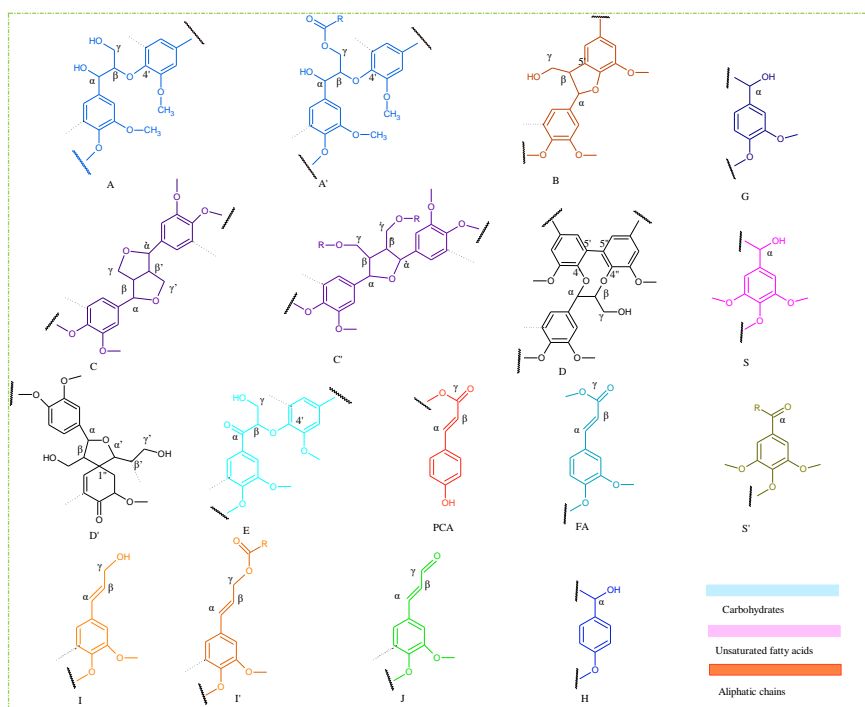
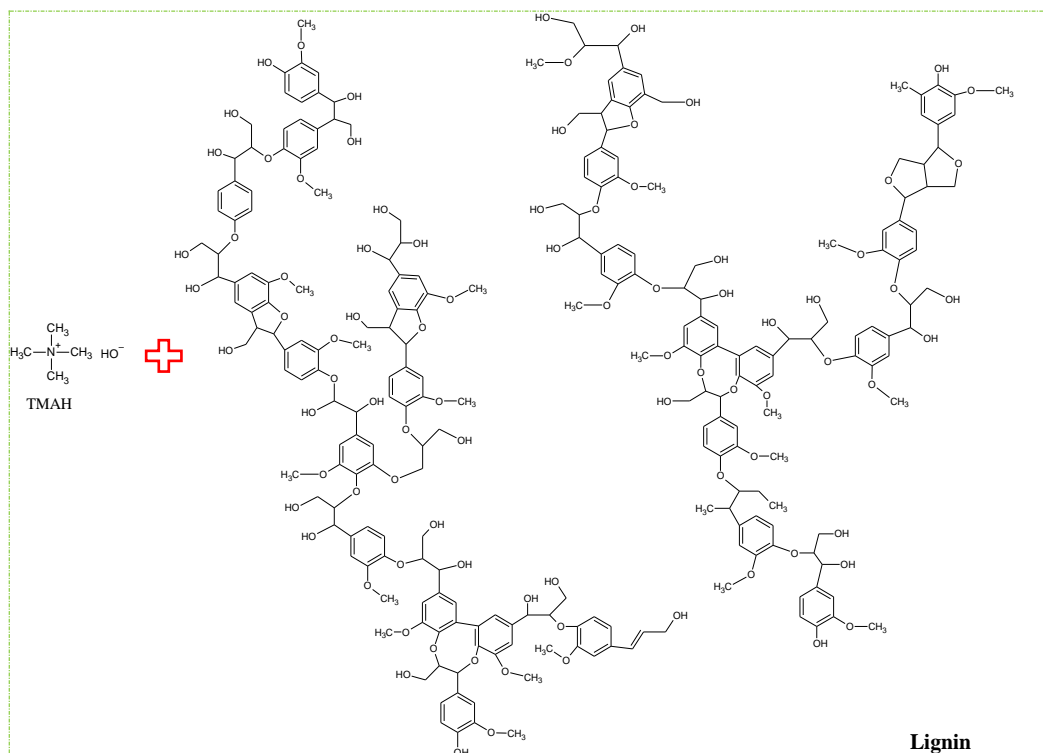


Figure 1-8 The structures of lignin that react with TMAH thermochemolysis, adapted from [4–8]. (A)  $\beta$ -O-4' alkyl-aryl ethers; (A')  $\gamma$ -acylated  $\beta$ -O-4' alkyl-aryl ethers; (B) phenylcoumarans; (C) resins; (C') tetrahydrofuran structures formed by  $\beta$ - $\beta$  coupling of monolignols acylated at the  $\gamma$ -carbon; (D) dibenzodioxocins; (D') spirodienone structures formed by  $\beta$ -1' coupling; (E) C $\alpha$ -oxidized  $\beta$ -O-4' structures; (I) cinnamyl alcohol end-groups; (I')  $\gamma$ -acylated cinnamyl alcohol end-groups; (J) cinnamyl aldehyde end-groups; (PCA) *p*-coumarate units; (FA) ferulates; (H) *p*-hydroxyphenyl units; (G) guaiacyl units; (S) syringyl units; (S') oxidized syringyl units bearing a carbonyl (R, lignin side-chain) or carboxyl (R, hydroxyl group) group at C $\alpha$ .

For plants, suberin and suberan are the important natural biopolymers. Their role is to provide a protective barrier between the plant and the environment [460]. The structure of this hydrolysable polyester is proposed to be comprised of long chain (C<sub>11</sub>-C<sub>24</sub>) polymethylenic domains with carboxylic acids held together by aromatic rings and esters [461]. Olivella [324,460] analyzed the suberin monomers isolated from cork by TMAH-Py-GC/MS. Their study showed that the major compounds of suberin from bark and cork layers were octadec-9-enedioic acid, docosanedioic acid, and 9,10-epoxyocta-decanedioic acid with mean values of 17.0%, 14.5%, and 11.0%, respectively. These isolated monomers were used to study the sorption of three pesticides (isoproturon, methomyl and oxamyl), and modeling calculations was used to study the interaction between the suberin monomers. Results showed that, in addition to the van der Waals interactions with the apolar region of sorbent and isoproturon, hydrogen bonds were also formed between the isoproturon NH group and a carboxylic oxygen atom of a suberin monomer.

We showed here that TMAH thermochemolysis was mainly used to analyze phenolic, ester, ether bonds and carboxyl functional groups of lignin, as well as their related degradation compounds, which demonstrates its suitability for the determination of the composition of large polymers. Soil is the necessary condition for plant, leaves, stem, roots or other organs of plants that are contained in soils, therefore TMAH thermochemolysis could also be used to analyze the degradation compounds of lignin or compounds derived from lignin in soil.

#### ***1.4.2.2 Coal***

Coal is a kind of flammable sedimentary rock in black or brown-black color, which is predominantly of vegetal origin. Lignin is possibly the most important vegetal precursor of vitrinite in coal in terms of quantity; monocyclic aromatic units are condensed with the aliphatic lignin forming polycyclic aromatic units, such as naphthalene, anthracene, or phenanthrene through the coalification process [462]. Figure 1-9 shows the structural model of high-volatile bituminous coal. Coal has a macromolecular three-dimensional cross-linked network (immobile phase) with a multitude of relatively small molecules with varying structures embedded therein (mobile phase). Coal has been widely used in many fields. For example, coal has been the main energy source for power generation in China. Coal char is used in the metallurgical industry, while coal tar is used to refine oil to different quality grades, such as the heavy oil used for aircraft oil and the light oil used in chemical products. Light oils include the light aromatic compounds, such as benzene, toluene, ethylbenzene, xylene and naphthalene. All

these light aromatic compounds are important raw materials for chemical products, such as fibers, plastics, pharmaceuticals, dyes, and other chemicals [463]. Coal gasification is a means to convert fossil fuels into a combustible gas or a synthesis gas, and this process plays an important role in the green energy conversion of coal into natural gas. Therefore, coal is one of the most important energy sources except for petroleum.

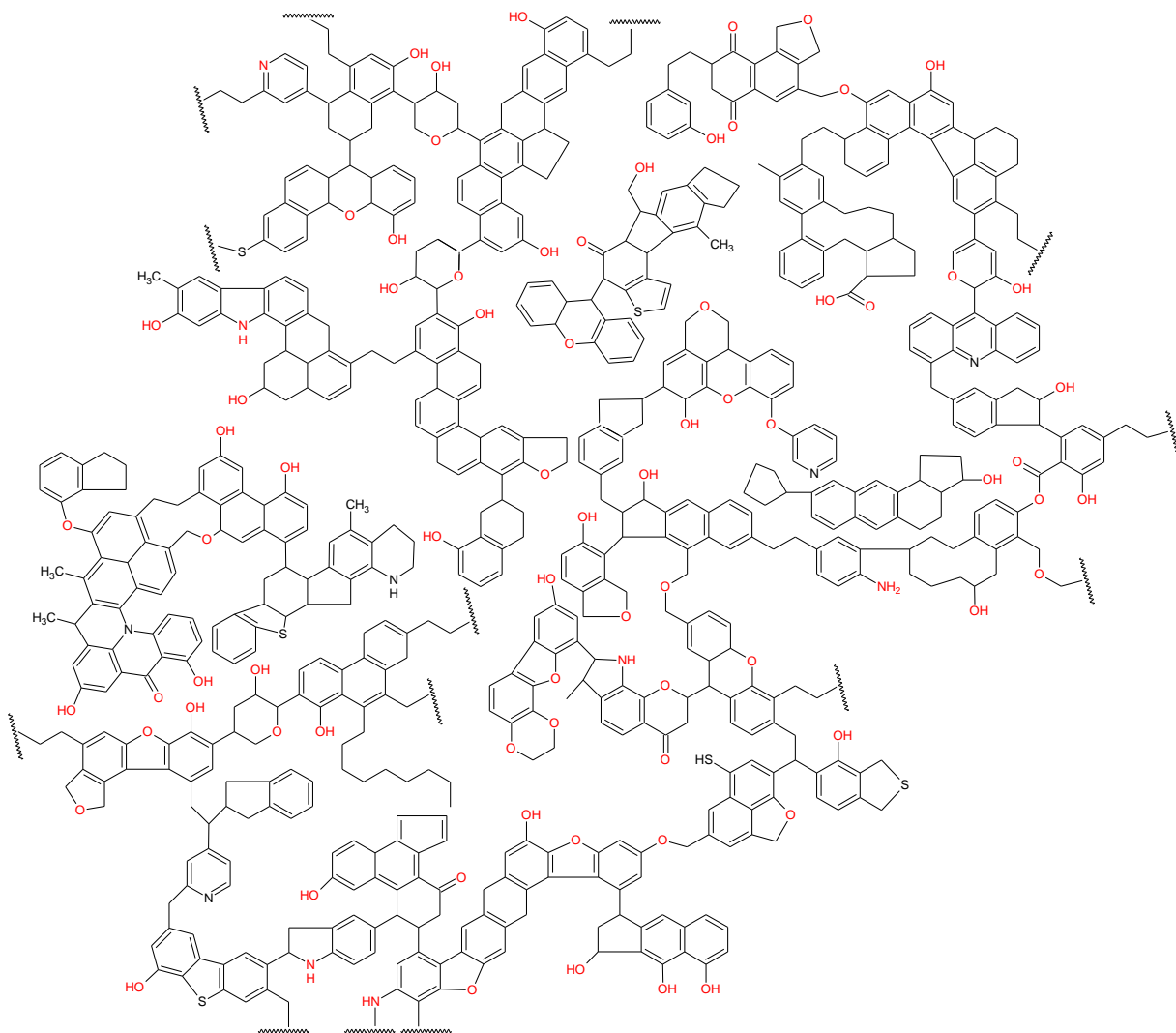


Figure 1-9 The structure of bituminous structure, adapted from [9].

The conversion rate of coal into “clean” energy depends on the utilization methods and the properties of coal. In fact, the structure of coal determines the conversion and utilization method, and plays an important role in the utilization of coal. Coal structure and the main organic matters of coal have been studied using XRD,  $^{13}\text{C}$  NMR, Raman, and FTIR spectroscopy. Organic matters, such as low molecular weight compounds, can be extracted from coal by organic solvents [270,464]. Pyrolysis GC/MS combined with extraction methods can result in the formation of light aromatics [465,466]. Although these are the traditional

methods, TMAH thermochemolysis has become an increasingly popular method for characterization of organic matter in coal. For example, TMAH-GC/MS was used to analyze the composition of filtrate coal after coal depolymerization [467]; identified compounds included fatty acids and derivatives, benzene related O-containing compounds, alcohols, heteroatom containing compounds, hydrocarbons, aromatics, and dicarboxylic acids.

Coal is composed of some macromolecular structures as shown in Figure 1-9. Humic acids, complex compounds containing hydroxyl and phenolic hydroxyl functional groups, are one of the important components of coal, and TMAH thermochemolysis has been used for the analysis of humic acids. For example, Grasset [468] characterized the lignin monomers in low rank coal humic acids using TMAH thermochemolysis followed by reductive cleavage. Results showed that the lignite (low rank coal) from the Czech Republic contains intact lignin monomers with a dominance of coniferyl units, which is in accordance with the gymnosperm origin of the lignite. The major methylated lignin derivatives included 3,4-dimethoxybenzaldehyde, 3,4-dimethoxyacetophenone and a 3,4-dimethoxybenzoic acid methyl ester. Nasir [469] also studied the structure of humic acids and nitrohumic acids (NHA) extracted from Pakistani lignite as well as the standard Leonardite humic acids (LHA) using Py-GC/MS with and without TMAH thermochemolysis and with a flash pyrolysis temperature of 721 °C. In addition, the FTIR and NMR techniques were used to elucidate the influence of coal rank on the regeneration and nitration processes related to the chemical composition of coal and derived materials. The most abundant aromatic derivatives were a 4-benzenedicarboxylic acid dimethyl ester and 1,6,7-trimethyl naphthalene. A high proportion of long-chain fatty acid methyl esters, nitrogen compounds and furan compounds were detected.

Extraction of organic matter from coal is a crucial method to first separate the free small molecules, including the aliphatics, and ether bridges within the skeleton structure of coal [9,270]. The organic compounds in coal extracts and extraction residues can then be studied combined with TMAH thermochemolysis. Stefanova [470] analyzed the components of CHCl<sub>3</sub> extraction residues of bitumen coal by using off-line TMAH-Py-GC/MS where the sample was pyrolyzed at 400 °C. Diterpenoids, *n*-Fatty acids, phenols and its alkylated homologues were detected. The long-chain homologues of *n*C<sub>24</sub> and *n*C<sub>26</sub> were maximal in the bitumen coal used herein; their results demonstrated that the predominance of conifers in the Bobov dol palaeomire was the biomarker assemblage of the “free” extractable bitumen [470]. The extracted component of the coal sample was influenced by the extraction solvent. Doskočil [272] studied the water-extractable fractions from South Moravian lignite, and results showed that the main contents of the off-line TMAH thermochemolysis of lignite were aromatic compounds

(77% of the total identified molecules), such as benzene carboxylic acids and their derivatives, especially methoxybenzoic acids, and to a lesser extent, methoxybenzenes. The identified aliphatic compounds consisted of short-chain diacids, fatty acids and polyols and were 23% of the identified compounds. Py-GC/MS can provide more insights into the chemistry of the resin-derived material, while THM-GC/MS is more informative about poly-methylene compounds. The two methods are complementary for detecting the aryl–O macromolecular backbone of kerogen. On the other side, the maturity of coal also influences the content and the type of its organic matter. The effect of coal rank on coal molecular properties has been investigated using 27 coal samples from lignite to high volatile bituminous rank using Py-GC/MS and THM-GC/MS methods [471]. Polyphenolic, polymethylenic and resin-derived constituents were detected. Lignin-derived material and long-chain ( $\geq C_{24}$ ) ester-bound polymethylene chains are the main components of immature coal, whereas the mature coals are enriched in short ( $C_{10}$ – $C_{25}$ ) free and/or trapped (isoprenoid) hydrocarbons, alkylated phenols and resinite aromatic derivatives.

Biodegradation or bioconversion of coal is a valuable form of clean energy conversion. In one study, asphaltenes were separated from a series of Liaohe biodegraded bitumens and the asphaltenes were analyzed using on-line flash pyrolysis-GC assisted by TMAH thermal hydrolysis and methylation [252]. Results showed that the alkyl moieties bonded to asphaltene macromolecules are dominated by C–C and ether (thioether) bonds but less so through ester and hydrogen bonds. Furthermore, the linear alkyl moieties bonded to the asphaltene structure by hydrogen and ester bonds are more susceptible to biodegradation than those bonded to the asphaltene core through stronger covalent bonds such as C–C and ether (thioether) bonds. On the other side, the TMAH-thermochemolysis method was also used to study the coal bioconversion activity of nonmycorrhizal fungi in the *C. dactylon*/coal rhizosphere [472]. The methylation compounds obtained from TMAH thermochemolysis were pyrolysed at 700 °C for 15 seconds and analyzed by GC/MS. Poly(tert-butylstyrene) (0.05 mg/mL in hexane) was used as an internal standard and benzeneamine, diazine, dimethylpyranone, furfural, hexadecanoic acid, methylaminophenol, and propanenitrile were semi-quantified. Results showed that low molecular weight organics can facilitate the bioconversion of coal and that the phyto-bioconversion of hard coal involving plants and microbes which occurs in the rhizosphere promotes the growth of *C. dactylon*.

In summary, TMAH has been mainly used for the characterization of coal or components extracted from coal through Py-GC/MS with or without an extraction method. Most of the studies focused on the qualification of coal composition, while few studies have

focused on the quantitative analysis of coal composition. Therefore, the composition of coal or coal-related components needs to be studied in the future. Low molecular weight compounds in coal play an important role in coal pyrolysis [270,464]. O-bearing compounds such as –OH, carbonyl group, phenols, alcohols, acids and esters have been detected in the extractions of a brown coal by FTIR characterization. While the abundance of each compound has not been quantified, TMAH thermochemolysis could be used to methylate these organic compounds and quantify the concentrations of the free organic compounds in coal samples.

#### ***1.4.2.3 Lacquer and heritage***

Lacquer is a glossy and durable coating material that has been used as an adhesive or painting material for crafts, weapons, wooden products, coffins, and daily necessities, since ancient times all over the world. Some examples of lacquer materials include natural lacquer sap, synthetic lacquer derivatives, and their films. The natural lacquer is made with the sap from lacquer trees, such as the *Rhus vernicifera* lacquer trees. They are also known as Asian lacquer trees or *Shengqi* in China and *Urushi* in Japan, with urushiol being the main lipid component. From the *Rhus succedanea* trees, which are used as Vietnamese and Chinese Taiwan lacquer, the main lipid component is laccol. Whereas thitsiol is the main lipid compound in the sap from the *Melanorrhoea (Gluta) usitata* trees; their sap has been used in lacquer from Myanmar, Laos, Cambodia, and Thailand [473]. The *Toxicodendron vernicifluum* trees grow naturally in Korea and various artifacts coated in the natural lacquer produced from their sap have been excavated there. European lacquers are complex decorative finishes imitating the appearance of Asian lacquer but made from locally available materials and techniques [325].

The sap was used alone or with additives such as flour or clay for the ground layers and they can be colored with pigments or metal fillers. The refined sap was applied on the surface of the relics for protection and/or decoration, and with multiple very thin layers on the top of the artwork. The multiple layers of lacquers can consist of a mixture of oils such as perilla oil, tung oil, tallow tree oil, linseed oil, sesame oil, tee seed oil, and Canola oil or *Rapa* oil [474]; resinous materials include waxes or synthetic resins; colorants and pigments; proteins such as pig's blood, animal glue, and egg; carbohydrates such as starchy materials (e.g., flour); miscellaneous materials such as the pig gall or bile; and the products of their interaction and degradation. Lacquer is dried under the specific conditions of over 70% relative humidity (RH) at room temperature overnight, which results in mainly the oxidation and polymerization of main lipid compounds, including the urushiol, laccol, and thitsiol by laccase [475–477]. The



unsaturated side-chain autoxidation process occurs after the concentration of lipid monomers decreases to less than 30%. Subsequently, a very sturdy and dense lacquer film is formed and its properties are of extreme hardness (approximately 6H pencil hardness) and insolubility due to accelerating nucleus-side chains (C–C, C–O–C) and side chain-side chain (C–C) cross-linkages [478]. These properties make it difficult to analyze the consistency of lacquers, especially the organic compounds that have been used in lacquers.

Lacquer is a glossy and durable coating material that has been used for thousands of years. The investigation of the composition of lacquer, with the aim of further enriching scholarship and contributing to our understanding of history, helps the archaeologist to understand global historical trade practices and heritage of the coating skills. Therefore, several analytical instruments have been used to characterize the composition of different lacquers, such as FTIR [479,480], which is commonly applied to the characterization of the organic functional groups in ancient artworks and ancient buildings because it is a non-destructive method. For example, it was shown that the utilization of natural organic compounds such as rice soup, the juice from vegetable leaves, egg whites, tung oil, fish oil, or even animal blood can greatly improve the performance of lime mortars [481]. Infrared spectroscopy in the range of 4000–600  $\text{cm}^{-1}$  (middle IR) is one of the most widely used techniques for the detection of organic materials [481], such as the CO stretching vibrations at around 1228, 1164, and 1087  $\text{cm}^{-1}$ , the ester carbonyl stretching band at around 1740  $\text{cm}^{-1}$ , NH bending vibrations at around 1584  $\text{cm}^{-1}$ , etc. [480]. However, FTIR was found to be unable to differentiate the organic structures of similar lacquers and the various organic and inorganic materials that were mixed with different lacquer saps [482], to differentiate the original lacquer tree of a given lacquer, and to distinguish macromolecular peptides and proteins. The peaks from the solid state nuclear magnetic resonance (NMR) spectroscopy could demonstrate the main carbon structures of the organic compounds; however, this technique cannot give precise information because it is difficult to analyze the peaks and obtain clear results [473]. Therefore, Py-GC/MS is widely used as the best method to characterize the components of the different organics. A macromolecular compound is heated at different temperatures and volatiles are formed. These volatiles are carried by a carrier gas into the GC for separation and the MS for detection. This method requires lower sample amounts and simple manipulation and pre-treatment of the sample. Though Py-GC/MS is an efficient instrument to acquire the fingerprint information of organic matter in lacquers, varnishes, and paintings, there are some refractory materials for which it is difficult to form volatiles with the pyrolysis process and thus it is difficult to detect these molecules directly by GC/MS. Therefore, wet chemistry, mainly derivatization reactions,

is combined with Py-GC/MS to elucidate the composition and structure of the target materials at the molecular level. Among various derivatization methods, as described in section 1.2, TMAH-Py-GC/MS has been shown to dramatically improve the sensitivity and specificity of organic analysis, such as in a study of the composition of Chinese lacquers [334,338,343,474,483–485]. These methods have been widely used for the analysis of artwork from many countries, including artwork from China, Korea and Japan, as well as some European countries such as Italy [336], the Netherlands [486], Spain [324] and Portugal [354].

TMAH-Py-GC/MS is a practical method for the characterization of ancient art works, especially the composition of lacquer, such as the black lacquers of 19th-century furniture [487], European lacquer [325], wooden chips [488], varnish [394,480,489], the paints of antiques, historical coatings on objects of art [490] and the organic matters of archaeological scenarios [301,350,491]. Lists of markers generated in this process could be added into a database to improve the interpretation of complex mixtures in lacquers and combined with other complementary techniques for the compositional analysis of coatings, lacquers, pigments and binders in different antique and ancient architecture. For example, Cauzzi [492] studied the chemical compositions of sculptural polychromy of employed materials and pigments of the Buddha in the *Zhongshan Grottoes* (R.P.C.) using Raman analysis, Fourier-transform infrared analysis, analysis through energy-dispersive X-ray spectrometry coupled to scanning electron microscopy and Py-GC/MS. TMAH was used to analyze the compositions of the pigments with Py-GC/MS [493]. Resinous constituents of varnishes on 19<sup>th</sup> and early 20<sup>th</sup> century tintypes were analyzed by TMAH-Py-GC/MS and the resinous materials of the collection tintypes were analyzed. This was the first large-scale analysis of tintype manufacturing and provided unique information on the working habits of photographers during the 19<sup>th</sup> and early 20<sup>th</sup> centuries. A summary of the applications of TMAH-Py-GC/MS and the main analyzed compositions of ancient art-objects are listed in Table 1-3.

Table 1-3 The organic compounds detected in ancient samples with TMAH-Py-GC/MS in previous studies

Sample	Compounds	TMAH volume	Derivatization method	T <sub>pyrolysis</sub>	Year	Publication
Bronze vessels	Glycero lipids of animals or animal+plant origin; PAHs	5 µl, 25% w/w in water	On-line	600 °C, 10 s	2011	[494]
Orange glaze	<i>p</i> -coumaric acid, linseed oil, colophony and sandarac	2–3.5 µl , 25% in methanol	On-line	550 °C	2011	[495]
Harpisichord	Cupressaceae or Araucariaceae resins, Pinaceae resin	0.5 µl, 25% in methanol	On-line	610 °C,10s	2012	[496]
Crucifix panel	Hexadecanoic acid; nonanedioic acid; the methyl ester of 7- <i>oxo</i> -dehydroabietic (7- <i>oxo</i> -DHA) acid; poly( <i>n</i> -butylmethacrylate) and diterpenoid Pinaceae resin; acrylic copolymer poly(ethylmethacrylate-methylacrylate)	3µl , 25% in water	On-line	600 °C	2013	[352]
Sculptural polychromy	Saccharidic derivative; Fatty acids	5 µl, at 25% w/w in water	On-line	750 °C, 10s	2013	[492]
Cartonnage masks	Permethylated and partially methylated 3-deoxyaldonic acids	5 µl, 25% in water	Off-line (30min)	300 °C to 700 °C	2014	[497]
Tintypes	Camphor, dammar, Pinaceae, sandarac, and shellac	3 µl, 25% in methanol	Off-line (3min)	550 °C, 6 s	2014	[493]
Wooden screen	Pine resin (colophony) and shellac, urushiol and different oils; blood (most likely pigs' blood).	3 µl , 25% in water	Off-line (3min)	550 °C,6 s	2016	[498]
Rectangular trays	Laccol (arlenic acid, C17), and drying oils, such as perilla oil, protein, soot; blood, pine resin, beeswax.	3 µl , 25% in methanol	Off-line (3min)	550 °C,6 s	2016	[499]
Gloss paints	Drying oil; such as palmitic, stearic, azelaic acid, suberic, sebacic acid, dehydroabietic acid, 7- <i>oxo</i> -dehydroabietic acid, 15-hydroxy-7- <i>oxo</i> -DHA.	2 µl, 25% in methanol	On-line	550 °C	2016	[500]
European scale armor	Wax and lipids, with fatty acids possibly from multiple sources (oils, fat, wax, soil)	3 µl, 25% in methanol	On-line	550 °C	2017	[501]
Wall paintings at Caere	No organic binding medium was detected.	1.6 µl, 25% in methanol	On-line	50 °C to 450 °C (3 min)	2017	[502]
Part of wall paintings	Fatty acid (especially high content of azelaic acid); rosin resin; protein; the binding medium includes animal glue; bovine (or yak) glue; Tung oil and rosin resin	3 µl, 25%	Off-line (60 min)	600 °C,10 s	2018	[503]
Tie lu	Animal glue, drying oils, beeswax	5 µl of 10% methanol	On-line	600 °C , 0.2 min	2018	[504]
Folding doors in foyer at Herlev Hospital	Phthalic acids, monocarboxylic acids caproic (C6:0), capric (C10:0), palmitic (C16:0), oleic (C18:1), stearic (C18:0), dicarboxylic acids suberic (2C8), azelaic (2C9), dehydroabietic acid (DHA), 7- <i>oxo</i> DHA, 7-methoxy-tetrahydroabietic acid.	15 µl, 2.5% in methanol	On-line	550 °C for 12 s	2018	[505]
Wooden panel of the Nongso offin	Markers of drying oil like azelaic acid and palmitic acid existed in large quantities.	3 µl, 25% in methanol	On-line	550 °C	2018	[506]
Furniture in black lacquer	Copal oil and Pinaceae resin	4 µl , 2.5% TMAH in methanol	-	480 °C	2019	[487]
Hillebrand Desk	Oils, pine resin, larch turpentine, sandarac, shellac, gum benzoin.	5 µl, 25% TMAH in methanol, diluted to 5% with methanol	On-line	360 °C to 660 °C at 500 °C min <sup>-1</sup>	2019	[325]
Four resins	Resins	2 µL 2.5 wt % in methanol from 25 wt % in methanol	On-line	480 °C	2019	[490]
“Tixi” carved lacquer	Pigment (soot, black layer), orpiment (yellow layer), cinnabar (red layer), lacquer sap, heat-bodied tung oil and tannins (partial layer); catechols, acid catechols, phenols, alkyl benzenes, and hydrocarbons of a maximum side chain length of 17 carbons; alcohols.	2 µl, 25 wt % in methanol	On-line	550 °C, 6 s	2019	[338]
Cabinet on stand	Shellac, pine resin	5 %	-	350 °C – 700 °C	2019	[486]
Bartolomeu Dias table	The binder is a mixture of proteins (primarily animal glue and blood) and drying oil; laccol was detected for the bottom lacquer layer and a mixture of laccol and urushi for the top lacquer layers	3 µl, 25% in methanol	Off-line(1 min)	600 °C, 12 s	2019	[479]
Lamp panel, fuel residue	Long-chain fatty acids, fatty alcohols and hydrocarbons, beeswax	3 µl of 25% in water	On-line	550 °C	2019	[507]

TMAH-Py-GC/MS can be used to analyze the organic components of different relics, other organic substances, and sap mixtures of urushiol, laccol, and thistsiol with two phenolic hydroxyls. Fatty acids reveal the presence of oils, which can be further identified according to the ratio of certain fatty acids. For example, drying oils can be identified by a ratio of azeleic acid to palmitic acid methyl esters (the so-called A/P ratio); the ratios of palmitic to stearic acid methyl esters (P/S ratios) at 1.0–1.2 show the presence of tung oil.

TMAH thermochemolysis is mainly the methylation of hydroxides of phenolic compounds, alcohols, saturated and unsaturated long-chain fatty acids, etc. [508,509]. Figure 1-10 shows the mechanism of TMAH thermochemolysis of different species, in which methylation plays a key role. Indeed, these compounds can be used as biomarkers to determine the origin of the lacquers or the trade among countries. TMAH thermochemolysis methods are not only used to study specific questions surrounding a material's composition, but also for elucidating aging/deterioration mechanisms and restoration treatments for long-term preservation of art-objects. For example, Katsibiri [347] characterized the properties, function and chemical composition of mordants and the deterioration that occurred during aging of the mordants. In this study, the TMAH was used as a methanolic solution for the samples to give complementary information combined with the EI-DTMS method. By comparing the differences and similarities of wall paintings across three churches, a common painter was identified. The compositional evolution of different ancient artworks is its own field of study since the natural aging or man-made decay problems of paintings is one of the most important problems in the hermitage science field.

Some researchers simulated the aging process and studied the effect of environmental conditions on the aging process of selected artworks [257,510,511]. For example, Ploeger [512] characterized the artists' alkyd paints and paint stability issues using characterization methods such as Fourier transform infrared spectroscopy attenuated total reflectance (FTIR-ATR) to analyze different functional groups. Py-GC/MS combined thermal hydrolysis and methylation methods to disclose the monomers used to manufacture an alkyd resin. Results showed that the aged films were brittle and difficult to handle, because of the high molecular weight of the alkyd polymer and faster stiffening from the excessive cross-linking and subsequent degradation reactions. The conclusion was that they should be preserved in conditions similar to those used for oil paintings.

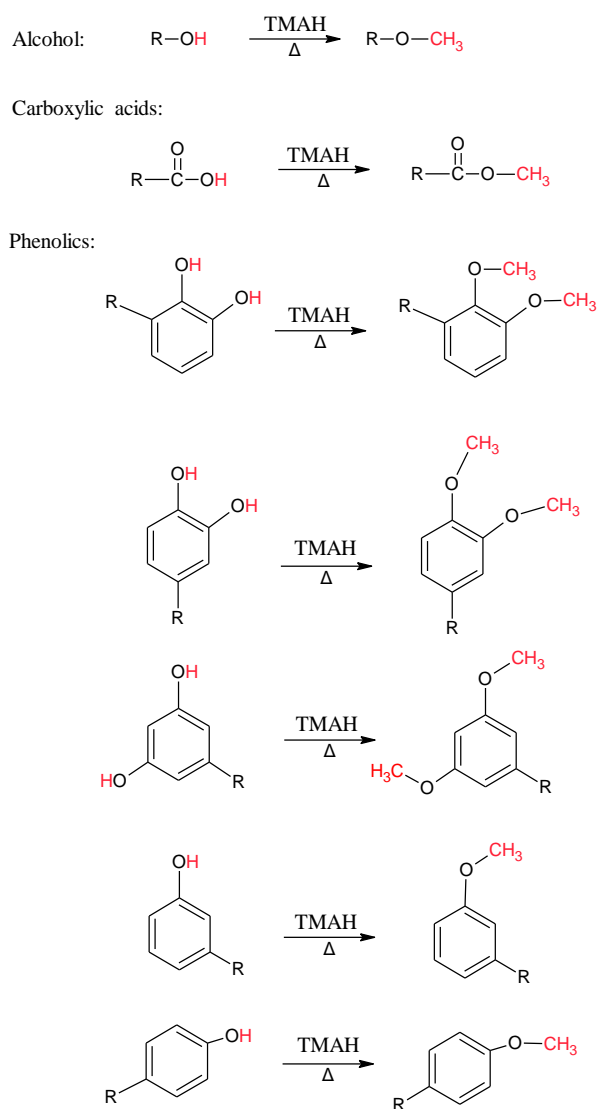


Figure 1-10 TMAH thermochemolysis with different organic compounds.

The amount of recorded literature on the application of TMAH thermochemolysis in archeology over the last 10 years is about 5 times higher than that during the ten-year period before 2010. A wide range of organic compounds were detected, including natural resins and fatty acids, which demonstrated that the TMAH-Py-GC/MS is an efficient method to analyze the organic compounds in coatings or paint layers of ancient artworks. This method could determine the compositions and the origin of lacquers, varnishes, and paints of relics, which played a key role in the conservation and restoration of ancient artworks. In addition, some advanced characterization technologies were used to characterize ancient artworks comprehensively, such as light microscopy (LM), optical microscopy (OM), direct temperature resolved mass spectrometry (DTMS), scanning electron microscopy–energy dispersive X-ray

spectroscopy (SEM–EDX), etc. However, few studies have focused on the quantitation of lacquer.

#### ***1.4.2.4 Soil***

The importance of organic matter within soil cannot be overemphasized because this organic matter plays a vital role for life, as a nutrient source, an energy and cation reservoir or source, a pH, temperature, and water storage buffer, an absorber of toxic organic compounds and inorganic ions, an enzyme activity controller, and finally, a major role player in greenhouse gas regulation [513]. The organic matter in soil is primarily responsible for the soil properties that control the productive capacity of soil and the sustainability of a productive soil system [514]. Therefore, it is of great importance to gain as much insight as possible into organic compounds within soils on the Earth. TMAH-Py-GC/MS is one of the most used methods for the characterization of organic compounds within soil samples. This method has been widely used in the analysis of forest soil [515], farmland [319], cattle husbandry soil [516], coastal Wetland soils [300], permafrost sediments [517], archaeological settings [301], peat soil [258,318,342], forensic soil [518], archaeological scenarios [301], and river sediments [249,390,519–521]. The organic compounds that have been detected in different soil samples are summarized and listed in Table 1-4.

The organic matter in soil can be classified into four categories : i) particulate organic matter, ii) humus, iii) resistant soil organic matter and iv) dissolved organic compounds [514,522]. The particulate organic matter, or particulate organic carbon (POC), is composed of decomposing plant residues, fungal hyphae, fine plant roots and associated biomasses, which are unstable and have a short turnover time less than 1-2 years. Lignin and its derivatives are the main decomposition products of plants and their organs. TMAH thermochemolysis has been widely used to characterize the decomposition products of plants and their organs in forest soil, farmland and Wetland soil. Lignin is also considered to be a major component of soil organic matter (SOM) [523], which mainly comes from the organs of plants such as leaves, roots, and grass litters [295,315,317]. The main structure of lignin and its derivatized compounds can be seen in Figure 1-8 in section 1.4.2.1 lignin and plants.

Table 1-4 The organic compounds detected in soil samples with TMAH-Py-GC/MS in previous studies.

Soil location	Organic compounds	TMAH volume	Derivatization mode	T <sub>Pyrolysis</sub>	Year	Publications
Mediterranean forest soil	Fatty acids, <i>n</i> -alkanols, $\alpha$ , $\omega$ -diacids, hydroxyacids, ligneous subunits, carbohydrates	2 mL 50% (w/w) in methanol	Off-line	400 °C	2009	[310]
Weerterbergen in The Netherlands.	Lignin, polysaccharides, phenols diketodipyrrole, <i>n</i> -alkenes/ <i>n</i> -alkanes (C10–C33), 2-methylketone; alkanolic acid	A droplet, 25% in water	-	600 °C, 5 s	2010	[292]
Acer pseudoplatanus on Petřín hill in Prague in May 2010.	litters	Excess, 25% in water	Off-line	550 °C, 10 s	2011	[314,315]
Loire and the Gartempe rivers	Heterocyclic compounds, N-containing compounds	25% (w/v) in methanol	-	650 °C, 10s	2012	[294]
Coastal Wetland soils	Aliphatic compounds, lignin-derived compounds, N-containing compounds, Polysaccharide-derived compounds, S-containing compounds	-	-	620 °C, 20 s	2012	[300]
A wet tropical forest on the island of Hawaii in the Kohala Mountains.	Aromatic, lipid, polysaccharide, N-bearing, lignin, phenol	5 $\mu$ L	Off-line (24 h)	590 °C	2012	[293]
Koroglu Mountain in Turkey	Amber extract, fossil resin	-	On-line	480 °C, 20 s	2014	[524]
Kervidy-Naizin catchment, in central Brittany, western France	Lignin and tannin markers, carbohydrates, and fatty acids.	Excess, solid TMAH	On-line	400 °C, 1 min	2014	[304]
Mega Rice Project area in Kalamangan village and Sebangau National Park in Central Kalimantan Province, Indonesia. Mega	Humic acids	25 $\mu$ l	Off-line	550 °C, 4 min	2015	[342]
Soil cores from Shark to Taylor Sloughs, the primary flowpaths of the southern Everglades	Kaurenes, cyclic diterpenoids; branched isoprenoids (C20HBIs) and Bot-ryococenes; lignin phenols.	100 mg of reagent	Off-line	-	2015	[525]
Soil from the permanent grassland in the south of France	Leaves and roots (aliphatic compounds, aromatics)	A few drops, at 25% ) in methanol	On-line	650 °C, 10 s	2016	[295]
Four forest sites situated in the Italian Alps	Aromatic compounds, polysaccharides, fatty acids, N-containing compounds.	Excess	On-line	550 °C, 10 s	2017	[316]
Sokolov brown-coal mining district, Czech Republic.	Litter (aliphatic and aromatic compounds and a decrease of carbohydrates)	Excess, in water	Off-line	550 °C, 10 s	2017	[317]
Abbaretz (BABZ <sup>^</sup> ), Mioche (BMCH <sup>^</sup> ) and La Petite Faye (BLPF <sup>^</sup> ), France	Products originated from proteins, carbohydrate, lignite, fatty acids, sterols and lipids fractions.	15 $\mu$ l	On-line	400 °C	2017	[321]
Wetland soil, in Brittany (France).	Lignin and tannin markers, carbohydrates and fatty acids.	Excess, solid TMAH	On-line	400 °C, 1 min	2018	[305]
Chateau de Versailles in Versailles; Rothamsted Research, United Kingdom; the Swedish University of Agricultural Sciences, Sweden; Askov Experimental Station, Denmark	Aromatic compounds, lignin-derived compounds and phenolic compounds, aliphatic compounds, carbohydrates and N-containing compounds	A few drops, 25% (w/w) in methanol	On-line	650 °C, 10 s	2018	[296]
Araguás catchment (Central Spanish Pyrenees)	Lignin (0–0.74 $\mu$ g mg in soil)	20 $\mu$ L, 25% (w/w) in water	Off-line(2 min)	600 °C, 5 s	2019	[297]
Archaeological Sites, The NW of the Iberian Peninsula	Monocyclic aromatic hydrocarbons, methylene chain compounds; N-compounds; short-chain FAMES (C16,C18); lignin	25% in water	-	750 °C, 20s	2019	[301]

The humus part of the soil has a longer turnover time, around 2-25 years, and includes partially stabilized organic materials and microbial metabolites. The resistant soil organic matter is strongly stable either chemically or physically and may be part of the humus fraction. Its turnover time is about 250 to 2500 years [514,522]. The humic substances represent approximately 40–60% of the soil organic matter, including humin, humic acid, and fulvic acid. Humin (C-based macromolecular compounds) is the insoluble fraction of humic substances. Humic acids are soluble under alkaline conditions and fulvic acid is the fraction that is soluble under both alkaline and acidic conditions. Humic substances can influence the soil buffering capacity, increase moisture retention, and supply plants with available micronutrients. These compounds can also interact with complex metals which alleviates both heavy metal toxicity and metal deficiency in soils [526]. Therefore, it's important to characterize the structure of humic substances in soil. Branched-chain fatty acids and methyl esters are related to a large amount of humic acid structures in the soil, and can be used as biomarkers in humic substances from matured compost samples. A higher level of branched-chain fatty acids indicates a higher aromaticity and lower molecular weight of humic substances and provides information on the history of microbial activities during the composting process [327]. The structures of humic substances are related to the soil function [249]. For example, humic substances from sugar cane cultivation areas were found to contain compounds rich in lipids and fatty acids [249,372]. The salinity of the soil can also affect the compositional formation of humic acids, with one study suggesting an increasing recalcitrance of humic acids along the salinity gradient. The same study observed a higher percentage of aromatics in humic acid compounds in soil with higher clay content [300]. Steel slag-compost fertilizer was shown to alter the steel slag during the fertilization period, mainly involving a decrease in phenolic moieties and a significant increase in the sulfur-containing pyrolysate compounds [306].

The dissolved organic compounds, mainly including sugars, amino acids, soluble P-containing compounds, and low molecular organic acids, make up a small but essential proportion of the soil organic compounds and serve a wide range of functions, most notably nutrient cycling [249]. Polysaccharides were used as an indicator and proxies have been proposed for the reconstruction of past peatland vegetation [527]. TMAH thermochemolysis has been proven to be able to analyze amino acids which consequently represent one of the most important components in the organic N cycle [286]. On the other side, microbial communities also play an important role for soil and drive the transformation of organic components in soil [452,516], TMAH thermochemolysis was used for the characterization of



changes in soil microbial communities by analyzing the changes in the inner composition of soil organics such as ligninocellulose or lignin [296,516].

Overall, TMAH thermochemolysis combined with Py-GC/MS or GC/MS has been used to analyze various organic compounds such as humic acids, fatty acids, lignin, N-containing compounds, and aliphatic and aromatic compounds in soil samples GC/MS.

#### ***1.4.2.5 Polymers***

To expand the applications of Py-GC/MS and THM, induced by the most widely applied thermochemolysis reagent, TMAH, we will cover the wide usage of this method for the structural characterization of various polymer samples [10,11,14–16]. During the pyrolysis and THM method, specific chemical bonds including ester, ether, and carbonate linkages of different polymers can be decomposed forming smaller methylated fragments which are amenable to GC/MS analysis. However, the products of polymers without ether, ester, and carboxylic bonds (polar compounds) are unaffected by TMAH thermochemolysis, such as polyethylene (PE), polypropylene (PP), polystyrene (PS), and polyvinyl chloride (PVC). However, TMAH thermochemolysis shows a good performance on the analysis of polyethylene terephthalate (PET), polycarbonate (PC), poly(methyl methacrylate) (PMMA), poly(alkyl methacrylate), polyamide 6 (PA6), and nylon. For those compounds the thermochemolytic transmethylation is the main mechanism of the TMAH reaction [16,298]. Though TMAH thermochemolysis did not show good performance on the analysis of polyethene, it can be used to predict the lifetime of artificial aging problems. By aging the unstablized polyethylene in water at elevated temperature and under a high pressure of oxygen, the TMAH thermochemolysis method can be applied to assess the degree of oxidation. In this study,  $\alpha,\omega$ -diacids are the valuable indicators to determine the degree of oxidation of PE aging, which is caused by the attraction of hydroxyl to the carbonyl group and cleavage of the C-C backbone to yield carboxylic acids [17].

Poly (butylene succinate-*co*-butylene adipate) (PBSA) is one of the popular commercial packaging and container materials that can be biodegraded, because its physical properties are similar to those of commodity plastics with a good biodegradability. TMAH thermochemolysis was applied to characterize its structure and the degradation byproducts of it. Baidurah [18,19] evaluated the biodegradability of PBSA based on its copolymer composition using THM-GC method. The butylene succinate (BS) and the butylene adipate (BA) units are the original components of PBSA. The copolymer composition of butylene adipate (BA) units decreases

with soil burial degradation time. Butanediol dimethyl ether (BD), butanediol monomethyl ether (BM), dimethyl succinate (SD), and dimethyl adipate (AD) were the characteristic peaks of PBSA degradation in the presence of TMAH, and they were used to calculate the content of BS and BA units in PBSA. Later, they clarified the cause of the changes of BS and BA units in copolymer composition, and studied the biodegradation behavior of PBSA with lowered crystallinity using the TMAH-GC method. Results showed that the butylene adipate (BA)-rich moieties in the copolymer chains could show relatively lower crystallinity than the butylene succinate (BS)-rich moieties and that they were preferentially biodegraded during soil burial tests, leading to the decrease in the BA content as the biodegradation proceeded.

Poly (3-hydroxybutyrate-*co*-3-hydroxyhexanoate) [P(3HB-*co*-3HHx)] is one of the biodegradable *co*-polyesters, which can be produced by several types of bacteria such as *Cupriavidus necator* and *Aeromonas caviae* and serve as their energy storage compounds. In order to control the biodegradability of the [P(3HB-*co*-3HHx)], it is of importance to analyze the structure of [P(3HB-*co*-3HHx)]. Baidurah [20,21] studied the composition of [P(3HB-*co*-3HHx)] accumulated in whole bacterial cells using TMAH THM-GC method. Characteristic compounds of 3HB and 3HHx units were determined. Methyl 3-butenate, methyl *cis*-2-butenate, methyl *trans*-2-butenate, and methyl 3-methoxybutanoate originated from 3HB. Methyl *cis*-2-hexenoate, methyl *trans*-3-hexenoate, methyl *cis*-3-hexenoate, methyl *trans*-2-hexenoate, and methyl 3-methoxyhexanoate are products of 3HHx. They also studied the soil burial biodegradation of [P(3HB-*co*-3HHx)]. The chemical composition of 3HB units increased while 3HHx units decreased with the soil burial time. In addition, THM-GC was also applied to direct analysis of poly(3-hydroxybutyrate-*co*-3-hydroxyvalerate) [P(3HB-*co*-3HV)] in *Cupriavidus necator* cells, without any appreciable pretreatment of the bacterial matrix [12]. Through analyzing the yield of the characteristic peaks 3HB and 3HV, results from THM-GC in the presence of TMAH were demonstrated in good agreement with those obtained from conventional technique, which is in alignment with the result obtained from study of polyhydroxybutyrate (PHB) film with TMAH-GC without any cumbersome sample pretreatment [13].

Tetramethylammonium acetate (TMAAc) was also used to analyze styrene/butyl acrylate/methacrylic acid terpolymer by a two-step reactive Py-GC process [10]. TMAAc was applied to control the undesirable transesterification. A solid ammonium Y zeolite was used as a thermochemolysis reagent for identification of polyethers and polyesters [11]. TMAH is the main thermochemolysis reagent used in the characterizations of various polymers. The main

structure of polymers can be seen in Figure 1-11. Aldehyde, carboxyl, ether, and ester functional groups are the main structures that react with TMAH and on which the methylation occurs.

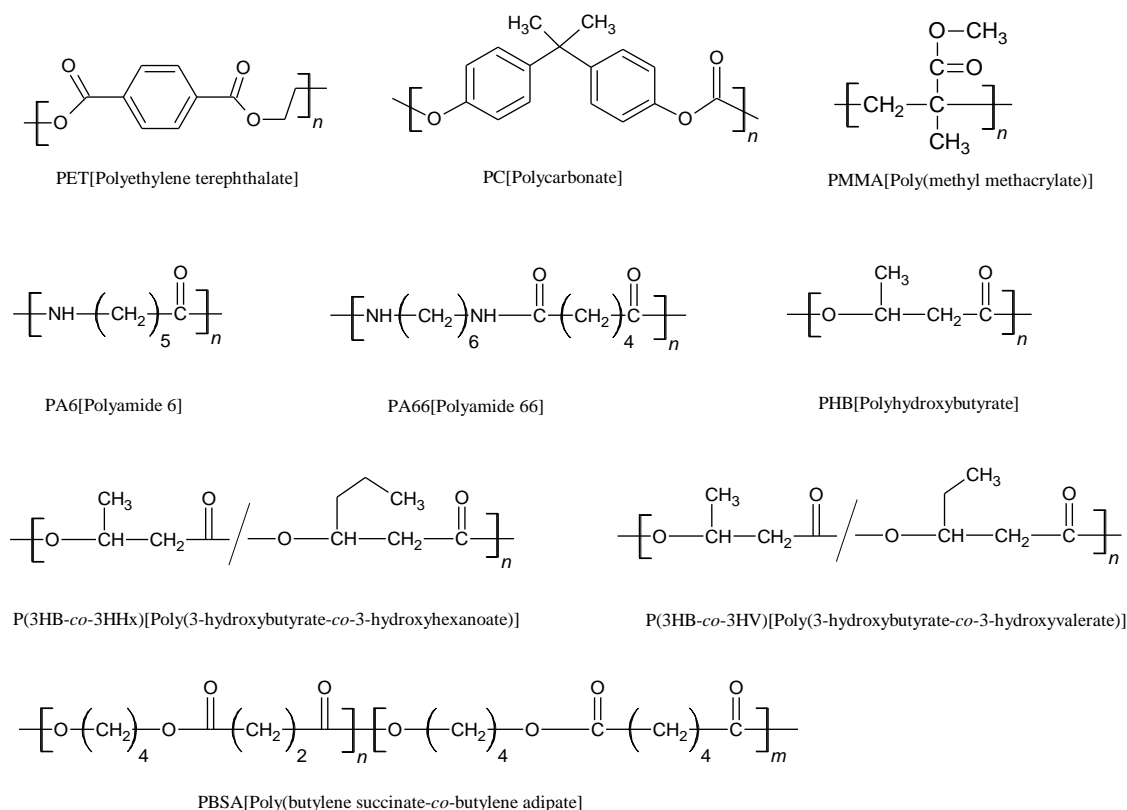


Figure 1-11 The structures of polymers that react with TMAH during thermochemolysis, adapted from [10–21].

#### 1.4.2.6 Thermochemolysis for space exploration

TMAH is used in space experimentation devoted to *in situ* characterization of the chemical composition of martian soils with automatized analytical laboratories. The SAM (Sample Analysis at Mars) experiment onboard the Curiosity rover of the Mars Science Laboratory mission, and MOMA (Mars Organic Molecule Analyzer), onboard the Rosalind Franklin rover of the Exomars mission, are able to implement TMAH thermochemolysis through an experimental set-up developed to meet the technical requirements for use on Mars. TMAH thermochemolysis will also be implemented in the future DraMS instrument onboard the Dragonfly drone that will explore the surface of Titan starting from 2034. However, only rare studies have been focused on the application of thermochemolysis in space. David [528] tested a pilot laboratory model for validation of the on-line pretreatment for analyses of organics by GC/MS, including the derivatization solvents N-Methyl-N-(tert-Butyldimethylsilyl)-trifluoroacetamide (MTBSTFA) as a silylating reagent, and N, N-Dimethylformamide Dimethylacetal (DMF-DMA) and TMAH as methylating agents.

#### 1.4.2.6.1 Thermochemolysis in the Sample Analysis at Mars (SAM) experiment

SAM is a complete *in situ* chemistry laboratory which is part of the Mars Science Laboratory mission and operates onboard the Curiosity rover. SAM includes a Gas Chromatograph (GC) and a Quadrupole Mass Spectrometer (QMS) which are coupled together to detect the organic molecules potentially present in the solid samples collected by the rover [1]. With this aim, a sample preparation and gas processing system is used to vaporize the molecules, and it includes three different techniques adapted to different organic molecules of interest: (i) a pyrolysis system heating the sample up to ~850 °C, (ii) derivatization using silylation process with MTBSTFA/DMF, (iii) TMAH (25% in methanol) thermochemolysis.

Derivatization and thermochemolysis have been developed and adapted for *in-situ* space applications by several authors [529–531]. For SAM, 500 µL of each derivatization reagent (MTBSTFA/DMF and TMAH) is placed in the bottom of nine (7 for MTBSTFA/DMF and 2 for TMAH) of the 74 metal ovens. The bottom (outer volume) of each cup which contains the derivatization reagent is closed with an aluminum foil which is punctured when the sample is delivered into the oven [2]. The inner volume of the cup contains a standard compound (nonanoic acid for TMAH and 3-fluoro-DL-valine for MTBSTFA). This internal standard is reactive with the reagent and it is used as a control compound to check the reaction worked well (Figure 1-12).

Up today, only pyrolysis and wet chemistry based on MTBSTFA/DMF have been used to extract and analyze organic molecules present in the martian samples collected. The instrument allowed to detect chlorinated (chlorobenzene, dichlorobenzene, etc.) and sulfur-bearing compounds [58,64,532] (thiophene and thiophene derivatives) proving for the time that organic matter is present at the Mars surface despite the harsh environmental conditions. Chlorinated compounds are most certainly the result of a reaction of martian perchlorate with endogenous martian organic compounds [222]. Because sulfur-bearing compounds have been detected at high temperature, two hypotheses have been proposed to explain their origin: i) they are refractory compounds endogenous to the martian sample, and ii) they are compounds released after reaction with sulfur-bearing compounds.

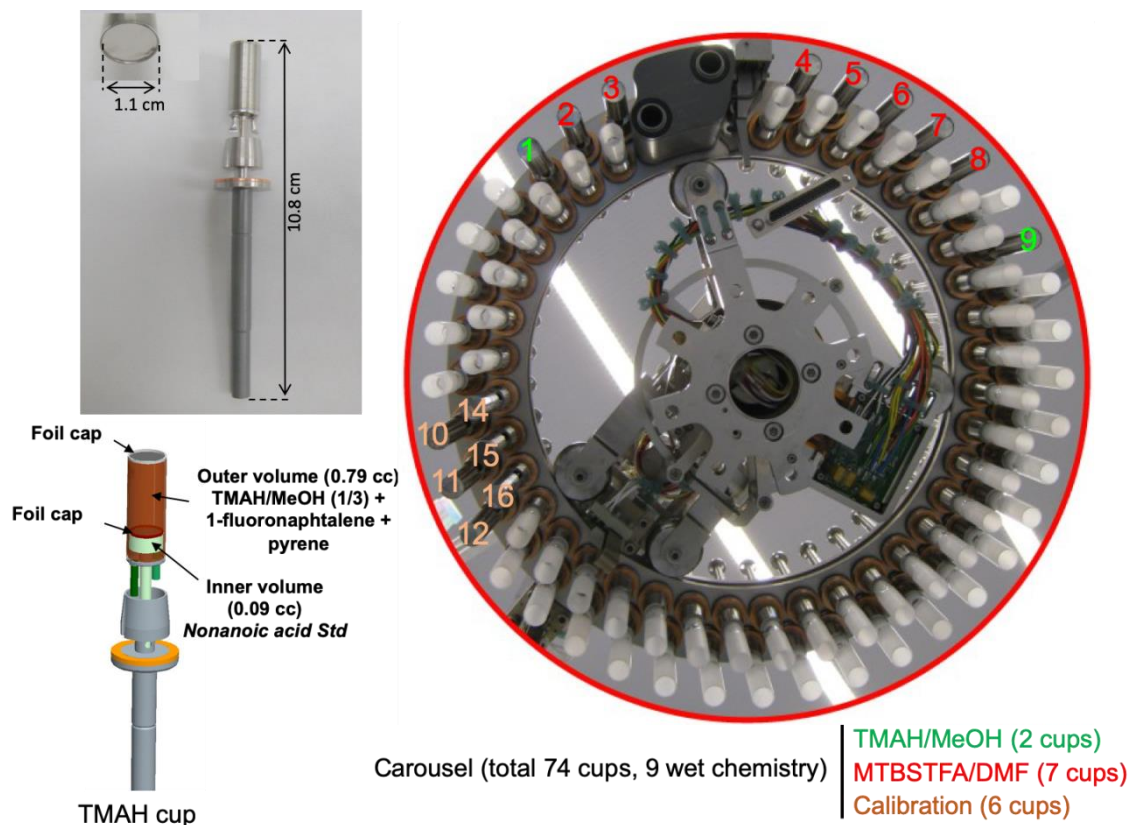


Figure 1-12 Sample Monitoring System (SMS) and close up of the SAM oven. Adapted from [22].

The strengths of TMAH thermochemolysis on SAM include desorption of organic compounds from the soil, a decrease in the polarity of the released products (through the methylation reaction) and a limitation of secondary reactions, resulting in improved chromatographic performance. Moreover, it is then easier to determine the analyte's parent molecular structure. Several authors showed that under SAM conditions TMAH thermochemolysis enabled the analysis of carboxylic acids (fatty acids), amino acids, and nucleobases [23,340,533] from standard samples but also from natural and analog samples [22]. Indeed, authors showed that under SAM-like pyrolysis conditions [22] TMAH thermochemolysis allows the extraction and analysis of fatty acid methyl esters (FAMES) from martian analog samples.

Because one (or more) of the SAM cups containing MTBSTFA/DMF leaks, it is possible that TMAH may be put in contact with MTBSTFA/DMF when it will be used for the first time. Williams [22] studied the recovery of fatty acids from mineralogical Mars analogs by TMAH-Py-GC/MS. The experimental parameters were analyzed, including the sample exposure time to TMAH, possible TMAH reactions with MTBSTFA, and loss of the TMAH solvent methanol prior to sample pyrolysis. Results showed that the MTBSTFA vapor could

react with TMAH in some ways that the evaporation of methanol will not have a significant effect on the TMAH thermochemolysis, and that TMAH shows a good performance on the methylation of FAMES. However, iron sulfide presents a challenge for thermochemolysis. Further studies need to be conducted in the future such as the recovery of TMAH thermochemolysis on other organics, such as carboxylic acids and complex organics such as DNA or RNA.

#### 1.4.2.6.2 Thermochemolysis in the Mars Organic Molecule Analyzer (MOMA)

The Mars Organic Molecule Analyzer (MOMA) experiment aboard the future ExoMars 2020 mission will continue the effort to search for organic compounds at the martian surface [3,534]. Compared to previous missions, samples will be collected as deep as 2 meters below the martian surface where organic materials are expected to be preserved from the effects of radiation and oxidation occurring at the surface. This will significantly improve the capacity for the instruments to detect traces of organic molecules indigenous to Mars. In order to analyze a wide range of potential organic compounds (volatile and non-volatile compounds) present in the martian soil, the MOMA instrument utilizes both UV laser desorption / ionization (LDI) and pyrolysis GC ion trap mass spectrometry (Py-GC-ITMS).

In order to analyze refractory organic compounds, and characterize the enantiomeric ratio for chiral species, the sample can be submitted to different sample preparation processes including derivatization. With this aim, MTBSTFA [529], DMF-DMA [222], TMAH [533] were selected as the derivatization agents in MOMA. To perform derivatization and thermochemolysis on MOMA, capsules have been designed to store 15  $\mu\text{L}$  of each corrosive reagent dedicated to the derivatization and thermochemolysis processes. Moreover, each liquid is released at a temperature corresponding to the melting temperature of different eutectics for each wet chemistry reaction. The temperature of each eutectic was chosen to optimize the chemical reaction during the sample treatment: DMF-DMA is released at 145  $^{\circ}\text{C}$ , MTBSTFA at 200  $^{\circ}\text{C}$ , and TMAH at 309  $^{\circ}\text{C}$ . Six capsules have been filled with MTBSTFA, six with DMF-DMA, and six with TMAH. Thermochemolysis and derivatization will be performed in an oven which is a part of the tapping station [3] (Figure 1-13). TMAH thermochemolysis will occur in three steps:

- i) Oven is heated with a ramp of 135  $^{\circ}\text{C min}^{-1}$  up to 309  $^{\circ}\text{C}$
- ii) At 309  $^{\circ}\text{C}$  derivatization capsule releases TMAH
- iii) Oven is heated up to 600  $^{\circ}\text{C}$

- iv) Thermochemolysis occurs during 30 s
- v) Oven valve is opened and volatile compounds are trapped at 0 °C on the Tenax® trap
- vi) Trap is heated and volatile compounds are injected into the gas chromatographic column



Figure 1-13 Tapping station with its oven (left) and derivatization capsule (right).

The chromatographic column dedicated to the analysis of the apolar and semi-polar compounds from the thermochemolysis reaction is an MXT5 metallic column (30m $\times$ 0.25mm $\times$ 0.25 $\mu$ m), its stationary phase is filled with diphenyl dimethyl polysiloxane, with a low-polarity. This is a column suitable for a broad range of applications, such as the analysis of hydrocarbons, polychlorinated biphenyl (PCB) congeners, drugs, solvent impurities, pesticides, essential oils and semi-volatiles. These advantages make it possible to reach the target of SAM and MOMA, characterizing organic compounds at a wide range of mass weight [3].

In order to prepare future thermochemolysis experiments on Mars, authors studied the thermal degradation byproducts of Tenax® in the presence of the derivatization reagent MTBSTFA/DMF and calcium perchlorate under SAM-like experimental conditions [60]. TMAH thermochemolysis experiments were also performed using chemical standards of seven kinds of nucleobases, important components of DNA and RNA, based on experimental conditions of the MOMA instrument [64]. In this study, properties of the TMAH thermochemolysis method were characterized and optimized for the detection of nucleobases under MOMA and SAM-like experimental conditions, as shown in Figure 1-14 (adenine, thymine, uracil, cytosine, guanine, xanthine, hypoxanthine, and fatty acids). Results showed that 600 °C is the optimal thermochemolysis temperature for all seven nucleobases. The methylated compounds and the methylation mechanisms of these seven nucleobases were

analyzed and there was no overlap among these seven nucleobases in the chromatographs. In addition, the limits of detection of these seven nucleobases were investigated and quantified, showing that adenine is the most probable nucleobase to be detected on Mars if its abundance is higher than the detection limit of the device.

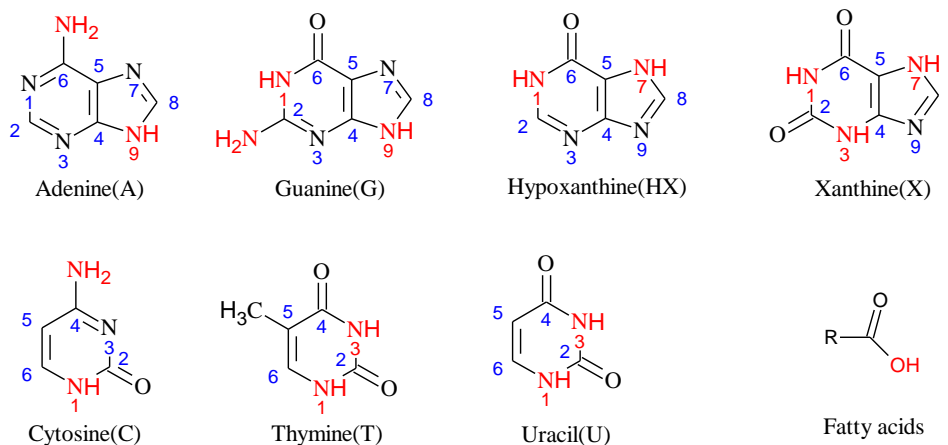


Figure 1-14 The structure of nucleobases and fatty acids, adapted from [22,23].

#### 1.4.2.7 Others

In addition to the application of TMAH for the analysis of soil, coal, lacquer, lignin and plants, polymers, and in space experimentation, TMAH has been used in other fields. It can be used as a strong base catalyst for increasing the transesterification of cotton seed oil and used frying oil [407] for biodiesel production. It can be used to analyze the biotransformation of organic matter during composting of solid waste from traditional tanneries, which involves the discrimination between four main families of compounds, including aromatic compounds, lipids, polysaccharides and nitrogen-containing substances, as well as the degradation of these compounds during the composting [401]. TMAH thermochemolysis has been used to characterize a rare tiny residue in a historic 18th century pharmaceutical vessel labelled MUMIA. The residue was microscopically subsampled and analyzed by Curie point Py-GC/MS (CP-Py-GC-MS) and GC/MS. Results demonstrated that the historic 18th century MUMIA vessel contained authentic mummy material [535].

Recently, TMAH has been used by the medical community. For example, TMAH was used to liberate and purify nanoparticles from tissues and showed a good performance compared with other alkaline compounds such as KOH and NaOH [536]. In this process, TMAH was used to dilute the blood sample and sonicated at 135W for 1 h to liberate the nanoparticles and avoid nanoparticle aggregation. Researchers also studied the component of triglycerides and cholesterol in serum samples [537], preserved bone tissue [330], and the



mycocerosic acid components of the phthiocerol dimycocerosate (PDIM) family of lipids [262] by using TMAH-GC/MS method. Additionally, TMAH methylation was used for the classification of bacteria based on an analysis of fatty acid methyl ester profiles [538]. TMAH-GC/MS was used to differentiate *Mycobacterium tuberculosis complex* (MTB) from non-tuberculous mycobacteria (NTM), tuberculostearic acid (TBSA) was used to check the sensitivity of the MS detector [539]. Results showed that the TMAH-GC/MS method provided a fast and reliable method for the differentiation of MTB and NTM bacteria after culture with an accuracy of greater than 95%; it was also used to analyze the degradation products of phthiocerol dimycocerosate waxes found in *Mycobacterium tuberculosis* [540].

### 1.4.3 Quantitative analysis

The TMAH-thermochemolysis method has been mainly used to qualify the organic compounds of different samples. Only a few studies have focused on the quantitation of organics. There are mainly two types of quantitative analytical methods: the external standard quantitation and internal standard quantitation. External standard quantitation is one of the most common approaches for calibration. The standard or known material is separated or external to the unknown material. The advantages of external standard calibration are that it is simple to perform this type of calibration and it can be applied to a wide variety of methods. However, it is greatly affected by the stability of the chromatographic detector system and the presence of chromatographic interferences in a sample or sample extract [541]. Table 1-5 shows the studies about external standard quantitative analysis of different compounds over the past 10 years. Py-GC/MS is the main instrument used for quantitative analysis of samples, including soil components, lignin analysis, and humic acid analysis. The pyrolysis experiment is mainly operated between 350 and 600 °C. However, the external standard quantitative method is not as popular as the internal standard quantitative method.

Table 1-5 Quantification using Py-GC/MS with the external calibration curves.

Sample	Chromatographic column	GC temperature program	T <sub>Pyrolysis</sub>	Year	Publications
Paddy soil from Wujiang Municipality, Suzhou City, Jiangsu Province, China Humic samples	Restek Rtx-5 MS fused silica capillary column (30 m × 0.25 mm × i.d., 0.25 μm film thickness)	1 min at 80 °C, from 80 to 180 °C at 4 °C min <sup>-1</sup> , 180 to 320 °C at 10 °C min <sup>-1</sup> , hold 10 min.	-	2010	[319]
	Fused-silica capillary column (Restek Rtx©-5MS, 30 m length × 0.25 mm I.D. × 0.25 μm film thickness)	From 100 °C to 300 °C at 4 °C min <sup>-1</sup> and hold 20 min.	600 °C	2012	[320]
Lignin standards, lipid standards and alkane standards	BPX-5 column (60 m x 0.25 mm, film thickness 0.25 μm)	5 min at 40 °C, 5 °C min <sup>-1</sup> to 270 °C and 30 °C min <sup>-1</sup> 1 to a 300 °C (hold 10 min).	590 °C	2012	[293]
Heptadecane, tridecanoic acid, cinnamic acid, octadecanol, 16-hydroxy hexadecanoic acid, docosanoic acid, and beta-sitosterol.	RTX-5MS WCOT capillary column (Restek, 30 m × 0.25 mm i.d.; film thickness = 0.25 μm)	1 min at 60 °C raise at 7 °C min <sup>-1</sup> to 100 °C and then at 4 °C min <sup>-1</sup> to 320 °C (hold 5 min).	400 °C	2012 2013	[284,311]
Bisphenol A and bisphenol S	A DB5 fused silica capillary column (30 m × 0.25 mm i.d., 0.25 μm film thickness)	100 °C to 250 °C at 10 °C min <sup>-1</sup> , and then to 275 °C at 5 °C min <sup>-1</sup> then at 15 °C min <sup>-1</sup> to 320 °C (hold for 5 min).	400 °C, 0.5s	2013	[238]
Gallic acid	A metal capillary column (Frontier Lab., Ultra ALLOY-5+, 30 m × 0.25 mm ID) coated with poly(5%-diphenyl-95%-dimethyl) siloxane (0.25 μm film thickness)	50 °C to 300 °C at a rate of 5 or 10 °C min <sup>-1</sup> .	350 °C	2015	[239]
Polymer standards	DB5 (J&W); 30 m x 0.25 mm ID, film thickness 0.25 μm	50 °C (1 min) to 310 °C (10 min) at 3 °C min <sup>-1</sup>	590 °C	2017	[298]
Tridecanoic acid, octadecanol, 16-hydroxyhexadecanoic acid, docosanoic acid, β-sitosterol, and cinnamic	Rtx-5MS WCOT (30 m × 0.25 mm id, 0.25 μm)	60 °C (1 min) to 100 °C at 7 °C min <sup>-1</sup> and then at 4 °C min <sup>-1</sup> to 320 °C (hold 10 min)	400 °C, 30 min	2013 2014	[312,313]

Table 1-6 Quantification using internal standards.

No.	Internal standard	Solvent	Sample	Analysis method	T <sub>Pyrolysis</sub>	Year	Publications
1.	Nonadecanoic acid	A mixture of acetone and methanol (v/v = 3/2)	Fertilizer samples, humic acid	Py-GC/MS	550 °C, 0.4 or 1 min	2009 2011 2012 2016	[306–309]
	Nonadecanoic acid	Hexane	Sediment sample (lignin analysis)	Py-GC/MS	590 °C, 20 s	2014	[299]
	Nonadecanoic acid	Acetone	Humic acid and fulvic acid samples	Py-GC/MS	550 °C, 0.4 min	2018	[327]
	Nonadecanoic-d <sub>37</sub> acid	Ethyl acetate	Sterols and stanols	GC/MS	300 °C	2017 2018	[519,521]
2.	<i>n</i> -Eicosane	TMAH	Freshly fallen litter and litter from litter bags	Py-GC/MS	350 °C	2011	[260,449]
	<i>n</i> -Eicosane	25% (wt%) TMAH methanol	Phenolic compounds	GC/MS	250 ± 2 °C for 30 min	2012	[542]
	<i>n</i> -Eicosane(C <sub>20</sub> )	EtOAc	Suberan	Py-GC/MS	610 °C, 15 s	2013	[461]
	<i>n</i> -Eicosane	Hexane	Lipid extraction of soil	GC/MS	280 °C	2015	[525]
3.	5 $\alpha$ -Androstane	TMAH	Peat litter and litterbag	Py-GC/MS	450 °C	2010	[456]
	5 $\alpha$ -Androstane	Dichloromethane	Wheat straw	Py-GC/MS	600 °C	2012	[302]
	5 $\alpha$ -Androstane	TMAH (25%; w/w)	Living plant tissues and litters	Py-GC/MS	610 °C, 10 s	2013	[303]
	5 $\alpha$ -Androstane	TMAH (25%, w/w)	Eight peat cores, sphagnum acid	Py-GC/MS	610 °C, 10 s	2013	[318]
	5 $\alpha$ -Androstane	Cyclohexane	Soil samples	Py-GC/MS	600 °C, 5 s.	2019	[297]
4.	<i>n</i> -Nonadecane	Dichloromethane	Methylated lignin derivatives	Py, GC/MS	-	1996	[9]
	<i>n</i> -Nonadecane	-	Lignite	Py-GC/MS	400 °C	2017	[271,272]
5.	3,5-dimethoxyphenol	-	Softwood lignin	Py-GC/MS	210 °C(3 min), 610 °C(1 min), and hold 56 min	2011	[444]
6.	<i>n</i> -Decylbenzene	TMAH	Winery wastewaters	Py-GC/MS	Pretreatment 340 °C then flash to 720 °C	2012	[543]
7.	Heptylbenzoic acid	Methanol	Fatty acids	GC/MS	-	2012, 2010	[544,545]
	Heptylbenzoic acid	-	Components of the “free” bitumen	Py-GC/MS	300 °C (S1), 600 °C (S2), 390 °C (S3)	2013	[470]
8.	Heneicosanoic acid	Methanol or dichloromethane	Guaiacyl palmitate and 2-nonyl palmitate	Py-GC/MS	600 °C, 2 s	2013	[254]
	Heptadecanoic acid	TMAH in methanol	Outer surfaces of archaeological pottery	Py-GC/MS	480 °C	2017	[491]
9.	Polymethylstyrene	Dichloromethane	asphaltene powders	Py-GC/MS	650 °C	2015	[252]
10.	Linolenic acid methyl ester	Ethyl acetate	Lignin	Py-GC/MS	-	2017	[457]
11.	<i>n</i> -Methyl- nonadecanoate	Dichloromethane	Lignin, carbohydrates, and lipids	GC/MS	250 °C	2018	[258]
12.	Tridecanoic acid (C13)	5% methanolic solution of TMAH	saturated fatty acid (SFA)	Py-GC/MS	360 °C to 700 °C (3 min)	2019	[257]
13.	Naphthalene-D8	Dichloromethane	Nucleobases	Py-GC/MS	600 °C, flash pyrolysis	2019	[23]
14	-	-	Amino acids	Py-GC/MS	400, 500, 700, and 900 °C	2010, 2011	[286,400]

For the internal standard quantitative analysis, an internal standard calibration involves the comparison of the instrument responses from the target compounds in the sample to the responses of other standards added to the sample or sample extract before injection. It can be used to account for routine variation in the response of the chromatographic system as well as variations in the exact volume of sample or sample extract introduced into the chromatographic system; however, the internal standard should not be the compounds that could be found in the samples or its related degradation products. Compared to external standard quantitative analysis, the internal standard quantitative method demonstrates better capabilities. For example, Seddon [546] studied the quantification method of UV-B absorbing compounds in *Pinus sylvestris* L. pollen. The study found that the quantification method can be improved using normalization by sporopollenin-based components, including external standards (*para*-coumaric acid stock solution), and internal standards (Vanillic acid (4-hydroxy-3-methoxybenzoic acid) and nonadecanoic acid in methanol). The THM–GC/MS method was used in order to identify the best analytical procedure to enable robust determination of UV-B absorbing compounds for future applications. Results showed that the internal standard methodology, using vanillic acid ensures more precise quantitative determination of UV-B absorbing compounds in *P. sylvestris* pollen, because the vanillic acid has a similar structure with *para*-coumaric (both include the combination of a carboxylic group and a phenolic hydroxyl group which react with TMAH). The similarity in chemical structure and in the reactions ensures comparable reactivities and transfer efficiencies during the analysis. The internal standard quantitative analysis that have been used in TMAH-thermochemolysis experiments are listed in Table 1-6. Only 13 kinds of internal standards were used to quantify organic compounds, including nonadecanoic acid, *n*-eicosane, 5 $\alpha$ -androstane, *n*-nonadecane, 3,5-dimethoxyphenol, *n*-decylbenzene, heptylbenzoic acid, and heneicosanoic acid, polymethylstyrene, *n*-methyl nonadecanoate, tridecanoic acid (C<sub>13</sub>), and Naphthalene-D8. Among these, the 5 $\alpha$ -androstane, nonadecanoic acid and *n*-eicosane are the most popular internal standards. Dichloromethane, methanol, TMAH and hexane are the solvents of these internal standards. Py-GC/MS or GC/MS is widely used for the quantitative analysis of TMAH thermochemolysis products, and the pyrolysis temperatures varied from 300 °C up to 900 °C according to the sample type, which included humic acids, nucleobases, lipids, and fatty acids.

However, more qualitative or semi-quantitative methods [547], rather than quantitative analysis of samples, were reported since 2010; only about 14% of these studies did quantitative analysis. Therefore, more efforts need to be put forward to develop a robust quantitative analysis method in the future.

## 1.4.4 The reactional mechanisms involved in TMAH thermochemolysis

### 1.4.4.1 The mechanism of TMAH thermochemolysis

TMAH works as a methylation agent boosting the cleavage of macromolecules during the TMAH thermochemolysis process. The TMAH thermochemolysis mechanism of using a certain compound with an acidic functional group was proposed by Kossa et al. in 1979 [24]. Trimethylamine was formed by the nucleonic attack by OH or methoxide ion. The methyl functional group can replace the active hydrogen of target compounds, such as the replacement of labile hydrogen in nucleobases [23]. A hydrolysis step was added by Challinor [26] where the OH<sup>-</sup> from the TMAH could cause a cleavage of ester or ether bonds. The Kossa methylation theory has been widely accepted, as shown in Figure 1-15. For example, Templier [548] studied the pyrolysis of 16 kinds of dipeptides with TMAH by GC/MS, in order to evaluate the effect of the peptide bond on the pyrolysis products released from proteinaceous materials. Results show that the direct methylation of peptide is the main pathway due to the presence of TMAH, along with the formation of piperazine-2,5-diones (DKPs) previously observed from single amino acids. In addition, the C- or N-terminal position of the amino acids is of importance for the formation of different products, such as imidazolidinedione. However, rarely new theories about the mechanism of TMAH thermochemolysis have been developed. There are mainly two methods to do TMAH thermochemolysis, including off-line and on-line thermochemolysis, TMAH has to be mixed with samples in both processes, which means that the methylation process happens when a sample is mixed with TMAH. However, it should be studied if TMAH could methylate a functional group such as -NH<sub>2</sub> in the gas phase. If the methyl functional group from TMAH in the gas phase could methylate samples, we could try to do further research in utilizing the derivatization reagent in gaseous form. New derivatization reagents need to be developed, such as derivatization substances in the solid or gas phase, which could increase the ease of delivery.

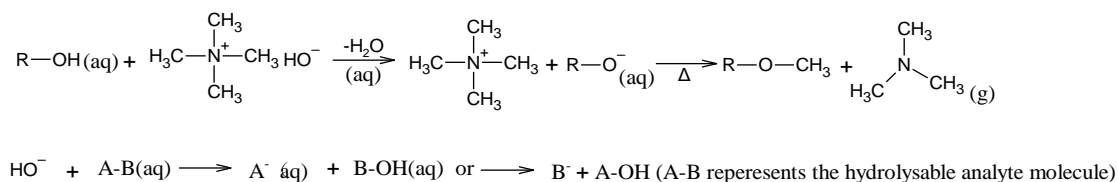


Figure 1-15 The mechanism of TMAH thermochemolysis, adapted from [24–26].

### 1.4.4.2 The mechanism of TMAH degradation

During the thermochemolysis process, TMAH undergoes two different pathways of degradation, the  $\text{SN}_2$  pathway and the ylide pathway. The  $\text{SN}_2$  pathway is the nucleophilic attack by  $\text{OH}^-$  on the  $\text{CH}_3$  group that produces trimethylamine and dimethyl ether [549]. For example, Macomber [550] studied the thermal decomposition pathways of TMAH using DSC, TG, and evolved gas analysis (EGA), finding that trimethylamine, methanol and dimethyl ether were the main byproducts. The methoxide formed in this way then reacts with  $[\text{Me}_4\text{N}]^+$  via an  $\text{SN}_2$  process to generate dimethyl ester. The ylide pathway is the decomposition of TMAH to give trimethylamine and dimethyl ether, caused by the initial removal of the proton from the quaternary ammonium salt followed by the decomposition of ylides [551]. The abstraction of the  $\alpha$ -proton to generate a nitrogen ylide is a very important degradation mechanism for methyl ammonium species. Deprotonation of the tetramethyl ammonium ion by hydroxide establishes a rapid equilibrium between tetramethylammonium ions and the nitrogen ylide species and water that scrambles the deuterium with the proton in the methyl groups.

However, some researchers think that the ylide pathway is more reasonable than the  $\text{SN}_2$  pathway [552]. The stability of tetramethylammonium ( $[\text{N}(\text{CH}_3)_4]^+$ ) under aqueous conditions in the presence of the  $\text{OH}^-$  ion was studied. Results showed that the ylide mechanism plays a crucial role in the decomposition of TMAH demonstrated by the TG-MS experiments which verified the H-D exchange. On the other side, the activation barrier for the ylide reaction is lower than for the  $\text{SN}_2$  pathway based on the calculations of the density functional theory. Also, the ylide pathway can give rise to unstable intermediates with side reactions including the Stevens rearrangement reaction [553], Sommelet-Hauser rearrangement, and Hofmann elimination [554]. Hofmann elimination is a vulnerable pathway for degradation of *n*-alkyl  $\text{TMA}^+$  cations [555]; the barrier is dependent on the carbon chain length because of steric interference and the number of hydrogens susceptible to Hofmann elimination [555]. On the other side, the Hofmann elimination is the preferred decomposition pathway for ammonium cations bearing  $\beta$ -hydrogens, and ylide formation scrambles protons from water into trimethylamine which is formed with a low activation barrier [27].

However, the degradation mechanism of TMAH has been studied at low temperatures (about 200 °C) and TMAH has been used extensively at high temperatures such as 600 °C. At this high temperature the degradation of TMAH could be different and the radical mechanisms that commonly occur at high pyrolysis temperatures should be studied. Moreover, TMAH biodegradation and the degradation under ultraviolet (UV) light have been investigated. For example, Wang [556] studied the oxidative degradation of a TMAH solution with UV light activated persulfate ( $\text{S}_2\text{O}_8^{2-}$ ). The effect of conditions such as the pH, dosages of persulfate, UV

intensities and system temperatures has been studied. Results showed that the TMAH decay increased with the increasing persulfate dosage; when the persulfate concentration was 50 mM, the highest degradation was observed. Higher reaction temperatures and strong UV irradiation increased the degradation of TMAH. Nitrate and ammonium are the degradation products of TMAH, which means that the demethylation mechanism is the main degradation pathway. The biodegradation of TMAH has a similar mechanism. The most proposed metabolic pathway for TMAH is that TMAH is first degraded into trimethylamine and methanol. In biological and chemical oxidative decompositions, it is proposed that TMAH will be decomposed into formaldehyde and ammonium. Finally, the TMAH will be decomposed to  $N_2$ ,  $H_2O$ , and  $CO_2$  by microorganism strains or thermal decomposition and oxidation catalysts [557], processes which could help to understand the TMAH degradation process during pyrolysis. However, the mechanism of TMAH degradation at high temperature as well as the byproducts of TMAH degradation still needs to be studied.

#### **1.4.5 Conclusions and future trends**

TMAH thermochemolysis has been widely used in various fields in recent years, especially for the analysis of organic compounds present in soils, lacquers, lignin and other related samples. TMAH thermochemolysis has become more and more popular for the study of artwork during the last ten years. The organic substances that could be analyzed by TMAH thermochemolysis include saturated and unsaturated long-chain fatty acids, humic acids, phenolic structures, alcohols, polymers containing aldehyde, carboxyl, ether, and ester functional groups, such as lignin, lignocellulose, and resins, and unnatural polymers such as polyethylene terephthalate (PET), polycarbonate (PC), poly(methyl methacrylate) (PMMA), poly(alkyl methacrylate), polyamide 6(PA6), and nylon, etc. These are the potential compounds that could be detected if related compounds exist on Mars.

This review gives an overview of the studies about TMAH thermochemolysis; however, most of the studies focus on the qualitative analysis of organic compounds, while the quantitative analysis of organic compounds and the use of internal or external standards require more study. For example, the quantitative analysis of lacquers in ancient artwork is useful for the repair and inheritance of these relics. On the other hand, the quantitative method needs to be developed, especially new internal standards. TMAH thermochemolysis has been used for the characterization of organics in soil samples. There is also ongoing development of the TMAH thermochemolysis technique for the analysis of organic compounds by space

experiments. Therefore, more studies need to be done under space conditions. It is useful to combine chemical and biological data on organic compounds in order to understand the properties of life on Earth or potentially on other planets; for example, TMAH studies can investigate if pretreatment of the TMAH chemical reagent will have an effect on microorganisms in a soil sample or the genetic information fundamental to life. An understanding of the relationship between organic matter, the parentage of that organic matter, and the environment across geological timescales can be constructed in order to improve our understanding of the origin of life. To achieve this goal, analytical methods and instrumentation must be developed which combine chemical and biological characterization methods. For example, most of the mass spectrometry used in previous studies targets compounds in a mass range below 500 u. An effective separation and detection device could be developed in the future which surpasses this range. Finally, the mechanism of TMAH thermochemolysis—as a methylation process—is well known; however, the degradation products of TMAH reagents at high temperatures and the effect of minerals on TMAH degradation or TMAH thermochemolysis should be studied, in order to optimize the experimental conditions of SAM and MOMA. In parallel, *in situ* technologies based on TMAH thermochemolysis and analysis are under development, and the application of TMAH thermochemolysis on the detection of organic compounds for space exploration is a new trend.

## **1.5 Conclusions**

### **1.5.1 Thesis scope, objectives and hypotheses**

The core objective of this thesis was to develop an understanding of how perchlorate influences the efficiency of the derivatization reagents, mainly MTBSTFA/DMF and TMAH. They are two main derivatization reagents that have been applied to search for life biosignatures on SAM and will be carried by MOMA. In addition, TMAH thermochemolysis, which will be applied in future missions, it's essential to have a better understanding of the application. It achieves this through a diverse set of studies involving analytical chemistry, biochemistry and pyrolysis method, etc. Effectively, three top level questions are addressed as below:

Q1. If perchlorates on Mars will influence the efficiency of the derivatization reagent on SAM onboard Curiosity? If there were some effects, what're the effects and how do they affect the reagents?



Hypothesis:

- (1). The presence of perchlorate or chlorine-bearing compounds could release oxygen to burn the organic compounds from the Martian sample or from the derivatization reagents.
- (2). There would be some chlorine-bearing compounds were formed during the reaction of perchlorate with the reagents.
- (3). The presence of perchlorate may or may not influence the mechanisms of the degradation of the reagents.

Q2. If it's possible to apply TMAH thermochemolysis on the analysis of DNA or RNA fragments? What's the optimal temperature of TMAH thermochemolysis, and what are the LOD and LOQ of our device?

Hypothesis:

- (1). It could be possible to characterize DNA or RNA fragments; however, it's difficult to determine the optimal temperature of different DNA or RNA fragments.
- (2). The nucleobases are the basic components of DNA or RNA, therefore, the LOD and LOQ of nucleobases are of importance.
- (3). Other important fragments of DNA or RNA such as the phosphate and ribose derivatives are still important.

Q3. If it's possible to analyze DNA or RNA or some other organic compounds from real life with TMAH thermochemolysis?

Hypothesis:

- (1). It could be possible to detect the DNA or RNA fragments from real life, however, maybe it will need a huge number of cells.
- (2). The complicity of real-life cells makes it difficult to predict the optimal temperature for the detection of DNA or RNA fragments or other organic compounds.

### **1.5.2 Thesis outline**

In this thesis, a range of different interlinked studies are documented. The methods and techniques used are detailed in each individual chapter. Figure 1-16 is the outline of this thesis.

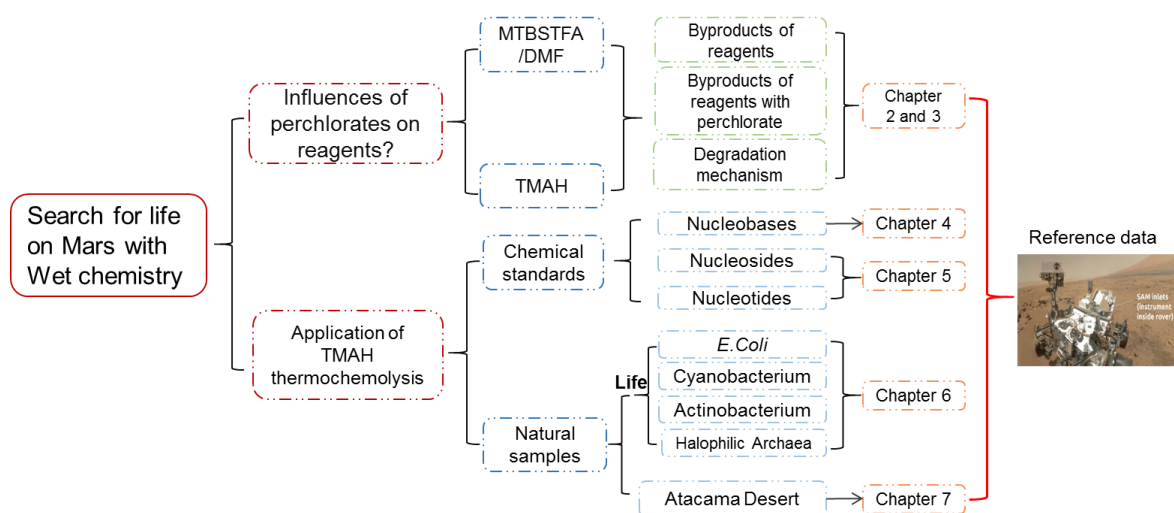


Figure 1-16 the Outline of this thesis.

The first chapter provides: a general introduction of the background of this study; a comprehensive literature review of previous work in related fields; the objectives and the outline of this thesis.

Chapter 2 and 3 provide detailed information about the influence of calcium perchlorate on the application of derivatisation reagents, mainly about MTBSTFA/DMF and TMAH. The byproducts of these two kinds of reagents, the influence of calcium perchlorate on the degradation of the reagents and their mechanisms of degradation were studied.

Chapter 4 is about the application of TMAH thermochemolysis on the detection of nucleobases. The optimal temperature of TMAH thermochemolysis and the LOD and LOQ were determined.

Chapter 5 then studied the application of TMAH thermochemolysis on a bit more complicated DNA and RNA fragments, such as nucleosides and nucleotides, and Poly A. The thermochemolysis temperature was optimized and all the products from nucleosides and nucleotides with TMAH thermochemolysis were studied.

Chapter 6 illustrated the application of TMAH thermochemolysis on real life. We studied the organic compounds from bacteria and Archaea that could be possibly survive in extremophile environment, mainly include *E.Coli* (for pre-experiments), cyanobacterium, actinobacterium, and halophilic Archaea.

Chapter 7 is about the application of TMAH thermochemolysis on the Martian analogues, Atacama Desert soil samples.

Chapter 8 summarizes and synthesis the overall findings and the perspectives for future workers.

# Chapter 2. Influence of pyrolysis and calcium perchlorate on the search for organic compounds using derivatization with MTBSTFA/DMF

## 2.1 Introduction

Searching for organic molecular biosignatures is one of the main goals of the Sample Analysis at Mars (SAM) experiment [2] onboard the NASA Curiosity rover. It is also a primary goal of the Mars Organic Molecule Analyzer (MOMA) instrument onboard the ESA/Roscosmos Rosalind Franklin rover, which will launch in 2022 and will land at Oxia Planum for the purpose of investigating Martian surface and subsurface sedimentary rocks [3]. For both missions, pyrolysis-gas chromatography and mass spectrometry (Py-GC-MS) combined with derivatization methods are employed to analyze the organic content of the collected samples. Three derivatization reagents have been selected for this purpose. MTBSTFA/DMF [532] and tetramethylammonium (TMAH) [558–560] are used for silylation and methylation derivatizations by both SAM and MOMA. Dimethylformamide-dimethylacetal (DMF-DMA) [222,561–564], a derivatization reagent specifically dedicated for chiral separation, is also used by MOMA.

MTBSTFA was chosen because it is one of the most popular silylation reagents. Silylation is a chemical reaction in which a labile hydrogen atom in OH, COOH, SH, NH, CONH, POH and SOH functional groups, or enolizable carbonyl, is replaced with a silyl group, most frequently with *tert*-butyldimethylsilane (TBDMS). An MTBSTFA/DMF mixture is often used, with the DMF acting as a solvent as well as a proton acceptor, significantly increasing the silylation reaction yield [234,529]. The MTBSTFA/DMF mixture has been shown to enable controlled reactions resulting in stable derivatives [565] and can maintain its derivatization efficiency after exposure to ionizing radiation [234], making it suitable for space applications. Figure 2-1 shows an example of derivatization of fatty and amino acids with MTBSTFA/DMF. This is a process related to the  $S_N2$  mechanism with the formation of a transition state derived from the nucleophilic attack of the analyte on the silicon atom [566]. Silylation of organic compounds results in better thermal stability, enhanced volatility, and reduced polarity of the silyl-derivatives with respect to the native analytes [368] and it improves the GC analysis [567].

However, the degradation of MTBSTFA/DMF may sometimes lead to misinterpretations in the characterization of organic compounds present in unknown samples.

Important ionized fragments of the MTBSTFA pyrolysis products include  $m/z$  75,  $m/z$  147,  $m/z$  134,  $m/z$  127,  $m/z$  41, and  $m/z$  15. The  $m/z$  75 fragment comes from the MTBSTFA pyrolysis product *tert*-butyldimethylsilanol (monosilylated H<sub>2</sub>O or MSW),  $m/z$  147 comes from 1,3-bis(1,1-dimethylethyl)-1,1,3,3-tetramethyldisiloxane (bisilylated H<sub>2</sub>O or BSW) [568],  $m/z$  124 from *tert*-butyldimethylfluorosilane (TBDMS-F), and  $m/z$  41 from 2-methylpropene (C<sub>4</sub>H<sub>8</sub>). A significant contribution at  $m/z$  15, either CH<sub>4</sub> or methylene ions, were found by Stern et al. (2015). The characteristic fragmentation patterns presented by MTBSTFA derivatives are mainly the fragments of the molecular ion [M]<sup>+</sup>, [M-57]<sup>+</sup> and [M-131]<sup>+</sup>, of which [M-57]<sup>+</sup> is generally dominant in the mass spectrum. [M-57]<sup>+</sup> results from cleavage of the *t*-butyl moiety (-C(CH<sub>3</sub>)<sub>3</sub>) while [M-131]<sup>+</sup> results from cleavage of the *t*-butyl-dimethyl silyl moiety. [M]<sup>+</sup>, [M-15]<sup>+</sup> and [M-89]<sup>+</sup> are the characteristic fragments of BSTFA-derivatives and [M]<sup>+</sup> is the main ion [231]. [M-15]<sup>+</sup> results from cleavage of the methyl group from the molecular ion while [M-89]<sup>+</sup> results from cleavage of the trimethylsilyl ether moiety.

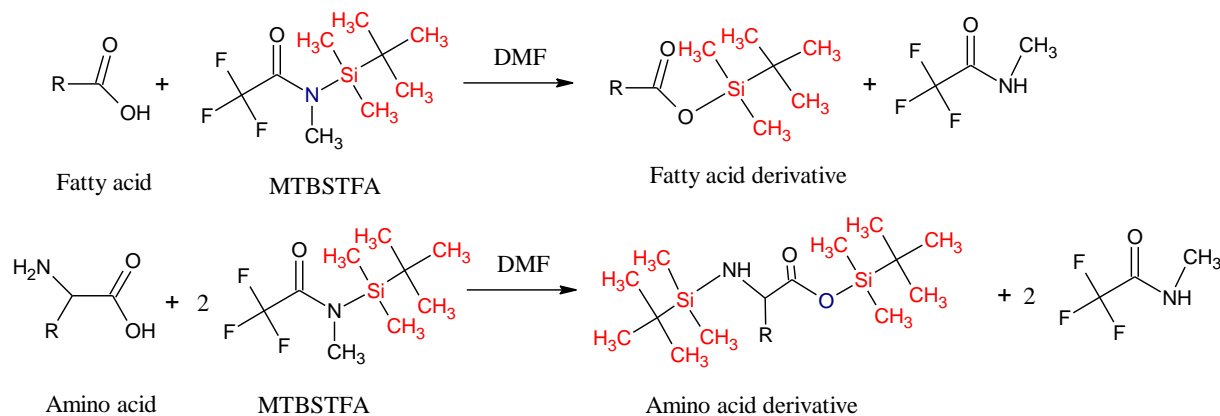


Figure 2-1: Example of fatty acids and amino acids derivatized by MTBSTFA.

The steric hindrance and molecular mass play a very important role in the choice of the best derivatization reagent. It is not always possible to use MTBSTFA, especially when the target compound presents sterically hindered sites or when the  $m/z$  of fragments resulting from the derivatized compounds is outside of the mass spectra range. The derivatization products of MTBSTFA/DMF are often detected in Py-GC-MS, but the lack of mass spectra of MTBSTFA-derivatized molecules in the NIST library is the main challenge for the identification of the chromatographic peaks [570]. MTBSTFA/DMF is usually used at low temperatures, varying from 50 to 150 °C [571]. However, the degradation products of MTBSTFA and DMF at different temperatures, especially at high temperatures, have not been systematically studied.

The Wet Chemistry Lab (WCL) onboard NASA's 2008 Phoenix Lander first detected the perchlorate ion ( $\text{ClO}_4^-$ ) in the Martian soil (0.4-0.6 wt.%), with calcium and magnesium perchlorate identified as its probable sources [54]. Later, oxychlorines were suggested to have been present at the Viking landing sites [55] and were also detected in Gale crater by SAM (~0.4 to 2 wt.% of  $\text{ClO}_4^-$ ) [56,63]. Some Cl-bearing compounds have also been detected by SAM, including hydrochloric acid, chloromethane, and dichloromethane [532]. Chlorobenzene and other chlorinated hydrocarbons detected on Mars may be the reaction products of oxychlorine species such as perchlorate and indigenous Martian organic carbon; e.g. benzene carboxylic acids may be the organic precursor of chlorobenzenes detected by SAM [57,223,572]. However, it is also possible that analytical components of the instrument, such as Tenax® adsorbent trapping [60,573] and derivatization reagents, contribute as sources of carbon- chloride-bearing compounds. For example, MTBSTFA/DMF has been considered as one of the possible precursors of the chlorine-bearing compounds, through the reaction of MTBSTFA/DMF with perchlorate [532].

To summarize, utilizing MTBSTFA/DMF with Py-GC-MS to analyze soils and rock samples on Mars raises several issues: i. the degradation of MTBSTFA/DMF can produce organic products that can interfere with the identification of indigenous organics present in the Martian sample; ii. the presence of calcium perchlorate could influence the degradation of MTBSTFA/DMF; iii. MTBSTFA/DMF could be the possible precursor of chlorine-bearing compounds in the presence of calcium perchlorate. For these reasons, it is of key importance to study the behavior of MTBSTFA/DMF under pyrolytic conditions, in the presence as well as in the absence of perchlorate.

In this study, we assessed the effects of pyrolysis temperature and heating mode on the degradation of MTBSTFA, DMF and an MTBSTFA/DMF (4:1) mixture. We also assessed the effect of calcium perchlorate on the degradation of MTBSTFA and DMF. All products of MTBSTFA and DMF were identified in order to form a database to support the interpretation of data obtained from the SAM and MOMA space instruments. Moreover, we propose a plausible mechanism of MTBSTFA and DMF degradation, which may shed additional light on the interpretation of SAM findings as well as future MOMA results. Finally, we note that this work is consistent with the conclusions of Freissinet et al. (2015), which proposes indigenous organics in Martian samples as the carbon source of detected chlorobenzene compounds.

## 2.2 Experimental

### 2.2.1 Chemical products

MTBSTFA (>97%, Sigma-Aldrich), DMF (anhydrous, 99.8%, Sigma-Aldrich), and a MTBSTFA/DMF mixture (v:v = 4:1) made from individual chemical compounds were used in this study. Calcium perchlorate tetrahydrate (99%, Aldrich) was used to make the calcium perchlorate solution (in ultra-pure water). Calcium perchlorate was considered to be a better candidate for the perchlorate species present in Martian samples analyzed by SAM than Fe-, Mg-, Na- and K-perchlorates, since the release temperature of oxygen from calcium perchlorate is consistent with rover data [57,62,64]. Naphthanlene-D8 (Sigma-Aldrich, isotopic purity, 99 atom % D) was used as an internal standard [23]. The concentration of calcium perchlorate solution (1.375 mol.L<sup>-1</sup>) was measured by Atomic Absorption Spectrometry (AAS) [574–577] (Varian Australia Pty Ltd ), using the air-acetylene flame, with a calcium cathode lamp set at the 422.7 nm resonance wavelength.

The abundance of  $ClO_4^-$  to MTBSTFA/DMF (wt.%) is given by the following equation:

$$wt. \% = \frac{2C_{Ca(ClO_4)_2} \cdot V_{Ca(ClO_4)_2} \cdot M_{ClO_4^-}}{V_{MTBSTFA/DMF} \cdot \rho_{MTBSTFA/DMF}} \%$$

Where  $C_{Ca(ClO_4)_2}$  is the concentration of the  $Ca(ClO_4)_2$  solution at 1.375 mol.L<sup>-1</sup>;  $M_{ClO_4^-}$  is the molar mass of  $ClO_4^-$ , 99.45 g/mol;  $V_{Ca(ClO_4)_2}$  is the volume of  $Ca(ClO_4)_2$  solution;  $V_{MTBSTFA/DMF}$  is the volume of the mixture of MTBSTFA/DMF solution, 3 $\mu$ l; and  $\rho_{MTBSTFA/DMF}$  is the density of the mixture of the MTBSTFA/DMF solution.

In the SAM experiment, each derivatization cup was filled with 500  $\mu$ l of the MTBSTFA/DMF (4:1) mixture. We note that the first measurements on Mars completed by SAM showed the presence of leaks from at least one cup [56]. Estimates led to the suggestion that that the maximum amount of MTBSTFA still present in the cup was ~100 nmol [56]. To be conservative, simulating a leak of MTBSTFA worse than that in the SAM case, 3  $\mu$ l of the MTBSTFA/DMF mixture was used in our experiments, representing about 10  $\mu$ mol MTBSTFA.

To test the influence of oxychlorines, different amounts of calcium perchlorate were introduced in the MTBSTFA/DMF mixture. Calcium perchlorate was used as the  $ClO_4^-$  carrier, and was dried under a flow of dinitrogen for 2 hours. It is possible that MTBSTFA could react

with water, forming mono- and bisilylated water compounds that could influence the background signals and compete with the derivatization process. We note that water abundance in the perchlorate has been measured by the Karl Fischer method with Aqua Processor Radiometer [60,578–582]. Detailed information could be seen in our previous work [560]. The hydration states of perchlorates could influence their thermal decomposition behavior [583]; therefore, the use of the same drying conditions could make it possible to test a sample containing calcium perchlorate with the same or with a very similar composition of hydration states. In addition, the products of calcium perchlorate under flash pyrolysis (600 °C) were analyzed to confirm the purity of its solution. As shown in Figure S2-1 in the supplementary material, only CO<sub>2</sub> at a low intensity was detected, which showed that there was no organic contamination in the solution of calcium perchlorate.

### 2.2.2 Pyrolysis experiments

An EGA/PY-3030D micro-oven pyrolyzer equipped with a MicroJet Cryo-trap (Frontier Lab) was used. It was installed on the split/splitless (SSL) injector of the gas chromatograph. Different volumes of Ca(ClO<sub>4</sub>)<sub>2</sub> solution were deposited in a capsule, followed by the drying process of Ca(ClO<sub>4</sub>)<sub>2</sub> solution under a stream of dinitrogen; then 3 µl of MTBSTFA/DMF (4:1, v/v) was injected into a capsule. That capsule, carried by an eco-stick (Frontier lab), was attached to the top of the pyrolyzer and the pyrolyzer head space was purged for 2 minutes before proceeding. Flash pyrolysis and SAM-like ramp pyrolysis, reaching maximum temperatures of 210, 300, 600, and 850 °C, were used for our study. For the flash pyrolysis, the sample was dropped inside the oven at a set temperature (with a 1 min hold). For the SAM-like ramp pyrolysis, the heart-cut EGA analysis method was used, using a capsule carried by an eco-stick (Frontier lab) which was attached and introduced inside the oven (initial temperature was 50 °C) and flushed by 1 mL·min<sup>-1</sup> of helium. The oven was programmed to reach the final temperature (hold 1 min) at the SAM heating rate of 35 °C·min<sup>-1</sup>. The liquid nitrogen MicroJet Cryo-trap was used to trap and pre-concentrate all products of pyrolysis at -180 °C at the chromatographic column inlet. When the pyrolysis process was finished, the liquid dinitrogen flow was stopped, and the temperature of the column inlet was quickly increased to 40 °C. All products then were released and sent to the GC/MS by helium flow (1.2 mL·min<sup>-1</sup>). In addition, to study the influence of calcium perchlorate on the pyrolysis of MTBSTFA/DMF, the step pyrolysis of MTBSTFA/DMF with and without calcium perchlorate

was performed on a Py-GC/MS using the SAM-like temperature ramp. The sample was injected into the pyrolyzer and heated from 50 °C to 100 °C, and then the temperature was increased up to 900 °C by steps of 100 °C.

Finally, for the analysis of the Murchison meteorite powder sample (Murchison USNM 5453), about 5 mg of meteorite was pyrolyzed in the flash mode at a temperature of 850 °C. The pyrolysis was done in the presence of 5 wt.% of calcium perchlorate.

### 2.2.3 Analysis of pyrolysis products

A gas chromatograph (Trace GC Ultra, Thermo Scientific) coupled to a quadrupole mass spectrometer (ISQ LT, Thermo Scientific) was used in this study. The GC instrument was equipped with a Supelco SLB-5MS Inferno column (30 m × 0.25 mm i.d. × 0.25 μm film thickness). More details have been described in a previous work [23]. The temperature programming of the column started at 40 °C and was held for 2 min, then ramped up to 300 °C at a heating rate of 3 °C·min<sup>-1</sup> and maintained for 1 min at this final temperature. Helium (Ultra-high purity grade >99.9999%, Air Liquide) was used as the carrier gas and its flow rate in the column was set to 1.2 mL·min<sup>-1</sup>. The split mode was used with a 24 mL·min<sup>-1</sup> split flow value. The temperature of the SSL injector was set to 280 °C. The ions were scanned between *m/z* 40 and *m/z* 500 (full scan mode), which revealed the total ion current (TICs) chromatograms. All the products were identified on the basis of their full scan mass spectra by comparison with the National Institute of Standards and Technology (NIST) library. The ionization energy of the electron impact source was set to 70 eV.

## 2.3 Results

### 2.3.1 MTBSTFA and DMF flash pyrolysis at different temperatures

#### 2.3.1.1 DMF flash pyrolysis at different temperatures

DMF was pyrolyzed at the temperature of 210, 300, 600, and 850 °C, respectively. Figure 2-2 shows the chromatograms that were obtained for each temperature and Table 2-1 lists the chemical compounds that were detected. These results show that the decomposition of DMF started between 300 and 600 °C (Figure 2-2). The abundance of DMF detected at 850 °C decreased drastically as it was thermally decomposed into several other products (see Appendix Figure S2-2). During the pyrolysis at 600 °C, more and new products were formed, such as acrylonitrile (containing a C≡N functional group) and benzene, as shown in Table 2-1.



Table 2-1: Products detected from DMF flash pyrolysis at 210, 300, 600, 850 °C

Compounds	Masses of fragments* and relative abundance: m/z (%)	Structure	T <sub>pyrolysis</sub> /°C			
			200	300	600	850
			Retention time/min			
Carbon dioxide	44	CO <sub>2</sub>	2.1	2.1	1.6	1.9
<i>N,N</i> -dimethylformamide (DMF)	73(100), 44(81), 42(56), 72(21), 74(17), 58(15)		6.9	4.6, 5.0	4.6-6.5	6.9
Trimethylamine	58(100), 59(55), 42(19)			2.26	2.16	
Dimethylamine	44(100), 42(23), 41(16), 45(12)				1.8	
Ethanolamine	41(100), 44(61), 40(34)				1.82	
<i>N,N,N',N'</i> -tetramethylmethanediamine	58(100), 42(12), 102(8)				2.8, 3.0	
Dimethylamino-acetonitrile	83(100), 84(64), 58(64), 42(59), 40(22), 43(15)				4.2	
Styrene	73(78), 44(89), 104(78), 40(54), 103(42), 78(42), 51(18)				8.7	8.6
1,3,5-triazine, hexahydro-1,3,5-trimethyl-	44(100), 86(42), 128(30), 43(18), 57(15)				12.2	12.2
<i>N,N</i> -dimethyldodecanamide	87(100), 100(21), 45(20), 72(19), 55(17)				61.1, 64.8	
Hydracrylonitrile	44(100), 41(94), 53(61), 52(47), 40(46), 51(20), 42(15)					2.1
Benzene	78(100), 44(40), 77(24), 44(19), 52(14)					3.0
Naphthalene	128(100)					22.8

Some of the byproducts of DMF detected at 850 °C were also observed at 600 °C, for example, *N,N,N',N'*-tetramethyl-methanediamine, dimethylamino-acetonitrile; olefins such as 1-decene, 1-undecene, and 1-dodecene. Hexahydro-1, 3, 5-trimethyl-1, 3, 5-triazine (TMTAC) were the main products of DMF pyrolyzed at 600 °C. However, no TMTAC was detected at 850 °C, which means TMTAC could be decomposed at high pyrolysis temperature, leading to secondary chemical reactions. Compared with the products obtained from DMF pyrolyzed at 600 °C, more aromatic were formed at 850 °C, probably through the aromatization of alkyl groups at this higher temperature [270]. Therefore, in order to prevent the decomposition of DMF and the formation of products, we conclude that DMF should be used at temperatures lower than 600 °C.

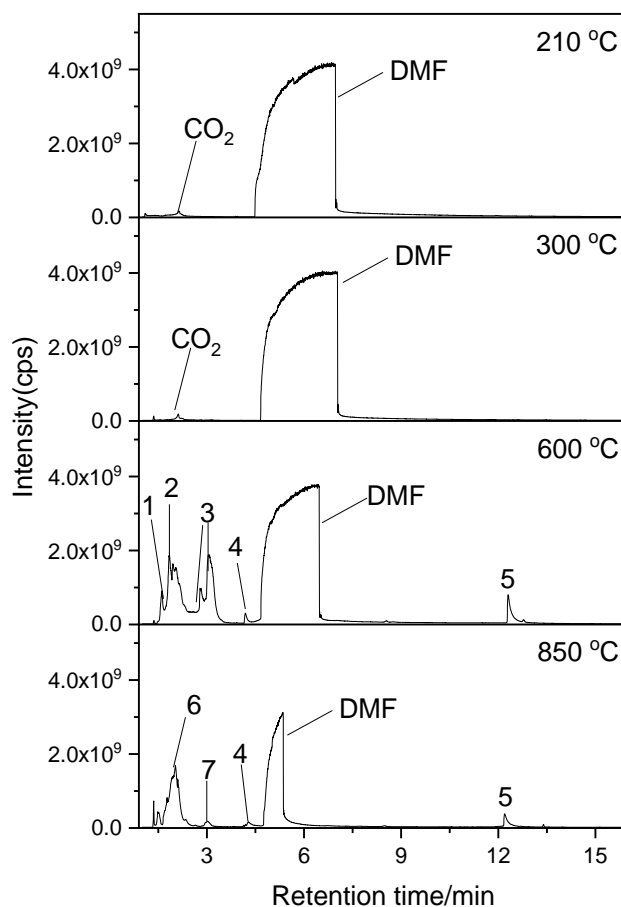


Figure 2-2: Chromatograms (TIC) of the compounds detected after DMF pyrolysis at different temperatures. Peak attributions: 1: Dimehtylamine; 2: Ethanolamine; 3: N, N, N', N'-tetramethylmethanediamine; 4: Dimethylamino-acetonitrile; 5: Hexahydro-1,3,5-trimethyl-1,3,5-triazine; 6: Hydracrylonitrile; 7: Benzene.

### 2.3.1.2 MTBSTFA flash pyrolysis at different temperatures

The flash pyrolysis of MTBSTFA at temperatures of 210, 300, 600 and 850 °C was also studied. The resulting chromatograms are shown in Figure 2-3, and in Table 2-2, provides a list of the chemical species detected as well as additional information about them. The number of compounds detected from the pyrolysis of MTBSTFA was significantly higher at 850 °C than 210 or 600 °C.

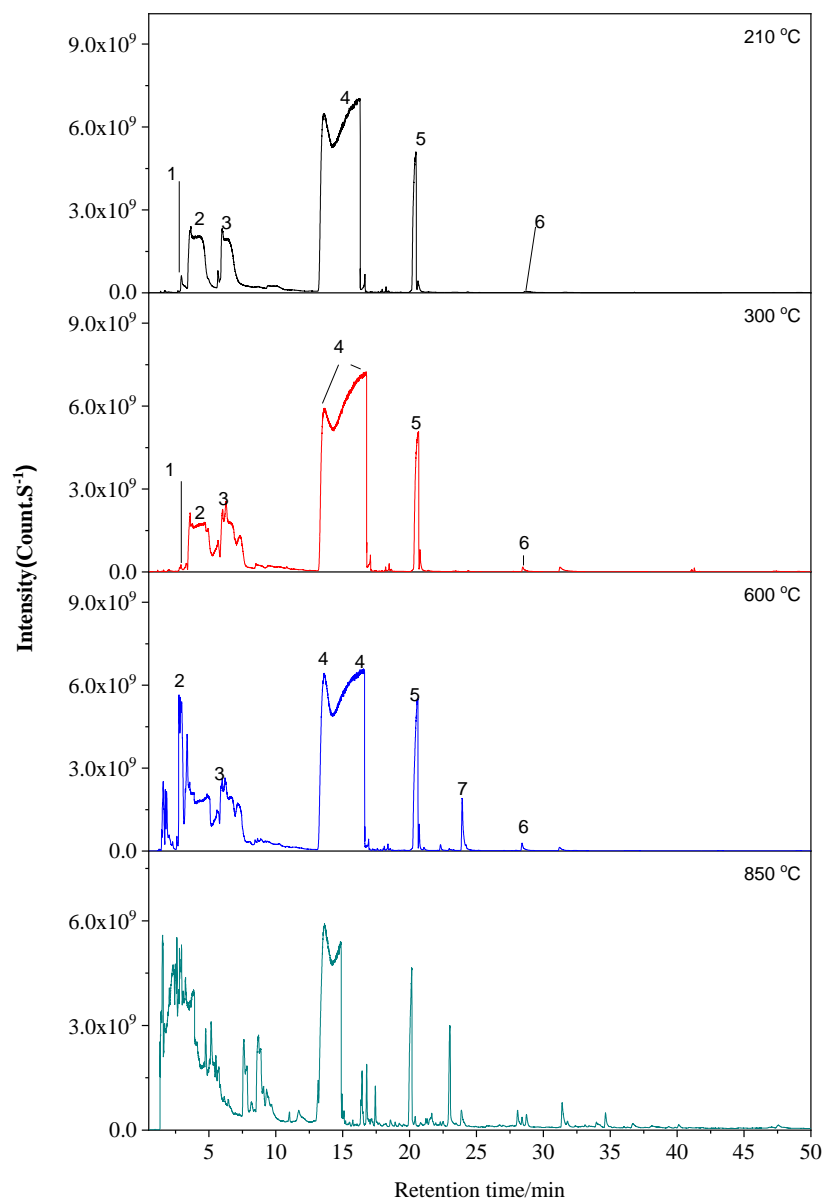


Figure 2-3 Chromatogram (TIC) of MTBSTFA flash pyrolysis at different temperatures. GC conditions can be seen in section 2.3 analysis of pyrolysis products. Peak attributions: 1: tert-butyldimethylsilylfluorosilane; 2: N-methyltrifluoroacetamide(TFMA); 3: tert-butyldimethylsilanol(MSW); 4: N-Methyl-N-trimethylsilyl-trifluoroacetamide(MSTFA); 5: BSW; 6: Tris(trimethylsilyl)borate; 7: 3-methyl-3H-cyclonona[def]biphenylene.

As also noted by Malespin et al. [568,584], when heated to 210 °C, the pyrolysis products of MTBSTFA were found to be dominated by *N*-methyl-*N*-(trimethylsilyl)trifluoroacetamide (MSTFA), *N*-methyltrifluoroacetamide (TFMA), *tert*-butyldimethylsilanol (MSW), and 1,3-ditert-butyl-1,1,3,3,-termethyldisiloxane (BSW). MSTFA is one of the products of MTBSTFA pyrolysis formed by the breakage of the Si-C bond connecting the *t*-butyldimethyl functional group. TFMA and *tert*-butyldimethyl radicals were formed by the cracking of the N-Si bond of MTBSTFA, while *tert*-butyldimethyl radicals were stabilized by other radicals, such as OH radicals, to form the MSW. BSW is a typical byproduct of MTBSTFA when there is H<sub>2</sub>O in the system [56]. Tris(trimethylsilyl)borate was detected from MTBSTFA pyrolysis at different temperatures. The borate could possibly originate from the borate glass used to contain MTBSTFA (Buch et al., 2019). At 210 °C, other pyrolysis products of MTBSTFA primarily included Si- and F- containing compounds, which were easily distinguishable from the natural samples during the derivatization analysis of organics. When the temperature was increased to 300 °C, no additional products were observed compared to the products from MTBSTFA degradation at 210 °C, as shown in Figure 2-3. When the temperature was increased to 600 °C, the distribution of the main products from MTBSTFA was almost the same as that at 210/300 °C, though some new products were detected at very low intensities when MTBSTFA were pyrolyzed at 600 °C.

However, many extra products were detected during the pyrolysis of MTBSTFA at 850 °C. As shown in Figure 2-3, the response from the original MTBSTFA molecule is significantly decreased at 850 °C (compared to lower pyrolysis temperatures), showing almost severe decomposition. Aromatic compounds and polyaromatic compounds were mainly formed. For example, light aromatic compounds such as toluene, xylene, and ethylbenzene were identified at retention times of 4.83, 7.31, and 7.76 mins, respectively. Naphthalene and related compounds were also detected, including methyl-naphthalene, dimethyl-naphthalene and their isomers, biphenyl and diphenylmethane, which both contain two benzene rings. Polyaromatic compounds were detected with retention times after 40.00 min and contained three (9H-fluorene, phenanthrene, methylphenanthrene, phenyl-naphthalene and their isomers), four (pyrene, fluoranthene, 3,4-benzophenanthrene, triphenylene and their isomers) or five (benzo[k]fluoranthene and 9H-cyclopenta[a]pyrene) carbon rings.

F-containing aromatics and benzonitrile compounds were also formed during the pyrolysis of MTBSTFA at 850 °C. F-bearing aromatics include fluorobenzene, *p*-fluoro-styrene, 2,3-dimethylfluorobenzene, difluorobenzene, difluorobiphenyl, trifluoromethyl-benzene, and 2,3,4-trifluorobenzaldehyde and their isomers. Fluoro-naphthalene and

fluorbenzol[a]anthracene were also detected, indicating that the fluorine radicals of MTBSTFA could combine during the aromatization process forming fluorine-containing polyaromatics. Benzonitrile compounds included benzonitrile, naphthonitrile and their derivatives and isomers. Pyridine and its derivatized compounds were also observed in the chromatograms, such as 5, 6-dimethyl-1,10-phenathroline, dimethyl-bipyridine, 1-hydroxyphenazine and its isomers. The main pyrolysis products are listed in Table 2-2, and a tabulation of all products of MTBSTFA at 850 °C can be found in the supplementary material in Table S2-1.

Table 2-2: The main products of MTBSTFA flash pyrolysis at different temperatures

T <sub>pyrolysis</sub>	RT (min)	Masses of fragments* and relative abundance: m/z (%)	Compounds	Structures
<b>210 °C/300 °C</b>				
1.	1.39	44	CO <sub>2</sub>	
2.	2.67, 2.94	77(100), 56(74), 58(40), 57(22), 69(13), 78(12), 134(10)	Tert-Butyldimethylfluorosilane	
3.	3.65	58(100), 69(45), 127(19), 78(18)	N-methyltrifluoroacetamide	
4.	5.98	75(100), 76(33), 47(22), 45(22), 132(16), 73(11)	Tert-butyldimethylsilanol	
5.	13.57-16.27	134(100), 184(95), 77(89), 73(36), 135(17), 185(17), 110(13), 118(15)	N-methyl-N-(trimethylsilyl)trifluoroacetamide	
6.	19.30, 20.42, 21.37, 49.22	147(100), 189(47), 148(31), 73(30), 149(16), 117(10), 133(10)	1,3-ditert-butyl-1,1,3,3,-termethyldisiloxane	
7.	19.07, 19.48	147(100), 191(53), 133(15), 68(10)	Bis(trimethylsilyl) carbonate	
8.	20.59	133(100), 147(68), 148(10), 73(10)	Disiloxane, pentamethyl-	
9.	24.44	146(100), 188(50), 130(20)	Bis(tert-butyldimethylsilyl)amine	
10.	29.10	221(100), 73(43), 263(23), 222(23)	Tris(trimethylsilyl)borate	
11.	32.34	147(100), 233(35), 73(21)	Bis(tert-butyldimethylsilyl) carbonate	
<b>600 °C</b>				
1.	1.94	44(100), 81(96), 69(68), 51(23), 76(20), 100(15), 50(17)	difluorodimethylsilane	
2.	2.4	57(100), 41(92), 56(79), 40(45), 91(27), 55(21), 58(10)	4-methyl-1-hexene	
3.	2.62, 2.93, 3.43	56(100), 76(72), 155(71), 57(49), 77(43), 134(35), 41(24), 49(19), 119(14)	Tert-Butyldimethylsilyl fluoride	
4.	5.71	58(100), 77(98), 93(82), 56(58), 121(50), 57(40), 127(36), 155(35), 95(29), 171(22)	tert-Butyldimethylsilyl 2,2,2-trifluoroacetate	

Table 2-2 (Continued)

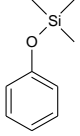
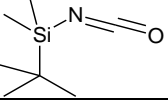
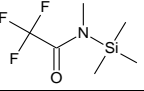
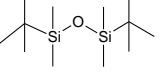
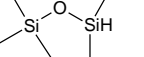
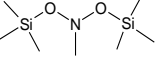
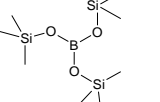
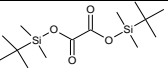
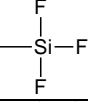
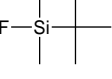
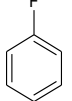
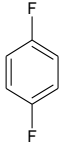
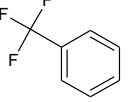
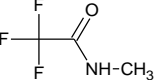
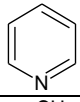
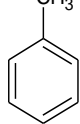
T <sub>pyrolysis</sub>	RT (min)	Masses of fragments* and relative abundance: m/z (%)	Compounds	Structures
5.	8.31	151(100), 152(24), 73(24), 75(23), 100(21), 152(25)	O-(trimethylsilyl)phenol	
6.	9.64, 20.47	100(100), 57(19), 56(17), 72(14), 85(12), 70(12)	Tert-Butyl-isocyanato-dimethylsilane	
7.	13.0, 16.62	134(100), 184(96), 77(77), 73(32), 135(17), 185(16), 118(13)	N-methyl-N-(trimethylsilyl)trifluoroacetamide	
8.	19.60	189(100), 147(91), 148(62), 73(48), 149(33), 190(21), 133(20), 117(15)	1,3-ditert-butyl-1,1,3,3,-termethylidisiloxane	
9.	20.10	133(100), 73(31), 147(30), 189(20), 134(14)	Pentamethylidisiloxane	
10.	23.91	73(100), 207(86), 208(18), 209(12), 211(11)	Bis(trimethylsiloxy)methylsilane	
11.	27.34	221(100), 73(32), 263(31), 222(25), 223(13)	Tris(trimethylsilyl)borate	
12.	31.21	73(100), 147(80), 189(54), 115(21), 57(22)	Bis[tert-butyl(dimethyl)silyl]oxalate	
<b>850 °C</b>				
1.	1.47, 1.53	85(100), 81(86), 80(23), 64(17), 44(16), 47(19), 100(18)	methyltrifluorosilane	
2.	2.79	77(100), 56(98), 57(69), 134(51), 151(27), 119(19), 96(16), 41(44), 49(27)	Tert-Butyldimethylfluorodilane	
3.	3.16-3.18	78(100), 77(92), 56(55), 96(29), 51(25), 52(24), 50(21), 57(17), 79(16), 114(13)	Fluorobenzene	
4.	3.40	114(100), 77(71), 58(48), 101(46), 88(25), 47(23), 155(16), 141(11)	1,4-difluoro-Benzene	
5.	3.65	58(100), 69(45), 77(10), 127(33), 146(27), 145(17), 56(13)	Benzene,(trifluoromethyl)-	
6.	3.92	58(58), 69(76), 127(25), 155(32), 181(28), 78(18), 73(16), 233(13)	N-methyltrifluoroacetamide	
7.	4.47	79(100), 52(62), 51(30), 50(23)	Pyridine	
8.	4.83	91(100), 92(77), 65(30), 63(15), 51(12), 7(11)	Toluene	

Table 2-2 (Continued)

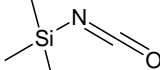
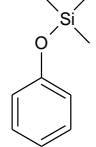
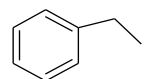
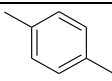
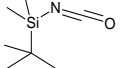
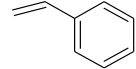
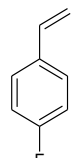
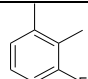
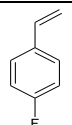
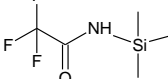
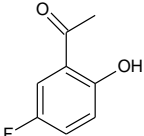
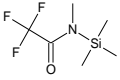
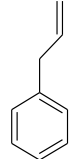
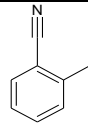
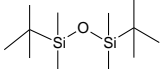
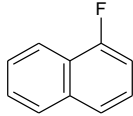
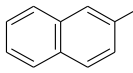
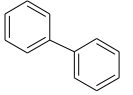
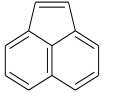
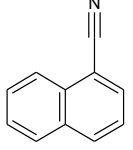
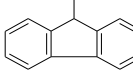
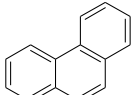
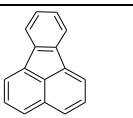
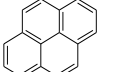
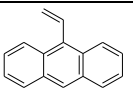
T <sub>pyrolysis</sub>	RT (min)	Masses of fragments* and relative abundance: m/z (%)	Compounds	Structures
9.	6.19	100(100), 126(48), 70(20), 86(12)	Isocyanatotrimethylsilane	
10.	7.18	151(100), 152(18), 73(10)	O-(Trimethyl)phenol	
11.	7.31	91(100), 143(26), 77(15), 106(34), 143(26), 158(12), 65(10), 167(11)	Ethylbenzene	
12.	7.76	91(100), 106(52), 111(23), 77(11), 51(10)	p-xylene	
13.	8.30	100(100), 101(34), 56(34), 72(31), 157(21), 41(17)	Tert-Butyl-isocyanato-dimethylsilane	
14.	8.67	104(100), 78(73), 103(71), 77(34), 51(30), 91(19), 105(16), 50(13)	Styrene	
15.	8.79,8.86,9.13	122(100), 121(39), 96(35), 101(36), 75(15)	p-fluoro-Styrene	
16.	9.26 ?	109(100), 91(58), 64(56), 124(43), 63(17), 159(14)	2,3-Dimethylfluorobenzene	
17.	9.90,10.06	122(100), 100(34), 100(25), 121(25), 159(23), 101(22), 140(14)	P-fluoron-Styrene	
18.	10.76	77(100), 120(67), 170(64), 143(23)	2,2,2-trifluoro-N-(trimethyl)acetamide	
19.	11.00	139(100), 154(30), 47(27), 91(18), 140(16)	2-Hydroxy-5-fluoroacetophenone	
20.	12.82	77(100), 134(97), 103(87), 184(57), 73(43), 121(10)	N-Methyl-N-(trimethyl)trifluoroacetamide	
21.	13.02, 13.18	117(100), 121(79), 118(60), 94(34), 115(30)	Benzene,2-propenyl-	
22.	16.40,17.52	117(100), 90(60), 116(58), 89(34), 63(12)	3-methyl-Benzonitrile	
23.	18.88	147(100), 73(21), 189(22), 148(18)	1,3-Ditert-butyl-1,1,3,3-tetramethyldisiloxane	

Table 2-2 (Continued)

T <sub>pyrolysis</sub>	RT (min)	Masses of fragments* and relative abundance: m/z (%)	Compounds	Structures
24.	22.05	146(100), 128(84), 129(20), 147(17), 145(16), 102(13), 120(12)	1-fluoro-Naphthalene	
25.	26.89	142(100), 141(88), 115(33), 160(30), 159(29), 139(13), 71(10)	2-methyl-naphthalene	
26.	30.53,3 2.66	154(100), 153(43), 152(32), 172(26), 76(18), 171(12), 151(10)	Biphenyl	
27.	33.39	152(100), 151(26), 150(19), 76(14)	Acenaphthylene	
28.	35.30,3 6.50	153(100), 126(25)	1-Naphthonitrile	
	41.06	165(100), 166(44), 179(21), 164(17), 82(18)	9-methyl-Fluorene	
29.	45.90,4 6.23	178(100), 176(21), 152(12), 76(14), 196(15), 76(14), 177(13)	phenanthrene	
30.	54.92,5 6.44	202(100), 200(22), 101(20), 203(18), 100(14)	Fluranthene	
31.	55.65	202(100), 200(23), 203(20), 220(15), 101(19), 88(10)	Pyrene	
32.	56.17	203(100), 202(87), 201(24), 200(21), 101(21), 88(21), 101(21), 175(11)	9-ethenyl-Anthracene	

### 2.3.1.3 MTBSTFA/DMF flash pyrolysis at different temperatures

The chromatograms obtained when pyrolyzing MTBSTFA alone and the MTBSTFA/DMF (4:1) mixture at different temperatures are shown in Figure 2-4. Compared with the pyrolysis of DMF and MTBSTFA respectively, no new main products were observed after the pyrolysis of the MTBSTFA/DMF (4:1, v/v) mixture across all temperatures. This suggests that there is no obvious cross-reaction between MTBSTFA and DMF during the pyrolysis process. Therefore, *N*-methyl-*N*-(trimethylsilyl)trifluoroacetamide, TFMA, MSW, and BSW are the main products of the mixture of MTBSTFA/DMF pyrolysis at temperatures of 210 and 300 °C, which is similar to our results for MTBSTFA and DMF pyrolysis individually. However, when the pyrolysis temperature was increased to 600 and 850 °C, the



mixture of MTBSTFA/DMF was completely cracked (Figure 2-4), resulting in a crowded chromatogram populated by the numerous products coming from both MTBSTFA and DMF. The main products are listed in Table 2-2.

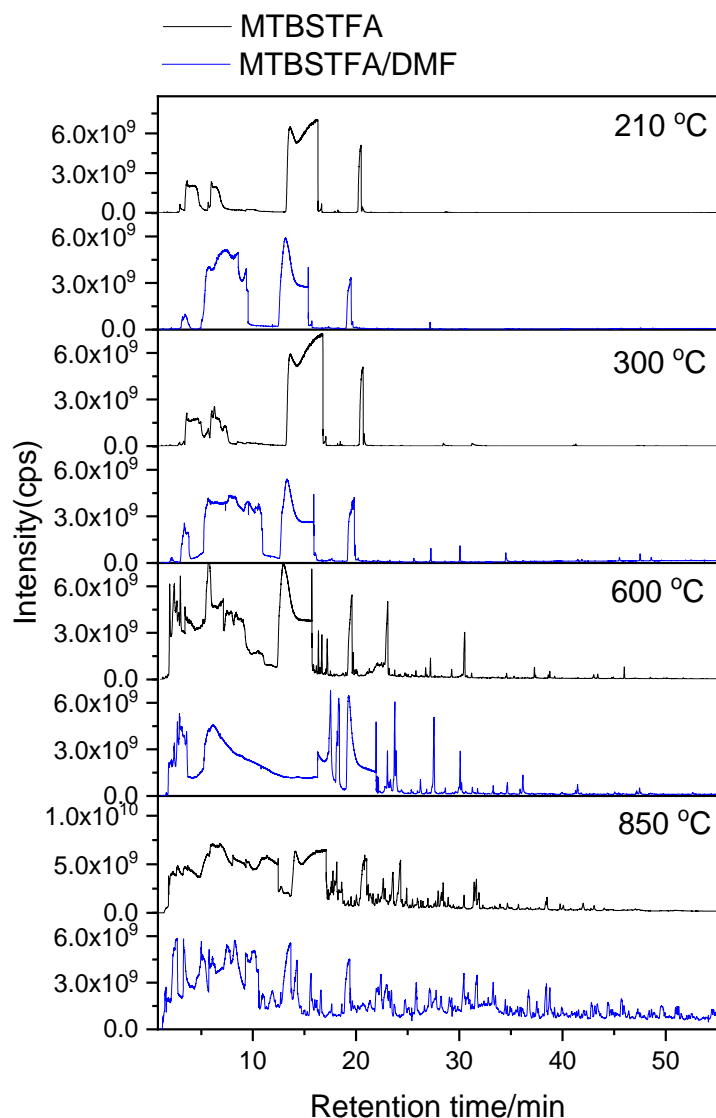


Figure 2-4: Chromatograms of MTBSTFA/DMF (4:1) pyrolyzed at different temperatures compared with those obtained with MTBSTFA only under the same conditions (as Section 2.3 analysis of pyrolysis products).

### 2.3.2 MTBSTFA/DMF flash pyrolysis with $\text{Ca}(\text{ClO}_4)_2$ at different temperatures

The effects of calcium perchlorate on MTBSTFA/DMF flash pyrolysis at different temperatures (210, 300, 600 °C) were also studied. Figure 2-5 shows that calcium perchlorate does not have any obvious qualitative effects on the pyrolysis of the MTBSTFA/DMF mixture at 210 °C (no new pyrolysis products were detected). This is assumed to be because calcium

perchlorate is thermally stable up to 210 °C, and it is expected that the reactivity of oxychlorine species in pyrolysis is effective only from the gaseous compounds it produces, such as HCl (for an example see [585]). However, the presence of oxychlorine can influence the quantity of products released by the mixture. Therefore, the effect of calcium perchlorate on the main pyrolysis products of MTBDTFA/DMF at 210 °C was studied. Figure 2-6 shows the effect of calcium perchlorate on the main products of MTBSTFA/DMF, including MSTFA, TFMA, BSW, and TBDMS-F. At 210 °C, the detection of DMF was not affected by calcium perchlorate. This suggests that the presence of calcium perchlorate should not affect the performance of DMF at least up to this temperature. The abundance of TFMA increased with the addition of calcium perchlorate when the abundance of  $\text{ClO}_4^-$  is lower than 20 wt.%. However, the presence of calcium perchlorate did not influence the formation of BSW, while it promoted the formation of TBDMS-F when the abundance of  $\text{ClO}_4^-$  was higher than 15 wt.%.

When MTBSTFA/DMF was pyrolyzed at 300 and 600 °C, the main degradation products were similar to those products detected at 210 °C, though there were more products compared to the pyrolysis results at 600 °C (see Figure S2-3). However, the presence of calcium perchlorate did not show any obvious influence on the degradation of MTBSTFA/DMF, as can be seen in Figure S2-4 and Figure S2-5 of the Appendix. On the other hand, we did not analyze the degradation of MTBSTFA/DMF in the presence of calcium perchlorate at a pyrolysis temperature of 850 °C, because the MTBSTFA/DMF was degraded severely and there were too many products. Hence, we conclude that the MTBSTFA/DMF mixture should not be applied for silylation at high temperatures, such as 850 °C.

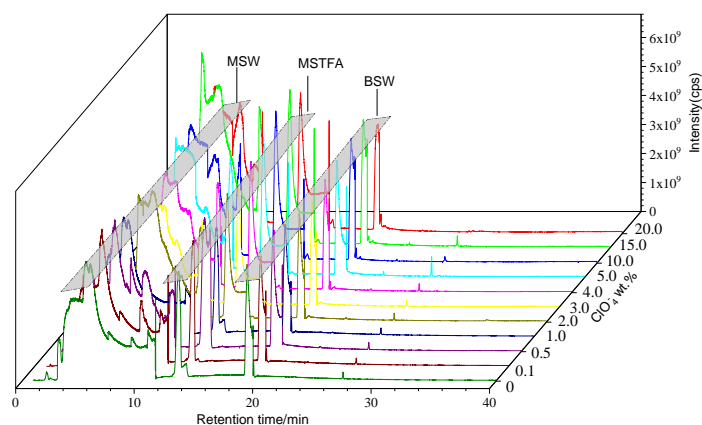


Figure 2-5: Chromatograms of MTBSTFA/DMF (4:1) pyrolysis with and without calcium perchlorate at 210 °C.

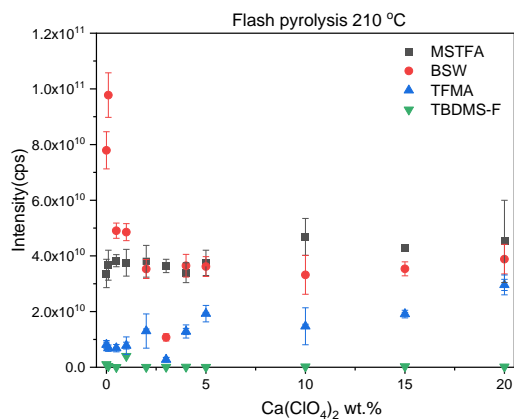


Figure 2-6: Influence of calcium perchlorate on the abundance of main products of MTBSTFA/DMF flash pyrolysis at 210 °C.

### 2.3.3 MTBSTFA/DMF and calcium perchlorate pyrolysis with SAM-like ramp

Figure 2-7 shows the chromatograph of a SAM-like ramp pyrolysis of MTBSTFA/DMF across different temperatures. The results show that there were not as many products of MTBSTFA/DMF pyrolysis after a SAM-like pyrolysis ramp compared to the number of products detected after a flash pyrolysis at the corresponding temperatures. MSTFA, TFA, MSW, and BSW were again the main pyrolysis products of the MTBSTFA/DMF mixture when the final pyrolysis temperatures were 300, 600, and 850 °C. In contrast to flash pyrolysis at 300 °C, no new products were produced from MTBSTFA/DMF pyrolysis using the SAM-like ramp pyrolysis. This demonstrated that the MTBSTFA/DMF mixture has the potential to be utilized under SAM-like ramp pyrolysis conditions at high temperatures, including 850 °C. The only chlorine-bearing compound detected was TBDMS-Cl and it was detected at relatively low levels. This chemical species has been detected among the pyrolysis products of the Rocknest soil sample that was analyzed on Mars [586]. It could be formed during the reaction of the TBDMS molecule with the Cl<sup>-</sup> ion when calcium perchlorate decomposed to CaCl<sub>2</sub> [587].

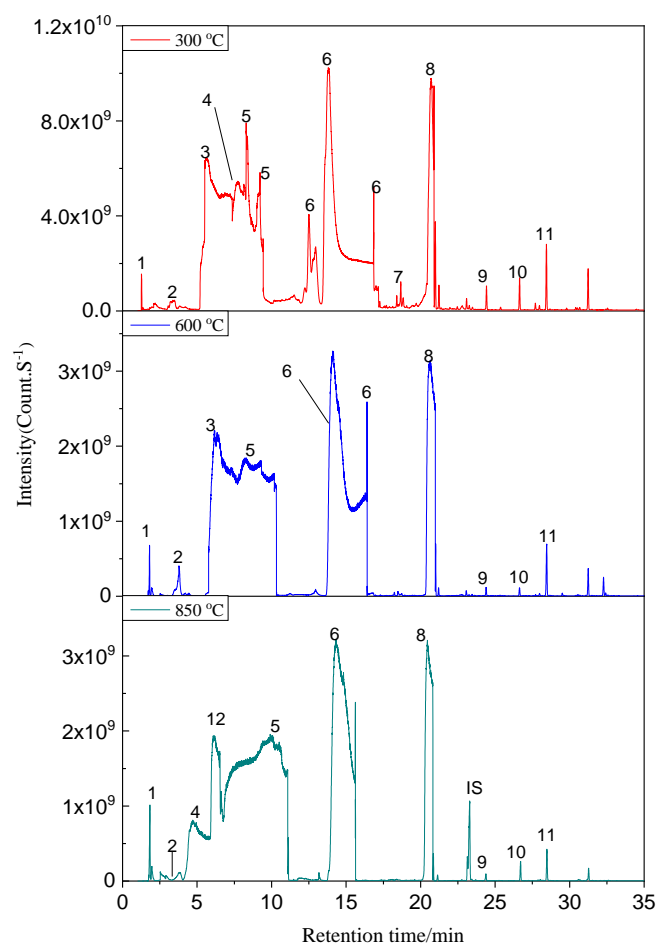


Figure 2-7: Chromatograms (TIC) of MTBSTFA/DMF (4:1) mixture pyrolyzed at different temperatures. Peak attributions 1: CO<sub>2</sub>; 2: TBDMS-F; 3: DMF, 4: TFMA; 5: MSW; 6: MSTFA; 7: Ethyl isopropyl(dimethyl)silyl ether; 8: BSW; 9: Bis(*tert*-butyldimethylsilyl)amine; 10: *Tert*-butyldimethylsilyl isocyanate; 11: Tris(trimethylsilyl)borate; 12: Bis(*tert*-butyldimethylsilyl)carbonate; 13 : *Tert*-butyl(methoxy)dimethylsilane; IS: Naphthalene-d<sub>8</sub>(Internal standard).

Figure 2-8 shows the effect of calcium perchlorate on the pyrolysis of MTBSTFA/DMF at SAM-like ramp pyrolysis at the final temperature of 300 °C. There was no obvious impact on the formation of most of the main products of MTBSTFA/DMF when the pyrolysis heating rate was 35 °C·min<sup>-1</sup> and the final temperature was 300 °C. Out of the main pyrolysis products of MTBSTFA/DMF (TFA, MSW, BSW, MSTFA), only the formation of MSTFA was affected by the presence of calcium perchlorate. The yield of MSTFA increased with the increasing abundance of perchlorate when the perchlorate abundance was higher than 3 wt.%. However, the presence of 20 wt.% of perchlorate promoted the decomposition of MSTFA. Therefore, the presence of calcium perchlorate did not influence the degradation of MTBSTFA/DMF during

a SAM-like pyrolysis with final temperatures up to 300 °C. Even at 850 °C, calcium perchlorate did not influence the degradation of MTBSTFA/DMF. The influence of the amount of calcium perchlorate on the main chemical products observed when MTBSTFA/DMF (4 :1) was pyrolyzed using a SAM-like ramp with a final temperature of 850 °C can be seen in Figure 2-8 in the supplementary material.

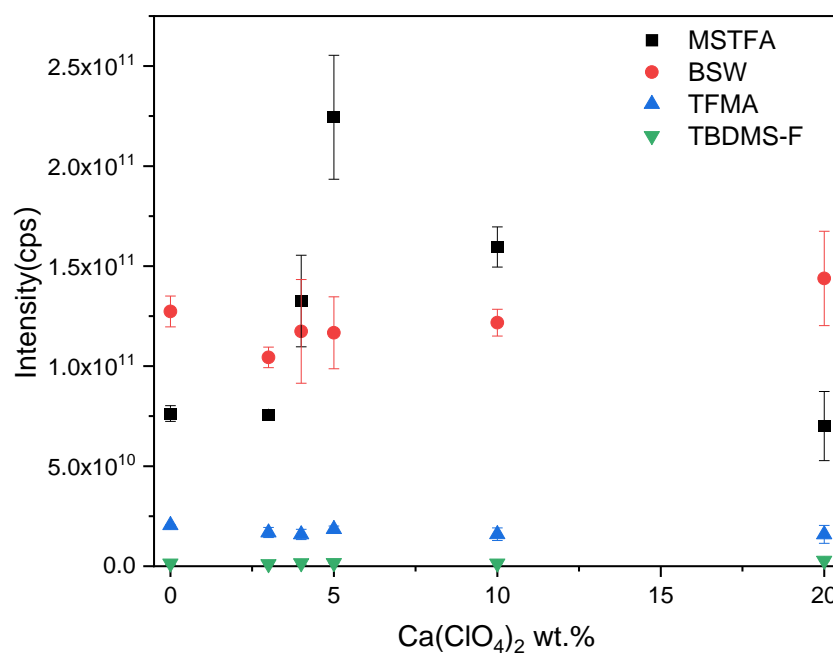


Figure 2-8: Influence of the amount of calcium perchlorate on the main chemical products observed when MTBSTFA/DMF (4 :1) is pyrolyzed using a SAM-like ramp with a final temperature of 300 °C.

### 2.3.4 Flash pyrolysis at 850 °C of Murchison meteorite and calcium perchlorate

Figure 2-9 shows a chromatogram of the flash pyrolysis (850 °C) of the Murchison meteorite. Most of the main compounds are aromatic compounds, including light aromatics such as benzene, toluene, *m,p*- or *o*-xylene and their isomers. Polyaromatic compounds were detected from the pyrolysis of the Murchison sample; for example, naphthalene, methyl-naphthalene, fluorene, phenanthrene, pyrene and their isomers were detected. Sulfur-containing compounds were also identified following pyrolysis of the Murchison meteorite, e.g. sulfur dioxide, *N*-methyltaurine, thiophene, benzenethiol, dibenzothiophene, and phenalenol[1,9-bc]thiophene. Among these S-bearing compounds, the abundance of *N*-methyltaurine is the highest. Acetonitrile was also detected with a retention time of 2.63 min.

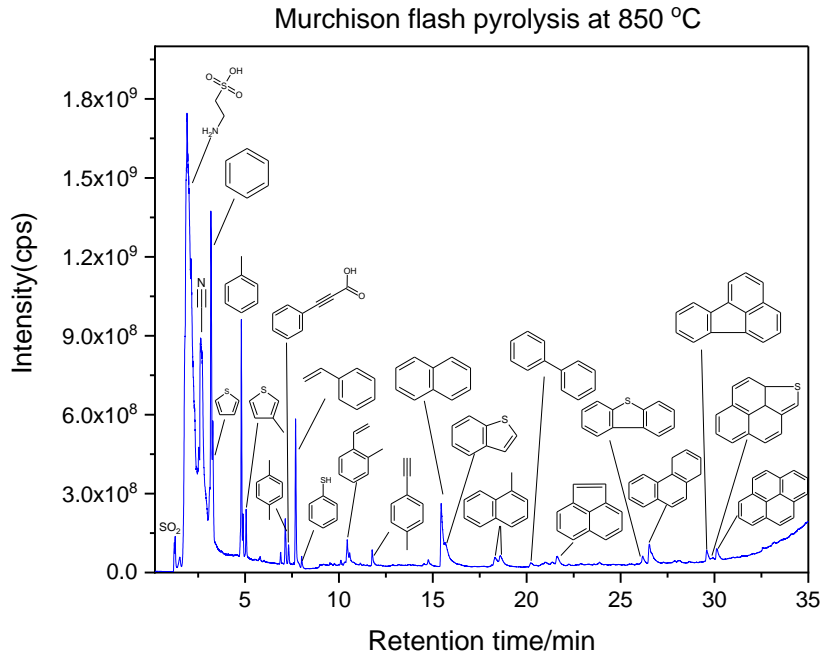


Figure 2-9: Chromatogram of flash pyrolysis at 850 °C of the Murchison meteorite.

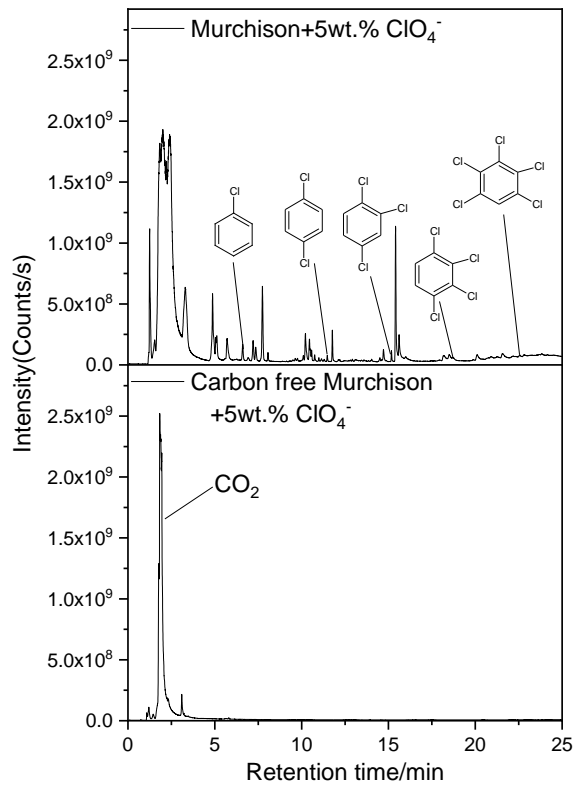


Figure 2-10: Chromatogram of flash pyrolysis of Murchison and carbon-free Murchison with calcium perchlorate (Chloro-bearing benzene and their isomers).

Figure 2-10 shows the chromatogram of the flash pyrolysis of Murchison and carbon-free Murchison both with calcium perchlorate. In addition to aromatic compounds, S-bearing compounds, and N-bearing compounds, chlorine-bearing compounds were also detected following the flash pyrolysis of the Murchison meteorite samples. These Cl-bearing organic compounds include chlorobenzene, dichlorobenzene, tri-chlorobenzene, tetra-chlorobenzene, and penta-chlorobenzene and have retention times of 6.60 min, 11.48 min, 15.17 min, 18.54 min, and 22.55 min, respectively. Murchison residue was collected after the pyrolysis (850 °C) of the Murchison meteorites. Then the Murchison residues were pyrolyzed at 850 °C in the presence of calcium perchlorate. Carbon dioxide was the main product and no other organics were identified in the chromatogram.

## **2.4 Discussion**

### **2.4.1 The mechanism of MTBSTFA/DMF degradation at different temperatures**

As flash pyrolysis, the distribution of the products of MTBSTFA changed with the pyrolysis temperature. The number of silicon bearing compounds increased with the pyrolysis temperature. However, the number of TBDMS-bearing compounds, TBDMS being the functional group of derivatization, decreased since these compounds decomposes at high temperature, while the formation of aromatic compounds was promoted. At the same time, the formation of nitrogenous heterocycles was also enhanced because of the high temperature, which may promote the cracking of F-C bonds forming the fluorine radicals. The formation of F-containing compounds also increased when the pyrolysis temperature increased from 210 to 850 °C. Figure 2-11 shows the distribution of the products of MTBSTFA flash pyrolysis at different temperatures. With increasing pyrolysis temperature, more aromatic compounds were formed from MTBSTFA pyrolysis.

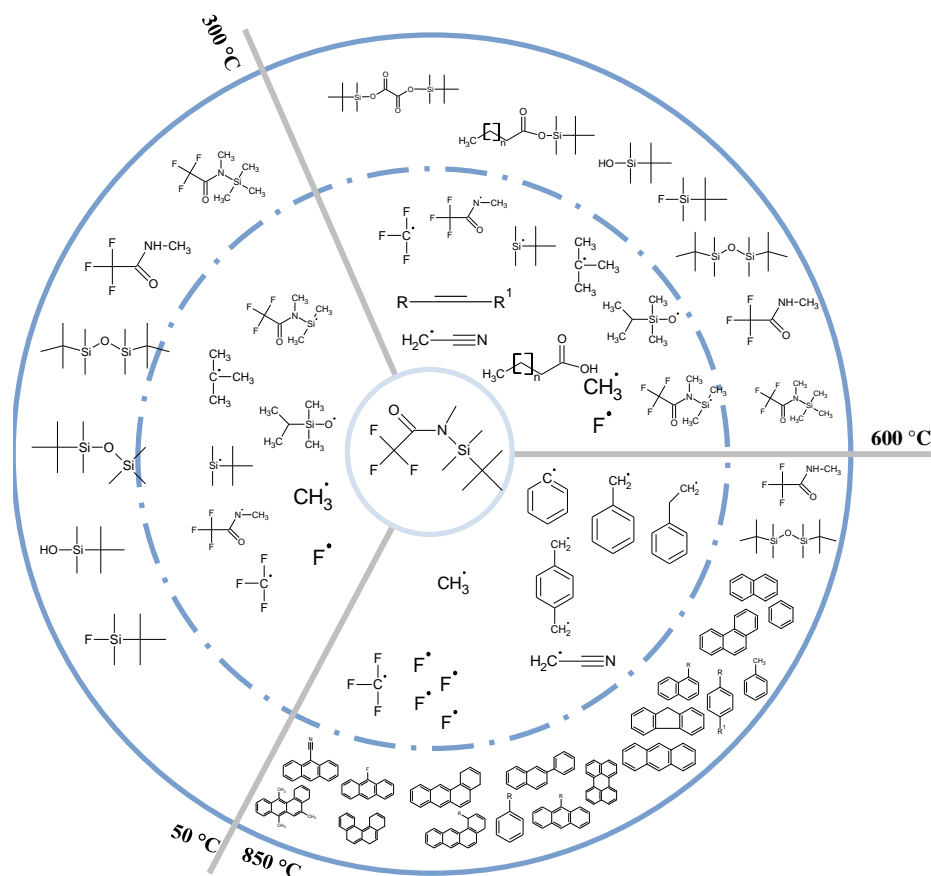


Figure 2-11: Distribution of the byproducts detected from MTBSTFA flash pyrolysis at different temperatures.

Figure 2-12 shows possible reaction pathways of MTBSTFA pyrolysis. When the pyrolysis temperature is lower than 600 °C, MSTFA, BSW, MSW, TBDMS and TBDMS-bearing compounds appear to be the main products of MTBSTFA pyrolysis; these are the classic products of MTBSTFA that have been reported in previous studies [231,568]. However, aromatization appears to be the main reaction occurring when the pyrolysis temperature reaches 850 °C. From these results, we conclude that high temperatures provide enough energy to crack chemical bonds, such as F-C, N-Si, Si-C, and N-C bonds of MTBSTFA. As a result, some active radicals are formed, such as  $F\cdot$ ,  $\cdot CH_3$ , and  $\cdot NH_2$ .

The cracking of MTBSTFA at high temperature during flash pyrolysis appears to significantly decrease the efficiency of derivatization. When the temperature is lower than 300 °C, fewer products were detected. The formation of TBMDMS functional group could improve the efficiency of derivatization process. We therefore conclude that the MTBSTFA derivatization should be operated below 300 °C for flash pyrolysis.



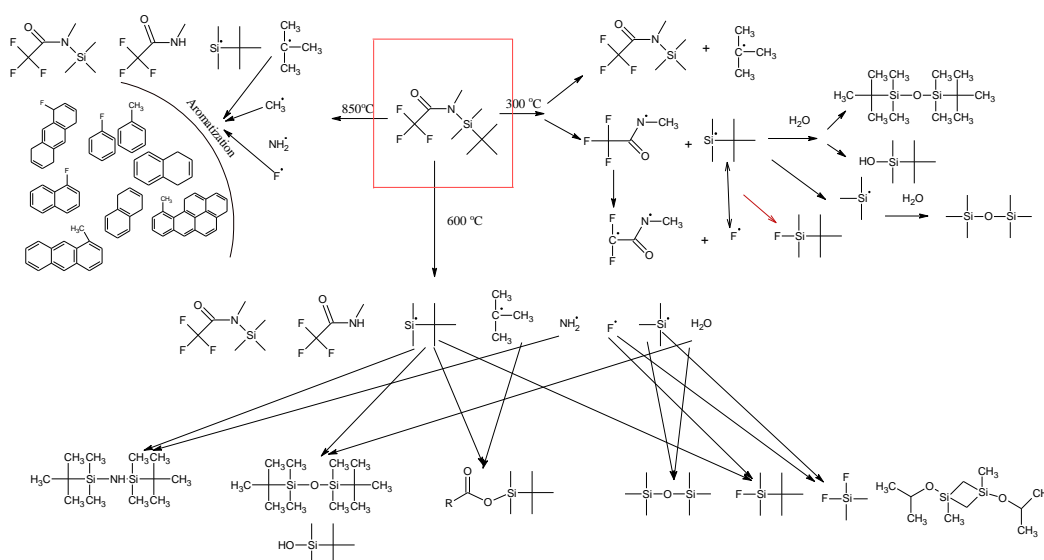


Figure 2-12: Possible reaction pathways of MTBSTFA pyrolyzed at different temperatures.

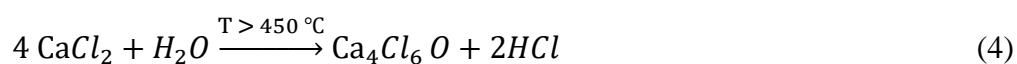
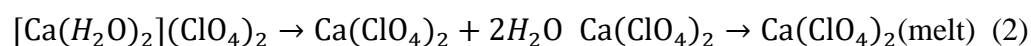
We observed that the products of MTBSTFA/DMF pyrolysis using SAM-like heating ramp were different than those resulting from flash pyrolysis, especially at high temperatures of 600 °C and 850 °C. This is because that the heating rate affects the distribution of pyrolysis products, even when the same final pyrolysis temperature is used [588]. The difference in retention times of the volatiles from MTBSTFA/DMF pyrolysis between the SAM-like pyrolysis and the flash pyrolysis indicates the difference in timing of the reactions, which in turn lead to different secondary reactions. When the pyrolysis temperature was lower than 300 °C, only some main products are formed, such as MSTFA, BSW, MSW. However, the products of MTBSTFA/DMF formed during the SAM-like ramp at 600 °C and 850 °C were almost in alignment with the products from the flash pyrolysis at 300 °C. As shown in Figures 2-4 and 2-7, the products of MTBSTFA/DMF from flash pyrolysis were very different than those resulting from SAM-like ramp pyrolysis at high temperature (850 °C), demonstrating that MTBSTFA/DMF can be used for derivatization using SAM-like heating ramp pyrolysis even for high final temperatures. This limitation of the number of products observed after a SAM-like ramp is obviously important for *in situ* analyses, as it will limit the risk of misinterpretation in attributing identifications to organic molecules detected to the analyzed sample.

Finally, under high temperature conditions, we conclude that it would be difficult to determine the origin of organic compounds detected in experiments performed on Mars. There are simply too many products from MTBSTFA and DMF flash pyrolysis. Therefore, the MTBSTFA/DMF mixture should be used at temperatures lower than 300 °C to limit this effect. The products of MTBSTFA/DMF pyrolysis should also be considered when MTBSTFA/DMF

is applied to analyze the organic compounds in natural samples. For example, oxalic acid were detected in MTBSTFA/DMF pyrolysis tests conducted in this study. However, MTBSTFA/DMF has primarily been used for the qualification and quantitation of organic compounds, such as amino acids, fatty acids, carboxylic acids, etc. Thus, it is essential to assess any possible contamination of the analysis system, including the instruments and the reagents, and to understand the products that can be produced from the derivatization reagents.

#### 2.4.2 The mechanism of MTBSTFA/DMF pyrolysis in the presence of calcium perchlorate

Calcium perchlorate can decompose in O<sub>2</sub> and Cl<sub>2</sub> when heated above their decomposition temperatures. As a result, organic matter that might be present in the samples could be combusted [56]. Carbon dioxide was observed from MTBSTFA degradation in the case of the SAM experiment [64]. For this reason, we analyzed the abundance of CO<sub>2</sub> detected from the pyrolysis of MTBSTFA/DMF at different temperatures. As shown in Figure 2-13, the abundance of CO<sub>2</sub> from MTBSTFA/DMF pyrolysis with Ca(ClO<sub>4</sub>)<sub>2</sub>, using a flash pyrolysis and SAM-like ramp pyrolysis was investigated. When MTBSTFA/DMF was pyrolyzed at temperatures below 300 °C, there were not obvious changes in the CO<sub>2</sub> abundance, even with an increase in calcium perchlorate. However, the CO<sub>2</sub> abundance increased with an increase in calcium perchlorate when the pyrolysis temperature was between 300 and 850 °C. This is due to the decomposition of calcium perchlorate, which includes three main stages [587]. The first stage is the process of dehydration, as shown in reaction (1); the second stage is the phase transition of solid to melted calcium perchlorate according to differential scanning calorimetry (DSC) curve at 346 to 416 °C, as shown in reaction (2); the third stage is the decomposition of Ca(ClO<sub>4</sub>)<sub>2</sub>, which happens concurrently with the formation of CaCl<sub>2</sub> and the release of O<sub>2</sub> at about 462 °C (3). When water is present, CaCl<sub>2</sub> could react with H<sub>2</sub>O and release HCl at the pyrolysis temperatures higher than 450 °C [56], as shown in reaction (4).



We observed that the abundance of O<sub>2</sub> released from the decomposition of calcium perchlorate increased slightly with the increase in the concentration of calcium perchlorate. As

more calcium perchlorate was added, more CO<sub>2</sub> was formed and detected when the pyrolysis temperature was higher than 600 °C. This demonstrates that some, but not all, of the carbon from the MTBSTFA/DMF derivatization reagent was oxidized by O<sub>2</sub> to CO<sub>2</sub>, rather than all MTBSTFA/DMF, since the abundance of the main products of MTBSTFA, such as MSTFA, BSW, and MSW, did not show a significant decrease with increasing calcium perchlorate. In addition, a large amount of MSTFA, BSW, and MSW were formed no matter the percentage of calcium perchlorate during the degradation of MTBSTFA/DMF from both flash pyrolysis and the SAM-like ramp pyrolysis. For example, the abundance of BSW was significantly higher than of CO<sub>2</sub> (*e.g.*, roughly 2800 times higher than the yield of CO<sub>2</sub> during the pyrolysis of MTBSTFA/DMF in the presence of 15 wt. % of calcium perchlorate). This suggests that the only a tiny part of carbon from MTBSTFA/DMF was combusted to CO<sub>2</sub>. This likely will not influence the performance of MTBSTFA/DMF during the derivatization process in the presence of natural samples, a result which is consistent with results obtained by Glavin et al. [56]. Furthermore, about 10 μmol of MTBSTFA was used, corresponding to 80 μmol of C, along with about 7.8 μmol of DMF mixed with the MTBSTFA, corresponding to an additional 23 μmol of C. Therefore, there was at least 103 μmol of C in the system, yet the maximum O<sub>2</sub> that could have been produced by calcium perchlorate at 15 wt. % would only be 8 μmol. Given that the abundance of carbon is about 12 times higher than that of O<sub>2</sub>, and there are 500 μl of MTBSTFA/DMF on SAM, we conclude that the presence of calcium perchlorate will not influence the performance of MTBSTFA/DMF, under either flash pyrolysis or SAM-like ramp pyrolysis conditions.

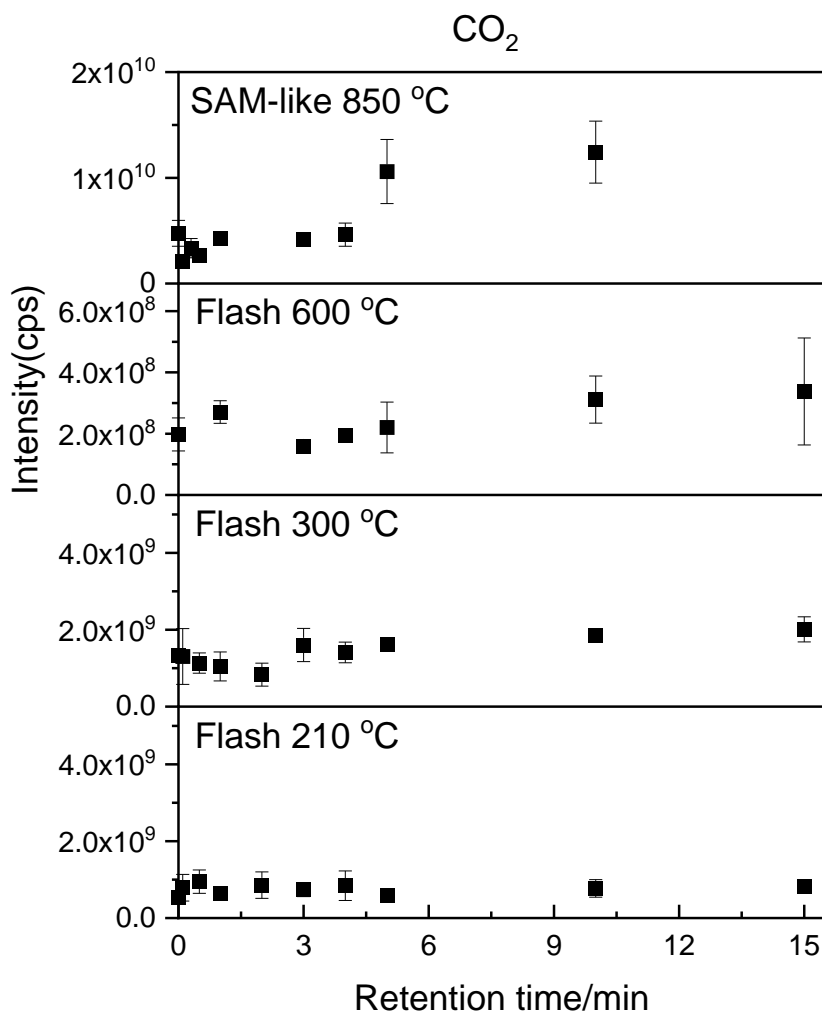


Figure 2-13: Abundance of CO<sub>2</sub> from MTBSTFA/DMF pyrolysis with Ca (ClO<sub>4</sub>)<sub>2</sub> at different conditions.

Chlorinated compounds have become a hot topic since the detection of chlorine-bearing products at Mars [53]. The origin of the carbon and chlorine components of these compounds is controversial. There are two main possible explanations for the carbon source and for the chlorine source of these chlorinated compounds, including either sources indigenous to the Martian sample and/or from contaminants present in the sample handling chain and from leaked reagents [56,57,66]. As MTBSTFA/DMF is one of the derivatization reagents onboard SAM and MOMA, it is essential to understand the possible chlorinated compounds that can be formed during the pyrolysis of MTBSTFA/DMF in the presence of perchlorate salts such as calcium perchlorate. In previous studies, some chlorinated compounds, such as chloromethane, chloromethylpropenes, and chlorobenzenes have been detected, as shown in Table 2-3.

However, in this study, only chloromethane and chloro-tertbutyldimethylsilane (TBDMS-Cl) were detected in the presence of calcium perchlorate. Chloromethane was only present following the SAM-like ramp pyrolysis. The abundance of chloromethane was relatively low at the final temperature of 300 °C with the SAM-like ramp pyrolysis. This is because the final temperature of 300 °C is lower than the decomposition temperature of calcium perchlorate, theoretically meaning that no chloride is released during the pyrolysis process. However, a low abundance of chloromethane detected following the SAM-like ramp pyrolysis showed that a low percentage of chloride from the GC/MS system may contribute to the formation of chloromethane. When the temperature was in the percentage increased up to 850 °C, the yield of chloromethane increased slightly with an increase of calcium perchlorate percentage, as shown in Figure 2-14. This result illustrated that the chloromethane detected in SAM experiments could be partially from MTBSTFA/DMF degradation in the presence of calcium perchlorate, as also suggested by previous studies [56,58].

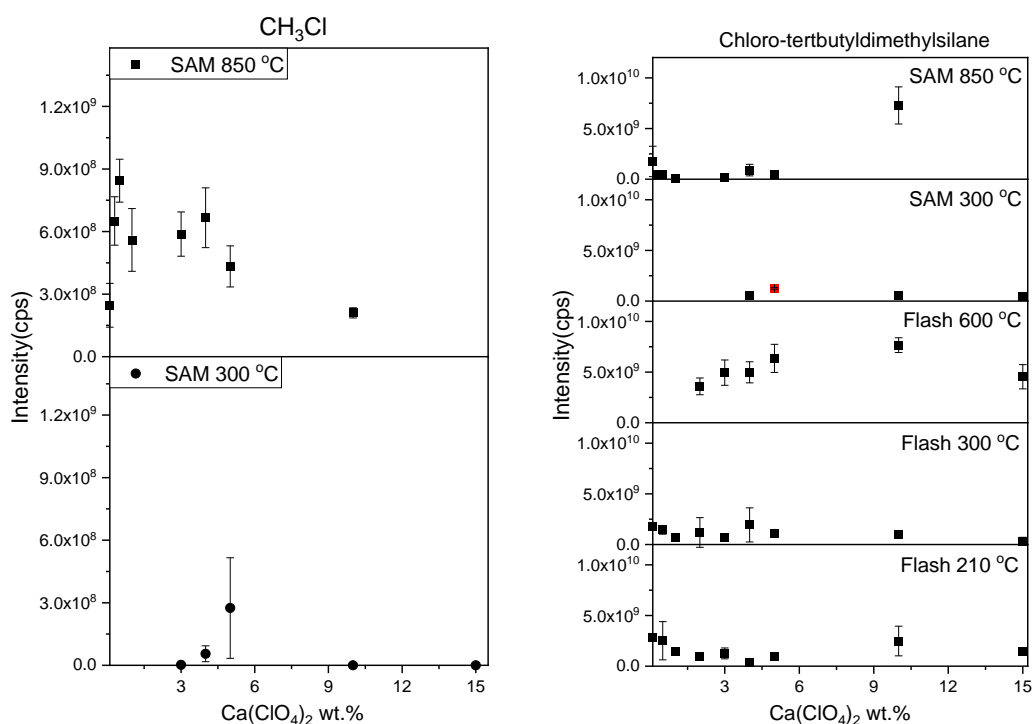


Figure 2-14: Chlorinated compounds detected from the pyrolysis of MTBSTFA/DMF with calcium perchlorate.

TBDMS-Cl, with important fragments at  $m/z$  of 93, 150, and 56, is the other chlorinated compound detected in our study from MTBSTFA/DMF pyrolysis in the presence of calcium perchlorate. As shown in Figure 2-14, TBDMS-Cl was detected both in the flash pyrolysis and the SAM-like ramp pyrolysis. Its abundance was the highest following flash pyrolysis at 600 °C,

and the yield of TBDMS-Cl increased consistently, with an increase in the percentage of calcium perchlorate. TBDMS was one of the expected products from MTBSTFA pyrolysis, and the chlorine element came from the decomposition of calcium perchlorate. The presence of this compound could be explained by the derivatization of HCl by TBDMS functional group. A low abundance of TBDMS-Cl was detected following flash pyrolysis at 210 and 300 °C and SAM-like pyrolysis at 300 °C, since the final pyrolysis temperature were lower than the degradation temperature of calcium perchlorate (expected to be around 400 ~500 °C). Therefore, no Cl<sub>2</sub> were released and no HCl was formed during the pyrolysis of calcium perchlorate at these temperatures.

Table 2-3: The chlorinated compounds have been detected in previous SAM and MOMA studies.

Compounds	Molecular formula	Mass fragments	Publications
Chloromethane	CH <sub>3</sub> Cl	50	[56,57,64,66,531]
Dichloromethane	CH <sub>2</sub> Cl <sub>2</sub>	84	[56,57,64,66,223,531,589]
Trichloromethane	CHCl <sub>3</sub>	83	[56,57,64,66,223,531]
Carbon tetrachloride	CCl <sub>4</sub>	117	[57,531]
Tetrachloroethene	C <sub>2</sub> Cl <sub>4</sub>	-	[57]
Chloroethane	C <sub>2</sub> H <sub>5</sub> Cl	64	[57]
Chloromethylpropene;(1-chloro-2-methyl-1-propene; 3-chloro-2-methyl-1-propene)	C <sub>4</sub> H <sub>7</sub> Cl	55	[56,57,64,223,531]
1,2-dichloroethane	C <sub>2</sub> H <sub>4</sub> Cl <sub>2</sub>	63	[57]
1,2-dichloropropane	C <sub>3</sub> H <sub>6</sub> Cl <sub>2</sub>	63	[57,531]
1,2-dichlorobutane	C <sub>4</sub> H <sub>8</sub> Cl <sub>2</sub>	90	[57,531]
2-chloro-2-methylpropane	C <sub>4</sub> H <sub>9</sub> Cl	-	[56,57]
Chlorobenzene	C <sub>6</sub> H <sub>5</sub> Cl	112	[56,57,60,64,223,531,589]
Dichlorobenzene	C <sub>6</sub> H <sub>4</sub> Cl <sub>2</sub>	146	[60,223]
Trichlorobenzene	C <sub>6</sub> H <sub>3</sub> Cl <sub>3</sub>	182	[60]
Tetrachlorobenzene	C <sub>6</sub> H <sub>2</sub> Cl <sub>4</sub>	216	[60]

It should be noted that neither dichloro-related compounds nor chlorobenzene were detected in this study. If chlorobenzene was one of the pyrolysis products of MTBSTFA/DMF and calcium perchlorate, benzene-bearing substances are expected to be formed. Chlorobenzene was detected from the pyrolysis of aromatic carboxylic acids along with products such as benzene and toluene, indicating that aromatic carboxylic acids could be one

of the possible precursors of chlorobenzene [572]. However, the aromatization of organic compounds occurs when pyrolysis temperature are higher than 600 °C [270,463]. As shown in Figure 2-11, only a few aromatic compounds formed from MTBSTFA/DMF pyrolysis at 600 °C. A higher temperature of 850 °C enhanced the formation of aromatics and polyaromatic hydrocarbons, such as benzene, toluene, ethylbenzene, naphthalene; fluorobenzene, dichlorobenzene, and trifluoromethylbenzene. However, following a SAM-like pyrolysis with a final temperature of 850 °C, no chlorobenzene was detected. To further study the mechanism of MTBSTFA/DMF degradation, the stepwise pyrolysis of MTBSTFA/DMF with and without calcium perchlorate from 50 to 1000 °C, with and without calcium perchlorate, was conducted. Figure 2-15 shows the chromatograms of MTBSTFA/DMF (4:1) following stepped pyrolysis with 15 wt.% of  $\text{ClO}_4^-$  at different temperatures. Most of the MTBSTFA/DMF was decomposed between 50 to 100 °C, and the TBMDS functional group was formed. This is an important advantage of MTBSTFA, which can be used as a derivatization reagent at a low temperature. With the increasing of pyrolysis temperature, only  $\text{CO}_2$  was detected, and the abundance of  $\text{CO}_2$  was the highest from 300 to 500 °C, which means that the  $\text{O}_2$  was formed during the decomposition of calcium perchlorate, combusting some of the carbon from the pyrolysis system. In addition, chloromethane was formed and detected primarily during the step pyrolysis of MTBSTFA/DMF from 200 to 500 °C, as shown in Figure 2-16. When the pyrolysis temperature was lower than 300 °C, the calcium perchlorate was not sufficiently degraded, so there was no overlap between the degradation of MTBSTFA/DMF and calcium perchlorate. Therefore, chlorobenzene was not been detected following SAM-like pyrolysis, demonstrating that MTBSTFA/DMF cannot be a source of chlorobenzene in SAM, This result is consistent with the conclusions of Freissinet et al. [57] for the chlorobenzene detected by SAM. In conclusion, the calcium perchlorate has no obvious influence on the performance of MTBSTFA/DMF.

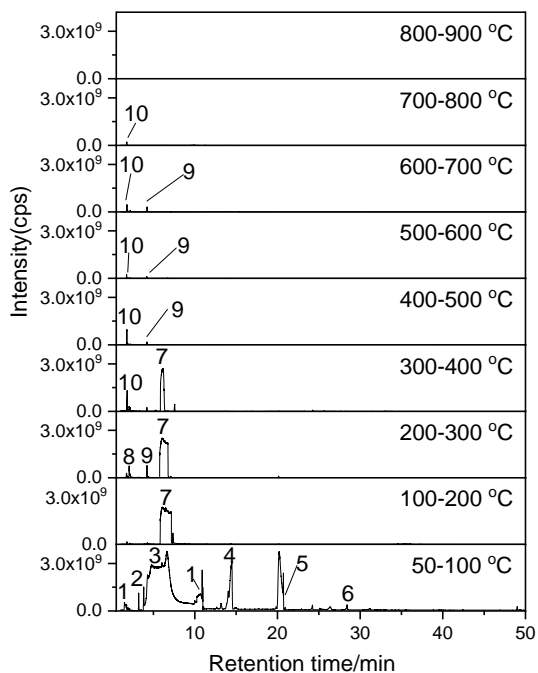


Figure 2-14: Chromatograms of MTBSTFA/DMF (4:1) stepped pyrolysis with 15wt% of  $\text{ClO}_4^-$  at different temperatures. Peak 1: tert-Butyldimethylsilanol; 2: tert-butyldimethylfluorosilane; 3: TFMA; 4: N-Methyl-N-(trimethylsilyl)trifluoroacetamide; 5: BSW; 6: Tris(trimethylsilyl)borate; 7: DMF; 8: trimethylamine; 9: N,N-dimethyltrifluoroacetamide; 10: Carbon dioxide.

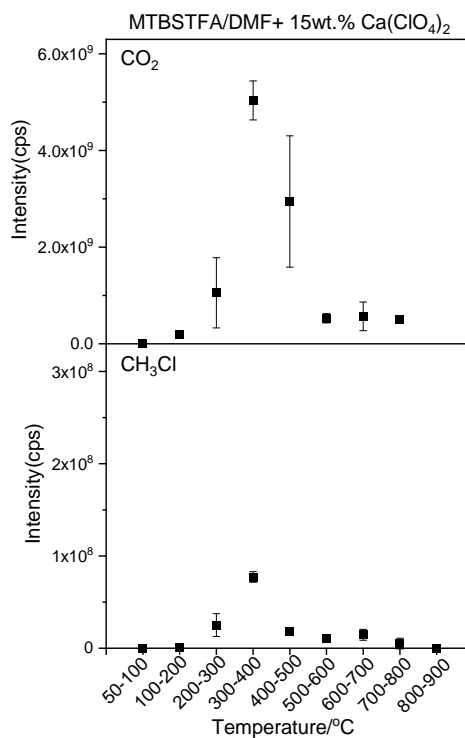


Figure 2-15: Distribution of  $\text{CO}_2$  and  $\text{CH}_3\text{Cl}$  of MTBSTFA/DMF (4:1) step pyrolysis with 15wt.% of  $\text{ClO}_4^-$  at different temperatures.



### **2.4.3 Consequences on the origin of chlorine bearing organic molecules detected from the pyrolysis of Martian rock samples with the SAM experiment**

Chlorobenzene (~150 to 300 ppbw) has been detected on Mars by the SAM experiment onboard the *Curiosity* Rover [57]. The possible sources of the carbon component of the chlorobenzene could be from the derivatization reagent MTBSTFA/DMF [56,64] or the indigenous functionalized aromatic compounds indigenous to the Martian sample. However, no chlorobenzene was detected in the pyrolysis of MTBSTFA/DMF in the presence of calcium perchlorate in this study. Therefore, MTBSTFA/DMF should not be a likely source of carbon of chlorobenzene in our experiments. Therefore, MTBSTFA/DMF should not be a likely source of the carbon component of the chlorobenzene detected by SAM based on our experiments. Thus, we can reasonably assume that indigenous organic compounds could be one of the possible sources of the chlorobenzene. In order to test our hypothesis, 5 wt.% calcium perchlorate was applied to a sample of the Murchison meteorite and underwent flash pyrolysis at 850 °C.

#### ***2.4.3.1 The formation of organic compounds from the pyrolysis of the Murchison meteorite***

Several organic compounds have been detected in samples of the Murchison meteorite. The soluble organic compounds include sugars derivatives [42], amino acids [39], nucleobases [40], amines and amides [41], etc. Among these soluble organic compounds, carboxylic acids (330 ppm) are the most abundant [215]. These compounds could be decomposed easily when the Murchison sample is pyrolyzed at high temperatures. The insoluble organic matter present in the Murchison meteorite is mainly in the form of aromatic structures; only 20 to 30 % of the carbon constitutes aliphatic bonds, which represents the aliphatic bridge among aromatic units [214]. These macromolecular structures could be destroyed by thermal pyrolysis and decomposed into light aromatics and polyaromatic compounds [270,463,464]. Indeed, mainly aromatic compounds were identified following the flash pyrolysis at 850 °C of the Murchison meteorite (Figure 2-9). Remusat et al. [590] also detected aromatic compounds such as benzene, naphthalene, and pyrene from the pyrolysis of the Murchison meteorite at 900 °C. In addition, phenylpropionic acid was detected in our results, which could be from the decomposition of the skeleton structure of inorganic matter present in the Murchison sample. This is consistent with results that suggest the presence of carboxylic acid functional groups in the molecular modeling of Murchison inorganic matters [591].

S-containing compounds, mainly occurring as thiophenes, have been detected in Murchison meteorite samples [214]. In this study, S-bearing compounds such as sulfur oxide, taurine, thiophene, benzenethiol, thianaphthene, phenaleno[1,9-bc]thiophene and their isomers have been detected from the pyrolysis of the Murchison sample. These sulfur-bearing compounds have been previously identified [45,590,592,593] in Murchison samples.

#### ***2.4.3.2 The formation of Cl-containing compounds from the pyrolysis of the Murchison meteorite***

It has been confirmed that carboxylic acids containing a benzene ring, rather than benzene or toluene, are the preferred precursor of chlorinated benzene detected by SAM [572]. The organic compounds contained in the Murchison sample, such as carboxylic acids, aromatic hydrocarbons, aliphatic hydrocarbons, etc. [214], could be the possible precursors of the Cl-containing aromatics detected following the reaction of the Murchison sample and calcium perchlorate. In addition, benzene can be readily chlorinated in gas phase reactions with Cl<sub>2</sub> at elevated temperatures through the mechanism of chlorine radicals [594]. However, when there is water, HCl would be released from the decomposition of calcium perchlorate at pyrolysis temperatures higher than 450 °C [56].

In this study, Murchison samples and calcium perchlorate were pyrolyzed at 850 °C, which was high enough to produce Cl• radicals. With the degradation of the skeleton structure of the Murchison sample, a huge number of aromatic units, especially benzene radicals with one or more active sites could be formed. The formation of benzene radicals could accelerate the formation of chlorine-bearing aromatics. Indeed, chlorobenzene, dichlorobenzene, trichlorobenzene, tetra-chlorobenzene, and penta-chlorobenzene were detected. Among these Cl-bearing aromatics, the intensity of chlorobenzene was the highest among these chlorinated benzenes following the pyrolysis of the Murchison meteorite in the presence of calcium perchlorate (Figure 10). No Cl-bearing aromatics were formed when the Murchison residue was pyrolyzed with calcium perchlorate, which demonstrates that the organic carbon present in the Murchison meteorite was the carbon source of Cl-bearing aromatic compounds.

In addition, dichlorobenzene isomers (~0.5 to 17 ppbw) and trichloromethylpropane were also detected by the SAM instrument [223]. Szopa et al. (2020) also reported that polycyclic aromatic hydrocarbons, amino acids, and carboxylic acids would be plausible organic precursors of the chlorinated aromatic molecules detected with SAM. Therefore, our results confirm that indigenous carbon, especially aromatic units, could be the carbon source of the chlorobenzene that has been detected on Mars by Viking and Curiosity's SAM [57,59].

However, the effect of sulfur- and nitrogen-bearing functional groups, especially as components of aromatic compounds, on the formation of Cl-bearing compounds will need a further study in the future.

## 2.5 Conclusion

Here we report the pyrolysis products of MTBSTFA/DMF at the different temperatures of 210, 300, 600 and 850 °C, both in the absence and presence of calcium perchlorate. Results demonstrate that MTBSTFA/DMF can be used effectively below 300 °C during flash pyrolysis, resulting in relatively few products. TFMA, MSW, and BSW were the main products, formed after the cracking of the N-Si bond from the TBDMS derivatization functional group during the pyrolysis process. Far more F-containing compounds were formed when the pyrolysis temperature was increased to 850 °C, which demonstrates the F-C bond breakage is enhanced at high temperature. Various aromatics were formed, such as benzene, toluene, naphthalene, fluoranthene, and pyrene. Chloromethane and chloro-*tert*-butylmethylsilane were also detected. In addition, compared with the numbers of products of MTBSTFA/DMF flash pyrolysis, less products of MTBSTFA/DMF were detected during SAM-like ramp pyrolysis across all final temperatures; therefore, we conclude that MTBSTFA/DMF can be used with a slow heating rate with a final temperature up to 850 °C. The presence of calcium perchlorate has no obvious effect on the ramp pyrolysis of MTBSTFA/DMF, additional validation that this reagent is a good fit for the SAM and MOMA experimental operations. Finally, our results confirm that the chlorobenzene that has been detected by SAM is probably from the indigenous carbon (especially macromolecular aromatic structures) present in the Martian sample.



# Chapter 3. Influence of calcium perchlorate on the search for organics on Mars with TMAH thermochemolysis

## 3.1 Introduction

NASA's 2008 Phoenix Mars lander and its wet chemistry laboratory (WCL) was the first experiment on Mars which detected ~0.4-0.6 wt.%  $\text{ClO}_4^-$  ions in the Martian soil [54]. After this initial *in situ* detection, calcium and magnesium perchlorates were identified at the landing site [54], and Kounaves *et al.*, (2014) [65] concluded that the soil samples analyzed by the Phoenix WCL could be composed of an ~3:2 ratio of  $\text{Ca}(\text{ClO}_4)_2$  to  $\text{Mg}(\text{ClO}_4)_2$  phases. Later, chlorine bearing compounds were detected by the Sample Analysis at Mars (SAM) instrument, one of ten instruments on the Mars Science Laboratory (MSL) Curiosity rover, such as hydrogen chloride gas, chloromethane, dichloromethane, chlorobenzene [61], and isomers of dichlorobenzene [62]. These chlorine-bearing hydrocarbons have been attributed to the reaction of oxychlorine related species with organic compounds during the pyrolysis of the samples analyzed with SAM [57,62]. From these results, a reinterpretation of the data obtained with the GCMS experiment onboard the 1976 Viking landers suggests that perchlorates and/or chlorates were also present in the samples analyzed by these experiments [59,63]. Further, analysis of the Rocknest wind ripple with the SAM instrument and a comparison with results obtained from laboratory measurements indicates that calcium perchlorate is a better candidate for the perchlorate species than Fe-, Mg-, Na- and K-perchlorates [64]. More recently, chloride-bearing hydrocarbons have been produced by the reaction of oxychlorine related species with organics in SAM's pyrolysis oven. This led to the conclusion that in modern sand deposits and some much older rocks, Ca and Mg perchlorate are the most likely sources of chlorine related products [57,62].

The detection of widespread perchlorates and likely chlorates on Mars led to several studies related to the potential effect of perchlorates on the detection of organic compounds with various instruments. Perchlorate is a strong oxidizing agent because oxygen can be released from the decomposition of perchlorates and could be the main cause of the degradation of organic compounds. The thermal decomposition of perchlorates, including lithium, sodium, potassium, magnesium, iron, aluminum, and calcium perchlorates, have been analyzed by using a thermobalance from previous experiments [595]. Two possible mechanisms for the thermal

decomposition of a perchlorate were proposed [595]: (1) by gradual hydrolysis of hydrated compounds to yield perchloric acid and an oxide, such as magnesium, iron, and aluminum perchlorates, and (2) by dehydration followed by decomposition to yield oxygen and chloride, as in the case of lithium (~440 °C), sodium (~480 °C), potassium (~540 °C), and calcium (~405 °C) perchlorates. The salts may be dehydrated first and then decomposed when the temperature is high enough to force their release.

The temperature of oxygen release from perchlorate can be affected by other minerals present in a solid sample. For example, the decomposition temperature of calcium perchlorate or another oxychlorine species can decrease due to the presence of iron phases [366,596]. Regardless of the perchlorate phase, oxygen will be released from any perchlorate in solid samples on Mars when the SAM instrument ovens are heated, leading to the oxidation of organic compounds into carbon dioxide. The main consequence of this is that organic matter is degraded and would not be detected [61]. Furthermore, the abundance of oxychlorides varies by one order of magnitude [597]. Some experiments have shown that there should be a minimum ratio of 4.7:1 between organic matter and perchlorate to ensure the detection of organic molecules with Pyr-GC/MS [598] without major impact from the perchlorate. In addition, hydrogen chloride (HCl) produced during the thermal decomposition of Martian perchlorate can react with soil carbonates leading to low temperature inorganic CO<sub>2</sub> release, and the presence of calcium chloride (CaCl<sub>2</sub>) which is formed from the reaction between calcite and hydrogen chloride, and has been confirmed by X-ray diffraction (XRD) experiments [599]. Therefore, the detection of organic fragments, not CO<sub>2</sub> alone, should be used as definitive evidence for organics in Martian soils [599].

Perchlorate not only affects the type and the number of organic compounds detected [600], it can also react with organic compounds to form chlorine-related compounds. For example, Guzman et al., (2018) [59] observed the presence of chlorobenzene at a concentration of 0.08 to 1.0 ppb (relative to sample mass) in Viking Lander 2 (VL-2) data at a pyrolysis temperature between 350 and 500 °C. They concluded that the reaction of indigenous organic carbon and instrument contamination with Martian perchlorate during the pyrolysis process is the likely source of the chlorobenzene. Laboratory experiments confirm that perchlorates mixed with organic molecules with different molecular weights (low, medium, or high) will form chloride related gases such as hydrogen chloride (HCl), carbonyl dichloride (CCl<sub>2</sub>O), and carbon tetrachloride (CCl<sub>4</sub>) [601]. However, Montgomery et al. [288] reported that the presence of perchlorate and other oxyanion salts inhibited the detection of organic compounds when

analyzed by Pyr-GC/MS; removing perchlorates and sulfates of Atacama Desert showed identifiable biomarkers associated with cyanobacteria.

Both the Mars Organic Molecule Analyzer (MOMA) instrument onboard the ESA/Roscosmos ExoMars rover and the SAM instrument on the NASA Curiosity rover can detect organic molecules. MOMA and SAM are both analytical suites that utilize Pyr-GC/MS. MOMA carries three derivatization/thermochemolysis agents [602], i.e. N-tert-Butyldimethylsilyl-N-methyltrifluoroacetamide/ N,N-Dimethylformamide (MTBSTFA/ DMF, for carboxylic and amino acids, nucleobases, amines, and alcohols), N,N-Dimethylformamide dimethyl acetal (DMF-DMA, for amino acids, fatty acids, and primary amines with chiral centers), and TMAH in methanol (for lipids and fatty acids, when driven to higher temperatures). SAM carries only MTBSTFA/ DMF and TMAH in methanol [2]. These derivatization/thermochemolysis agents increase the volatility of organic molecules with labile groups such as amino acids, carboxylic acids, nucleobases [558], etc. TMAH is very useful for the liberation of polar molecules from macromolecules and the volatilization of fatty acids but the decomposition of TMAH at elevated temperatures above 500 °C [340] can cause additional issues that complicate organics detection. The degradation of TMAH at relatively low temperatures (lower than 200 °C) has been studied and different TMAH degradation mechanisms have been reported [549,552,554,555], but no study has reported on the byproducts of TMAH pyrolysis at elevated temperatures.

The thermal degradation of TMAH can proceed via two different pathways. The first pathway is a nucleophilic substitution reaction mechanism (the bi-molecular or S<sub>N</sub>2 pathway) defined by the synchronous formation of one bond as another bond is broken. In this case it is the nucleophilic attack by OH<sup>-</sup> on the CH<sub>3</sub> group that produces trimethylamine (TMA) and dimethyl ether [549]. The second pathway is the ylide one wherein the decomposition of TMAH to give TMA and dimethyl ether results from the initial removal of a proton from the quaternary ammonium salt followed by the decomposition of the resulting ylide [551]. For example, Macomber et al., (2008) [550] actually have been doing experiments with D-labeled TMAH in order to work out the mechanism of TMAH decomposition, using Differential Scanning Calorimetry (DSC), Thermal Gravimetry (TG), and Evolved Gas Analysis (EGA). They concluded that TMA, methanol and dimethyl ether were the main resulting products. The extraction of the  $\alpha$ -proton to generate a nitrogen ylide is an important degradation mechanism for methyl ammonium species. Deprotonation of the tetramethyl ammonium ion by hydroxide establishes a rapid equilibrium between the tetramethylammonium ion and the nitrogen ylide species and water that combines the deuterium with the proton in the methyl groups. Then, the

methoxide formed in this way reacts with  $[\text{Me}_4\text{N}]^+$  via an  $\text{S}_{\text{N}}2$  process to generate dimethyl ester. However, Chempath et al., (2008) [552] proposed that the ylide pathway is more reasonable than the  $\text{S}_{\text{N}}2$  pathway. These researchers performed TG-MS experiments in order to evaluate the stability of tetramethylammonium ( $[\text{N}(\text{CH}_3)_4^+]$ ) under aqueous conditions in the presence of  $\text{OH}^-$  ions. They verified the H-D exchange and their results demonstrated that the ylide mechanism plays a crucial role on the decomposition of TMAH. Moreover, they confirmed this pathway by calculation of the energy of the activation barrier and they proved that it is lower than for the  $\text{S}_{\text{N}}2$  pathway. Finally, the ylide pathway can give rise to unstable intermediates with side reaction including the Stevens rearrangement reactions [553], Sommelet-Hauser rearrangement, and Hofmann elimination [554]. Hofmann elimination is a vulnerable pathway for degradation of n-alkyl- tetramethylammonium ( $\text{TMA}^+$ ) cations [555]. However, this barrier is also found to depend on the carbon chain length because of steric interference and number of hydrogens susceptible to Hofmann elimination [555].  $\text{OH}^-$  can attack the  $\alpha$ -carbon atom and the cation degrades by the  $\text{S}_{\text{N}}2$  pathways. Edson et al., (2012) [27] studied the effect of the number of  $\beta$ -hydrogen atoms susceptible to Hofmann elimination and the mechanism of different alkyltrimethylammonium cations in deuterioxide form using evolved gas analysis (EGA) (Figure 3-1). The Hofmann elimination is the preferred decomposition pathway for ammonium cations bearing  $\beta$ -hydrogens, and ylide formation reorganizes protons from water into TMA that is formed with a low activation barrier. The stability of cations increased with the blocking of  $\beta$ -hydrogens, and without  $\beta$ -hydrogen,  $\text{S}_{\text{N}}2$  reactions occurred, as shown in Figure 3-1. However, no studies report the degradation mechanism of TMAH at high temperature.

To distinguish the source of chlorinated organic compounds detected by the SAM instrument [51], Miller et al., (2015) [573] evaluated possible carbon sources with and without the Tenax® trap, which is used to concentrate the evolved species from the Martian samples. They found that perchlorates have nearly no effect on the Tenax® trap on board SAM when the trap is not heated above 300°C. In laboratory experiments there is rare degradation of the trap after hundreds of pyrolysis experiments of Mars analogue soils doped with perchlorates (calcium perchlorate, magnesium perchlorate, or iron chloride). Moreover, the effect of calcium perchlorate on the degradation of Tenax® and the subsequent byproducts have been studied [60]. The byproducts of perchlorates have an impact on the degradation products of Tenax®, such as chlorinated phenyl molecules, chlorobenzaldehyde, chlorophthalic acid, chlorobiphenyl etc. To date, few studies have reported on the effect of perchlorate on the function of derivatization agents, especially TMAH, at high temperature (600°C). Thus, the influence of



perchlorate on the function of TMAH thermochemolysis must be studied to best understand the potential influence of perchlorates on the TMAH experiment on the SAM and MOMA instruments.

This study explores the degradation of TMAH and the effect of calcium perchlorate on TMAH pyrolysis at 600 °C (with different heating ramps, including flash pyrolysis and SAM-like ramp pyrolysis at 35°C.min<sup>-1</sup>) using Pyr-GC/MS with a hydrocarbon trap. From these results we propose a mechanism for TMAH degradation at a high pyrolysis temperature (600 °C) in the presence of calcium perchlorate. These results provide important foundational data for the interpretation of the origin of organic molecules detected by SAM and MOMA.

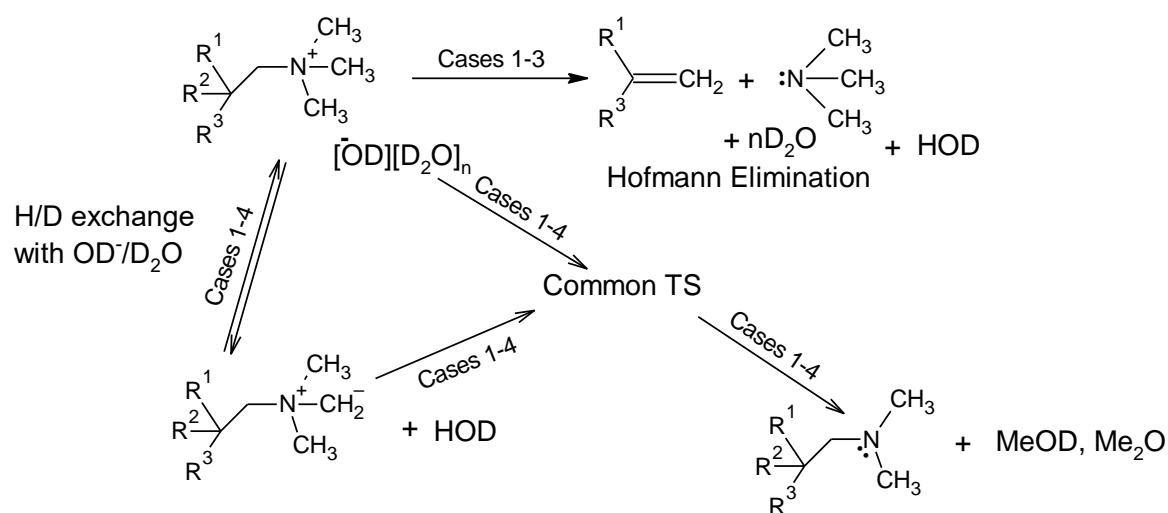


Figure 3-1 Thermal decomposition of alkyltrimethylammonium deuterioxide[27]. Case 1: R<sup>1</sup>, R<sup>2</sup>, and R<sup>3</sup> =H; Case 2: R<sup>1</sup>=CH<sub>3</sub>, R<sup>2</sup> and R<sup>3</sup>=H; Case 3: R<sup>2</sup>=H, R<sup>1</sup>and R<sup>3</sup>=CH<sub>3</sub>; Case 4: R<sup>1</sup>, R<sup>2</sup>, and R<sup>3</sup>=CH<sub>3</sub>. TS=Transition State.

## 3.2. Experimental design

### 3.2.1 Samples and chemical products

A TMAH solution (25% by weight in methanol, Sigma-Aldrich) was used in this study and calcium perchlorate tetrahydrate (99%, Aldrich) was used to make the calcium perchlorate solution. Naphthalene-d<sub>8</sub> (Sigma-Aldrich, isotopic purity, 99 atom % D) was used as an internal standard. The concentration of calcium perchlorate solution (0.85 mol.L<sup>-1</sup>) was measured by Atomic Absorption Spectrometry [574–577] (Varian Australia Pty Ltd ), using air-acetylene flame test, with a calcium cathode lamp set at the 422.7 nm resonance wavelength.

The abundance of  $ClO_4^-$  to TMAH solution (wt.%) is given by the following equation (1):

$$wt. \% = \frac{2C_{Ca(ClO_4)_2} \cdot V_{Ca(ClO_4)_2} \cdot M_{ClO_4^-}}{V_{TMAH} \cdot \rho_{TMAH}} \% \quad (1)$$

where  $C_{Ca(ClO_4)_2}$  is the concentration of  $Ca(ClO_4)_2$  solution of  $0.85 \text{ mol.L}^{-1}$ ;

$M_{ClO_4^-}$  is the molar mass of  $ClO_4^-$ ,  $99.45 \text{ g.mol}^{-1}$ ;

$V_{Ca(ClO_4)_2}$  is the volume of  $Ca(ClO_4)_2$  solution ;

$V_{TMAH}$  is the volume of TMAH,  $3\mu\text{l}$ ; and

$\rho_{TMAH}$  is the density of TMAH solution :  $0.866 \mu\text{g.mL}^{-1}$ .

The effect of different wt.% of  $ClO_4^-$ , (0.1, 0.5, 1.0, 2.0, 3.0, 4.0, 5.0, 10.0, 15.0, 20.0, 30.0, 40.0 wt.% ) on TMAH pyrolysis at  $600^\circ\text{C}$  was studied. The calcium perchlorate was dried at room temperature under a dinitrogen flow for 3 hours and the water abundance in the sample was measured by Karl Fischer method with an Aqua processeur radiometer[578–582]. The calibration curve of the moisture detection is shown in Figure 3-2. Results show that the content of moisture within the capsule is less than 1.6 % and 0.7% when the calcium perchlorate abundance is 40 wt. % and 15 wt. %, respectively, which ensured that the experimental conditions are more Mars like.

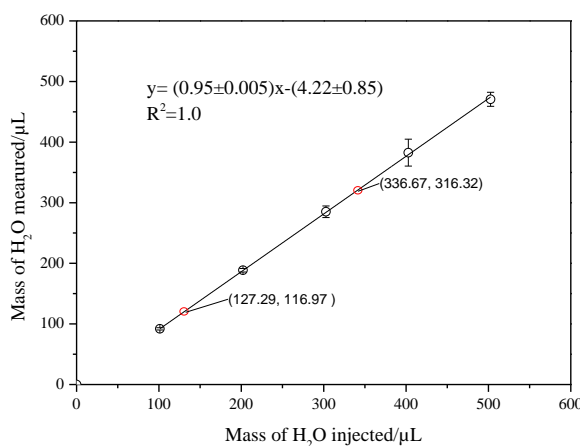


Figure 3-2 The calibration curve of  $H_2O$  detection

Individual solutions of octanoic acid (C8, Aldrich,  $\geq 98\%$ ), nonanoic acid, Kosher (C9, SAFC,  $\geq 96\%$ ), decanoic acid (C10, Sigma Grade,  $\geq 98.0\%$ ), undecanoic acid (C11, Fluka,  $\geq 97.0\%$ ), Lauric acid (C12, sigma-aldrich,  $\geq 98.0\%$ ), tridecanoic acid (C13, Sigma Grade,  $\geq 98.0\%$ ), myristic acid (C14, Sigma Grade, 99-100%), pentadecanoic acid (C15, Sigma Grade, approx.99%), palmitic acid (C16, Sigma Grade,  $\geq 99.0\%$ ), heptadecanoic acid (C17, Sigma

Grade,  $\geq 98.0\%$ ), stearic acid (C18, Sigma Grade,  $\geq 98.5\%$ ), and arachidic acid (C20, sigma-Aldrich,  $\geq 99.0\%$ ) were prepared by diluting the pure fatty acids into pyridine (Aldrich, 99+%) solvent. The concentration of each fatty acid is  $0.67 \text{ mmol}\cdot\text{L}^{-1}$ . For the recovery of fatty acids with  $3 \mu\text{L}$  TMAH,  $2 \mu\text{L}$  of the fatty acid solution was used. For the recovery of fatty acids under similar conditions used on Mars by the SAM and MOMA instruments, the original fatty acids solution was diluted to 1000 times, about  $2.2 \mu\text{L}$  of diluted fatty acid solution and  $0.2 \text{ mg}$  of  $\text{ClO}_4^-$  was used, respectively.

### 3.2.2 Pyrolysis experiments

The pyrolysis experiments were performed with an EGA/PY-3030 D micro-oven pyrolyser, Frontier Lab, installed on the Split/SplitLess (SSL) injector of a Trace GC Ultra gas chromatograph (Thermo Scientific) coupled to a quadrupole mass spectrometer (ISQ LT, Thermo Scientific). Varying volumes of  $\text{Ca}(\text{ClO}_4)_2$  solution were injected in a capsule (Eco-Cup, Frontier lab) under a stream of nitrogen to dry the  $\text{Ca}(\text{ClO}_4)_2$  solution; and then  $3 \mu\text{L}$  of TMAH was injected into the capsule. That capsule carried by an eco-stick (Frontier lab) was attached to the top of the pyrolyzer.

Two kinds of pyrolysis ramps were used in this study. The first one is flash pyrolysis wherein the sample is pushed into a heated and stabilized oven at  $600 \text{ }^\circ\text{C}$  for 30 seconds, after which the sample is removed from the oven. Helium is used as the carrier gas to carry the pyrolysis volatile products into the GC/MS. The second ramp is the SAM-like ramp pyrolysis. During this process, the heart-cut EGA analysis method was used. For that, the sample cup was attached to the pyrolyzer and the pyrolyzer head space was purged for 2 minutes before proceeding. Then the sample cup was pushed inside the oven (initial temperature was  $50 \text{ }^\circ\text{C}$ ), and the oven was heated to the final temperature of  $600 \text{ }^\circ\text{C}$  (with a 1 min hold) at the SAM heating rate of  $35^\circ\text{C}\cdot\text{min}^{-1}$ . The MicroJet Cryo-trap (Frontier Lab) was used to trap and pre-concentrate at  $-180 \text{ }^\circ\text{C}$  all the released products. When the pyrolysis process was finished, the temperature of the trap was quickly increased to  $40 \text{ }^\circ\text{C}$ . All of the products then were released and sent to the GC/MS through the helium flow. Lastly, to explore the products of TMAH pyrolysis with calcium perchlorate, a stepped pyrolysis of TMAH with and without calcium perchlorate was performed. For this study, the sample was injected into the pyrolyzer and was heated at a SAM-like heating rate of  $35^\circ\text{C}\cdot\text{min}^{-1}$  from  $50 \text{ }^\circ\text{C}$  to  $100 \text{ }^\circ\text{C}$ , every increase in  $100 \text{ }^\circ\text{C}$  up to  $1000 \text{ }^\circ\text{C}$ , as  $100\text{-}200 \text{ }^\circ\text{C}$ ,  $200\text{-}300 \text{ }^\circ\text{C}$ ,  $300\text{-}400 \text{ }^\circ\text{C}$ ,  $400\text{-}500 \text{ }^\circ\text{C}$ ,  $500\text{-}600 \text{ }^\circ\text{C}$ ,  $600\text{-}700 \text{ }^\circ\text{C}$ ,  $700\text{-}800 \text{ }^\circ\text{C}$ ,  $800\text{-}900 \text{ }^\circ\text{C}$ , and  $900\text{-}1000 \text{ }^\circ\text{C}$ . All experiments were repeated more than 3 times.

### 3.2.3 GC/MS analysis

Analyses were conducted with a Trace GC Ultra gas chromatograph (Thermo Scientific) coupled to a quadrupole mass spectrometer (ISQ LT, Thermo Scientific). The GC is equipped with a Supelco SLB-5MS Inferno column (30 m × 0.25 mm i.d. × 0.25 μm film thickness) with 5m integrated guard column. For the flash pyrolysis, the temperature programming of the column starts at 40 °C held for 2 min, then at a heat rate of 3 °C min<sup>-1</sup> up to 200 °C then raised to 300 °C at a rate of 6 °C min<sup>-1</sup> and maintained for 1 min. To mimic the SAM ramp, the temperature programming of the column starts at 40 °C hold for 2 min, then at a heat rate of 6 °C min<sup>-1</sup> up to 300 °C and maintained 1 min. In both ramps, helium was used as the carrier gas and the helium flow rate in the column was 1.2 mL.min<sup>-1</sup>. The split flow was 24 mL.min<sup>-1</sup>. The temperature of the SSL injector was set at 280 °C. The masses were scanned between *m/z* 40 and *m/z* 500. The ionization energy was 70 eV.

The relative abundance of the compounds was obtained through the following formula:

$$C_i = \frac{\frac{A_i}{A_{is}}}{\sum \frac{A_i}{A_{is}}} \times 100\%$$

Where  $A_i$  and  $A_{is}$  refer to the peak areas of the products and the peak area of the internal standard, respectively.

## 3.3 Results and discussion

### 3.3.1 Flash pyrolysis of TMAH at 600 °C

#### 3.3.1.1 Products of TMAH treated with flash pyrolysis at 600 °C

Flash pyrolysis is a high temperature process, in which the sample is rapidly heated at a very high heating and heat transfer rate in the absence of air[603]. Samples treated with the flash pyrolysis method almost always yield a greater number and diversity of fatty acid methyl esters than ramped pyrolysis, because the flash pyrolysis step of macromolecules with TMAH thermochemolysis is higher efficient [22]. Therefore, the flash pyrolysis products of TMAH at 600 °C were analyzed. Figure 3-3 shows the chromatogram of TMAH pyrolysis at 600 °C, and all products released from flash pyrolysis are listed in Table 3-1. Most of the byproducts of TMAH pyrolysis were detected from the retention time of 1.0 to 5.0 min; the naphthalene-d8 (internal standard) was eluted at the retention time of 14.80 min. TMA ( eluted at 2.06-2.29 min) and dimethyl ether (eluted at 1.95 min) are the main products of TMAH flash pyrolysis degradation at 600 °C. The production yield of TMA and dimethyl ether is *ca.* 48% and 25%,

respectively, and carbon dioxide formed during the TMAH pyrolysis process accounts for 15% of all pyrolysis products from TMAH pyrolysis. Other nitrogen bearing compounds account for 12% of all pyrolysis products from TMAH flash pyrolysis, such as N- methyl-ethylamine, N, N-dimethyl-ethylamine, and the N-O containing compounds such as urea. Various siloxane compounds were detected at different retention times of 6.60, 6.80, 10.69, 11.0, and 13.79 min, which were caused by the column bleeding, a loss of its stationary phase (5% diphenyl/95% dimethyl siloxane).

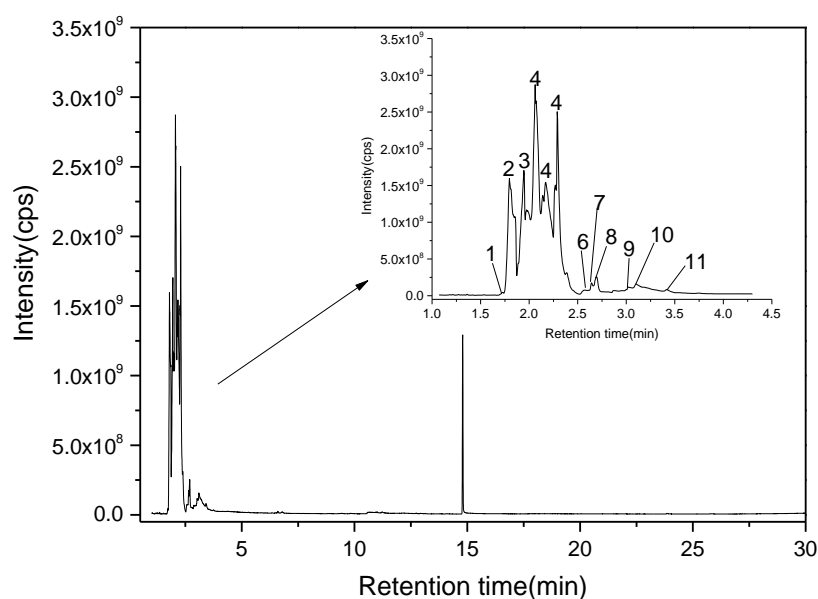


Figure 3-3 The chromatogram of TMAH flash pyrolysis at 600 °C. Peak 1: CO<sub>2</sub>; Peak 2: 3-Aminobutanoic acid; Peak 3: Dimethyl ether; Peak 4: Trimethylamine; Peak 5: Dimethoxy-methane; Peak 6: N- methyl-ethylamine; Peak 7: Urea; Peak 8, 9: N,N-dimethyl-ethylamine; Peak 10: Betaine; Peak 11: 1, 2-dimethoxy-ethane.

During the flash pyrolysis of TMAH at 600 °C, radicals such as  $\cdot\text{H}$ ,  $\cdot\text{CH}_3$ ,  $\cdot\text{CH}_2$ ,  $\cdot\text{CH}_2$  ( $\text{CH}_3$ )<sub>3</sub>N<sup>+</sup>,  $\cdot\text{CH}_2$ ( $\text{CH}_3$ )<sub>2</sub>N<sup>+</sup>, etc., were formed because of the cracking of the bond of nitrogen and a methyl group, the bond of C-H bond in the methyl functional group, and the recombination of these radicals. For example, the hydrogen radicals stabilize the structure of ( $\text{CH}_3$ )<sub>2</sub>N<sup>+</sup>CH<sub>2</sub>- and TMA was formed [556]. The Hoffman elimination plays a key role in alkene formation, the aromatization of alkenes producing aromatics, such as benzene, and N, N-dimethyl-benzenemethanamine formation from the combination of benzene radicals and ( $\text{CH}_3$ )<sub>2</sub>N<sup>+</sup>CH<sub>2</sub>-. Methanol could be formed through the demethylation of TMAH and the combination of methyl functional group with the OH radicals, and dimethyl ether was formed through the dehydration of methanol. The aldehyde product ( $\text{CH}_3$ )<sub>3</sub>N<sup>+</sup>CHO, could be generated

by the hydrolysis reaction of carbon center radicals, and the aldehyde products could be oxidized by the oxygen radicals from the system and to form the carboxylic acids at high temperature. The possible route of TMAH degradation is shown in Figure 3-4.

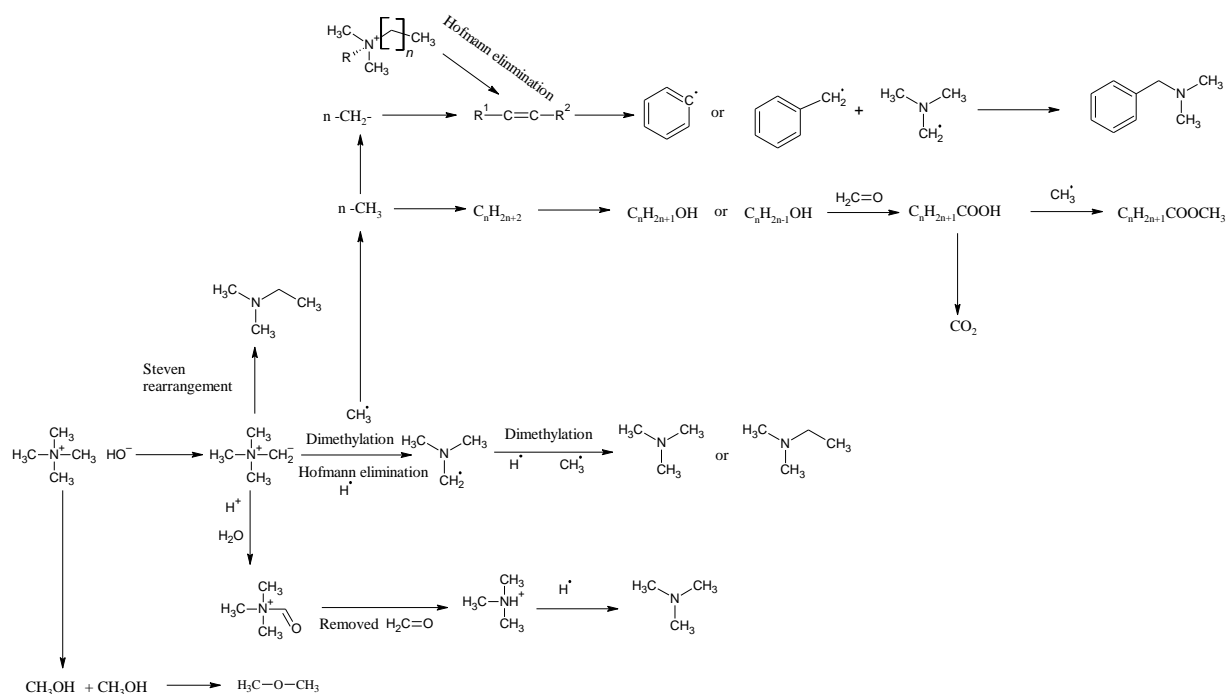


Figure 3-4 The mechanism of TMAH degradation via flash pyrolysis.


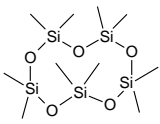
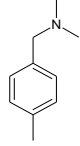
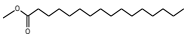
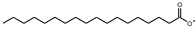
Table 3-1 The pyrolysis products of TMAH flash pyrolysis at 600 °C, refers to Figure 3-3.

Num.	RT/ min	Masses of fragments* and relative abundance: m/z (%)	Empirical formula	Compounds	Structure
1	1.73	44(100)	CO <sub>2</sub>	Carbon dioxide	CO <sub>2</sub>
2	1.80	44(100), 45(54), 46(28)	C <sub>2</sub> H <sub>5</sub> NO <sub>3</sub>	3-Aminobutanoic acid	
3	1.95	45(100), 46(74)	C <sub>2</sub> H <sub>6</sub> O	Dimethyl ether	
4	2.06- 2.29	58(100), 59(69), 42(36), 57(15), 45(12), 56(10)	C <sub>3</sub> H <sub>9</sub> N	Trimethylamine	
5	2.38	45(100), 75(81), 58(64), 59(31), 42(18), 44(14)	C <sub>3</sub> H <sub>8</sub> O <sub>2</sub>	Dimethoxy-methane	
6	2.58	44(100), 58(69), 59(34), 42(19)	C <sub>3</sub> H <sub>9</sub> N	N- methyl-ethylamine	
7	2.64/ 2.69	61(100), 58(19), 42(17), 45(16), 44(16)	CH <sub>4</sub> N <sub>2</sub> O	Urea	

Table 3-1 (Continued)

Num.	RT/ min	Masses of fragments* and relative abundance: m/z (%)	Empirical formula	Compounds	Structure
8	2.87, 3.02	73(100),72(81),58(77),56(18)	C <sub>4</sub> H <sub>11</sub> N	N,N-dimethyl-ethylamine	
9	3.10	58(100), 57(51), 73(33), 72(25), 44(14), 88(13), 56(12)	C <sub>5</sub> H <sub>13</sub> N	Betaine	
10	3.42	45(100), 60(24), 78(22), 58(12), 90(7)	C <sub>4</sub> H <sub>10</sub> O <sub>2</sub>	1, 2-dimethoxy-ethane	
11	3.75	58(100), 42(30), 43(31), 44(29), 45(28), 59(22), 73(18), 72(16), 41(16), 71(12)	C <sub>4</sub> H <sub>11</sub> N	N, 1-dimethyl-ethylamine	
12	6.60, 6.80	207(100), 44(48), 208(19), 96(12), 191(12), 209(12), 133(7)	C <sub>6</sub> H <sub>18</sub> O <sub>3</sub> Si <sub>3</sub>	Hexamethyl-Cyclotrisiloxane (from column bleeding)	
13	9.30	58(100), 117(10), 44(27), 42(10)	C <sub>5</sub> H <sub>11</sub> NO <sub>2</sub>	Glycine, N,N-dimethyl, methyl ester[ Methyl(dimethylamino) acetate]	
14	9.41	59(100), 89(76), 45(50), 58(50), 43(23), 102(23), 88(15), 71(14)	C <sub>6</sub> H <sub>14</sub> O <sub>3</sub>	1,2,3- trimethoxy-propane Glycerol trimethyl ether	
15	9.82	72(100),74(21), 43(12), 42(10)	C <sub>5</sub> H <sub>11</sub> N <sub>3</sub> O <sub>2</sub>	N,N,1-trimethyl-Ethylamine	
16	10.69 ,11.0	281(100), 58(87), 282(29), 265(21), 42(19), 249(14), 207(7), 191(10), 133(12)	C <sub>8</sub> H <sub>24</sub> O <sub>4</sub> Si <sub>4</sub>	Octamethyl- Cyclotetrasiloxane (from column bleeding)	
17	11.22	91(100), 121(63), 122(55), 92(31), 77(30), 65(20), 56(14), 69(11)	C <sub>8</sub> H <sub>10</sub> O	Benzyl methyl ether	
18	12.20	87(100), 57(79), 102(54), 59(30), 101(20), 115(17), 130(12), 55(12), 129(11)	C <sub>9</sub> H <sub>18</sub> O <sub>2</sub>	Hexanoic acid-2-ethyl-methyl ester	
19	12.72	45(100), 75(34), 144(26), 85(23), 99(18), 69(18), 129(14), 41(13), 97(10), 55(10)	C <sub>10</sub> H <sub>22</sub> O <sub>4</sub>	2-[2-(2- butoxyethoxy)ethoxy]-ethanol/ Buyoxytriethylene glycol	
20	12.93	58(100), 91(70), 135(61), 134(40), 57(57), 65(17), 44(43), 92(14), 42(25), 118(11)	C <sub>9</sub> H <sub>13</sub> N	N,N,4-Ddimethyl- Benzenemethamine	

Table 3-1 (Continued)

Num.	RT/ min	Masses of fragments* and relative abundance: m/z (%)	Empirical formula	Compounds	Structure
21	13.13	58(100), 56(41), 55(40), 41(27), 70(28), 57(21), 83(21), 91(21), 97(11), 134(14)	C <sub>13</sub> H <sub>28</sub> O	n-Tridecanol	
22	13.79	73(100), 267(67), 355(39), 74(34), 105(20), 268(16), 356(14), 269(12), 357(11)	C <sub>10</sub> H <sub>30</sub> O <sub>5</sub> Si <sub>5</sub>	Decamethyl- Cyclopentasiloxane (from column bleeding)	
23	14.06	104(100), 58(88), 149(58), 105(56), 44(46), 77(26), 78(18), 79(16), 42(15), 41(11)	C <sub>12</sub> H <sub>20</sub> N <sub>2</sub>	N,N,4-tetramethyl-1,3- Benznedimethanamine	
24	23.85	74(100), 87(69), 143(19), 55(26), 43(24), 129(10), 227(15), 171(8), 199(8), 207(15)	C <sub>17</sub> H <sub>34</sub> O <sub>2</sub>	Hexadecanoic acid methyl ester	
25	25.78	74(100), 87(73), 207(55), 55(32), 43(23), 69(21), 143(18), 75(19), 96(15), 281(14), 199(13), 255(10), 97(9), 191(9)	C <sub>19</sub> H <sub>38</sub> O <sub>2</sub>	Methyl stearate	

### 3.3.1.2 Effect of Ca(ClO<sub>4</sub>)<sub>2</sub> on flash pyrolysis of TMAH

As described previously, perchlorates have been detected on Mars, with calcium perchlorate thought to be the main source of chlorine [61]. Therefore, the influence of calcium perchlorate on the pyrolysis behavior of TMAH was investigated; in particular the pyrolysis behavior of TMAH with calcium perchlorate in different concentrations (0.1, 0.5, 1.0, 2.0, 3.0, 4.0, 5.0, 10.0 and 15.0 wt. %) was studied. The resulting chromatograms are shown in Figure 3-5. When the perchlorate abundance is lower than 2 wt.%, few new products formed during the flash pyrolysis of TMAH. When the abundance of perchlorate is higher than 2 wt.%, new products were detected such as (dimethylamino)acetonitrile (Rt : 5.33 min) and dimethyl cyanamide (RT : 5.80 min) with the C≡N bond, N, N-dimethylformamide (DMF) with the aldehyde functional group eluted at 6.26 min, hexahydro-1,3,5-trimethyl-1, 3, 5-triazine (TMTAC) with a six-membered heterocyclic aromatic ring eluted at 11.10 min. Pyrrole was formed during the pyrolysis of TMAH, such as 2,5-dimethyl-pyrrole at the retention time of 7.49 min and 4-ethyl-2-methyl-pyrrole at the retention time of 9.83 min. The products of TMAH pyrolysis with calcium perchlorate at a concentration over 10 wt.% are listed in Table



3-2. There are only three possible Cl-containing compounds at low abundance detected in this study, including 5-chloro-2-pyridinol (RT=10.12, 12.57 min), 5-chloro-1-methylimidazole (RT=10.18, 12.0, and 12.69 min), and 4, 5-dichloro-1-methyl-imidazole (RT=15.72 min). The intensity of these peaks are at the detection limit of the instrument.

Table 3-2 The products of TMAH flash pyrolysis with calcium perchlorate over 10 wt.% at 600 °C, refers to Figure 3-5.

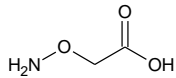
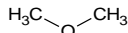
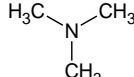
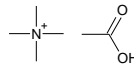
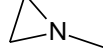
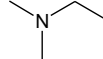
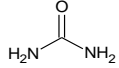
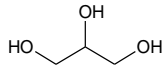
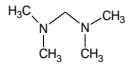
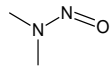
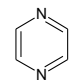
RT/ min	Masses of fragments* and relative abundance: m/z (%)	Empirical formula	Compounds	Structure
1.72,1. 91	44(100), 45(54), 46(28)	C <sub>2</sub> H <sub>5</sub> NO <sub>3</sub>	O- (Carboxymethyl)hydro xylamine	
1.79	45(100), 46(74)	C <sub>2</sub> H <sub>6</sub> O	Dimethyl ether	
2.07- 2.31	58(84),59(100),42(40),57(21)	C <sub>3</sub> H <sub>9</sub> N	Trimethylamine	
2.39	58(100), 42(44), 59(41), 43(31), 74(17)	C <sub>6</sub> H <sub>5</sub> NO <sub>2</sub>	Tetramethylammoniu m acetate	
2.52	42(100),57(61),41(13)	C <sub>3</sub> H <sub>7</sub> N	1-methyl-aziridine	
2.67,2. 97	58(100),73(29),72(24), 42(21),44(16)	C <sub>4</sub> H <sub>11</sub> N	N,N-dimethyl- ethylamine	
2.71	61(100)	CH <sub>4</sub> N <sub>2</sub> O	Urea	
2.83	61(100),45(79), 44(68), 42(27)	C <sub>3</sub> H <sub>8</sub> O <sub>3</sub>	Glycerin	
3.38,4. 67	58(100),44(20), 45(11),42(9),102 (6)	C <sub>5</sub> H <sub>14</sub> N <sub>2</sub>	N,N,N',N'- Tetramwthyl- methanediamine	
4.85	74(100),42(37),43(18)	C <sub>2</sub> H <sub>6</sub> N <sub>2</sub> O	N- Nitrosodimethylamine	
5.03	80(100) ,53(42),52(12)	C <sub>4</sub> H <sub>4</sub> N <sub>2</sub>	Pyrazine	

Table 3-2 (continued)

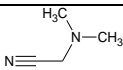
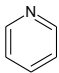
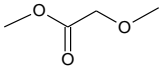
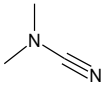
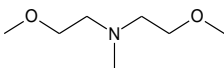
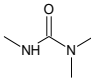
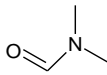
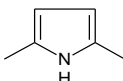
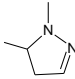
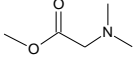
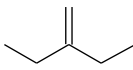
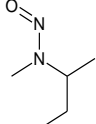
RT/ min	Masses of fragments* and relative abundance: m/z (%)	Empirical formula	Compounds	Structure
5.26	83(100),84(58),58(55),42(46), 43(10)	C <sub>4</sub> H <sub>8</sub> N <sub>2</sub>	Dimethylamino- acetonitrile	
5.58	79(100),52(57),51(30),50(21),69( 14),78(13)	C <sub>5</sub> H <sub>5</sub> N	Pyridine	
5.64	45(100),74(46),75(9)	C <sub>4</sub> H <sub>8</sub> O <sub>3</sub>	Acetic acid, methoxy,- methyl ester	
5.80	69(100),70(49),58(37),44(31),42( 25), 74(26),53(12)	C <sub>3</sub> H <sub>6</sub> N <sub>2</sub>	Dimethyl-cyanamide	
6.11	102(100),44(94),59(35),72(37),10 3(25)	C <sub>7</sub> H <sub>17</sub> NO <sub>2</sub>	2-methoxy-N-(2- methoxyethyl)-N- methyl-Ethanamine	
6.20,8. 47	44(100), 42(99), 102(71), 58(60),43(47), 72(23),103(18),41(17), 74(10)	C <sub>4</sub> H <sub>10</sub> N <sub>2</sub> O	Trimethyl-urea	
6.52	59(100), 58(21),44(10)	C <sub>2</sub> H <sub>3</sub> N	Acetonitrile	$\text{H}_3\text{C}-\text{C}\equiv\text{N}$
6.56	73(100), 44(53), 42(28), 72(14),43(9)	C <sub>3</sub> H <sub>7</sub> NO	Dimethylformide	
7.49	94(100),95(66),42(12),93(12),78( 11)	C <sub>6</sub> H <sub>9</sub> N	2,5-dimethyl-pyrrole	
7.71	83(100),42(32),98(13),43(11)	C <sub>5</sub> H <sub>10</sub> N <sub>2</sub>	1,5-dimethyl-2- pyrazoline	
8.02	58(100), 114(14),42 (16), 87(7)	C <sub>5</sub> H <sub>11</sub> NO <sub>2</sub>	N,N-dimethyl-glycine- methyl ether	
8.09	69(100),84(54),55(27),56(25),42( 21)	C <sub>6</sub> H <sub>12</sub>	3-methylene-pentane	
8.63	57(100), 116(70),86(24),87(34), 87(33), 56(33),85(21), 86(24), 84(19),55(19) , 102(15),117(13)	C <sub>5</sub> H <sub>12</sub> N <sub>2</sub> O	N-methyl-N-nitroso-2- butanamine	

Table 3-2 (continued)

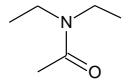
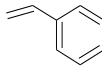
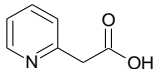
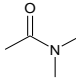
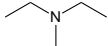
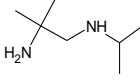
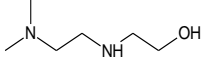
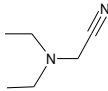
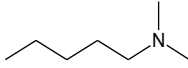
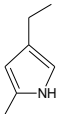
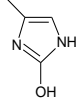
RT/ min	Masses of fragments* and relative abundance: m/z (%)	Empirical formula	Compounds	Structure
8.77	58(100),115(28),78(14)	C <sub>6</sub> H <sub>13</sub> NO	N,N-diethyl-acetamide	
8.82	104(100),103(53), 78(51),114(28),77(25),51(25), 52(20)	C <sub>8</sub> H <sub>8</sub>	Styrene	
8.81	93(100),87(66),44(69),66(41),92(39), 65(35)	C <sub>7</sub> H <sub>7</sub> NO <sub>2</sub>	2-Pyridineacetic acid	
8.94	44(100),87(51),42(38/), 72(30),58(23),43(19)	C <sub>4</sub> H <sub>9</sub> NO	N,N-dimethylacetamide	
9.00	72(100), 42(38),44(36),43(17)	C <sub>5</sub> H <sub>13</sub> N	N-methyl-diethylamine	
9.07	58(100),72(67),44(40), 42(72),87(12)	C <sub>7</sub> H <sub>18</sub> N <sub>2</sub>	N1-Isopropyl-2-methyl-1,2-propanediamine	
9.36	58(100),44(64),42(48), 43(29), 87(14), 59(11)	C <sub>6</sub> H <sub>16</sub> N <sub>2</sub> O	N-(N,N-Dimethylaminoethyl)aminoethanol	
9.56	97(100),69(85),42(84),108(45),78(36),44(24), 56(20),112(18)	C <sub>6</sub> H <sub>12</sub> N <sub>2</sub>	2-(diethylamino)acetonitrile	
9.71	58(100),83(9),42(22)44(17)	C <sub>7</sub> H <sub>17</sub> N	N,N-dimethyl-1-pentanamine	
9.83	94(100),109(52),42(43),43(17),93(16), 53(8)	C <sub>7</sub> H <sub>11</sub> N	4-ethyl-2-methylpyrrole	
10.02	42(100),43(33), 98(19), 41(17), 69(12),40(11)	C <sub>4</sub> H <sub>6</sub> N <sub>2</sub> O	2-hydroxyl-4-methylimidazole	

Table 3-2 (continued)

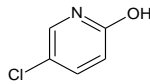
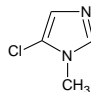
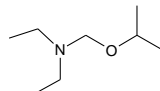
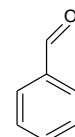
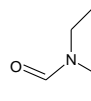
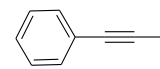
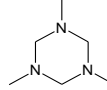
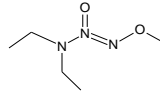
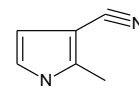
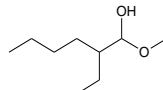
RT/ min	Masses of fragments* and relative abundance: m/z (%)	Empirical formula	Compounds	Structure
10.12,1 2.57 ?	129(100),58(97), 101(92),106(90),78(61),42,114(4 5), 131(31), 80(26), 52(22), 79(21)?	C <sub>5</sub> H <sub>4</sub> ClNO	5-chloro-2-pyridinol	
10.18,1 2.0,12. 69	42(100),116(99), 43(58),44(40), 118(35), 54(22), 79(20),81(20), 109(12),117(17),87(17),73(15)?	C <sub>4</sub> H <sub>5</sub> ClN <sub>2</sub>	5-chloro-1- methylimidazole	
10.65	42(100),43(50),44(40), 58(45),86(35),71(23),40(15)	C <sub>8</sub> H <sub>19</sub> NO	N-ETHYL-n-[1- methylethoxy)methyl]- ethanamine	
10.68	77(100),105(94), 106(77), 44(48),51(44)	C <sub>7</sub> H <sub>6</sub> O	Benzaldehyde	
10.71	58(100),42(87),101(57),86(44)	C <sub>5</sub> H <sub>11</sub> NO	N,N-dimethyl- Formamide	
10.77?	115(100), 78(44),80(21),58(17)	C <sub>9</sub> H <sub>8</sub>	1-Propynyl-benzene	
11.14	44(100), 86(66),42(62), 128(40),43(29), 57(25)	C <sub>6</sub> H <sub>15</sub> N <sub>3</sub>	1,3,5-Trimethyl-1,3,5- triazacyclohexane	
11.65	102(100),44(58),42(57),132(39), 43(34),133(13), 72(12),58(6)	C <sub>5</sub> H <sub>13</sub> N <sub>3</sub> O <sub>2</sub>	1-methoxy-3, 3- diethyltriazene-2-oxide	
11.88	106(100),105(83),78(34),74(20),4 3(18)	C <sub>6</sub> H <sub>6</sub> N <sub>2</sub>	2-methyl-(1H)pyrrole- 3-carbonitrile	
12.17	44(100),57(73),87(75),102(57),41 (27), 42(25), 43(22), 59(15), 69(10)	C <sub>9</sub> H <sub>18</sub> O <sub>2</sub>	Hexanoic acid, 2-ethyl- methyl ester	

Table 3-2 (continued)

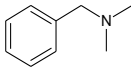
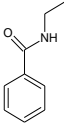
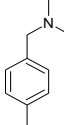
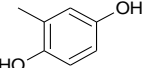
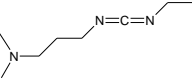
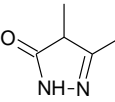
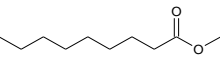
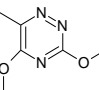
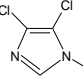
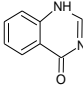

RT/ min	Masses of fragments* and relative abundance: m/z (%)	Empirical formula	Compounds	Structure
12.45	58(100),91(98),135(71),134(67),65(28),118(11)	C <sub>9</sub> H <sub>13</sub> N	N,N-dimethyl-benzenemethanamine	
13.25	105(100),77(70),149(54),136(41),151(34),51(26),73(25),112(18)	C <sub>9</sub> H <sub>11</sub> NO	N-ethyl-benzamide	
13.82	58(98),104(100),105(58),149(49),77(22),107(23),114(15)	C <sub>10</sub> H <sub>15</sub> N	N,N,4-Trimethyl-benzenemethanamine	
14.12	95,124,67,66,81,107	C <sub>7</sub> H <sub>8</sub> O <sub>2</sub>	2-methyl-1,4-Benzenediol	
14.42	58(100),112(92),116(43),83(26),56(18)	C <sub>8</sub> H <sub>17</sub> N <sub>3</sub>	1-Ethyl-3-(3-dimethylaminopropyl)carbodiimide	
14.47	112(100),83(27),60(13),117(170)	C <sub>5</sub> H <sub>8</sub> N <sub>2</sub> O	2,4-dimethyl-3H-Pyrazol-3-one	
15.26	74(100),87(48),141(11),55(22),59(11)	C <sub>10</sub> H <sub>20</sub> O <sub>2</sub>	Nonanoic acid, methyl ester	
15.56	70(100),155(87),55(21)	C <sub>6</sub> H <sub>9</sub> N <sub>3</sub> O <sub>2</sub>	6-Azathymine , Bis(methyl) ether	
15.72?	150(100),109(75),152(64),110(44),76(31),88(26),154(12),47(11)	C <sub>4</sub> H <sub>4</sub> Cl <sub>2</sub> N <sub>2</sub>	4,5-dichloro-1-methylimidazole	
15.80	42(100),146(77) 148(26),117(26),57(13),44(12)	C <sub>8</sub> H <sub>6</sub> N <sub>2</sub> O	4(1H)-Quinazolinone	
16.12	71(100),56(46),44(41),113(20),156(20),98(13)	C <sub>11</sub> H <sub>24</sub>	Undene	

Table 3-2 (continued)

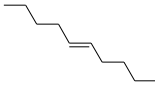
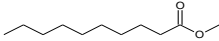
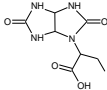

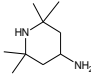
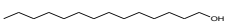
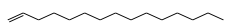
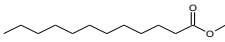
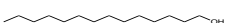
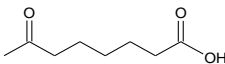
RT/ min	Masses of fragments* and relative abundance: m/z (%)	Empirical formula	Compounds	Structure
16.28,1 6.54,16 .72	42(100),140(64),69(26),83(22),97 (13),112(10)	C <sub>10</sub> H <sub>20</sub>	E-5-Decene	
16.72	42(100), 74(94),140(62),87(50),43(22), 143(19),55(16),112(10)	C <sub>11</sub> H <sub>22</sub> O <sub>2</sub>	Decanoic acid, methyl ester	
16.95,2 2.72	42(100),76(50),140(70),180(36),1 12(15),124(8)	C <sub>8</sub> H <sub>12</sub> N <sub>4</sub> O <sub>4</sub>	Imidazo[4,5- d]imidazole-1-acetic acid, a-ethyloctahydro- 2,5-dioxo-	
17.67	42(100),69(76),55(56),41(55),83( 52),43(54),112(59),97(40),140(39 )	C <sub>12</sub> H <sub>26</sub> O	1-dodecanol	
17.84	58(100),42(29),98(20),141(21),44 (19)	C <sub>9</sub> H <sub>20</sub> N <sub>2</sub>	2,2,6,6-tetramethyl- 4-Piperidinamine	
18.59	58(100),42(76),83(53),111(52), 41(37), 82(36), 138(26), 69(25), 112(23), 168(15)	C <sub>14</sub> H <sub>30</sub> O	1-Tetradecanol	
18.97	55(100),43(82), 69(80), 57(74), 83(67), 70(53), 41(51), 71(35),84(33),85(16)	C <sub>15</sub> H <sub>30</sub>	1-pentadecene	
19.35	74(100),87(65),43(20),55(22),143 (12)	C <sub>13</sub> H <sub>26</sub> O <sub>2</sub>	Dodecanoic acid, methyl ester	
20.19	71(100),43(91),83(71),69(69), 97(46),41(51),70(51),57(51), 55(61)	C <sub>14</sub> H <sub>30</sub> O	1-tetradecanol	
20.46	42(100),42(95),57(78), 41(73), 43(63),82(50), 55(46),71(33), 96(33)	C <sub>8</sub> H <sub>14</sub> O <sub>3</sub>	7-oxo-Octanoic acid	

Table 3-2 (continued)

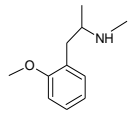
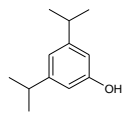
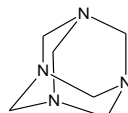
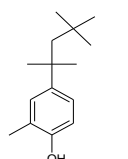
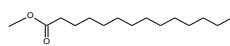
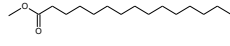
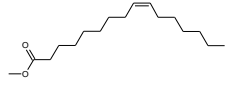
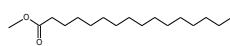
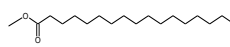

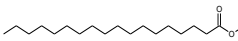
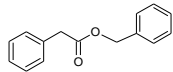
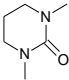
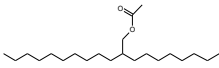
RT/ min	Masses of fragments* and relative abundance: m/z (%)	Empirical formula	Compounds	Structure
20.86	149(100),140(14),121(13)	C <sub>11</sub> H <sub>17</sub> NO	Methoxyphenamine/ion trap	
20.98	163(100), 121(64), 140(62), 135(61), 205(23)	C <sub>12</sub> H <sub>18</sub> O	3, 5-disopropyl-phenol	
15.97, 21.35	42(100),140(65),42(22), 150(17), 69(14),83(11),163(11)	C <sub>6</sub> H <sub>12</sub> N <sub>4</sub>	Methenamine	
21.42	149(100),140(58),121(15),193	C <sub>15</sub> H <sub>24</sub> O	4-Tert-Octyl-oCresol	
21.69	74(100),42(50),87(66),199(16),14 0(41), 55(19) ,69(15),	C <sub>15</sub> H <sub>30</sub> O <sub>2</sub>	Tetradecanoic acid, methyl ester	
22.77	74(87),140(100),87(65),42(40),85 (23),71(16)	C <sub>16</sub> H <sub>32</sub> O <sub>2</sub>	Pentadecanoic acid, methyl ester	
23.57	55(79),96(100),97(96), 74(85),140(92), 84(68) ,98(43), 110(35)	C <sub>17</sub> H <sub>32</sub> O <sub>2</sub>	Methyl palmitoleate	
23.80	74(100),87(71),143(18),227(13),5 5(22),270(13) 97(9),129(7)	C <sub>17</sub> H <sub>34</sub> O <sub>2</sub>	Hexadecanoic acid, methyl ester	
24.77	74(100),87(73),96(54), 97(46),143(24),207(22), 241(10)	C <sub>18</sub> H <sub>36</sub> O <sub>2</sub>	Heptadecanoic acid, methyl ester	
25.49	55(100),96(97), 97(90),69(56),83(62),98(123,180, 207,264,235	C <sub>19</sub> H <sub>36</sub> O <sub>2</sub>	Oleic acid, ,ethyl ester	

Table 3-2 (continued)

RT/ min	Masses of fragments* and relative abundance: m/z (%)	Empirical formula	Compounds	Structure
25.72	74(100),87(70),143(22),199(11),2 55(13),55(24),43(17),57(17),	C <sub>19</sub> H <sub>38</sub> O <sub>2</sub>	Methyl stearate	
26.64	91(100),180(11),224(10), 65(10)	C <sub>15</sub> H <sub>14</sub> O <sub>2</sub>	Benzeneacetic acid, phenylmethyl ester	
27.34	42(100),99(90),128(62),56(26),71 (24), 212(22), 85(14),143(14),	C <sub>6</sub> H <sub>12</sub> N <sub>2</sub> O	1,3- Dimethyltetrahydro- 2(1H)-pyrimidinone	
28.08	57(100),42(79), 207(58), 43(47), 97(39),96(31),71(30), 69(25), 55(24), 103(22),111(22),208(16)	C <sub>22</sub> H <sub>44</sub> O <sub>2</sub>	2-octyldodecyl acetate	

The distribution of the main products of TMAH flash pyrolysis with 10 wt.% calcium perchlorate is shown in Table 3-3. Most of the products are N-containing compounds. These include TMA, N,N,N',N'-tetramethyl-methanedi-amine and TMTAC at 12.7 %, 21.3 %, and 16.7%, respectively. Dimethyl ether and CO<sub>2</sub> are also main products at 11.0% and 13.9%, respectively. The newly formed products of dimethylamino acetonitrile and DMF, of 6.2% and 6.7% respectively, account for a relatively high proportion compared with other nitrogen containing byproducts.



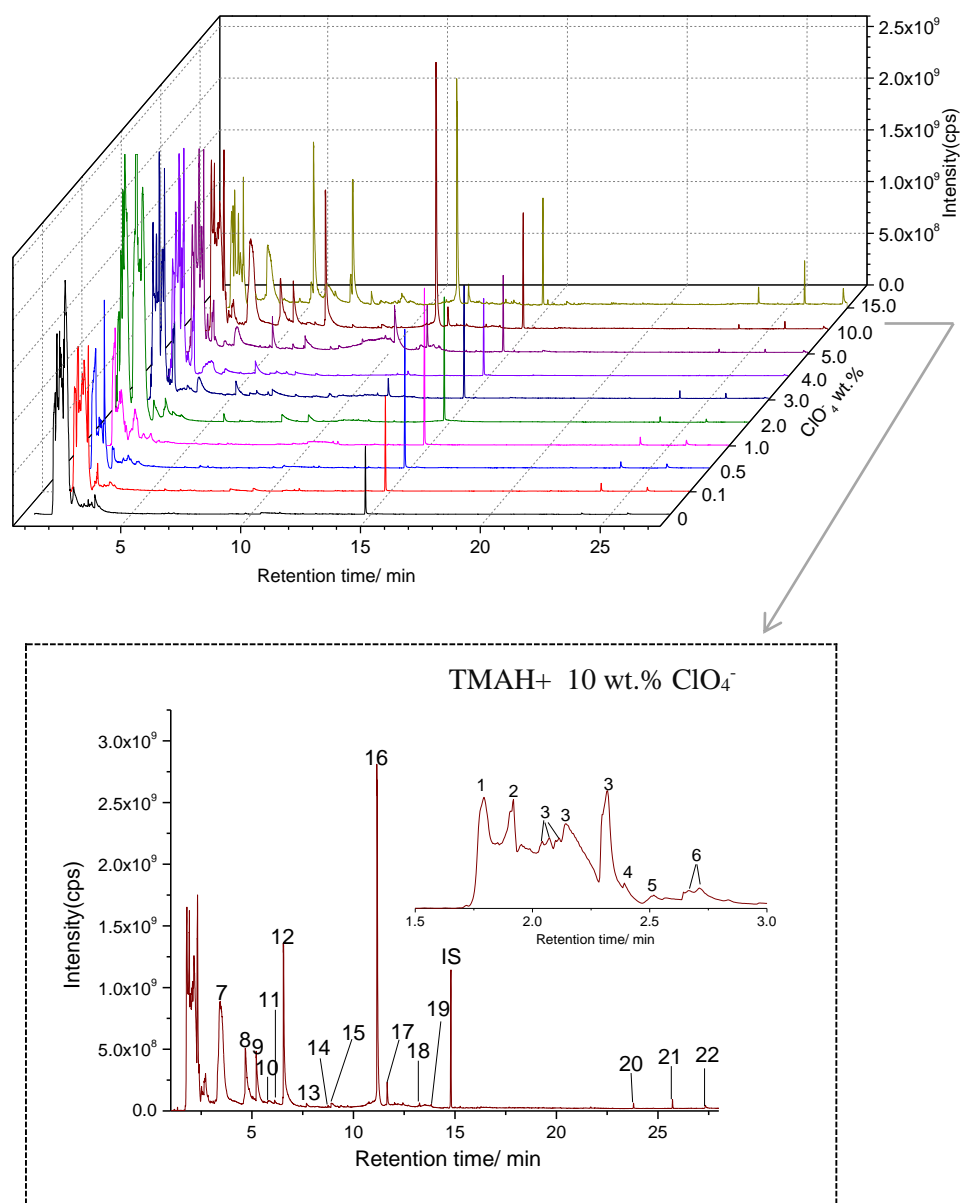


Figure 3-5 Chromatograms of TMAH pyrolysis with Ca (ClO<sub>4</sub>)<sub>2</sub> in different abundance at 600 °C. (Peak 1: dimethyl ether; 2: 2-methoxyethoxy-ethene; 3: N,N-dimethyl-methylamine; 4: Tetramethylammonium acetate?; 5: 1-methylaziridine; 6: N,N-dimethyl-ethylamine; 7,8 : N,N,N',N'-tetramethyl-methanediamine; 9: dimethylamino-acetonitrile; 10: dimethyl-cyanamide; 11: N-methyl-N-(2-hydroxyethyl)carbamic acid, methyl ester; 12: N,N-dimethyl-formamide; 13: propenal dimethylhydrazone; 14: 1-methyl-3-piirtidinol; 15: N,N-dimethylacetamide; 16: hexahydro-1,3,5-trimethyl-1,3,5-triazine; 17: N-methyl-N-(2-hydroxyethyl)carbamic acid, methyl ether; 18: benzoic acid, methyl ester; 19: N,N,4-trimethyl-benzenemethanamine; 20: hexadecanoic acid, methyl ester(plalmitic acid, methyl ester); 21: octadecanoic acid; methyl ester ( Stearic acid, methyl ester); 22: 2-butenedioic acid(Z)-diethyl ester( Maleic acid diethyl ester).

Table 3-3 the distribution of the pyrolysis products of TMAH with 10 wt. % of perchlorate during the flash pyrolysis at 600 °C

Compounds	Yields(%)	Compounds	Yields(%)
CO <sub>2</sub>	13.9	Dimethylamino-acetonitrile	6.2
Dimehtyl ether	11.0	Dimethylformamide	6.7
Trimethylamine	12.7	Dimethyl-cyanamide	1.0
N,N-dimethyl-ethylamine	1.3	Hexahydro-1,3,5-trimethyl-1,3,5-triazine	16.7
N,N,N',N'-tetramethanediamine	21.3	1-methoxy-3,5-diethyltriazene-2-ox	1.2
Others	8.0		

Figure 3-6 shows the effects of calcium perchlorate on the main products produced during the flash pyrolysis of TMAH at 600 °C. Trimethylamine and dimethyl ether are the main compounds from the flash pyrolysis of TMAH with the presence of calcium perchlorate as shown in Table 3-3, and their abundance did not show obvious changes with the increase of calcium perchlorate when its abundance is lower than 5 wt.%. TMA abundance increases as calcium perchlorate reaches 2 wt.%, and the TMA abundance remains stable as the calcium perchlorate concentration increases to 10 wt.%. However, TMA decreases with an increase of calcium perchlorate up to 15 wt.%, which means other N-bearing compounds are formed. Dimethyl ether shows a similar trend as TMA. Nitrogen containing compounds such as DMF and dimethylamino acetonitrile, TMTAC and dimethyl cyanamide are formed when calcium perchlorate is over 5 wt.%, and the yield of DMF and dimethylamino acetonitrile increases with an increase in calcium perchlorate when its abundance is higher than 5 wt.%. For example, the amount of DMF formed after the TMAH pyrolysis with the presence of 15 wt.% ClO<sub>4</sub><sup>-</sup> is *ca.* 2.7 times higher than that from TMAH pyrolysis with calcium perchlorate with the presence of 5 wt.% ClO<sub>4</sub><sup>-</sup>; the TMTAC and dimethyl cyanamide shows a slight increase with the increase of perchlorate over 5 wt. %. N,N,N',N'-tetramethyl-methanediamine is one of the most important byproducts from TMAH pyrolysis and the abundance of N,N,N',N'-tetramethyl-methanediamine increases with an increase in calcium perchlorate up to 10 wt.%. N,N,N',N'-tetramethyl-methanediamine could possibly be decomposed or transferred to other nitrogen contain compounds, such as cyanamide or triazine. 1-methoxy-3, 3-diethyltriazene 2-oxide at the retention time of 11.66 min is an intermediate compound and the abundance of N,N-dimethyl-ethylamine increases slightly with increasing perchlorate concentration. And N,N-dimethylbenzenamide was detected at a low concentration, indicating that additional perchlorate promotes the formation of these products.

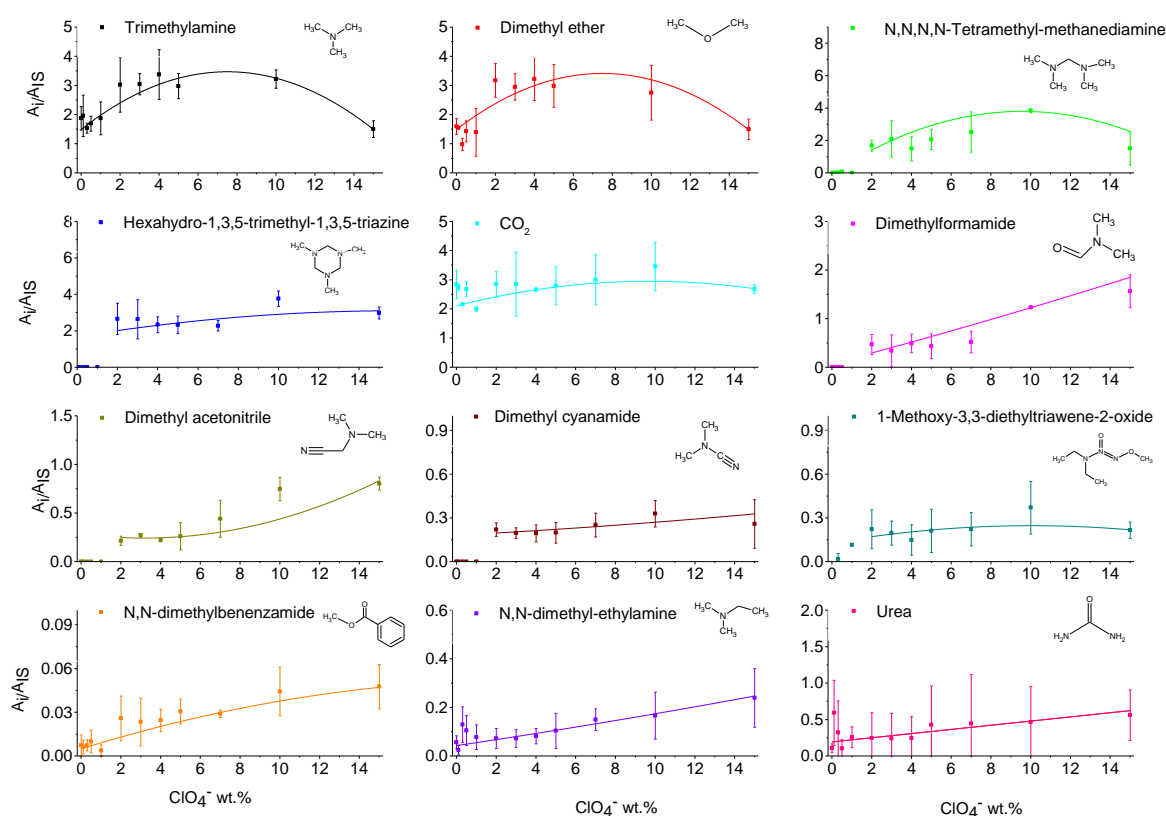


Figure 3-6 Effect of perchlorate on the main products of TMAH pyrolysis at 600 °C ( $A_I/A_S$  represents the peak area of the internal standard divided by the peak area of the target compounds)

### 3.3.2 The pyrolysis of TMAH under SAM experimental conditions

#### 3.3.2.1 Products of TMAH pyrolysis under SAM experiment conditions

The chromatogram for TMAH pyrolysis using the SAM-like ( $35^{\circ}\text{C}\cdot\text{min}^{-1}$ ) heating ramp (Figure 3-7) is similar to the results of TMAH flash pyrolysis from  $50^{\circ}\text{C}$  to  $600^{\circ}\text{C}$ . Indeed, no compounds of interest were detected after 5 minutes retention time. Trimethylamine (TMA) and dimethyl ether are the main products of TMAH pyrolysis. Other pyrolysis products of TMAH include nitrogen and oxygen containing compounds (Table 3-4). Compared with TMAH flash pyrolysis, there are fewer byproducts with TMAH pyrolysis at the SAM-like ramp. This is due to radical fragments being formed simultaneously and in a highly reactive state [604,605] during TMAH flash pyrolysis at  $600^{\circ}\text{C}$ . Thus the radicals interact with each other forming more byproducts. The pyrolysis products of TMAH pyrolysis at *ca.* 135 to  $140^{\circ}\text{C}$  has been previously studied [606], with the main products of dimethyl ether and TMA being consistent with our study.

Table 3-4 The products of TMAH pyrolysis at 600 °C at a heating rate of 35°C .min<sup>-1</sup> from 50°C to 600 °C, refers to Figure 3-7.

	Peak No.	Retention time/min	Masses of fragments* and Relative abundance: m/z (%)	Empirical formula	Compounds
N-containing	5	1.64, 1.95, 2.77	58(100), 59(51), 42(33), 45(29), 46(15)	C <sub>3</sub> H <sub>9</sub> N	Trimethylamine
	6	2.37	58(100), 44(29), 59(26), 42(26), 73(15), 72(10)	C <sub>4</sub> H <sub>11</sub> N	N,N-dimethyl-Ethylamine
	7	2.61	44(100), 58(20), 42(7), 57(7)	C <sub>4</sub> H <sub>12</sub> N <sub>2</sub>	N,N'-dimethyl-Ethylenediamine
	8	2.68	44(100), 58(17), 59(7), 42(6)	C <sub>3</sub> H <sub>9</sub> N	2-propanamine
	9	2.90	44(100), 58(52), 42(19), 59(12)	C <sub>4</sub> H <sub>11</sub> N	Diethylamine
	10	4.96	75(100), 73(70), 58(59), 44(58), 43(21)	C <sub>4</sub> H <sub>11</sub> NO <sub>2</sub>	2,2-dimethoxy-ethanamine
O-containing	1	1.24	44	CO <sub>2</sub>	Carbon dioxide
	2, 4	1.27	45(100), 46(80), 44(11)	C <sub>2</sub> H <sub>6</sub> O	Dimethyl ether
	3	1.46	45(100), 46(80), 44(54)	C <sub>2</sub> H <sub>2</sub> O <sub>4</sub>	Ethanedioic acid

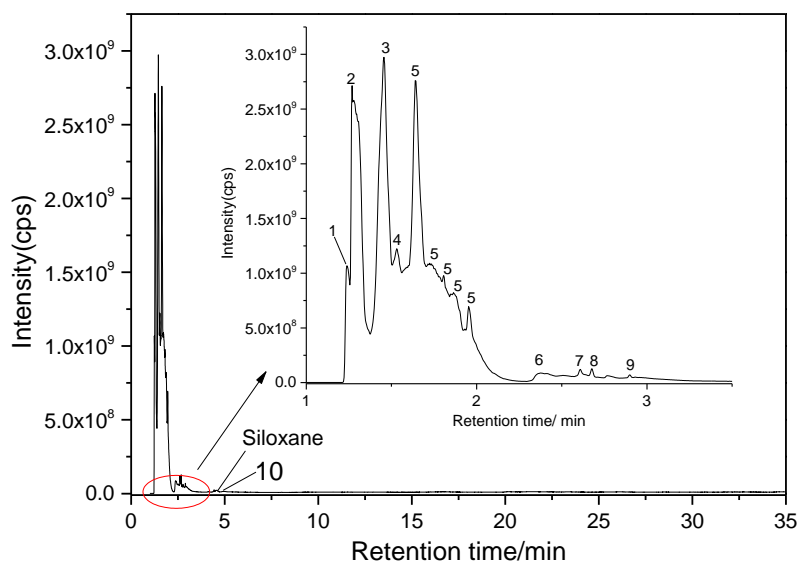


Figure 3-7 Chromatography of TMAH pyrolysis at SAM ramp. Peak 1: CO<sub>2</sub>; peak 2,4 : Dimethyl ether; peak 3: Ethanedioic acid; peak 5: Trimethylamine; peak 6: N, N-dimethyl-Ethylamine; peak 7: N, N'-dimethyl-Ethylenediamine; peak 8: 2-propanamine; peak 9: Diethylamine; peak 10: 2, 2-dimethoxy-ethanamine.

### 3.3.2.2 The effect of calcium perchlorate on TMAH under SAM-like pyrolysis experimental conditions

In order to study the effect of calcium perchlorate on TMAH pyrolysis under SAM-like ramp conditions ( $35\text{ }^{\circ}\text{C}\cdot\text{min}^{-1}$  up to a final temperature of  $600\text{ }^{\circ}\text{C}$ ), the pyrolysis products of TMAH with different calcium perchlorate concentrations were analyzed. Figure 3-8 shows the chromatograms of TMAH pyrolysis with  $\text{Ca}(\text{ClO}_4)_2$  at the SAM-like ramp from  $50$  to  $600\text{ }^{\circ}\text{C}$ . Results show that chloromethane is formed during the pyrolysis of TMAH when calcium perchlorate concentrations are  $> 3\text{ wt.}\%$ , and chloromethane abundance increases with an increase in calcium perchlorate percentage. This trend may be caused by the decomposition of tetramethylammonium chloride. This reaction can be expressed by the following equation [607]:



Figure 3-9 shows the results of calcium perchlorate on TMAH pyrolysis at the SAM-like heating ramp. Dimethyl ether and TMA do not show obvious changes with the increase of calcium perchlorate until the perchlorate percentage is higher than  $10\text{ wt.}\%$ . After  $10\text{ wt.}\%$  perchlorate, the abundance of dimethyl ether and TMA decrease slightly with the increase in perchlorates. At the same time, DMF and TMTAC are formed and become the main pyrolysis products, with a stable trend in their yield with the increase in calcium perchlorate. This demonstrates that the presence of calcium perchlorate can cause the formation of N-containing compounds, and the transfer of N from TMA to other nitrogen containing compounds was promoted. However, the reaction among these cracking fragments and how these byproducts are formed during the TMAH flash pyrolysis and at SAM-like ramp pyrolysis need to be studied.

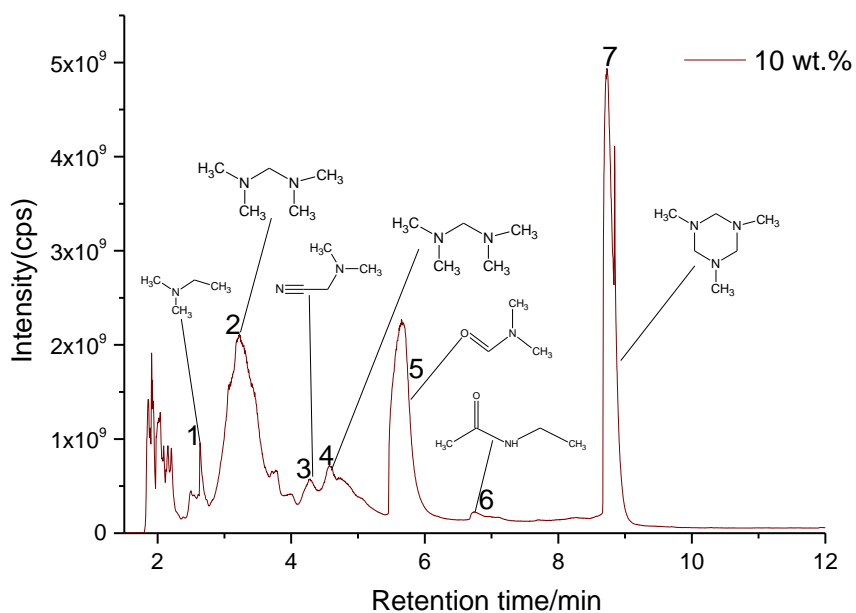
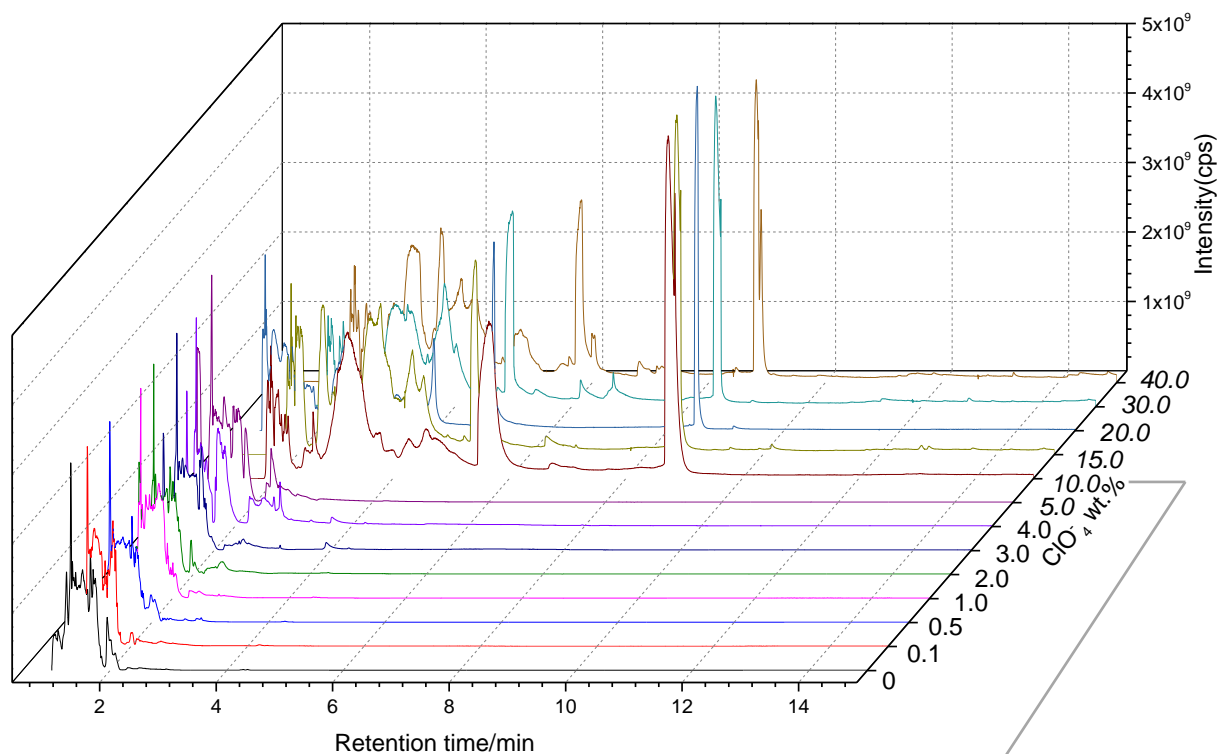


Figure 3-8 Chromatograms of TMAH pyrolysis with  $\text{Ca}(\text{ClO}_4)_2$  at SAM ramp. Peak 1: N,N-dimethyl-ethylamine; peak 2 and 4 : N,N,N',N'-tetramethyl-methanediamine; peak 3: Dimethylamino-acetonitrile; peak 5: DMF; peak 6: N-ethyl-acetamide; peak 7: TMTAC.

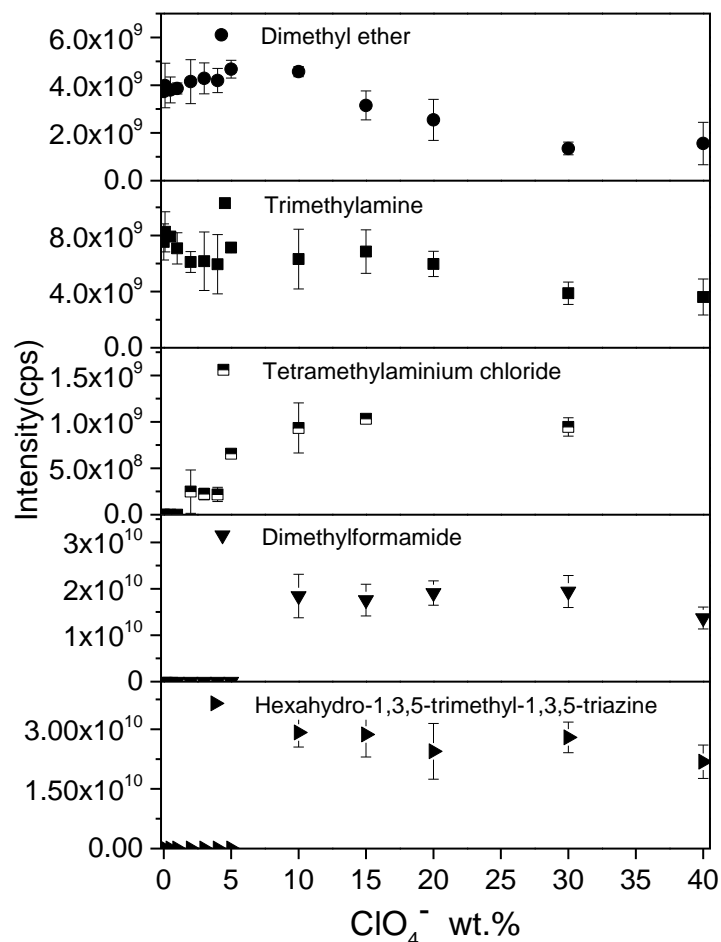


Figure 3-9 The effect of  $\text{Ca}(\text{ClO}_4)_2$  on the pyrolysis products of TMAH at a heating rate of  $35\text{ }^\circ\text{C}\cdot\text{min}^{-1}$  from 50 to  $600\text{ }^\circ\text{C}$ .

### 3.3.3 Mechanism of reaction of perchlorate with TMAH during the pyrolysis

To elucidate how calcium perchlorate influences the formation of byproducts from TMAH pyrolysis at  $600\text{ }^\circ\text{C}$ , a step pyrolysis experiment was conducted to assess the products of TMAH with calcium perchlorate (at 20 wt.%) and without calcium perchlorate. Compared with the SAM-like pyrolysis products of TMAH, there was no obvious difference between the experiments except for the TMAH + 20 wt %  $\text{Ca}(\text{ClO}_4)_2$  from the 400 to  $500\text{ }^\circ\text{C}$  temperature range (Figure 3-10). Table 3-5 summarizes all products of TMAH with and without 20 wt% calcium perchlorate. TMA is the main pyrolysis product and was detected at temperature steps ranging from 100 to  $400\text{ }^\circ\text{C}$ . This indicates that TMAH can be decomposed at temperatures as low as *ca.*  $100\text{ }^\circ\text{C}$ , and a variety of N-bearing compounds were formed. In the 400 to  $700\text{ }^\circ\text{C}$  range, lower abundances of TMA are detected. At temperatures  $>800\text{ }^\circ\text{C}$ , only  $\text{CO}_2$  was

detected. In the 200 to 500 °C range, chloromethane was detected at higher concentrations, indicating methyl groups are formed during TMAH pyrolysis, as shown in Figure 3-11.

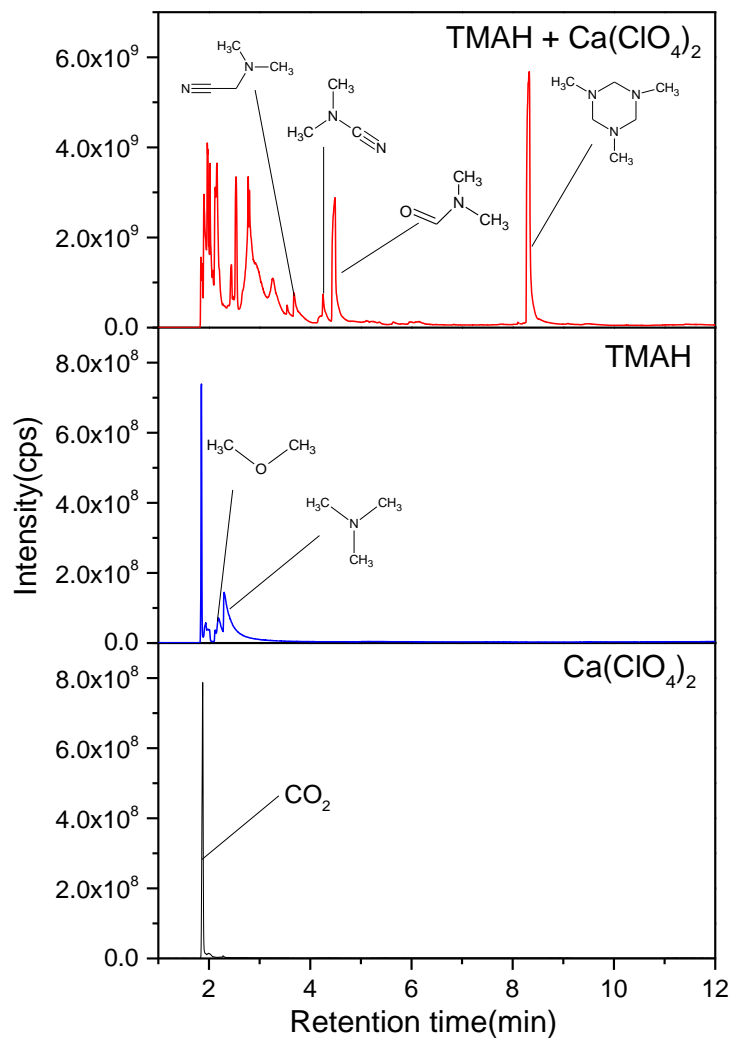


Figure 3-10 The chromatography of TMAH with 20 wt.% ClO<sub>4</sub><sup>-</sup>, TMAH, and Ca(ClO<sub>4</sub>)<sub>2</sub> pyrolysis at 400 to 500 °C at a heating rate of 35 °C.min<sup>-1</sup>.



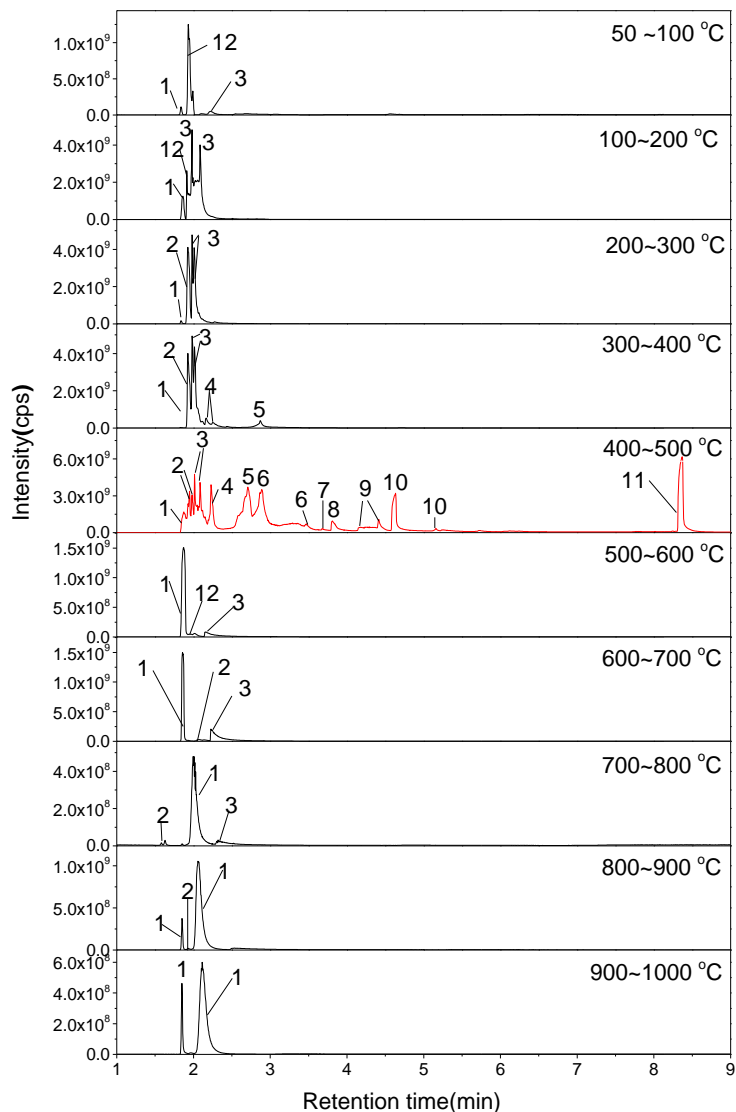


Figure 3-11 Chromatograms of TMAH pyrolysis (a heating rate of 35 °C.min<sup>-1</sup>) with 20 wt. % calcium perchlorate at different temperatures ( Peak 1: CO<sub>2</sub>; 2: chloromethane; 3 and 5: TMA; 4: N,N-dimethyl-ethylamine; 5, 6: N,N,N',N'-tetramethyl-methanediamine; 7: 1-Methyl-pyrrole; 8: Dimethylamino-acetonitrile; 9: Dimethyl-cyanamide; 10: N,N-dimethylformamide; 11: TMTAC; 12: Dimethyl ether.)

Table 3-5 The step pyrolysis products of TMAH with 20 wt. % calcium perchlorate at a heating rate of 35 °C.min<sup>-1</sup>.

Compounds			Pyrolysis Temperature/°C																			
			50-100		100-200		200-300		300-400		400-500		500-600		600-700		700-800		800-900		900-1000	
Name	Mass	Empirical formula	0	20	0	20	0	20	0	20	0	20	0	20	0	20	0	20	0	20	0	20
Carbon dioxide	44	CO <sub>2</sub>	√	√	√	√	√	√	√	√	√	√	√	√	√	√	√	√	√	√	√	√
Trimethylamine	58,59,42,43,63	C <sub>3</sub> H <sub>9</sub> N	√	√	√	√		√	√	√	√	√	√	√	√	√	√	√				
Chloromethane	52,50	CH <sub>3</sub> Cl		√		√		√		√		√		√		√		√		√		
Dimethyl ether	45,46	C <sub>2</sub> H <sub>6</sub> O	√	√	√	√								√	√							
N,N-dimethyl-Ethylamine	58,59,42,73	C <sub>14</sub> H <sub>12</sub> N <sub>2</sub>			√		√	√	√	√		√										
Acetonitrile	41,44	C <sub>2</sub> H <sub>7</sub> NO																		√		
O-(Carboxymethyl)hydroxylamine	44,42,46,50	C <sub>2</sub> H <sub>5</sub> NO <sub>3</sub>												√		√						
2-propanamine	44 ;58 ;72	C <sub>3</sub> H <sub>9</sub> N																		√		
Tetramethylammonium chloride	58,59,50	C <sub>4</sub> H <sub>12</sub> ClN								√		√										
Betaine Hydrochloride	58,59,45,49,73,91,104	C <sub>5</sub> H <sub>12</sub> ClNO <sub>2</sub>		√																		
Dimethoxydimethylsilane	105,75,58,45	C <sub>4</sub> H <sub>12</sub> O <sub>2</sub> Si		√																		
Methamphetamine	58,59,42,75,91,105	C <sub>11</sub> H <sub>17</sub> NO		√																		
Metamfetamine	58,59,91,44	C <sub>10</sub> H <sub>15</sub> N		√																		
Tetramethylammonium perchlorate	58,59,44,45,74	C <sub>4</sub> H <sub>12</sub> ClNO <sub>4</sub>				√		√														
N-methyl- ethylamine	44,58,59	C <sub>3</sub> H <sub>9</sub> N				√																
Betaine	58,59,105,42,75	C <sub>5</sub> H <sub>11</sub> NO <sub>2</sub>				√				√												
1-methoxy-2-(vinylxy)-ethane	58,59,45,46	C <sub>5</sub> H <sub>10</sub> O <sub>2</sub>			√	√		√										√				
Tetramethylammonium acetate	43,58,74	C <sub>6</sub> H <sub>15</sub> NO <sub>2</sub>			√			√														
Bis(dimethylamino)methane	58,42,102	C <sub>5</sub> H <sub>14</sub> N <sub>2</sub>								√	√	√										
1-methyl-pyrrole	58,81,80,72,42	C <sub>5</sub> H <sub>7</sub> N										√										
Dimethylamino-acetonitrile	83,58,42,74	C <sub>4</sub> H <sub>8</sub> N <sub>2</sub>										√										
Dimethyl-cyanamide	69,70,58,42,53	C <sub>3</sub> H <sub>6</sub> N <sub>2</sub>										√										
Dimethylformamide	73,44,58	C <sub>3</sub> H <sub>7</sub> NO						√				√										
4,5-Dimethyl-DELTA.[2]-pyrazoline	83,59 ;42,73,98,44	C <sub>5</sub> H <sub>10</sub> N <sub>2</sub>										√										
N-n-Butylaminoacetonitrile	42,59,58,83,73,102,98,116	C <sub>8</sub> H <sub>12</sub> N <sub>2</sub>										√										
2-ethyl-1-Butene	69,58,42,84,113,73	C <sub>6</sub> H <sub>12</sub>										√										
(1E)-Ethanal o-ethylxime	59,58,42,87,72,69,	C <sub>4</sub> H <sub>9</sub> NO										√										
Methyl-dimethyl ester Malonic acid	59 ;58,44,87,72,115	C <sub>5</sub> H <sub>8</sub> O <sub>4</sub>										√										
2-Methyl-2,4-pentanediamine	59 ;42 ;58 ;44 ;73 ;97	C <sub>6</sub> H <sub>16</sub> N <sub>2</sub>										√										
Cycloserine	42 ;59,73,104	C <sub>3</sub> H <sub>6</sub> N <sub>2</sub> O <sub>2</sub>										√										
Hexahydro-1,3,5-trimethyl-S-Triazine	44,86,128,57,50	C <sub>6</sub> H <sub>15</sub> N <sub>3</sub>										√										
2-Chloro-N,N-diethyl-3-oxo-Butanamide	42,44,59,58,73,102,149,134,151	C <sub>8</sub> H <sub>14</sub> ClNO <sub>2</sub>										√										
1,3,5,7-Tetraazaadamantane	42, 140,58,69,85,112	C <sub>6</sub> H <sub>12</sub> N <sub>4</sub>										√										
4,5-Dichloro-1methyl-1H-imidazole	42,44,58,109,150	C <sub>4</sub> H <sub>4</sub> Cl <sub>2</sub> N <sub>2</sub>										√										

Compared with TMAH-only experiment, the numbers of pyrolysis products were increased in TMAH SAM-like ramp pyrolysis in the presence of 20 wt. %  $\text{ClO}_4^-$ . Figure 3-11 shows the chromatograms of TMAH pyrolysis with the presence of 20 wt.% of  $\text{ClO}_4^-$  at different temperatures. Dimethyl ether and TMA are the main products the pyrolysis. There are also other O- and N-containing compounds that were detected when the pyrolysis temperature was lower than 400 °C, such as 1-methoxy-2-(vinylloxy)-ethane and N,N-dimethyl-ethylamine. There was no significant change in the number of byproducts when the pyrolysis temperature was lower than 400 °C; however, more than 20 compounds were detected during the TMAH pyrolysis from the 400 to 500 °C temperature range. Approximately 50% of these compounds contain nitrogen. Among these compounds, a high concentration of TMTAC was detected. Other related nitrogen-containing and nitrogen-oxygen containing compounds were identified, such as dimethyl-cyanamide, dimethylamino-acetonitrile, N-dimehtyl-N-D-aspartic acid, pyrrole, and DMF. TMTAC, DMF, and TMA are the main products obtained from the pyrolysis of TMAH with  $\text{Ca}(\text{ClO}_4)_2$ , and the intensity of TMTAC is the highest, which means the TMTAC is the most stable form of a nitrogen containing compound in these experiments.

TMTAC, with a chair conformer with the axial orientation of one  $\text{CH}_3$  group based on electron diffraction data [608], is a kind of nucleophilic acyl group transfer reagent and can provide a convenient alternative to the established dialkoxymethyl lithium compounds and lithiodithianes commonly employed as one-carbon nucleophiles, a building block for imidazoles[609]. It is well known that hexamethylenetetramine (HMT) or hexamine can be formed by the reaction of formaldehyde and ammonia, and they are stable intermediates during the reaction. Ogata[610] explained the mechanism and kinetics of the formaldehyde and ammonia reaction, wherein the formation of methylenediamine ( $\text{NH}_2\text{CH}_2\text{CH}_2$ ) is faster than that of hexamine, and a higher ratio of  $\text{CH}_2\text{O}$  vs.  $\text{NH}_3$  is favorable for the formation of hexamine. They proposed the dimethylamine pathway for the formation of HMT during the reaction of formaldehyde and ammonia, which has been confirmed by Zeffiro[611]. Their results showed that dimethylamine plays a key role in the formation of HMT, which are stable intermediates. Through a dehydration process, methylenediamine reacts with dimethylamine and forms the cyclotrimethylenetriamine, which is the related heterocyclic compound of  $(\text{CH}_2\text{NR})_3$ , where R is hydrogen; however, if R represents a methyl group, the product should be TMTAC.

This reaction led to the conclusion that the presences of aldehyde and amine functional group-containing compounds are key factors for the formation of TMTAC. Results from our study indicate that DMF, with both aldehyde and amine functional groups, could be the main compound formed simultaneously with the formation of TMTAC. Thus, we speculate that DMF

is a vital intermediate and plays a key role in the formation of TMTAC. DMF is a polar solvent used widely in industrial processes that can dissolve a wide range of both organic and inorganic compounds because of its large dipole moment, a high dielectric constant and its donor-acceptor properties[612]. It can also be used as a dehydrating agent and catalyst in the dehydration of aldoximes to nitriles[613]. The oxygen atom in DMF is the negative pole and is an ideal hydrogen bond acceptor that extends out from the rest of the molecule. The TMTAC cannot be the condensation product of nitriles because the lack of methyl groups on the nitrile N atom makes it impossible to form TMTAC.

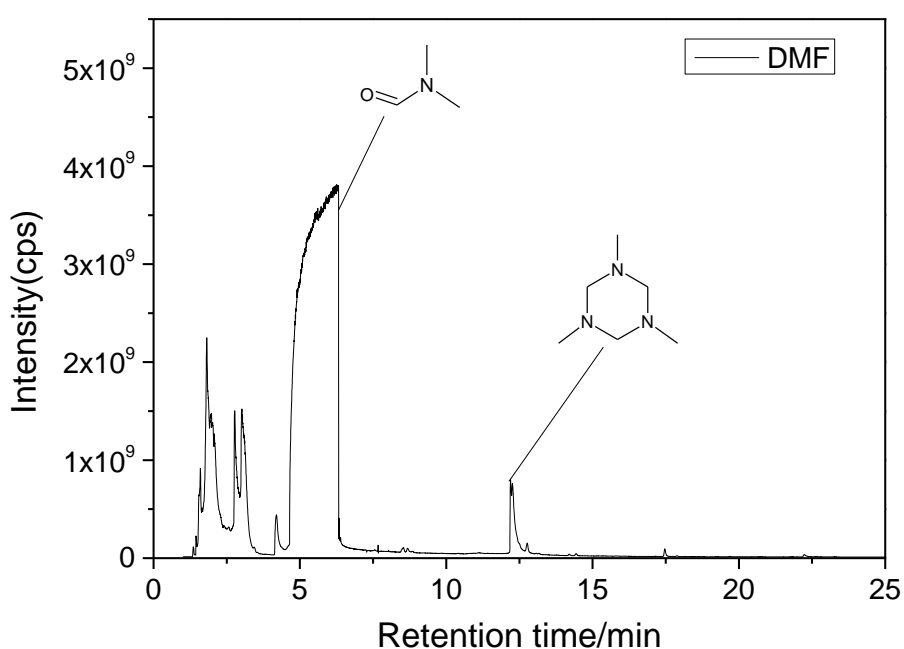


Figure 3-12 The chromatography of DMF flash pyrolysis at 600 °C.

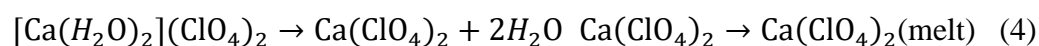
To confirm the function of DMF during the formation of TMTAC, the flash pyrolysis products of DMF at 600 °C were studied. Figure 3-12 shows the chromatogram of DMF flash pyrolysis at 600 °C and the main pyrolysis products are listed in Table 3-6. Results show that the TMTAC was formed during the pyrolysis of DMF at 600 °C, and N, N, N', N'-tetramethylmethanediamine (RT=2.77 and 3.02 min), dimethylamino-acetonitrile (RT=4.02 min), and some olefins such as 1-nonene (RT=8.53 min) and 1-decene (12.78 min) were detected. These results indicate that DMF is the main intermediate for the formation of these compounds.

Table 3-6 The pyrolysis products of DMF flash pyrolysis at 600 °C, refers to Figure 3-12.

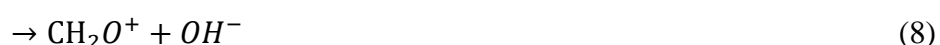
Num.	Retention time/ min	Masses of fragments* and relative abundance: m/z (%)	Empirical formula	Compounds	Structure
1	1.36	44(100)	CO <sub>2</sub>	Carbon dioxide	
2	1.61	42(100),43(52),44(21),40(18)	C <sub>2</sub> H <sub>5</sub> N	Ethylenimine	
3	1.80	44(100), 45(54), 46(28)	C <sub>2</sub> H <sub>7</sub> NO	Ethanolamine	
4	1.97	44(100), 42(38), 43(21), 41(15), 58(10)	C <sub>3</sub> H <sub>9</sub> N	2-Propanamine	
5	2.77, 3.02	58(100), 42(11), 102(6)	C <sub>5</sub> H <sub>14</sub> N <sub>2</sub>	N,N,N',N'-tetramethyl- methane diamine	
6	4.02	83(100),84(58),58(55),42(46), 43(10)	C <sub>4</sub> H <sub>8</sub> N <sub>2</sub>	Dimethylamino-acetonitrile	
7	4.65-6.31	73(100), 44(53), 42(28), 72(14),43(9)	C <sub>3</sub> H <sub>7</sub> NO	Dimethylformide	
8	8.53	56(100),43(87), 55(82), 41(63), 69(61),70(49),42(34), 83(26),97(24),	C <sub>9</sub> H <sub>18</sub>	1-Nonene	
9	8.68	104(100), 78(51), 103(49), 77(24), 51(22)	C <sub>8</sub> H <sub>8</sub>	Styrene	
10	12.20	44(100), 86(66),42(62), 128(40),43(29), 57(25)	C <sub>6</sub> H <sub>15</sub> N <sub>3</sub>	1,3,5-Trimethyl-1,3,5-triazacyclohexane	
11	12.77	56(100),55(97), 70(87),41(79),57(60)43(62), 83(41),97(28),111(14),	C <sub>10</sub> H <sub>20</sub>	1-Decene	
12	14.20, 14.44	93(100),92(40),68(40),79(32),107(16), ,59(11), 121(9)	C <sub>10</sub> H <sub>16</sub>	1-methyl-4-(1-methylethyl)-(S)-Cyclohexene	
13	17.47	55(100),70(91), 41(80), 43(76), 83(61), 97(35), 111(15)	C <sub>11</sub> H <sub>24</sub> O	1-Undecanol	
14	17.87	57(100), 43(74), 71(55), 41(32), 70(15)	C <sub>11</sub> H <sub>24</sub>	Undecane	
15	22.43	55(100),69(93),56(89),70(78),83(71),97(50), 98(20)	C <sub>12</sub> H <sub>24</sub>	1-Dodecene	
16	22.63	57(100),71(67), 43(49), 85(37),55(30), 70(25), 41(24), 97(11)	C <sub>12</sub> H <sub>26</sub> O	2-Butyl-1-Octanol	

The question remains of how DMF is formed during the TMAH pyrolysis at 600 °C in the presence of calcium perchlorate. The thermal decomposition process of calcium perchlorate is an integral step in understanding this process. Migdał-Mikuli[587] studied the thermal

decomposition of calcium perchlorate, which includes three main stages: and the first stage is the process of dehydration as shown in reaction (3), between 184 and 287 °C; the phase transition of solid to melted calcium perchlorate is the second stage according to differential scanning calorimetry (DSC) curve at 346 to 416 °C as shown in reaction (4); the third stage is the decomposition of  $\text{Ca}(\text{ClO}_4)_2$  concurrent with the formation of  $\text{CaCl}_2$  and the release of  $\text{O}_2$  at about 462 °C (5). When water is present,  $\text{CaCl}_2$  could react with  $\text{H}_2\text{O}$  and release  $\text{HCl}$  at the pyrolysis temperatures higher than 450 °C[56]. The oxidation of TMAH was caused by the oxygen released during the thermal decomposition of calcium perchlorate from 400 to 500 °C, which can provide enough energy needed for the thermal decomposition of calcium perchlorate, as shown in Figure 3-10 and 11.



During the pyrolysis of TMAH, TMA was detected, which is the most possible likely precursor of DMF, which means the methyl functional group of TMA or tetramethylammonium ion could be oxidized by  $\text{O}_2$  released from the degradation of calcium perchlorate. The reaction between  $\text{CH}_3$  and  $\text{O}_2$  may proceed through three different channels, as shown in equations (6), (7), and (8)[614].



Reaction (6) is the main channel at low temperatures about 300 K. The reaction (7) and (8) play a major role in the consumption of  $\text{CH}_3$  during methane oxidation at elevated temperatures. For the oxidation of TMA in this study, result showed that channel (8) is the main process of TMAH oxidation, because the hydrogens are active and can be transited among different methyl groups [615,616]. Therefore, the oxidation of the methyl functional groups of the TMA or TMAH ion by oxygen released during the decomposition of calcium perchlorate is the main source of DMF formation. However, oxygen has consistently been present such that formation of the intermediate  $(\text{CH}_3)_2\text{NCH}_2\text{O}_2$  was not rate determining [617]. Therefore, the formation of DMF with different percentages of calcium perchlorate did not substantially change with the 35 °C.min<sup>-1</sup> heating rate. However, the potential energy surface of OH formation is pressure dependent [617]. The pressure of TMAH flash pyrolysis increases

immediately when the sample is injected into the pyrolysis chamber. At the same time, many radical fragments are formed and volatile volumes increase to facilitate the combination among these radicals and form different chemical products. Therefore, the yield of DMF during the flash pyrolysis increased with the increasing amount of calcium perchlorate, and there are many more byproducts of TMAH with the SAM-like ramp pyrolysis. For the same reason, the formation of TMTAC showed a relatively stable trend with SAM-like ramp pyrolysis. Additionally, TMTAC increased with an increase of calcium perchlorate, which could also be facilitated by the higher formation and mass transfer rate of hydrogen radicals during the flash pyrolysis.

The cyanamide and acetonitrile feature a nitrogen atom ( $sp^3$  or  $sp^2$ ) bearing a nitrile group and possess unique properties as building blocks for organic synthesis owing to their original unique structures [618]. Cyanamide and acetonitrile bearing compounds are formed during TMAH pyrolysis at 600 °C with the presence of calcium perchlorate. Examples of these products include dimethylamino-acetonitrile (RT=5.26 min, Figure 3-5) and dimethylcyanamide (5.80 min, Figure 3-5), which indicates not only oxidation but also cyanations occur during the TMAH pyrolysis with calcium perchlorate. The simplest form of cyanamide can be formed naturally. Cyanamide is also considered as an important molecule in prebiotic chemistry with the condensation of cyanamide 1 with  $\alpha$ -hydroxy aldehydes being a possible prebiotic route to cytosine-type nucleosides [619]. Cyanamide can be formed through several different methods, including the alkylation and acylation of cyanamides, the cyanation of amines and their derivatives, and dehydration of urea and amide oximes [620]. Doubly labeled nitrile compounds have been synthesized by combining the source of  $-CN$  from DMF (96%  $^{13}C$  source) and ammonia (98%  $^{15}N$  source) in the palladium-catalyzed cyanation of aryl C-H bonds [621]. Cyanamide can also be formed by the direct transformation of DMF[622]. Both element N and C of cyano functional group derived from DMF ( $C_3H_7NO$ ),  $O_2$  and  $-CH_3$  are the sources of element O and C in the generated  $-CHO$  group, individually; which demonstrated that the functional group  $-CHO$  were generated from the methyl oxidation by  $O_2$ . Results showed that the presence of  $H_2O$  decreases the yield of  $-CN$  formation, which could be caused by the  $-CN$  group hydration to amine[623]. The formation of various intermediates could also be formed through the Ritter reaction[624,625]. Therefore, hydration processes could occur during TMAH degradation. As shown in Figure 3-10, some urea related products are formed, such as urea and N,N-dimethyl urea. Therefore, DMF is the key intermediate for the formation of cyanamide and (dimethylamino)acetonitrile during the TMAH pyrolysis in presence of calcium perchlorate over 15 wt.%. This is demonstrated by the pyrolysis of DMF at 600 °C.

Therefore, the formation of cyanamide and nitriles, CO<sub>2</sub>, and other byproducts related to DMF formation are influenced by the formation rate of DMF, hence these compounds' formation remains stable. The reaction route can be seen in Figure 3-13. There are two competitive processes involved: the oxidation by O<sub>2</sub> and hydrogenation reduction by hydrogen radicals including ·H radicals and ·CH<sub>3</sub> radicals formed from the demethylation reactions of TMAH. The nitrogen ylide could be oxidized to acyl containing compounds, and then further oxidized to carboxyl by O<sub>2</sub>, followed by the methylation process, or by the formation of CO<sub>2</sub> through carboxyl elimination; and the intermediate products could be stabilized by hydrogen radicals. CO<sub>2</sub> could also result from the partial hydrolysis of secondary and tertiary amide groups formed in branching and crosslinking reactions[623]. Alternatively, the methyl groups could form the alkyl chain products via the free radical polymerization mechanism[626]. At the same time, the aromatization of these active free radicals could occur according to the aromatization mechanism[463]. The cyclization reaction also plays a key role during the degradation of TMAH at 600 °C, such as the formation of pyrrole compounds that may be formed through the reaction of amine functional groups with α-hydrogen[400]. However, no researchers have reported the direct formation of –CN from TMAH pyrolysis, which would represent a new pathway for cyanamide and nitrile formation. However, the hydroxyl ion can catalyze the hydrolysis of cyanamide, which could be decomposed in alkaline solutions to urea [627] as well as polymerized to dicyanodiamide.



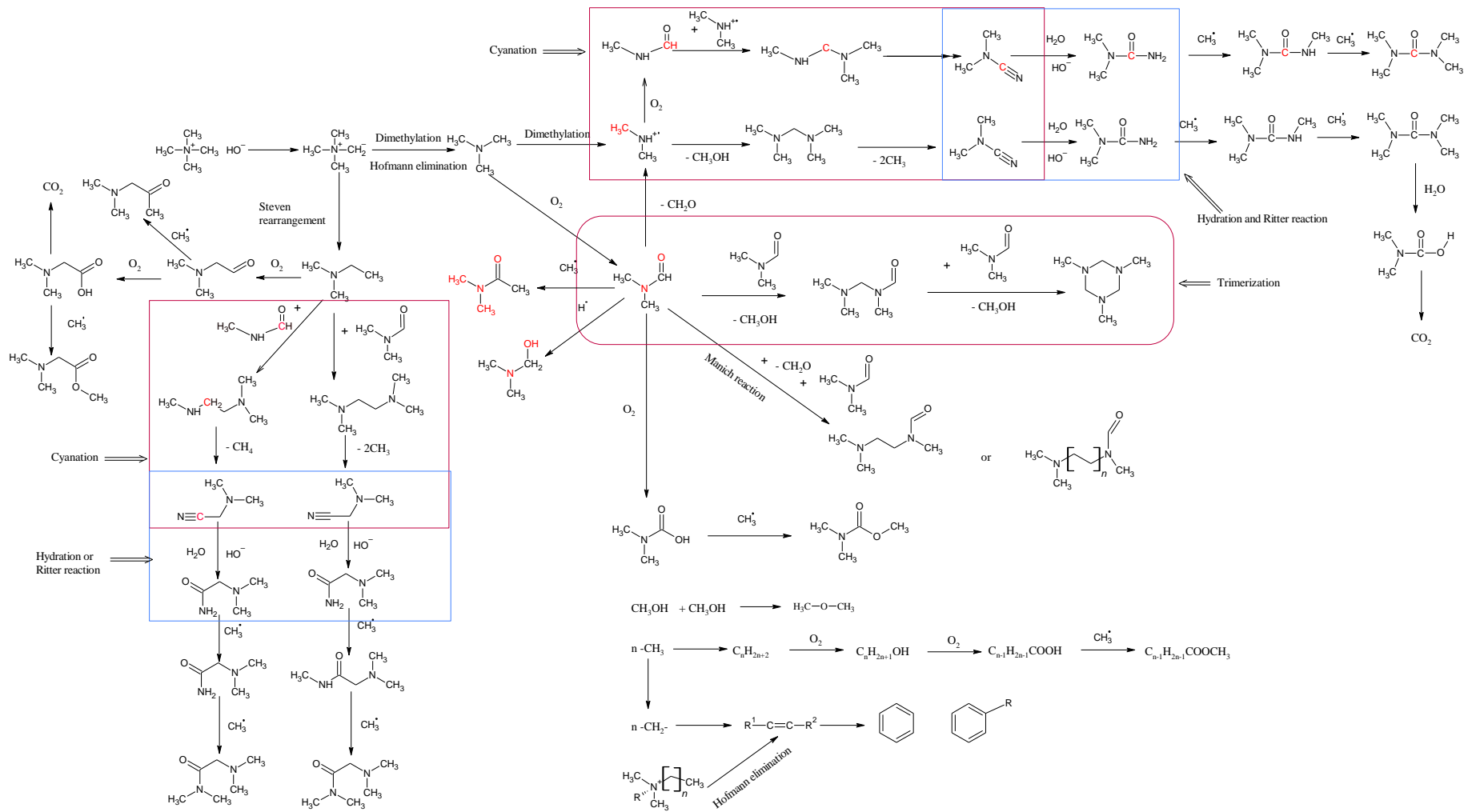


Figure 3-13 The plausible mechanism of TMAH degradation with the presence of calcium perchlorate at 600 °C.

As mentioned before, the decomposition of TMAH at low temperatures (*ca.* 200 °C) has two possible pathways: the S<sub>N</sub>2 and the ylide pathway. Based on the TMAH pyrolysis products at 600 °C, the nucleophilic attack of TMAH and the ylide intermediate pathway is a more satisfactory explanation. Ylide is another important compound for the formation of nitrogen containing byproducts, including dimethyl-methanolamine, dimethylamine, and N, N, N',N'-tetramethyl-methanediamine [623], all formed during the TMAH pyrolysis process. For example, unstable ylides can decompose to produce dimethyl ethylamine and polyethylene, and the ylide would be involved in the formation of the dimethyl ether [628]. The ylide can rearrange via intramolecular hydrogen exchange to form the dimethyl ether products mixed with CH<sub>3</sub>OCH<sub>3</sub>, CH<sub>2</sub>-DOCHs, CHD<sub>2</sub>OCH<sub>3</sub>, and CD<sub>3</sub>OCH<sub>3</sub> [66,629]. The charge distribution of N-containing ylides is largely affected by the electron withdrawing properties of the quaternary nitrogen [630]. Other than the Mannich reaction [631,632], *in situ* dehydration of water from the hemiaminal products of the reaction between formaldehyde containing compounds and an amine also plays an important role in the formation of different alkyl ylides, as shown in Figure 3-13.

#### **3.3.4 Fatty acid recovery with TMAH thermochemolysis in the presence of calcium perchlorate**

Lastly, the performance of TMAH on the recovery of fatty acids (16 nmol) was studied. Although there are several new products formed during the pyrolysis of TMAH with >10 wt. % calcium perchlorate, the highest concentrations of ClO<sub>4</sub><sup>-</sup> detected on Mars is *ca.* ~1 wt.% [633,634]. Therefore the effect of calcium perchlorate (< 5 wt. %) on the detection of fatty acids was studied. Naphthalene-d<sub>8</sub> was used as the internal standard and the fatty acids were quantified by rationing the peak area of the fatty acid divided by the peak area of naphthalene-d<sub>8</sub>. Figure 3-14 shows the recovery of fatty acids without and with different percentages of calcium perchlorate. Results demonstrate that the increase in calcium perchlorate up to 5 wt. % has nearly no effect on the detection of fatty acids. Additionally, the concentration of the methyl group (about 86 μmol, calculation can be seen in supplementary materials) used to derivatize the fatty acids is much greater than (in excess) the concentration needed to complete fatty acid methylation (of 16 nmol). Therefore, the calcium perchlorate has no obvious effect on the recovery of the fatty acids.

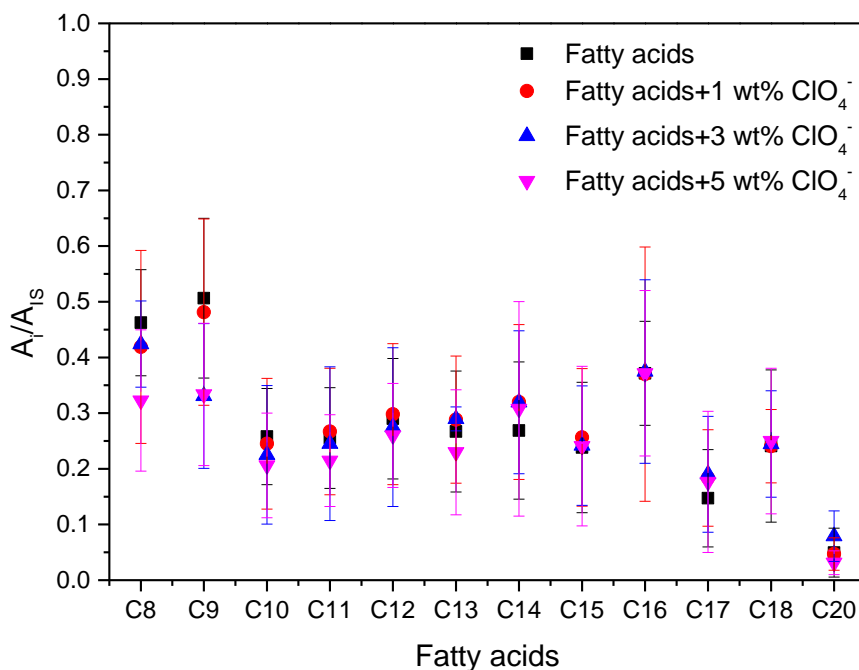


Figure 3-14 The effect of calcium perchlorate on the recovery of fatty acids by TMAH thermochemolysis

To further explore how calcium perchlorate may affect the detection of organics on Mars, experiments were conducted that utilized the same concentration of fatty acids and perchlorate as has been reported from Mars [59]. Chlorobenzene has been detected on Mars at 300 ppb and is used as a proxy for the concentration of organics on Mars for this experiment. Perchlorate on Mars has been detected at about *ca.* 1 % [61]. The *Curiosity* rover which carries the SAM instrument is capable of delivering *ca.* 20 mg of sample to SAM for a TMAH thermochemolysis experiment. Therefore, *ca.*  $6 \times 10^{-9}$  g ( $300 \text{ ppb} \times 20 \text{ mg} = 6 \times 10^{-9}$  g) of fatty acids and 0.2 mg ( $1\% \times 20 \text{ mg}$ )  $\text{ClO}_4^-$  were set to simulate the Mars conditions for this experiment. Figure 3-15 shows the recovery of fatty acids with and without calcium perchlorate on Mars-like conditions. Different percentages of calcium perchlorate have nearly no effect on the detection of fatty acids at these ratios. The calcium perchlorate used in this study can release  $4 \times 10^{-6}$  mol of  $\text{O}_2$ , the abundance of TMAH is about 4.4 times higher than the amount of  $\text{O}_2$ , and the C abundance is 17.6 times higher than that of  $\text{O}_2$  (calculation can be seen in supplementary materials). However, TMAH can be degraded to methyl radicals which more readily react with  $\text{O}_2$ . The fatty acids used in these experiments are very stable [635] and have been derivatized to methyl

esters by TMAH thermochemolysis, the methylation of the groups containing esters and ethers could increase the thermodynamic stability and chromatographic detection by GC/MS [249]. However, methyl groups can be formed when TMAH pyrolysis temperatures reach to 100 °C, readily driving forward reactions with O radicals [636]. The presence of calcium perchlorate did not show obvious effects on fatty acid recovery (about 11.8 pmol, calculation can be seen in the supplementary materials). Hence, the excess TMAH to sample ratio is essential for the detection of organics with the SAM and MOMA instruments. However, fatty acid detection becomes more difficult with both long alkyl chains or with lower abundance of fatty acids.

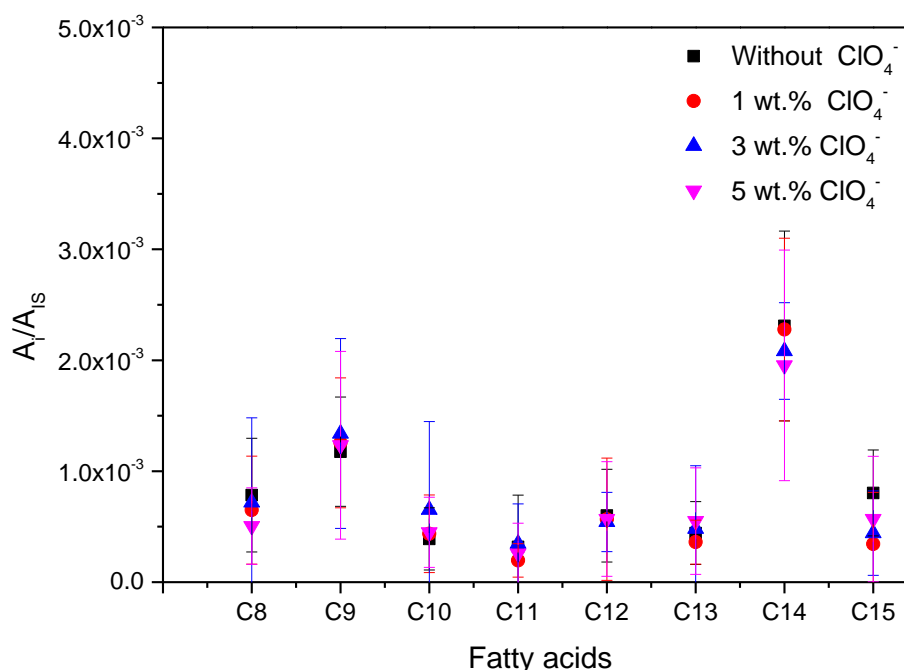


Figure 3-15 The recovery of fatty acids with TMAH thermochemolysis on Mars-like conditions. The concentration of perchlorate is the ratio of perchlorate to organics (300 ppb of fatty acids).

### 3.4 Conclusions

In this study, the degradation of TMAH with and without the presence of calcium perchlorate at flash pyrolysis and SAM-like ramp pyrolysis to 600 °C was studied. Some chloride related compounds were detected during TMAH pyrolysis with >10 wt. % calcium perchlorate, including chloromethane, tetramethylammonium chloride, 5-chloro-2-pyridinol, 5-chloro-1-methylimidazole, and 4,5-dichloro-1-methyl-imidazole. Though the peak intensity of these chlorinated compounds was over 1000 times lower than that of the

main products, they are the potential candidates for the chloride containing byproducts of TMAH. Therefore, TMAH showed little reactivity with chlorine-containing substances.

We also conclude that calcium perchlorate does not affect TMAH degradation at a SAM-like ramp pyrolysis temperature 600 °C when calcium perchlorate concentrations are lower than 10 wt.%. Although TMA and dimethyl ether are the main byproducts of TMAH pyrolysis, some new byproducts are formed when the calcium perchlorate concentrations is higher than 10 wt.%. DMF is formed because of methyl group oxidation by O<sub>2</sub> released from the decomposition of calcium perchlorate and followed by the formation of cyanamide and acetonitrile through the cyanation route of amines. TMTAC is formed by the trimerization of DMF, which is a crucial intermediate for the formation of other nitrogen containing byproducts of TMAH. Urea is formed through the Ritter reaction and Manich reaction, and the Steven rearrangement and Hofmann elimination are involved in the formation of various intermediates and ylides. However, in our experimental conditions, calcium perchlorate did not affect the recovery of fatty acids with TMAH thermochemolysis, even when the fatty acid volume was low. These lines of evidence demonstrate that TMAH is a good thermochemolysis reagent at high temperature (600 °C) for the methylation and detection of organics on Mars with the SAM and MOMA instruments.



# Chapter 4. Application of TMAH thermochemolysis to the detection of the nucleobases: application to the MOMA and SAM space experiment.

## 4.1 Introduction

Searching for the biochemical precursors at the Mars surface is one of the main goals of the Sample Analysis at Mars (SAM) and Mars Organic Molecule Analyzer (MOMA) experiments onboard the Curiosity and ExoMars 2020 rovers, respectively. Among the chemical compounds, organic molecules are of particular importance and key species include carboxylic acids, amino acids, and nucleobases. Seven nucleobases are of particular importance in terrestrial biology. Five — adenine (A), guanine (G), thymine (T), cytosine (C), and uracil (U) — are contained within DNA and/or RNA. These nucleobases build codons, and each codon corresponds to an amino acid. Two others — xanthine (X) and hypoxanthine (HX) — are important metabolic intermediates. Here we show that if these seven nucleobases were present in Martian samples, they could be detected *in situ* by instruments on current Mars rover missions even at low concentrations.

Low concentrations of nucleobases have been identified in carbonaceous chondrite-type meteorites [40,41,225,637–643]. Callahan [644] analyzed the component of five different martian meteorites after formic acid extraction, purification and concentration followed by liquid chromatography-mass spectrometry. However, no nucleobases or nucleobase analogs were observed above their detection limit of 1 ppb in any of the martian meteorite samples studied [13]. These laboratory studies of carbonaceous chondrites and martian meteorites provide a solid baseline for future searches for nucleobases on the martian surface.

Though Basiuk and Doua [645] investigated the recovery rate of underivatized adenine, guanine, cytosine, and uracil after sublimation at temperatures between 400°C and 1000°C using a laboratory furnace under a N<sub>2</sub> or CO<sub>2</sub> atmosphere. Results indicated that the temperature range from 500-600°C represented the best compromise between the thermal decomposition and volatilization rate, suggesting that thermal introduction of nucleobases is a viable strategy for sample analysis. Pyrolysis-Gas Chromatography-Mass Spectrometry (Pyr-GC/MS) is one of the operational modes used to detect the organic compounds as part of the SAM and MOMA experiments. Unlike sublimation, pyrolysis does not preserve the initial organic compounds,

some derivatization solvent should be used, such as N,N-tert-butyl-dimethylsilyl-trifluoroacetamide (MTBSTFA) and dimethylformamide (DMF) and tetramethylammonium hydroxide (TMAH) will be used on MOMA and SAM to protect polar compounds released from the pyrolysis experiment. MTBSTFA and DMF have been proved as good derivatization solvent. For example, Glavin [646] detected the adenine, thymine, uracil, cytosine, and xanthine (interpreted as a product of guanine degradation) in the extract of *Escherichia coli* strains (*E. coli*) inoculated with serpentine samples. Results showed that sublimation coupled with chemical derivatization using MTBSTFA and DMF as the derivatization solvent, with GC/MS analysis, could detect nucleobases in Martian soil analogs. TMAH works as a methylation agent boosting the cleavage of macromolecules, thereby methylating the products released from sample pyrolysis, and giving rise to improved detection by GC/MS. For example, thymine can react with TMAH [24,647]. TMAH thermochemolysis can provide much more important information about organic compounds of different samples [294,563,648–650], such as amino acids [250,286,548,651–653], aliphatic and aromatic carboxylic acids [654], natural water, soil samples, and kerogen [655,656]. TMAH derivatization can increase the volatility of the nucleobases by decreasing the polarity of the labile molecules, which makes it easier to identify nucleic acids in the complex mixtures [647].

However, the classical process of offline thermochemolysis requires several steps, including the process of solvent derivatization, the thermochemolysis products extraction, and the supernatant drying under a flow of N<sub>2</sub> to remove solvent or separate derivatives prior to GC/MS analysis [264,657]. At present, these steps are too technically complex to be fully automated for *in situ* analysis in space, especially for the detection of organic compounds on Mars. Therefore, a simpler “on-line” thermochemolysis method suited to such an application has been implemented for SAM and MOMA. 500 μL of 25% TMAH in methanol and 15 μL of TMAH are stored in the SAM oven [2] and MOMA derivatization capsules [3], respectively. The TMAH thermochemolysis process needs to be tested and optimized according to the analysis conditions of the SAM and MOMA experiments, i.e. by contacting the sample and the TMAH directly in contact inside the pyrolysis furnace without any further sample processing. The results of TMAH derivatization are affected by the experimental conditions, such as TMAH concentrations, pyrolysis temperature, and volume of TMAH (which in turns affects pH) [286,287]. TMAH thermochemolysis, however, has rarely been considered for the analysis of nucleobases based on the SAM and MOMA missions, thus the experimental conditions as well



as the direct TMAH thermochemolysis process in SAM and MOMA conditions have yet to be optimized.

In this study, the TMAH thermochemolysis products of seven nucleobase standards and mixtures pyrolyzed at different temperatures were analyzed individually by Pyr-GC/MS. The derivatizations of all nucleobases at the optimal pyrolysis temperature, as well as the limit of detection (LOD) and limit of quantification (LOQ) of the nucleobases were determined. In addition, the thermochemolysis mechanisms of all nucleobases in TMAH were analyzed. This data is the first of its kind, benchmarking whether it would be possible to detect all or some of the studied nucleobases with the *in situ* TMAH thermochemolysis experiments on the SAM and MOMA experiments of the Mars Science Laboratory and ExoMars 2020 space missions. However, it should be noted that on Mars the nucleobases are contained in a solid matrix from which they will have to be extracted.

## 4.2 Experiments

### 4.2.1 Materials and methods

In this study, individual solutions of adenine (Sigma, purity > 99%), thymine (Fluka, purity > 99%), uracil (Alfa Aesar, purity > 99%), cytosine (Fluka, purity ~ 97%), guanine (Fluka, purity > 99%), xanthine (Alfa Aesar, purity > 99%) and hypoxanthine (Sigma, purity > 99%) were prepared by diluting the pure solid nucleobases in TMAH solutions (25% by weight in methanol, Sigma-Aldrich). The concentration of each nucleobase and their mixtures used in this study are shown in Table 4-1. TMAH was always in excess compared to the nucleobase, with a minimum of six molecules of TMAH for three methylation sites in the case of cytosine. Naphthalene-d8 (Sigma-Aldrich, isotopic purity: 99 atom % D) was used as an internal standard. All of the samples were stored in the refrigerator at 3°C.

Table 4-1 Detailed information of nucleobases used in this study.

Nucleobases	Amount (nmol)	Injection volume (μl)	Concentration (mol·L <sup>-1</sup> )
Adenine	0.125	0.05	2.5×10 <sup>-3</sup>
	0.25	0.10	2.5×10 <sup>-3</sup>
	2.50	0.01	0.25
Thymine	0.26	0.10	2.6×10 <sup>-3</sup>
Uracil	0.26	0.10	2.6×10 <sup>-3</sup>
Cytosine	15.0	0.05	0.3

Table 4-1 (continued)

Nucleobases	Amount (nmol)	Injection volume ( $\mu\text{l}$ )	Concentration ( $\text{mol}\cdot\text{L}^{-1}$ )
Guanine	11.0	0.05	0.22
Xanthine	0.22	0.10	$2.2\times 10^{-3}$
Hypoxanthine	1.20	0.10	$1.2\times 10^{-2}$
Adenine	18	0.10	0.18
Guanine	31	0.10	0.31
Cytosine	43	0.10	0.43
Mixtures	Thymine	0.19	$1.86\times 10^{-3}$
	Uracile	0.19	$1.86\times 10^{-3}$
	Xanthine	0.18	$1.57\times 10^{-3}$
	Hypoxanthine	0.86	$8.57\times 10^{-3}$

#### 4.2.2 Pyrolysis-GC/MS and methods

During the pyrolysis experiments, several amount of each nucleobase solution was pyrolyzed at 400°C, 500°C, and 600 °C, and 0.1  $\mu\text{l}$  of the mixture of seven nucleobases in solution were pyrolyzed at 600°C. The pyrolysis experiments were performed with an EGA/PY-3030D micro-oven pyrolyzer (Frontier Lab), installed on the Split/SplitLess (SSL) injector of a gas chromatograph (Trace GC Ultra, Thermo Scientific) coupled to a quadrupole mass spectrometer (ISQ LT, Thermo Scientific). An Optic 4 injector (GL Sciences) was used for the low temperature analyses (injection at 250°C and 300°C). It was connected to a GC (Trace GC Ultra, Thermo Scientific) coupled to a quadrupole mass spectrometer (DSQ II, Thermo Scientific). The GC was equipped with a Zebron ZB-5HT Inferno column (30 m  $\times$  0.25 mm i.d.  $\times$  0.25  $\mu\text{m}$  film thickness) with a 5 m integrated guard column. The temperature programming of the column started at 50°C, was held for 5 min, then heated at a rate of 6°C.min<sup>-1</sup> up to 240°C, then raised to 300°C at a rate of 10°C.min<sup>-1</sup> and held for 2 min. Helium was used as the carrier gas, with the helium flow rate in the column at 1.5 mL min<sup>-1</sup>. The split flow was 50 mL min<sup>-1</sup>. The temperature of the SSL injector was 280°C. The masses were scanned between m/z 40 and m/z 500. The ionization energy was 70 eV. These conditions are similar to those on SAM and MOMA since it can be used to analyze whether or not it will be able to detect nucleobases on Mars.

#### 4.2.3 Quantification of all nucleobases

A solution of naphthalene-d8 in dichloromethane was prepared at a concentration of  $0.05 \text{ mol}\cdot\text{L}^{-1}$ , and  $0.4 \mu\text{l}$  of naphthalene-d8 internal standard solution was added in each solution of the nucleobase. A standard solution of all seven nucleobases (A, G, T, U, C, X, and HX) at a concentration of  $0.01 \text{ mol}\cdot\text{L}^{-1}$  was prepared with the mix of TMAH (25% by weight in methanol) and  $\text{H}_2\text{O}$  in the same volume. For the calibration curve of guanine, different amounts of guanine (0, 15, 20, 40, 80, 120 nmol) were injected; for the other six nucleobases, 0, 5, 10, 15, 20, 30, 50 nmol were injected. The main peaks of each nucleobase ( $m/z = 177, 154, 140, 153, 194, 194, 164$ ) were chosen respectively as target products for A, T, U, C, G, X, and HX quantification.

In order to analyze the mixtures of all nucleobases, a new GC temperature program was used. The initial column temperature was set at  $40^\circ\text{C}$  and held for 2 min, followed by a ramp of  $3^\circ\text{C min}^{-1}$  up to  $200^\circ\text{C}$ . The temperature raised to  $300^\circ\text{C}$  at a rate of  $6^\circ\text{C min}^{-1}$  and maintained at this temperature for 2 min. The split ratio was set at 20:1. All of the nucleobase solutions were sampled in a clean capsule (pre-cleaned at  $1000^\circ\text{C}$  for 30 sec) and dried completely with a stream of nitrogen. Then  $3.0 \mu\text{l}$  of TMAH was added. All points were repeated more than three times. The quantification curves of all nucleobases were used to quantify the corresponding nucleobase.

## 4.3 Results and Discussion

### 4.3.1 Optimization of the thermochemolysis for nucleobases

To determine the optimal temperature of TMAH thermochemolysis by direct Pyr-GC/MS analysis, each of the seven nucleobases diluted in TMAH was pyrolyzed at  $400^\circ\text{C}$ ,  $500^\circ\text{C}$ , and  $600^\circ\text{C}$ .

#### 4.3.1.1 Adenine

2.5 nmol of adenine dissolved in TMAH was injected successively at  $400^\circ\text{C}$ ,  $500^\circ\text{C}$ , and  $600^\circ\text{C}$ , and all derivatives of adenine were analyzed. The chromatograms obtained are given in Figure 4-1A. At  $500^\circ\text{C}$ , 3-methyl-adenine was not detected. The five peaks 5, 6, 7, 8 and 9 were methylated derivatives of adenine which cannot be detected at  $400^\circ\text{C}$ , however, their exact tautomeric forms cannot be determined. The major peak is N, N, 9-trimethyl-adenine (or N, N, 9-trimethyl-9H-purin-6-amine, peak 2), and its three labile hydrogen sites are fully methylated at every tested temperature. At this amount of adenine (2.5 nmol), these two compounds were detected from  $400^\circ\text{C}$  to  $600^\circ\text{C}$ . However, it should be noted that the intensity

of all peaks increased strongly with the increase of pyrolysis temperature, and the optimal detection temperature of adenine in TMAH thermochemolysis was 600°C. According to our previous work, when the temperature is higher than 600°C, TMAH can be degraded. This gives rise to more byproducts [658], which are degradational to the thermochemolysis of nucleobases in TMAH; hence 600 °C is considered the optimal temperature for TMAH thermochemolysis experiments. Some siloxane peaks were detected in the thermochemolysis products of seven nucleobases at different temperatures, there are also siloxane in the blank experiments. Thus, these siloxanes may originate either from the thermal degradation of the septum of the GC injector or from the degradation of the stationary phase of the column caused by the corrosive effect of TMAH, or both.

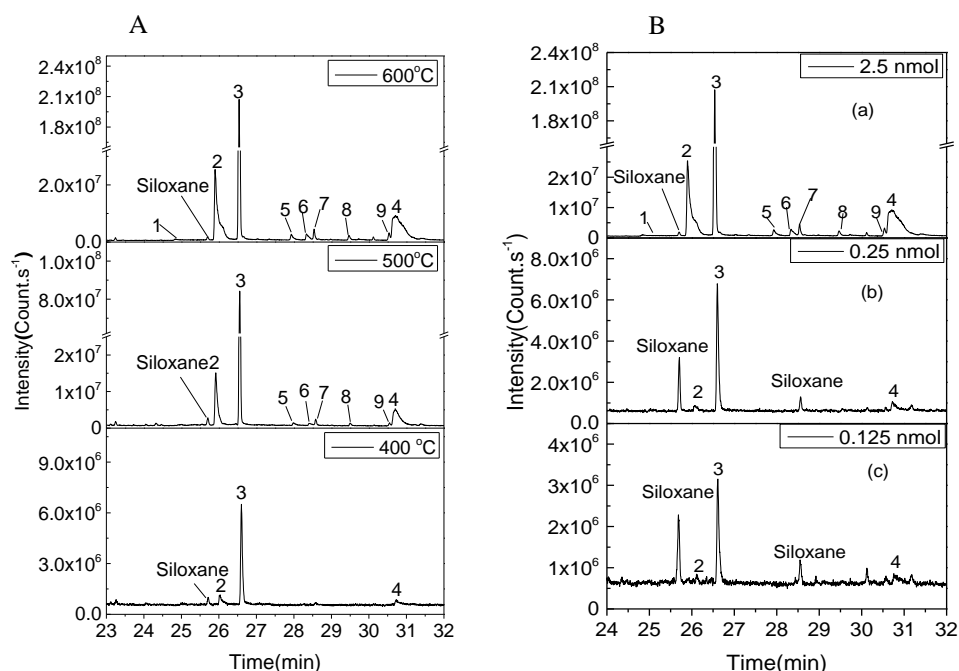


Figure 4-1: Chromatograms of adenine thermochemolysis in TMAH performed at different temperature (A: 600°C, 500°C, and 400°C.) and different amount (B: (a) 0.125 nmol (b) 0.25 nmol (c) 2.5 nmol). Chromatogram A: Peak 1: 3-methyl-3H-purin-6-amine; Peak 2: N, 9-dimethyl-9H-purin-6-amine; Peak 3: N, N, 9-trimethyl-9H-purin-6-amine; Peak 4: N, N, 3-trimethyl-3H-purin-6-amine; Peak 5: dimethyl adenine; Peak 6,7,8,9: trimethyl adenine. Note the break in the intensity scale to show the height of peak 3; Chromatogram B: Peak 1: 3-methyl-adenine; Peak 2: N, 9-dimethyl-adenine; Peak 3: N, N, 9-trimethyl adenine; Peak 4: N, N, 3-trimethyl-adenine; Peak 5: dimethyl adenine; Peak 6,7,8,9: trimethyl adenine. Note the break in the intensity scale to show the height of peak 3 in the 2.5 nmol chromatogram.

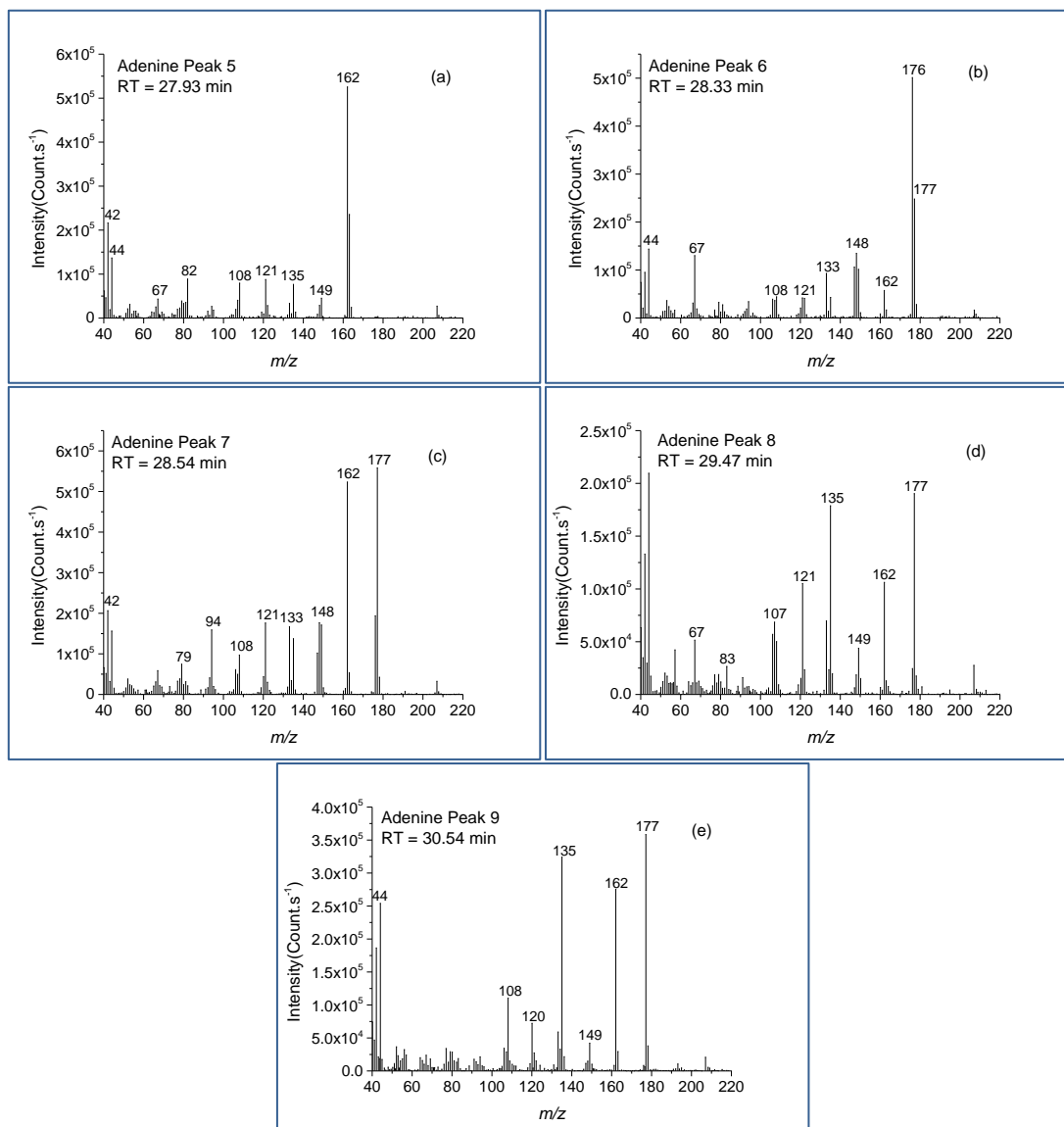


Figure 4-2: Mass spectra of adenine methylated through thermochemolysis. (a-e) 162 m/z corresponds to the molecular ion of dimethyladenine and (b-e) 177 m/z corresponds to the molecular ion of trimethylated adenine.

Figure 4-1B shows the chromatograms of different amounts of adenine thermochemolyzed at 600°C. For the 0.125 nmol adenine solution (Figure 4-1B(a)), three different methylated derivatives of adenine were identified, with low intensity peaks: a dimethylated form (peak 2: N, 9-dimethyl-adenine) and two kinds of trimethylated tautomeric forms (peak 3: N, N, 9-trimethyl-adenine, and peak 4: N, N, 3-trimethyl-adenine). No additional peaks were observed for an injection of 0.25 nmol (Figure 4-1B (b)). There were six adenine related peaks in addition to the three mentioned previously when 2.5 nmol of adenine was analyzed (Figure 4-1B (c)). Peak 1 is 7-methyl-adenine, which corresponds to the methylation

of adenine. The other five products could not be unambiguously attributed to specific derivatives of adenine. However, if the peaks with the highest  $m/z$  values represent the molecular ion (and not the fragment of a heavier molecule), the chromatographic data of five peaks correspond to a dimethyl derivative of adenine (peak 5:  $m/z$  163) and four trimethylated tautomeric forms (peaks 6, 7, 8 and 9:  $m/z$  177). The mass spectra corresponding to peaks 5 to 9 are given in Figure 4-2. All of the corresponding retention times, and the masses of the molecular ions and main fragments are given in Table 4-2. It should be noted that there are some other peaks on the chromatograms that are not related to adenine.

#### 4.3.1.2 Thymine and Uracil

Once thermochemolysis occurs, there are similar derivatized pyrimidine bases between thymine and uracil since they differ only by the presence of an additional methyl group at carbon position 5 in the thymine (i.e. 5-methyl-uracil, see Figure 4-3). Thymine and uracil solutions at a concentration of  $2.6 \times 10^{-3} \text{ mol} \cdot \text{L}^{-1}$  in TMAH were analyzed by Pyr-GC/MS.

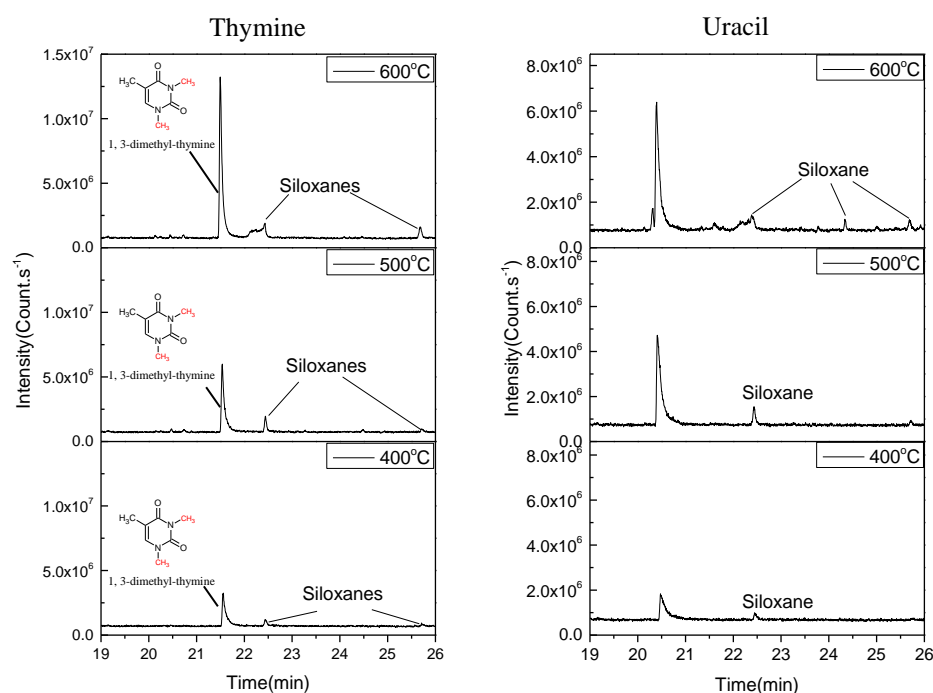


Figure 4-3: Chromatograms of thymine (0.26 nmol) and uracil (0.26 nmol) thermochemolysis in TMAH at different temperatures.

Since the compounds respond well to that concentration (high signal intensity), there was no need to inject a larger amount of thymine and uracil. The chromatograms of thymine

and uracil obtained at 400°C, 500°C, and 600°C are shown in Figure 4-3, respectively. 1, 3-dimethyl-thymine (1, 3, 5-trimethyl-2, 4 (1H, 3H) -pyrimidinedione) was the only compound derived from thymine detected at a retention time of 21.5 min. The only derivative of uracil was 1, 3-dimethyl-uracil (1, 3-dimethyl-2, 4 (1H, 3H) -pyrimidinedione) at a retention time of 20.4 min. The molecular ion masses of 1, 3-dimethyl-thymine and 1, 3-dimethyl-uracil and their major fragments are shown in Table 4-2, respectively.

For thymine and uracil, the thermochemolysis temperature had no effect on the number of derivatives detected, since only the canonical form was observed. However, the signal intensities of thymine and uracil were stronger at a higher pyrolysis temperature (i.e. 600°C), suggesting a high reaction rate. The optimal temperature for analysis of thymine and uracil pyrolysis products is 600°C, same as the case of adenine. As for adenine, siloxane peaks, coming from the column bleeding or septum decomposition, were detected.

#### **4.3.1.3 Cytosine**

Cytosine solution at a concentration of 0.3 mol·L<sup>-1</sup> in TMAH was analyzed by Pyr-GC/MS. Because injection of 0.3 and 2.5 nmol of cytosine in TMAH gave no chromatographic response, 15 nmol of cytosine in TMAH was used to prevent a possible decrease in the response of the cytosine derivatization at a lower temperature. Compared with the nucleobases studied above, the cytosine solution was much more concentrated. The difficulty of detecting cytosine is probably due to the high polar primary amino group. The analysis of amines is particularly problematic with Pyr-GC/MS not only because of their adsorption on the transfer line and the liner of the pyrolyzer, but also because of their interaction with the stationary phase of the chromatographic column (5% diphenyl/95% dimethyl polysiloxane), which results in significant spreading peaks.

The chromatograms of 15 nmol cytosine pyrolyzed at 400°C, 500°C, and 600°C are shown in Figure 4-4. Whatever the pyrolysis temperature, the same molecules were detected, including N, N, N-trimethyl-cytosine corresponding to the canonical form of the three methylated cytosine, and 2-O-methyl-cytosine corresponding to an enol form of the cytosine methylated on the oxygen atom site. Besides, peak 2 (m/z = 139), peaks 3 and 5 (m/z = 153) correspond to a dimethyl and trimethyl forms of cytosine, respectively. All of the cytosine derivatives in TMAH are summarized in Table 4-2. The mass spectra corresponding to peak 2, 3, and 5 are given in Figure 4-5, respectively. The spectrum of peak 5 spreads over several

minutes, and may overlap with other coeluted tautomers; however, according to the mass spectra, the main compound is trimethyl-cytosine. In summary, the major peaks correspond to two tautomeric forms of trimethyl-cytosine: N, N, N'-trimethyl-cytosine, which is the canonical form of the fully methylated cytosine, and another trimethylated tautomeric form.

As in the case of thymine, the thermochemolysis temperature of cytosine had no effect on the number of functionalized derivatives detected; six methylated derivatives of cytosine were observed at 400°C, 500°C, and 600°C, respectively. However, from a quantitative point of view, the intensity of cytosine peaks is higher at 600°C than that at other temperatures. Hence, 600°C is the optimal temperature.

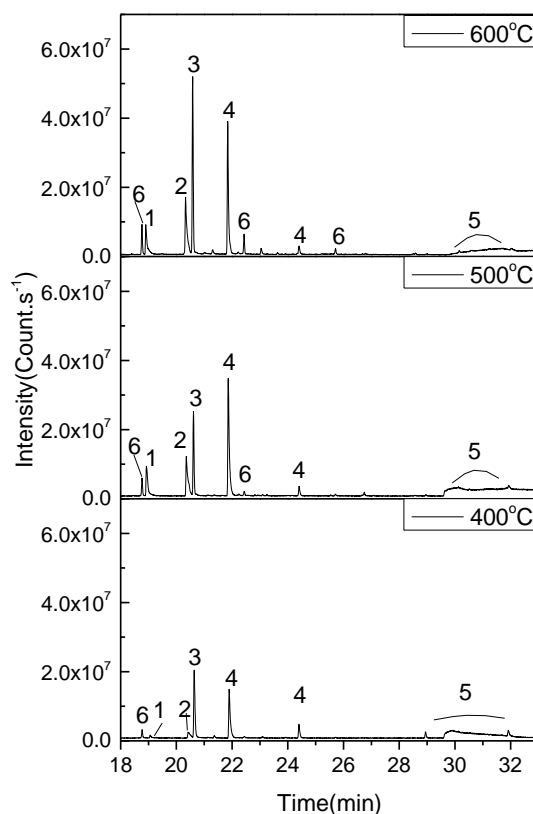


Figure 4-4: Chromatograms of cytosine (15 nmol) thermochemolysis in TMAH thermochemolysis at different temperatures (1: 4-amino-2-methoxy-pyrimidine; 2: dimethyl cytosine; 3: trimethyl-cytosine; 4: N, N, N'-trimethyl-cytosine; 5: trimethyl-cytosine; 6: siloxane).



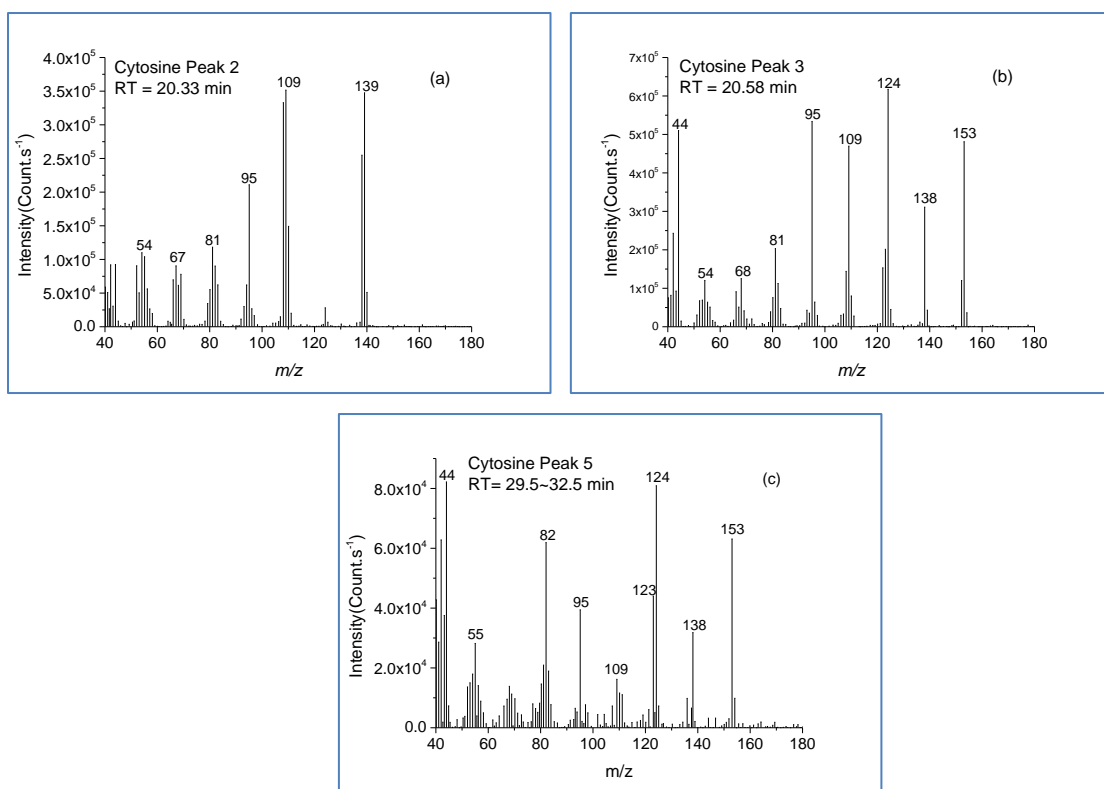


Figure 4-5: Mass spectra of methylated cytosine. 139  $m/z$  corresponds to the molecular ion of the dimethylated cytosine and 153  $m/z$  corresponds to the molecular ion of the trimethylated cytosine.

#### 4.3.1.4 Guanine

11 nmol of guanine in TMAH solution was injected to study the effect of thermochemolysis temperature. The chromatograms of guanine thermochemolyzed at 400°C, 500°C, and 600°C are shown in Figure 4-6. 1, 3, 7-trimethylxanthine (caffeine) was identified using the NIST database when guanine is thermochemolyzed at 500°C and 600°C. The other peaks were identified from the  $m/z$  ratios of their supposed molecular ions, including dimethyl-guanine (peak 2,  $m/z$  179), three tautomers of trimethyl-guanine (peaks 3, 5 and 9,  $m/z$  193) and four tautomers of tetramethyl-guanine (peaks 4, 6, 7 and 8,  $m/z$  207). The mass spectra corresponding to peaks 2 to 9 are given in Figure 4-7. Some other compounds are also detected with lower intensity, such as glycoamine (RT=20.0 min) and mesalamine (RT=21.3 min).

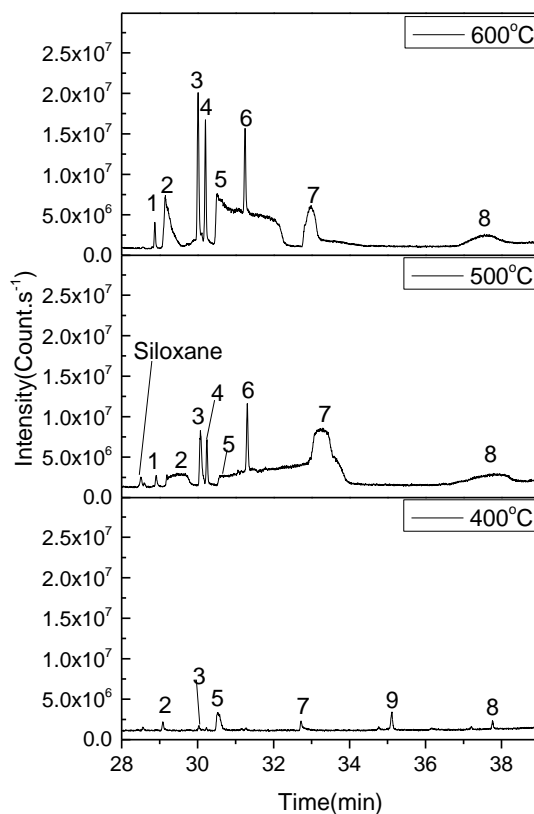


Figure 4-6: Chromatograms of guanine (11 nmol) thermochemolysis in TMAH at 600 °C, 500 °C, and 400 °C. (1: caffeine; 2: dimethyl-guanine; 3 and 5: trimethylguanaine; 4, 6, 7, 8: tetramethylguanaine; 9: trimethylguanaine).

The intensity of peaks generally increased with the increase in temperature. However, Peak 9 (trimethyl-guanine) was observed only at 400°C while peaks 1, 4, and 6 were not detected at 400 °C. Peak 1 corresponds to the methylated xanthine from the degradation of guanine as mentioned before, which probably occurs at temperatures above 400°C. Peaks 4 and 6 correspond (according to the  $m/z$  ratios of the molecular ion) to two tautomers of tetramethylated guanaine. Trimethyl-guanine (peak 9) certainly coeluted with peak 7 at a higher temperature than 400°C. All detected compounds of guanaine can be seen in Table 4-2.

Compared with adenine and cytosine, guanaine is the third nucleobase with a primary amine moiety that can decrease the effectiveness of GC/MS analysis dramatically. At low temperatures of 250°C and 300°C, no thermochemolysis products of guanaine in TMAH solutions were detected. Thus, we conclude that thermochemolysis reactions barely occur at temperatures lower than 400°C to 600°C. However, it was difficult to analyze guanaine because of the numerous derivatives and the spread and often coeluted peaks.

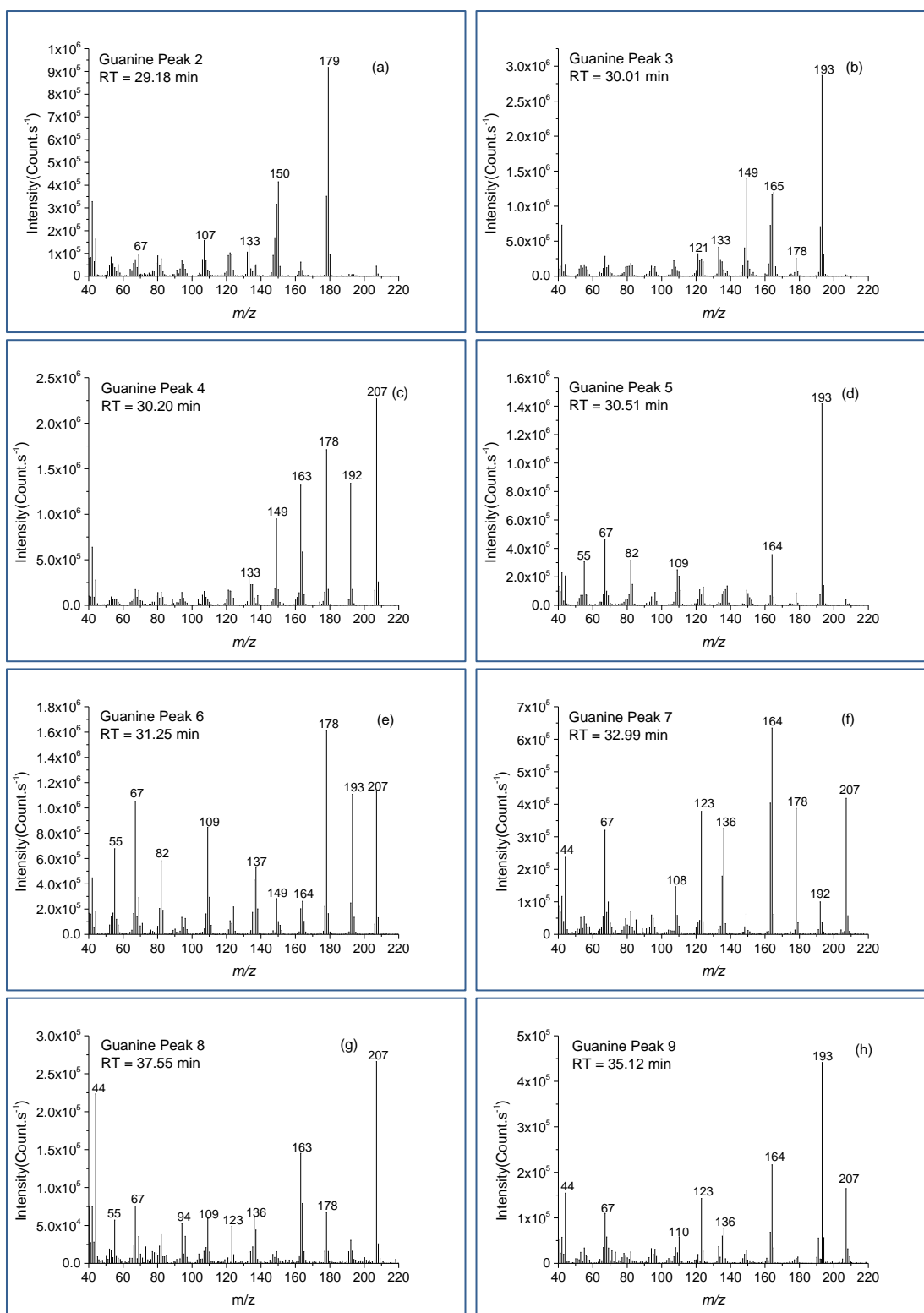


Figure 4-7: Mass spectrum of methylated guanine. 179 *m/z* corresponds to the molecular ion of dimethyl guanine, 193 *m/z* corresponds to the molecular ion of trimethylated guanine, and 207 *m/z* corresponds to the molecular ion of tetramethylated guanine.

#### 4.3.1.5 Xanthine

$2.2 \times 10^{-3}$  mol·L<sup>-1</sup> of xanthine in TMAH was used. Like thymine and uracil, xanthine responded well at the lower concentration. The chromatograms of xanthine obtained at 400°C, 500°C, and 600°C are shown in Figure 4-8. The only derivative of xanthine detected was 1, 3, 7-trimethylxanthine (caffeine; TR = 28.90 min at 600°C), which is the trimethylated form of xanthine, with a mass of the molecular ion of 194 g·mol<sup>-1</sup>. As shown in Figure 4-8, the signal intensity increased with the increase of thermochemolysis temperature, and the optimal analysis temperature was 600°C.

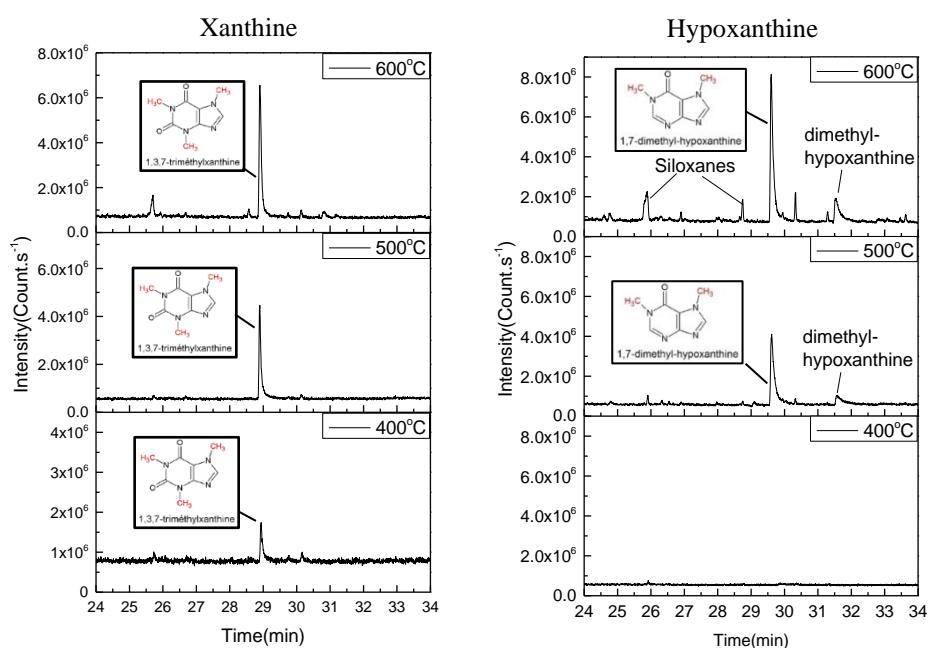


Figure 4-8: Chromatograms of xanthine (0.22 nmol) and hypoxanthine (1.2 nmol) thermochemolysis in TMAH at different temperatures.

#### 4.3.1.6 Hypoxanthine

The chromatograms of hypoxanthine in TMAH solutions obtained at the pyrolyzed temperature of 400 °C, 500 °C and 600 °C are given in Figure 4-8. There are two derivatives of hypoxanthine, 1, 7-dimethyl-hypoxanthine (the main peak, at a retention time of 29.60 min at 600 °C) with relatively higher intensity and dimethyl-hypoxanthine tautomer (at a retention time of 31.52 min at 600 °C) with lower intensity. There were virtually no compounds released at 400 °C; the derivative compounds were only detectable above 500 °C. Some nucleobases—such as thymine, uracil, xanthine, and hypoxanthine, which were completely methylated on

their intracyclic nitrogen (trimethyl substitutions of xanthine, dimethyl substitutions of hypoxanthine)—were detectable at low concentration.

#### 4.3.2 Thermochemolysis patterns

All derivatized compounds detected are listed in Table 4-2. It can be seen that most of the derivatized compounds are the methylated products of the seven nucleobases. However, the nucleobases exist in different tautomeric forms because of the presence of  $\pi$  bonds and non-binding doublet. Tautomerism of the nucleobases is manifested by the delocalization of  $\pi$  electrons and the displacement of a hydrogen atom, thus the protons move from one site to another and transform from a functional group into another within the same molecule. There are two kinds of prototropic tautomerisms in nucleobases, one is the keto-enol tautomerism, where the ketone form is in equilibrium with the enol form (C=C with OH functional group in the vinyl position) and imine-enamine tautomerism, where the enamine forms (ethylenic alpha amine) and is in equilibrium with the ketimine form. Imine-enamine tautomerism is involved in all the above-mentioned nucleic bases. In all cases, different tautomeric forms of the same molecule coexist in an equilibrium that can be displaced towards one or the other, depending on pH, temperature, and solvent (with the pH value of dependent on the solvent). As a result, the position of the methylation sites varies with labile protons moving within the molecule. The proton is substituted by the methyl group and acquires the stable form. Hence, there are different methylation forms of nucleobases besides the canonical form.

For adenine, there are three possible methylation sites: one is at the N9 position, and the two others are at the N10 position, as shown in Figure 4-9. During the TMAH thermochemolysis process, dimethyl and trimethyl-adenine were detected. As shown in Figure 4-1A, the peak intensity of N, N, 9-trimethyl-adenine, which is the methylated products of the N9H form of adenine, was the highest. This is because the N9H tautomeric form is the major form of adenine and the N7H and N3H tautomeric forms are minor forms [659,660], however, the formation and observation of the 7(H) and 3(H) tautomers may be facilitated in the solution phase [661]. The N, 9-dimethyl-adenine form was the second highest peak at 600°C, which is also the methylated derivative of the N9H form of adenine. According to Fonseca Guerra [660], the natural N9H form of adenine was the most stable tautomer of the twelve systems studied and the stability of the N3H form of adenine was preceded only by the N9H form. Hence, the methylated derivatives of the N7H form of adenine were also detected during the TMAH thermochemistry process. 7-methyl-adenine and N, N, 3-trimethyl-adenine are the monomethyl

substitution and trimethyl substitution, respectively. The content of trimethyl substitution products was higher than that of monomethyl substitution or dimethyl substitution, which demonstrates that the trimethyl substitution products are more stable than other substitutions.

Table 4-2: The thermochemolysis products detected from different nucleobases.

Nucleobases	Retention time	Base peak	Masses of fragments* and relative abundance: <i>m/z</i> (%)	Compounds
Adenine	24.84	149	<b>149(100)</b> , 44(86), 148(27), 42(26), 122(23), 121(11), 207(10), 53(10), 68(9)	7-methyl-adenine
	25.90	163	<b>163(100)</b> , 107(72), 135(69), 134(55), 80(31), 133(30), 162(27)	N, 9-dimethyl-adenine
	26.54	148	<b>148(100)</b> , 162(38), 177(34), 107(22), 133(22), 135(15), 106(12)	N, N, 9-trimethyl-adenine
	27.93	162	<b>162(100)</b> , 163(45), 42(41), 82(17), 121(17), 108(15), 135(15)	dimethyl-adenine
	28.33	176	<b>176(100)</b> , 177(56), 148(33), 147(23), 67(24), 133(20), 42(16)	trimethyl-adenine
	28.54	162	<b>162(100)</b> , 177(91), 176(44), 148(37), 42(38), 133(30), 94(30), 121(29)	trimethyl-adenine
	29.47	177	<b>177(100)</b> , 135(93), 44(92), 42(83), 121(63), 162(44), 133(41), 107(32)	trimethyl-adenine
	30.54	177	<b>177(100)</b> , 135(81), 162(66), 44(50), 42(49), 108(21), 120(15), 133(10)	trimethyl-adenine
	30.72	148	<b>148(100)</b> , 162(59), 177(34), 134(30), 107(21), 135(21), 119(18)	N, N, 3-trimethyl-adenine
Thymine	21.49	154	<b>154(100)</b> , 68(93), 69(46), 42(41), 97(15), 96(11), 56(9.0)	1,3-dimethyl-thymine
Uracil	20,40	140	<b>140(100)</b> , 42(62), 55(53), 83(43), 82(29), 54(15), 56(11)	1,3-dimethyl-uracile
Cytosine	18.90	95	<b>95(100)</b> , 125(72), 124(50), 68(38), 67(19), 96(16), 41(15)	4-amino-2-methoxy-pyrimidine
	20.33	139	<b>139(100)</b> , 109(80), 108(63), 138(59), 95(53), 110(32), 81(22)	dimethyl-cytosine
	20.58	153	<b>153(100)</b> , 124(39), 152(7), 123(7), 138(5), 44(1.14), 95(1)	trimethyl-cytosine
	21.36	72	<b>72(100)</b> , 44(68), 153(15), 71(17), 207(10)	2-(dimethylamino)-1-phenyl-1-propanone

Table 4-2 (continued)

Nucleobases	Retention time	Base peak	Masses of fragments* and relative abundance: <i>m/z</i> (%)	Compounds
	21.84	124	<b>124(100)</b> , 153(75), 55(44), 95(43), 96(36), 42(29), 54(13)	N, N, N'-trimethyl-cytosine
	24.40	123	<b>123(100)</b> , 96(76), 42(72), 154(58), 44(46), 80(37)	2-amino-4,6-dimethyl-pyrimidine
	28.95	166	<b>166(100)</b> , 44(65), 197(26), 139(23), 109(20), 83(19), 138(11)	3,4,5-trimethoxybenzylamine
	30-37	153	<b>153(100)</b> , 124(44), 42(13), 138(11), 125(6), 154(5), 123(4), 152(3)	trimethyl-cytosine
Guanine	19.98	122	<b>122(100)</b> , 123(7)	Glycocyanine
	21.28	136	<b>136(100)</b> , 108(7)	Mesalamine
	28.88	194	<b>194(100)</b> , 109(62), 55(44), 82(29), 44(27), 67(26), 193(20),	Caffeine (1, 3, 7-trimethyl-xanthine)
	29.18	179	<b>179(100)</b> , 150(49), 42(45), 178(40), 149(37), 107(27), 44(24)	dimethyl-guanine
	30.01	193	<b>193(100)</b> , 149(65), 164(51), 165(52), 42(48), 192(21), 163(28)	trimethyl-guanine
	30.20	207	<b>207(100)</b> , 178(94), 163(71), 192(54), 42(54), 149(48), 44(31), 164(28)	tetramethyl-guanine
	30.51-32.21	193	<b>193(100)</b> , 82(32), 55(31), 42(29), 67(27), 164(24), 109(22)	trimethyl-guanine
	31.25	178	<b>178(100)</b> , 67(70), 207(67), 109(52), 55(41), 82(40), 137(36)	tetramethyl-guanine
	32.99	164	<b>164(100)</b> , 207(65), 123(64), 163(60), 178(50), 136(40), 67(23)	tetramethyl-guanine
	37.10-38.00	207	<b>207(100)</b> , 44(66), 163(49), 178(30), 42(30), 164(29), 67(24), 109(14)	tetramethyl-guanine
	35.12	193	<b>193(100)</b> , 164(92), 123(60), 67(32), 163(24), 110(28), 136(20)	trimethyl-guanine(400°C)
Xanthine	28.90	194	<b>194(100)</b> , 109(52), 67(47), 55(38), 82(32), 193(21), 42(13)	1, 3,7-trimethyl-xanthine (caffeine)
Hypoxanthine	29.60	164	<b>164(100)</b> , 163(58), 42(44), 110(14), 68(14), 67(13), 53(9)	1,7-dimethyl-hypoxanthine
	31.52	164	<b>164(100)</b> , 135(56), 42(56), 82(21), 163(16), 67(10), 108(9)	dimethyl-hypoxanthine

Note: \* the masses of the main fragments are in order of decreasing abundance; the mass marked in bold is the main peak.

For thymine and uracil, only the methylated canonical forms were detected during the TMAH thermochemolysis. Although the keto form, enol form, and keto-enol tautomerism of thymine and uracil have been reported before [662–666], the canonical tautomer is thermodynamically more stable than all enol and dienol forms. Therefore, the canonical tautomer is the main thermochemolysis product of thymine and uracil in TMAH solution as shown in Figure 4-3. There are two active sites (secondary amine) on the thymine and uracil at N1 and N3 position, and they are replaced by a methyl group during TMAH thermochemolysis, as shown in Figure 4-9. The absence of methylation of the enolactic tautomeric forms of thymine and uracil is explained by the keto-enolic thermodynamic equilibrium shifted very strongly in favor of the ketone form. Therefore, 1, 3-dimethyl-thymine and 1, 3-dimethyl-uracil are detected, which are the most stable methylated products of thymine and uracil, respectively.

For cytosine, various tautomeric forms have been detected in different studies [667]. These are mainly amino-oxo, imino-oxo and amino-hydroxy forms of cytosine. The computational investigations have obtained different results via different methods. The amino-hydroxy tautomer was found to be the most stable in the gas phase, and the canonical amino-oxo form seemed to be the most stable one under aqueous solvation [668–670]. In TMAH solutions, methylated cytosine in canonical forms, such as trimethyl-cytosine and N, N, N'-trimethyl-cytosine, were the main products, which means that the canonical amino-oxo form of cytosine was also the most stable form in TMAH solutions. In addition, there are relatively weak peaks of the methylated compounds of cytosine in enol form, such as 4-amino-2-methoxy-pyrimidine (Figure 4-4, peak 1), 2-(dimethylamino)-1-phenyl-1-propanone (Figure 4-4, RT=21.36 min), 2-amino-4,6-dimethyl-pyrimidine (Figure 4-4, RT=24.40 min), and 3,4,5-trimethoxybenzylamine (Figure 4-4, RT=28.95 min).

According to the guanine thermochemolysis chromatograph, there were more tautomeric transformations of guanine compared with cytosine. The keto (amino-oxo) and enol (amino-hydroxy) forms were the most stable forms according to the value of the relative energies of the tautomers of guanine and both exist in approximately equal concentrations [671]. The 7-, 9- or 1-methylations of guanine and dimethylated guanine were identified by some researchers using Infrared spectroscopy (IR) [672–674]. In our study, the dimethyl, trimethyl, and tetramethyl-guanine were detected and are probably the methylated products of the 9NH or 7NH form of guanine. These are the products of methylation and oxidative deamination of guanine, as shown in Figure 4-9. The deamination and oxidation of guanine to xanthine, which



was methylated by TMAH on its three labile hydrogen atoms, 1, 3, 7-trimethylxanthine (caffeine) was consequently detected.

Hypoxanthine and guanine are structurally very similar, and they play an important role during the DNA replication process and can form a base pair with cytosine. From this point of view, therefore, hypoxanthine also has keto-enol and prototropic tautomeric phenomena [672,675,676]. The keto-N7H and keto-N9H forms are the most stable forms of hypoxanthine, and there are two possible substituted sites at N1 and N7 position. According to the chromatograph of the hypoxanthine, dimethyl products were detected in excessive TMAH solutions, which must be the most stable methylated forms of hypoxanthine. Xanthine also has a similar structure with hypoxanthine, there are three possible substituted sites, N1, N3, and N7 position. Therefore, the trimethyl form must be the most stable methylated product of xanthine.

TMAH can improve pyrolysis by mild thermal decomposition and a selective cleavage of ester and ether bonds as opposed to random and uncontrolled thermal decomposition and fragmentation of the organic material via standard pyrolysis [2]. During the thermochemolysis of nucleobases, tautomerism transformations of all nucleobases occur. TMAH also plays an important role by promoting the cracking of N-H bonds at 600°C; thus the fragments of nucleobases in stable tautomerism forms are methylated and form the stable derivatives. It is not surprising that the methylated compounds of all of the nucleobases detected by GC/MS were their most stable forms in an aqueous phase. Their characteristic methylated compounds are summarized in Table 4-3. Thymine, uracil, and xanthine each have only one unique characteristic peak individually; however, the case is different for the other four kinds of nucleobases, as at least two characteristic peaks correspond to their identification. Hence, the characteristic thermochemolysis products of each nucleobases (list in Table 4-3) could be used to identify these nucleobases on MOMA or SAM.

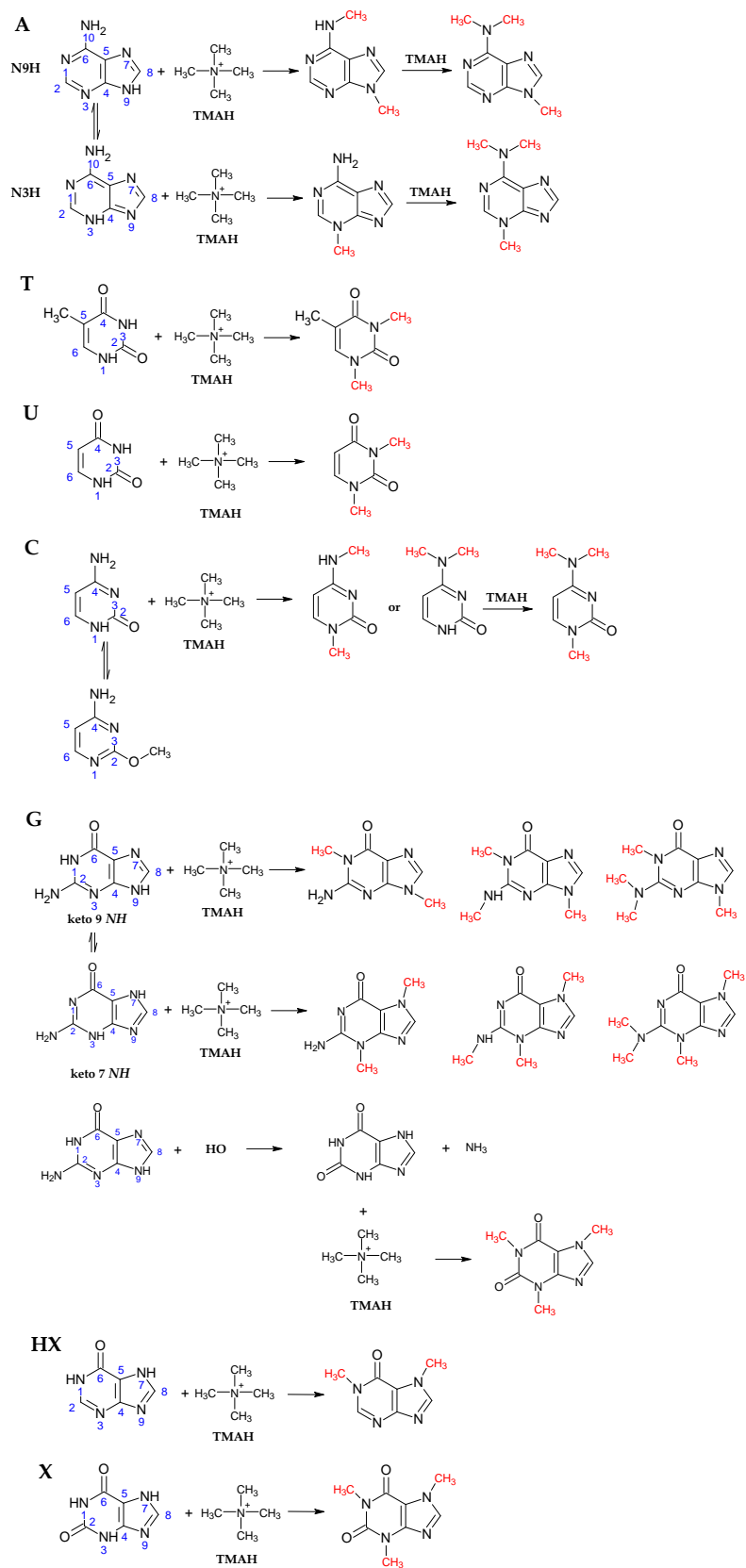


Figure 4-9: The TMAH thermochemolysis schemes of seven nucleobases.

### 4.3.3 Analysis of the mixture of nucleobases

The chromatogram corresponding to the thermochemolysis of 0.1  $\mu\text{l}$  of the nucleobases mixture detected at 600°C is shown in Figure 4-10, and the concentration and the amount of each nucleobase are shown in Table 4-1. The methylated derivatives of the nucleobases detected as well as their retention times and the associated parent molecules are listed in Table 4-4. The characteristic peak of each nucleobase appears at different retention times but in the same order as shown in Table 4-3 because the temperature programming of the column was changed (starting at 50°C held for 2 min, then at a heating rate of 3°C min<sup>-1</sup> up to 170°C then raised to 300°C at a rate of 10°C min<sup>-1</sup> and maintained for 3 min).

Each of the seven nucleobases was identified when more samples were used, and the derivatives of thymine, uracil, xanthine, and hypoxanthine were uniquely identified. All compounds were the methylated canonical form of all their labile hydrogens, except for dimethyl-hypoxanthine, where a second tautomer was detected. Compared with five different methylated derivatives during the injection of 15 nmol of cytosine, only the trimethylated canonic form, one of the weakest peaks, was detected.

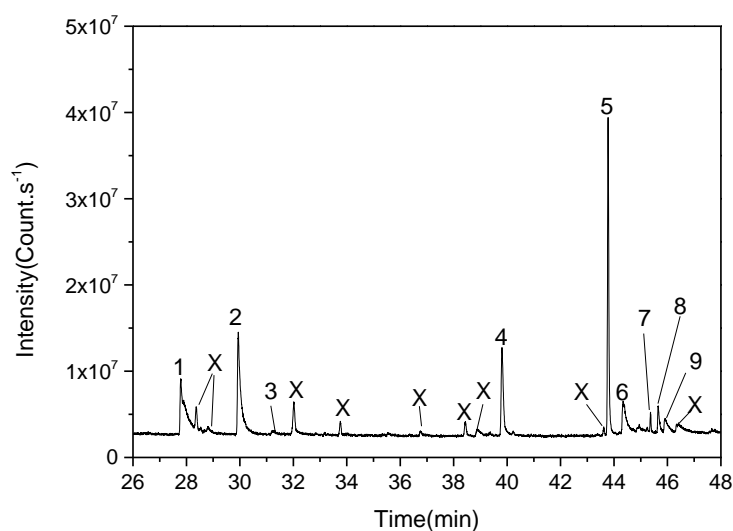


Figure 4-10: Chromatogram of seven nucleobases mixtures dissolved in TMAH thermochemolysis at 600°C. Peak 1: 1, 3-dimethyl-uracil; Peak 2: 1, 3-dimethyl-thymine; Peak 3: N, N, N'-trimethyl-cytosine; Peak 4: N, N, 9-trimethyl-adenine; Peak 5: 1, 3, 7-trimethyl-xanthine (caffeine); Peak 6: 1,7-dimethyl-hypoxanthine; Peak 7: methyl ester hexadecanoic acid; Peak 8: trimethyl-guanine; Peak 9: trimethyl-adenine Peak X: Siloxane.

Table 4-3: The characteristic peaks of the seven nucleobases in TMAH.

Nucleobase	Retention time (min)	Characteristic peak
Uracil	20.40	1, 3-dimethyl-uracil
Thymine	21.49	1, 3-dimethyl-thymine
Cytosine	21.84	N, N, N'-trimethyl-cytosine
Adenine	26.54	N, N, 9-trimethyl-adenine
Xanthine	28.90	1, 3, 7-trimethylxanthine
Hypoxanthine	29.60	1,7-dimethyl-hypoxanthine
Guanine	30.01	trimethyl-guanine

Table 4-4: The methylated components detected from pyrolysis of the nucleobases mixture.

Retention time (min)	Component	Parent compound
27.79	1, 3-dimethyl-uracil	Uracil
29.94	1, 3-dimethyl-thymine	Thymine
31.19	N, N, N'-trimethyl-cytosine	Cytosine
39.81	N, N, 9-trimethyl-adenine	Adenine
43.78	1, 3, 7-trimethyl-xanthine (caffeine)	Xanthine
44.34	1,7-dimethyl-hypoxanthine	Hypoxanthine
45.66	trimethyl-guanine	Guanine
45.91	trimethyl-adenine	Adenine

Compared with the nine derivatives obtained by the pyrolysis of 2.5 nmol of adenine, two derivatives were observed in the 0.1 $\mu$ L mixture. The predominant peak of adenine corresponded to the trimethylated canonical structure whereas the second peak of low intensity was a trimethyl tautomer form of adenine. A single derivative of guanine with low intensity was also detected. Guanine was the only nucleobase whose methylation was uncompleted: only three out of four labile hydrogens were replaced by methyl groups. A small amount of guanine was detected due to the oxidative deamination of guanine which degraded to xanthine. This is also the reason for the high intensity of the 1, 3, 7-trimethyl xanthine peak, which is preponderant in the chromatogram. In addition, there were no interactions among seven nucleobases, because there were nearly no obvious cracking reactions of nucleobases at low temperature.

We conclude that among the seven nucleobases, four peaks with high intensity should be easily detected by thermochemolysis if there were in the nanomole range or higher amounts

in natural samples, including xanthine, adenine, thymine, and uracil. Due to the oxidative deamination of guanine to xanthine during thermochemolysis, detection of xanthine may also be a strong indicator of the presence of guanine.

#### 4.3.4 Quantification study of nucleobases

Limit of detection (LOD) and limit of quantitation (LOQ) can be determined by signal-to-noise (S/N) and relative standard deviation (RSD). A value of S/N=3 or RSD $\approx$ 17% can be used for LOD, S/N=10 or RSD $\approx$ 5% can be used for LOQ[677–681]. Therefore, S/N=3 and S/N=10 were used to determine the LOD and LOQ of the nucleobases in this study. The calibration curves of nucleobases were obtained by plotting peak area ratio values (the peak area of nucleobases/internal standard peak area) against the concentration ratio of nucleobases (nucleobases amount/internal standard amount).

Naphthalene-d8 was used as the internal standard, and the stability was tested five times at 600°C. The average peak area of Naphthalene-d8 was about  $3.2 \times 10^8$  cps.s<sup>-1</sup>.min; the % RSD was about 6.96%, which is calculated by the average divided by the standard deviation (about  $2.26 \times 10^7$  cps.s<sup>-1</sup>.min). Moreover, we observed no degradation of the Naphthalene-d8 after a pyrolysis at 600°C compared at the same GCMS injection at 270°C in the GC injector. Therefore, because of its good stability at 600°C, naphthalene-d8 was used as our internal standard.

Table 4-5 LOD and LOQ values and the standard curves of each nucleobase.

Nucleobases	LOD(nmol)	LOQ(nmol)	Linear regression equation	Correlation coefficient
Adenine	0.075	0.15	$y = 0.0190x - 0.00001$	0.9975
Thymine	0.075	0.15	$y = 0.0250x + 0.0259$	0.9989
Uracil	0.075	0.30	$y = 0.0023x - 0.0038$	0.9973
Cytosine	0.55	0.65	$y = 0.0004x - 0.0015$	0.9898
Guanine	0.40	0.675	$y = 0.0002x - 0.0004$	0.9958
Xanthine	0.15	0.275	$y = 0.0090x + 0.0018$	0.9992
Hypoxanthine	0.75	0.95	$y = 0.0006x - 0.0019$	0.9805

To confirm the value of LOD and LOQ for each sample, all experiments were run in triplicate. The LOD and LOQ value and the linearity of standard curves for each nucleobase are summarized in Table 4-5. We conclude that the relativity of standards curves is not a sufficient metric, as shown in Figure 4-11, possibly because of the interaction of TMAH with the column.

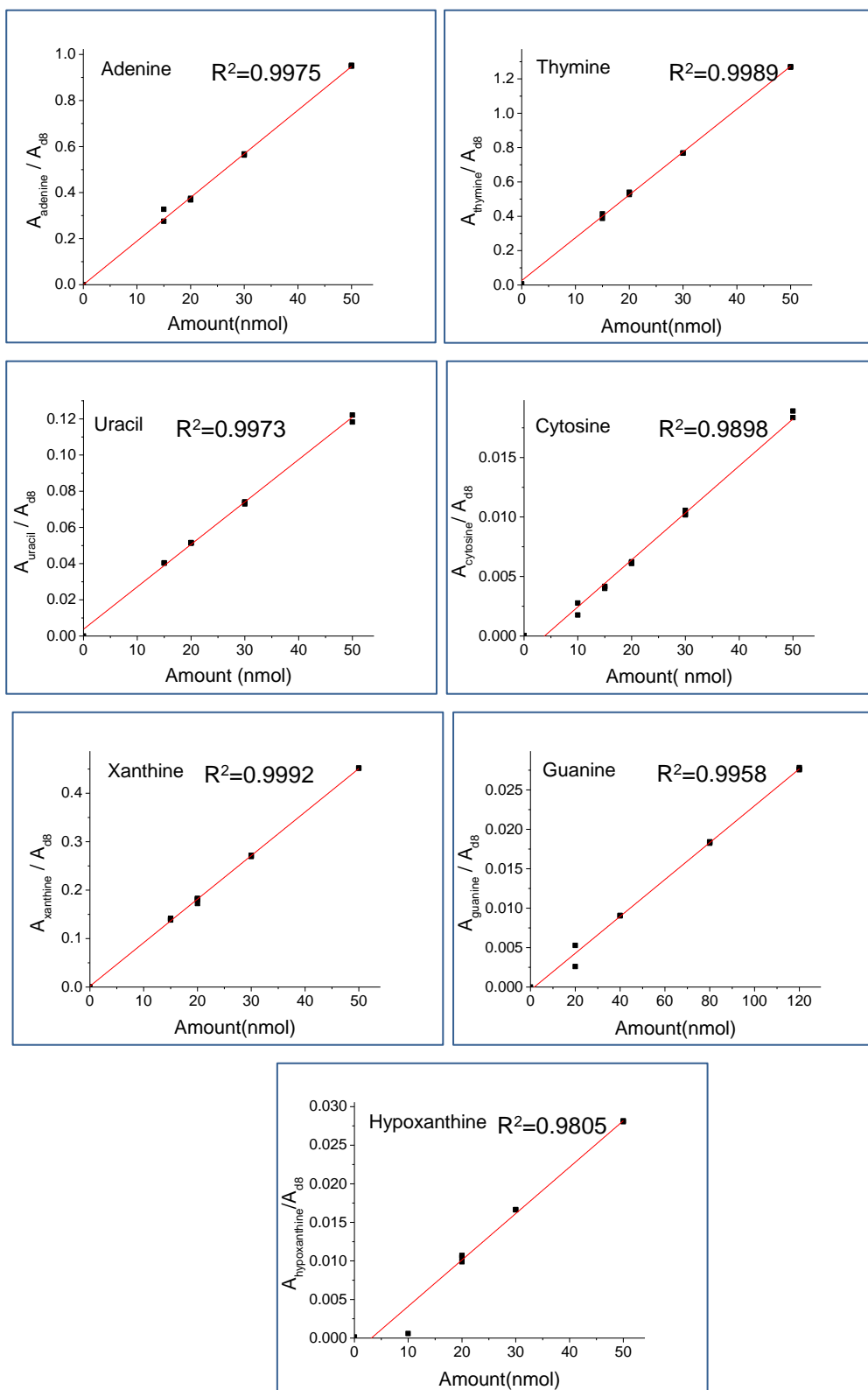


Figure 4-11: Calibration curves for the seven nucleobases.

## 4.4 Conclusion

We conclude that TMAH thermochemolysis allows for the methylation and detection of the seven nucleobases investigated in this study. The optimal temperature for nucleobase thermochemolysis under SAM and MOMA conditions was 600°C. Trimethyl-adenine, 1,3-dimethyl-thymine, 1,3-dimethyl-uracil, trimethyl-cytosine, 1,3,7-trimethyl-xanthine (caffeine) and dimethyl-hypoxanthine were the main methylated products of adenine, thymine, uracil, cytosine, guanine, and xanthine, and hypoxanthine, respectively, because they are the most stable forms of each nucleobase in a gas phase or in aqueous form. In addition, there was no interaction among these nucleobases when pyrolyzed in a mixture, which makes it possible to detect different nucleobases in natural samples. However, oxidative deamination of guanine to xanthine may also lead to misidentifications when these molecules are detected in unknown samples. The presence of the  $-NH_2$  group also induces a tautomerization of the molecule and therefore multiplies the number of methylated derivatives detected for each of these nitrogenous bases. Based on the values of LOD and LOQ for each nucleobase, adenine, thymine, and uracil are easier to be detected, as they can be detected at about 0.15 nmol. It is possible, though more difficult, to detect the guanine, cytosine and hypoxanthine (LOD=0.40, 0.55 and 0.75 nmol, respectively). However, the complex matrix needs to be pretreated with the extraction process in order to detect the nucleobases on Mars, the LOD may be higher than value of our study.

According to the observed retention times, potential coelutions may occur in studies of mixtures of different nucleobases at high concentrations. This was mainly due to the spread of cytosine peaks (between 30 and 37 min), guanine (between 30.5 and 32.2 min) and, to a lesser extent, adenine (around 30.7 min). There was also a coelution between dimethyl-uracil (at the retention time of 20.40 min) and dimethyl cytosine (at the retention time of 20.33 min), though these problems can be avoided by using a lower column heating rate. In addition, some nucleobases with a primary amine function ( $-NH_2$ ), such as adenine, guanine, and cytosine, displayed a spreading of the chromatographic peaks because of the interaction of the amine group with the stationary phase of the column.

All nucleobases detected here had relatively high retention times in the range of 27 to 47 minutes of elution with the temperature programming of the column used here (50°C for 2 min, then 3°C min<sup>-1</sup> up to 170 °C then 10 °C.min<sup>-1</sup> up to 300°C, held 3 min), the column of MOMA flight instruments is shorter than the column used herein; Therefore, it would be more easier to detect the nucleobases related compounds *in situ*, such as trimethyl-guanine, trimethyl-

adenine and dimethyl-hypoxanthine; and signs of adenine and hypoxanthine can be detected when the temperature is lower than 250°C. What's more, the separation and detection abilities of the device on SAM and MOMA will be tested in the coming missions, and SAM is ready to do the TMAH analysis experiments soon; MOMA will be ready in 2022. In a word, it would be possible to detect the nucleobases if the samples are fresh and their content are higher than the limit of detection of the device on Mars and MOMA, and our results laid the data foundation for the implementation of SAM and MOMA missions.



## **Chapter 5. Application of TMAH thermochemolysis to the detection of nucleic acids: application to the MOMA and SAM space experiment.**

Deoxyribonucleic acid (DNA), as information carrier, stores the information that defines the organism in unique orders of four bases (A, T, C, G) located in tiny molecules, and this way of storing information has continued for three billion years, and some studies have suggested that DNA can be placed in the extremely cold regions of the Earth or even on Mars for millennium-long storage [144]. RNA probably formed the basis of first life, which is made up of sequences of four different nucleotides, the latter of which can be formed through reaction source. RNA polymers must have emerged very quickly after the deposition of meteorites (less than a few years), and the synthesis of nucleotides and their polymerization into RNA occurred in just one to a few wet-dry cycles [145]. Even artificial nucleic acids may exist in a large number of chemical alternatives; however, biological RNA and DNA are universal, unique, and very conservative. The role of RNA in the origin of life is well established, and how RNA emerged on the early Earth is one of the first steps in understanding the origin of life [682]. Therefore, it's essential to study the detection efficiency of DNA or RNA and their fragments. Nucleobases, nucleosides, and nucleotides are the components of DNA and RNA. Nucleobases are of the most important building blocks of DNA and RNA; nucleosides consist of nucleobases and ribose. Nucleotides and nucleotriphosphates are organic molecules consisting of a nucleoside and a phosphate. Since their structures are different though with some similarities, their behaviors could be different when thermochemolysis with TMAH. Therefore, in this chapter, nucleosides, nucleotides, and nucleotides triphosphate of DNA and RNA were analyzed with TMAH thermochemolysis, in order to evaluate the efficiency and the potential of TMAH thermochemolysis on the analyze with real DNA or RNA samples. At last, TMAH thermochemolysis was applied to analyze poly A, which is the RNA tail and plays an important role in protecting the RNA molecular.

## 5.1 Experiment conditions

### 5.1.1 Samples

In this study, nucleosides, nucleotides, and nucleotides triphosphate were used. Nucleosides include deoxyadenosine (dA, Sigma,  $\geq 99\%$ , stored 2-8 °C), deoxyguanosine (dG, Sigma, 99-100%); 2'-deoxycytidine (dC, Sigma,  $\geq 99\%$ , HPLC, stored -20 °C); thymidine (dT, Sigma,  $\geq 99\%$ ), 2'-deoxyuridine (dU, Sigma, 99-100%), deoxyinosine (dI, Sigma,  $\geq 98\%$ , stored -20 °C). Nucleotides include 2'-deoxyadenosine 5'-monophosphate (dAMP, Sigma grade, 98-100%, stored -20 °C); 2'-deoxyguanosine monophosphate (dGMP, Sigma, 99-100%), 2'-deoxycytidine 5'-monophosphate (dCMP, Sigma,  $\geq 99\%$ , stored -20 °C), thymidine 5'-monophosphate disodium, salt hydrate (dTMP, Sigma,  $\geq 99\%$ , stored -20 °C), 2'-deoxyuridine 5'-monophosphatedisodium salt (dUMP, Sigma grade, stored -20 °C), 2'-deoxyinosine 5'-monophosphate sodium salt (dIMP, Sigma,  $\geq 97\%$ , HPLC, stored -20 °C), 2'-deoxyguanosine 5'- monophosphate sodium salt hydrate (dGMP, Sigma,  $\geq 99\%$ , HPLC, stored -20 °C) . Nucleotides triphosphates include deoxyadenosine triphosphate (dATP, PCR grade, Roche Diagnostics GmbH, Germany), deoxyguanosine triphosphate (dGTP, PCR grade, Roche Diagnostics GmbH, Germany), deoxycytosine triphosphate (dCTP, PCR grade, Roche Diagnostics GmbH, Germany), deoxythymine triphosphate (dTTP, PCR grade, Roche Diagnostics GmbH, Germany), deoxyuridine triphosphate (dUTP, PCR grade, Roche Diagnostics GmbH, Germany), deoxyinosine triphosphate (dITP, molecular biology grade, thermoscientific). All nucleotides triphosphates were bought from Roche diagnostics GmbH, Germany, and they were stored at -15 to -20 °C. All the structures of nucleosides, nucleotides, and nucleotides triphosphate can be seen in Figure 5-1. Polyadenylic acid (Poly A, Sigma, stored -20 °C) was used herein. The concentration of each nucleoside, nucleotide, nucleotides triphosphate, and their mixtures have been shown in Table 5-1. 3  $\mu$ l TMAH was applied in this study, which is always in excess compared to the nucleosides, nucleotides, and nucleotides triphosphate. Naphthalene D8 (Sigma-Aldrich, isotopic purity, 99 atom % D) was used as the internal standard.

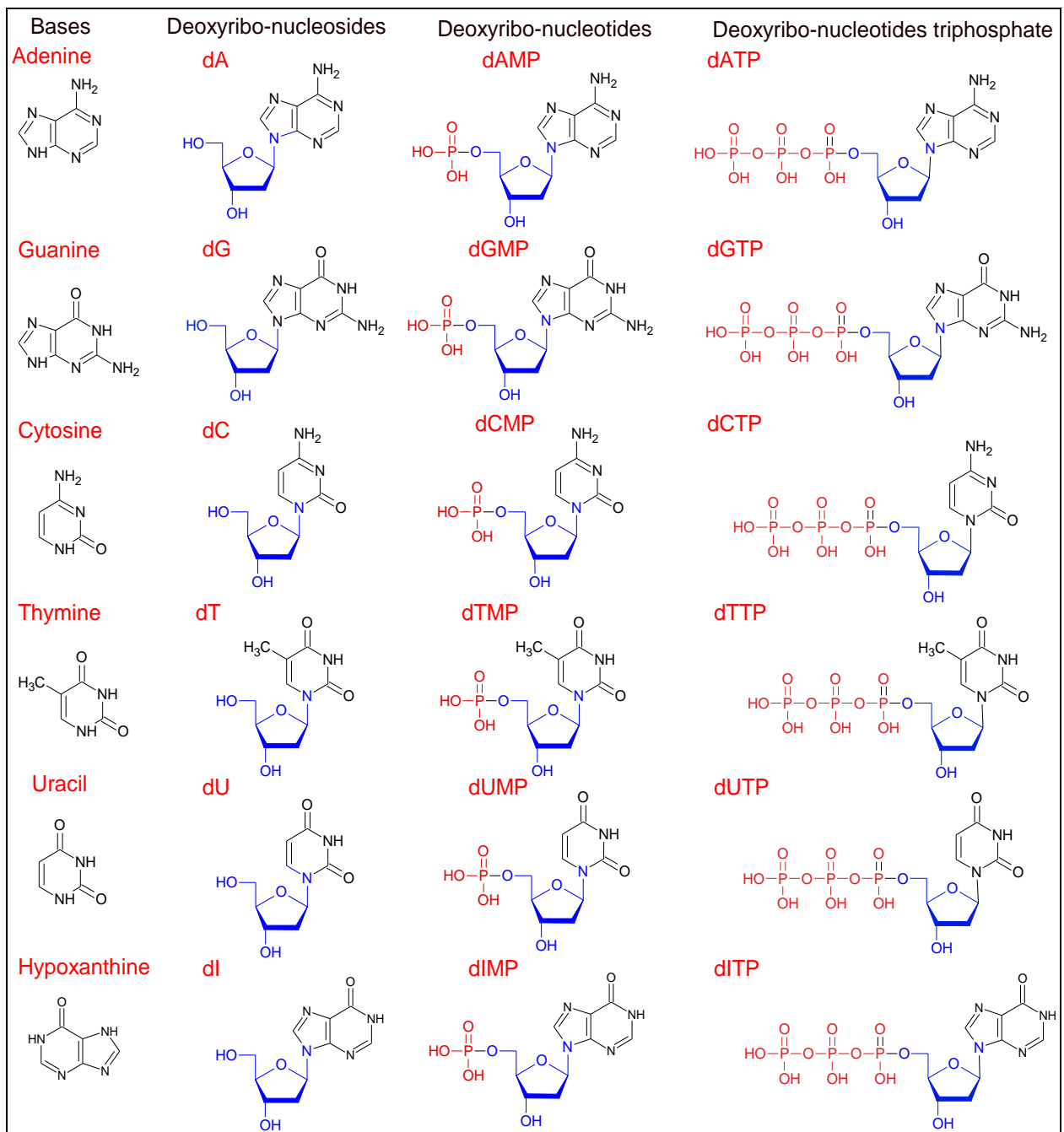


Figure 5-1 The structures of nucleobases, nucleosides, nucleotides, and nucleotides triphosphate.

Table 5-1 Detailed informations of samples used in this study.

	<b>Compounds</b>	<b>Amount (nmol)</b>	<b>Injection volume (<math>\mu</math>l)</b>	<b>Concentration (mol·L<sup>-1</sup>)</b>	
<b>Nucleosides</b>	dA	10	0.5	0.05	
	dG	10	1.0	0.01	
	dT	10	0.5	0.05	
	dU	10	0.5	0.05	
	dC	10	0.5	0.05	
	dI	10	0.5	0.05	
		dA	2	0.2	0.01
		dT	2	0.2	0.01
	Mixtures	dU	2	0.2	0.01
		dC	2	0.2	0.01
		dI	2	0.2	0.01
<b>Nucleotides</b>	dAMP	10	0.25	0.04	
	dGMP	10	1.0	0.01	
	dTMP	10	0.25	0.04	
	dUMP	10	0.25	0.04	
	dCMP	10	0.25	0.04	
	dIMP	10	0.25	0.04	
	Mixtures	dAMP	2.5	0.25	0.01
		dTMP	2.5	0.25	0.01
		dUMP	2.5	0.25	0.01
		dCMP	2.5	0.25	0.01
	dGMP	10	1	0.01	
<b>Nucleotides triphosphate</b>	dATP	10	0.1	0.1	
	dGTP	10	0.1	0.1	
	dTTP	10	0.1	0.1	
	dUTP	10	0.1	0.1	
	dCTP	10	0.1	0.1	
	dITP	10	0.1	0.1	
	Mixtures	dATP	10	0.1	0.1
		dGTP	10	0.1	0.1
		dTTP	10	0.1	0.1
		dUTP	10	0.1	0.1
	dCTP	10	0.1	0.1	
<b>DNA</b>	Poly A	5	1	0.005	

### 5.1.2 Py-GC/MS and methods

The pyrolysis experiments were performed with an EGA/PY-3030D micro-oven pyrolyser, Frontier Lab, installed on the Split/SplitLess (SSL) injector of a Trace GC Ultra gas chromatograph (Thermo Scientific) coupled to a quadrupole mass spectrometer (ISQ LT, Thermo Scientific). Flash pyrolysis and SAM-like ramp pyrolysis were applied in this chapter. For flash pyrolysis, the final temperatures are the following: 200, 300, 400, 500, 600 °C. The sample is pushed into a heated and stabilized oven at the designed final temperatures for 30 seconds, after which the sample is removed from the oven. Helium is used as the carrier gas to carry the pyrolysis volatile products into the GC/MS. SAM-like ramp pyrolysis is the same as the previous work, which can be seen in the experiment section of the chapter 2 and 3. All of the products then were released and sent to the GC/MS through the helium flow. All experiments were repeated 6 times.

Analyses were conducted with GC/MS that has been described in the previous chapter. The temperature programming of the column starts at 40 °C held for 2 min, then at a heat rate of 6 °C min<sup>-1</sup> up to 130 °C then raised to 300 °C at a rate of 10 °C min<sup>-1</sup> and maintained for 1 min. In both ramps, helium flow rate in the column was set at 1.2 mL.min<sup>-1</sup>. The split flow was 12 mL.min<sup>-1</sup>. The temperature of the SSL injector was set at 280 °C. The masses were scanned between *m/z* 40 and *m/z* 500. The ionization energy was 70 eV.

## 5.2 TMAH thermochemolysis of nucleosides

### 5.2.1 TMAH thermochemolysis for nucleosides

In order to determine the main products of nucleosides with TMAH thermochemolysis, the thermochemolysis products of each nucleoside were analyzed at flash pyrolysis at 200 °C, including dI, dC, dU, dT, dG, and dA. Figure 5-2 shows the chromatogram of nucleosides with TMAH thermochemolysis at flash pyrolysis of 200 °C. The target compounds of nucleosides with TMAH thermochemolysis at 200 °C was shown in Figure 5-2. Though there are various methylated compounds of nucleobases as in our previous study [23], the methylated compounds with the highest intensity were selected as the target compounds of nucleosides with TMAH thermochemolysis. Table 5-2 shows the main products of nucleosides with TMAH thermochemolysis at flash 200 °C.

For dI, 1,7-dimethyl-hypoxanthine is the target compound at the retention time of 27.60 min; N, N, N'-trimethyl-cytosine at the retention time of 27.42 min is the main methylated compounds of dC with TMAH thermochemolysis; 1,3-dimethyl-uracil at the retention time of 20.22 min is the main methylated compounds of dU; 1,3-dimethyl-thymine at the retention time of 21.27 min is the key products of thymine with TMAH thermochemolysis; tetramethyl-guanine is the main methylated compounds of dG at the retention time of 28.08 and 29.39 min. This is because guanine has different cases for the replacement of polar hydrogen with methyl functional group from TMAH, there are several peaks of methylated guanine [23]; N, N, 9-trimethyl-adenine or N, N, 3-trimethyl-adenine at the retention time of 25.44 min and 28.13 min is the main methylated compounds of dA with TMAH thermochemolysis. This is caused by the different abundances of each mass fragment, which means even trimethyl-adenine has the almost the same mass fragments, their abundances of each m/z are not completely the same. For example, trimethyl-adenine at the retention time of 28.13 min, the mass fragments and their abundances are of 148(100), 162(54), 177(39), 134(32), 107(20), 133(13), which is a bit different from that of 25.41 min, 148(100), 177(51), 162(48), 107(27), 133(27), 134(13). However, the compounds from 28.13 min still should be trimethyl-adenine. This principle could be used to explain why some compounds are at different retention times in the chromatograms.

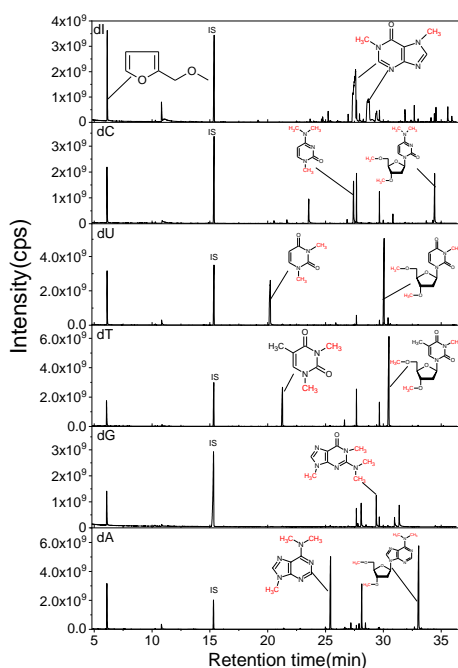


Figure 5-2 The chromatogram of nucleosides with TMAH thermochemolysis at flash pyrolysis of 200 °C.

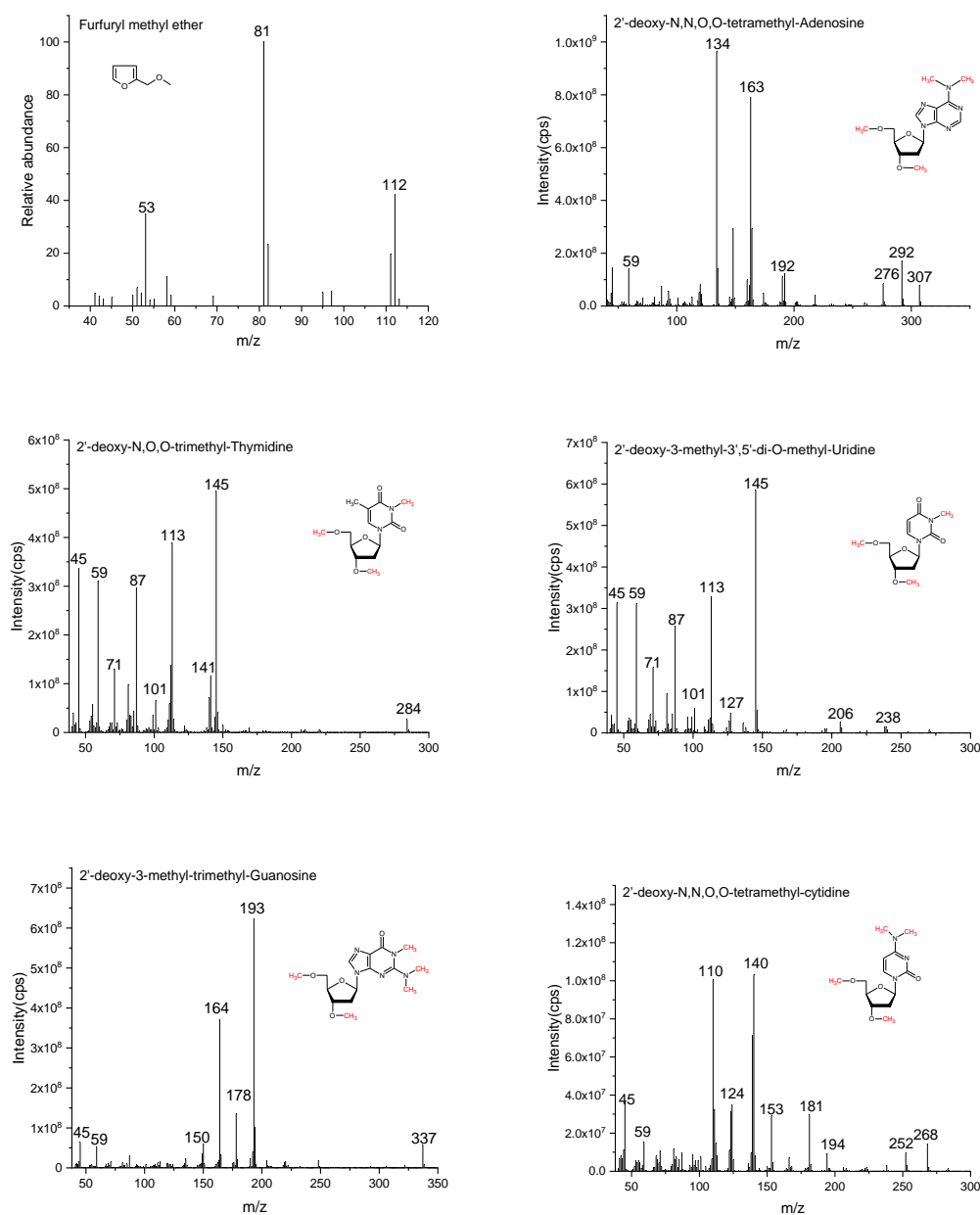


Figure 5-3 Mass spectrums of the organic compounds from nucleosides obtain after TMAH thermochemolysis.

In addition, not only the methylated nucleobases derivated from each nucleoside was detected, the characteristic peak of methylated ribose of nucleosides was also found at the retention time of 6.0 min, named 2-methoxymethyl-furan or furfuryl methyl ether, it's the methylated products of ribose from nucleosides. As we mentioned, nucleosides consist of one basic nucleobase and one ribose, and their methylated compounds were detected when nucleosides thermochemolysis with TMAH, which could be an evidence for the detection of

nucleosides. On the other side, the methylated nucleosides were also detected in our study, such as the methylated dC at the retention time of 34.44 min, the methylated dU at the retention time of 30.07 min, named 2'-deoxy-3-methyl-3,5'-di-O-methyl-uridine; the methylated dT at the retention time of 30.48 min is 2'-deoxy-N,N,O-trimethyl-thymidine; 2'-deoxy-N,N,O,O-tetramethyl-adenosine at the retention time of 33.06 min is methylated dA. Their peaks intensities are high, which demonstrated that the methylated nucleosides are stable and could be the direct evidence of the presence of DNA molecule fragments. Figure 5-3 shows the mass spectrum of different methylated compounds from nucleosides thermochemolysis with TMAH.

In addition to the main methylated compounds of nucleoside obtain after flash TMAH thermochemolysis at 200°C, there are some byproducts of nucleobases. Hexadecanoic acid and methyl stearate methyl esters, at the retention time of 27.68 and 29.66 min, respectively, have been detected from the reaction of nucleosides with TMAH thermochemolysis. Their intensities are relatively higher than other byproducts.

Table 5-2 The compounds of nucleosides and nucleotides with TMAH thermochemolysis at 200 °C.

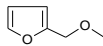
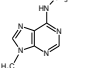
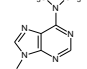
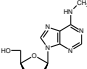
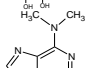
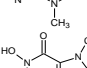
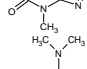
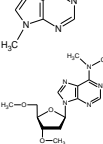
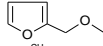
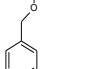
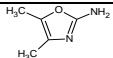
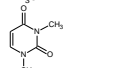
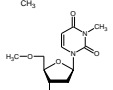
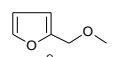
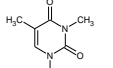
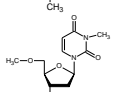
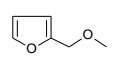
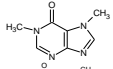
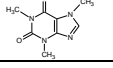
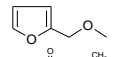
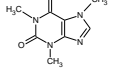
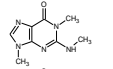
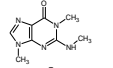
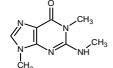
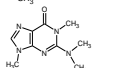
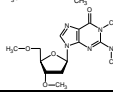
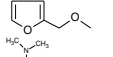
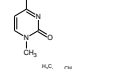
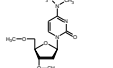
Mother Molecule	RT (min)	Masses of fragments* and relative abundance: m/z (%)	Empirical formula	Compounds	Compounds Structure
dA	6.10	81,112,53,97	C <sub>6</sub> H <sub>8</sub> O <sub>2</sub>	2-methoxymethyl-furan	
	24.99	163,107,135,148,80,42,53	C <sub>7</sub> H <sub>9</sub> N <sub>5</sub>	9H-Purin-6-amine,N,9-dimethyl-	
	25.45	148,162,177,107,133,80,42,52	C <sub>8</sub> H <sub>11</sub> N <sub>5</sub>	N,N,9-Trimethyl-9H-purin-6-amine	
	26.67	178,192,207,149,135,109,80,67,44	C <sub>11</sub> H <sub>15</sub> N <sub>5</sub> O <sub>4</sub>	N-methyl-adenosine	
	26.78	134,162,177,148,121,93,42,58	C <sub>8</sub> H <sub>11</sub> N <sub>5</sub>	N,N,3-trimethyl-3H-6-amine	
	26.94	194,109,67,55,82,162,177,148,121,133	C <sub>8</sub> H <sub>10</sub> N <sub>4</sub> O <sub>2</sub>	Caffeine or 3,7-dihydro-1,3,7-trimethyl-1H-purine-2,6-dione	
	27.90	177,135,162,120,108,42,79,	C <sub>7</sub> H <sub>7</sub> N <sub>5</sub> O	Trimethyl-adenine	
	33.06,33.29	134,163,148,192,292,307,120	C <sub>14</sub> H <sub>21</sub> N <sub>5</sub> O <sub>3</sub>	2'-deoxy-N,NO,O-tetramethyl-adenosine	
dU	6.11	81,112,53,97	C <sub>6</sub> H <sub>8</sub> O <sub>2</sub>	2-methoxymethyl-furan	
	10.28	91;121;77;65;105	C <sub>8</sub> H <sub>10</sub> O	Methoxymethyl-benzene	



Table 5-2 (continued)

Mother Molecule	RT (min)	Masses of fragments* and relative abundance: m/z (%)	Empirical formula	Compounds	Compounds Structure
dU	10.85	111,45,81,99,71,53	C <sub>5</sub> H <sub>8</sub> N <sub>2</sub> O	4,5-dimethyl-2-oxazolamine	
	20.22	140,83,42,55,111	C <sub>6</sub> H <sub>8</sub> N <sub>2</sub> O <sub>2</sub>	1,3-dimethyl-uracil	
	30.01	145,113,87,59,45,127	C <sub>12</sub> H <sub>18</sub> N <sub>2</sub> O <sub>5</sub>	2'-Deoxy-3-methyl-3',5'-di-O-methyl-uridine	
dT	6.04	81,112,53,97	C <sub>6</sub> H <sub>8</sub> O <sub>2</sub>	2-methoxymethyl-furan	
	21.54	154,68,97,42,140	C <sub>7</sub> H <sub>10</sub> N <sub>2</sub> O <sub>2</sub>	1,3-Dimethyl-thymidine	
	30.13	145,113,87,59,45,127	C <sub>12</sub> H <sub>18</sub> N <sub>2</sub> O <sub>5</sub>	2'-Deoxy-3-methyl-3',5'-di-O-methyl-uridine	
dI	6.13	81,112,53,97	C <sub>6</sub> H <sub>8</sub> O <sub>2</sub>	2-methoxymethyl-furan	
	27.54	164,107,134,81,67,53,42	C <sub>7</sub> H <sub>8</sub> N <sub>4</sub> O	1,7-Dimethyl-hypoxanthine	
	26.95	194,109,55,67,82,137,165,42	C <sub>8</sub> H <sub>10</sub> N <sub>4</sub> O <sub>2</sub>	Caffeine	
dG	6.07	81,112,53,97	C <sub>6</sub> H <sub>8</sub> O <sub>2</sub>	2-methoxymethyl-furan	
	26.96	194,109,55,67,82,137,165,42	C <sub>8</sub> H <sub>10</sub> N <sub>4</sub> O <sub>2</sub>	Caffeine	
	27.79	207,178,192,163,149,133,121,107,42,67	C <sub>8</sub> H <sub>11</sub> N <sub>5</sub> O	Trimethyl-guanine	
	29.42	164,207,123,136,178,192,67,108	C <sub>8</sub> H <sub>11</sub> N <sub>5</sub> O	Tetramethyl-guanine	
	30.99	178,109,164,67,82,55,207,192,137	C <sub>9</sub> H <sub>13</sub> N <sub>5</sub> O	Tetramethyl-guanine	
	31.40	207,163,136,123,94,192,67,178	C <sub>9</sub> H <sub>13</sub> N <sub>5</sub> O	Tetramethyl-guanine	
	34.51	193,164,178,150,45,59,87,37	C <sub>15</sub> H <sub>22</sub> N <sub>5</sub> O <sub>4</sub>	Methyl guanosine	
dC	6.10	81,112,53,97	C <sub>6</sub> H <sub>8</sub> O <sub>2</sub>	2-methoxymethyl-Furan	
	27.44	153,124,138,109,82,95,42,55	C <sub>7</sub> H <sub>11</sub> N <sub>3</sub> O	4-Dimethylamino-1-methyl-2(1H)-pyrimidinone	
	34.44	110,140,124,153,181,45,268,252,268	C <sub>13</sub> H <sub>20</sub> N <sub>2</sub> O <sub>5</sub>	2'-deoxy-N,N,O,O-tetramethyl- Cytidine	

### 5.2.2 Optimization of thermochemolysis for nucleosides

In order to optimize the temperature of TMAH thermochemolysis of nucleosides, the TMAH thermochemolysis were operated at different temperatures, from 200 °C to 600 °C.

Figure 5-4 shows the chromatograms of each nucleoside after TMAH thermochemolysis at different temperatures. We have compared the main compounds from nucleosides with TMAH thermochemolysis at different temperatures. Whatever the temperature the target compounds of each nucleoside thermochemolysis products are the same.

However, the amounts of their target compounds are of differences, as shown in Figure 5-5. The target peak intensity of each nucleoside with TMAH thermochemolysis is the highest at flash pyrolysis of 200 °C, including the methylated nucleobases and the methylated nucleosides. For dA, dT, and dU, their methylated compounds were detected, as 2'-deoxy-N,N,O,O-tetramethyl-adenosine, 2'-deoxy-N,O,O-trimethyl-thymine, 2'-deoxy-3-methyl-3',5'-di-O-methyl-uridine, respectively. With the temperature increasing, the methylated nucleosides decreased, while the abundances of methylated nucleobases were increased. This demonstrated that the bond between the ribose and the nucleobase was cracked because of the high temperature. Thus, the yield of methylated nucleobases increased when the temperature increases from 300 to 600 °C.

Figure 5-6 shows the abundance of methyl furfuryl obtained from nucleosides with TMAH at different temperatures. The yield of methylated ribose, 2-methoxymethyl-furan, increased with the rise of temperature, which also demonstrated that the high temperature destroyed the nucleosides and separated them into two parts, the nucleobases and the ribose. The decomposition of nucleosides could also be demonstrated from Figure 5-5. The abundance of methylated nucleotides decreased with an increase of thermochemolysis temperature. However, the abundance of the methyl furfuryl showed the opposite trends with that of methylated nucleotides. The methylated nucleobases from nucleosides with TMAH thermochemolysis were detected at high temperature of 600 °C, which showed that TMAH thermochemolysis could be applied at 600 °C.

However, 200 °C is the optimal temperature for the detection of nucleosides chemical standards with TMAH thermochemolysis. On the other side, it could be different cases when applying TMAH thermochemolysis on the detection of nucleotides from natural samples. The optimal temperature could be different because of the adsorption of nucleosides on rocks or soil samples [683]. And also, maybe a higher temperature would be needed to analyze the nucleotides from natural samples with TMAH thermochemolysis.

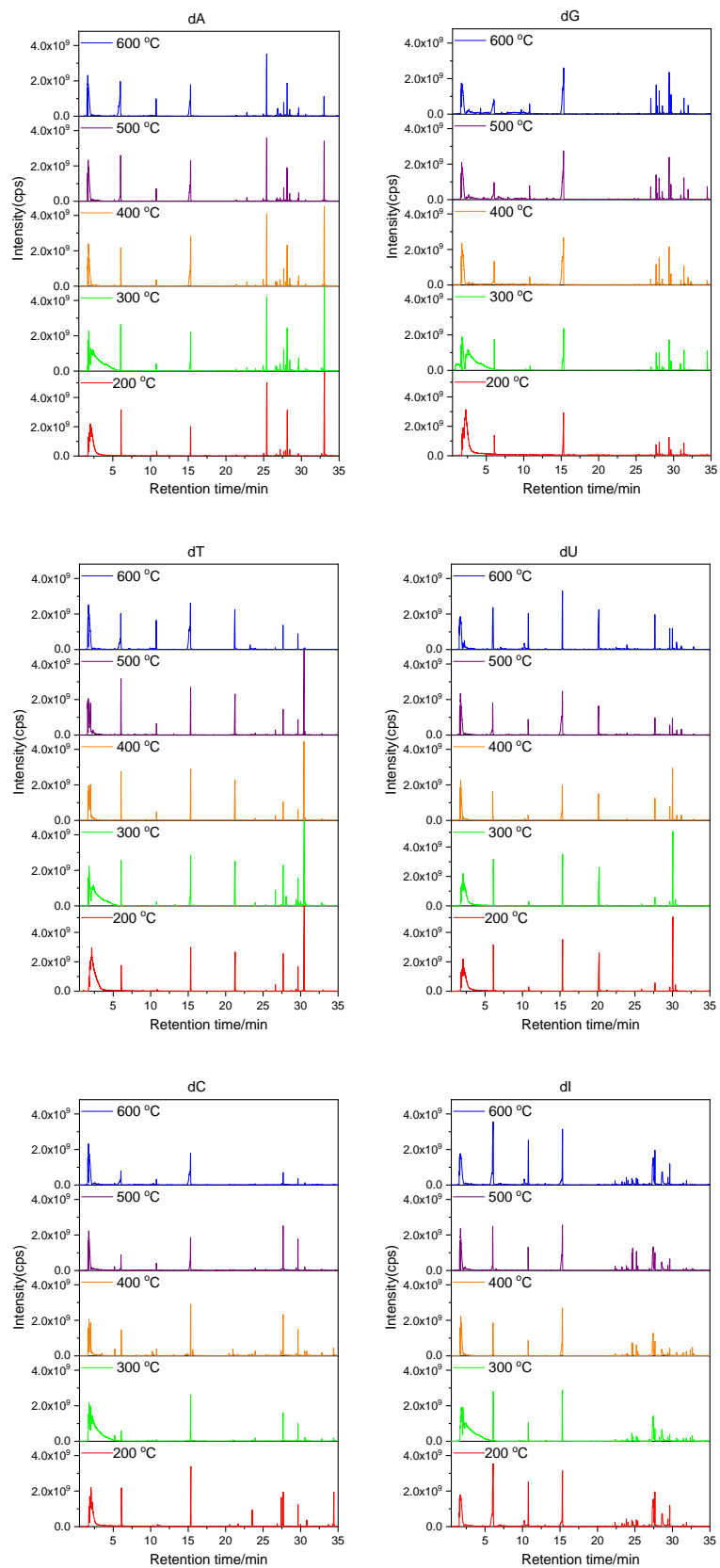


Figure 5-4 The chromatograms of nucleosides with TMAH thermochemolysis at different flash pyrolysis temperatures.

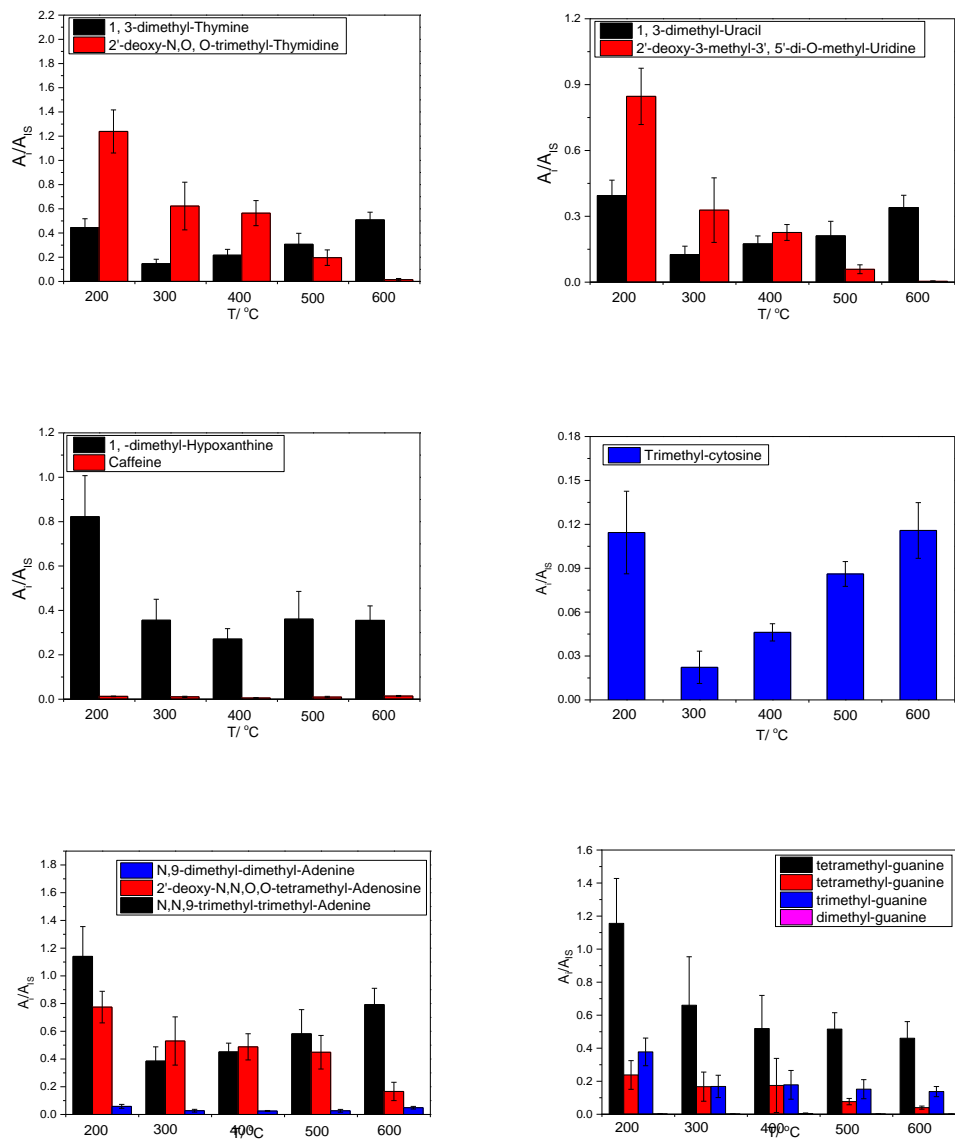


Figure 5-5 Distribution of thermochemolysis products of nucleosides in TMAH at different temperatures ( $A_i/A_{IS}$  is the ratio of area of organics and the area of internal standard).



Figure 5-6 The abundance of methyl fufuryl obtained from nucleosides with TMAH at different temperatures ( $A_i/A_{IS}$  is the ratio of area of organics and the area of internal standard).

### 5.2.3 Analysis of the mixture of nucleosides at different temperatures

The methylated products of nucleosides and their target compounds at different temperatures have been analyzed. Then, in order to determine whether or not there are overlaps among these nucleosides, the mixtures of nucleosides, including dA, dU, dC, dT, and dI with TMAH thermochemolysis have been analyzed between the temperatures of 200 to 600 °C, as shown in Figure 5-7. According to the previous research, dG was not mixed with the other five kinds of nucleosides, because we found it could be decomposed into caffeine, which is one of the byproducts from hypoxanthine after TMAH thermochemolysis [23]. The target peak of each nucleoside has been found in the chromatogram. For example, the methylated compounds of dU and dT were separated completely, even if their structure is similar, methylated uracil (peak 4) at the retention time of 20.17 min, methylated thymine (peak 5) at the retention time of 21.25 min. In addition, some of the methylated nucleosides were detected directly, including 2'-deoxy-3-methyl-3',5'-di-O-methyl-uridine (peak 10), 2'-deoxy-N,O,O-trimethyl-thymidine (peak 11), 2'-deoxy-N,O,O,O-tetramethyl-adenosine(peak 12). These methylated nucleosides are more stable and with simpler structures and their mass fragments are within the limitation of detection of our device.

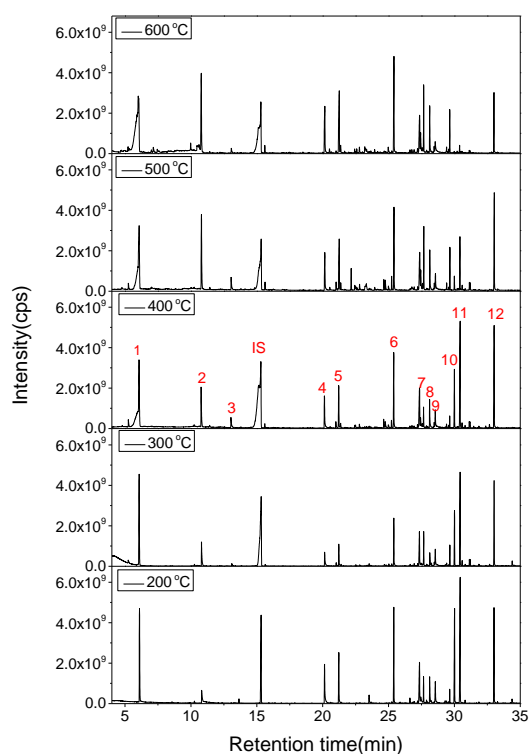


Figure 5-7 Chromatograms of nucleosides (10 nmol each) after TMAH thermochemolysis at different temperatures. Peak 1 : Furfuryl methyl ether; Peak 2 : 2'-deoxy-Cytidine?; peak 3 : 3-methyl-1,2-cyclopentanedione?; peak 4 : 1,3-dimethyl-uracil ; peak 5 : 1,3-dimethyl-thymine; peak 6 : N,N,9-trimethyl-adenine; peak 7,9 : 1,7-dimethyl-hypoxanthine; peak 8 : N,N,3-trimethyl-adenine; peak 10: 2'-deoxy-3-methyl-3',5'-di-O-methyl-Uridine; peak 11: 2'-deoxy-N,O,O-trimethyl-thymidine ; peak 12 : 2'-deoxy-N,O,O,O- tetramethyl-Adenosine.

#### 5.2.4 SAM-like ramp pyrolysis

The methylated products of nucleosides and their target compounds at SAM-like ramp pyrolysis were studied, in order to simulate the condition of SAM instrument on Mars. Figure 5-8 shows the products from nucleosides with TMAH thermochemolysis at SAM-ramp pyrolysis. Compared with the chromatogram of nucleosides with TMAH thermochemolysis at flash pyrolysis (Figure 5-2), it could be found that the methylated compounds of each nucleoside and the byproducts from nucleoside with TMAH thermochemolysis at SAM-like ramp pyrolysis are almost the same. Table 5-3 shows the main products of nucleosides with TMAH thermochemolysis at SAM-like ramp pyrolysis.

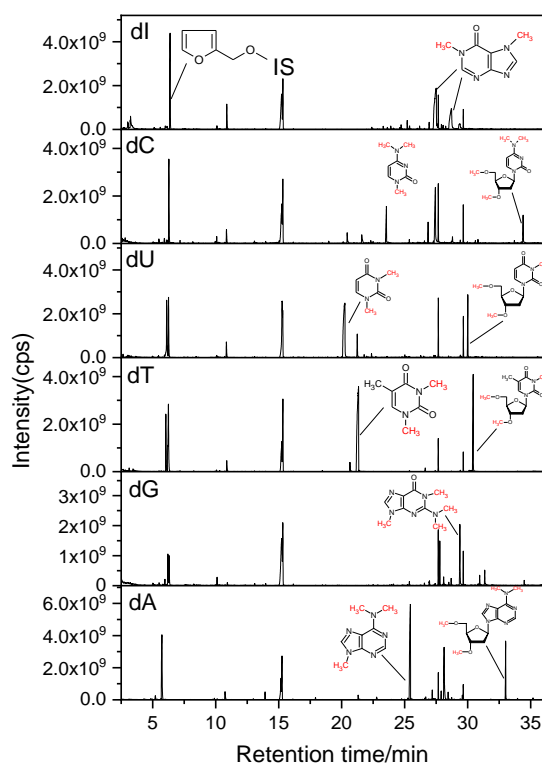
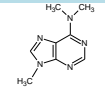
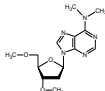
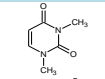
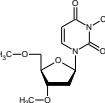
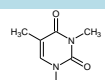
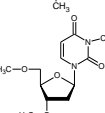
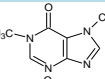
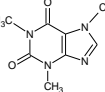
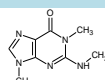
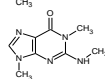
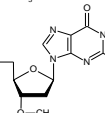
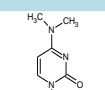
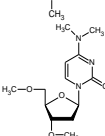


Figure 5-8 The pyrolysis products of nucleosides at SAM-like ramp pyrolysis.

Figure 5-9 is the chromatogram of the mixtures of five kinds of nucleosides with TMAH thermochemolysis. dG was not mixed with other five kinds of nucleosides because we have already known that the guanine could decompose into caffeine, hence influence the quantitation of the hypoxanthine. Results showed that there was no overlap among these five kinds of nucleosides after TMAH thermochemolysis. The target compounds of each nucleoside with TMAH thermochemolysis can be seen in Figure 5-9. Figure 5-10 shows the relative abundance of the target compounds from each nucleoside with TMAH thermochemolysis. Compared the peak intensities of these nucleosides, the responding values of these nucleosides detected by GC/MS decreased as  $dA > dG > dT > dU > dI > dC$ . This demonstrates that dA is the most possible compounds that could be detected among the mixtures of nucleosides. The result is in consistent with the conclusion in our previous work [23]. As adenine is the most possible nucleobases that could be detected on Mars, if the abundance of nucleobases is higher than the detect limitation of our device [23]. This means adenine is one of the nucleobases that give the best response after TMAH thermochemolysis

Table 5-3 The target compounds of nucleosides with TMAH thermochemolysis

RT ( min)	Masses of fragments* and relative abundance: m/z (%)	Empirical formula	Compounds	Compounds Structure
<b>dA</b>				
25.45	148,162,177,107,133,80,42,52	C <sub>8</sub> H <sub>11</sub> N <sub>5</sub>	N,N,9-Trimethyl-adenine	
33.06	134,163,148,192,292,307,120	C <sub>14</sub> H <sub>21</sub> N <sub>5</sub> O <sub>3</sub>	2'-deoxy-N,N,O,O-tetramethyl-adenosine	
<b>dU</b>				
20.22	140,83,42,55,111	C <sub>6</sub> H <sub>8</sub> N <sub>2</sub> O <sub>2</sub>	1,3-Dimethyl-Uracil	
30.01	145,113,87,59,45,127	C <sub>12</sub> H <sub>18</sub> N <sub>2</sub> O <sub>5</sub>	2'-Deoxy-3-methyl-3',5'-di-O-methyl-Uridine	
<b>dT</b>				
21.54	154,68,97,42,140	C <sub>7</sub> H <sub>10</sub> N <sub>2</sub> O <sub>2</sub>	1,3-Dimethyl-Thymidine	
30.13	145,113,87,59,45,127	C <sub>12</sub> H <sub>18</sub> N <sub>2</sub> O <sub>5</sub>	2'-Deoxy-3-methyl-3',5'-di-O-methyl-Uridine	
<b>dI</b>				
27.54	164,107,134,81,67,53,42	C <sub>7</sub> H <sub>8</sub> N <sub>4</sub> O	1,7-Dimethyl-hypoxanthine	
26.95	194,109,55,67,82,137,165,42	C <sub>8</sub> H <sub>10</sub> N <sub>4</sub> O <sub>2</sub>	Caffeine	
<b>dG</b>				
27.79	207,178,192,163,149,133,121,107,42,67	C <sub>8</sub> H <sub>11</sub> N <sub>5</sub> O	Trimethyl-guanine	
29.38	164,207,123,136,178,192,67,108	C <sub>8</sub> H <sub>11</sub> N <sub>5</sub> O	Tetramethyl-guanine	
34.51?	193,164,178,150,45,59,87,337	C <sub>15</sub> H <sub>22</sub> N <sub>5</sub> O <sub>4</sub>	Methyl guanosine	
<b>dC</b>				
23.52	153,124,138,109,82,95,42,55	C <sub>7</sub> H <sub>11</sub> N <sub>3</sub> O	4-dimethylamino-1-methyl-2(1H)-pyrimidinone	
34.44	110,140,124,153,181,45,268,252,268	C <sub>13</sub> H <sub>20</sub> N <sub>2</sub> O <sub>5</sub>	2'-deoxy-N,N,O,O-tetramethyl-Cytidine	



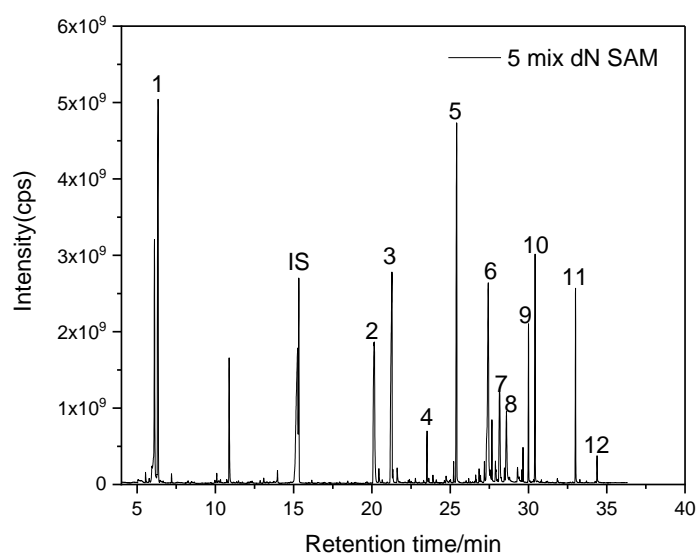


Figure 5-9 The chromatogram of the mixtures of nucleosides at SAM-like ramp pyrolysis. Peak 1: Furfuryl methyl ether; 2: 1,3-dimethyl-uracil; 3: 1,3-dimethyl- thymine; 4: trimethyl-cytosine; 5: N,N,9-Trimethyl-adenine; 6,8: 1,7-dimethyl-hypoxanthine; 7: N,N,3-Trimethyl-adenine; 9: 2'-Deoxy-3-methyl-3',5'-di-O-methyl-Uridine; 10: 2'-Deoxy-3-methyl-3',5'-di-O-methyl-Uridine; 11: 2'-deoxy-N,N,O,O-tetramethyl-adenosine; 12: 2'-deoxy-N,N,O,O-tetramethyl-Cytidine.

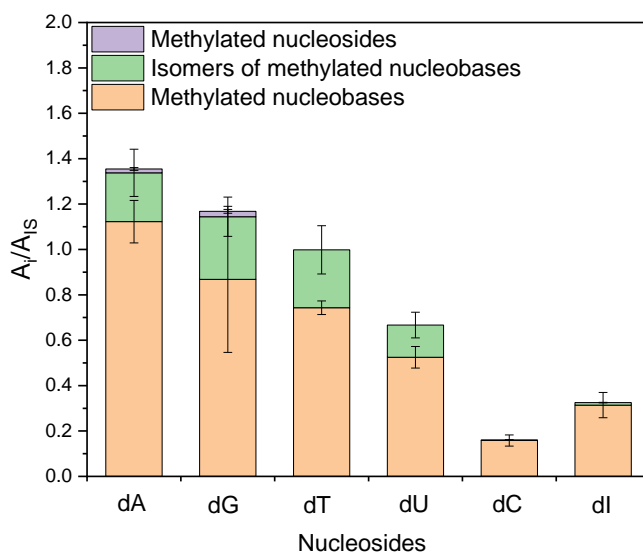


Figure 5-10 the abundance of each nucleoside detected by Py-GC/MS at SAM-like ramp pyrolysis with TMAH thermochemolysis.

### 5.3 TMAH thermochemolysis of nucleotides

Nucleotides are important compositions of DNA. The application of TMAH thermochemolysis on the detection of nucleosides was studied in this section. The products from nucleosides with TMAH thermochemolysis at 200 °C were analyzed, the target compounds of each nucleoside were determined firstly. In order to obtain the highest intensity of the target compounds of each nucleoside, the temperature of TMAH thermochemolysis were optimized. Furthermore, the products of nucleosides with TMAH thermochemolysis at different temperatures were analyzed. The possible mechanisms of TMAH thermochemolysis with nucleosides were investigated. Therefore, the nucleosides samples were thermochemolysis at temperatures of 200, 300, 400, 500, and 600 °C, at flash pyrolysis and SAM-like ramp pyrolysis.

#### 5.3.1 TMAH thermochemolysis for nucleotides

The products of nucleotides with TMAH thermochemolysis were analyzed at 200 °C, including dIMP, dCMP, dUMP, dTMP, dGMP, and dAMP. Figure 5-11 shows the chromatogram of nucleotides with TMAH flash thermochemolysis at 200 °C, including the structures of the main products of each nucleotide. Results show that 1,7-dimethyl-hypoxanthine, at the retention time of 27.5 min, is the main products of dIMP after TMAH thermochemolysis. N,N,N'-trimethyl-cytosine, at the retention time of 20.44 and 27.38 min, is the main thermochemolysis products of dCMP. For dUMP, 1,3-dimethyl-uracil is the methylated compounds of dUMP. 2'-deoxy-3-methyl-3',5'-di-O-methyl-uridine, the methylated dU was detected at the retention time of 29.98 min. However, compared with the intensity of 1,3-dimethyl-uracil, the peak intensity of methylated dU is about 27 time lower than that of 1,3-dimethyl-uracil. 1,3-dimethyl-thymine, at the retention time of 21.32 min, is the main methylated products of dTMP. 2'-deoxy-N,O,O-trimethyl-thymine at a low intensity is detected at the retention time of 30.41 min. N,N,9-trimethyl-adenine at the retention time of 25.44 min and the N,N,3-Trimethyl-adenine at the retention time of 28.14 min are the main methylated compounds of dAMP. In addition, 2'-deoxy-N,N,O,O-tetramethyl-adenosine, the methylated dA, was detected at the retention time of 33.0 min. For dGMP, the main products from TMAH thermochemolysis were trimethyl- and tertamethyl-guanine. Trimethyl-guanine was detected at the retention time of 28.27 min. However, the highest peak at the rethention time of 29.79 min is the target peak for dGMP, i.e. tetramethyl-guanine. Because of isomers of guanine and different cases for the replace of polar hydrogen with methyl functional group from TMAH, there are several peaks of methylated guanine. For example, in addition to the retention

time of 29.79 min, the products of dGMP with TMAH thermochemolysis are also tetramethyl-guanine at the retention time of 28.00 min, 28.27 min, 31.23 min and 31.58 min. All the target compounds of each nucleotide with TMAH thermochemolysis are the methylated compounds of their corresponding nucleobases. The mass fragments of the methylated nucleobases can be seen in Table 4-2.

The methylated compounds of nucleotides with flash TMAH thermochemolysis were detected at 200 °C, as well as some byproducts are from the degradation of TMAH, such as trimethylamine, dimethyl ether, as what we have shown in Chapter 4. All the byproducts of TMAH pyrolysis at 600 °C. Other byproducts are from the degradation of nucleotides under TMAH thermochemolysis. Table 5-4 lists the main products of nucleotides with TMAH thermochemolysis at flash 200 °C.

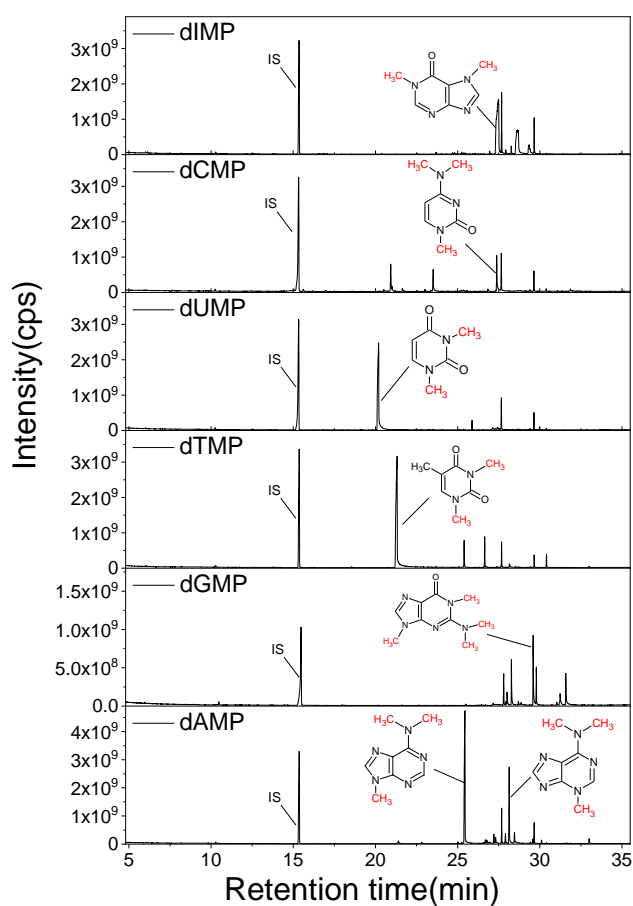


Figure 5-11 The chromatography of nucleotides with TMAH thermochemolysis at flash 200 °C.

Table 5-4 The main products of nucleotides with TMAH thermochemolysis at flash 200 °C

RT/ min	Masses of fragments* and relative abundance: m/z (%)	Empirical formula	Compounds	Compounds Structure
<b>dAMP</b>				
24.99	163,107,135,148,80,42,53	C <sub>7</sub> H <sub>9</sub> N <sub>5</sub>	9H-Purin-6-amine,N,9-dimethyl-	
25.45	148,162,177,107,133,80,42,52	C <sub>8</sub> H <sub>11</sub> N <sub>5</sub>	N,N,9-Trimethyl-9H-Purin-6-amine	
26.78	134,162,177,148,121,93,42,58	C <sub>8</sub> H <sub>11</sub> N <sub>5</sub>	N,N,3-trimethyl-3H-6-amine	
26.94	194,109,67,55,82,162,177,148,121,133	C <sub>8</sub> H <sub>10</sub> N <sub>4</sub> O <sub>2</sub>	Caffeine Or 3,7-dihydro-1,3,7-trimethyl-1H-Purine-2,6-dione	
33.06, 20	134,163,148,192,292,307,120	C <sub>14</sub> H <sub>21</sub> N <sub>5</sub> O <sub>3</sub>	2'-deoxy-N,N,O,tetramethyl-adenosine	
<b>dUMP</b>				
20.19	140,58,83,42,155	C <sub>6</sub> H <sub>8</sub> N <sub>2</sub> O <sub>2</sub>	1,3-Dimethyl-Uracil	
29.98	145,113,87,59,45,71,101,127	C <sub>12</sub> H <sub>18</sub> N <sub>2</sub> O <sub>5</sub>	Uridine,2'-deoxy-3-methyl-3',5'-di-o-methyl-	
<b>dTMP</b>				
21.52	154,68,97,42,140	C <sub>7</sub> H <sub>10</sub> N <sub>2</sub> O <sub>2</sub>	1,3-Dimethyl-Thymidine	
30.40	145,113,45,59,87,71,112,284	C <sub>13</sub> H <sub>20</sub> N <sub>2</sub> O <sub>5</sub>	2'-deoxy-N,O,O-trimethyl-Thymidine	
<b>dIMP</b>				
26.95	194,109,55,67,82,137,165,42	C <sub>8</sub> H <sub>10</sub> N <sub>4</sub> O <sub>2</sub>	Caffeine	
27.45	164,110,42,68,82,138,	C <sub>7</sub> H <sub>8</sub> N <sub>4</sub> O	1,7-Dimethyl-Hypoxanthine	
<b>dCMP</b>				
21.64	153,124,138,95,109,44,81,68,54	C <sub>7</sub> H <sub>11</sub> N <sub>3</sub> O	4-Dimethylamino-1-methyl-2(1H)-pyrimidinone	
<b>dGMP</b>				
28.00	207,178,192,163,149,133,42	C <sub>9</sub> H <sub>13</sub> N <sub>5</sub> O	Tetramethyl-Guanine	
28.27	193,164,109,67,82,55,138,149	C <sub>8</sub> H <sub>11</sub> N <sub>5</sub> O	Trimethyl-Guanine	
29.58	164,123,136,178,207,67,192,149,108	C <sub>9</sub> H <sub>13</sub> N <sub>5</sub> O	Tetramethyl-Guanine	
31.23	178,109,164,67,55,82,193,207,137,123	C <sub>9</sub> H <sub>13</sub> N <sub>5</sub> O	Tetramethyl-Guanine	
31.58	207,163,136,123,94,67,42,192,178,	C <sub>9</sub> H <sub>13</sub> N <sub>5</sub> O	Tetramethyl-Guanine	

### 5.3.2 Optimization of thermochemolysis for nucleotides

The target compounds of each nucleotide with TMAH thermochemolysis have been determined in the last section. In this part, the abundances of products from nucleotides thermochemolysis with TMAH at different temperatures were studied, at flash temperature of 200, 300, 400, 500, 600 °C. Figure 5-12 shows the chromatograms of nucleotides with TMAH thermochemolysis at different temperatures. With the increase of temperatures, the target compounds of each nucleotide with TMAH thermochemolysis did not show obvious changes, which demonstrated that there is no new compounds were formed with the increase of temperature. Only the methyl phosphate was detected at 300-500 °C, as shown in Figure 5-13. The mass spectrum of methyl phosphate can be seen in Figure 5-14. Its main mass fragments should be 110; the mass weight of 140 is also important as it's the total mass weight of methyl phosphate. All the products of nucleotides thermochemolysis with TMAH at different temperatures were analyzed, from 300 to 600 °C. Compared the products of different temperatures, a few new products were formed during the pyrolysis of these methylated nucleotides. Therefore, the abundance of the target nucleobases from the thermochemolysis of nucleotides with TMAH differs with the increase of temperature; barely new compounds were formed during the pyrolysis process.

The relative intensity of each target compounds of each nucleotide was analyzed. Figure 5-15 shows the distribution of the methylated compounds of nucleotides with TMAH thermochemolysis at different temperatures. Compared the relative intensity of the target compounds of each nucleotide, 200 °C is the optimal temperature of each nucleotide with TMAH thermochemolysis. For cytosine, N,N,N'-trimethyl-cytosine is the only methylated compounds of dCMP, the intensity of N,N,N'-trimethyl-cytosine detected at different temperatures are similar except that at 400 °C. The yields of the methylated products of other nucleotides with TMAH thermochemolysis decreased with the increase of pyrolysis temperature, including dAMP, dTMP, and dUMP. However, dGMP showed different results. It shows that at 600 °C, the abundance of methylated guaninie is the highest. At 200 and 300 °C, its abundance is similar. Therefore, for dGMP, the TMAH thermochemolysis could also be applied at 200 or 300 °C.

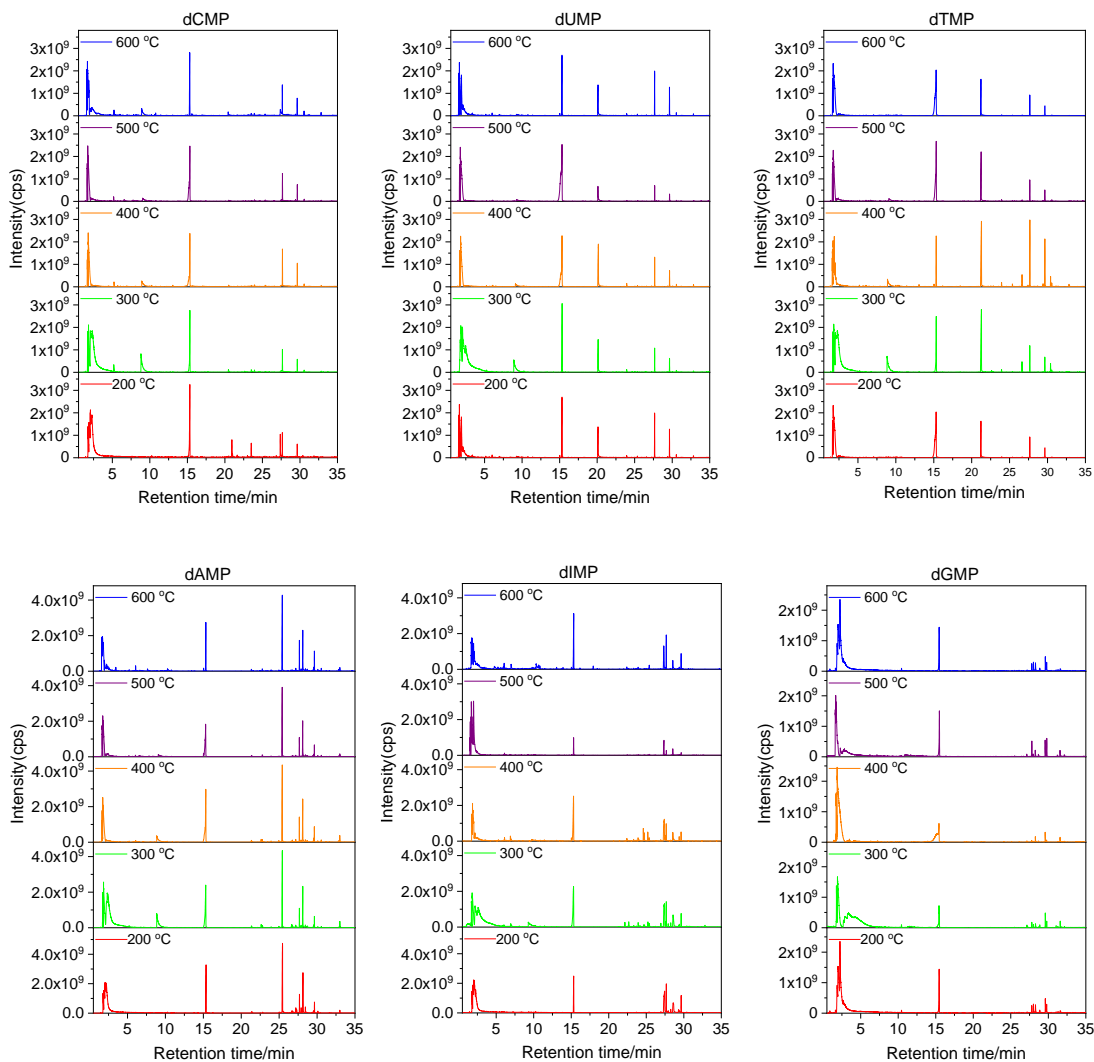


Figure 5-12 Chromatograms of nucleotides with TMAH thermochemolysis at different flash temperatures.

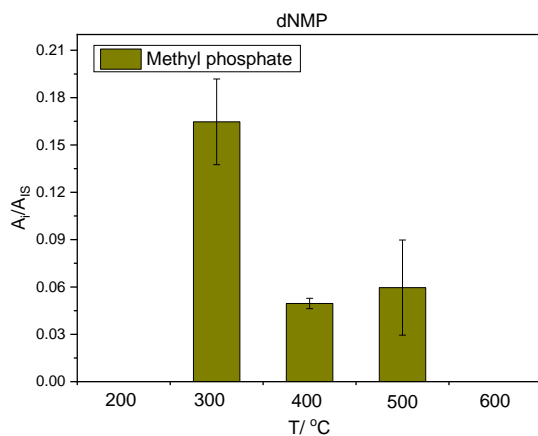


Figure 5-13 the abundance of methyl phosphate from four mix of nucleotides monphosphate with TMAH thermochemolysis at different temperatures.

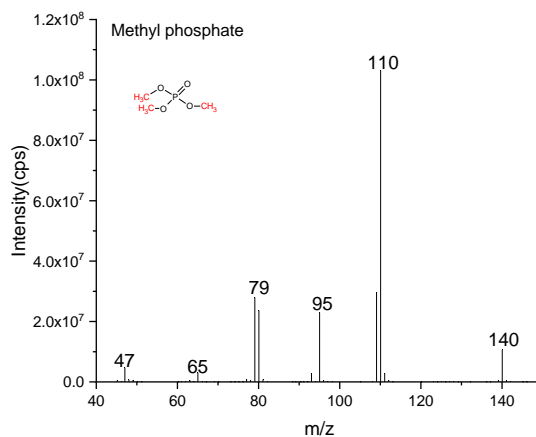


Figure 5-14 The mass spectrum of methylated phosphate.

Figure 5-15 shows that the methylated nucleobases are the main methylated byproducts of nucleotides whatever the temperature. Though the methylated nucleosides, such as dA, dT, and dU, have been detected from 200 to 500 °C. However, their abundances are much lower than that of the methylated nucleobases. The abundance of methylated nucleosides decreases with the increase of pyrolysis temperature. This demonstrates that the structure of these methylated nucleosides become unstable at high temperatures. Most of the methylated ribose was removed from nucleotides when the temperature is higher than 200 °C. This is mainly because of the cleavage of the N-C bond, which connects the nucleobases and the ribose of the nucleosides. Methylated phosphates were detected when the temperature is higher than 300 °C. The abundance of methylated phosphates decreased with the increase of temperature, from 300 to 500 °C. When thermochemolysis temperature is lower than 200 °C or higher than 600 °C, the methylated phosphate of nucleotides thermochemolysis with TMAH could not be detected. At low temperature, the phosphate groups are stable; they are attached with the ribose stably. However, increasing temperature leads the cleavage of O-C bonds connecting the phosphate and the ribose structure. On the other side, methylated phosphates could be decomposed at high temperatures. Therefore, the abundance of methyl phosphate decreases drastically with the increase of temperature. However, no methyl phosphate was detected at 600 °C, which demonstrated that methyl phosphate was decomposed completely when the temperature is higher than 600 °C. The abundance of the methylated phosphates is the highest at 300 °C. Methyl phosphate could be one of the target compounds of nucleotides, but the optimal temperature should be 300 °C.

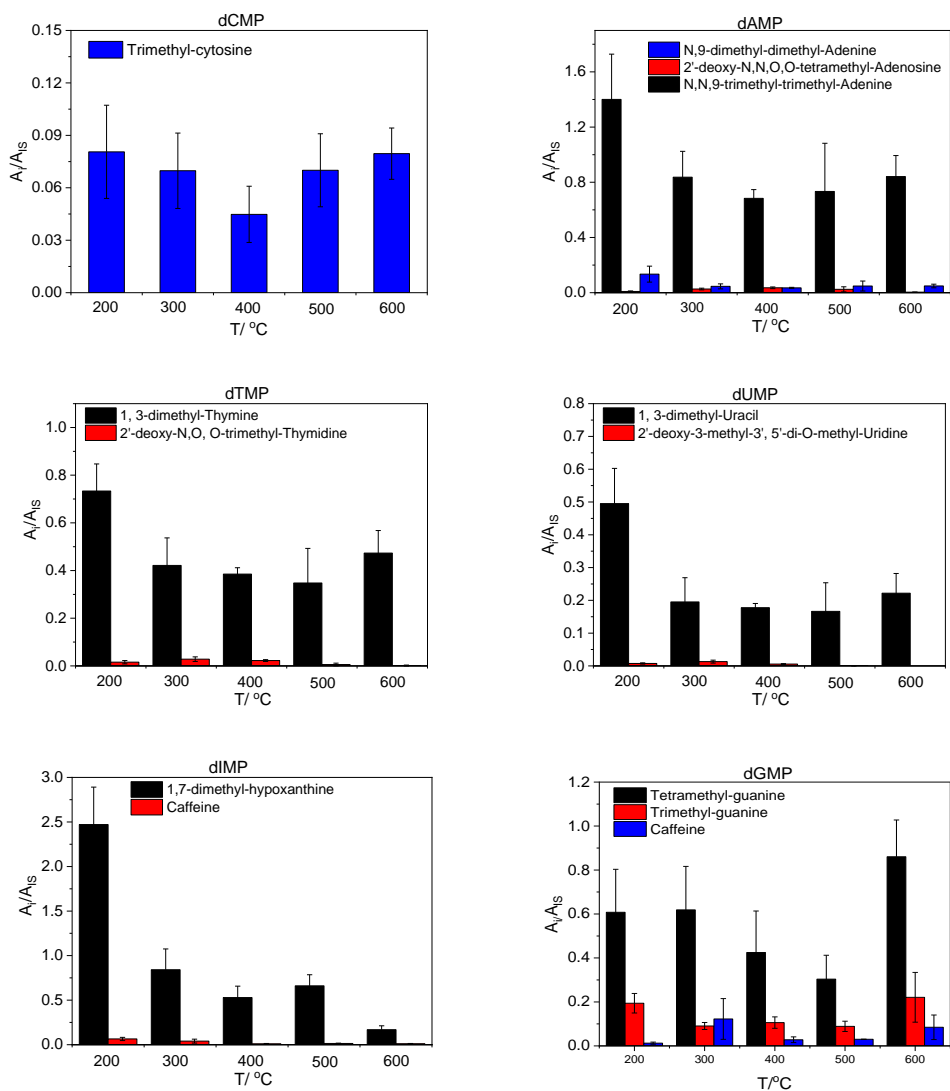


Figure 5-15 Distribution of thermochemolysis products of nucleotides in TMAH at different temperatures ( $A_i/A_{IS}$  is the ratio of area of organics and the area of internal standard).

In addition, thermochemolysis temperature still influences the detection of methylated nucleosides. Higher temperature could lead the fission of N-O bonds connecting the nucleobases and the ribose structure, which could be concluded from the intensity of the methylated adenosine, the methylated uridine, and thymine, as shown in Figure 5-15. Therefore, the optimal temperature for the detection of methylated nucleotides should be from 200 to 300 °C. However, if there are nucleotides in Martian soil samples, the optimal temperature could be different from that of the nucleotides chemical standards with TMAH thermochemolysis. Owing the fact that the strong adsorption by the matrix can result in the poor recovery of organic compounds [684], hence the detection of organics from solid matrix could be difficult even combined with extraction process [685]. Therefore, a higher temperature



would be needed for the detection of organics from soil matrix. From the results of nucleotides with TMAH thermochemolysis at different temperatures, as in Figure 5-15, the methylated nucleobases obtained from nucleotides with TMAH thermochemolysis could be detected even at high temperature of 600 °C.

### 5.3.3 Analysis of the mixture of nucleosides at different temperatures

The chromatography corresponding to the thermochemolysis of the nucleotides mixtures detected at different temperatures (from 200 to 600 °C) is shown in Figure 5-16. Each of methylated nucleotide with TMAH thermochemolysis was identified and they are the derivatives of uracil, thymine, and adenine.

The predominate peak of adenine corresponded to trimethylated canonical structure whereas the second peak of low intensity was a trimethyl tautomer form of adenine, at the retention time of 25.43 min and 28.15 min, respectively. A single derivative of dUMP and dTMP were detected, 1,3-dimethyl-uracil and 1,3-dimethyl-thymine at the retention time of 20.18 min and 21.28 min, respectively. Therefore, all the methylated nucleotides were separated and detected by our programs.

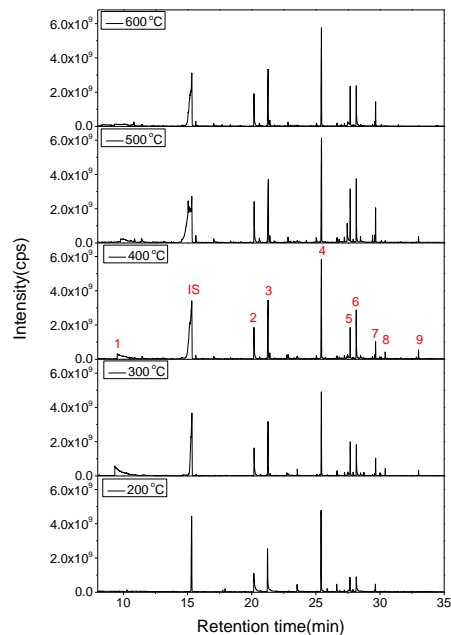


Figure 5-16 Chromatograms of nucleotides (10 nmol) thermochemolysis in TMAH at different temperatures. Peak 1: Methyl phosphate ; peak 2 :1,3-dimethyl-uracil ; peak 3 : 1,3-dimethyl-thymine; peak 4: N,N,9-trimethyl-adenine; peak 5: Hexadecanoic acid, methyl ester; peak6: N,N,3-trimethyl-adenine; peak 7: octadecanoic acid, methyl ester; peak 8: 2'-deoxy-N,O,O-trimethyl-thymidine(trimethyl-dT) ; peak 9: 2'-deoxy-N,O,O,O- tetramethyl-Adenosine(tetramethyl-dA).

#### 5.3.4 SAM-like ramp pyrolysis

In order to mimic the experimental conditions of SAM on board Curiosity on Mars, the products of nucleotides with TMAH thermochemolysis at SAM-like ramp pyrolysis were studied. Figure 5-17 shows the chromatograms of nucleotides (10 nmol) thermochemolysis in TMAH at SAM-like ramp pyrolysis. The target compound of each nucleotide with TMAH thermochemolysis has been presented in Figure 5-17. The target compounds of each nucleotide are almost the same as the products are obtained from nucleosides and nucleotides thermochemolysis with TMAH, as shown in section 5.1 and 5.2. The main differences of these products are the degradation of the ribose. Furfuryl methyl ether, at the retention time of 6.31 min, is one of the main typical products from nucleosides and nucleotides degradation at flash pyrolysis and SAM-like ramp pyrolysis. However, some ribose derivatives were detected when the nucleotides thermochemolysis with TMAH at SAM-like ramp pyrolysis. Furfuryl alcohol and furfuryl formate were detected, at the retention time of 7.26 and 8.15 min, respectively. Furfuryl formate could be formed through the reaction of furfuryl alcohol and acetyl formate at 60 °C [686]. The nucleotides were analyzed at high temperature as 200 °C leading to the formation of furfuryl formate. In addition, 2,5-dimethyl-furan at the retention time of 6.52 min was detected. This demonstrates that there are the transformations of furfuryl methyl ether during the heating of nucleotides with TMAH thermochemolysis. At SAM-like ramp pyrolysis, the volatiles that formed from the nucleotides with TMAH thermochemolysis have a longer retention time at the pyrolyser. Therefore, some secondary reactions could produce the derivatives of furans.

Figure 5-18 shows the chromatograms of the mixtures of nucleotides (10 nmol) thermochemolysis in TMAH at SAM-like ramp pyrolysis. Methyl phosphate and methyl furfuryl ester were detected at 6.32 min and 9.28 min, respectively. The methylated uracil, thymine, adenine, guanine, and cytosine were detected. The intensity of methylated cytosine was the lowest; this demonstrated that cytidine could not be detected easily compared with other nucleotides. There was no overlap among these nucleobases. This demonstrated that nucleobases could be well separated and detected by Py-GC/MS combined TMAH at SAM-like ramp pyrolysis.

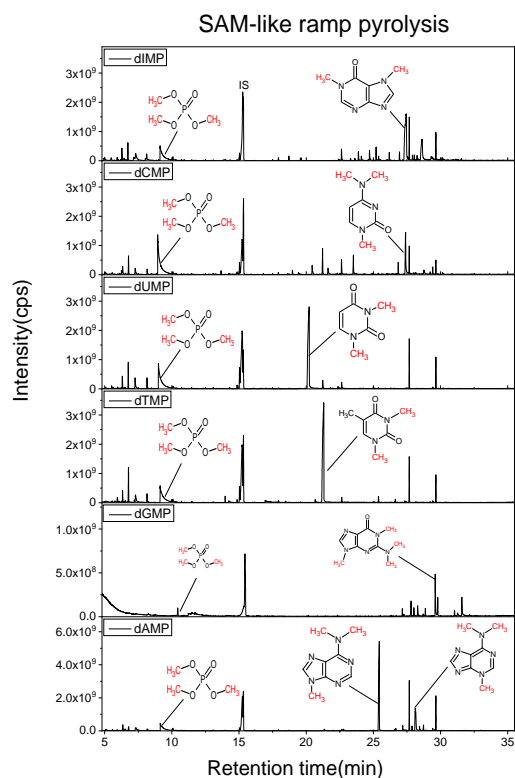


Figure 5-17 Chromatograms of nucleotides (10 nmol) thermochemolysis in TMAH at SAM-like ramp pyrolysis.

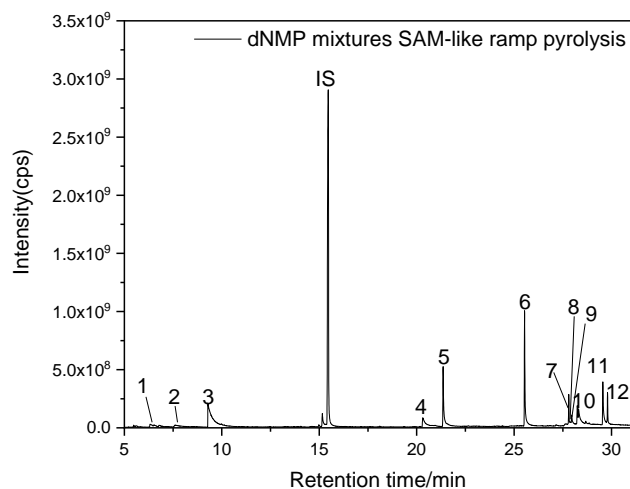


Figure 5-18 Chromatograms of the mixtures of nucleotides (10 nmol) thermochemolysis in TMAH at SAM-like ramp pyrolysis. Peak 1: Furfuryl methyl ether; 2: furfuryl alcohol; 3: Methyl phosphate; 4: 1,3-dimethyl-uracil; 5: 1,3-dimethyl-thymine; 6: N,N,9-trimethyl-adenine; 7: Hexadecanoic acid, methyl ester; 8: trimethyl-cytosine; 9: Tetramethyl-guanine; 10: N,N,3-trimethyl-adenine; 11: tetramethyl-guanine; 12: Octadecanoic acid methyl ester.

## 5.4 TMAH thermochemolysis of nucleotides triphosphate

Nucleotides triphosphate is the most important components of DNA or RNA. The products of each nucleotide and their mixtures with TMAH thermochemolysis at different temperatures were analyzed, at flash pyrolysis from 200 to 600 °C and SAM-like ramp pyrolysis at the final temperature of 850 °C.

### 5.4.1 Flash pyrolysis

The methylated products of each nucleotide with TMAH thermochemolysis at different temperatures were analyzed. Figure 5-19 shows the chromatogram of nucleotides triphosphate with TMAH thermochemolysis at different temperatures. Their target compounds have been presented as well, which are consistent with the target compounds from nucleosides and nucleotides with TMAH thermochemolysis at different flash temperatures. Furthermore, the target compounds of each nucleotides triphosphate with TMAH thermochemolysis are the same under different thermochemolysis temperatures. Therefore, we did not list the main products herein. However, their intensities increase with the increasing of temperatures.

The abundance of methyl phosphate was analyzed. Figure 5-20 shows the abundance of methyl phosphate from 5mix of nucleotides triphosphate with TMAH thermochemolysis at different temperatures. No methylated phosphate was detected when the temperature is lower than 300 °C. At 300 °C, the relative intensity of methyl phosphate is the highest, and its intensity declined dramatically with the raising of the temperature of thermochemolysis. The yield of methyl phosphate of nucleotides at flash 300 °C is about 5.6 times higher than that from the 600 °C; at 600 °C, only a few amounts of methyl phosphate was detected with the lowest abundance. The relative intensity of methyl phosphate from nucleotides triphosphate thermochemolysis with TMAH at flash 400 °C is about 0.6 times lower than that obtained from 300 °C. Methyl phosphate is one of the significant units of nucleotides triphosphate; therefore, it is necessary to optimize the detection conditions of methyl phosphate. Results demonstrate that the optimal temperature for the characterization of methyl phosphate is at 300 °C.

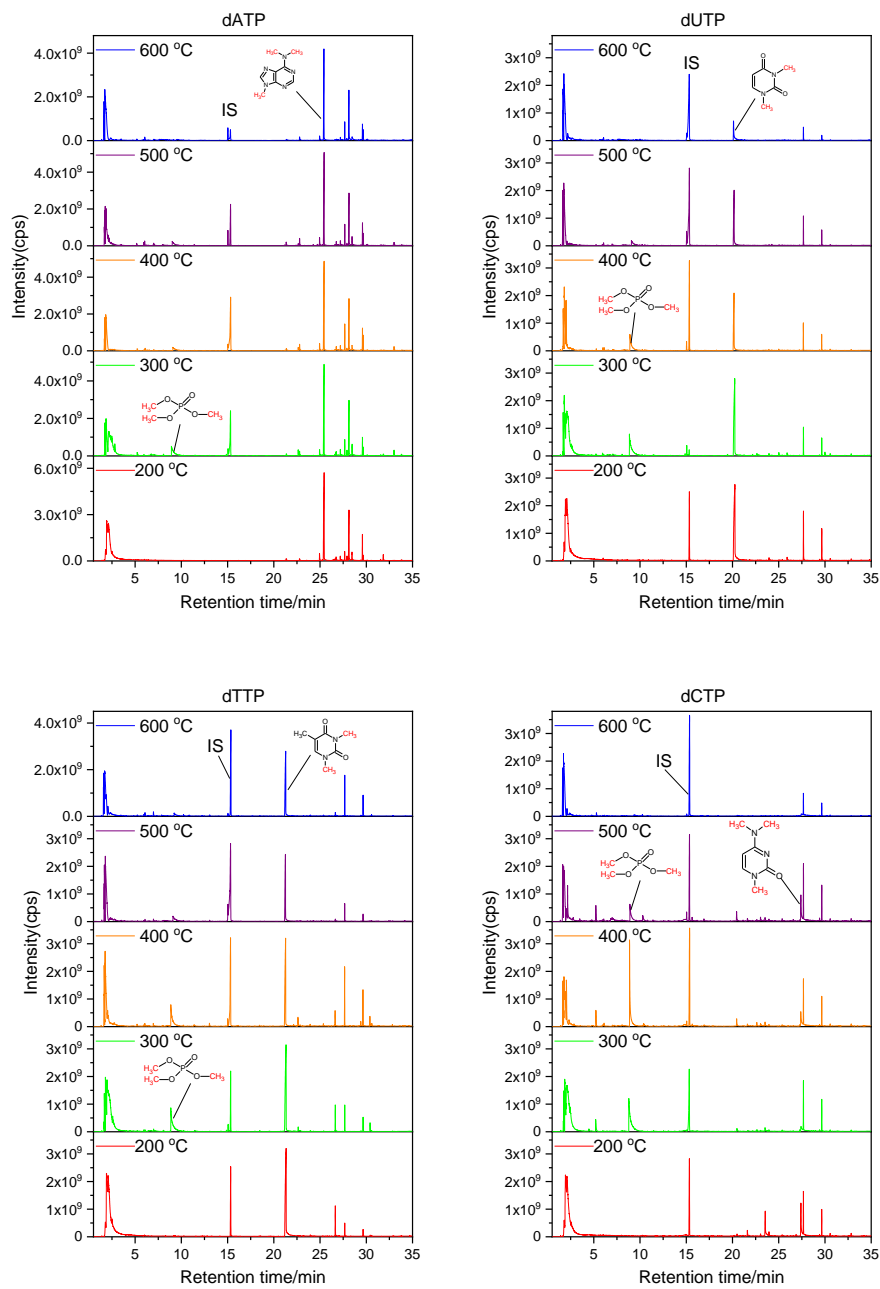


Figure 5-19 Chromatograms of nucleotides after flash TMAH thermochemolysis at different temperatures (200°C-600°C).

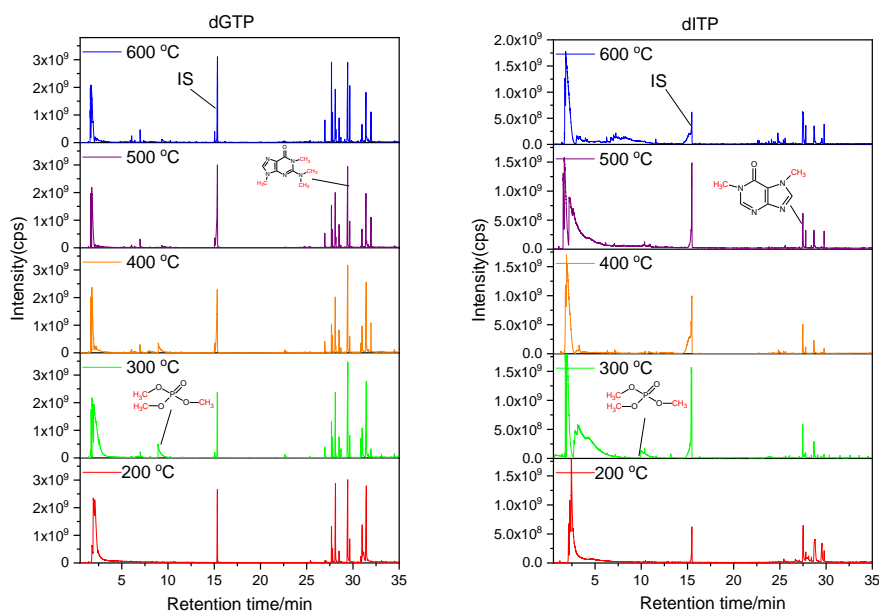


Figure 5-19 (continued) Chromatograms of nucleotides after flash TMAH thermochemolysis at different temperatures (200°C-600°C).

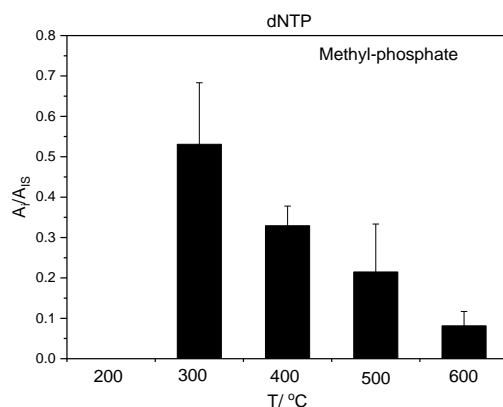


Figure 5-20 The abundance of methyl phosphate from 5mix of nucleotides triphosphate with TMAH thermochemolysis at different temperatures.

Figure 5-21 shows the distribution of thermochemolysis products of nucleotides triphosphate in TMAH at different temperatures. Since the methylated nucleobases are also the main compounds from nucleotides triphosphate with TMAH thermochemolysis, as Figure 5-19. Therefore, the abundance of the methylated nucleobases is the criterion for selecting the optimal temperature of nucleotides detection with TMAH thermochemolysis. For the detection of methylated nucleobases, 200 °C is the optimal temperature for methylated adenine, guanine, uracil, thymine, and cytosine. The abundances of methylated nucleobases reduced significantly with an increase in temperature of flash thermochemolysis. For example, the relative intensity

of trimethyl-cytosine obtained from 200 °C is 5.2 times of that from the 600 °C. This is similar with the case of deoxyuridine triphosphate and deoxyguanosine triphosphate, which is the abundance of methylated uracil and methylated guanine decreased with an increasing of temperature. Only deoxyadenosine triphosphate showed a relative stable property. The abundance of the methylated adenine from flash 200 °C is 1.4 times higher than that of the methylated adenine from flash 600 °C. This is different from the case of detection of nucleobases with TMAH thermochemolysis, 600 °C is the optimal temperature for the detection of nucleobases. Since nucleotides and nucleobases are different from their structures, the addition of ribose and phosphate changed their stabilities when thermochemolysis at different temperatures. Nucleobases showed better stabilities than nucleotides. In addition, the methylated nucleosides were also detected but at a low intensity, such as the methylated deoxyadenosine, deoxyuridine, deoxythymine, deoxyguanosine. High temperature prohibited the preservation of these methylated nucleosides because of the degeneration of these nucleotides triphosphate. Therefore, 200 °C is the optimal temperature for the detection of these methylated nucleobases.

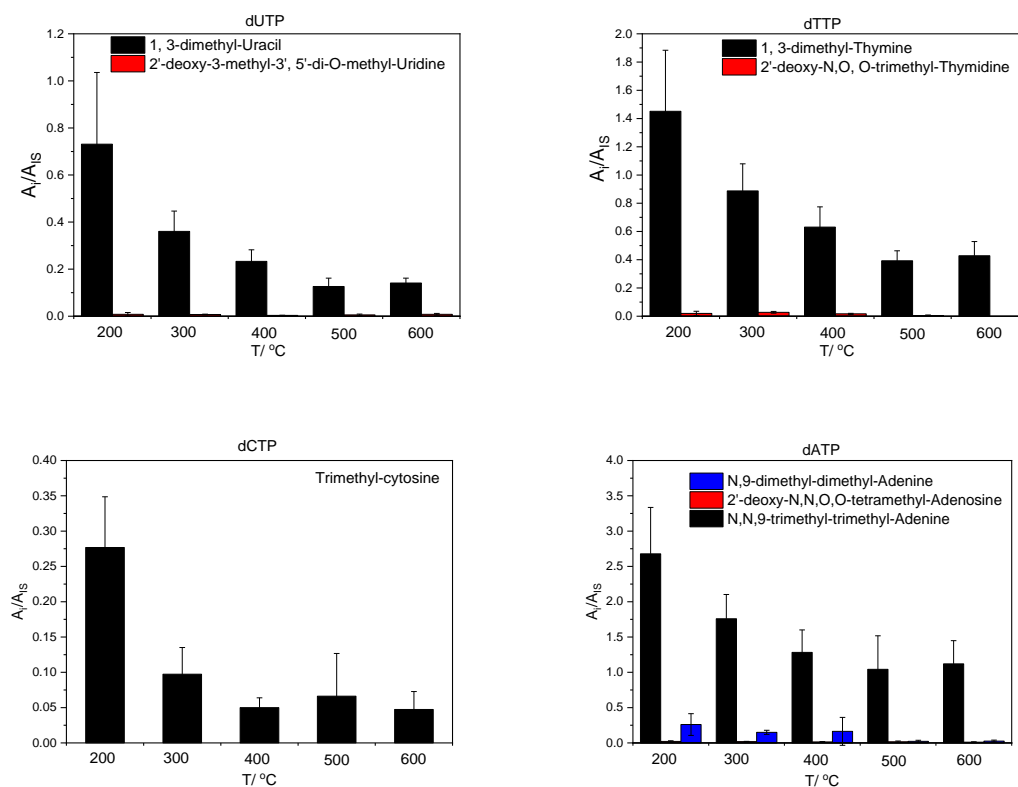


Figure 5-21 Distribution of thermochemolysis byproducts of nucleotides triphosphate in TMAH at different temperatures ( $A_i/A_{IS}$  is the ratio of area of organics and the area of internal standard).

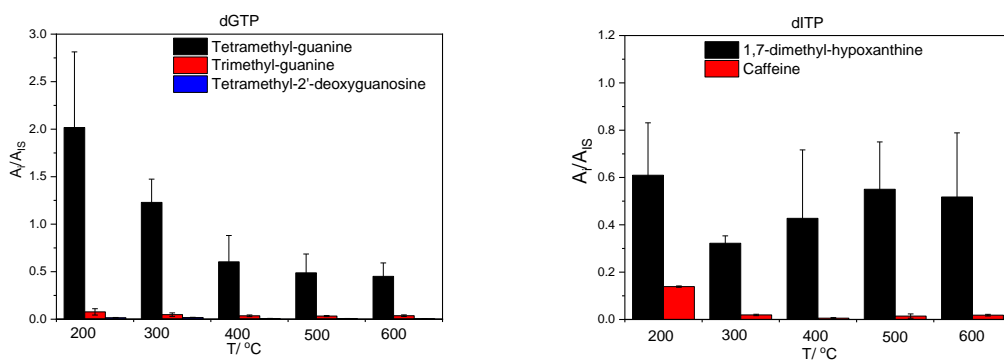


Figure 5-21(continued) Distribution of thermochemolysis byproducts of nucleotides triphosphate in TMAH at different temperatures ( $A_i/A_{IS}$  is the ratio of area of organics and the area of internal standard).

The solution of dAMP, dGMP, dTMP, dUMP, and dCMP standard was mixed and their thermochemolysis byproducts were studied. Figure 5-22 shows the chromatograms of the mixtures of the five nucleotides triphosphate after flash TMAH thermochemolysis at different temperatures. The target compounds of each nucleotide triphosphate were detected respectively. And they have the same retention time as we mention in section 5.1 and 5.2. This demonstrates that increasing the thermochemolysis temperature does not influence the separation and detection of these nucleotides triphosphate.

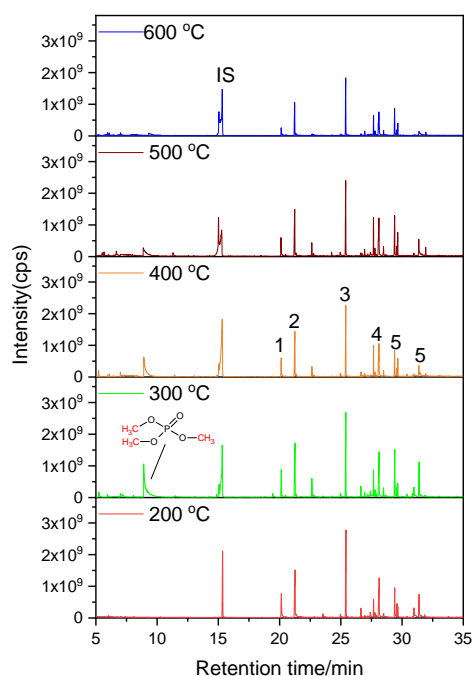


Figure 5-22 The mixtures of nucleotides triphosphate with TMAH thermochemolysis at different temperatures. Peak 1: 1,3-dimethyl-uracil; 2: 1,3-dimethyl-thymine; 3: N,N,9-trimethyl-adenine; 4: N,N,3-trimethyl-adenine; 5: Tetramethyl-guanine.



### 5.4.2 SAM-like ramp pyrolysis

Figure 5-23 shows the pyrolysis products of nucleotides triphosphate with TMAH at SAM-like ramp pyrolysis. Same as the results of nucleotides triphosphate with TMAH thermochemolysis, the methylated nucleobases are the target compounds of each corresponding nucleotides with TMAH thermochemolysis at SAM-like ramp pyrolysis, such as 1,3 dimethyl-uracil at the retention time of 20.13 min, 1,3-dimethyl-thymine at the retention time of 21.26 min, N,N,9-trimethyl-adenine at the retention time of 25.41 min, tetramethyl guanine at 29.41 min. Hence we did not list the main target compounds here. In addition, the methylated phosphate was detected at a relatively high intensity. The mixture of five kinds of nucleotides triphosphate, including dATP, dGTP, dTTP, dUTP, and dCTP with TMAH thermochemolysis has been analyzed, as shown in Figure 5-24. Results show that all of the target compounds have been separated and detected efficiently. Therefore, there is no overlap among these nucleotides triphosphate, and their target methylated nucleobases, furfuryl methyl ether, and the methylated phosphate have been detected at a high intensity.

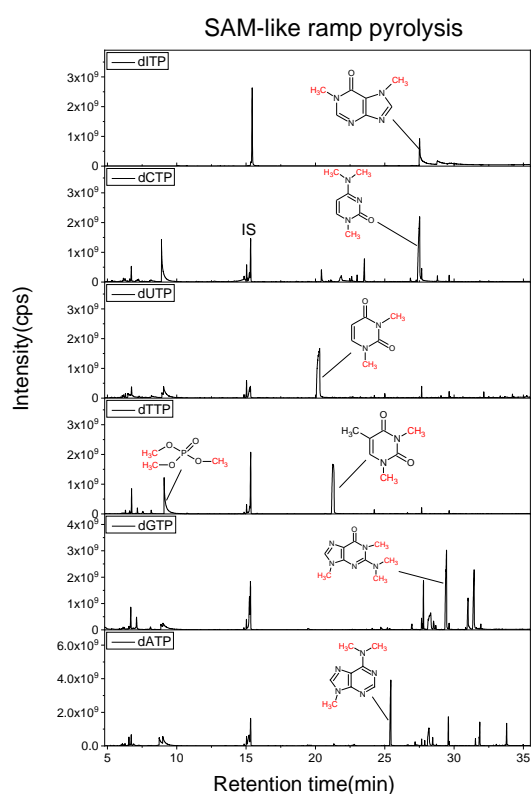


Figure 5-23 The pyrolysis products of nucleotides triphosphate with TMAH at SAM-like ramp pyrolysis.

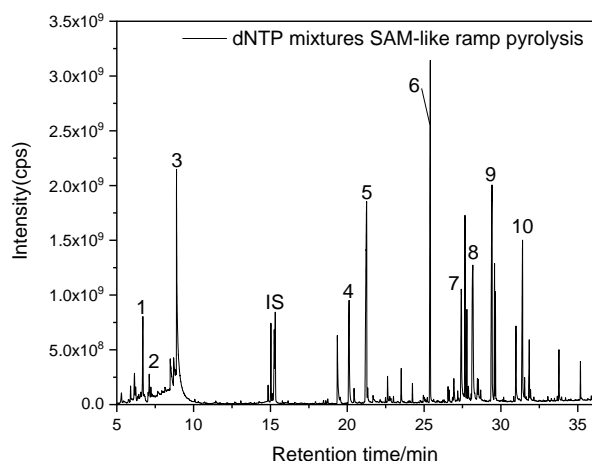
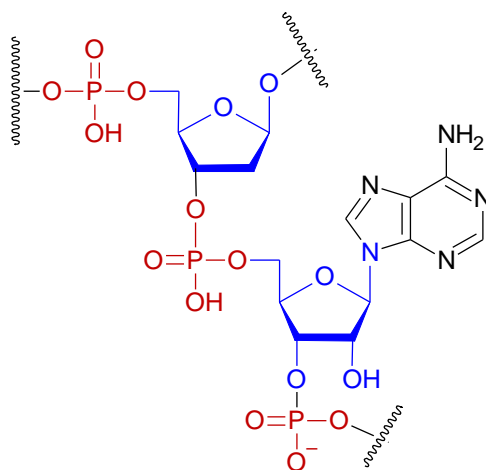


Figure 5-24 Chromatograms of mixtures of nucleotides triphosphate thermochemolysis in TMAH at SAM-like ramp pyrolysis. Peak 1: 1-chlorocyclohexene; 2: Furfuryl methyl ether; 3: methyl phosphate; 4: 1,3-dimethyl-uracil; 5: 1,3-dimethyl-thymine; 6: N,N,9-Trimethyl-adenine; 7: trimethyl-cytosine; 8: N,N,3-Trimethyl-adenine; 9,10:tetramethyl-guanine.

## 5.5 TMAH thermochemolysis of poly A

The products of poly A after TMAH thermochemolysis were analyzed herein, Figure 5-25 shows the structure of poly A. In this section, the temperature of poly A with TMAH thermochemolysis was optimized, at both flash pyrolysis (from 100 to 700 °C) and SAM-like ramp pyrolysis at the final temperature of 850 °C. The target products of poly A with TMAH thermochemolysis were listed and analyzed.



Poly A (RNA tail)

Figure 5-25 The structures of Poly A.

### 5.5.1 Flash pyrolysis

The methylated compounds of poly A with TMAH thermochemolysis were analyzed, at flash pyrolysis from 100 to 700 °C. Figure 5-26 shows the chromatograms of poly A (5.15 nmol) thermochemolysis in TMAH (25% in methanol) at different temperatures. No byproduct was detected from poly A thermochemolysis at 100 °C. The byproducts of poly A thermochemolysis with TMAH were detected when the temperature is higher than 200 °C. This means that the degradation of poly A occurred only when the thermochemolysis temperature is higher than 100 °C. N,N,9-Trimethyl-adenine is the main methylated byproducts of poly A after TMAH thermochemolysis. At the retention time of 25.42, 26.89, 27.08, 27.27, and 27.92 min, respectively. N,9-dimethyl-adenine at the retention time of 25.19 min is detected. In addition, methylated adenosine is also detected but at a very low intensity. The intensity of N,N,9-Trimethyl-adenine is the highest. Therefore, N,N,9-trimethyl-adenine is the target compounds of poly A thermochemolysis with TMAH at different temperatures. The main products from poly A with TMAH thermochemolysis are listed in Table 5-5.

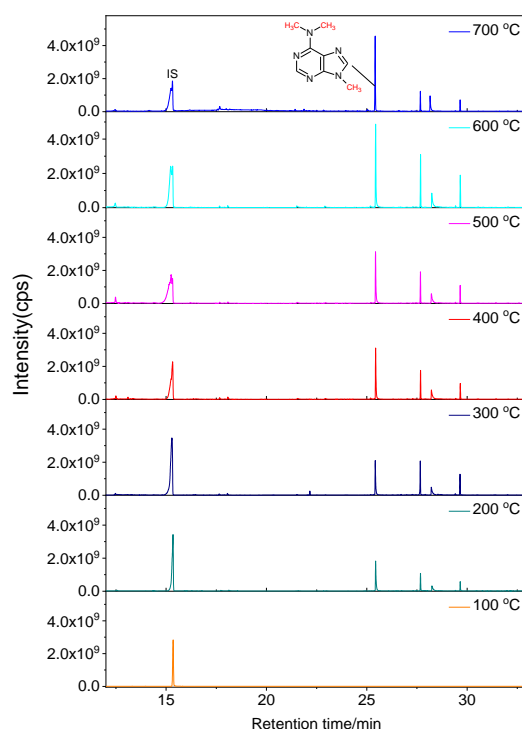
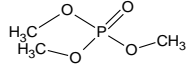
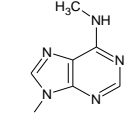
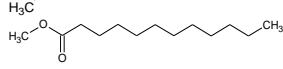
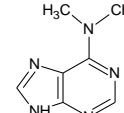
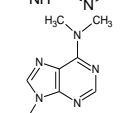
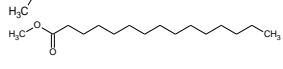
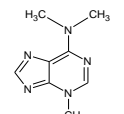
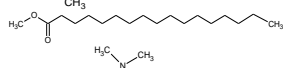
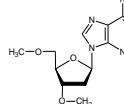


Figure 5-26 Chromatograms of PolyA (5.15 nmol) thermochemolysis in TMAH at different temperatures.

Table 5-5 The main compounds detected from Poly A with TMAH thermochemolysis at flash pyrolysis

RT/ min	Masses of fragments* and relative abundance: m/z (%)	Empirical formula	Compounds	Compounds Structure
11.25	110,79,95,58,140	C <sub>3</sub> H <sub>9</sub> O <sub>4</sub> P	Methyl phosphate	
25.19	163,107,135,148,80,42,53	C <sub>7</sub> H <sub>9</sub> N <sub>5</sub>	9H-Purin-6-amine,N,9-dimethyl-	
25.37	74,87,143,107,129,199,242	C <sub>15</sub> H <sub>30</sub> O <sub>2</sub>	Tetradecanoic acid, methyl ester	
26.89	134,148,163,119,93,66,44	C <sub>7</sub> H <sub>9</sub> N <sub>5</sub>	N,N-dimethyl-adenine	
25.42	148,162,177,107,133,80,42,52	C <sub>8</sub> H <sub>11</sub> N <sub>5</sub>	N,N,9-Trimethyl-9H-Purin-6-amine	
27.67	74,87,143,129,227,171,185,199,270,43,55	C <sub>17</sub> H <sub>34</sub> O <sub>2</sub>	Hexadecanoic acid, methyl ester	
28.22	148,162,177,134,107,119,94,67	C <sub>8</sub> H <sub>11</sub> N <sub>5</sub>	N,N,3-Trimethyl-3H-Purine-6-amine	
29.65	74,87,143,199,255,298	C <sub>19</sub> H <sub>38</sub> O <sub>2</sub>	Methyl stearate	
33.06	134,163,148,192,292,307,120	C <sub>14</sub> H <sub>21</sub> N <sub>5</sub> O <sub>3</sub>	2'-deoxy-N,N,O-tetramethyl-adenosine	

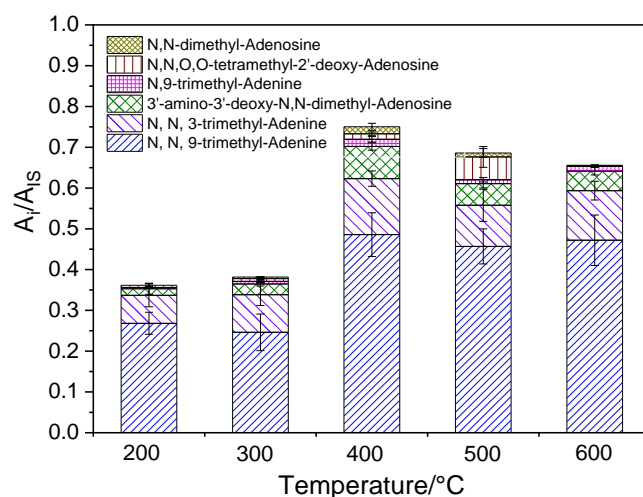


Figure 5-27 Distribution of TMAH thermochemolysis byproducts of Poly A at different temperatures ( $A_i/A_{IS}$  is the ratio of area of organics and the area of internal standard).

Figure 5-27 shows the distribution of thermochemolysis products of poly A in TMAH at different temperatures ( $A_i/A_{IS}$  is the ratio of area of organics and the area of internal standard). Trimethyl-adenine is the main methylated compounds of poly A with TMAH thermochemolysis at different temperatures. With the increase of thermochemolysis temperature, the intensity of nucleobases containing compounds increased from 200 to 400 °C. The abundances of N,N,9-trimethyl-adenine and N,N,3-trimethyl-adenine are similar at 400, 500, and 600 °C. However, the total abundance of methylated adenine and adenosine is the highest at 400 °C. When the temperature was at below 400 °C, poly A was decomposed into adenine or adenosine, which could react with TMAH and produced methylated adenine and adenosine. However, when the temperature is higher than 400 °C, poly A could degrade into smaller fragments; therefore, less methylated adenosine was formed.

In addition, methyl phosphate, one of the most important structures of poly A, was detected at the retention time of 11.25 min. The byproducts from poly A obtained after TMAH thermochemolysis mainly include the degradation products of TMAH and poly A. The byproducts from TMAH degradation were released mainly at the retention time before 8 min. Some fatty acids methyl esters were detected, such as succinic acid dimethyl ester at the retention time of 11.57 min, decanoic acid methyl ester at 18.51 and 22.51 min, tetradecanoic acid, methyl ester at 25.37 min, pentadecanoic acid, and methyl ester at the retention time of 36.57 min. However, these fatty acids methyl esters could be originated from the byproducts of poly A degradation. They were also detected from the reactions of nucleosides, nucleotides, and nucleotides triphosphate with TMAH thermochemolysis. And some other N-containing compounds such as N,N-dimethyl-benzenemethanamine at the retention time of 12.98 min, are the byproducts from TMAH degradation. The intensities of these byproducts are very low; therefore, it's easier to discriminate the target compounds of poly A with TMAH thermochemolysis from the byproducts.

### 5.5.2 SAM-ramp like pyrolysis

Figure 5-28 is the chromatogram of poly A with TMAH thermochemolysis at SAM ramp like pyrolysis. Compared with the results from flash pyrolysis, the target compounds from poly A with TMAH thermochemolysis are almost the same. Trimethyl adenine is the main compounds from poly A with TMAH thermochemolysis at SAM-like ramp pyrolysis. The methylated adenosine, 2'-deoxy-N,N,O,O-tetramethyl-adenosine was detected, at the retention

time of 33.35 min. The relative intensity of trimethyl adenine of poly A with TMAH at SAM-like ramp thermochemolysis is almost the same as that from flash pyrolysis. This demonstrates that the distribution of the main compounds of poly A with TMAH thermochemolysis is not influenced by the mode of thermochemolysis (no matter flash or SAM-like ramp thermochemolysis).

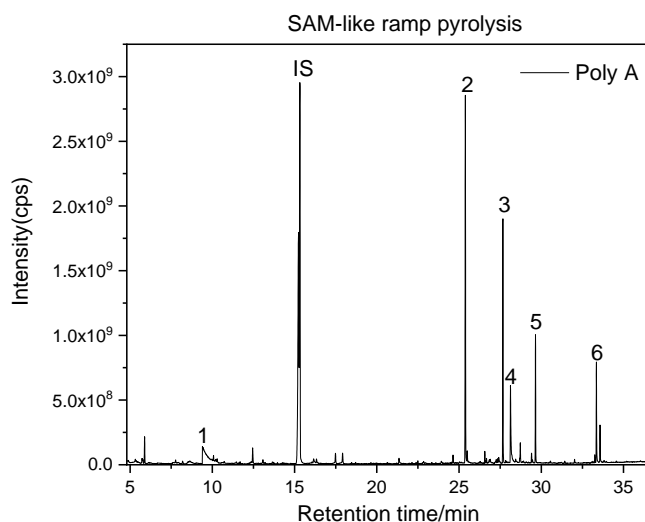


Figure 5-28 Chromatogram of Poly A (5.15 nmol) thermochemolysis in TMAH at SAM-like ramp pyrolysis. Peak 1: methyl phosphate; 2: N,N,9-Trimethyl-9H-Purin-6-amine or N,N,9-Trimethyl-adenine; 3: Hexadecanoic acid, methyl ester; 4: N,N,3-Trimethyl-3H-Purine-6-amine N,N,9-Trimethyl-adenine; 5: Methyl stearate; 6: 2'-deoxy-N,NO,O-tetramethyl-adenosine.

However, the abundance of methyl phosphate is different between flash pyrolysis and SAM-like ramp pyrolysis. Figure 5-29 shows the relative intensity of methyl phosphate from poly A with TMAH thermochemolysis at different conditions, including the flash pyrolysis at different temperatures and SAM-like ramp pyrolysis. The abundances of methyl phosphate released from poly A with TMAH thermochemolysis at flash pyrolysis are different. It increases with the increasing of temperature, and the yield of methyl phosphate is the highest at flash pyrolysis 400 °C. Higher temperatures precede the decomposition of methylated phosphate, caused the lower intensity of methylated phosphate. However, the relative intensity of methyl phosphate from thermochemolysis of poly A at SAM-like ramp is higher than that from flash pyrolysis, even at the final temperature of 850 °C. Therefore, SAM-like ramp pyrolysis is more conducive to the detection of methylated phosphate. Flash pyrolysis at 400 °C is the optimal temperature of the detection of methylated phosphate.

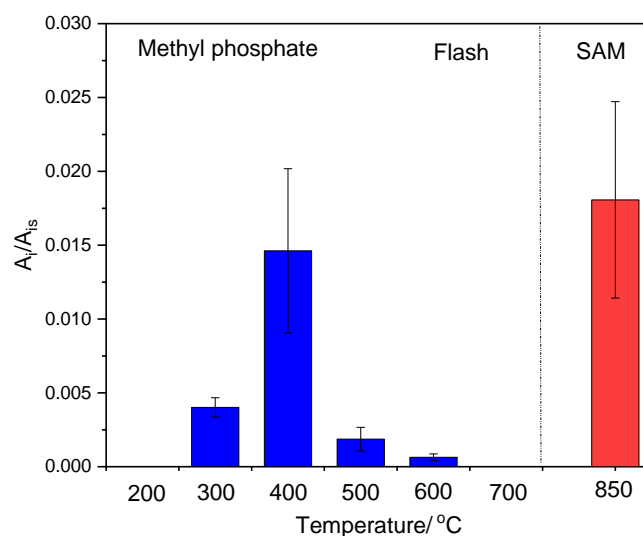


Figure 5-29 The relative intensity of methyl phosphate from poly A with TMAH thermochemolysis at different conditions.

Figure 5-30 shows the plausible mechanism of poly A with TMAH thermochemolysis at flash and SAM-like ramp pyrolysis. For poly A thermochemolysis with TMAH, there are two main reactions. One is the decomposition of poly A, the other is the methylation of poly A by TMAH thermochemolysis. Therefore, temperature is one of the main factors that affects the degradation efficiency of poly A. The efficiency of TMAH methylation of poly A is also influenced by temperature. Increasing the heating temperature enables poly A fully degrade, and to be methylated sufficiently with TMAH. Therefore, 400 °C is the optimal temperature for poly A with flash TMAH thermochemolysis.

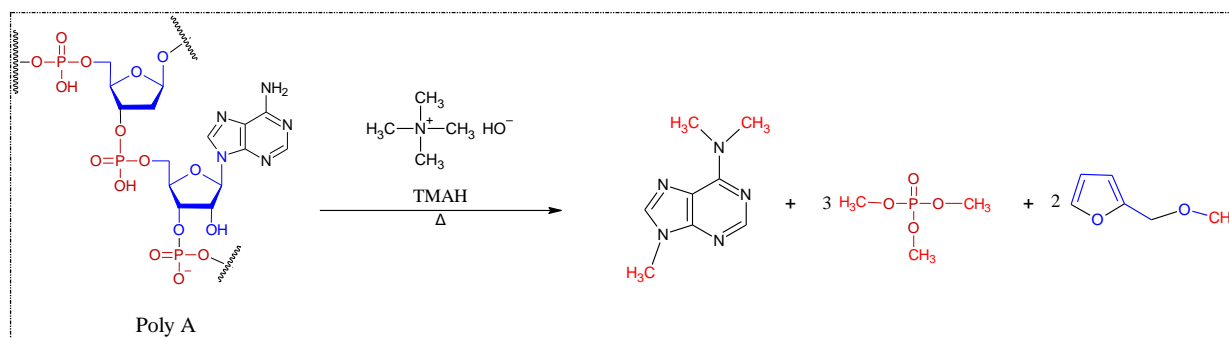


Figure 5-30 the plausible mechanism of poly A with TMAH thermochemolysis

## 5.6 Thermochemolysis patterns

The products of nucleosides, nucleotides, nucleotides triphosphate and DNA with TMAH thermochemolysis were analyzed at flash pyrolysis and SAM-like ramp pyrolysis. Figure 5-31 shows the plausible pathway of nucleosides, nucleotides, nucleotides triphosphate with TMAH thermochemolysis at different temperatures. The deoxyribose sugar conjugates only to the nitrogenous base form deoxyribonucleosides, and the methylated nucleosides could be detected when the temperature is higher than 200 °C, 200 °C is the optimal temperature for the detection of methylated nucleosides. Phosphate group is one of the characteristics constitutes of deoxynucleotides monophosphate and deoxynucleotides triphosphate. When the thermochemolysis temperature is higher than 300 °C up to 500 °C, methyl phosphate of the nucleotides thermochemolysis could be detected. Furfuryl methyl ether could be detected from 200 °C to 600 °C at different intensities; 200 °C is the optimal temperature for the detection of ribose sugar. The target compounds of these nucleosides, nucleotides and nucleotides triphosphate are their corresponding methylated nucleobases. The methylated nucleobases are stable and could be detected even at high temperature as 600 °C; they could be detected when the temperature is higher than 200 °C. This is mainly because the C-N sugar-bases (293 kJ/mol) and PO-C sugar-phosphate (358 kJ/mol) exocyclic are the thermally weakest bonds in DNA structure [687]. During the degradation of DNA without TMAH methylation, from 180~230 °C, ammonia was detected among volatiles besides water and CO<sub>2</sub>. From 50-180 °C, there is only 10% weight loss of DNA, mainly the release of isocyanic acid (HNCO), water, and CO<sub>2</sub>. NH<sub>3</sub>, water, and CO<sub>2</sub> were detected from 180 to 230 °C; H<sub>2</sub>O, CO<sub>2</sub> and NH<sub>3</sub> were detected from 230-400 °C; only CO and CO<sub>2</sub> were released from 400-700 °C. Thus there is 17 %, 27%, 36%, 42%, 47%, 51%, 53% of weight loss of DNA at 230 °C, 300 °C, 350 °C, 400 °C, 450 °C, 500 °C, 600 °C, and 700 °C, respectively [687]. After thermal polymerization, polymer surface of DNA residues and a higher thermally stable ceramic-like material are formed.

However, in this study, TMAH thermochemolysis of nucleosides, nucleotides, and nucleotides triphosphate allows to increase the stability of their characteristic groups, including the methylated nucleobases, furfuryl methyl ethers, and methyl phosphates. The addition of phosphate group of nucleosides has a light influence of the detection of the methylated nucleosides, and the methylated nucleobases should be the main byproducts from the degradation of DNA fragments. Therefore, TMAH thermochemolysis plays an essential



role and should be applied for the detection of the life signatures on Mars or other space missions for the detection of organic compounds with polar functional groups.

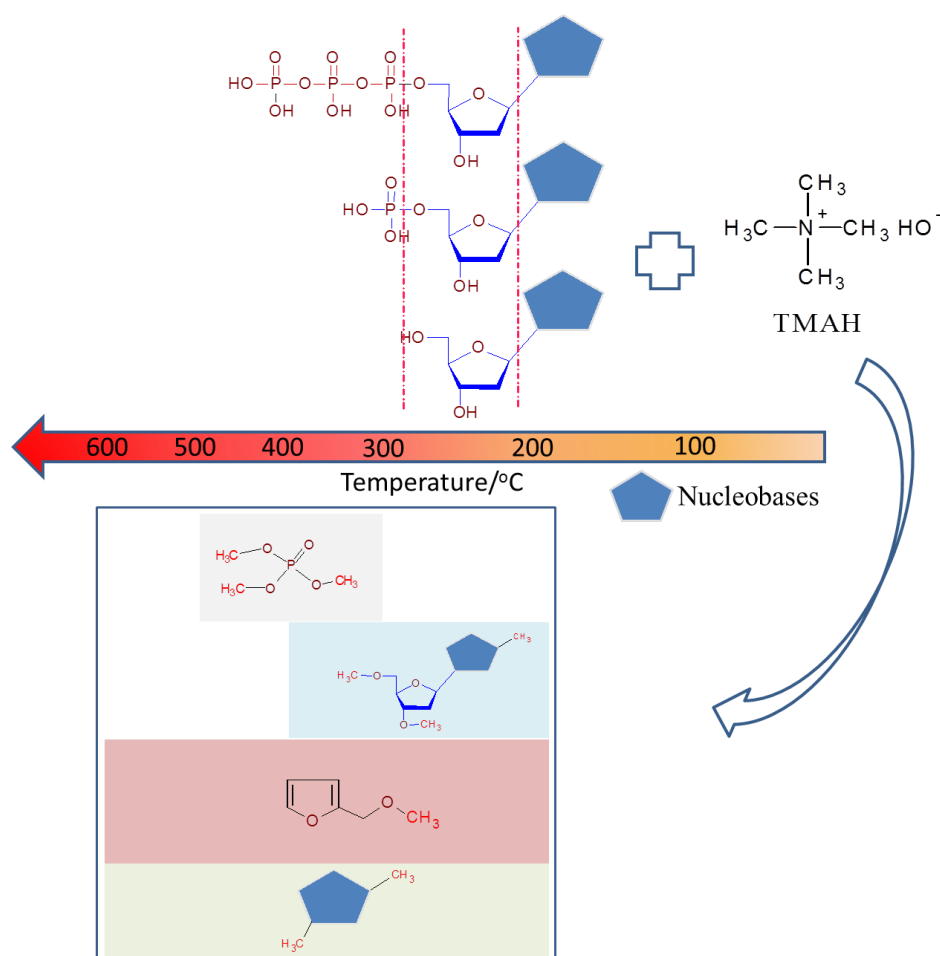


Figure 5-31 The thermal stability of nucleosides, nucleotides, nucleotides triphosphate and their plausible pathway with TMAH thermochemolysis at different temperatures.

## 5.7 Conclusions

The products of nucleosides, nucleotides, and nucleotides phosphates with TMAH thermochemolysis were studied at flash pyrolysis and SAM-like ramp pyrolysis. We conclude that the methylated nucleobases are the main compounds of nucleosides, nucleotides and nucleotides triphosphate with TMAH thermochemolysis. The optimal temperature for the detection of methylated nucleobases, nucleosides and ribose derivatives such as furfuryl methyl ether is 200 °C; 300 °C is the optimal temperature for the detection of methyl phosphate.

However, a higher temperature may be needed for the detection of nucleosides, nucleotides and nucleotides triphosphate because of the strong adsorption of organics with solid matrix. Our results demonstrated the methylated nucleobases could be detected even at high temperature of 600 °C. Therefore, the nucleosides, nucleotides, and nucleotides triphosphate could still be detected if they were contained in Martian soil samples. The structure of the original nucleobases influence the detection of the characteristic compounds. For example, the abundance of methylated nucleosides from the methylation of nucleosides and nucleotides are different. The intensity of methylated nucleosides from the nucleosides thermochemolysis with TMAH is higher than that from the nucleotides thermochemolysis with TMAH. Although 200 °C is the optimal temperature for the detection of methylated nucleobases, for poly A, the abundance of methylated adenine is the highest at 400 °C. This demonstrates that the efficiency of TMAH thermochemolysis depends on the degradation of DNA fragments. Hence, the temperature of TMAH thermochemolysis affects the efficiency of detection of DNA fragments. Therefore, if there is life on Mars such as the bacteria in Martian soil, the experimental conditions of the detection of life should be optimized in the future.

## **Chapter 6. Application of TMAH thermochemolysis to the detection of bacteria: application to the MOMA and SAM space experiment.**

The applications of TMAH thermochemolysis on the detection of DNA fragments and a short DNA have been studied in the previous chapter, and the results demonstrate that TMAH thermochemolysis is an efficient way to analyze the consistent of DNA or RNA molecules. One of the main goals of SAM is to make the inventory of organic compounds on Mars through analyzing the organic compounds in Martian soil. Since the harsh environment of Mars, life habitation problems are huge challenges for life. However, we think that microorganisms could possibly survive under extreme conditions. In addition, some bacteria such as cyanobacteria have been detected in the Atacama Desert sample, which is a Martian analogue on Earth; it could be not exclude the possibility that there are some bacteria alive on Mars. If there are bacteria on Mars, the application of TMAH thermochemolysis on the detection of bacteria could be essential. Therefore, in this chapter, the application of TMAH thermochemolysis on the detection of organic compounds from *E.coli* (*Escherichia coli*) were studied, and the experimental conditions were optimized. For further study, cyanobacteria (*chroococciopsis cubana*), anctinobacteria (*Rubrobacter radiotolerans*) that have been detected in Atacama sample, and halophilic Archaea (*halobacterium salinarum*) that could possibly survive in extreme environment were studied with TMAH thermochemolysis. The main products from these real lives with TMAH thermochemolysis were studied, and the thermochemolysis temperature was optimized.

### **6.1 Experimental**

#### **6.1.1 Cultures**

##### **6.1.1.1 *E.coli* culture**

*E. coli* cultures were grown in 250 mL Erlenmeyer flask filled with 50 mL of YPG medium (yeast, peptone and glucose medium; REF). Cultures were grown a couple of days and the optical density at a wavelength of 600 nm (OD600) was determined by diluting the bacterial suspension in a polystyrene cuvette (Fisher scientific 14-955-127), 1 ml of water was used as the blank with uv/Vis spectrophotometer (Evolution 60S Thermoscientific).

#### **6.1.1.2 *Chroococcidiopsis cubana* culture**

*Chroococcidiopsis cubana* DSM 107010 was bought from DSMZ (Leibniz institute, DSMZ-German collection of Microorganisms and Cell Culture GmbH). They were isolated from dry soil, Cuba, Pinar del Rio. They were cultivated in 250 mL Erlenmeyer flask filled with 50 mL of 3N-Bristol medium (Table S6-1 in the appendix), under a continuous photon flux density of 20  $\mu\text{mol photons m}^{-2}\text{s}^{-1}$ . The cultures were grown for approximately 10 days before harvesting.

#### **6.1.1.3 *Rubrobacter radiotolerans* culture**

*Rubrobacter radiotolerans* DSM 5868 was bought from DSMZ (Leibniz institute, DSMZ-German collection of Microorganisms and Cell Culture GmbH). They were isolated from thermos-mineral water spring, Missa, Tottori Pref. Japan. They were cultivated in 250 mL Erlenmeyer flask filled with 50 mL Halobacteria medium at 37°C and in the dark (Table S6-2 in the appendix). The cultures were grown for approximately 4 days before harvesting.

#### **6.1.1.4 *Halobacterium salinarum* culture**

*Halobacterium salinarum* DSM 671 was bought from DSMZ (Leibniz institute, DSMZ-German collection of Microorganisms and Cell Culture GmbH). They were cultivated in 250 mL Erlenmeyer flask filled with 50 mL Halobacteria medium at 37°C and in the dark (Table S6-3 in the appendix). The cultures were grown for approximately 4 days before harvesting.

### **6.1.2 Separation of cells**

In order to separate the cells from the respective growth media, aliquots of cultures of these bacteria sample were centrifuged at 8000 rpm from 5 mins. The supernatant was then discharged and the pellet suspended in normal saline (0.85% NaCl in distilled water). The whole process was repeated for at least 3 times to ensure that no media residues were present in the sample. Figure 6-1 is the samples of *Chroococcidiopsis cubana*(C.C.), *Rubrobacter radiotolerans*(R.R.), and *Halobacterium salinarum*(H.S).



Figure 6-1 The samples of *Chroococcidiopsis cubana*(C.C.), *Rubrobacter radiotolerans*(R.R.), and *Halobacterium salinarum*(H.S). Bacteria in saline of 1000 mL (left); pure cells with less normal saline (right). R.R., 0.85% normal saline; C.C. in distilled water; H.S. 12.5% NaCl in water).

### 6.1.3 Py-GC/MS

The pyrolysis experiments of different bacteria samples were performed with an EGA/PY-3030D micro-oven pyrolyser, the organic volatiles from the pyrolysis of bacteria were analyzed by GC/MS as described in previous chapters. Flash pyrolysis at different temperatures was applied in this chapter. The final temperatures are the following: 200, 300, 400, 500, 600 °C. The sample is pushed into a heated and stabilized oven at the designed final temperatures. Helium is used as the carrier gas to carry the pyrolysis volatile products into the GC/MS. The temperature programming of the column is the same as the programming of nucleosides, nucleotides, and nucleotides triphosphate. The temperature programming starts at 40 °C held for 2 min, then at a heat rate of 6 °C min<sup>-1</sup> up to 130 °C then raised to 300 °C at a rate of 10 °C min<sup>-1</sup> and maintained for 1 min. In both ramps, helium flow rate in the column was set at 1.2 mL.min<sup>-1</sup>. The split flow was 12 mL.min<sup>-1</sup>. The temperature of the SSL injector was set at 280 °C. The masses were scanned between  $m/z$  40 and  $m/z$  500. The ionization energy was 70 eV. All experiments were repeated 6 times.

## 6.2 Organic compounds from *E.coli* with TMAH thermochemolysis

### 6.2.1 Flash pyrolysis

In this section, the organic compounds from *E.coli* with TMAH thermochemolysis have been studied, mainly at flash pyrolysis at different temperatures, 100 °C, 200 °C, 300 °C, 400 °C, 500 °C, and 600 °C. However, when the pyrolysis temperature is at 100 °C, no organic compound was detected from *E.coli* with TMAH thermochemolysis. Therefore, only organic

compounds obtained from *E.coli* with TMAH thermochemolysis between 200 to 600 °C were analyzed herein.

#### **6.2.1.1 Organic compounds from *E.coli* with TMAH thermochemolysis**

Figure 6-2 shows the chromatograms of *E.coli* with TMAH thermochemolysis at different temperatures. Many fatty acids methyl esters were detected during the flash pyrolysis of *E.coli* with TMAH, mainly from the retention time of 22 min to 30 min, the fatty acids include methyl vanillate (RT=20.50 min), dodecanoic acid methyl ester (RT=22.50 min); tetradecanoic acid methyl ester (RT=25.37 min), methyl myristoleate (RT=26.01 min), Methyl palmitoleate (RT=27.45 min), etc. The abundance of hexadecanoic acid methyl ester at the retention time of 27.69 min is the highest; cis-10-heptadecenoic acid methyl ester at the retention time of 28.56 min is the second highest peak in the chromatogram, indicating that hexadecanoic acid and heptadecenoic acid are the main fatty acids compounds of *E.coli* with TMAH thermochemolysis. In addition, 9-Octadecenoic acid(Z)- methyl ester, octadecanoic acid methyl ester, cis-10-Nonadecenoic acid methyl ester were also detected. These results are similar with the results obtained by Dworzanski [131]. Phospholipid fatty acids or fatty acids are commonly used as biomarkers to trace viable bacteria in environmental samples [688], and they have been detected in ultra-low organic carbon Atacama desert samples [689].

In addition to the fatty acids, nucleobases were also found from *E.coli* with TMAH thermochemolysis. Figure 6-3 shows the chromatograms of nucleobases detected from *E.coli* with TMAH thermochemolysis at flash 300 °C. The abundance of each nucleobase was lower compared with the abundance of fatty acids. This depends on the content of organics in parent *E.coli*, because the relative abundance of DNA in *E.coli* was only about 3.1 % of dry weight, lipopolysaccharide (3.4%), peptidoglycan (2.5%), and intracellular metabolites, cofactors, and ions (3.5%), proteins ( about 50%) [128]. Though some amino acids, proteins, and saccharide derivatives have been detected from *E.coli*, in this chapter we mainly focus on the main products.

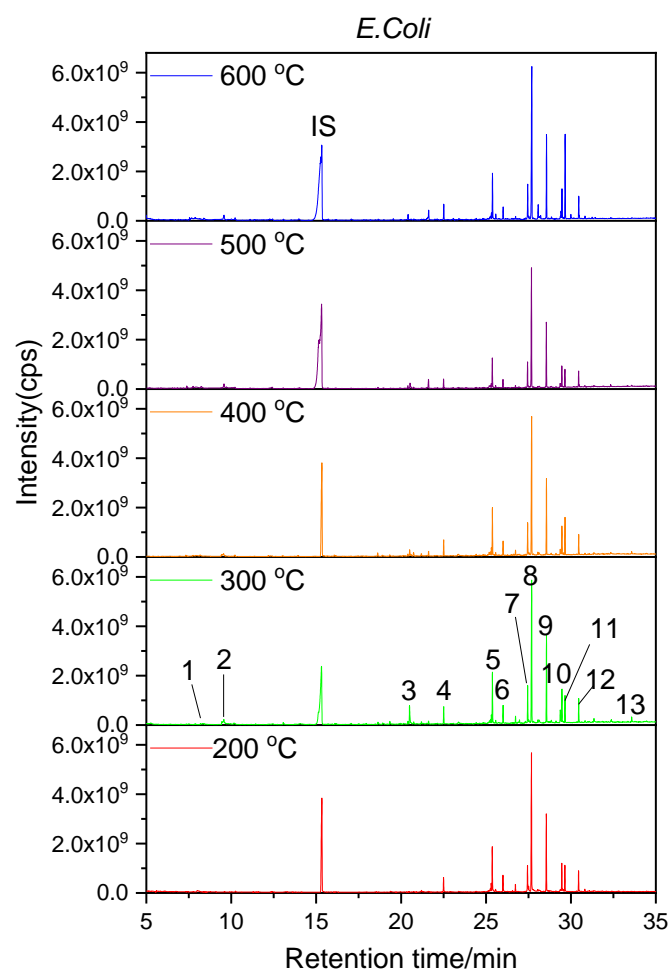


Figure 6-2 The chromatograms of *E.coli* with TMAH thermochemolysis at different flash pyrolysis temperatures. Peak 1: Furfuryl methyl ether; 2: Methyl phosphate; 3: Methyl vanillate; 4: Dodecanoic acid, methyl ester; 5: Tetradecanoic acid, methyl ester; 6: Methyl myristoleate; 7: Methyl palmitoleate; 8: Hexadecanoic acid, methyl ester; 9: cis-10-Heptadecenoic acid, methyl ester; 10: 9-Octadecenoic acid(Z)-,methyl ester; 11: Octadecanoic acid, methyl ester; 12: cis-10-Nonadecenoic acid, methyl ester; 13: N,N-dimethyl-Adenosine.

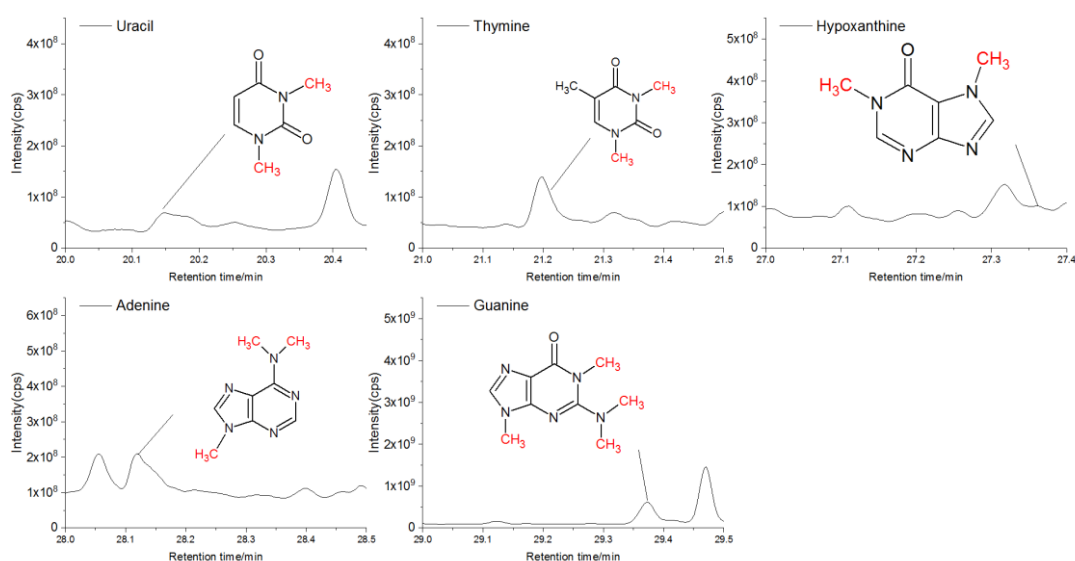


Figure 6-3 The nucleobases detected from *E. coli* with TMAH thermochemolysis at flash 300 °C.

### 6.2.1.2 The distribution of organic compounds from *E. coli*

To optimize the temperature of *E. coli* with TMAH thermochemolysis, the abundance of main target organics obtained from *E. coli* with TMAH thermochemolysis at different temperatures was studied. Figure 6-4 showed the distribution of fatty acids from *E. coli* with TMAH thermochemolysis at different temperatures (200 °C to 600 °C). The abundance of hexadecanoic acid is the highest among these fatty acids from *E. coli* with TMAH thermochemolysis. The abundance of *cis*-10-heptadecenoic acid is the second highest. This demonstrated that the C16 and C17 fatty acids account for a high content of *E. coli* cells. On the other side, hexadecanoic acid could also be from TMAH degradation. This has been proved from our previous study, as shown in the chapter 3 about “Influence of calcium perchlorate on the search for organics on Mars with TMAH thermochemolysis”. Therefore, hexadecanoic acid is not only from *E. coli* cells, the degradation of TMAH thermochemolysis could contribute to the total amount of hexadecanoic acid. However, *cis*-10-heptadecenoic acid was not found from TMAH degradation. Therefore, *cis*-10-heptadecenoic acid could be one of the biomarkers from *E. coli* with TMAH thermochemolysis. Its content is about 2 times of the other fatty acids detected from *E. coli* with TMAH thermochemolysis.



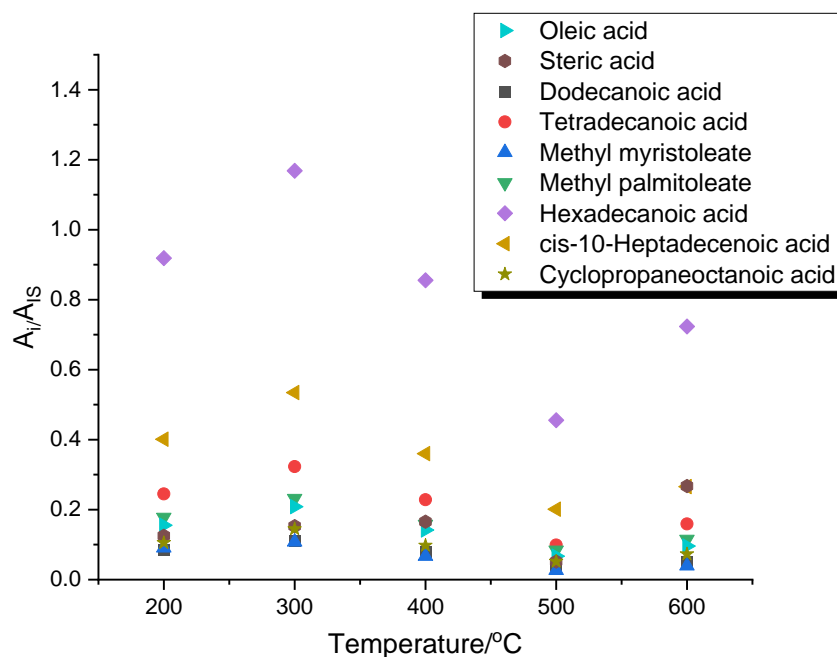


Figure 6-4 the distribution of fatty acids from *E.coli* with TMAH thermochemolysis at different temperatures (200 °C to 600 °C).

In addition, 300 °C is the optimal temperature for the detection of fatty acids from *E.coli* with TMAH thermochemolysis, as the abundance of each fatty acid from *E.coli* is the highest at 300 °C; 200 °C presents the second highest intensities. On the other side, methyl phosphate was found from *E.coli* with TMAH thermochemolysis. Figure 6-5 shows the abundance of methyl phosphate detected from *E.coli* with TMAH thermochemolysis at different temperatures (200 °C to 600 °C). The relative abundance of methyl phosphate from *E.coli* with TMAH thermochemolysis is much lower than other organics such as fatty acids. 300 °C is also the optimal temperature for the detection of methyl phosphate, because the abundance of methyl phosphate is the highest, about 4 times higher than that from *E.coli* with TMAH thermochemolysis at 400 °C. And also, methyl phosphate could be detected only when the thermochemolysis temperature is higher than 300 °C. However, the relative abundance of methyl phosphate declined with an increase of temperature. This reveals that the decomposition of methyl phosphate occurs with an increase of temperature.

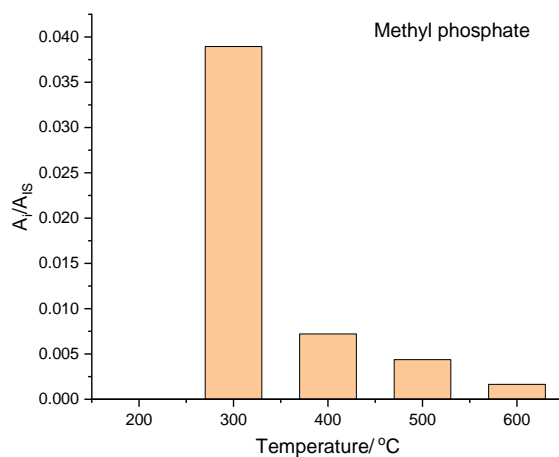


Figure 6-5 The abundance of methyl phosphate detected from *E.coli* after TMAH thermochemolysis at different temperatures (200 °C to 600 °C).

Methyl fufuryl is another characteristic peak we obtained from nucleosides, nucleotides, and nucleotides triphosphate. Therefore, the abundance of methyl fufuryl was analyzed. Figure 6-6 shows the abundance of methyl fufuryl detected from *E.coli* with TMAH thermochemolysis at different temperatures (200 °C to 600 °C). Methyl fufuryl could be detected from 200 °C to 600 °C, however, 200 °C is the optimal temperature for its detection. Therefore, the optimal temperature for the detection of organic biomarkers from *E.coli* with TMAH thermochemolysis should be at 300 °C.

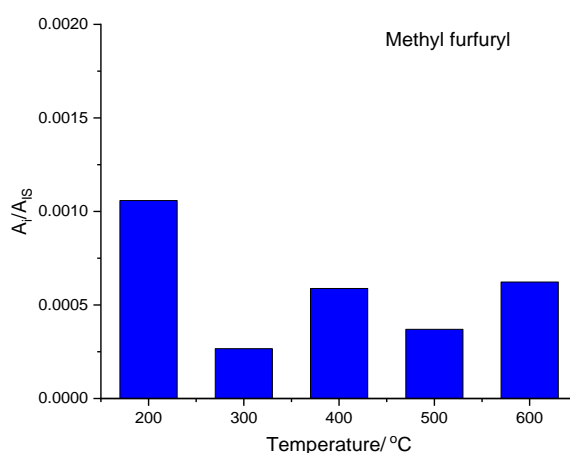


Figure 6-6 The abundance of methyl fufuryl detected from *E.coli* with TMAH thermochemolysis at different temperatures (200 °C to 600 °C). Only one replicate done.

## 6.2.2 SAM-like ramp pyrolysis

SAM-like ramp pyrolysis was applied in this study to mimic the SAM conditions on Mars. Therefore, the organic compounds from *E.coli* with TMAH thermochemolysis at SAM-like ramp were analyzed in this section. Figure 6-7 shows the chromatograms of *E.coli* with TMAH thermochemolysis at SAM-like ramp. However, the repeatability of SAM-like ramp for *E.coli* is not good enough. As shown in Figure 6-7, the peaks and their intensities are not well stable. This could be caused by the temperature program process, and during the heating process of *E.coli*, it could possibly blow to the trap and frozen there, as a result, the heating process of column is not be able to release organics from *E.coli*. Hence, compared with the results from flash pyrolysis, SAM-like ramp pyrolysis is not suitable for the characterizations of *E.coli*, or possibly the same for other bacteria, which needs a further research. Therefore, only flash pyrolysis will be applied to study the organic compounds from other typical bacteria that have been detected in Martian samples.

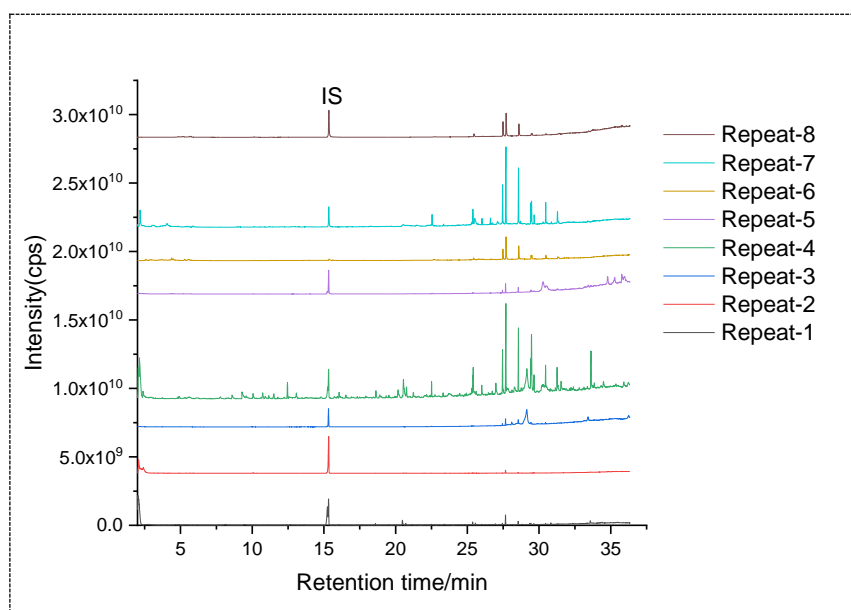


Figure 6-7 Chromatograms of *E.coli* with TMAH thermochemolysis at SAM-like ramp pyrolysis.

## 6.3 TMAH thermochemolysis of cyanobacteria

### 6.3.1 Organics from cyanobacteria

The organic compounds from cyanobacteria were analyzed with TMAH thermochemolysis. Figure 6-8 showed the chromatograms of *chroococcidiopsis cubana* with

TMAH thermochemolysis at different flash pyrolysis temperatures, from 100 °C to 600 °C. Results showed that cyanobacteria decomposed when thermochemolysis temperature is higher than 100 °C. Plenty of organic compounds have been detected from *chroococcidiopsis cubana* with TMAH thermochemolysis when the temperature is higher than 200 °C. The main compounds from cyanobacteria with TMAH thermochemolysis have been numbered in Figure 6-8. Table 6-1 lists all the main products from *chroococcidiopsis cubana* with TMAH thermochemolysis at flash pyrolysis. Fatty acids are the main organic compounds from cyanobacteria with TMAH thermochemolysis, such as 9-hexadecenoic acid (RT=27.59 min), hexadecanoic acid (RT=27.82 min), octadecanoic acid (RT= 29.79 min), 9,12-octadecadienoic acid (RT= 30.36 min). Glucopyranoside is also one of the most important organic compounds. For example, L(-)-Fucose tetramethyl ether (RT=17.87 min), α-D- methyl 2,3,4,6-tetra-O-methyl-galactopyranoside (RT= 23.90, 27.85, 32.20, 32.30 min), α-D-methyl 2,3,4,6-tetra-O-phenyl- glucopyranoside (RT= 30.75 min), α-D-methyl 2,3,4,6-tetra-O-glucopyranoside (RT= 33.09 and 35.51 min).

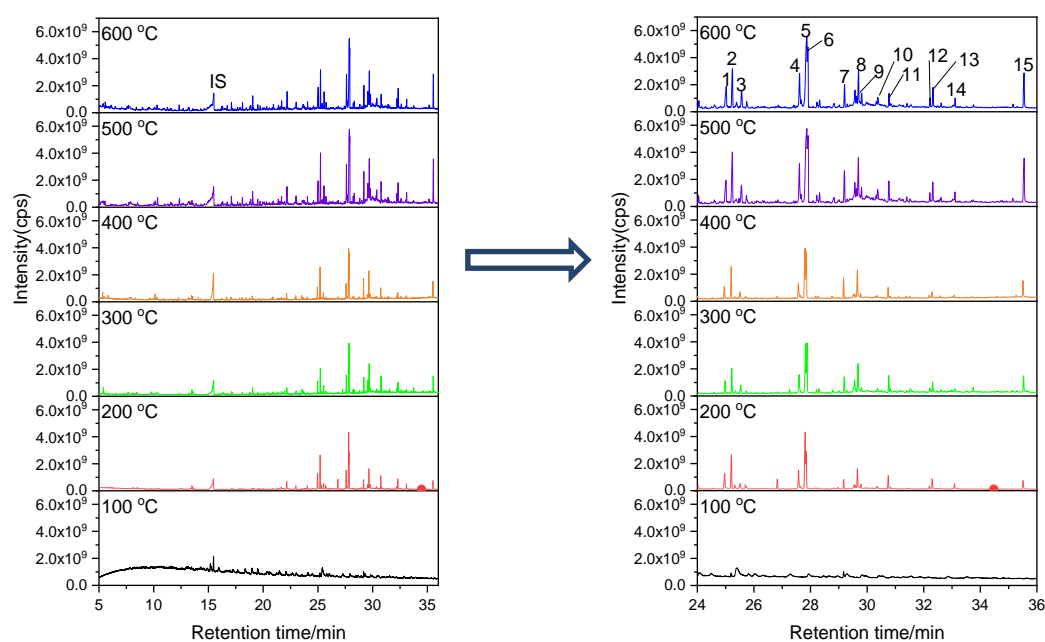


Figure 6-8 The chromatograms of *chroococcidiopsis cubana* with TMAH thermochemolysis at different flash pyrolysis temperatures. Peak 1: p-methoxy-cinnamic acid, methyl ester; 2: Heptadecane; 3: N,N,9-trimethyl-Adenine; 4: Methyl palmitoleate; 5: Palmitic acid, methyl ester ; 6,15: GlcA-DG, permethylated; 7: 2(3H)-Furanone,5-heptyldihydro-; 8: Phytol; 9: Octadecanoic acid, emthyl ester; 10: Linoleic acid, methyl ester; 11: Glucopyranoside, phenyl 2,3,4,6-tetra-O-methyl, A-d-; 12: Manmopyranoside,methyk 2,3,4,6-tetra-O-methyl, a-D-; 13,14: Glucopyranoside, methyl 2,3,4,6-tetra-O-methyl-,a-D-.

On the other side, lignin derivatives have been detected in this study. 1,2,4-trimethoxybenzene at the retention time of 19.69 min is the guaiacyl units; PCA (p-coumarate units) were detected, include p-methoxy-cinamic acid methyl ester at the retention time of 23.61, 23.73, 24.97, and 28.75 min, 1-(4-methoxyphenyl)-4-methyl-1-penten-3-one at the retention time of 28.97 min. Cinnamic acid, methyl ester (RT=20.10 min) could be possibly derived from PCA or (FA) ferulates. 3,4-Dimethoxytoluene (RT=16.67 min), 4-methoxybenzyl alcohol methyl ether (RT=16.85 min), and 2,5-dimethoxy-toluene (RT=16.95 min) could be the products of lignin degradation. Isopropyl styryl ketone (RT=25.70 min) and a-methoxy-,(n)-benzeneacetic acid (RT=29.26 min) are also the degradation compounds of lignin from cyanobacteria with TMAH thermochemolysis. This demonstrates that lignin-derivatives from cyanobacteria could be one of the possible biomarkers from life on Mars.

Besides, the degradation products of chlorophyll have been detected. Phytol and its derivatives have been found in the chromatograms. Phytol acetate (RT=26.83 min) and phytol (RT=29.66 min) could be degraded from the chlorophyll in cyanobacteria. Bute hydrocarbon at the retention time of 25.74 min could be source from the long chain structure of chlorophyll, the chlorophyll structure has been determined several years before [205,206].

In addition, the methylated nucleobases such as N,N,3-trimethyl-adenine (RT=25.51 min), N,N,9-trimethyl-adenine (28.26 min), 1,3-dimethyl-uracil (RT=20.30 min), trimethyl-thymine (RT=21.35 min) and guanine (RT=29.51 min) have been detected. Nucleotides such as 2'-deoxy-N,N,O,O-tetramethyl-adenosine at the retention time of 33.50 min, N-methyl-2',3',5'-trimethyl ether-cytidine (RT=30.49 min) have been detected. When the temperature is higher than 300 °C, 1-methyl-5-oxo- L-Proline methyl ester (RT=23.55 min) was the only new product from Cyanobacteria with TMAH thermochemolysis.

Overall, several life biomarkers have been detected from cyanobacteria with TMAH thermochemolysis even at high temperatures. Therefore, TMAH thermochemolysis could be able to analyze the organic compounds from real life in Martian soil, if there is life on Mars. However, the experimental condition needs to be optimized, especially the thermochemolysis temperature.

Table 6-1 The organic compounds from Cyanobacteria with TMAH thermochemolysis at 200 °C.

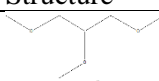
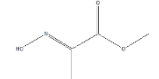
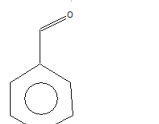
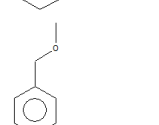
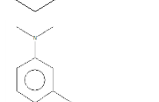
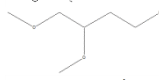
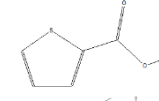
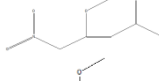
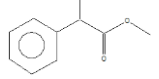
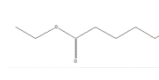
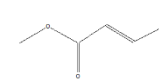
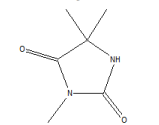
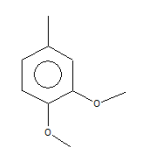
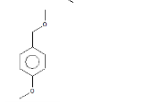
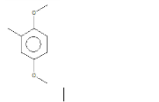
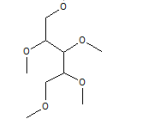
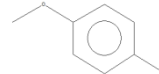
RT/ min	Masses of fragments : m/z (%)	Empirical formula	Compounds	Compounds Structure
8.10	59,89,102,45,71	C <sub>6</sub> H <sub>14</sub> O <sub>3</sub>	Glycerol trimethyl ether	
8.51	85,58,42,116,69	C <sub>4</sub> H <sub>7</sub> NO <sub>3</sub>	Pyruvic acid, methyl ester, oxime	
9.73	77,105,106,51	C <sub>7</sub> H <sub>6</sub> O	Benzaldehyde	
10.39	91,121,77,65,51	C <sub>8</sub> H <sub>10</sub> O	Benzyl methyl ether	
12.30	135,72,91,118,65	C <sub>9</sub> H <sub>13</sub> N	N,N,3-Trimethyl-benzenamine	
12.41	45,103,71,89,135	C <sub>7</sub> H <sub>16</sub> O <sub>3</sub>	1,2,4-Trimethoxy-Butane	
12.57	111,68,142,83,	C <sub>6</sub> H <sub>6</sub> O <sub>2</sub> S	Methyl thiophene-2-carboxylate	
13.37	129,144,55,101,85,45,69	C <sub>6</sub> H <sub>9</sub> NO <sub>5</sub>	2-Butenoic acid,3-methoxy-4-nitro-,methyl ester, E-	
15.86	121,77,91,105	C <sub>10</sub> H <sub>12</sub> O <sub>3</sub>	Benzeneacetic acid,a-methoxy-, methyl ester	
16.01	128,111,45,43,69,56,101,142,174	C <sub>8</sub> H <sub>14</sub> O <sub>4</sub>	Hexanedioic acid, monoethyl ester	
16.11	98,55,140,70,114,82,129	C <sub>6</sub> H <sub>11</sub> NO <sub>2</sub>	Acrylic acid, 3-dimethylamino-, methyl ester	
16.32	127,142,42,74,57,87,154	C <sub>6</sub> H <sub>10</sub> N <sub>2</sub> O <sub>2</sub>	3,5,-trimethyl-Hydantoin	
16.67	152,137,109,91,79,65,51,39	C <sub>9</sub> H <sub>12</sub> O <sub>2</sub>	3,4-Dimethoxytoluene	
16.85	121,152,77,42,91	C <sub>9</sub> H <sub>12</sub> O <sub>2</sub>	4-Methoxybenzyl alcohol, methyl ether	
16.95	137,152,98,109	C <sub>9</sub> H <sub>12</sub> O <sub>2</sub>	2,5-Dimethoxy-Toluene	
17.10	71,142,104,45	C <sub>10</sub> H <sub>22</sub> O <sub>5</sub>	L-(-)-Arabitol, permethyl-	
17.19	71,135,77,107,45,92	C <sub>8</sub> H <sub>8</sub> O <sub>2</sub>	4-Methoxy-benzaldehyde	

Table 6-1 (continued)

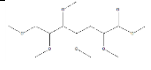
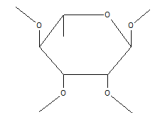
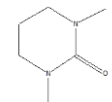
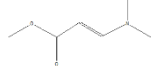
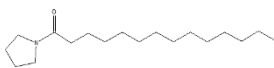
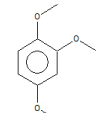
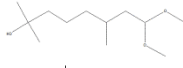
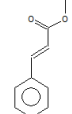
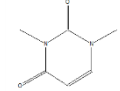
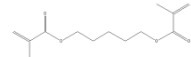


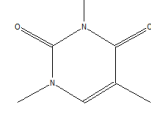
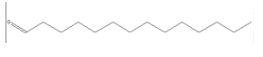
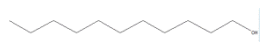
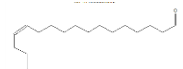
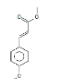
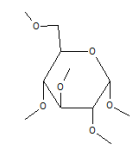

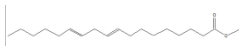
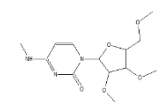

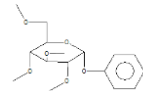
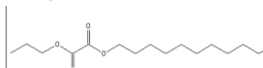
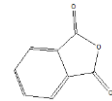
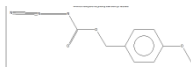
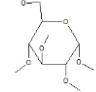
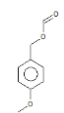
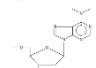
RT/ min	Masses of fragments : m/z (%)	Empirical formula	Compounds	Compounds Structure
17.68	129,115,75,59,71,161	C <sub>13</sub> H <sub>26</sub> O <sub>7</sub>	2,4,5,6,7- Pentamethoxyheptanoic acid, methyl ester	
17.87	88,75,101,73,71,45	C <sub>10</sub> H <sub>20</sub> O <sub>5</sub>	L(-)-Fucose,tetramethyl ether	
18.82,20. 89	128,42,71,84,100,115,55	C <sub>6</sub> H <sub>12</sub> N <sub>2</sub> O	1,3-Dimethyltetrahydro- 2(1H)-pyrimidinone	
19.11	98,129,71	C <sub>6</sub> H <sub>11</sub> NO <sub>2</sub>	2-propenoic acid,3- (dimethylamino)-, methyl ester	
19.51	113,98,72,85,126,59,58	C <sub>21</sub> H <sub>41</sub> NO	Pyrrolidine,1-(1- oxoheptadecyl)-	
19.69	153,125,168,110,93,69,79, 52	C <sub>9</sub> H <sub>12</sub> O <sub>3</sub>	1,2,4-trimethoxy-benzene	
19.95	85,75,115,45,55,127,155	C <sub>12</sub> H <sub>26</sub> O <sub>3</sub>	2-Octanol,8,8-dimethoxy- 2,6-dimethyl-	
20.10	131,103,162,77,51	C <sub>10</sub> H <sub>10</sub> O <sub>2</sub>	Cinnamic acid, methyl ester	
20.30	140,83,42,55	C <sub>6</sub> H <sub>8</sub> N <sub>2</sub> O <sub>2</sub>	1,3-Dimethyl-Uracil	
20.54	69,41,67,126,154,97	C <sub>13</sub> H <sub>20</sub> O <sub>4</sub>	1,5-Pentane dimethacrylate	
20.61	71,100,82,135,166,180,20 9	C <sub>17</sub> H <sub>34</sub> O	1-Hexadecenyl methyl ether	
20.76	128	C <sub>9</sub> H <sub>18</sub> N <sub>2</sub> O <sub>4</sub>	Lle-ser	
21.35	154,68,69,97,42,56	C <sub>7</sub> H <sub>10</sub> N <sub>2</sub> O <sub>2</sub>	1,3,5-trimethyl-uracil	
21.51,21. 94	57,70,95,82,41,109	C <sub>14</sub> H <sub>28</sub> O	Tetradecanal	
21.75	97,70,43,55,83,111,128,15 4,165	C <sub>11</sub> H <sub>24</sub> O	1-Undecanol	
22.98	97,71,55,81,111,135,123,4 3	C <sub>18</sub> H <sub>34</sub> O	13-Octadecenal,(Z)-	
23.61,23. 73,24.97, 28.75	161,133,192,118,89,100,6 3	C <sub>11</sub> H <sub>12</sub> O <sub>3</sub>	Cinamic acid,p- methoxy-,methyl ester	
23.90,27. 85,32.20, 32.30	88,101,75,45,163,127	C <sub>11</sub> H <sub>22</sub> O <sub>6</sub>	Galactopyranoside, methyl 2,3,4,6-tetra-O-methyl-, a- D-	

Table 6-1 (continued)

RT/ min	Masses of fragments : m/z (%)	Empirical formula	Compounds	Compounds Structure
25.20	57,71,85,99,43,113,127	C <sub>17</sub> H <sub>36</sub>	Heptadecane	
25.32	98	C <sub>6</sub> H <sub>7</sub> NO <sub>2</sub>	n-Ethymaleimide	
25.51	148,107,133,162,177,80,44	C <sub>8</sub> H <sub>11</sub> N <sub>5</sub>	N,N,9-Trimethyl-adenine	
25.70	131,103,77,175,51	C <sub>12</sub> H <sub>14</sub> O	Isopropyl styryl ketone	
25.74	57,71,85,88,103,131,152,43,168	C <sub>19</sub> H <sub>40</sub>	Bute hydrocarbon	
26.29	101,88,141,169,201,45	C <sub>15</sub> H <sub>28</sub> O <sub>9</sub>	GlcA-DG, permethylated	
26.83	68,95,82,57,43,123,109,166,278	C <sub>20</sub> H <sub>40</sub> O	Phytol, acetate	
27.58	55,69,74,83,87,96,98,110,111,124,152,194,236	C <sub>17</sub> H <sub>32</sub> O <sub>2</sub>	Methyl palmitoleate	
27.64	212,153,181,58,86,50,64	C <sub>14</sub> H <sub>12</sub> O <sub>2</sub>	Methyl biphenyl-4-carboxylate	
27.81, 28.53	74,87,143,101,129,55	C <sub>17</sub> H <sub>34</sub> O <sub>2</sub>	Hexadecanoic acid, methyl ester	
28.26	148,134,162,177,119,107	C <sub>8</sub> H <sub>11</sub> N <sub>5</sub>	N,N,3-Trimethyl-adenine	
28.59	55,69,83,87,97,98,110,148,123,134,166,179,194,223,208,250	C <sub>19</sub> H <sub>36</sub> O <sub>2</sub>	Oleic acid, methyl ester	
28.81	74,87,210,143,164,269	C <sub>18</sub> H <sub>36</sub> O <sub>2</sub>	Heptadecanoic acid, methyl ester	
28.97	161,133,205,89,118,77	C <sub>13</sub> H <sub>16</sub> O <sub>2</sub>	1-Penten-3-one, 1-(4-methoxyphenyl)-4-methyl-	
29.17	85,123,55,43	C <sub>10</sub> H <sub>18</sub> O <sub>2</sub>	c-Decatactone	
29.26	121,77,91	C <sub>9</sub> H <sub>10</sub> O <sub>3</sub>	Benzeneacetic acid, alpha-methoxy-, (n)-	
29.51	164,123,67,136,178,207,192,108	C <sub>9</sub> H <sub>13</sub> N <sub>5</sub> O	Tetramethyl-Guanine	
29.55,29.60	55,69,74,83,97,87,111,125,138,152,166,180,222,264	C <sub>19</sub> H <sub>36</sub> O <sub>2</sub>	Oleic acid, methyl ester	
29.66	71,81,95,123,57,55	C <sub>20</sub> H <sub>40</sub> O	Phytol	
29.78	74,87,143,199,213,241,255,298	C <sub>19</sub> H <sub>38</sub> O <sub>2</sub>	Methyl stearate	



Table 6-1 (continued)

RT/ min	Masses of fragments : m/z (%)	Empirical formula	Compounds	Compounds Structure
29.94,30.19,30.35	81,79,95,96,109,130,141,188,198,294,262,41,57	C <sub>19</sub> H <sub>34</sub> O <sub>2</sub>	Linoleic acid, methyl ester	
30.30	67,81,95,96,109,110,149,294	C <sub>19</sub> H <sub>34</sub> O <sub>2</sub>	9,12-Octadecenoic acid, methyl ester	
30.49	101,45,168,71,87,143,115	C <sub>13</sub> H <sub>21</sub> N <sub>3</sub> O <sub>5</sub>	N-methyl-2',3',5'-trimethyl ether-cytidine	
30.59	69,55,83,98,154,111,141,43,278	C <sub>19</sub> H <sub>36</sub> O <sub>2</sub>	Oleic acid, methyl ester	
30.75	111,101,187,71,75,45,89,127,155,159	C <sub>16</sub> H <sub>24</sub> O <sub>6</sub>	Glucopyranoside, phenyl 2,3,4,6-tetra-O-methyl-, α-D-	
30.83	97,83,71,69,57,55,111,125,43,269	C <sub>21</sub> H <sub>40</sub> O <sub>4</sub>	Oxalic acid, hexadecyl propyl ester	
31.38	121,77	C <sub>8</sub> H <sub>4</sub> O <sub>3</sub>	Phthalic anhydride	
31.49	98,121,163,207,42,77	C <sub>9</sub> H <sub>9</sub> N <sub>3</sub> O <sub>3</sub>	P-Methoxybenzylazido formate	
33.09,35.51	88,101,12+,75,71,187,263,45,187	C <sub>11</sub> H <sub>22</sub> O <sub>6</sub>	Glucopyranoside, methyl 2,3,4,6-tetra-O-methyl-, α-D	
33.20	121,166,144,100,69,70,228,251	C <sub>9</sub> H <sub>10</sub> O <sub>3</sub>	p-methoxy-benzenemethanol, formate	
33.50	134,164,114,192,220,306	C <sub>14</sub> H <sub>21</sub> N <sub>5</sub> O <sub>3</sub>	2'-Deoxy-N,N,O,O-tetramethyl-Adenosine	

### 6.3.2 Optimal temperature for the detection of organic compounds

In order to optimize the temperature of *chroococcidiopsis cubana* with TMAH thermochemolysis, we compared the abundance of each organic compound from *chroococcidiopsis cubana* at different temperatures. Figure 6-9 shows the distribution of organic compounds from *chroococcidiopsis cubana* with TMAH thermochemolysis at different flash pyrolysis temperatures. It is obvious that the abundance of each organic compound is the highest at flash 500 °C, which demonstrated that 500 °C is the optimal temperature for the organics detection of *chroococcidiopsis cubana* after TMAH thermochemolysis. For example, the abundance of glucopyranoside increase with an increase of temperature until 500 °C, the peak intensity of glucopyranoside at 600 °C is much lower than that at 500 °C, which demonstrates that higher temperature could lead to the decomposition of the glucopyranoside,

or other organic compounds. Therefore, the optimal temperature should be 500 °C, when TMAH thermochemolysis will be applied to analyze the organic compounds from cyanobacteria.

Therefore, for the detection of organic compounds from cyanobacteria from TMAH thermochemolysis, the target organic compounds could be fatty acids (such as Methyl palmitoleate, Oleic acid, methyl ester etc.), glucopyranoside and its derivatives (eg. methyl 2,3,4,6-tetra-O-methyl-,  $\alpha$ -D-galactopyranoside)-, lignin derivatives (such as p-methoxy-cinamic acid methyl ester) and nucleobases such as adenine, uracil and thymine. And the optimal temperature is 500 °C when analyzing the organic compounds from cyanobacteria with TMAH thermochemolysis.

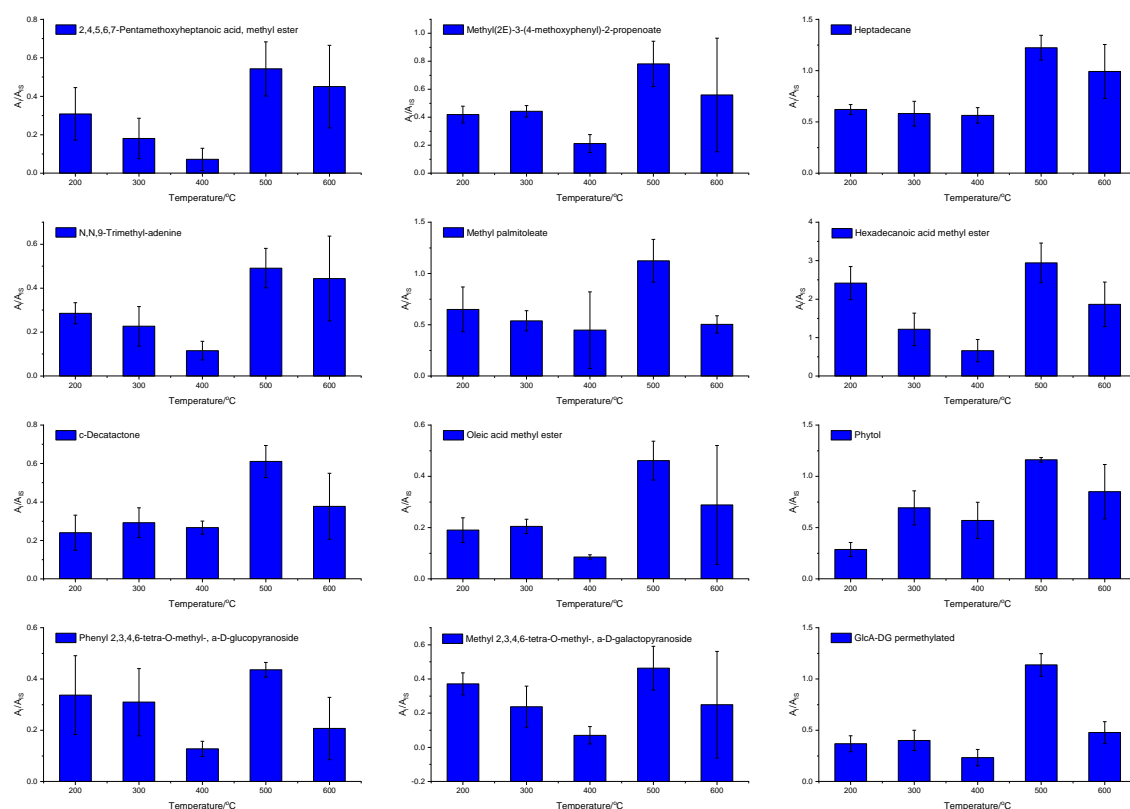


Figure 6-9 the distribution of organic compounds from *chroococcidiopsis cubana* with TMAH thermochemolysis at different flash pyrolysis temperatures (from 200 to 600 °C).

## 6.4 TMAH thermochemolysis of Anctinobacteria

### 6.4.1 Organics from *Rubrobacter radiotolerans*

*Rubrobacter radiotolerans* is known to be extremely high gamma radiation resistant [110]. Here *Rubrobacter radiotolerans* was chosen as one kind of extreme bacteria that could possibly survive in a Martian environment. The organic compounds in *Rubrobacter radiotolerans* sample were analyzed with TMAH thermochemolysis at different temperatures, from 200 to 600 °C. Figure 6-10 shows the chromatograms of *Rubrobacter radiotolerans* with TMAH thermochemolysis at different flash pyrolysis temperatures. Table 6-2 listed all organic compounds that have been detected from *Rubrobacter radiotolerans* with TMAH thermochemolysis at different flash pyrolysis temperatures. A huge number of organic compounds have been detected from *Rubrobacter radiotolerans* with TMAH thermochemolysis. Among these organic compounds, fatty acids, glucopyranoside, and the products of pigments are the main products. And these main products were mainly released after the retention time of 25 min, which means these organic compounds need to be released at relatively high column temperatures. Fatty acids include lauryl acetate (RT=25.23 min), 1-hexadecanol, acetate (RT=26.73 min), heptadecanoic acid, methyl ester (RT=28.36 min), octadecanoic acid, methyl ester (RT=29.79 min), methyl nonadecanoate (RT=26.73 min), eicosanoic acid, methyl ester (RT=30.54 min), tetradecanedioic acid (RT=31.93 min), (Z)-13-Docosanoic acid, methyl ester (RT=33.03 min). Some alkanols were also detected, such as 1-nonadecanol (RT=27.30 min), 1-octadecanol (RT= 28.85 min), 1-hexadecanol (RT=29.33 min), 1-docosanol (RT=29.90min). These long chains containing fatty acids and alkanols could be the products from the degradation of cell membranes of *Rubrobacter radiotolerans*. Carreto [690] also studied the fatty acid composition of *Rubrobacter radiotolerans* with GC/MS combined with trimethylsilylation by bis-(trimethylsilyl)-trifluoroacetamide, 12-methylhexadecanoic acid (12-methyl-16:0) and 14-methyloctadecanoic acid (14-methyl-18:0) were determined as the major fatty acids.

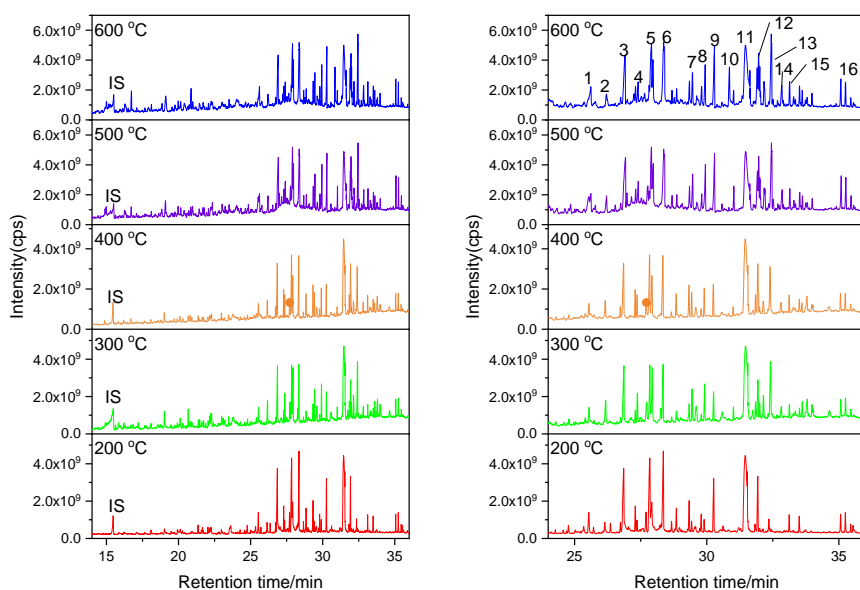


Figure 6-10 The chromatograms of *Rubrobacter radiotolerans* with TMAH thermochemolysis at different flash pyrolysis temperatures. Peak 1: N,N,9-trimethyl-adenine; 2: Cyclohexane, 1R-acetamido-4-cis-acetoxy-5,6Zcisepoxy-2-cis,3trans-dimethoxy-3: a-D-Glucopyranoside, phenyl 2,3,4,6-tetra-O-methyl-; 4: 1-Nonadecanol; 5: Methyl 3-methoxy-2-[(2,3,4,6-tetra-O-methylhexopyranosyl)oxy]propanoate; 6: Heptadecanoic acid, methyl ester; 7:1-Docosanol; 8: 1-Hexadecanol; 9: Methyl nonadecanoate; 10: a-D-Glucopyranoside,2,3,4,6-tetra-O-methyl-a-glucopyranosyl 2,3,4,6-tetra-O-methyl-; 11: a-D-Glucopyranoside, phenyl 2,3,4,6-tetra-O-methyl-; 12:Triethylene glycol monododecyl ether; 13: 1,5-Anhydro-2,3,4,6-tetra-O-methyl-D-mannitol; 14: 1,2,3,4-Tetramethylmannose; 15: 2-hydroxy-tetradecanoic acid; 16: Squalene.

Compared with the organic compounds from *E.Coli* degradation, sugars or sugar-bearing compounds account for a large proportion of products from *Rubrobacter radiotolerans*. Glycosides such as methyl 2,3,5-tri-O-methyl-a-D-Xylofuranoside was detected at the retention of 17.26 min. Glucopyranoside derivatives include methyl 3-O-acetyl-2-deoxy-4,6-di-O-methyl-a-D-glucopyranoside (RT=21.66 min), methyl 3-O-acetyl-2-deoxy-4,6-di-O-methyl-a-D-glucopyranoside (RT=26.03 min), phenyl 2,3,4,6-tetra-O-methyl-a-D-glucopyranoside (RT=26.86 min), and 2,3,4,6-tetra-O-methyl-a-glucopyranosyl 2,3,4,6-tetra-O-methyl- a-D-glucopyranoside (RT=30.62 min). Among these glucopyranoside derivatives, the abundance of phenyl 2,3,4,6-tetra-O-methyl-a-D-glucopyranoside is the highest. These glycosides derivatives could be the degradation products of polysaccharides from *Rubrobacter radiotolerans*. This is because sugars plays an important role for desiccation tolerance and they are thought to occupy some space between lipid molecules [116].

On the other side, pigments are essential for *Rubrobacter radiotolerans*. Bacterioruberin and monoanhydrobacterioruberin are the two main carotenoid pigments that have been detected

from *Rubrobacter radiotolerans* [109]. As shown in Chapter 1, The 50-carbon carotenoid  $\alpha$ -bacterioruberin was detected as the major carotenoid in all archaeal strains. When *Rubrobacter radiotolerans* thermochemolysis in TMAH at different temperatures, the pigments inside of *Rubrobacter radiotolerans* could be released because of the decomposition of cell membranes. At the same time, the organic pigments could be degraded caused by the high temperature. Therefore, bacterioruberin and monoanhydrobacterioruberin were deteriorated and some degradation products were formed. Squalene and its isomers, at the retention time of 35.07, 35.25, and 35.45 min, were detected and its peak intensity was high, as shown in Figure 6-10. From the structural point of view, squalene is the products of bacterioruberin or monoanhydrobacterioruberin with the loss of hydroxyl groups.

In addition, amino acids are important life biomarkers. Some methylated amino acids and their derivatives were detected from *Rubrobacter radiotolerans* with TMAH thermochemolysis. For example, L-proline, N-pivaloyl-methyl ester (RT=21.73 min), N-glycyl-DL-Threonine (RT=22.10 min), N-[p-Vinylbenzoyl]-l-alanine (RT=25.72 min), L-Alanyl-l-glutamine (RT=26.14 min). However, their abundance are very low compared with the major components.

Nucleobases and nucleotides are the basements of DNA or RNA. Not only nucleobases but also nucleotides were detected herein. Such as the N,N,9-trimethyl-adenine (RT=25.54 min), N,N,3-trimethyl-adenine (RT=28.28 min), 1,3-dimethyl-uracil (RT=20.27 min) and dimethyl-thymine (RT=21.36 min). Nucleotides include adenosine include 3'-amino-3'-deoxy – adenosine (RT=29.58min) and 3'-amino-3'-deoxy-N,N-dimethyl-adenosine (RT= 33.74 min), cytidine, N-methyl-, 2',3',5'-trimethyl ether (RT=32.45 min). However, only the abundance of methylated adenine and adenosine are relatively higher than that of other nucleobases detected herein. This demonstrated that the methylated adenine should be treated as the characteristic compounds of nucleobases from *Rubrobacter radiotolerans* with TMAH thermochemolysis.

Methyl phosphate is one of the most important compounds for life. When the temperature of TMAH thermochemolysis increases to 300 °C, methyl phosphate was detected. As with the results from Chapter 5, when the nucleotides monophosphate and triphosphate with TMAH thermochemolysis, methyl phosphate could be detected only when the temperature is higher than 300 °C. Some new products were detected when the temperature is higher than 300 °C, however, those could be the byproducts from TMAH degradation and no interesting products were found.

Table 6-2 The organic compounds from Anctinobacterium with TMAH thermochemolysis.

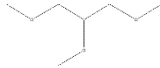
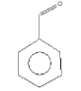
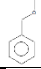
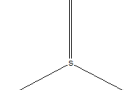
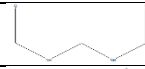
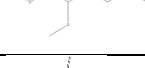
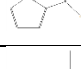
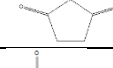
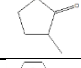
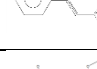
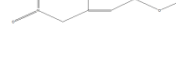
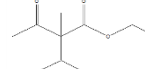
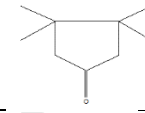

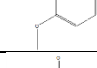
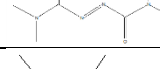
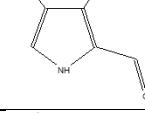

RT/ min	Masses of fragments* and relative abundance: m/z (%)	Empirical formula	Compounds	Compounds Structure
200 °C				
8.08	89,59,102,45,71	C <sub>6</sub> H <sub>14</sub> O <sub>3</sub>	1,2,3-Trimethoxy- propane	
9.73	77,105,51,86	C <sub>7</sub> H <sub>6</sub> O	Benzaldehyde	
10.48	91,121,77,65,51	C <sub>8</sub> H <sub>10</sub> O	Benzyl methyl-ether	
11.79	59,72,101,111,142	C <sub>2</sub> H <sub>6</sub> OS	Dimethyl sulfoxide	
12.10	72,73,58,102,84,45	C <sub>3</sub> H <sub>6</sub> N <sub>2</sub> O <sub>2</sub>	Methylenediformamide	
12.36	45,71,58,103	C <sub>7</sub> H <sub>16</sub> O <sub>3</sub>	1,2,4-Trimethoxy- Butane	
12.56	111,68,142,118,127,83	C <sub>6</sub> H <sub>6</sub> O <sub>2</sub> S	Methyl thiophene-2- carboxylate	
13.16	113,56,85	C <sub>5</sub> H <sub>7</sub> NO <sub>2</sub>	N-methyl-succinimide	
13.23	112,69,41,55,83	C <sub>6</sub> H <sub>8</sub> O <sub>2</sub>	3-methyl-1,2- Cyclopentanedione	
13.35	129,144,105,101,77,85,4 5	C <sub>10</sub> H <sub>8</sub> O	4-Phenyl-3-butyn-2-one	
13.49	129,144,101,55,85,45,75	C <sub>6</sub> H <sub>9</sub> NO <sub>5</sub>	2-Butenoic acid,3- methoxy-4-nitro, methyl ester,(E)-	
13.61	129,144,101,55,45,85,59 ,42	C <sub>10</sub> H <sub>18</sub> O <sub>3</sub>	Ethyl 2-acetyl-2,3- dimethylbutanoate	
13.70	56,42,140,110,78	C <sub>9</sub> H <sub>16</sub> O	3,3,4,4-Tetramethyl- cyclopentanone	
14.03	104,58,72,149,44	C <sub>9</sub> H <sub>11</sub> NO	N- formylphenylethylamine	
14.43	138,95,77,123,65,52,51	C <sub>8</sub> H <sub>10</sub> O <sub>2</sub>	1,2-dimethoxy-benzene	
14.51	72,87,129,98,43	C <sub>6</sub> H <sub>12</sub> N <sub>4</sub> O <sub>2</sub>	Diamide	
14.76	123,72,94,108,53,43	C <sub>7</sub> H <sub>9</sub> NO	3,4-Dimethyl-1H- pyrrole-2-carbaldehyde	
14.92	138,123,95,58	C <sub>8</sub> H <sub>10</sub> O <sub>2</sub>	1,4-Dimethoxy-benzene	

Table 6-2 (continued)

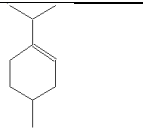
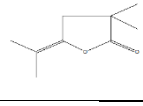
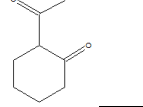
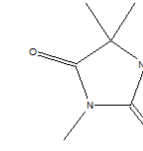
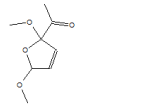
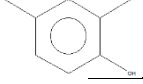
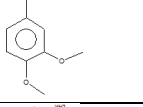
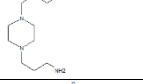
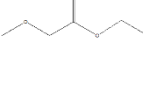
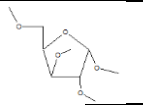
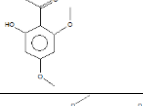
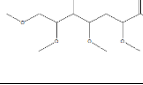
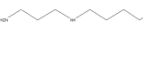
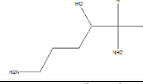
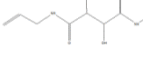
RT/ min	Masses of fragments* and relative abundance: m/z (%)	Empirical formula	Compounds	Compounds Structure
15.01	95,138,123,112,67,81,55, 54	C <sub>10</sub> H <sub>18</sub>	p-Menth-3-ene	
15.14	70,154,152,42,97	C <sub>9</sub> H <sub>14</sub> O <sub>2</sub>	5-Isopropylidene-3,3-dimethyl-dihydrofuran-2-one	
15.85	70,121,140,54,75,97	C <sub>8</sub> H <sub>12</sub> O <sub>2</sub>	2-Acetyl-cyclohexanone	
16.21	127,142,101,57,42,84	C <sub>6</sub> H <sub>10</sub> N <sub>2</sub> O <sub>2</sub>	3,5,5-trimethyl-Hydantoin	
16.32	129,101,142,56,45	C <sub>8</sub> H <sub>12</sub> O <sub>4</sub>	Ketone,2,5-dihydro-2,5-dimethoxy-2-furyl methyl	
16.38	127,94,67,68,54,42,43	C <sub>7</sub> H <sub>9</sub> NO	3-Pyridinol,2,6-dimethyl-	
16.67	152,137,109,94,91,77,53, 65	C <sub>9</sub> H <sub>12</sub> O <sub>2</sub>	3,4-Dimethoxytoluene	
16.76	70,84,99,114,140,155	C <sub>10</sub> H <sub>24</sub> N <sub>4</sub>	1,4-Bis(3-aminopropyl)piperazine	
17.08	71,84,45,115,147	C <sub>8</sub> H <sub>14</sub> O <sub>4</sub>	Tetrahydro-2-furanylmethyl methoxyacetate	
17.26	101,71,75,83,45,56,115, 140,161	C <sub>9</sub> H <sub>18</sub> O <sub>5</sub>	α-D-Xylofuranoside, methyl 2,3,5-tri-O-methyl-	
17.45	181,166,196,138,125,71, 56,45,83	C <sub>10</sub> H <sub>12</sub> O <sub>4</sub>	Xanthoxylin	
17.66	129,115,101,75,89,59,16 1	C <sub>13</sub> H <sub>26</sub> O <sub>7</sub>	2,4,5,6,7-Pentamethoxyheptanoic acid, methyl ester	
18.62	85,70,57,98,45,42,139,1 72	C <sub>9</sub> H <sub>20</sub> N <sub>2</sub>	Spermine	
18.78	128,42,70,113	C <sub>6</sub> H <sub>14</sub> N <sub>2</sub> O <sub>3</sub>	DL-α-Hydroxylsine	
18.85	84,144,128,42,70,127	C <sub>10</sub> H <sub>16</sub> N <sub>2</sub> O <sub>4</sub>	N,N'-Diallyl tartardiamide	

Table 6-2 (continued)

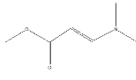

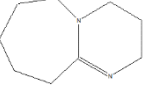
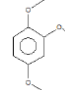
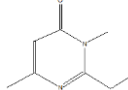
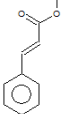
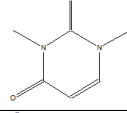
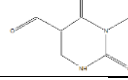
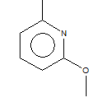
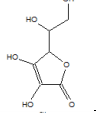
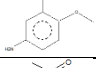
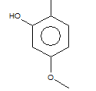
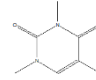
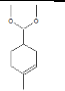
RT/ min	Masses of fragments* and relative abundance: m/z (%)	Empirical formula	Compounds	Compounds Structure
19.02	98,129,70,71	C <sub>6</sub> H <sub>11</sub> NO <sub>2</sub>	2-Propenoic acid,3-(dimethylamino), methyl ester	
19.48	98,113,44,85,72,126,55	C <sub>6</sub> H <sub>14</sub> N <sub>2</sub>	N-Aminohexamethylenimine	
19.61	70,98,152,137,42,113,54	C <sub>9</sub> H <sub>16</sub> N <sub>2</sub>	Pyrimido-[1,2,a]azepine,2,3,4,6,7,8,9,10-octahydro-	
19.70	153,125,168,98,110,70,93	C <sub>9</sub> H <sub>12</sub> O <sub>3</sub>	1,2,4-Trimethoxybenzene	
19.92	70,152,137,124,98,80	C <sub>8</sub> H <sub>12</sub> N <sub>2</sub> O	2-Ethyl-3,6-dimethyl-4(3H)-pyrimidinone	
20.12	131,103,162,77,84,51	C <sub>10</sub> H <sub>10</sub> O <sub>2</sub>	Cinnamic acid, methyl ester	
20.27	140,83,55,42	C <sub>6</sub> H <sub>8</sub> N <sub>2</sub> O <sub>2</sub>	1,3-dimethyl-Uracil	
20.41	69,126,154	C <sub>6</sub> H <sub>6</sub> N <sub>2</sub> O <sub>3</sub>	5-Formyl-3-methyluracil	
20.52	139,124,153,182,95,109,72	C <sub>7</sub> H <sub>9</sub> NO <sub>2</sub>	2,6-dimethoxy-Pyridine	
20.81	116,86,71,101,128,179,218,45	C <sub>6</sub> H <sub>8</sub> O <sub>6</sub>	Vitamin C/L-Ascorbic acid	
20.93	139,124,96,42,111,68,83	C <sub>7</sub> H <sub>9</sub> NO <sub>2</sub>	5-Amino-2-methoxyphenol	
21.16	70,151,166,94,42,137	C <sub>9</sub> H <sub>10</sub> O <sub>3</sub>	1-(2-hydroxy-4-methoxyphenyl)-Ethanone	
21.36	68,154,97,42,56	C <sub>7</sub> H <sub>10</sub> N <sub>2</sub> O <sub>2</sub>	1,3,5-trimethyl-uracil	
21.48	75,123,45,58,109,139,150,182,157	C <sub>10</sub> H <sub>18</sub> O <sub>2</sub>	Cyclohexene,4-(dimethoxymethyl)-1-methyl-	



Table 6-2(Continued)

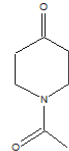
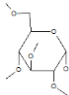
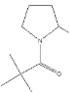
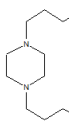
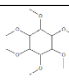
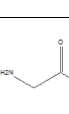
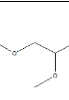
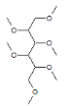
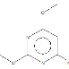
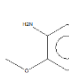
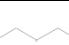
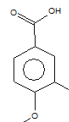
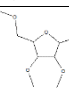
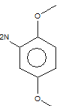
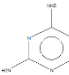
RT/ min	Masses of fragments* and relative abundance: m/z (%)	Empirical formula	Compounds	Compounds Structure
21.59	113,42,57,71,142,156,99, 85	C <sub>7</sub> H <sub>11</sub> NO <sub>2</sub>	1-Acetyl-4-piperidone	
21.66	88,101,75,129,45,59	C <sub>11</sub> H <sub>22</sub> O <sub>6</sub>	Glucopyranosine, methyl 2,3,4,6-tetra-O- methyl-, a, D-	
21.73	154,128,68,98,70,56,185, 43,56	C <sub>11</sub> H <sub>19</sub> NO <sub>3</sub>	L-proline, N-pivaloyl-, methyl ester	
21.88	58,127,42,71,70,101,85, 139,170,180	C <sub>10</sub> H <sub>24</sub> N <sub>4</sub>	1,4-Bis(3- aminopropyl)piperazine	
22.04	101,75,88,114,144,201,4 5	C <sub>12</sub> H <sub>24</sub> O <sub>6</sub>	Myo-inositol, 1,2,3,4,5,6-hexa-O- methyl-	
22.10	114,85,142,57,44	C <sub>6</sub> H <sub>12</sub> N <sub>2</sub> O <sub>4</sub>	DL-Threonine, N- glycyl-	
22.15	129,154,75,101,68,45,11 4	C <sub>13</sub> H <sub>26</sub> O <sub>7</sub>	2,4,5,6,7- Pentamethoxyheptanoic acid, methyl ester	
22.24	101,89,45,59,145,75,133	C <sub>12</sub> H <sub>26</sub> O <sub>6</sub>	Dulcitol, hexamethyl ether	
22.27	154,128,68,98,185,56	C <sub>6</sub> H <sub>9</sub> N <sub>3</sub> O <sub>2</sub>	2,6-Dimethoxy-4- aminopyrimidine	
22.48	152,167,124,180,109,79, 94,65	C <sub>8</sub> H <sub>9</sub> NO <sub>3</sub>	3-Amino-4-anisic acid	
22.74	89,101,59,118,45,71,131 ,143	C <sub>7</sub> H <sub>14</sub> O <sub>3</sub>	Propionic acid,3- ethoxy-, ethyl ester	
22.80	182,197,112,121,139,16 7,70	C <sub>9</sub> H <sub>10</sub> O <sub>4</sub>	Veratric acid	
22.97	71,89,101,115,143,152,1 75	C <sub>10</sub> H <sub>20</sub> O <sub>5</sub>	2,5-Anhydro-1,3,4,6- tetra-O-methyl-d- mannitol	
23.01	138,56,110,153,126,97	C <sub>8</sub> H <sub>11</sub> NO <sub>2</sub>	2,5-dimethoxy-Aniline	
23.17	101,121,139,162,182,42, 53	C <sub>6</sub> H <sub>6</sub> N <sub>6</sub>	2,4-Diaminopteridine	

Table 6-2(Continued)

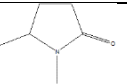
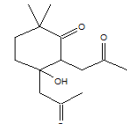
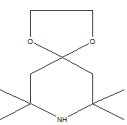
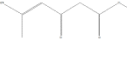
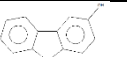
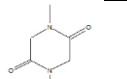
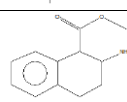
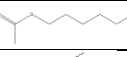
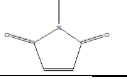
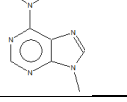
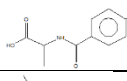
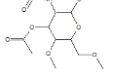
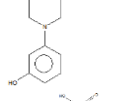
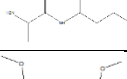
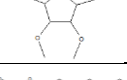

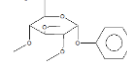
RT/ min	Masses of fragments* and relative abundance: m/z (%)	Empirical formula	Compounds	Compounds Structure
23.59	98,113,142,42,70	C <sub>6</sub> H <sub>11</sub> NO	1,5-Dimethyl-2-pyrrolidinone	
23.97	98,125,153,154,138,70,5 5,42,196	C <sub>14</sub> H <sub>22</sub> O <sub>4</sub>	5-Hydroxy-2,2-dimethyl-5,6-bis-(2-oxopropyl)-cyclohexanone	
24.06	98,184,45,68,75,128,113 ,215	C <sub>11</sub> H <sub>21</sub> NO <sub>2</sub>	7,7,9,9-Tetramethyl-1,4-dioxaspiro[4,5]decane	
24.13	84,157,98,128,112,70	C <sub>7</sub> H <sub>11</sub> NO <sub>3</sub>	4-Hexenoic acid,5-amino-3-oxo, methyl ester	
24.27	184,98,101,45,128,215	C <sub>12</sub> H <sub>8</sub> O <sub>2</sub>	2-Dibenzofuranol	
24.57	142,113,42,57,72	C <sub>6</sub> H <sub>10</sub> N <sub>2</sub> O <sub>2</sub>	Sarcosine anhydride	
25.03	129,84,156,188,58,64	C <sub>12</sub> H <sub>15</sub> NO <sub>2</sub>	Methyl 2-amino-1,2,3,4-tetrahydro-1-naphthalenecarboxylate	
25.23	83,70,111,140,168,44,55	C <sub>12</sub> H <sub>28</sub> O <sub>2</sub>	Lauryl acetate	
25.35	98,70	C <sub>6</sub> H <sub>7</sub> NO <sub>2</sub>	N-Ethylmaleimide	
25.54	148,162,177,107,133,80, 44	C <sub>8</sub> H <sub>11</sub> N <sub>5</sub>	N,N,9-trimethyl-adenine	
25.72	131,103,77,175,51	C <sub>12</sub> H <sub>13</sub> NO <sub>3</sub>	N-[p-Vinylbenzoyl]-l-alanine	
26.03	101,71,102,141,169,242, 273	C <sub>13</sub> H <sub>23</sub> NO <sub>7</sub>	Methyl 3-O-acetyl-2-deoxy-4,6-di-Omethyl-a-D-glucopyranoside	
26.08	150,165,122,55,698,94	C <sub>10</sub> H <sub>15</sub> NO	3-diethylamino-phenol	
26.14	182,115,84,58,71,100,14 0,42	C <sub>8</sub> H <sub>15</sub> N <sub>3</sub> O <sub>4</sub>	L-Alanyl-l-glutamine	
26.36	101,143,175,115,58,71,7 4,117	C <sub>10</sub> H <sub>20</sub> O <sub>5</sub>	2,5-Anhydro-1,3,4,5-tetra-O-methyl-d-mannitol	
26.73	83,69,97,58,45,111,125, 139,161	C <sub>18</sub> H <sub>36</sub> O <sub>2</sub>	1-Hexadecanol, acetate	
26.86	101,111,187,88,71,45,59 ,127,155,219	C <sub>16</sub> H <sub>24</sub> O <sub>6</sub>	a-D-Glucopyranoside, phenyl 2,3,4,6-tetra-O-methyl-	

Table 6-2(Continued)

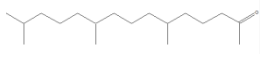
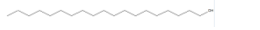

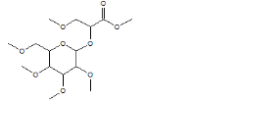

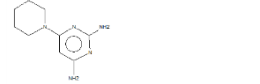
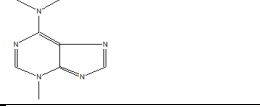
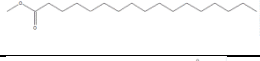
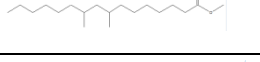
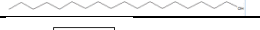
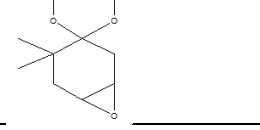
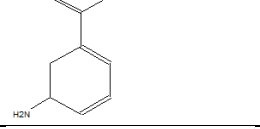

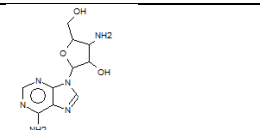
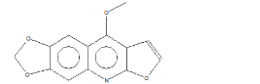
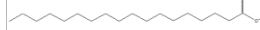

RT/ min	Masses of fragments* and relative abundance: m/z (%)	Empirical formula	Compounds	Compounds Structure
27.04	58,75,101,111,187,124,152,168,210	C <sub>18</sub> H <sub>36</sub> O	Hexahydrofarnesyl acetone	
27.30	69,83,97,57,55,111,125,153,181,41	C <sub>19</sub> H <sub>40</sub> O	1-Nonadecanol	
27.70	130,115,101,89,143,45,58	C <sub>5</sub> H <sub>6</sub> S <sub>2</sub>	3-Methylthio-thiophene	
27.84	88,101,75,117,177,45,219	C <sub>15</sub> H <sub>28</sub> O <sub>9</sub>	Methyl 3-methoxy-2-[(2,3,4,6-tetra-O-methylhexopyranosyl)oxy]propanoate	
27.92	69,83,97,57,111,41,125,140,168	C <sub>19</sub> H <sub>38</sub>	1-Nonadecene	
28.23	193,67,82,110,164,138,55	C <sub>9</sub> H <sub>15</sub> N <sub>5</sub>	Desoxy-minoxidyl	
28.28	148,162,177,137,107,94,80,44	C <sub>8</sub> H <sub>11</sub> N <sub>5</sub>	N,N,3-trimethyl-adenine	
28.36	74,87,97,143,199,241,43,69,55	C <sub>18</sub> H <sub>36</sub> O <sub>2</sub>	Heptadecanoic acid, methyl ester	
28.67	74,87,143,57,97,101,185,213	C <sub>19</sub> H <sub>38</sub> O <sub>2</sub>	Methyl 8,10-dimethyl-hexadecanoate	
28.85	18H38O	C <sub>18</sub> H <sub>38</sub> O	1-Octadecanol	
28.97	98,112,141,84,42,257	C <sub>10</sub> H <sub>16</sub> O <sub>3</sub>	4,5-Epoxy-2,2-dimethylcyclohexanone ethylene ketal	
29.28	121,77,87	C <sub>7</sub> H <sub>9</sub> NO <sub>2</sub>	3-Amino-2,3-dihydrobenzoic acid	
29.33	97,83,69,57,85,111,43,45,111,125,139,153,168,181,209	C <sub>16</sub> H <sub>34</sub> O <sub>2</sub>	1-Hexadecanol	
29.58	123,164,136,84,67,178,207,192,271	C <sub>10</sub> H <sub>14</sub> N <sub>6</sub> O <sub>3</sub>	3'-Amino-3'-deoxy-Adenosine	
29.74	243,200,148,133,110,95,82,228,79,67	C <sub>13</sub> H <sub>9</sub> NO <sub>4</sub>	Maculin	
29.79	74,87,143,129,97,43,55,199,255,271	C <sub>19</sub> H <sub>38</sub> O <sub>2</sub>	Octadecanoic acid, methyl ester	
29.90	69,57,83,97,43,125,139,153,41	C <sub>22</sub> H <sub>46</sub> O	1-Docosanol	

Table 6-2(Continued)

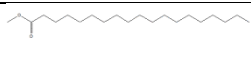
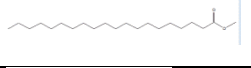
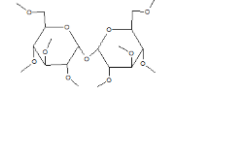
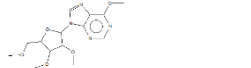

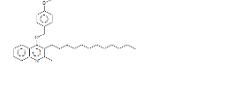
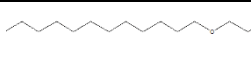
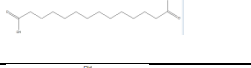
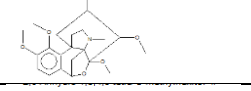
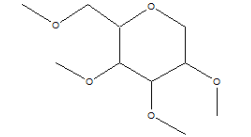
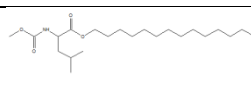
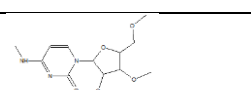
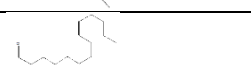
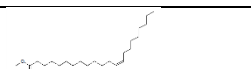
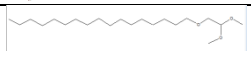
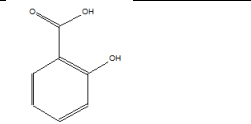
RT/ min	Masses of fragments* and relative abundance: m/z (%)	Empirical formula	Compounds	Compounds Structure
30.26	74,87,43,55,143,97,199, 213,269,312	C <sub>20</sub> H <sub>40</sub> O <sub>2</sub>	Methyl nonadecanoate	
30.54	87,74,58,143,168,210,45, 326	C <sub>21</sub> H <sub>42</sub> O <sub>2</sub>	Eicosanoic acid, methyl ester	
30.62, 31.83	101,111,75,187,147,127, 115	C <sub>20</sub> H <sub>38</sub> O <sub>11</sub>	α-D- Glucopyranoside,2,3,4,6- tetra-O-methyl-α- glucopyranosyl 2,3,4,6- tetra-O-methyl-	
30.82	101,111,72,174,145,45,5 9,247,261,324	C <sub>14</sub> H <sub>20</sub> N <sub>4</sub> O <sub>5</sub>	Tetramethyl ether, Inosine	
31.93	89,58,71,85,43,99,101,1 21	C <sub>21</sub> H <sub>44</sub> O <sub>3</sub>	Chimilether	
32.0	121,87,74,101,57,143	C <sub>30</sub> H <sub>41</sub> NO <sub>2</sub>	3-Dodecyl-4-[(4- methoxybenzyl)oxy]-2- methylquinoline	
32.13	57,71,85,45,59,72,101,1 11,113,127,155	C <sub>16</sub> H <sub>34</sub> O <sub>3</sub>	Diethylene glycol monododecyl ether	
32.23	98,86,112,125,147,222,5 8,295	C <sub>14</sub> H <sub>26</sub> O <sub>4</sub>	Tetradecanedioic acid	
32.29	70,244,131,103,374	C <sub>21</sub> H <sub>29</sub> NO <sub>6</sub>	Dihydrostephamiesine	
32.35	101,111,71,45,89,143,17 5	C <sub>10</sub> H <sub>20</sub> O <sub>5</sub>	1,5-Anhydro-2,3,4,6- tetra-O-methyl-D- mannitol	
32.39	58,144,75,71,43,107,98	C <sub>24</sub> H <sub>47</sub> NO <sub>4</sub>	L-Leucine, N- methoxycarbonyl-, hexadecyl ester	
32.45	101,112,115,139,147,70, 45,56,89,169,237	C <sub>13</sub> H <sub>21</sub> N <sub>3</sub> O <sub>5</sub>	Cytidine, N-methyl-, 2',3',5'-trimethyl ether	
32.93	98,141,126,69,83,59,193 ,171	C <sub>14</sub> H <sub>26</sub> O	9-Tetradecenal,(Z)-	
33.03,	69,55,91,97,101,111,125 ,144,155,184,320,41	C <sub>23</sub> H <sub>44</sub> O <sub>2</sub>	13-Docosenoic acid, methyl ester,(Z)-	
33.12	58,71,89,99,113,43,127, 281	C <sub>21</sub> H <sub>44</sub> O <sub>3</sub>	Chimilether	
33.21	121,70,139	C <sub>7</sub> H <sub>6</sub> O <sub>3</sub>	Salicylic acid	

Table 6-2(Continued)

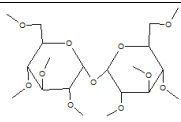
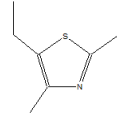
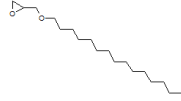
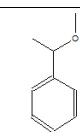
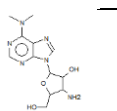
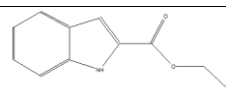
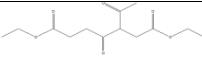
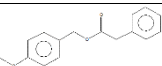
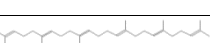
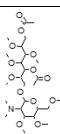
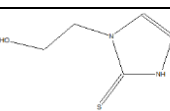

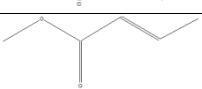
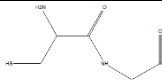
RT/ min	Masses of fragments* and relative abundance: m/z (%)	Empirical formula	Compounds	Compounds Structure
33.33	101,59,71,89,111,144,15 5,187	C <sub>20</sub> H <sub>38</sub> O <sub>11</sub>	Glucopyranoside,2,4,6- tetra-O-methyl- $\alpha$ -D- glucopyranosyl 2,3,4,6- tetra-O-methyl-, $\alpha$ -D-	
33.43	141,126,58,59,71,89,163	C <sub>7</sub> H <sub>11</sub> NS	5-ethyl-2,4-dimethyl- Thiazole	
33.50	58,71,89,43,41,99,113,1 21,134,164,281	C <sub>19</sub> H <sub>38</sub> O <sub>2</sub>	Oxirane,[(hexadecycloxy) methyl]-	
33.67	121,105,85,71,57,42,153	C <sub>9</sub> H <sub>12</sub> O	1-methoxyethyl-benzene	
33.74	134,164,114,192,220,87, 45,292	C <sub>12</sub> H <sub>8</sub> N <sub>6</sub> O <sub>3</sub>	Adenosine,3'-amino-3'- deoxy-N,N-dimethyl-	
33.77	144,134,115,91	C <sub>11</sub> H <sub>11</sub> NO <sub>2</sub>	Ethyl indole-2- carboxylate	
33.94	101,129,185,43,55,73,23 0	C <sub>13</sub> H <sub>20</sub> O <sub>6</sub>	Diethyl 3-acetyl-4- oxoheptanedioate	
34.19	121,98,257,58	C <sub>16</sub> H <sub>16</sub> O <sub>3</sub>	Benzeneacetic acid,(4- methoxyphenyl)methyl ester	
35.07, 35.25, 35.45	59,81,95,109,123,136,55	C <sub>30</sub> H <sub>50</sub>	Squalene and its isomers	
35.54, 35.88	101,114,114,86,232,200, 144,147	C <sub>26</sub> H <sub>49</sub> NO <sub>13</sub>	1,5-Di-O-acetyl-7-O-(2- dimethylamino)-3,4,6- tri-O- methylhexopyranosyl]- 2,3,4,6-tetra-O- methylheptitol	
35.59	87,144,100,101,72,114,4 5	C <sub>5</sub> H <sub>8</sub> N <sub>2</sub> OS	3-(2- Hydeoxyethyl)imidazole -2-thione	
>300 °C				
4.32	69,100,85,41,59	C <sub>5</sub> H <sub>8</sub> O <sub>2</sub>	2-Butenoic acid, methyl ester,(Z)-	
4.91	69,85,100,41,59	C <sub>5</sub> H <sub>8</sub> O <sub>2</sub>	Crotonic acid, methyl ester,E-	
5.41	59,88,43	C <sub>5</sub> H <sub>10</sub> N <sub>2</sub> O <sub>3</sub> S	Cys-Gly	

Table 6-2(Continued)

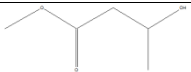
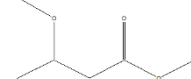
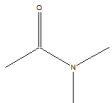
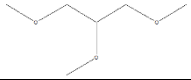


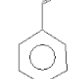

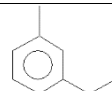
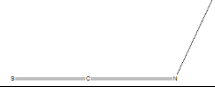
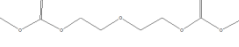
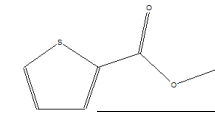
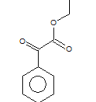
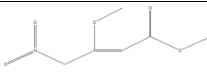
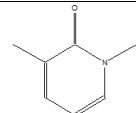
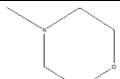
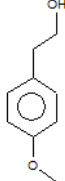
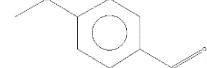

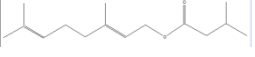
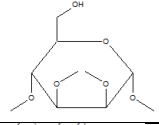
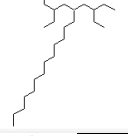
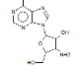
RT/ min	Masses of fragments* and relative abundance: m/z (%)	Empirical formula	Compounds	Compounds Structure
7.49	74,43,45,71,59,87,103	C <sub>5</sub> H <sub>10</sub> O <sub>3</sub>	Butanoic acid, 3-hydroxy-, methyl ester	
7.63	59,75,117,102,43	C <sub>6</sub> H <sub>12</sub> O <sub>3</sub>	Methyl (3R)-methoxybutanoate	
7.73	87,44,45,75	C <sub>4</sub> H <sub>9</sub> NO	N,N-Dimethylacetamide	
7.97	59,89,44,87,102	C <sub>6</sub> H <sub>14</sub> O <sub>3</sub>	1,2,3-Trimethoxypropane	
8.51	45,58,75,89	C <sub>6</sub> H <sub>14</sub> O <sub>4</sub>	Triethylene glycol	
9.41	110,79,80,95,44,65	C <sub>3</sub> H <sub>9</sub> O <sub>4</sub> P	Methyl phosphate	
9.43	77,105,44,51	C <sub>7</sub> H <sub>6</sub> O	Benzaldehyde/artificial almond oil	
10.25	59,87,89,45,29	C <sub>6</sub> H <sub>14</sub> O <sub>3</sub>	1,1'-Oxybis[2-methoxy-]ethane	
11.25	122,113,77,85,107,59,44,91	C <sub>8</sub> H <sub>10</sub> O	m-methyl-Anisole	
11.99	73,72,44,58	C <sub>2</sub> H <sub>3</sub> NS	Isothiocyanato-Methane	
12.28	45,103,58,73	C <sub>8</sub> H <sub>14</sub> O <sub>7</sub>	Dimethyl diglycolcarbonate	
12.56	111,68,142,83,45,99	C <sub>6</sub> H <sub>6</sub> O <sub>2</sub> S	Methyl-2-thiophene carboxylate	
13.18	105,77,112,85,41,51	C <sub>10</sub> H <sub>10</sub> O <sub>3</sub>	Glyoxylic acid, phenyl-, ethyl ester	
13.46	129,144,101,85,55,45,75	C <sub>6</sub> H <sub>9</sub> NO <sub>5</sub>	2-Butenoic acid,3-methoxy-4-nitro-, methyl ester, (E)-	
14.87	123,94,67,44,42	C <sub>7</sub> H <sub>9</sub> NO	2(1H)-Pyridone,1,3-dimethyl-	
16.68	71,70,101,99,102,43,59	C <sub>5</sub> H <sub>11</sub> NO	4-methyl-Morpholine	

Table 6-2(Continued)

RT/ min	Masses of fragments* and relative abundance: m/z (%)	Empirical formula	Compounds	Compounds Structure
16.85	121,77,78,152,91,51	C <sub>9</sub> H <sub>12</sub> O <sub>2</sub>	4-Methoxyphenethyl alcohol	
17.20	135,77,92,107,63,51	C <sub>8</sub> H <sub>8</sub> O <sub>2</sub>	4-methoxy- benzaldehyde	
31.00	57,69,83,98,111,43,41,1 25,254	C <sub>18</sub> H <sub>34</sub> O <sub>2</sub>	Oleic acid	
32.17	71,57,85,45,121,97,141, 155	C <sub>15</sub> H <sub>26</sub> O <sub>2</sub>	Geranyl isovalerate	
32.84	101,45,71,87,187,145	C <sub>10</sub> H <sub>20</sub> O <sub>6</sub>	1,2,3,4- Tetramethylmannose	
33.61	58,75,71,85	C <sub>26</sub> H <sub>54</sub>	Octadecane,3-ethyl-5- (2-ethylbutyl)-	
33.80	134,164,192,114,202,29 4	C <sub>12</sub> H <sub>18</sub> N <sub>6</sub> O <sub>3</sub>	3'-amino-3'-deoxy-N,N- dimethyl-Adenosine	

#### 6.4.2 Optimal temperature for the detection of organic compounds

Figure 6-11 shows the distribution of long-chain bearing fatty acids and alkanes from *Rubrobacter radiotolerans* with TMAH thermochemolysis at different flash pyrolysis temperatures. The abundance of the long-chain bearing compounds increased with an increase of the temperature of TMAH thermochemolysis, especially when the temperature is higher than 300 °C. This demonstrated that the high temperature enables the decomposition of cell membranes or other lipids-bearing structures in cells. Therefore, more long-chain bearing compounds were formed. For squalene, it's one of the products from pigment; here could be carotenoid, which could be treated as the characteristic compounds or life biomarker of *Rubrobacter radiotolerans*. The abundance of squalene from 200 °C is almost consistent with that from 400, 500, 600 °C. This demonstrated that 200 °C is already enough for the detection of the fragments from pigment degradation. However, if we consider other compounds from

*Rubrobacter radiotolerans*, 400 °C could be the optimal temperature for the detection of organic compounds from bacteria herein.

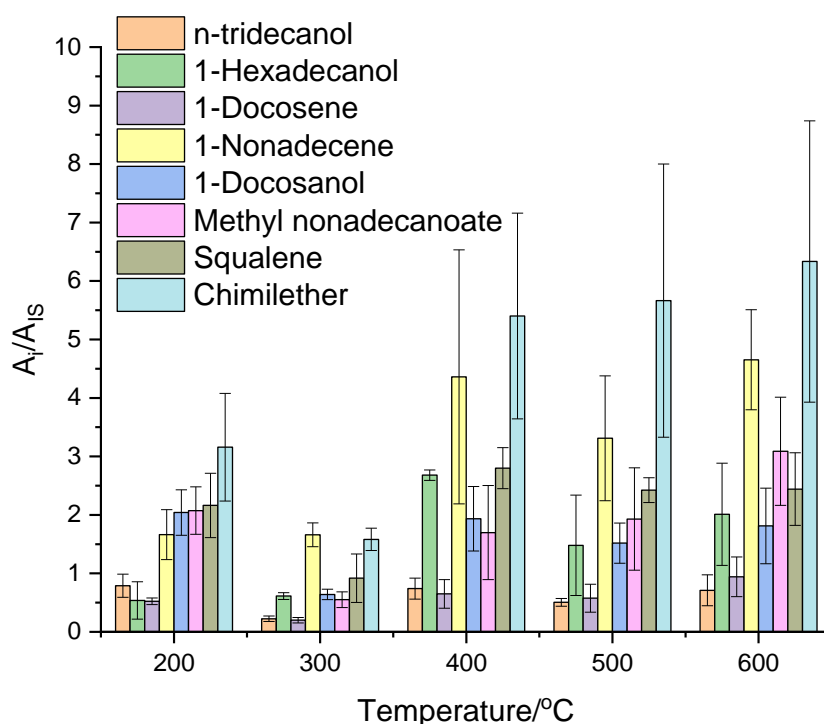


Figure 6-11 The distribution of long-chain bearing fatty acids and alkanes from *Rubrobacter radiotolerans* with TMAH thermochemolysis at different flash pyrolysis temperatures. RT=25.61 min: n-tridecanol; 27.30 min: 1-Hexadecanol; 27.92 min: 1-Docosene; 28.86 min: 1-Octadecanol; 29.34 min: 1-Hexadecanol; 29.46 min: 1-Nonadecene; 29.94 min: 1-Docosanol; 30.29 min: Methyl nonadecanoate; 33.14 min: Chimilether; 35.07 min: Squalene.

Figure 6-12 shows some major components that have been detected from *Rubrobacter radiotolerans* with TMAH thermochemolysis. Results also shows that high temperature enables the detection of adenine, cytidine. For glucopyranoside, except at 300 °C, its abundances are similar at other different temperatures. The abundance of phenyl 2,3,4,6-tetra-O-methyl-  $\alpha$ -D-Glucopyranoside is the highest compared with other organic compounds that have been detected from *Rubrobacter radiotolerans* with TMAH thermochemolysis. This demonstrated that the high abundance of phenyl glucopyranoside may be one of the causes of radiotolerant property for *Rubrobacter radiotolerans*. In addition, some nucleobases were detected. The abundance of the methylated nucleobases increased with an increase of temperature, such as the methylated adenine. From the results, 600 °C is the optimal temperature for the detection



of methylated nucleobases, which is in consistent with the result we obtained from our previous work, as shown in the Chapter 4 [23].

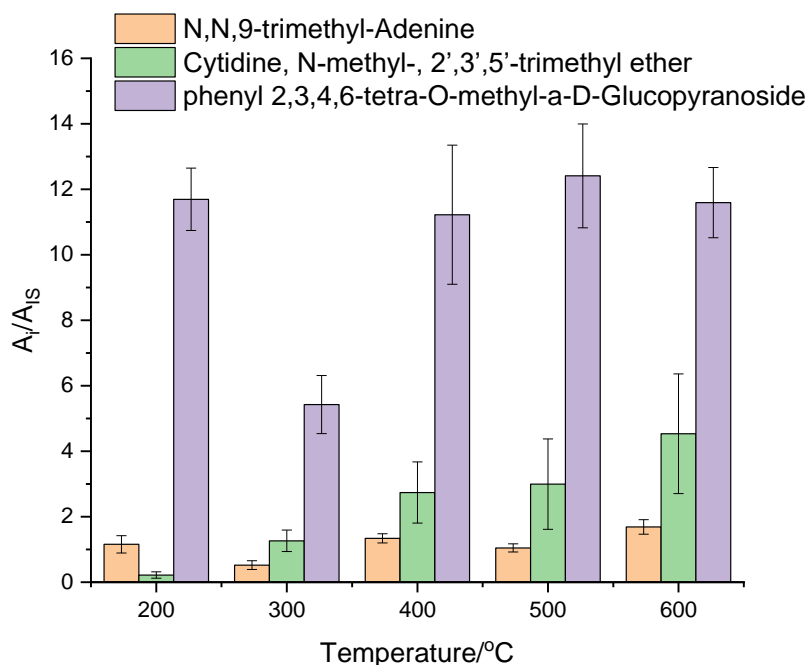


Figure 6-12 The abundance of adenine, cytidine and glucopyranoside from *Rubrobacter radiotolerans* with TMAH thermochemolysis at different flash pyrolysis temperatures.

The main organic compounds from Anctinobacterium with TMAH thermochemolysis, mainly include glucopyranosides, alcohols such as 1-nonadecanol, 1-octadecanol, 1-docosanol, etc. nucleobases such as adenine and adenosine. The aduncance of these organic compounds increased with an increasing of temperatures. When the temperarure was higher than 400 °C, the abundance of organic compounds increased sslightly. Therefore, the thermochemolysis temperature of anctinobacteria should be higher than 400 °C. In addition, a higher volume of TMAH should be applied when analyzing the organic compounds from anctinobacaterium, because of the unmethylated alcohols. This demonstrated that when the anctinobacterium cells were heated, more organic compounds were relased from cells. Therefore, according to the cells number, the optimal volum of TMAH should be optimized in the furture study.

## 6.5 TMAH thermochemolysis of halophilic bacteria

Laboratory strain *Halobacterium salinarum* NRC-1 is one of the best-studied representatives to date, and they are ideal candidates for space related studies [88]. Studies have investigated how this strain reacts to desiccation, shifts in osmotic pressure [84,95], heat [96], oxidative stress [97], ionizing radiation [98,99], oxygen limitation [97], and a broad range of different UV radiation regimes [100,101]. Therefore, *Halobacterium salinarum* was chosen as one of the samples in this study. In this section, the organic compounds from *Halobacterium salinarum* with TMAH thermochemolysis at different temperatures have been studied. Figure 6-13 shows the chromatograms of *halobacterium salinarum* with TMAH thermochemolysis at different flash pyrolysis temperatures. Only when the temperature is higher than 200 °C, organic compounds can be detected. Cells of *halobacterium salinarum* with TMAH thermochemolysis have been tested; however, no organic compound was detected. The peaks' intensities were increased with an increase of temperature, and some new organic compounds were formed and identified. Table 6-3 lists the organic compounds from *halobacterium salinarum* after TMAH thermochemolysis at different temperatures. From the results, the compounds at the retention time of 25.57 min and 35.06 min are the highest peaks, they are N,N,9-trimethyl-adenine and squalene, respectively. Adenine could be possible from the degradation of ATP, which is a molecular related to energy transformation to maintain cell viability. The previous studies also showed that the flagellar motor of swimming *Halobacterium salinarum* may be driven either by ATP directly or by an ATP-generated ion gradient that is not coupled directly to the proton gradient or the proton motive force of the cell [691,692]. This demonstrated that the viability of the *halobacterium salinarum* cell samples we've used herein. Figure 6-14 shows the abundance of some major organics that have been detected from *Halobacterium salinarum* with TMAH thermochemolysis. As shown in Figure 6-14, the optimal temperature for the detection of adenine-derivate is either 200 °C or 600 °C. In addition, methylated uracil, thymine, and cytosine were detected, this demonstrated that TMAH thermochemolysis have a great potential for the *in-situ* detection of nucleobases from natural life samples.

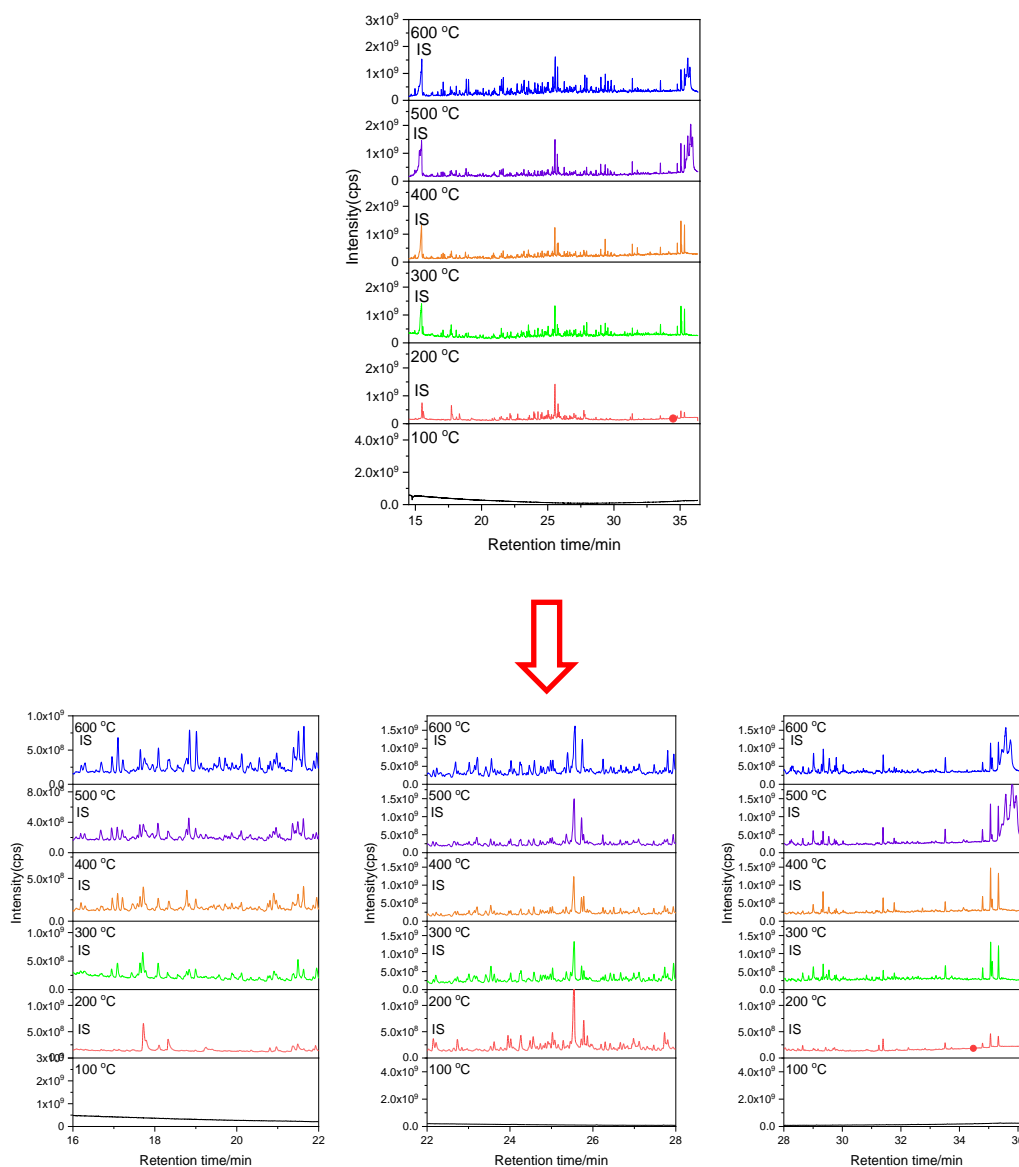


Figure 6-13 The chromatograms of *halobacterium salinarum* with TMAH thermochemolysis at different flash pyrolysis temperatures.

Squalene, a 30-carbon isoprenoid, is the primary component of the non-polar fraction, known primarily for its association with bacteriorhodopsin [693]. *Halobacterium salinarum* is one of the well-known extremophiles to withstand particular environmental hardships. They have pigments in their membrane to protect the cells from harsh environment. *Halobacterium salinarum* is colored brightly red-orange mainly due to the high content of carotenoid pigments in their cell membrane [167]. Squalene is one part of the bacteriorhodopsin, and also, it's the products of bacteriorhodopsin pyrolysis at high temperatures. Therefore, the abundance of

squalene is relatively high compared with other organics detected from *Halobacterium salinarum* with TMAH thermochemolysis. Figure 6-14 shows the abundance of some major organics that have been detected from *Halobacterium salinarum* with TMAH thermochemolysis. Results demonstrated that the abundance of squalene decreased slightly with an increase of temperature. This demonstrated that high temperature could cause the decomposition of squalene. Therefore, 200 °C is the optimal temperature for the detection of squalene from *Halobacterium salinarum*. As the highest peak intensity of squalene, it could be one of the characteristic compounds from *Halobacterium salinarum*.

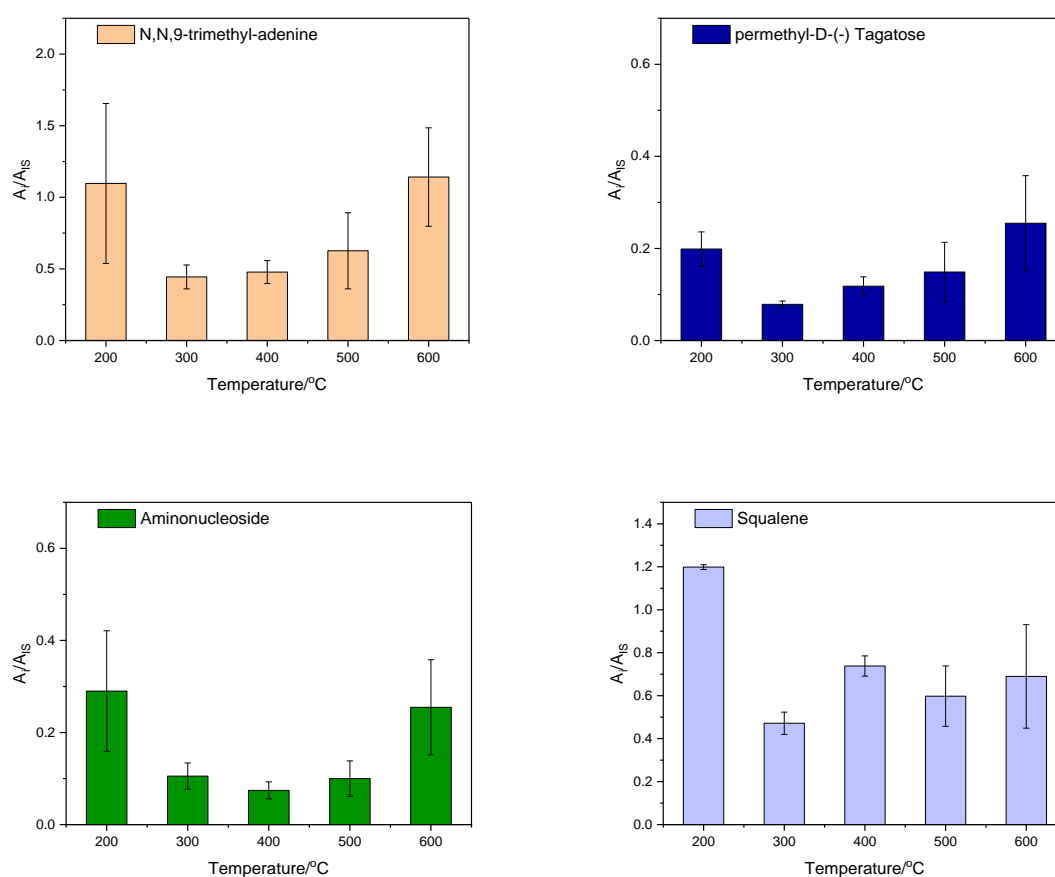


Figure 6-14 The distribution of main organics from *halobacterium salinarum* with TMAH thermochemolysis at different flash pyrolysis temperatures.

In addition, fatty acids are another important compound found from *Halobacterium salinarum*. Membranes of extremophiles are the first line of defense against environmental assaults. The polar lipid portion of the membrane of *Halobacterium salinarum* is primarily

composed of phospholipids and glycolipids based on archaeol, a glycerol diether lipid containing phytanyl chains derived from isoprenoids [693]. Phosphatidylglycerol (PG) and phosphatidylglycerophosphate methyl ester (PGP-Me) are primary compounds, which account for about 85% of the polar lipid content [694]. This means C18:1 and C16:0 should be the main lipids from the membranes of *Halobacterium salinarum*. Oleic acid (RT=34.79 min) and palmitic acid (RT=27.80 min) have been detected in this study. However, their abundances are not as high as the fatty acids that have been detected in *Rubrobacter radiotolerans* and *chroococciopsis cubana*. On the other hand, the abundance of phenyl 2,3,4,6-tetra-O-methyl- $\alpha$ -D-glucopyranoside from *Halobacterium salinarum* is much lower than that from *Rubrobacter radiotolerans*. The abundance of phenyl 2,3,4,6-tetra-O-methyl- $\alpha$ -D-glucopyranoside from *Halobacterium salinarum* is about 40 times lower than that of *Rubrobacter radiotolerans*. This may due to the different properties of these different species.

There are still some of the organic compounds detected from *Halobacterium salinarum* with TMAH thermochemolysis; however, more experiments need to be done to determine the organic compounds. On the other hand, we met huge obstacles to give a reasonable explanation of the organic compounds detected from *Halobacterium salinarum* because of lack of investigation of the organics in the previous study.

Table 6-3 The organic compounds from *halobacterium salinarum* with TMAH thermochemolysis.

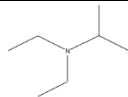
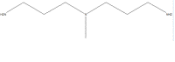
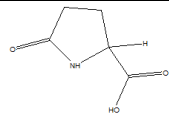
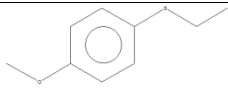
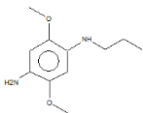
RT/ min	Masses of fragments* and relative abundance: m/z (%)	Empirical formula	Compounds	Compounds Structure
200 °C				
17.72	100,58,44,72,115	C <sub>7</sub> H <sub>17</sub> N	N,N-Diethyl-2-propanamine	
18.10	58,101,75,86,42	C <sub>7</sub> H <sub>19</sub> N <sub>3</sub>	Dipropylamine,3,3'-diamino-N-methyl-	
18.32	84,542	C <sub>5</sub> H <sub>7</sub> NO <sub>3</sub>	DL-pyroglutamic acid	
18.66	70,58,139,153,168,126,96,113	C <sub>9</sub> H <sub>12</sub> OS	p-Methoxyethylthiobenzene	
18.99	181,125,166,153,210,195,56,68	C <sub>11</sub> H <sub>18</sub> N <sub>2</sub> O <sub>2</sub>	4-[n-Propylamino]-2,5-dimethoxyaniline	

Table 6-3 (continued)

RT/ min	Masses of fragments* and relative abundance: m/z (%)	Empirical formula	Compounds	Compounds Structure
19.24	70,108,140,116,59	C <sub>13</sub> H <sub>24</sub> N <sub>6</sub> O <sub>4</sub>	Pro-Gly-Arg	
19.28	70,141,168	C <sub>10</sub> H <sub>17</sub> NO <sub>3</sub>	L-proline, N-butyl-, methyl ester	
20.07	140,125,70,97,112,153	C <sub>7</sub> H <sub>8</sub> OS	4-methylthio-Phenol	
20.35	141,56,209	C <sub>11</sub> H <sub>16</sub> N <sub>4</sub> O <sub>4</sub>	Razoxane	
20.81	116,71,86,101,45,218	C <sub>12</sub> H <sub>22</sub> O <sub>7</sub>	Methyl 3-O-acetyl- 2,4,6-tri-O- methylhexopyranoside	
20.97	114,86,72,58,42	C <sub>9</sub> H <sub>21</sub> N	1-Propanamine, N,N- dipropyl-	
21.37	68,69,154,42,97	C <sub>7</sub> H <sub>10</sub> N <sub>2</sub> O <sub>2</sub>	1,3,5-trimethyl-Uracil	
21.49	150,121,135,67,42,81	C <sub>9</sub> H <sub>14</sub> N <sub>2</sub>	2,3-diethyl-5-methyl- Pyrazine	
21.63	86,128,72,113,156	C <sub>10</sub> H <sub>23</sub> N	3-Octanamine, N,N- dimethyl-	
21.76	124,153,96,55,180,42	C <sub>7</sub> H <sub>11</sub> N <sub>3</sub> O	4-Dimethylamino-1- ethyl-2(1H)- pyrimidinone	
21.87, 22.22	58,127,85,170,99,113,12 8,155	C <sub>9</sub> H <sub>17</sub> NO <sub>2</sub>	2-Methylamino-3,5- octanedione	
21.92	56,72,155,183,127,140	C <sub>12</sub> H <sub>24</sub> O	3-Dodecanone	
22.03	98,72,142,58	C <sub>9</sub> H <sub>19</sub> N	1-butyl-piperidine	
22.15	141,56,72,169,99	C <sub>3</sub> H <sub>7</sub> O <sub>7</sub> P	3-Phosphoglyceric acids	
22.40	140,167,124,85	C <sub>7</sub> H <sub>9</sub> NO <sub>2</sub>	5-Amino-2- methoxyphenol	
22.53	164,195,151,137,94,71,5 9,42	C <sub>20</sub> H <sub>25</sub> NO <sub>5</sub>	2-[2-(3,4- dimethoxyphenyl)ethyl] -3,4-dimethoxy- Benzeneacetamide	
22.64	128,72,86,60,100,44,144 ,154	C <sub>11</sub> H <sub>25</sub> N	N-butyl-N-propyl-1- butanamine	

Table 6-3 (continued)

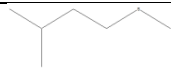
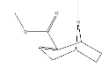
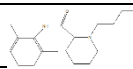
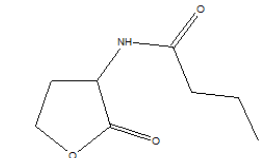
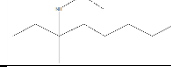
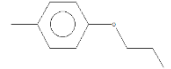
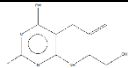
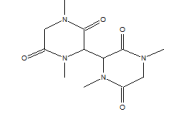
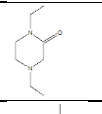
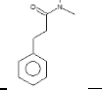
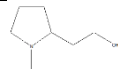
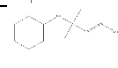
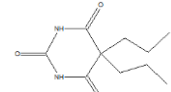
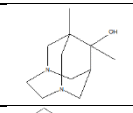

RT/ min	Masses of fragments* and relative abundance: m/z (%)	Empirical formula	Compounds	Compounds Structure
22.73	118,70,61,128,42	C <sub>6</sub> H <sub>14</sub> S	Isopentyl methyl-sulfide	
22.84	152,123,181,137,166,10 9,95,70,82,44	C <sub>10</sub> H <sub>15</sub> NO <sub>2</sub>	2-Carbomethoxy-8- methyl-8- azabicyclo[3.2.1]oct-2- ene	
22.96	140	C <sub>18</sub> H <sub>28</sub> N <sub>2</sub> O	Bupivacaine	
23.03	140,126,112,166,61,68	C <sub>8</sub> H <sub>13</sub> NO <sub>3</sub>	N-Butyryl-DL- homoserine lactone	
23.20	100,126,142,151,166,15 6,57	C <sub>11</sub> H <sub>25</sub> N	N-ethyl-3-methyl-3- octabamine	
23.26	108,152,80,53,73	C <sub>9</sub> H <sub>12</sub> O <sub>2</sub>	2-(4-Methylphenoxy)- ethanol	
23.39	178,131,103,151,137,20 9,194,59,77	C <sub>10</sub> H <sub>15</sub> N <sub>3</sub> O <sub>2</sub>	Pyrimidin-4-ol,5-allyl- 6-(2- hydroxyethylamino)-2- methyl-	
23.53	113,142,42,71,99	C <sub>12</sub> H <sub>18</sub> N <sub>4</sub> O <sub>4</sub>	Piperazine-2,5- dione,1,4-dimethyl-3,3'- bis-	
23.62	127,156,58,42,99,113,14 1	C <sub>8</sub> H <sub>16</sub> N <sub>2</sub> O	1,4-Diethyl-2- piperazinone	
23.69	91,58,72,108,45,177,133 ,152	C <sub>11</sub> H <sub>15</sub> NO	N,N-dimethyl- Benzenepropanamide	
23.78	84,42,57,100,124,138	C <sub>7</sub> H <sub>15</sub> NO	1-Methyl-2- pyrrolidineethanol	
23.88	56,141,140,169,84,125,4 1	C <sub>10</sub> H <sub>20</sub> N <sub>2</sub> O	2-(cyclohexylamino)-2- methyl-propanal oxime	
23.95	141,170,72,113,42,155	C <sub>10</sub> H <sub>16</sub> N <sub>2</sub> O <sub>3</sub>	Di-2-Propylbarbituric acid	
24.02	196,152,125,96,124,82,7 2,56,42	C <sub>11</sub> H <sub>20</sub> N <sub>2</sub> O	1,8-Dimethyl-3,6- diazahomoadamantan-9- ol	
24.08	155,183,127,141	C <sub>12</sub> H <sub>9</sub> NO	3-Dibenzofuranamine	

Table 6-3 (continued)

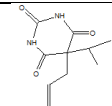
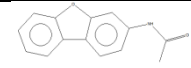
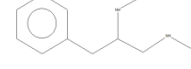
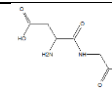

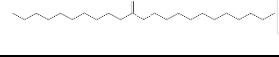
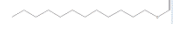
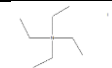
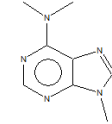
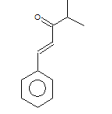
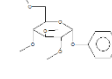
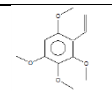
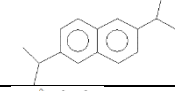
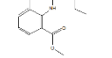
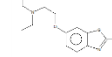
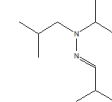
RT/ min	Masses of fragments* and relative abundance: m/z (%)	Empirical formula	Compounds	Compounds Structure
24.26	141,169,56,70,98,112,126	C <sub>10</sub> H <sub>14</sub> N <sub>2</sub> O <sub>3</sub>	Aprobarbital	
24.56	183,155,56,169,72,98,143,142	C <sub>14</sub> H <sub>11</sub> NO <sub>2</sub>	2-3-Dibenzofuranyl-Acetamide	
24.65	134,115,119,91,72,	C <sub>11</sub> H <sub>18</sub> N <sub>2</sub>	1,2-Peopanediamine,N,N'-dimethyl-3-phenyl-,(S)-	
24.73	156,127,141,113,99	C <sub>6</sub> H <sub>10</sub> N <sub>2</sub> O <sub>5</sub>	Alpha-Asp-Gly	
24.96	58,86,120,129	C <sub>8</sub> H <sub>19</sub> N	2-Pentanamine,2,4,4-trimethyl-	
25.28	84,56,70,173,182,139,195,215,45	C <sub>24</sub> H <sub>48</sub>	1-Tetradecene,2-decyl-	
25.39	84,98,111,112,168,55,140	C <sub>13</sub> H <sub>26</sub> O <sub>2</sub>	Formic acid, dodecyl ester	
25.46	86,127,156,42,71,99,98	C <sub>8</sub> H <sub>20</sub> IN	Ethanaminium, N,N,N-triethyl-,iodide	
25.55	148,107,133,162,177,80,44	C <sub>8</sub> H <sub>11</sub> N <sub>5</sub>	N,N,9-Trimethyl-Adenine	
25.72	131,103,77,51,175	C <sub>12</sub> H <sub>14</sub> O	Isopropyl styryl ketone	
25.78	101,111,71,75,89,187,45,59,218	C <sub>16</sub> H <sub>24</sub> O <sub>6</sub>	Glucopyranoside, phenyl 2,3,4,6-tetra-O-methyl-, alpha-D-	
25.95	209,180,122,100,138,224	C <sub>12</sub> H <sub>16</sub> O <sub>4</sub>	2,3,4,6-Tetramethoxystyrene	
25.98	197,155,169,127,139,98,56,41,68	C <sub>16</sub> H <sub>20</sub>	2,6-Diisopropyl-naphthalene	
26.20	86	C <sub>15</sub> H <sub>22</sub> N <sub>2</sub> O <sub>3</sub>	Tolycaine	
26.30	86,100,72,55,44,155,183	C <sub>15</sub> H <sub>23</sub> N <sub>3</sub> OS	Diamthazole	
26.41	141,113,100,72,86,184,169	C <sub>11</sub> H <sub>24</sub> N <sub>2</sub>	Isobutyraldehyde isopropylisobutylhydrazone	



Table 6-3 (continued)

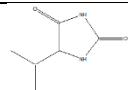
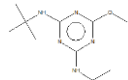
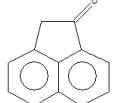
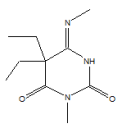
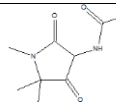
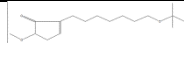
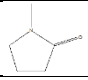
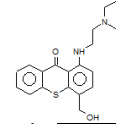
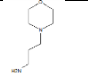
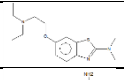
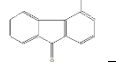
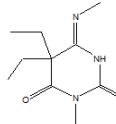
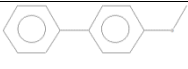
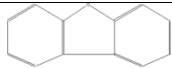
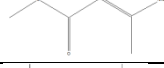
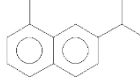
RT/ min	Masses of fragments* and relative abundance: m/z (%)	Empirical formula	Compounds	Compounds Structure
26.50	100,72,86,57,141	C <sub>6</sub> H <sub>10</sub> N <sub>2</sub> O <sub>2</sub>	5-Isopropyl-2,4- imidazolidinedione	
26.61	209,114,141,169,225,19 7,98,86,56,72,238	C <sub>10</sub> H <sub>19</sub> N <sub>5</sub> O	Terbumeton	
26.66	139,168,70,100,42	C <sub>12</sub> H <sub>8</sub> O	1-Acenaphthenone	
26.74	125,84,153,182,211,139, 42,70,55	C <sub>10</sub> H <sub>17</sub> N <sub>3</sub> O <sub>2</sub>	5,5-Diethyl-3-methyl-6- methylimino- hexahydro-pyrimidine- 2,4-dione	
26.80	141,198,113,100,155,18 3,56,42,71,127	C <sub>9</sub> H <sub>14</sub> N <sub>2</sub> O <sub>3</sub>	3-Acetamido-1,5,5- trimethyl-pyrrolidin-2,4- dione	
26.84	56,68,82,95,123,225,178 ,197,149,169	C <sub>17</sub> H <sub>30</sub> O <sub>3</sub>	2-(7-t-Butoxy-heptyl)-5- methoxy-cyclopent-2- enone	
26.95	100,86,72,58	C <sub>5</sub> H <sub>9</sub> NO	1-Methyl-2- pyrrolidinone	
26.98	86,58,100,141,113,200,2 42	C <sub>20</sub> H <sub>24</sub> N <sub>2</sub> O <sub>2</sub> S	Hycanthon	
27.12	100,58,86,42,114	C <sub>7</sub> H <sub>16</sub> N <sub>2</sub> O	4- Morpholinerpropanamin e	
27.21	100,86,58,72,42,155	C <sub>15</sub> H <sub>23</sub> N <sub>3</sub> OS	Diamthazole	
27.31	195,167,139,153,181,98, 84,71	C <sub>13</sub> H <sub>9</sub> NO	4-Amino-9-fluorenone	
27.47	168,139,84,125,182,70,4 2,57,111	C <sub>10</sub> H <sub>17</sub> N <sub>3</sub> O <sub>2</sub>	5,5-Diethyl-3-methyl-6- methylimino- hexahydro-pyrimidine- 2,4-dione	
27.58	184,169,155,70,96,115	C <sub>13</sub> H <sub>12</sub> O	1,1'-Biphenyl,4- methoxy-	
27.69	168,139,81,114	C <sub>12</sub> H <sub>8</sub> O	Dibenzofuran	
27.73	115,84,100,164,42,72	C <sub>5</sub> H <sub>9</sub> NO <sub>2</sub>	2-Butenoic acid, 3- amino-, methyl ester	
27.80	169,184,100,115,141,15 5	C <sub>14</sub> H <sub>16</sub>	1-methyl-7-(1- methylethyl)- Naphthalene	

Table 6-3 (continued)

RT/ min	Masses of fragments* and relative abundance: m/z (%)	Empirical formula	Compounds	Compounds Structure
27.94	100,207,149,153,192,84, 121,59,42	C <sub>11</sub> H <sub>13</sub> NO <sub>3</sub>	3,4,5-Trimethoxy- Benzeneacetonitrile	
28.05	100,170,70,58,155,101,1 14,127	C <sub>11</sub> H <sub>16</sub> IN	Ethyltri- propylammonium iodide	
28.30	230,100,148,115,245,56, 77	C <sub>16</sub> H <sub>23</sub> NO	2,6-Bis(1,1- dimethylethyl)-4- cyanomethylphenol	
28.33	156,141,114,100,75	C <sub>12</sub> H <sub>12</sub>	1,2-dimethyl- naphthalene	
28.48	84,100,114	C <sub>9</sub> H <sub>9</sub> NO <sub>2</sub>	c-Aminobutyric acid	
28.54	84,100,72,58	C <sub>5</sub> H <sub>7</sub> NO <sub>3</sub>	D-Pyroglutamic acid	
28.64	84,69,57,43,97,125,178	C <sub>17</sub> H <sub>34</sub>	1-Heptadecene	
28.72	136,111,121,275,232,18 9,83,57,67	C <sub>18</sub> H <sub>29</sub> NO	10a- Methylhexadecahydrona phtho[2,1-f]quinolin- 2(1H)-one	
28.84	58,237,69,83,97,111,123 ,152,194,296	C <sub>19</sub> H <sub>36</sub> O <sub>2</sub>	n-Propyl 9- hexadecenoate	
29.01	155,198,127,161,84,56,7 5,133,169	C <sub>15</sub> H <sub>19</sub> F <sub>2</sub> NO <sub>3</sub>	D-Alanine,N-(2,6- difluoro-3- methylbenzoyl)-, isobutyl ester	
29.06	183,155,140,127,69,72,1 27	C <sub>7</sub> H <sub>13</sub> N <sub>5</sub> O	1,3,5-Triazin-2(1H)- one,4,6-bis(ethylamino)-	
29.17	114,142,169,86,44,58,70 ,226,198	C <sub>12</sub> H <sub>22</sub> N <sub>2</sub> O <sub>2</sub>	1,8- Diazacyclotetradecane- 2,7-dione	
29.43	169,226,56,44,70,141,12 8,98	C <sub>12</sub> H <sub>11</sub> N	4-Biphenylamine	
29.53	272,230,287,187,172,14 1,128,68	C <sub>16</sub> H <sub>20</sub> N <sub>4</sub> O <sub>5</sub>	Porfiromycin	
29.69	169,226,128,115,141,15 5,57,89	C <sub>15</sub> H <sub>14</sub> O <sub>2</sub>	Oxirane,(1,1'-biphenyl- 2-yloxy)methyl-	

Table 6-3 (continued)

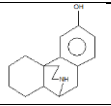
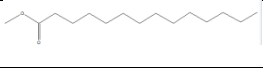
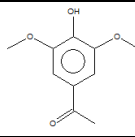
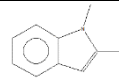
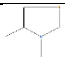
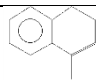
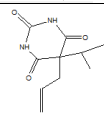
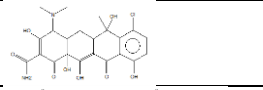
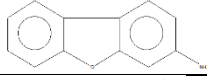
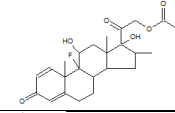
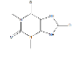
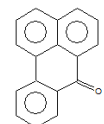
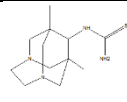
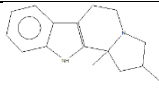
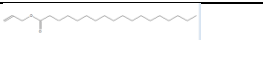
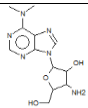
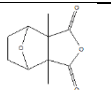
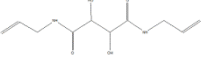
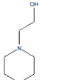
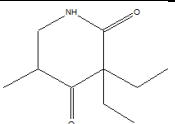
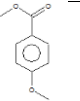
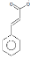
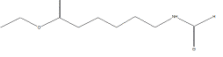

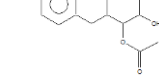
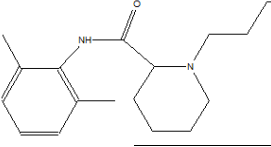
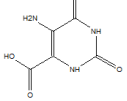

RT/ min	Masses of fragments* and relative abundance: m/z (%)	Empirical formula	Compounds	Compounds Structure
29.73	243,200,169,148,133,110,77,45	C <sub>16</sub> H <sub>21</sub> NO	Norlevorphanol	
29.79	74,87,155,212,128,142,114,43,243	C <sub>15</sub> H <sub>30</sub> O <sub>2</sub>	Methyl tetradecanoate	
30.26	181,196,139,128,84,86,58,61,43	C <sub>10</sub> H <sub>12</sub> O <sub>4</sub>	4'-HYDROXY-3',5'-dimethoxy-Acetophenone	
30.82	144,115,77,96	C <sub>10</sub> H <sub>11</sub> N	1,2-dimethyl-Indole	
30.87	96,144,56,81	C <sub>5</sub> H <sub>8</sub> N <sub>2</sub>	1,5-Dimethyl-1H-imidazole	
30.92	129,144,115,72,96,86,64	C <sub>11</sub> H <sub>12</sub>	1,2-dihydro-4-methyl-Naphthalene	
31.01	169,141,121,96,54,	C <sub>10</sub> H <sub>14</sub> N <sub>2</sub> O <sub>3</sub>	Aprobarbital	
31.19	84,112,98,136,207,172,42	C <sub>22</sub> H <sub>23</sub> ClN <sub>2</sub> O <sub>8</sub>	Chlortetracycline	
31.25	183,121,155,56,96,72	C <sub>12</sub> H <sub>9</sub> NO	3-Dibenzofuranamine	
31.60	121,141,169,58,101,86,73,142	C <sub>24</sub> H <sub>31</sub> FO <sub>6</sub>	Betamethasone acetate	
31.86	197,162,152,121,86,56,78,216	C <sub>7</sub> H <sub>8</sub> N <sub>4</sub> O <sub>3</sub>	1,3-Dimethyluric acid	
32.11	230,96,98,136,182	C <sub>17</sub> H <sub>10</sub> O	Benzanthreneone	
32.25	70,72,85,100,115,155,254	C <sub>12</sub> H <sub>22</sub> N <sub>4</sub> S	1,8-Dimethyl-9-thioureido-3,6-diazahomoadamantane	
32.58	225,98,100,141,114,86,70,56	C <sub>16</sub> H <sub>20</sub> N <sub>2</sub>	11H-Indolo[3,2-g]indolizine,1,2,3,5,6,11b-hexahydro-2,11b-dimethyl-	
33.20	100,121,70,164,207,225,234,268	C <sub>21</sub> H <sub>40</sub> O <sub>2</sub>	Octadecanoic acid,2-propenyl ester	
33.51	134,164,114,129,192,101,71,45,143,174,220,306	C <sub>12</sub> H <sub>18</sub> N <sub>6</sub> O <sub>3</sub>	Adenosine,3'-amino-3'-deoxy-N,N-dimethyl-	

Table 6-3 (continued)

RT/ min	Masses of fragments* and relative abundance: m/z (%)	Empirical formula	Compounds	Compounds Structure
33.73	144	C <sub>10</sub> H <sub>7</sub> NO <sub>3</sub>	Kynurenic acid	
34.79	83,69,57,95,97,109,123, 144,207,57	C <sub>25</sub> H <sub>48</sub>	1,7-Dicyclopentyl-4-n- octylheptane	
35.09	69,81,83,95,97,121,136, 167,169	C <sub>30</sub> H <sub>50</sub>	Squalene	
>300 °C				
11.23	122,58,59,77,107,91	C <sub>8</sub> H <sub>10</sub> O	p-methyl-Anisole	
11.54	115,87,55,65,40	C <sub>6</sub> H <sub>10</sub> O <sub>4</sub>	Butanedioic acid, dimethyl ester	
11.76	100,111,58,42,126	C <sub>11</sub> H <sub>18</sub> O <sub>6</sub>	Methyl 4,6-di-O-acetyl- 2,3- dideoxyhexopyranoside	
11.91	84,118,42,73	C <sub>6</sub> H <sub>13</sub> NO	N-methyl-L-prolinol	
12.29	45,103,71,73,142	C <sub>7</sub> H <sub>16</sub> O <sub>3</sub>	1,2,4-Trimethoxy butane	
12.41	89,119,63,97,129	C <sub>8</sub> H <sub>8</sub> O	Phenyl-oxirane	
12.55	111,142,68,83,99,127,45 ,55	C <sub>8</sub> H <sub>14</sub> O <sub>2</sub>	2-Hexenoic acid, 3- methyl-, methyl ester	
12.72	114,72,102,58,71	C <sub>8</sub> H <sub>17</sub> NO <sub>2</sub>	N,N-Dimethyl-l-leucine	
13.19	105,77,136,51	C <sub>8</sub> H <sub>8</sub> O <sub>2</sub>	Benzoic acid, methyl ester	
13.44	56,58,140,112,42,72	C <sub>9</sub> H <sub>16</sub> O	Cyclopentanone,2,2,5,5- tetramethyl-	
13.66	121,136,56,105	C <sub>11</sub> H <sub>15</sub> NO <sub>2</sub>	Carbamic acid, methyl-,o-cumenyl ester	
13.89	139,127,98,54,55,71,98	C <sub>14</sub> H <sub>22</sub> N <sub>4</sub> O <sub>2</sub>	Cuprizone	
13.97	104,149,72,88	C <sub>8</sub> H <sub>7</sub> NO <sub>2</sub>	2-Pyridineacrylic acid	
14.68	134,119,91,65,44,63	C <sub>9</sub> H <sub>10</sub> O	4'-methyl-acetophenone	

Table 6-3 (continued)

RT/ min	Masses of fragments* and relative abundance: m/z (%)	Empirical formula	Compounds	Compounds Structure
18.77	128,70,42,113,151,180	C <sub>10</sub> H <sub>12</sub> O <sub>4</sub>	Cantharidin	
18.84	84,114,116,42,70	C <sub>10</sub> H <sub>16</sub> N <sub>2</sub> O <sub>4</sub>	N,N'-Diallyl tartardiamide	
18.98	98,70,41	C <sub>7</sub> H <sub>15</sub> NO	1-Piperidineethanol	
19.57	140,124,155,83,56,110	C <sub>10</sub> H <sub>17</sub> NO <sub>2</sub>	Methyprylon	
19.88	135,166,77,107,92,50,64	C <sub>9</sub> H <sub>10</sub> O <sub>3</sub>	p-Anisic acid, methyl ester	
21.12	131,103,77,51,162	C <sub>10</sub> H <sub>10</sub> O <sub>2</sub>	Cinnamic acid, methyl ester	
20.55	100,142,154,70,58,43,11 3,129	C <sub>9</sub> H <sub>17</sub> NO <sub>3</sub>	Ethyl 6- formamidohexanoate	
20.76	128	C <sub>9</sub> H <sub>18</sub> N <sub>2</sub> O <sub>4</sub>	Ile-Ser	
22.68	84,144,100,58,139,145	C <sub>14</sub> H <sub>19</sub> NO <sub>4</sub>	Anisomycin	
22.96	140,150,98	C <sub>18</sub> H <sub>28</sub> N <sub>2</sub> O	Bupivacaine	
23.01	126,153	C <sub>5</sub> H <sub>5</sub> N <sub>3</sub> O <sub>4</sub>	5-Aminoorotic acid	
35.59	71,57,85,99,113,127,141 ,155,169,183,197	C <sub>27</sub> H <sub>56</sub>	Heptacosane	

## 6.6 Conclusions

*E. coli* as well as three other extremophiles bacteria or Archaea samples were chosen as the possible candidates that could possibly survive under Martian environment. These samples are cyanobacteria (*Chroococcidiopsis cubana*), anctinobacteria (*Rubrobacter radiotolerans*), and halophilic Archaea (*Halobacterium salinarum*). The organic compounds from these four natural bacteria samples were analyzed by Py-GC/MS combined with TMAH

thermochemolysis. The organic compounds vary with different species. The main compounds from cyanobacteria and anctinobacterium samples are fatty acids and alcohols, varying from C<sub>11</sub>~C<sub>19</sub>, they are the most detectable organic compounds. However, only few long chain organic compounds were detected from halophilic Archaea. Adenine-derivatives are the easiest and has the highest abundance compared with other nucleobases. Glucopyranoside is one of the most important target compounds from the three extremophiles bacteria used herein; however, its abundance was different in each sample. The abundance of glucopyranoside-derivate is the lowest in *halobacterium salinarum*, the highest in cyanobacterium. The abundance of phenyl glucopyranoside is the highest in *Rubrobacter radiotolerans*. Carotenoids are the main pigments in *Rubrobacter radiotolerans* and *halobacterium salinarum*. Squalene is their target compound for the presence of carotenoids. From the results, we could conclude that 200 °C could be enough for the decomposition of cell membranes, though higher temperature could promote the detection of some organic compounds. Many organic compounds have been detected from these natural life samples; however, more experiments will need to be done to determine the organic compounds. This could be a new way and a new project to study the characteristic compounds from natural samples.

## **Chapter 7. Application of TMAH thermochemolysis on the analysis of Atacama sample.**

Atacama Desert is an ancient temperate hyperarid desert, which runs nearly 1000 km along the Pacific coast of South America from 30 °S to 20 °S. Its extreme aridity can be attributed to the constant temperature inversion caused by the cool, north- flowing Humboldt Current and the presence of the strong Pacific anticyclone [67,68]. It's one of the most important Martian analogues on Earth, and it is hotpot for extremophiles and extremotolerant microorganisms where the chemical and physical limits for life may be studied [76]. Therefore, it's essential to study the organic compounds from Atacama sample with TMAH thermochemolysis, in order to optimize the experimental conditions for the *in-situ* analysis of Martian sample. In this chapter, the organic compounds of Atacama Desert sample (AT05-177 and AT05-22) were analyzed with and without TMAH thermochemolysis, and at different heating rates, with three types of programe, including flash pyrolysis, MOMA-like rampe, and SAM-like ramp pyrolysis.

### **7.1 Experimental conditions**

#### **7.1.1 Sample preparation**

The Atacama samples collected by Rafael Navaroo Gonzalez [695], named AT 05-177 and AT 02-22 were grounded by Cryogenic Mixer Mill CryoMill, Retsch, Germany. Figure 7-1 is the picture of the CryoMill used in this study. The soil samples were grounded with cooling by liquid nitrogen at -196 °C to avoid the oxidation and thermal degradation of soil samples. The first grinding cycle consists of a pre-cooling of 4 mins (frequency 5/s), followed by 5 mins grinding process (frequency 25/s), with 2 Cryo cycles. The grounded samples were collected after cooling the sample cup at room temperature.



Figure 7-1 Cryogenic Mixer Mill CryoMill, Retsch, Germany.

### 7.1.2 Extraction of Atacama sample

To well understand the organic compounds of Atacama samples, the extraction process was applied. As shown in Figure 7-2, it is the extraction method that was applied in this study. About 3 g of AT05-177 sample were put inside of the extraction thimble, which was laid in the extraction tube connected with a round-bottomed flask. The extraction solvents used for this study is a mixture of water and isopropanol (1:1) [529], 75 mL. 3-4-zeolite grains were used to avoid bumping in the flask. The sample was extracted for 24 h at a temperature of 75 °C. Excess solvent was removed by a rotary evaporator, and the final volume of the extracts was 5 mL. The soil residues were dried in vacuum at 70 °C for 12 h, and the final weight was recorded. The whole extraction experiments were repeated 3 times. However, this extraction process was failed because of we did not found something interesting in the extraction process, neither amino acids nor nucleobases. On the other hand, maybe the extraction method will need to be optimized. We did not optimize the experimental conditions since the time limit. Therefore, more work will need to be done for further study with extraction method. What's more, the preparation and extraction process are time-consuming, therefore, the extraction method could not be the optimal method to analyze the organic compounds from Martian soil.



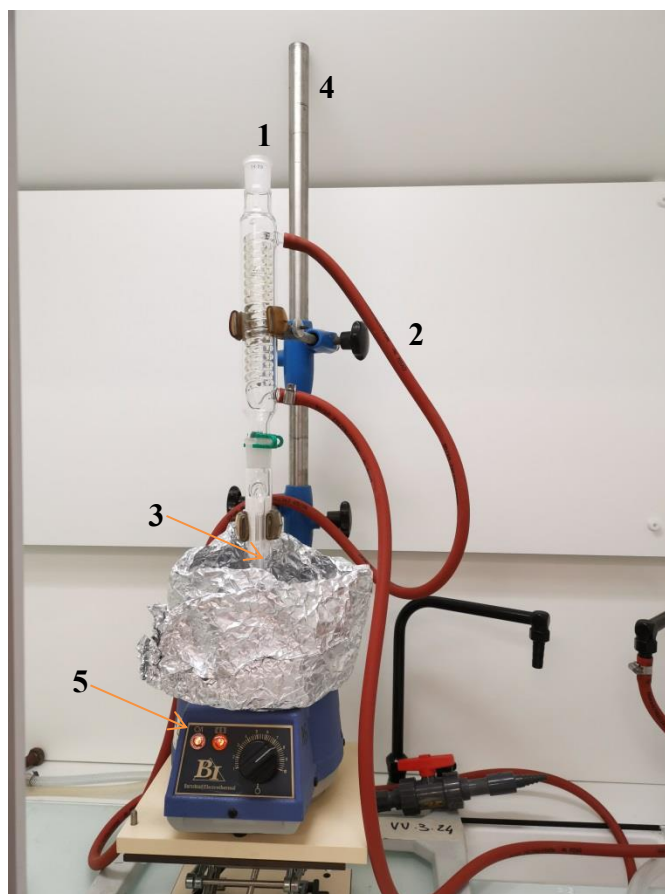


Figure 7-2 the extraction device of Atacama sample. 1: Serpentine condenser; 2: Condensate pipe; 3: Extraction tube and round-bottomed flask; 4: Iron stand; 5: Electric heating mantle.

### 7.1.3 Pyrolysis and GC/MS

The organic compounds of Atacam sample were analyzed by Pyrolysis-GC/MS, as we described in other chapters. The samples were pyrolyzed at three different mode, flash pyrolysis, MOMA-like ram pyrolysis, and SAM-like ramp pyrolysis. For the flash pyrolysis, the sample was dropped inside the oven at a set temperature °C (with 1 min hold). For MOMA and SAM-like ramp pyrolysis, the heart-cut EGA analysis method was used, with a capsule carried by an eco-stick (Frontier lab) attached and introduced inside the oven (initial temperature was 50 °C) flushed by 1 mL min<sup>-1</sup> of helium, and the oven was programmed to reach the final temperature (hold 1 min) at the MOMA heating rate of 200 °C.min<sup>-1</sup> and SAM heating rate of 35 °C.min<sup>-1</sup>, respectively. The liquid dinitrogen MicroJet Cryo-trap was used to trap and pre-concentrate all products of pyrolysis at -180 °C at the chromatographic column inlet. When the pyrolysis process was finished, the liquid dinitrogen flow was stopped, and the temperature of the column inlet was quickly increased to 40 °C.

## 7.2 Organic compounds of Atacama sample

### 7.2.1 Pyrolysis-GC/MS

The organic compounds from Atacama Desert samples were analyzed by Py-GC/MS. Figure 7-3 is the chromatograms of AT 05-177 and AT 02-22 with TMAH thermochemolysis at flash pyrolysis, MOMA-like ramp pyrolysis, and SAM-like ramp pyrolysis. Table 7-1 and Table 7-2 listed all organic compounds detected from AT05-177 and AT 02-22 sample flash pyrolysis at 600 °C, respectively. The main compounds in AT 05-177 are light aromatic compounds and alkene. Light aromatics are mainly benzene-bearing aromatics. For example, benzene (RT=3.33 min), toluene (RT=4.99 min), *m,p*-xylene(RT= 7.94 min), trimethylbenzene (RT=9.73, 9.86 min), cymene (RT=11.39 min). Alkenes are also the major products, including 1-hexene (RT=2.63 min), 2-methyl-1-hexene (RT=3.65 min), 1-octene (RT=5.46 min) and their isomers, 3,5-dimethyl-3-heptene (RT=7.73 min). Similar analysis result was found for AT 02-22 samples with alkenes and light aromatic compounds. In addition, sulfur dioxide was only found in AT05-177 samples, and its intensity is relatively high. This demonstrates that the elements from Atacama sample depend on the ancient environment and the sample sites.

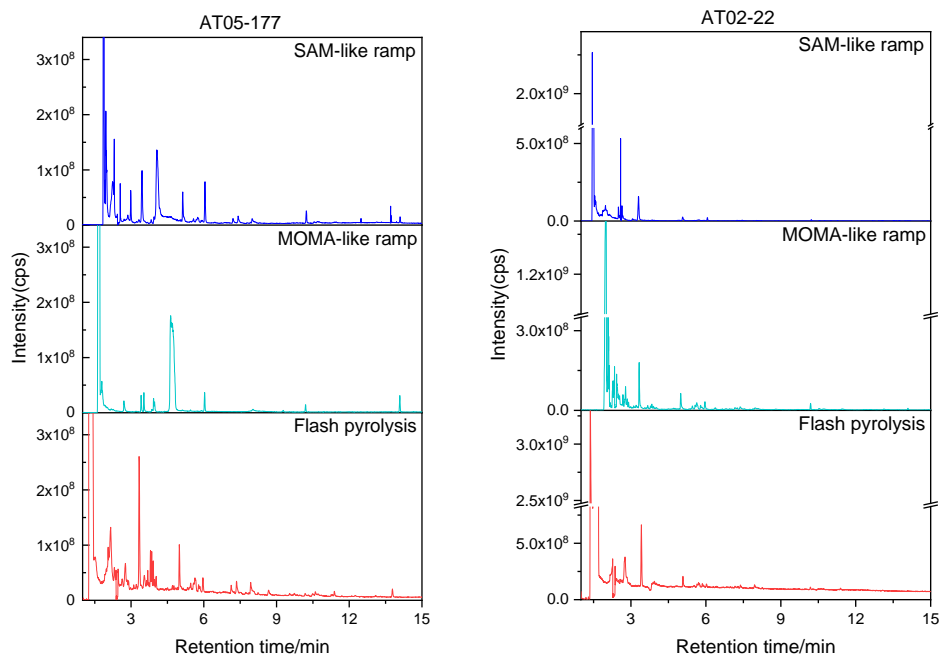


Figure 7-3 The chromatograms of AT 05-177 and AT 02-22 with TMAH thermochemolysis at flash pyrolysis, MOMA-like ramp pyrolysis, and SAM-like ramp pyrolysis.

When comparing the products from Atacama sample used herein, three different pyrolysis programs did not show obvious influence on the detection of organics, even the same organics were released at different retention time. Different heating rate could have a little influence on the retention time in the oven; therefore, the volatiles from Atacama sample would need different time to reach to the column. Hence, their peaks of retention time shift slightly. That is why we only give the products from flash pyrolysis at 600 °C.

Table 7-1 Organic compounds detected from AT 05-177 sample flash pyrolysis at 600 °C.


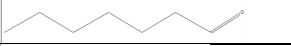
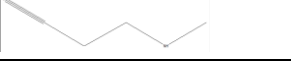
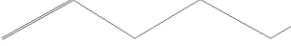
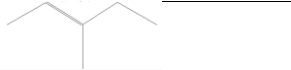
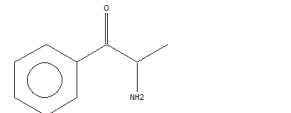
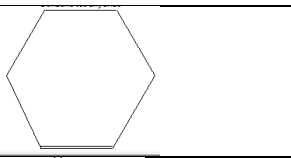
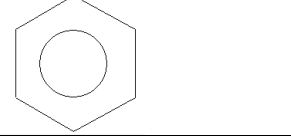

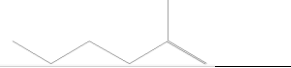
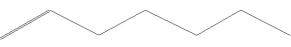
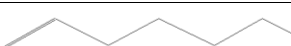
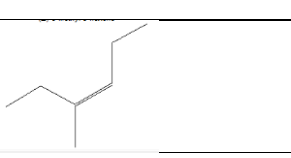

<b>AT 05-177</b>			
RT/min	Mass fragments	Compounds	Structure
1.56	44	Ethanolamine	
2.16	41,44,55,70	Heptanal	
2.31	44,53,67	3-methylation-propaneitrile	
2.63	44,56,69,84	1-Hexene	
2.77,2.89	44,55,69,84	E-3-methyl-2-pentene	
3.11	44,78,52	Cathinone	
3.21	67,55,44,82,98	Cyclohexene	
3.33	78,52	Benzene	
3.54	64,48	Sulfur dioxide	
3.65	56,41,70,83,98	2-methyl-1-Hexene	
3.69	56,70,69,41,98	1-Heptene	
3.80	41,56,69,98,43	1-Heptene	
3.85	69,41,55,98,83	Z-3-methyl-3-Hexene	
3.91	55,69,98,83,41	E-2-Heptene	

Table 7-1 (continued)


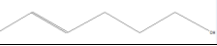
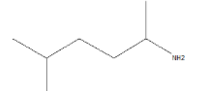
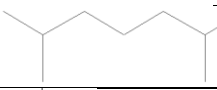
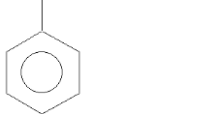
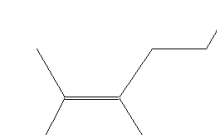
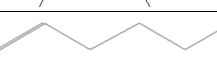
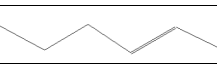
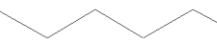
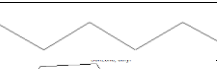
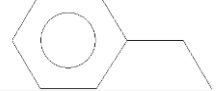
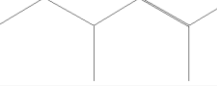


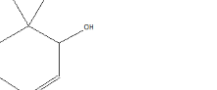
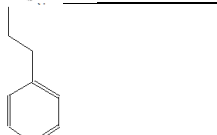
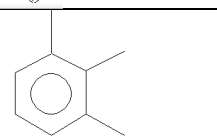
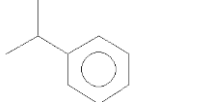
RT/min	Mass fragments	Compounds	Structure
3.97	69,83	3-methyl-1-pentyn-3-ol	
4.03	55,81,96	4-Hexene-1-ol	
4.71	44,55,69,83	5-methyl-2-Hexanamine	
4.77	44,55,69	Octodrine	
4.99	91,92,44,65	Toluene	
5.37	55,69,83,112	2,3-dimethyl-2-hexene	
5.46	55,70,69,43,83,112	1-Octene	
5.58	55,70,83,112,41	E-4-Octene	
5.64	41,55,70,112,85	2-Octene	
5.79	55,41,70,112	E-2-Octene	
7.13,7.35	91,106	Toluene	
7.73	55,97,126,70	3,5-dimethyl-3-heptene	
7.88	56,43,70,97,84	1-Nonene	
7.94	91,104,77,78,51	p-Xylene	
8.23	70,126,55,95	6,6-dimethyl-cyclohex-2-en-1-ol	
9.55	91,120,65,140,50	Propyl-Benzene	
9.73,9.86	105,120	1,2,3-trimethyl-benzene	
10.50	105,120	1-methylethyl-benzene	

Table 7-1 (continued)

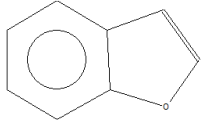

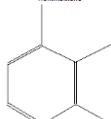
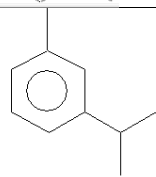
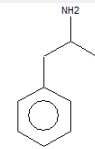
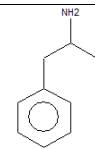
RT/min	Mass fragments	Compounds	Structure
10.70	118,89,103,63	Benzofuran	
11.25	119,91,134,117,103	p-Cymene	
11.32	105,120,79	1,2,3-trimethyl-benzene	
11.39	119,91,134,117,65	m-Cymene	
11.70,12.24	44,117,64,91	Amphetamine	
12.09	44,64,105,134	2-amino-1-(4-methylphenyl)propane	

Table 7-2 Organic compounds detected from AT 02-22 sample flash pyrolysis at 600 °C.




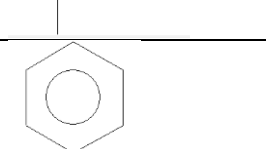

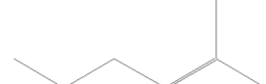
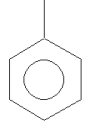

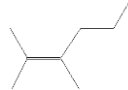
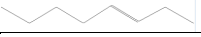
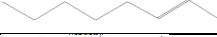

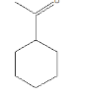

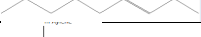
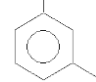

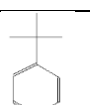
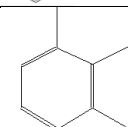
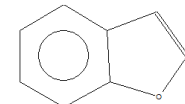
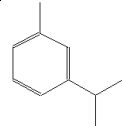
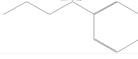

AT 02-22				
RT/min	Mass fragments	Formula	Compounds	Structure
1.65,2.27	44	CO <sub>2</sub>	Carbon dioxide	O=C=O
2.16	44,58,59	C <sub>3</sub> H <sub>9</sub> N	N-methyl-ethanamine	
2.36	47,44	CH <sub>2</sub> O <sub>2</sub>	Formic acid	
2.50	56,55,41,69,84	C <sub>6</sub> H <sub>12</sub>	2-Methyl-1-pentene	
2.74,3.29	78,44,52	C <sub>6</sub> H <sub>6</sub>	Benzene	
2.84	55,84,69,44,41	C <sub>6</sub> H <sub>12</sub>	3-Hexene,(Z)-	
3.89	69,41,98,55,81	C <sub>7</sub> H <sub>14</sub>	2-Methyl-2-hexene	

Table 7-2 (continued)

RT/min	Mass fragments	Formula	Compounds	Structure
5.01	91,92,44,65	C <sub>7</sub> H <sub>8</sub>	Toluene	
5.51	55,70,83,112,97,42,41	C <sub>8</sub> H <sub>16</sub>	Cyclooctane	
5.65	55,83,112,44,70	C <sub>8</sub> H <sub>16</sub>	2,3-Dimethyl-2-hexene	
5.71	55,70,41,112,83	C <sub>8</sub> H <sub>16</sub>	E-3-Octene	
5.86	55,70,83,41,112,197	C <sub>8</sub> H <sub>16</sub>	2-Octene	
5.91	70,55,41,112,83,95	C <sub>8</sub> H <sub>16</sub>	3-methylene-Heptane	
6.42	83,55,97,43,126	C <sub>8</sub> H <sub>14</sub> O	1-cyclohexyl-Ethanone	
7.16	91,106,65,77	C <sub>8</sub> H <sub>10</sub>	Ethylbenzene	
7.28	70,55,41,126,97,110	C <sub>9</sub> H <sub>18</sub>	E-3-Nonene	
7.39,7.95	91,106,77,65,51	C <sub>8</sub> H <sub>10</sub>	1,3-dimethyl-benzene(isotope)	
7.89	56,41,69,70,84,83	C <sub>9</sub> H <sub>20</sub> O	1-Nonanol	
10.51	119,91,70,57,41,81,134,140	C <sub>10</sub> H <sub>14</sub>	Tert-butyl-Benzene	
10.62	106,120,140,77,76,42	C <sub>9</sub> H <sub>12</sub>	1,2,3-trimethyl-benzene	
10.71	118,89,	C <sub>8</sub> H <sub>6</sub> O	Benzoduran	
11.39	119,134,91,42,65,77,117,140	C <sub>10</sub> H <sub>14</sub>	m-Cymene	
12.23	91,134,105,119,65	C <sub>10</sub> H <sub>14</sub>	n-Butylbenzene	
13.09	55,70,83,97,41,154,117,31	C <sub>11</sub> H <sub>24</sub> O	1-Undecanol	

### 7.2.2 Atacama sample with TMAH thermochemolysis

From the analysis of Atacama sample, all organic compounds containing in Atacama sample were determined. To test the efficiency of TMAH thermochemolysis, it was applied to analyze the organic compounds from natural soil sample. Figure 7-4 and Figure 7-5 showed the chromatograms of AT 05-177 and 02-22 samples with and without TMAH thermochemolysis at flash pyrolysis, MOMA-like ramp, and SAM-like ramp pyrolysis. However, the results were not the same as what it was supposed to be. The peaks of the organic compounds from Atacama samples were inhibited by the peaks of byproducts from TMAH degradation. For example, the benzene peak at the retention time of 3.42 min was overlapped by the peaks of trimethylamine, which is one of the major byproducts from TMAH degradation. This could also be caused by the chromatographic problems, such as the programming process of column. In addition, other byproducts, such as the palmitic acid and methyl stearate, from TMAH degradation could lead to a miss understanding or miss explanation of the organic compounds from Atacama sample. In addition, these results indicate that the efficiency of TMAH thermochemolysis is not suitable for the analysis of soil samples with less abundance of organic compounds, especially those samples without polar organic compounds. It means TMAH thermochemolysis should not be applied to analyze the organic compounds inside of soil samples, that if i) the content of organic compounds in soil sample is pretty low; 2) there are no polar functional groups-bearing compounds inside of the soil sample, such as amino acids, fatty acids, or nucleobases. Therefore, if Martian soil doesn't contain a high amount of organic compounds, we should be careful in explaining the organic compounds that have been detected with TMAH thermochemolysis on SAM. Therefore, new methods need to be proposed to search for life biosignatures on Mars.

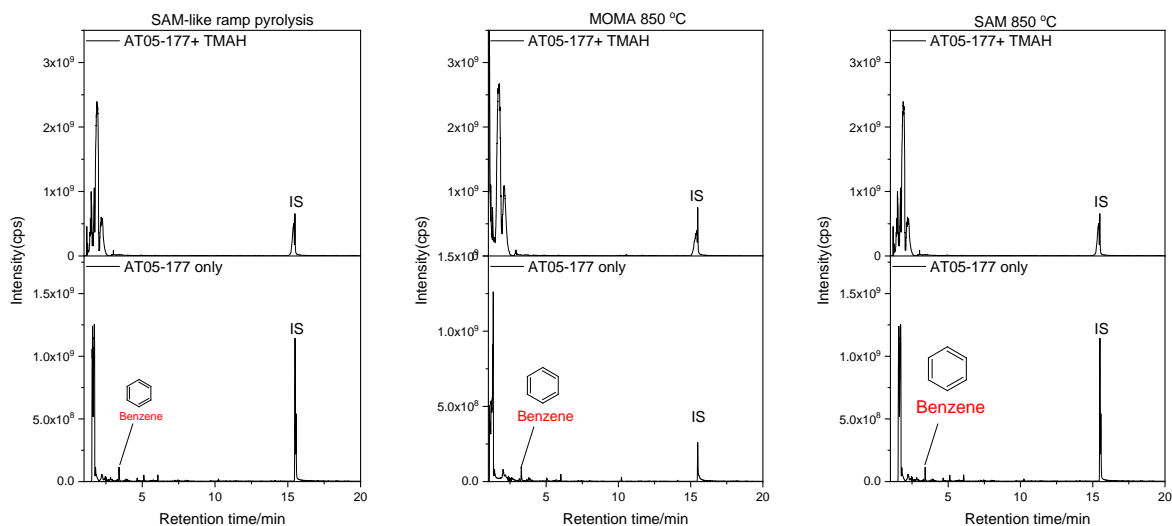


Figure 7-4 The chromatograms of AT05-177 sample without and with TMAH thermochemolysis at flash pyrolysis, MOMA-like ramp, and SAM-like ramp pyrolysis.

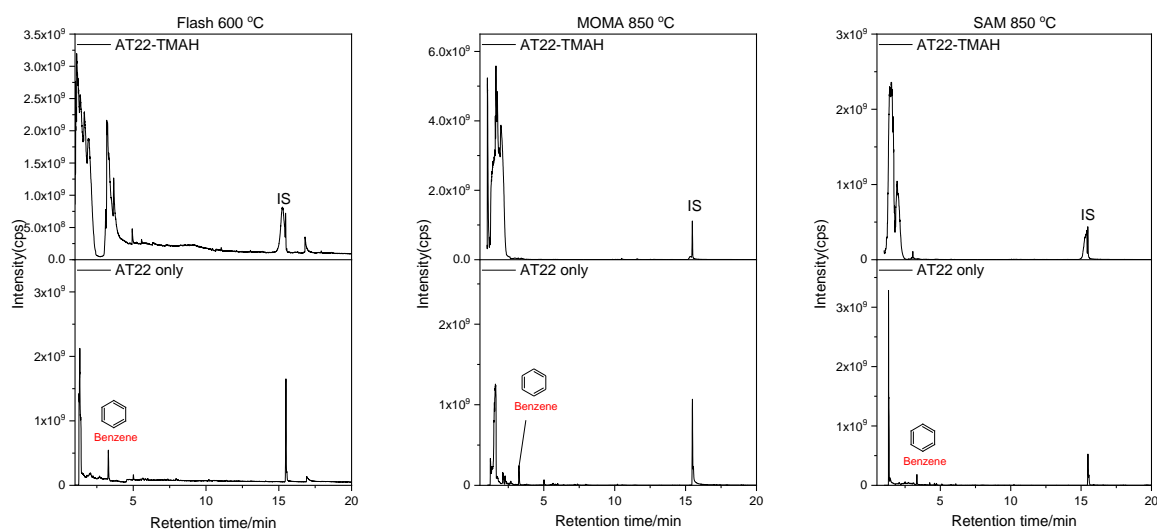


Figure 7-5 The chromatograms of AT02-22 sample without and with TMAH thermochemolysis at flash pyrolysis, MOMA-like ramp, and SAM-like ramp pyrolysis.

### 7.3 Conclusions

Py-GC/MS combined with extraction and TMAH thermochemolysis were applied to analyze the organic compounds of the natural Atacama sample. Light aromatic compounds and alkenes are the major compounds that have been detected in Atacama sample used herein. Sulfur oxides were also found in Atacama sample, this demonstrated that the sulfur-bearing



compounds could be one of the interesting compounds in the future missions. In addition, our result showed that Py-GC/MS is the optimal method to analyze the organic compounds from natural sample containing less abundance of organic compounds. TMAH thermochemolysis is not able to improve the detection efficiency when study the organic compounds from natural soil samples, especially the samples with less organic compounds. Therefore, new advanced characteristic methods need to be developed in the future missions.

## Chapter 8. Conclusions and perspectives

This final chapter summarizes the main findings of each previous chapter and attempts to provide a direction for future works.

### 8.1 General conclusion

The core objective of this thesis was to develop an understanding of how perchlorate influences the efficiency of the derivatization reagents, mainly MTBSTFA/DMF and TMAH, and develop the knowledge of TMAH application in DNA and RNA fragments and the detection of organic compounds from natural samples.

Chapter 1 presents the background of this study with a review of life biomarkers and the application of TMAH thermochemolysis in the last 10 years.

In chapter 2, the influence of calcium perchlorate on the detection of organic compounds with MTBSTFA/DMF has been studied. Result showed that MTBSTFA/DMF should be applied at low temperature ( $< 300\text{ }^{\circ}\text{C}$ ) for flash pyrolysis, to avoid the production of a huge amount of byproducts from MTBSTFA/DMF degradation. High temperature leads to the formation of aromatic compounds and F-bearing compounds. For SAM-like ramp pyrolysis, MTBSTFA/DMF performed well even at  $850\text{ }^{\circ}\text{C}$ . Meanwhile, the presence of calcium perchlorate has no obvious effect on the pyrolysis of MTBSTFA/DMF, making it a good fit for the SAM and MOMA missions. Finally, our results confirm that the chlorobenzene that has been detected by SAM is certainly from the indigenous carbon in the Martian sample.

In chapter 3, we studied the influence of calcium perchlorate on the search for organics on Mars with TMAH thermochemolysis. The byproducts of TMAH with and without the presence of calcium perchlorate were studied. The presence of a high content of calcium perchlorate would probably influence the route of TMAH degradation, and we note that DMF is an important intermediate for the formation of Hexahydro-1,3,5-trimethyl-1,3,5-triazine. In addition, the application of TMAH thermochemolysis on the detection of fatty acids were studied. In our experimental conditions, calcium perchlorate did not affect the recovery of fatty acids during TMAH thermochemolysis, even when the fatty acid amount was low ( $300\text{ ppb}$ ). This demonstrated that TMAH is a good thermochemolysis reagent at high temperature ( $600\text{ }^{\circ}\text{C}$ ) for the methylation and detection of organics on Mars with the SAM and MOMA instruments.

Since it has been proved that TMAH is a good thermochemolysis reagent in Chapter 3, the application of TMAH thermochemolysis on the detection of nucleobases were carried out in Chapter 4. TMAH allows the methylation and detection of seven nucleobases. Its optimal temperature is at flash 600 °C. Each target compounds of the corresponding nucleobase are listed, and the mechanisms of TMAH thermochemolysis have been proposed. What's more, we note that adenine is the most detectable nucleobase among these seven nucleobases. Based on the values of LOD and LOQ for each nucleobase, adenine, thymine, and uracil are easier to be detected, as they can be detected at about 0.15 nmol. It is possible, though more difficult, to detect the guanine, cytosine and hypoxanthine (LOD=0.40, 0.55 and 0.75 nmol, respectively). However, the complex matrix needs to be pretreated with the extraction process in order to detect the nucleobases on Mars, the LOD may be higher than value of our study.

To have a better understanding of TMAH thermochemolysis on the detection of DNA/RNA, chemical standards of nucleosides, nucleotides, nucleotide mon- and tri-phosphates were studied in Chapter 5. We note that the target compounds of these DNA/RNA fragments are the methylated nucleobases, also with the methylated ribose derivatives and methylated phosphate. Surprisingly, the methylated nucleosides were found in our results. This demonstrated that TMAH thermochemolysis could protect the nucleosides or nucleotides from decomposition at high temperatures.

A further study of TMAH application to natural life samples were conducted in Chapter 6, mainly about *E.coli*, cyanobacteria (*chroococcidiopsis cubana*), anctinobacteria (*Rubrobacter radiotolerans*) that has been detected in Atacama sample, and halophilic Archaea (*halobacterium salinarum*) that could possibly survive in extreme environment. We note that the organic compounds vary with different species. The main compounds from these natural samples are fatty acids; they are the most detectable organic compounds. Adenine-derivatives have the highest abundance compared with other nucleobases and therefore are the easiest ones to be detected. Glucopyranoside is one of the most important target compounds from the three extremophiles bacteria used herein. Carotenoids are the main pigments in *Rubrobacter radiotolerans* and *halobacterium salinarum*. Squalene is their target compound for the presence of carotenoids, and it could be the biomarkers for life.

Chapter 7 studied the application of TMAH thermochemolysis on the Atacama Desert sample. Light aromatic compounds and alkenes are the major compounds that have been detected in Atacama sample used herein. Sulfur oxides were also found in Atacama sample, this demonstrated that the sulfur-bearing compounds could be one of the interesting compounds

in the future missions. However, TMAH thermochemolysis was not able to help the detection of organic compounds of Atacama Desert sample. Therefore, new advanced characteristic methods need to be developed in the future missions.

## **8.2 Future work**

Even this work has advanced the knowledge of the calcium perchlorate on the application of derivatization reagents, the application of TMAH thermochemolysis on the detection of DNA/RNA fragments and natural samples, about real life and Martian samples. However, we only analyzed the influence of perchlorate on the application of the reagents, the influence of perchlorate and other minerals on the application of reagents and the detection of organic compounds in natural samples will also need to be studied. In addition, the optimal experimental conditions of the natural samples have not been optimized, such as the selection of a better derivatization reagent, the volume of thermochemolysis reagents, the analysis of organic compounds from SAM and MOMA ramp pyrolysis. Therefore, a range of works should be considered in the future, they are listed below:

- 1) The influence of other minerals on the derivatization reagents should be studied, such as silicates, phyllosilicates, sulfates, carbonates, etc. They are important Martian minerals, which could have effects on the application of derivatization reagents.
- 2) More chemical standards representing life biomarkers should be studied with TMAH thermochemolysis, such as lipids, amino acids, polysaccharides, proteins and pigments. In addition, their degradation products should also be studied. For example, carotenoids, as one of the important pigments, play a key role in extremophiles residing to extreme conditions. And it was detected from Anctinobacteria and halophilic bacteria in this study. The byproducts of carotenoids at different pyrolysis conditions should be studied.
- 3) The organic compounds from various extremophile microorganisms should be studied with and without TMAH thermochemolysis. The characteristic compounds of each microorganism should be addressed. The experimental conditions of TMAH thermochemolysis should be optimized, such as the volume of TMAH with a certain number of cells, the optimal temperature of TMAH thermochemolysis, etc.
- 4) The effect of oxychlorides such as perchlorates on the distribution of organic compounds in extremophile microorganisms should be investigated, in order to have a

further understanding on the influence of chlorine bearing compounds on the growth of bacteria.

- 5) New *in situ* methods need to be developed, to analyze organic compounds with TMAH thermochemolysis. For example, we could try to cultivate the bacteria in soil, centrifuge cells and soil samples, and analyze the organic compounds from the mixture of cells and soil samples. Then a new system of “cultivation+clean+separation+detection” should be developed.
- 6) The application of TMAH thermochemolysis on the detection of organic compounds from different types of soils should be studied. These soil samples should enrich in organic compounds with carboxyl, hydroxyl, amino, and acyl et al. function groups.
- 7) New derivatization reagents should be developed to improve the efficiency of the detection of life biomarkers On Mars. TMAH (25% methanol), as both solvent and the reagent of thermochemolysis, is not able to dissolve some of organic compounds. In addition, the degradation byproducts from TMAH could be confusing when analyzing the data collected from space. Therefore, new derivatization reagents with higher solubility of organic compounds and with less byproducts should be developed.

## Reference:

- [1] J.P. Grotzinger, J. Crisp, A.R. Vasavada, R.C. Anderson, C.J. Baker, R. Barry, D.F. Blake, P. Conrad, K.S. Edgett, B. Ferdowski, R. Gellert, J.B. Gilbert, M. Golombek, J. Gómez-Elvira, D.M. Hassler, L. Jandura, M. Litvak, P. Mahaffy, J. Maki, M. Meyer, M.C. Malin, I. Mitrofanov, J.J. Simmonds, D. Vaniman, R. V. Welch, R.C. Wiens, Mars Science Laboratory mission and science investigation, 2012. <https://doi.org/10.1007/s11214-012-9892-2>.
- [2] P.R. Mahaffy, C.R. Webster, M. Cabane, P.G. Conrad, P. Coll, S.K. Atreya, R. Arvey, M. Barciniak, M. Benna, L. Bleacher, W.B. Brinckerhoff, J.L. Eigenbrode, D. Carignan, M. Cascia, R.A. Chalmers, J.P. Dworkin, T. Errigo, P. Everson, H. Franz, R. Farley, S. Feng, G. Frazier, C. Freissinet, D.P. Glavin, D.N. Harpold, D. Hawk, V. Holmes, C.S. Johnson, A. Jones, P. Jordan, J. Kellogg, J. Lewis, E. Lyness, C.A. Malespin, D.K. Martin, J. Maurer, A.C. McAdam, D. McLennan, T.J. Nolan, M. Noriega, A.A. Pavlov, B. Prats, E. Raaen, O. Sheinman, D. Sheppard, J. Smith, J.C. Stern, F. Tan, M. Trainer, D.W. Ming, R. V. Morris, J. Jones, C. Gundersen, A. Steele, J. Wray, O. Botta, L.A. Leshin, T. Owen, S. Battel, B.M. Jakosky, H. Manning, S. Squyres, R. Navarro-González, C.P. McKay, F. Raulin, R. Sternberg, A. Buch, P. Sorensen, R. Kline-Schoder, D. Coscia, C. Szopa, S. Teinturier, C. Baffes, J. Feldman, G. Flesch, S. Forouhar, R. Garcia, D. Keymeulen, S. Woodward, B.P. Block, K. Arnett, R. Miller, C. Edmonson, S. Gorevan, E. Mumm, The sample analysis at mars investigation and instrument suite, *Space Sci. Rev.* 170 (2012) 401–478. <https://doi.org/10.1007/s11214-012-9879-z>.
- [3] F. Goesmann, W.B. Brinckerhoff, F. Raulin, W. Goetz, R.M. Danell, S.A. Getty, S. Siljeström, H. Mißbach, H. Steininger, R.D. Arevalo, A. Buch, C. Freissinet, A. Grubisic, U.J. Meierhenrich, V.T. Pinnick, F. Stalport, C. Szopa, J.L. Vago, R. Lindner, M.D. Schulte, J.R. Brucato, D.P. Glavin, N. Grand, X. Li, F.H.W. van Amerom, the MOMA Science Team, The Mars Organic Molecule Analyzer (MOMA) instrument: characterization of organic material in martian sediments, *Astrobiology.* 17 (2017) 655–685. <https://doi.org/10.1089/ast.2016.1551>.
- [4] A. Brandt, L. Chen, B.E. Van Dongen, T. Welton, J.P. Hallett, Structural changes in lignins isolated using an acidic ionic liquid water mixture, *Green Chem.* 17 (2015) 5019–5034. <https://doi.org/10.1039/c5gc01314c>.
- [5] A.V. Marques, J. Rencoret, A. Gutiérrez, J.C. Del Río, H. Pereira, Ferulates and lignin structural composition in cork, *Holzforschung.* 70 (2016) 275–289. <https://doi.org/10.1515/hf-2015-0014>.

- [6] J.C. Del Río, P. Prinsen, J. Rencoret, L. Nieto, J. Jiménez-Barbero, J. Ralph, Á.T. Martínez, A. Gutiérrez, Structural characterization of the lignin in the cortex and pith of elephant grass (*Pennisetum purpureum*) stems, *J. Agric. Food Chem.* 60 (2012) 3619–3634. <https://doi.org/10.1021/jf300099g>.
- [7] C. Crestini, M. Crucianelli, M. Orlandi, R. Saladino, Oxidative strategies in lignin chemistry: A new environmental friendly approach for the functionalisation of lignin and lignocellulosic fibers, *Catal. Today.* 156 (2010) 8–22. <https://doi.org/10.1016/j.cattod.2010.03.057>.
- [8] R. Vanholme, B. Demedts, K. Morreel, J. Ralph, W. Boerjan, Lignin biosynthesis and structure, *Plant Physiol.* 153 (2010) 895–905. <https://doi.org/10.1104/pp.110.155119>.
- [9] J.H. Shinn, From coal to single-stage and two-stage products: A reactive model of coal structure, *Fuel.* 63 (1984) 1187–1196. [https://doi.org/10.1016/0016-2361\(84\)90422-8](https://doi.org/10.1016/0016-2361(84)90422-8).
- [10] K. Takeuchi, H. Aoi, H. Ohtani, Precise compositional analysis of styrene/butyl acrylate/methacrylic acid terpolymer by two-step reactive pyrolysis-gas chromatography with tetramethylammonium acetate, *J. Anal. Appl. Pyrolysis.* 113 (2015) 22–26. <https://doi.org/10.1016/j.jaap.2014.09.018>.
- [11] M. Blazsó, J. Bozi, Ammonium Y zeolite applied as a thermochemolysis reagent for identification of polyethers and polyesters, *J. Chromatogr. A.* 1271 (2013) 217–220. <https://doi.org/10.1016/j.chroma.2012.11.050>.
- [12] S. Baidurah, Y. Kubo, M.K. Kuno, K.K. Kadera, Y.I. Ishida, T. Yamane, H. Ohtani, Rapid and direct compositional analysis of poly ( 3-hydroxybutyrate- co -3-hydroxyvalerate ) in whole bacterial cells by thermally assisted hydrolysis and methylation – gas chromatography, *Anal. Sci.* 31 (2015) 79–83.
- [13] S.B. Y S Khok, M Suwa, H Ito, M Hazwan Hussin, Y Ishida, K Sudesh, Comparison of quantification methods and subsequent characterization of polyhydroxybutyrate film sample utilizing pretreated cane molasses as carbon source Comparison of quantification methods and subsequent characterization of polyhydroxybutyrate film sa, in: *IOP Conf. Ser. Mater. Sci. Eng.*, 2020: p. 012013. <https://doi.org/10.1088/1757-899X/716/1/012013>.
- [14] H. Ohtani, K. Takeuchi, Y. Iiguni, A. Kaneko, M. Kiura, H. Momose, End group analysis of styrene-butyl acrylate copolymers initiated with benzoyl peroxide by stepwise chemolysis-pyrolysis gas chromatography, *J. Anal. Appl. Pyrolysis.* 124 (2017) 677–681. <https://doi.org/10.1016/j.jaap.2016.12.004>.

- [15] R. Spaccini, D. Todisco, M. Drosos, A. Nebbioso, A. Piccolo, Decomposition of biodegradable plastic polymer in a real on-farm composting process, *Chem. Biol. Technol. Agric.* 3 (2016) 1–12. <https://doi.org/10.1186/s40538-016-0053-9>.
- [16] A. Hosaka, C. Watanabe, N. Teramae, H. Ohtani, Development of a new micro reaction sampler for pyrolysis-GC/MS system facilitating on-line analytical chemolysis of intractable condensation polymers, *J. Anal. Appl. Pyrolysis.* 106 (2014) 160–163. <https://doi.org/10.1016/j.jaap.2014.01.014>.
- [17] C. Schwarzinger, I. Hintersteiner, B. Schwarzinger, W. Buchberger, B. Moser, Analytical pyrolysis in the determination of the aging of polyethylene, *J. Anal. Appl. Pyrolysis.* 113 (2015) 315–322. <https://doi.org/10.1016/j.jaap.2015.02.005>.
- [18] S. Baidurah, S. Takada, K. Shimizu, K. Yasue, S. Arimoto, Y. Ishida, T. Yamane, H. Ohtani, Evaluation of biodegradation behavior of poly(butylene succinate-co-butylene adipate) with lowered crystallinity by thermally assisted hydrolysis and methylation-gas chromatography, *Int. J. Polym. Anal. Charact.* 17 (2012) 29–37. <https://doi.org/10.1080/1023666X.2012.638439>.
- [19] S. Baidurah, S. Takada, K. Shimizu, Y. Ishida, T. Yamane, H. Ohtani, Evaluation of biodegradation behavior of poly(butylene succinate-co-butylene adipate) with lowered crystallinity by thermally assisted hydrolysis and methylation-gas chromatography, *J. Anal. Appl. Pyrolysis.* 103 (2013) 73–77. <https://doi.org/10.1016/j.jaap.2012.08.011>.
- [20] S. Baidurah, P. Murugan, L. Joyyi, J. Fukuda, M. Yamada, K. Sudesh, Y. Ishida, Validation of thermally assisted hydrolysis and methylation-gas chromatography for rapid and direct compositional analysis of poly(3-hydroxybutyrate-co-3-hydroxyhexanoate) in whole bacterial cells, *J. Chromatogr. A.* 1471 (2016) 186–191. <https://doi.org/10.1016/j.chroma.2016.10.019>.
- [21] S. Baidurah, P. Murugan, K.Y. Sen, Y. Furuyama, M. Nonome, K. Sudesh, Y. Ishida, Evaluation of soil burial biodegradation behavior of poly(3-hydroxybutyrate-co-3-hydroxyhexanoate) on the basis of change in copolymer composition monitored by thermally assisted hydrolysis and methylation-gas chromatography, *J. Anal. Appl. Pyrolysis.* 137 (2019) 146–150. <https://doi.org/10.1016/j.jaap.2018.11.020>.
- [22] A.J. Williams, J. Eigenbrode, M. Floyd, M.B. Wilhelm, S. O'Reilly, S.S. Johnson, K.L. Craft, C.A. Knudson, S. Andrejkovičová, J.M.T. Lewis, A. Buch, D.P. Glavin, C. Freissinet, R.H. Williams, C. Szopa, M. Millan, R.E. Summons, A. McAdam, K. Benison, R. Navarro-González, C. Malespin, P.R. Mahaffy, Recovery of fatty acids from mineralogic Mars analogs by TMAH thermochemolysis for the Sample Analysis at Mars wet chemistry experiment on the



- Curiosity Rover, *Astrobiology*. 19 (2019) 522–546. <https://doi.org/10.1089/ast.2018.1819>.
- [23] Y. He, A. Buch, M. Morisson, C. Szopa, C. Freissinet, A. Williams, M. Millan, M. Guzman, R. Navarro-Gonzalez, J.Y. Bonnet, D. Coscia, J.L. Eigenbrode, C.A. Malespin, P. Mahaffy, D.P. Glavin, J.P. Dworkin, P. Lu, S.S. Johnson, Application of TMAH thermochemolysis to the detection of nucleobases: Application to the MOMA and SAM space experiment, *Talanta*. 204 (2019) 802–811. <https://doi.org/10.1016/j.talanta.2019.06.076>.
- [24] A.J. Kossa, W. C., MacGee, J., Ramachandran, S., Webber, Pyrolytic methylation/gas chromatography: A short review, *J. Chromatogr. Sci.* 17 (1979) 177–187.
- [25] F. Shadkami, R. Helleur, Recent applications in analytical thermochemolysis, *J. Anal. Appl. Pyrolysis*. 89 (2010) 2–16. <https://doi.org/10.1016/j.jaap.2010.05.007>.
- [26] J.M. Challinor, Review: The development and applications of thermally assisted hydrolysis and methylation reactions, *J. Anal. Appl. Pyrolysis*. 61 (2001) 3–34. [https://doi.org/10.1016/S0165-2370\(01\)00146-2](https://doi.org/10.1016/S0165-2370(01)00146-2).
- [27] J.B. Edson, C.S. Macomber, B.S. Pivovar, J.M. Boncella, Hydroxide based decomposition pathways of alkyltrimethylammonium cations, *J. Memb. Sci.* 399–400 (2012) 49–59. <https://doi.org/10.1016/j.memsci.2012.01.025>.
- [28] and R.T. Chicarro, Augustin, Patrick Martin, The Mars Express Mission: An overview, *Mars Express Sci. Payload*. 1240 (2004) 3–13.
- [29] N. Dauphas, A. Pourmand, Hf-W-Th evidence for rapid growth of Mars and its status as a planetary embryo, *Nature*. 473 (2011) 489–492. <https://doi.org/10.1038/nature10077>.
- [30] K. Mezger, V. Debaille, T. Kleine, Core formation and mantle differentiation on Mars, *Space Sci. Rev.* 174 (2013) 27–48. <https://doi.org/10.1007/s11214-012-9935-8>.
- [31] G. Di Achille, B.M. Hynek, Ancient ocean on Mars supported by global distribution of deltas and valleys, *Nat. Geosci.* 3 (2010) 459–463. <https://doi.org/10.1038/ngeo891>.
- [32] M.H. Carr, J.W. Head, Geologic history of Mars, *Earth Planet. Sci. Lett.* 294 (2010) 185–203. <https://doi.org/10.1016/j.epsl.2009.06.042>.
- [33] A.S. Khayat, G.L. Villanueva, M.J. Mumma, A.T. Tokunaga, A search for SO<sub>2</sub>, H<sub>2</sub>S and SO above Tharsis and Syrtis volcanic districts on Mars using ground-based high-resolution submillimeter spectroscopy, *Icarus*. 253 (2015) 130–141. <https://doi.org/10.1016/j.icarus.2015.02.028>.

- [34] R. Sullivan, D. Banfield, J.F. Bell, W. Calvin, D. Fike, M. Golombek, R. Greeley, J. Grotzinger, K. Herkenhoff, D. Jerolmack, M. Malin, D. Ming, L.A. Soderblom, S.W. Squyres, S. Thompson, W.A. Watters, C.M. Weitz, A. Yen, Aeolian processes at the Mars Exploration Rover Meridiani Planum landing site, *Nature*. 436 (2005) 58–61.  
<https://doi.org/10.1038/nature03641>.
- [35] A. Mittelholz, C.L. Johnson, J.M. Feinberg, B. Langlais, R.J. Phillips, Timing of the martian dynamo: New constraints for a core field 4.5 and 3.7 Ga ago, *Sci. Adv.* 6 (2020) 1–8.  
<https://doi.org/10.1126/sciadv.aba0513>.
- [36] S. Ruhunusiri, J.S. Halekas, J.P. McFadden, J.E.P. Connerney, J.R. Espley, Y. Harada, R. Livi, K. Seki, C. Mazelle, D. Brain, T. Hara, G.A. DiBraccio, D.E. Larson, D.L. Mitchell, B.M. Jakosky, H. Hasegawa, MAVEN observations of partially developed Kelvin-Helmholtz vortices at Mars, *Geophys. Res. Lett.* 43 (2016) 4763–4773.  
<https://doi.org/10.1002/2016GL068926>.
- [37] S.C. Werner, B.A. Ivanov, G. Neukum, Theoretical analysis of secondary cratering on Mars and an image-based study on the Cerberus Plains, *Icarus*. 200 (2009) 406–417.  
<https://doi.org/10.1016/j.icarus.2008.10.011>.
- [38] H.B. Franz, P.R. Mahaffy, C.R. Webster, G.J. Flesch, E. Raaen, C. Freissinet, S.K. Atreya, C.H. House, A.C. McAdam, C.A. Knudson, P.D. Archer, J.C. Stern, A. Steele, B. Sutter, J.L. Eigenbrode, D.P. Glavin, J.M.T. Lewis, C.A. Malespin, M. Millan, D.W. Ming, R. Navarro-González, R.E. Summons, Indigenous and exogenous organics and surface–atmosphere cycling inferred from carbon and oxygen isotopes at Gale crater, *Nat. Astron.* (2020).  
<https://doi.org/10.1038/s41550-019-0990-x>.
- [39] M.P. Callahan, M.G. Martin, A.S. Burton, D.P. Glavin, J.P. Dworkin, Amino acid analysis in micrograms of meteorite sample by nanoliquid chromatography-high-resolution mass spectrometry, *J. Chromatogr. A*. 1332 (2014) 30–34.  
<https://doi.org/10.1016/j.chroma.2014.01.032>.
- [40] Z. Martins, O. Botta, M.L. Fogel, M.A. Sephton, D.P. Glavin, J.S. Watson, J.P. Dworkin, A.W. Schwartz, P. Ehrenfreund, Extraterrestrial nucleobases in the Murchison meteorite, *Earth Planet. Sci. Lett.* 270 (2008) 130–136. <https://doi.org/10.1016/j.epsl.2008.03.026>.
- [41] R. Hayatsu, M.H. Studier, L.P. Moore, E. Anders, Purines and triazines in the Murchison meteorite, *Geochim. Cosmochim. Acta*. 39 (1975) 471–488. [https://doi.org/10.1016/0016-7037\(75\)90101-5](https://doi.org/10.1016/0016-7037(75)90101-5).

- [42] G. Cooper, N. Kimmich, W. Belisle, J. Sarinana, K. Brabham, L. Garrel, Carbonaceous meteorites as a source of sugar-related organic compounds for the early Earth, *Nature*. 414 (2001) 879–883. <https://doi.org/10.1038/414879a>.
- [43] Y.I. Yashin, A.Y. Yashin, Miniaturization of Gas-Chromatographic Instruments, *J. Anal. Chem.* 56 (2001) 902–914.
- [44] D. Meunier, R. Sternberg, F. Mettetal, A. Buch, D. Coscia, C. Szopa, C. Rodier, P. Coll, M. Cabanec, F. Raulin, A laboratory pilot for in situ analysis of refractory organic matter in Martian soil by gas chromatography-mass spectrometry, *Adv. Sp. Res.* 39 (2007) 337–344. <https://doi.org/10.1016/j.asr.2005.05.008>.
- [45] P. Schmitt-Kopplin, Z. Gabelica, R.D. Gougeon, A. Fekete, B. Kanawati, M. Harir, I. Gebefuegi, G. Eckel, N. Hertkorn, High molecular diversity of extraterrestrial organic matter in Murchison meteorite revealed 40 years after its fall, *Proc. Natl. Acad. Sci. U. S. A.* 107 (2010) 2763–2768. <https://doi.org/10.1073/pnas.0912157107>.
- [46] Z. Martins, Q.H.S. Chan, L. Bonal, A. King, H. Yabuta, Organic Matter in the Solar System—Implications for Future on-Site and Sample Return Missions, *Space Sci. Rev.* 216 (2020) 1–3. <https://doi.org/10.1007/s11214-020-00679-6>.
- [47] L.B. Browning, H.Y. McSween, M.E. Zolensky, Correlated alteration effects in CM carbonaceous chondrites, *Geochim. Cosmochim. Acta.* 60 (1996) 2621–2633. [https://doi.org/10.1016/0016-7037\(96\)00121-4](https://doi.org/10.1016/0016-7037(96)00121-4).
- [48] E.E. Palmer, D.S. Lauretta, Aqueous alteration of kamacite in CM chondrites, *Meteorit. Planet. Sci.* 46 (2011) 1587–1607. <https://doi.org/10.1111/j.1945-5100.2011.01251.x>.
- [49] V. Vinogradoff, C. Le Guillou, S. Bernard, L. Binet, P. Cartigny, A.J. Brearley, L. Remusat, Paris vs. Murchison: Impact of hydrothermal alteration on organic matter in CM chondrites, *Geochim. Cosmochim. Acta.* 212 (2017) 234–252. <https://doi.org/10.1016/j.gca.2017.06.009>.
- [50] C.R. Webster, P.R. Mahaffy, S.K. Atreya, G.J. Flesch, M.A. Mischna, P.Y. Meslin, K.A. Farley, P.G. Conrad, L.E. Christensen, A.A. Pavlov, J. Martín-Torres, M.P. Zorzano, T.H. McConnochie, T. Owen, J.L. Eigenbrode, D.P. Glavin, A. Steele, C.A. Malespin, P.D. Archer, B. Sutter, P. Coll, C. Freissinet, C.P. McKay, J.E. Moores, S.P. Schwenzer, J.C. Bridges, R. Navarro-Gonzalez, R. Gellert, M.T. Lemmon, Mars methane detection and variability at Gale crater, *Science* (80-. ). 347 (2015) 415–417. <https://doi.org/10.1126/science.1261713>.
- [51] J.L. Eigenbrode, R.E. Summons, A. Steele, C. Freissinet, M. Millan, R. Navarro-gonzález, B.

- Sutter, A.C. Mcadam, P.G. Conrad, J.A. Hurowitz, J.P. Grotzinger, S. Gupta, H.B. Franz, D.P. Glavin, P.D. Archer, P.R. Mahaffy, P.G. Conrad, J.A. Hurowitz, J.P. Grotzinger, S. Gupta, D.W. Ming, D.Y. Sumner, C. Szopa, C. Malespin, A. Buch, P. Coll, Organic matter preserved in 3-billion-year-old mudstones at Gale crater, Mars, *Science* (80-. ). 360 (2018) 1096–1101. <https://doi.org/10.1126/science.aas9185>.
- [52] J. Heinz, D. Schulze-Makuch, Thiophenes on mars: Biotic or abiotic origin?, *Astrobiology*. 20 (2020) 552–561. <https://doi.org/10.1089/ast.2019.2139>.
- [53] K. Biemann, J. Oro, P. Toulmin, L.E. Orgel, A.O. Nier, D.M. Anderson, P.G. Simmonds, D. Flory, A. V. Diaz, D.R. Rushneck, J.E. Biller, A.L. Lafleur, The search for organic substances and inorganic volatile compounds in the surface of Mars, *J. Geophys. Res.* 82 (1977) 4641–4658. <https://doi.org/10.1029/js082i028p04641>.
- [54] M.H. Hecht, S.P. Kounaves, R.C. Quinn, S.J. West, S.M.M. Young, D.W. Ming, D.C. Catling, B.C. Clark, W. V. Boynton, J. Hoffman, L.P. DeFlores, K. Gospodinova, J. Kapit, P.H. Smith, Detection of perchlorate and the soluble chemistry of martian soil at the phoenix lander site, *Science*. 325 (2009) 64–67. <https://doi.org/10.1126/science.1172466>.
- [55] R. Navarro-González, E. Vargas, J. De La Rosa, A.C. Raga, C.P. McKay, Reanalysis of the Viking results suggests perchlorate and organics at midlatitudes on Mars, *J. Geophys. Res. E Planets*. 115 (2010) 1–11. <https://doi.org/10.1029/2010JE003599>.
- [56] D.P. Glavin, C. Freissinet, K.E. Miller, J.L. Eigenbrode, A.E. Brunner, A. Buch, B. Sutter, P.D. Archer, S.K. Atreya, W.B. Brinckerhoff, M. Cabane, P. Coll, P.G. Conrad, D. Coscia, J.P. Dworkin, H.B. Franz, J.P. Grotzinger, L.A. Leshin, M.G. Martin, C. McKay, D.W. Ming, R. Navarro-González, A. Pavlov, A. Steele, R.E. Summons, C. Szopa, S. Teinturier, P.R. Mahaffy, Evidence for perchlorates and the origin of chlorinated hydrocarbons detected by SAM at the Rocknest aeolian deposit in Gale Crater, *J. Geophys. Res. E Planets*. 118 (2013) 1955–1973. <https://doi.org/10.1002/jgre.20144>.
- [57] C. Freissinet, D.P. Glavin, P.R. Mahaffy, K.E. Miller, J.L. Eigenbrode, R.E. Summons, A.E. Brunner, A. Buch, C. Szopa, P.D. Archer, H.B. Franz, S.K. Atreya, W.B. Brinckerhoff, M. Cabane, P. Coll, P.G. Conrad, D.J. Des Marais, J.P. Dworkin, A.G. Fairén, P. François, J.P. Grotzinger, S. Kashyap, I.L. Kate, L.A. Leshin, C.A. Malespin, M.G. Martin, A.C. Mcadam, D.W. Ming, A.A. Pavlov, B.D. Prats, S.W. Squyres, A. Steele, J.C. Stern, D.Y. Sumner, B. Sutter, M.P. Zorzano, D.J. Des Marais, J.P. Dworkin, A.G. Fairén, P. François, J.P. Grotzinger, S. Kashyap, I.L. Ten Kate, L.A. Leshin, C.A. Malespin, M.G. Martin, F.J. Martin-Torres, A.C. Mcadam, D.W. Ming, R. Navarro-González, A.A. Pavlov, B.D. Prats, S.W. Squyres, A. Steele,

- J.C. Stern, D.Y. Sumner, B. Sutter, M.P. Zorzano, Organic molecules in the Sheepbed Mudstone, Gale Crater, Mars, *J. Geophys. Res. Planets.* 120 (2015) 495–514.  
<https://doi.org/10.1002/2014JE004737>.Received.
- [58] C. Szopa, C. Freissinet, D.P. Glavin, M. Millan, A. Buch, H.B. Franz, R.E. Summons, D.Y. Sumner, B. Sutter, J.L. Eigenbrode, R.H. Williams, R. Navarro-González, M. Guzman, C. Malespin, S. Teinturier, P.R. Mahaffy, M. Cabane, First detections of dichlorobenzene isomers and trichloromethylpropane from organic matter indigenous to Mars mudstone in Gale Crater, Mars: results from the Sample Analysis at Mars Instrument onboard the Curiosity Rover, *Astrobiology.* 20 (2020) 292–306. <https://doi.org/10.1089/ast.2018.1908>.
- [59] M. Guzman, C.P. McKay, R.C. Quinn, C. Szopa, A.F. Davila, R. Navarro-González, C. Freissinet, Identification of chlorobenzene in the Viking gas chromatograph-mass spectrometer data sets: reanalysis of Viking mission data consistent with aromatic organic compounds on Mars, *J. Geophys. Res. Planets.* 123 (2018) 1674–1683. <https://doi.org/10.1029/2018JE005544>.
- [60] A. Buch, I. Belmahdi, C. Szopa, C. Freissinet, D.P. Glavin, M. Millan, R. Summons, D. Coscia, S. Teinturier, J.Y. Bonnet, Y. He, M. Cabane, R. Navarro-Gonzalez, C.A. Malespin, J. Stern, J. Eigenbrode, P.R. Mahaffy, S.S. Johnson, Role of the Tenax® adsorbent in the interpretation of the EGA and GC-MS analyses performed with the sample analysis at Mars in Gale Crater, *J. Geophys. Res. Planets.* 124 (2019) 2819–2851.  
<https://doi.org/10.1029/2019JE005973>.
- [61] D.W. Ming, P.D.A. Jr, D.P. Glavin, J.L. Eigenbrode, H.B. Franz, B. Sutter, A.E. Brunner, J.C. Stern, C. Freissinet, A.C. Mcadam, P.R. Mahaffy, M. Cabane, P. Coll, J.L. Campbell, S.K. Atreya, P.B. Niles, J.F.B. Iii, D.L. Bish, W.B. Brinckerhoff, A. Buch, P.G. Conrad, D.J. Des Marais, B.L. Ehlmann, I. Pradler, S.W. Squyres, R.E. Summons, A. Steele, E.M. Stolper, D.Y. Sumner, J. Klein, MSL Science Team, Volatile and Organic Compositions of Sedimentary Rocks in Yellowknife, *Science.* 343 (2014) 1–10. <https://doi.org/10.1126/science.1245267>.
- [62] M. Millan, C. Szopa, A. Buch, M. Cabane, S. Teinturier, P. Mahaffy, S.S. Johnson, Performance of the SAM gas chromatographic columns under simulated flight operating conditions for the analysis of chlorohydrocarbons on Mars, *J. Chromatogr. A.* 1598 (2019) 183–195. <https://doi.org/10.1016/j.chroma.2019.03.064>.
- [63] B. Sutter, R.C. Quinn, P.D. Archer, D.P. Glavin, T.D. Glotch, S.P. Kounaves, M.M. Osterloo, E.B. Rampe, D.W. Ming, Measurements of oxychlorine species on Mars, *Int. J. Astrobiol.* 16 (2017) 203–217. <https://doi.org/10.1017/S1473550416000057>.

- [64] L.A. Leshin, P.R. Mahaffy, C.R. Webster, M. Cabane, P. Coll, P.G. Conrad, P.D. Archer, S.K. Atreya, A.E. Brunner, A. Buch, J.L. Eigenbrode, G.J. Flesch, H.B. Franz, C. Freissinet, D.P. Glavin, A.C. McAdam, K.E. Miller, D.W. Ming, R. V. Morris, R. Navarro-González, P.B. Niles, T. Owen, R.O. Pepin, S. Squyres, A. Steele, J.C. Stern, R.E. Summons, D.Y. Sumner, B. Sutter, C. Szopa, S. Teinturier, M.G. Trainer, J.J. Wray, J.P. Grotzinger, Volatile, isotope, and organic analysis of martian fines with the Mars curiosity rover, *Science* (80-. ). 341 (2013) 1238937. <https://doi.org/10.1126/science.1238937>.
- [65] S.P. Kounaves, N.A. Chaniotakis, V.F. Chevrier, B.L. Carrier, K.E. Folds, V.M. Hansen, K.M. McElhoney, G.D. O’Neil, A.W. Weber, Identification of the perchlorate parent salts at the Phoenix Mars landing site and possible implications, *Icarus*. 232 (2014) 226–231. <https://doi.org/10.1016/j.icarus.2014.01.016>.
- [66] Fabien Kenig, Luoth Chou, Christopher P. McKay, W. Andrew Jackson, Peter T. Doran, Alison E. Murray, and Christian H. Fritsen, Perchlorate and volatiles of the brine of Lake Vida (Antarctica): Implication for the in situ analysis of Mars sediments, *J. Geophys. Res. Planets*. 121 (2016) 1190–1203. <https://doi.org/10.1002/2014JD021488>.Received.
- [67] P.W. Rundel, M.O. Dillon, B. Palma, H.A. Mooney, S.L. Gulmon, *Aliso: A Journal of Systematic and Evolutionary Botany The Phytogeography and Ecology of the Coastal Atacama and Peruvian Deserts*, *Aliso A J. Syst. Evol. Bot.* 13 (1991). <http://scholarship.claremont.edu/aliso>[http://scholarship.claremont.edu/aliso%0Ahttp://scholarship.claremont.edu/aliso/vol13/iss1/2](http://scholarship.claremont.edu/aliso/vol13/iss1/2%0Ahttp://scholarship.claremont.edu/aliso%0Ahttp://scholarship.claremont.edu/aliso/vol13/iss1/2).
- [68] J.D.A. Clarke, Antiquity of aridity in the Chilean Atacama Desert, *Geomorphology*. 73 (2006) 101–114. <https://doi.org/10.1016/j.geomorph.2005.06.008>.
- [69] C.P. McKay, E.I. Friedmann, B. Gómez-silva, L. Cáceres-villanueva, D.T. Andersen, Temperature and Moisture Conditions for Life in the Extreme Arid Region of the Atacama Desert: Four Years of Observations Including the El Niño of 1997–1998, *Astrobiology*. 3 (2003) 393–406.
- [70] J. Wei, A. Wang, J.L. Lambert, D. Wettergreen, N. Cabrol, K. Warren-Rhodes, K. Zacny, Autonomous soil analysis by the Mars Micro-beam Raman Spectrometer (MMRS) on-board a rover in the Atacama Desert: A terrestrial test for planetary exploration, *J. Raman Spectrosc.* 46 (2015) 810–821. <https://doi.org/10.1002/jrs.4656>.
- [71] J.C. Viennet, S. Bernard, C. Le Guillou, P. Jacquemot, L. Delbes, E. Balan, M. Jaber, Influence of the nature of the gas phase on the degradation of RNA during fossilization processes, *Appl.*

- Clay Sci. 191 (2020) 105616. <https://doi.org/10.1016/j.clay.2020.105616>.
- [72] A.M. Skelley, A.D. Aubrey, P.A. Willis, X. Amashukeli, P. Ehrenfreund, J.L. Bada, F.J. Grunthaner, R.A. Mathies, Organic amine biomarker detection in the Yungay region of the Atacama Desert with the Urey instrument, *J. Geophys. Res. Biogeosciences*. 112 (2007) 1–10. <https://doi.org/10.1029/2006JG000329>.
- [73] J.W. Aerts, A. Riedo, D.J. Melton, S. Martini, J. Flahaut, U.J. Meierhenrich, C. Meinert, I. Myrgorodska, R. Lindner, P. Ehrenfreund, Biosignature Analysis of Mars Soil Analogs from the Atacama Desert: Challenges and Implications for Future Missions to Mars, *Astrobiology*. 20 (2020) 766–784. <https://doi.org/10.1089/ast.2019.2063>.
- [74] L. Sánchez-García, M.A. Fernández-Martínez, M. Moreno-Paz, D. Carrizo, M. García-Villadangos, J.M. Manchado, C.R. Stoker, B. Glass, V. Parro, Simulating Mars Drilling Mission for Searching for Life: Ground-Truthing Lipids and Other Complex Microbial Biomarkers in the Iron-Sulfur Rich Río Tinto Analog, *Astrobiology*. 20 (2020) 1–19. <https://doi.org/10.1089/ast.2019.2101>.
- [75] Y. Blanco, L.A. Rivas, V. Parro, Searching for organic matter on Mars by immunological assays: Detection of mellitic acid in the surface and subsurface of the Atacama Desert terrestrial analog, 7 (2012).
- [76] I.F. Santiago, V.N. Gonçalves, B. Gómez-Silva, A. Galetovic, L.H. Rosa, Fungal diversity in the Atacama Desert, *Antonie van Leeuwenhoek, Int. J. Gen. Mol. Microbiol.* 111 (2018) 1345–1360. <https://doi.org/10.1007/s10482-018-1060-6>.
- [77] M.G.C.A.D. BILLI, *Chroococciopsis* from desert to mars, *Environments*. 1965 (2007) 553–568.
- [78] R. Amils, C. Ellis-Evans, H. Hinghofer-Szalkay, Life in extreme environments, *Life Extrem. Environ.* 409 (2007) 1–450. <https://doi.org/10.1007/978-1-4020-6285-8>.
- [79] K.M. Finstad, A.J. Probst, B.C. Thomas, G.L. Andersen, C. Demergasso, A. Echeverría, R.G. Amundson, J.F. Banfield, Microbial community structure and the persistence of cyanobacterial populations in salt crusts of the hyperarid atacama desert from genome-resolved Metagenomics, *Front. Microbiol.* 8 (2017) 1–10. <https://doi.org/10.3389/fmicb.2017.01435>.
- [80] R. Ruginescu, C. Purcărea, C. Dorador, P. Lavin, R. Cojoc, S. Neagu, I. Lucaci, M. Enache, Exploring the hydrolytic potential of cultured halophilic bacteria isolated from the Atacama Desert, *FEMS Microbiol. Lett.* 366 (2019) 1–9. <https://doi.org/10.1093/femsle/fnz224>.

- [81] W. Stoeckenius, The purple membrane of salt-loving bacteria., *Sci. Am.* 234 (1976) 38–46.
- [82] R. L. Armstrong, Radiogenic isotopes: the case for crustal recycling on a near-steady-state non-continental-growth Earth, *Philos. Trans. R. Soc. London. Ser. A, Math. Phys. Sci.* 301 (1981) 443–472. <https://doi.org/10.1098/rsta.1981.0122>.
- [83] C.K. Robinson, K. Webb, A. Kaur, P. Jaruga, M. Dizdaroglu, N.S. Baliga, A. Place, J. DiRuggiero, A major role for nonenzymatic antioxidant processes in the radioresistance of *Halobacterium salinarum*, *J. Bacteriol.* 193 (2011) 1653–1662. <https://doi.org/10.1128/JB.01310-10>.
- [84] M. Kottemann, A. Kish, C. Iloanusi, S. Bjork, J. DiRuggiero, Physiological responses of the halophilic archaeon *Halobacterium* sp. strain NRC1 to desiccation and gamma irradiation, *Extremophiles.* 9 (2005) 219–227. <https://doi.org/10.1007/s00792-005-0437-4>.
- [85] K. Sankaranarayanan, T.K. Lowenstein, M.N. Timofeeff, B.A. Schubert, J.K. Lum, Characterization of ancient DNA supports long-term survival of haloarchaea, *Astrobiology.* 14 (2014) 553–560. <https://doi.org/10.1089/ast.2014.1173>.
- [86] H. Stan-lotter, C. Gruber, Ch. Radax, *Halococcus dom-browskii* sp. nov., an archaeal isolate from a Permian alpine salt deposit, *Int. J. Syst. Evol. Microbiol.* 52 (2002) 1807–1814. <https://doi.org/10.1099/ijs.0.02278-0.The>.
- [87] H. Stan-lotter, S. Fendrihan, M. Dornmayr-pfaffenhuemer, A. Holzinger, Halophilic life on Mars ?, in: *Geophys. Res. Abstr.*, 2010: p. 4594.
- [88] S. Leuko, P. Rettberg, A.L. Pontifex, B.P. Burns, On the response of halophilic archaea to space conditions, *Life.* 4 (2014) 66–76. <https://doi.org/10.3390/life4010066>.
- [89] C.D. Litchfield, Survival strategies for microorganisms in hypersaline environments and their relevance to life on early Mars, *Meteorit. Planet. Sci.* 33 (1998) 813–819. <https://doi.org/10.1111/j.1945-5100.1998.tb01688.x>.
- [90] G.A. Landis, Martian Water: Are There Extant Halobacteria on Mars?, *Astrobiology.* 1 (2001) 161–164. <https://doi.org/10.1021/cen-v027n032.p2282>.
- [91] A. Oren, R. Elevi Bardavid, L. Mana, Perchlorate and halophilic prokaryotes: Implications for possible halophilic life on Mars, *Extremophiles.* 18 (2014) 75–80. <https://doi.org/10.1007/s00792-013-0594-9>.
- [92] J. Heinz, T. Krahn, D. Schulze-Makuch, A new record for microbial perchlorate tolerance:



- fungal growth in  $\text{NaClO}_4$  brines and its implications for putative life on Mars, *Life*. 10 (2020) 4–11. <https://doi.org/10.3390/life10050053>.
- [93] D.C. Fernández-Remolar, G. Chong-Díaz, M. Ruíz-Bermejo, M. Harir, P. Schmitt-Kopplin, D. Tziotis, D. Gómez-Ortíz, M. García-Villadangos, M.P. Martín-Redondo, F. Gómez, J.A. Rodríguez-Manfredi, M. Moreno-Paz, G. De Diego-Castilla, A. Echeverría, V.N. Urtuvia, Y. Blanco, L. Rivas, M.R.M. Izawa, N.R. Banerjee, C. Demergasso, V. Parro, Molecular preservation in halite- and perchlorate-rich hypersaline subsurface deposits in the Salar Grande basin (Atacama Desert, Chile): Implications for the search for molecular biomarkers on Mars, *J. Geophys. Res. Biogeosciences*. 118 (2013) 922–939. <https://doi.org/10.1002/jgrg.20059>.
- [94] V.J. Laye, S. Dassarma, An Antarctic Extreme Halophile and Its Polyextremophilic Enzyme: Effects of Perchlorate Salts, *Astrobiology*. 18 (2018) 412–418. <https://doi.org/10.1089/ast.2017.1766>.
- [95] J.A. Coker, P. DasSarma, J. Kumar, J.A. Müller, S. DasSarma, Transcriptional profiling of the model Archaeon *Halobacterium* sp. NRC-1: responses to changes in salinity and temperature, *Saline Systems*. 3 (2007) 6. <https://doi.org/10.1186/1746-1448-3-6>.
- [96] H.D. Shukla, Proteomic analysis of acidic chaperones, and stress proteins in extreme halophile *Halobacterium* NRC-I: A comparative proteomic approach to study heat shock response, *Proteome Sci*. 4 (2006) 1–11. <https://doi.org/10.1186/1477-5956-4-6>.
- [97] P. DasSarma, R.C. Zamora, J.A. Müller, S. Dassarma, Genome-wide responses of the model archaeon *Halobacterium* sp. strain NRC-1 to oxygen limitation, *J. Bacteriol*. 194 (2012) 5530–5537. <https://doi.org/10.1128/JB.01153-12>.
- [98] K. Whitehead, A. Kish, M. Pan, A. Kaur, D.J. Reiss, N. King, L. Hohmann, J. DiRuggiero, N.S. Baliga, An integrated systems approach for understanding cellular responses to gamma radiation, *Mol. Syst. Biol*. 2 (2006). <https://doi.org/10.1038/msb4100091>.
- [99] L.C. DeVeaux, J.A. Müller, J. Smith, J. Petrisko, D.P. Wells, S. DasSarma, Extremely radiation-resistant mutants of a halophilic archaeon with increased single-stranded DNA-binding protein (RPA) gene expression, *Radiat. Res*. 168 (2007) 507–514. <https://doi.org/10.1667/RR0935.1>.
- [100] N.S. Baliga, S.J. Bjork, R. Bonneau, M. Pan, C. Iloanusi, M.C.H. Kottmann, L. Hood, J. DiRuggiero, Systems level insights into the stress response to UV radiation in the halophilic archaeon *Halobacterium* NRC-1, *Genome Res*. 14 (2004) 1025–1035. <https://doi.org/10.1101/gr.1993504>.

- [101] S. McCready, J. Müller, I. Boubriak, B. Berquist, W. Ng, S. DasSarma, UV irradiation induces homologous recombination genes in the model archaeon, *Halobacterium* sp. NRC-1., *Saline Systems*. 1 (2005) 3. <https://doi.org/10.1186/1746-1448-1-3>.
- [102] A. Irimia, C. Ebel, D. Madern, S.B. Richard, L.W. Cosenza, G. Zaccai, F.M.D. Vellieux, The oligomeric states of *Haloarcula marismortui* malate dehydrogenase are modulated by solvent components as shown by crystallographic and biochemical studies, *J. Mol. Biol.* 326 (2003) 859–873. [https://doi.org/10.1016/S0022-2836\(02\)01450-X](https://doi.org/10.1016/S0022-2836(02)01450-X).
- [103] C. Ebel, L. Costenaro, M. Pascu, P. Faou, B. Kernel, F. Proust-De Martin, G. Zaccai, Solvent interactions of halophilic malate dehydrogenase, *Biochemistry*. 41 (2002) 13234–13244. <https://doi.org/10.1021/bi0258290>.
- [104] L. Costenaro, G. Zaccai, C. Ebel, Link between protein-solvent and weak protein-protein interactions gives insight into halophilic adaptation, *Biochemistry*. 41 (2002) 13245–13252. <https://doi.org/10.1021/bi025830z>.
- [105] P. Vauclare, F. Natali, J.P. Kleman, G. Zaccai, B. Franzetti, Surviving salt fluctuations: stress and recovery in *Halobacterium salinarum*, an extreme halophilic Archaeon, *Sci. Rep.* 10 (2020) 1–10. <https://doi.org/10.1038/s41598-020-59681-1>.
- [106] A. Kish, G. Kirkali, C. Robinson, R. Rosenblatt, P. Jaruga, M. Dizdaroglu, J. Diruggiero, Salt shield: Intracellular salts provide cellular protection against ionizing radiation in the halophilic archaeon, *Halobacterium salinarum* NRC-1, *Environ. Microbiol.* 11 (2009) 1066–1078. <https://doi.org/10.1111/j.1462-2920.2008.01828.x>.
- [107] A. Kish, P.L. Griffin, K.L. Rogers, M.L. Fogel, R.J. Hemley, A. Steele, High-pressure tolerance in *Halobacterium salinarum* NRC-1 and other non-piezophilic prokaryotes, *Extremophiles*. 16 (2012) 355–361. <https://doi.org/10.1007/s00792-011-0418-8>.
- [108] I. Siotis, E. Aloupi-Siotis, Experimental interpretation of the presence of female genitalia in Early Bronze Age ‘frying pan’-type ceramics from the Cyclades\*, *Archaeometry*. 62 (2020) 285–296. <https://doi.org/10.1111/arc.12525>.
- [109] T. Saito, H. Terato, O. Yamamoto, Pigments of *Rubrobacter radiotolerans*, *Arch. Microbiol.* 162 (1994) 414–421. <https://doi.org/10.1007/BF00282106>.
- [110] A.C. Ferreira, M.F. Nobre, E. Moore, F.A. Rainey, J.R. Battista, M.S. Da Costa, Characterization and radiation resistance of new isolates of *Rubrobacter radiotolerans* and *Rubrobacter xylanophilus*, *Extremophiles*. 3 (1999) 235–238.

<https://doi.org/10.1007/s007920050121>.

- [111] N. Stivaletta, R. Barbieri, D. Billi, Microbial Colonization of the Salt Deposits in the Driest Place of the Atacama Desert (Chile), *Orig. Life Evol. Biosph.* 42 (2012) 187–200.  
<https://doi.org/10.1007/s11084-012-9289-y>.
- [112] C.S. Cockell, D.S.S. Lim, S. Braham, P. Lee, B. Clancey, Exobiological protocol and laboratory for the human exploration of Mars - Lessons from a polar impact crater, *JBIS - J. Br. Interplanet. Soc.* 56 (2003) 74–86.
- [113] H.D. Smith, M. Baqué, A.G. Duncan, C.R. Lloyd, C.P. McKay, D. Billi, Comparative analysis of cyanobacteria inhabiting rocks with different light transmittance in the Mojave Desert: A Mars terrestrial analogue, *Int. J. Astrobiol.* 13 (2014) 271–277.  
<https://doi.org/10.1017/S1473550414000056>.
- [114] E. Imre Friedmann, R. Ocampo-Friedmann, A primitive cyanobacterium as pioneer microorganism for terraforming Mars, *Adv. Sp. Res.* 15 (1995) 243–246.  
[https://doi.org/10.1016/S0273-1177\(99\)80091-X](https://doi.org/10.1016/S0273-1177(99)80091-X).
- [115] C.S. Cockell, A.C. Schuerger, D. Billi, E.I. Friedmann, C. Panitz, Effects of a Simulated Martian UV Flux on the Cyanobacterium, *Chroococcidiopsis* sp. 029, *Astrobiology.* 5 (2005).
- [116] M. Potts, Mechanisms of desiccation tolerance in cyanobacteria, *Eur. J. Phycol.* 34 (1999) 319–328. <https://doi.org/10.1080/09670269910001736382>.
- [117] D. Billi, M. Baqué, H.D. Smith, C.P. McKay, Cyanobacteria from Extreme Deserts to Space, *Adv. Microbiol.* 03 (2013) 80–86. <https://doi.org/10.4236/aim.2013.36a010>.
- [118] M.G. Caiola, D. Billi, E.I. Friedmann, Effect of desiccation on envelopes of the cyanobacterium *chroococcidiopsis* sp. (chroococcales), *Eur. J. Phycol.* 31 (1996) 97–105.  
<https://doi.org/10.1080/09670269600651251a>.
- [119] D.J. Wright, S.C. Smith, V. Joardar, S. Scherer, J. Jervis, A. Warren, R.F. Helm, M. Potts, UV irradiation and desiccation modulate the three-dimensional extracellular matrix of *Nostoc commune* (Cyanobacteria), *J. Biol. Chem.* 280 (2005) 40271–40281.  
<https://doi.org/10.1074/jbc.M505961200>.
- [120] J.H. Crowe, Trehalose As a “Chemical Chaperone,” in: *Mol. Asp. Stress Response Chaperones, Membr. Networks*, 2007: pp. 143–158. [https://doi.org/10.1007/978-0-387-39975-1\\_13](https://doi.org/10.1007/978-0-387-39975-1_13).

- [121] L.M. Crowe, J.H. Crowe, Anhydrobiosis: A strategy for survival, *Adv. Sp. Res.* 12 (1992) 239–247. [https://doi.org/10.1016/0273-1177\(92\)90178-Z](https://doi.org/10.1016/0273-1177(92)90178-Z).
- [122] F.S. Lee, R. Shapiro, B.L. Vallee, Tight-Binding Inhibition of Angiogenin and Ribonuclease A by Placental Ribonuclease Inhibitor, *Biochemistry.* 28 (1989) 225–230. <https://doi.org/10.1021/bi00427a031>.
- [123] J.F. Carpenter, J.H. Crowe, An infrared spectroscopic study of the interactions of carbohydrates with dried proteins, *Biochemistry.* 28 (1989) 3916–3922. <https://doi.org/10.1021/bi00435a044>.
- [124] H. Stan-Lotter, S. Fendrihan, Desert cyanobacteria: potential for space and Earth applications, in: *Adapt. Microb. Life to Environ. Extrem. Nov. Res. Results Appl. Second Ed.*, 2017: pp. 1–342. <https://doi.org/10.1007/978-3-319-48327-6>.
- [125] M. Musilova, G. Wright, J.M. Ward, L.R. Dartnell, Isolation of Radiation-Resistant Bacteria from Mars Analog Antarctic Dry Valleys by Preselection, and the Correlation between Radiation and Desiccation Resistance, *Astrobiology.* 15 (2015) 1076–1090. <https://doi.org/10.1089/ast.2014.1278>.
- [126] M.J. Daly, Death by protein damage in irradiated cells, *DNA Repair (Amst).* 11 (2012) 12–21. <https://doi.org/10.1016/j.dnarep.2011.10.024>.
- [127] M.J. Daly, A new perspective on radiation resistance based on *Deinococcus radiodurans*, *Nat. Rev. Microbiol.* 7 (2009) 237–245. <https://doi.org/10.1038/nrmicro2073>.
- [128] Christopher P. Long and Maciek R. Antoniewicz, Quantifying Biomass Composition by Gas Chromatography/ Mass Spectrometry, *Anal Chem.* 86 (2014) 9423–9427. <https://doi.org/10.1016/j.physbeh.2017.03.040>.
- [129] Geoffrey M. Cooper, *the Cell Molecular Approach*, 2006. <https://doi.org/10.1017/CBO9781107415324.004>.
- [130] R. Zhu, G.J.M. Versteegh, K.U. Hinrichs, Detection of microbial biomass in subseafloor sediment by pyrolysis-GC/MS, *J. Anal. Appl. Pyrolysis.* 118 (2016) 175–180. <https://doi.org/10.1016/j.jaap.2016.02.002>.
- [131] J.P. Dworzanski, L. Berwald, H.L.C. Meuzelaar, Pyrolytic methylation-gas chromatography of whole bacterial cells for rapid profiling of cellular fatty acids, *Appl. Environ. Microbiol.* 56 (1990) 1717–1724. <https://doi.org/10.1128/AEM.56.6.1717-1724.1990>.
- [132] J.P. Dworzanski, L. Berwald, W.H. McClennen, H.L.C. Meuzelaar, Mechanistic aspects of the

- pyrolytic methylation and transesterification of bacterial cell wall lipids, *J. Anal. Appl. Pyrolysis*. 21 (1991) 221–232. [https://doi.org/10.1016/0165-2370\(91\)80027-6](https://doi.org/10.1016/0165-2370(91)80027-6).
- [133] Y. Ishida, S. Isomura, S. Tsuge, H. Ohtani, T. Sekino, M. Nakanishi, T. Kimoto, Discriminative analysis of zooplankton individuals by pyrolysis-gas chromatography combined with on-line methylation, *Analyst*. 121 (1996) 853–856. <https://doi.org/10.1039/an9962100853>.
- [134] F. Basile, M.B. Beverly, K.J. Voorhees, T.L. Hadfield, J.M. Challinor, Pathogenic bacteria: Their detection and differentiation by rapid lipid profiling with pyrolysis mass spectrometry, *TrAC - Trends Anal. Chem.* 17 (1998) 15–24. [https://doi.org/10.1016/0165-2370\(91\)80059-H](https://doi.org/10.1016/0165-2370(91)80059-H).
- [135] L. Krásný, R. Hynek, I. Hochel, Identification of bacteria using mass spectrometry techniques, *Int. J. Mass Spectrom.* 353 (2013) 67–79. <https://doi.org/10.1016/j.ijms.2013.04.016>.
- [136] S.S. Johnson, M. Millan, H. Graham, K.C. Benison, A.J. Williams, A. McAdam, C.A. Knudson, S. Andrejkovičová, C. Achilles, Lipid Biomarkers in Ephemeral Acid Salt Lake Mudflat/Sandflat Sediments: Implications for Mars, *Astrobiology*. 20 (2020) 167–178. <https://doi.org/10.1089/ast.2017.1812>.
- [137] W.N. Millar, L.E. Casida, Evidence for muramic acid in soil., *Can. J. Microbiol.* 16 (1970) 299–304. <https://doi.org/10.1139/m70-054>.
- [138] T.H. Evans, H. Hibbert, *Bacterial Polysaccharides*, ACADEMIC PRESS, INC., 1946. [https://doi.org/10.1016/S0096-5332\(08\)60011-9](https://doi.org/10.1016/S0096-5332(08)60011-9).
- [139] G. Guggenberger, S.D. Frey, J. Six, K. Paustian, E.T. Elliott, Bacterial and Fungal Cell-Wall Residues in Conventional and No-Tillage Agroecosystems, *Soil Sci. Soc. Am. J.* 63 (1999) 1188–1198. <https://doi.org/10.2136/sssaj1999.6351188x>.
- [140] J.R. GOLECKI, Studies on Ultrastructure and Composition of the Cyanobacterium *Anacystis nidulans*, *Arch. Microbiol.* 114 (1977) 35–41.
- [141] J.M. Shick, W.C. Dunlap, Mycosporine-like amino acids and related gadusols: Biosynthesis, accumulation, and UV-protective functions in aquatic organisms, *Annu. Rev. Physiol.* 64 (2002) 223–262. <https://doi.org/10.1146/annurev.physiol.64.081501.155802>.
- [142] P. Gabani, O. V. Singh, Radiation-resistant extremophiles and their potential in biotechnology and therapeutics, *Appl. Microbiol. Biotechnol.* 97 (2013) 993–1004. <https://doi.org/10.1007/s00253-012-4642-7>.
- [143] F. de la Coba, J. Aguilera, M. V. de Gálvez, M. Álvarez, E. Gallego, F.L. Figueroa, E. Herrera,

- Prevention of the ultraviolet effects on clinical and histopathological changes, as well as the heat shock protein-70 expression in mouse skin by topical application of algal UV-absorbing compounds, *J. Dermatol. Sci.* 55 (2009) 161–169.  
<https://doi.org/10.1016/j.jdermsci.2009.06.004>.
- [144] Y. Dong, F. Sun, Z. Ping, Q. Ouyang, L. Qian, DNA storage : research landscape and future prospects, *Natl. Sci. Rev.* (2020) 0–1.
- [145] B.K.D. Pearce, R.E. Pudritz, D.A. Semenov, T.K. Henning, Origin of the RNA world: The fate of nucleobases in warm little ponds, *Proc. Natl. Acad. Sci. U. S. A.* 114 (2017) 11327–11332.  
<https://doi.org/10.1073/pnas.1710339114>.
- [146] G. Dandanell, B. Hove-Jensen, M. Willemoës, K.F. Jensen, Nucleotides, Nucleosides, and Nucleobases, *EcoSal Plus.* 3 (2008). <https://doi.org/10.1128/ecosalplus.3.6.2>.
- [147] K.A. Jacobson, M.F. Jarvis, M. Williams, Purine and pyrimidine (P2) receptors as drug targets, *J. Med. Chem.* 45 (2002) 4057–4093. <https://doi.org/10.1021/jm020046y>.
- [148] D.B. Davies, Conformations of nucleosides and nucleotides, *Prog. Nucl. Magn. Reson. Spectrosc.* 12 (1978) 135–225. [https://doi.org/10.1016/0079-6565\(78\)80006-5](https://doi.org/10.1016/0079-6565(78)80006-5).
- [149] S. Steenken, Purine Bases, Nucleosides, and Nucleotides: Aqueous Solution Redox Chemistry and Transformation Reactions of Their Radical Cations and e<sup>-</sup> and OH Adducts, *Chem. Rev.* 89 (1989) 503–520. <https://doi.org/10.1021/cr00093a003>.
- [150] C. Altona, M. Sundaralingam, Conformational analysis of the sugar ring in nucleosides and nucleotides. Improved method for the interpretation of proton magnetic resonance coupling constants, *J. Am. Chem. Soc.* 95 (1973) 2333–2344. <https://doi.org/10.1021/ja00788a038>.
- [151] C. Altona, M. Sundaralingam, Conformational Analysis of the Sugar Ring in Nucleosides and Nucleotides. a New Description Using the Concept of Pseudorotation, *J. Am. Chem. Soc.* 94 (1972) 8205–8212. <https://doi.org/10.1021/ja00778a043>.
- [152] Forrest S. Anderson and Robert C. Murphy, Isocratic Separation of some purine nucleotide, nucleoside, and base metabolites from biological extracts by high-performance liquid chromatography, *J. Chromatogr.* 121 (1976) 251–262.
- [153] L.P. Turner, Characterization of nucleotides and nucleosides by pyrolysis-gas chromatography, *Anal. Biochem.* 28 (1969) 288–294. [https://doi.org/10.1016/0003-2697\(69\)90181-X](https://doi.org/10.1016/0003-2697(69)90181-X).
- [154] B. Peng, H. Li, X.X. Peng, Functional metabolomics: from biomarker discovery to metabolome

- reprogramming, *Protein Cell*. 6 (2015) 628–637. <https://doi.org/10.1007/s13238-015-0185-x>.
- [155] S. ichiro Fujii, K. Inagaki, K. Chiba, A. Takatsu, Quantification of phosphorus in DNA using capillary electrophoresis hyphenated with inductively coupled plasma mass spectrometry, *J. Chromatogr. A*. 1217 (2010) 7921–7925. <https://doi.org/10.1016/j.chroma.2010.10.066>.
- [156] S. Neubauer, A. Rugova, D.B. Chu, H. Drexler, A. Ganner, M. Sauer, D. Mattanovich, S. Hann, G. Koellensperger, Mass spectrometry based analysis of nucleotides, nucleosides, and nucleobases-application to feed supplements, *Anal. Bioanal. Chem.* 404 (2012) 799–808. <https://doi.org/10.1007/s00216-012-6170-9>.
- [157] S. ichiro Fujii, K. Inagaki, A. Takatsu, T. Yarita, K. Chiba, Determination of phosphorus using capillary electrophoresis and micro-high-performance liquid chromatography hyphenated with inductively coupled plasma mass spectrometry for the quantification of nucleotides, *J. Chromatogr. A*. 1216 (2009) 7488–7492. <https://doi.org/10.1016/j.chroma.2009.05.019>.
- [158] S. Guo, J.A. Duan, D. Qian, H. Wang, Y. Tang, Y. Qian, D. Wu, S. Su, E. Shang, Hydrophilic interaction ultra-high performance liquid chromatography coupled with triple quadrupole mass spectrometry for determination of nucleotides, nucleosides and nucleobases in ziziphus plants, *J. Chromatogr. A*. 1301 (2013) 147–155. <https://doi.org/10.1016/j.chroma.2013.05.074>.
- [159] C. Maggiori, J. Stromberg, Y. Blanco, J. Goordial, E. Cloutis, M. García-Villadangos, V. Parro, L. Whyte, The Limits, Capabilities, and Potential for Life Detection with MinION Sequencing in a Paleochannel Mars Analog, *Astrobiology*. 20 (2020) 1–19. <https://doi.org/10.1089/ast.2018.1964>.
- [160] T.D. Niederberger, N.N. Perreault, S. Tille, B.S. Lollar, G. Lacrampe-Couloume, D. Andersen, C.W. Greer, W. Pollard, L.G. Whyte, Microbial characterization of a subzero, hypersaline methane seep in the Canadian high arctic, *ISME J.* 4 (2010) 1326–1339. <https://doi.org/10.1038/ismej.2010.57>.
- [161] C.T. Adcock, E.M. Hausrath, P.M. Forster, Readily available phosphate from minerals in early aqueous environments on Mars, *Nat. Geosci.* 6 (2013) 824–827. <https://doi.org/10.1038/ngeo1923>.
- [162] F.H. Westheimer, Why Nature Chose Phosphates, *Science*. 235 (1987) 1173–1178.
- [163] T. Satyanarayana, A. Prakash, B.N. Johri, *Microorganisms in environmental management: Microbes and environment*, 2012. <https://doi.org/10.1007/978-94-007-2229-3>.
- [164] A. Ellery, D. Wynn-Williams, *Methodologies and Techniques for Detecting Extraterrestrial*

- (Microbial) Life Why Raman Spectroscopy on Mars?—A Case of the Right Tool for the Right Job, *Astrobiology*. 3 (2003) 565–579.
- [165] J. Parnell, D. Cullen, M.R. Sims, S. Bowden, C.S. Cockell, R. Court, P. Ehrenfreund, F. Gaubert, W. Grant, V. Parro, M. Rohmer, M. Sephton, H. Stan-Lother, A. Steele, J. Toporski, J. Vago, Searching for life on Mars: Selection of molecular targets for ESA's Aurora ExoMars mission, *Astrobiology*. 7 (2007) 578–604. <https://doi.org/10.1089/ast.2006.0110>.
- [166] A. Oren, Characterization of Pigments of Prokaryotes and Their Use in Taxonomy and Classification, Elsevier Ltd, 2011. <https://doi.org/10.1016/B978-0-12-387730-7.00012-7>.
- [167] W. Children, Chapter 5 Pigments of Halophilic Microorganisms, in: *Growth* (Lakeland), 2001: pp. 173–206.
- [168] H.A. Frank, V. Chynwat, R.Z.B. Desamero, R. Farhoosh, J. Erickson, J. Bautista, On the photophysics and photochemical properties of carotenoids and their role as light-harvesting pigments in photosynthesis, *Pure Appl. Chem.* 69 (1997) 2117–2124. <https://doi.org/10.1351/pac199769102117>.
- [169] N.I. Krinsky, The biologic properties of carotenoids, *Pure Appl. Chem.* 66 (1994) 1003–1010. [https://doi.org/10.1016/0375-9474\(74\)90146-8](https://doi.org/10.1016/0375-9474(74)90146-8).
- [170] M. Baqué, A. Napoli, C. Fagliarone, R. Moeller, J.P. de Vera, D. Billi, Carotenoid raman signatures are better preserved in dried cells of the desert cyanobacterium *Chroococcidiopsis* than in hydrated counterparts after high-dose gamma irradiation, *Life*. 10 (2020) 1–13. <https://doi.org/10.3390/life10060083>.
- [171] F. Imperi, G. Caneva, L. Cancellieri, M.A. Ricci, A. Sodo, P. Visca, The bacterial aetiology of rosy discoloration of ancient wall paintings, *Environ. Microbiol.* 9 (2007) 2894–2902. <https://doi.org/10.1111/j.1462-2920.2007.01393.x>.
- [172] H. Morillas, M. Maguregui, I. Marcaida, J. Trebolazabala, I. Salcedo, J.M. Madariaga, Characterization of the main colonizer and biogenic pigments present in the red biofilm from La Galea Fortress sandstone by means of microscopic observations and Raman imaging, *Microchem. J.* 121 (2015) 48–55. <https://doi.org/10.1016/j.microc.2015.02.005>.
- [173] J. Jehlička, H.G.M. Edwards, K. Osterrothová, J. Novotná, L. Nedbalová, J. Kopecký, I. Němec, A. Oren, Potential and limits of Raman spectroscopy for carotenoid detection in microorganisms: Implications for astrobiology, *Philos. Trans. R. Soc. A Math. Phys. Eng. Sci.* 372 (2014). <https://doi.org/10.1098/rsta.2014.0199>.



- [174] B.F. Lutnaes, A. Oren, S. Liaaen-Jensen, New C40-carotenoid acyl glycoside as principal carotenoid in *Salinibacter ruber*, an extremely halophilic eubacterium, *J. Nat. Prod.* 65 (2002) 1340–1343. <https://doi.org/10.1021/np020125c>.
- [175] C.P. Marshall, S. Leuko, C.M. Coyle, M.R. Walter, B.P. Burns, B.A. Neilan, Carotenoid analysis of halophilic archaea by resonance Raman spectroscopy, *Astrobiology.* 7 (2007) 631–643. <https://doi.org/10.1089/ast.2006.0097>.
- [176] J. Jehlička, A. Oren, Raman spectroscopy in halophile research, *Front. Microbiol.* 4 (2013) 1–7. <https://doi.org/10.3389/fmicb.2013.00380>.
- [177] M.T.A. Alexandre, K. Gundermann, A.A. Pascal, R. Van Grondelle, C. Büchel, B. Robert, Probing the carotenoid content of intact *Cyclotella* cells by resonance Raman spectroscopy, *Photosynth. Res.* 119 (2014) 273–281. <https://doi.org/10.1007/s11120-013-9942-y>.
- [178] S. Fendrihan, M. Musso, H. Stan-Lotter, Raman spectroscopy as a potential method for the detection of extremely halophilic archaea embedded in halite in terrestrial and possibly extraterrestrial samples, *J. Raman Spectrosc.* 40 (2009) 1996–2003. <https://doi.org/10.1002/jrs.2357>.
- [179] A. Garrido Frenich, M.E. Hernández Torres, A. Belmonte Vega, J.L. Martínez Vidal, P. Plaza Bolaños, Determination of ascorbic acid and carotenoids in food commodities by liquid chromatography with mass spectrometry detection, *J. Agric. Food Chem.* 53 (2005) 7371–7376. <https://doi.org/10.1021/jf050973o>.
- [180] M. Manikandan, N. Hasan, H.F. Wu, Rapid detection of haloarchaeal carotenoids via liquid-liquid microextraction enabled direct TLC MALDI-MS, *Talanta.* 107 (2013) 167–175. <https://doi.org/10.1016/j.talanta.2013.01.005>.
- [181] P. Sricharoen, N. Limchoowong, S. Techawongstien, S. Chanthai, A novel extraction method for  $\beta$ -carotene and other carotenoids in fruit juices using air-assisted, low-density solvent-based liquid-liquid microextraction and solidified floating organic droplets, *Food Chem.* 203 (2016) 386–393. <https://doi.org/10.1016/j.foodchem.2016.02.093>.
- [182] L. Vernès, M. Vian, F. Chemat, Ultrasound and microwave as green tools for solid-liquid extraction, *Liq. Extr.* (2019) 355–374. <https://doi.org/10.1016/B978-0-12-816911-7.00012-8>.
- [183] Y. Sun, D. Liu, J. Chen, X. Ye, D. Yu, Effects of different factors of ultrasound treatment on the extraction yield of the all-trans- $\beta$ -carotene from citrus peels, *Ultrason. Sonochem.* 18 (2011) 243–249. <https://doi.org/10.1016/j.ultsonch.2010.05.014>.

- [184] I.F. Strati, V. Oreopoulou, Effect of extraction parameters on the carotenoid recovery from tomato waste, *Int. J. Food Sci. Technol.* 46 (2011) 23–29. <https://doi.org/10.1111/j.1365-2621.2010.02496.x>.
- [185] M. Careri, L. Furlattini, A. Mangia, M. Musci, E. Anklam, A. Theobald, C. Von Holst, Supercritical fluid extraction for liquid chromatographic determination of carotenoids in *Spirulina Pacifica* algae: A chemometric approach, *J. Chromatogr. A.* 912 (2001) 61–71. [https://doi.org/10.1016/S0021-9673\(01\)00545-3](https://doi.org/10.1016/S0021-9673(01)00545-3).
- [186] N. Saim, J.R. Dean, M.P. Abdullah, Z. Zakaria, Extraction of polycyclic aromatic hydrocarbons from contaminated soil using soxhlet extraction, pressurised and atmospheric microwave-assisted extraction, supercritical fluid extraction and accelerated solvent extraction, *J. Chromatogr. A.* 791 (1997) 361–366. [https://doi.org/10.1016/S0021-9673\(97\)00768-1](https://doi.org/10.1016/S0021-9673(97)00768-1).
- [187] F.P. Cardenas-Toro, S.C. Alcázar-Alay, J.P. Coutinho, H.T. Godoy, T. Forster-Carneiro, M.A.A. Meireles, Pressurized liquid extraction and low-pressure solvent extraction of carotenoids from pressed palm fiber: Experimental and economical evaluation, *Food Bioprod. Process.* 94 (2015) 90–100. <https://doi.org/10.1016/j.fbp.2015.01.006>.
- [188] M. Castro-Puyana, A. Pérez-Sánchez, A. Valdés, O.H.M. Ibrahim, S. Suarez-Álvarez, J.A. Ferragut, V. Micol, A. Cifuentes, E. Ibáñez, V. García-Cañas, Pressurized liquid extraction of *Neochloris oleoabundans* for the recovery of bioactive carotenoids with anti-proliferative activity against human colon cancer cells, *Food Res. Int.* 99 (2017) 1048–1055. <https://doi.org/10.1016/j.foodres.2016.05.021>.
- [189] K. Zaghdoudi, S. Pontvianne, X. Framboisier, M. Achard, R. Kudaibergenova, M. Ayadi-Trabelsi, J. Kalthoum-Cherif, R. Vanderesse, C. Frochot, Y. Guiavarc'h, Accelerated solvent extraction of carotenoids from: Tunisian Kaki (*Diospyros kaki* L.), peach (*Prunus persica* L.) and apricot (*Prunus armeniaca* L.), *Food Chem.* 184 (2015) 131–139. <https://doi.org/10.1016/j.foodchem.2015.03.072>.
- [190] E. Damergi, J.P. Schwitzguébel, D. Refardt, S. Sharma, C. Holliger, C. Ludwig, Extraction of carotenoids from *Chlorella vulgaris* using green solvents and syngas production from residual biomass, *Algal Res.* 25 (2017) 488–495. <https://doi.org/10.1016/j.algal.2017.05.003>.
- [191] H. V. Chuyen, P.D. Roach, J.B. Golding, S.E. Parks, M.H. Nguyen, Ultrasound-assisted extraction of GAC peel: An optimization of extraction conditions for recovering carotenoids and antioxidant capacity, *Processes.* 8 (2020). <https://doi.org/10.3390/pr8010008>.
- [192] M. Civan, S. Kumcuoglu, Green ultrasound-assisted extraction of carotenoid and capsaicinoid

- from the pulp of hot pepper paste based on the bio-refinery concept, *Lwt.* 113 (2019) 108320.  
<https://doi.org/10.1016/j.lwt.2019.108320>.
- [193] H. V. Chuyen, M.H. Nguyen, P.D. Roach, J.B. Golding, S.E. Parks, Microwave-assisted extraction and ultrasound-assisted extraction for recovering carotenoids from Gac peel and their effects on antioxidant capacity of the extracts, *Food Sci. Nutr.* 6 (2018) 189–196.  
<https://doi.org/10.1002/fsn3.546>.
- [194] K.T. Amorim-Carrilho, A. Cepeda, C. Fente, P. Regal, Review of methods for analysis of carotenoids, *TrAC - Trends Anal. Chem.* 56 (2014) 49–73.  
<https://doi.org/10.1016/j.trac.2013.12.011>.
- [195] R.M. Pop, Y. Weesepeol, C. Socaciu, A. Pintea, J.P. Vincken, H. Gruppen, Carotenoid composition of berries and leaves from six Romanian sea buckthorn (*Hippophae rhamnoides* L.) varieties, *Food Chem.* 147 (2014) 1–9. <https://doi.org/10.1016/j.foodchem.2013.09.083>.
- [196] G.E. Hegazy, M.M. Abu-Serie, G.M. Abo-Elela, H. Ghozlan, S.A. Sabry, N.A. Soliman, Y.R. Abdel-Fattah, In vitro dual (anticancer and antiviral) activity of the carotenoids produced by haloalkaliphilic archaeon *Natrialba* sp. M6, *Sci. Rep.* 10 (2020) 1–14.  
<https://doi.org/10.1038/s41598-020-62663-y>.
- [197] A. Ilg, P. Beyer, S. Al-Babili, Characterization of the rice carotenoid cleavage dioxygenase 1 reveals a novel route for geranyl biosynthesis, *FEBS J.* 276 (2009) 736–747.  
<https://doi.org/10.1111/j.1742-4658.2008.06820.x>.
- [198] J.R. Mein, G.G. Dolnikowski, H. Ernst, R.M. Russell, X.D. Wang, Enzymatic formation of apo-carotenoids from the xanthophyll carotenoids lutein, zeaxanthin and  $\beta$ -cryptoxanthin by ferret carotene-9', 10'-monooxygenase, *Arch. Biochem. Biophys.* 506 (2011) 109–121.  
<https://doi.org/10.1016/j.abb.2010.11.005>.
- [199] H. Zheng, Q. Zhang, J. Quan, Q. Zheng, W. Xi, Determination of sugars, organic acids, aroma components, and carotenoids in grapefruit pulps, *Food Chem.* 205 (2016) 112–121.  
<https://doi.org/10.1016/j.foodchem.2016.03.007>.
- [200] A. Rubio, J.L. Rambla, M. Santaella, M.D. Gómez, D. Orzaez, A. Granell, L. Gómez-Gómez, Cytosolic and plastoglobule-targeted carotenoid dioxygenases from *Crocus sativus* are both involved in  $\beta$ -ionone release, *J. Biol. Chem.* 283 (2008) 24816–24825.  
<https://doi.org/10.1074/jbc.M804000200>.
- [201] S. Ruch, P. Beyer, H. Ernst, S. Al-Babili, Retinal biosynthesis in Eubacteria: In vitro

- characterization of a novel carotenoid oxygenase from *Synechocystis* sp. PCC 6803, *Mol. Microbiol.* 55 (2005) 1015–1024. <https://doi.org/10.1111/j.1365-2958.2004.04460.x>.
- [202] A.A. Pulschen, F. Rodrigues, R.T.D. Duarte, G.G. Araujo, I.F. Santiago, I.G. Paulino-Lima, C.A. Rosa, M.J. Kato, V.H. Pellizari, D. Galante, UV-resistant yeasts isolated from a high-altitude volcanic area on the Atacama Desert as eukaryotic models for astrobiology, *Microbiologyopen.* 4 (2015) 574–588. <https://doi.org/10.1002/mbo3.262>.
- [203] J. Jehlicka, A. Culka, L. Mana, A. Oren, Comparison of miniaturized raman spectrometers for discrimination of carotenoids of halophilic microorganisms, *Front. Microbiol.* 10 (2019) 1–12. <https://doi.org/10.3389/fmicb.2019.01155>.
- [204] A. Oren, Halophilic archaea on Earth and in space: Growth and survival under extreme conditions, *Philos. Trans. R. Soc. A Math. Phys. Eng. Sci.* 372 (2014). <https://doi.org/10.1098/rsta.2014.0194>.
- [205] D. Mauzerall, Chlorophyll and photosynthesis, *Philos. Trans. R. Soc. London. Sci. B, Biol. Sci.* 273 (1976) 287–294.
- [206] R.C. Dougherty, H.H. Strain, W.A. Svec, R.A. Uphaus, J.J. Katz, The Structure, Properties, and Distribution of Chlorophyll c, *J. Am. Chem. Soc.* 92 (1970) 2826–2833. <https://doi.org/10.1021/ja00712a037>.
- [207] H.G.M. Edwards, S.E.J. Villar, J. Parnell, C.S. Cockell, P. Lee, Raman spectroscopic analysis of cyanobacterial gypsum halotrophs and relevance for sulfate deposits on Mars, *Analyst.* 130 (2005) 917–923. <https://doi.org/10.1039/b503533c>.
- [208] P. Víttek, J. Jehlička, H.G.M. Edwards, I. Hutchinson, C. Ascaso, J. Wierzchos, The miniaturized Raman system and detection of traces of life in halite from the Atacama desert: Some considerations for the search for life signatures on Mars, *Astrobiology.* 12 (2012) 1095–1099. <https://doi.org/10.1089/ast.2012.0879>.
- [209] J. Rydberg, C.A. Cooke, J. Tolu, A.P. Wolfe, R.D. Vinebrooke, An assessment of chlorophyll preservation in lake sediments using multiple analytical techniques applied to the annually laminated lake sediments of Nylandssjön, *J. Paleolimnol.* 64 (2020) 379–388. <https://doi.org/10.1007/s10933-020-00143-z>.
- [210] K. Kebelmann, A. Hornung, U. Karsten, G. Griffiths, Intermediate pyrolysis and product identification by TGA and Py-GC/MS of green microalgae and their extracted protein and lipid components, *Biomass and Bioenergy.* 49 (2013) 38–48.

<https://doi.org/10.1016/j.biombioe.2012.12.006>.

- [211] A. Oren, Probing saltern brines with an oxygen electrode: What can we learn about the community metabolism in hypersaline systems?, *Life*. 6 (2016) 1–11.  
<https://doi.org/10.3390/life6020023>.
- [212] B. Schobert, J.K. Lanyi, Halorhodopsin is a light-driven chloride pump., *J. Biol. Chem.* 257 (1982) 10306–10313.
- [213] W.D. Hoff, P. Düx, K. Hård, B. Devreese, I.M. Nugteren-Roodzant, W. Crielaard, R. Boelens, R. Kaptein, J. Van Beeumen, K.J. Hellingwerf, Thiol Ester-Linked p-Coumaric Acid as a New Photoactive Prosthetic Group in a Protein with Rhodopsin-Like Photochemistry, *Biochemistry*. 33 (1994) 13959–13962. <https://doi.org/10.1021/bi00251a001>.
- [214] L. Remusat, Organic material in meteorites and the link to the origin of life, *BIO Web Conf.* 2 (2014) 03001. <https://doi.org/10.1051/bioconf/20140203001>.
- [215] R. V. Krishnamurthy, S. Epstein, J.R. Cronin, S. Pizzarello, G.U. Yuen, Isotopic and molecular analyses of hydrocarbons and monocarboxylic acids of the Murchison meteorite, *Geochim. Cosmochim. Acta.* 56 (1992) 4045–4058. [https://doi.org/10.1016/0016-7037\(92\)90015-B](https://doi.org/10.1016/0016-7037(92)90015-B).
- [216] A. Gulick, Phosphorus as a factor in the origin of life, *Am. Sci.* 43 (1955) 479–489.
- [217] M.A. Pasek, M. Gull, B. Herschy, Phosphorylation on the early earth, *Chem. Geol.* 475 (2017) 149–170. <https://doi.org/10.1016/j.chemgeo.2017.11.008>.
- [218] A.W. Schwartz, Phosphorus in prebiotic chemistry, *Philos. Trans. R. Soc. B Biol. Sci.* 361 (2006) 1743–1749. <https://doi.org/10.1098/rstb.2006.1901>.
- [219] J.D. Toner, D.C. Catling, A carbonate-rich lake solution to the phosphate problem of the origin of life, *Proc. Natl. Acad. Sci. U. S. A.* 117 (2020) 883–888.  
<https://doi.org/10.1073/pnas.1916109117>.
- [220] J. Xu, G.J. Ramian, J.F. Galan, P.G. Savvidis, A.M. Scopatz, R.R. Birge, S.J. Allen, K.W. Plaxco, Terahertz circular dichroism spectroscopy: A potential approach to the in situ detection of life's metabolic and genetic machinery, *Astrobiology*. 3 (2003) 489–504.  
<https://doi.org/10.1089/153110703322610609>.
- [221] D.S. McKay, E.K. Gibson, K.L. Thomas-Keprta, H. Vali, C.S. Romanek, S.J. Clemett, X.D.F. Chillier, C.R. Maechling, R.N. Zare, Search for past life on Mars: Possible relic biogenic activity in martian meteorite ALH84001, *Science* (80-. ). 273 (1996) 924–930.

<https://doi.org/10.1126/science.273.5277.924>.

- [222] C. Freissinet, A. Buch, R. Sternberg, C. Szopa, C. Geffroy-Rodier, C. Jelinek, M. Stambouli, Search for evidence of life in space: Analysis of enantiomeric organic molecules by N,N-dimethylformamide dimethylacetal derivative dependant Gas Chromatography-Mass Spectrometry, *J. Chromatogr. A.* 1217 (2010) 731–740. <https://doi.org/10.1016/j.chroma.2009.11.009>.
- [223] C. Szopa, C. Freissinet, D.P. Glavin, M. Millan, A. Buch, H.B. Franz, R.E. Summons, D.Y. Sumner, B. Sutter, J.L. Eigenbrode, R.H. Williams, R. Navarro-González, M. Guzman, C. Malespin, S. Teinturier, P.R. Mahaffy, M. Cabane, First detections of dichlorobenzene isomers and trichloromethylpropane from organic matter indigenous to Mars mudstone in Gale Crater, Mars: results from the Sample Analysis at Mars Instrument onboard the Curiosity Rover, *Astrobiology.* 20 (2020) 292–306. <https://doi.org/10.1089/ast.2018.1908>.
- [224] P.G. Simmonds, Organic analysis by pyrolysis-gas chromatography-mass spectrometry a candidate experiment for the biological exploration of mars, *J. Chromatogr. Sci.* 7 (1969) 36–41. <https://doi.org/10.1093/chromsci/7.1.36>.
- [225] O. Botta, J.L. Bada, Extraterrestrial organic compounds in meteorites, *Surv. Geophys.* 23 (2002) 411–467. <https://doi.org/10.1023/A:1020139302770>.
- [226] P.R. Solomon, M.A. Serio, E.M. Suuberg, Coal pyrolysis: Experiments, kinetic rates and mechanisms, *Prog. Energy Combust. Sci.* 18 (1992) 133–220. [https://doi.org/10.1016/0360-1285\(92\)90021-R](https://doi.org/10.1016/0360-1285(92)90021-R).
- [227] X. Li, J. ichiro Hayashi, C.Z. Li, FT-Raman spectroscopic study of the evolution of char structure during the pyrolysis of a Victorian brown coal, *Fuel.* 85 (2006) 1700–1707. <https://doi.org/10.1016/j.fuel.2006.03.008>.
- [228] H. Yang, R. Yan, H. Chen, D.H. Lee, C. Zheng, Characteristics of hemicellulose, cellulose and lignin pyrolysis, *Fuel.* 86 (2007) 1781–1788. <https://doi.org/10.1016/j.fuel.2006.12.013>.
- [229] H.Y. Cai, A.J. Güell, I.N. Chatzakis, J.Y. Lim, D.R. Dugwell, R. Kandiyoti, Combustion reactivity and morphological change in coal chars: Effect of pyrolysis temperature, heating rate and pressure, *Fuel.* 75 (1996) 15–24. [https://doi.org/10.1016/0016-2361\(94\)00192-8](https://doi.org/10.1016/0016-2361(94)00192-8).
- [230] K.R. Doolan, J.C. Mackie, R.J. Tyler, Coal flash pyrolysis: secondary cracking of tar vapours in the range 870-2000 K, *Fuel.* 66 (1987) 572–578. [https://doi.org/10.1016/0016-2361\(87\)90166-9](https://doi.org/10.1016/0016-2361(87)90166-9).

- [231] C. Schummer, O. Delhomme, B.M.R. Appenzeller, R. Wennig, M. Millet, Comparison of MTBSTFA and BSTFA in derivatization reactions of polar compounds prior to GC/MS analysis, *Talanta*. 77 (2009) 1473–1482. <https://doi.org/10.1016/j.talanta.2008.09.043>.
- [232] L. Degani, C. Riedo, O. Chiantore, Identification of natural indigo in historical textiles by GC–MS, *Anal. Bioanal. Chem.* 407 (2015) 1695–1704. <https://doi.org/10.1007/s00216-014-8423-2>.
- [233] K. Hiroyuki, Derivatization reactions for the determination of amines by gas chromatography and their applications in environmental analysis, *J. Chromatogr. A.* 733 (1996) 19–34. [https://doi.org/10.1016/0021-9673\(95\)00726-1](https://doi.org/10.1016/0021-9673(95)00726-1).
- [234] C. Freissinet, M. Millan, D.P. Glavin, X. Li, A. Grubisic, J.E. Eigenbrode, J.C. Stern, J.P. Dworkin, A. Buch, C. Szopa, M.A. Guzman, M.A. Carts, S.A. Getty, W.B. Brinckerhoff, Investigating the effects of gamma radiation on selected chemicals for use in biosignature detection instruments on the surface of Jupiter’s moon Europa, *Planet. Space Sci.* 175 (2019) 1–12. <https://doi.org/10.1016/j.pss.2019.05.009>.
- [235] J.M. Challinor, A pyrolysis-derivatisation-gas chromatography technique for the structural elucidation of some synthetic polymers, *J. Anal. Appl. Pyrolysis.* 16 (1989) 323–333. [https://doi.org/10.1016/0165-2370\(89\)80015-4](https://doi.org/10.1016/0165-2370(89)80015-4).
- [236] E.W. Robb, J.J. Westbrook, Preparation of methyl esters for gas liquid chromatography of acids by pyrolysis of tetramethylammonium salts, *Anal. Chem.* 35 (1963) 1644–1647. <https://doi.org/10.1021/ac60204a029>.
- [237] Y. Sun, C. Tang, X. Wu, Z. Pan, L. Wang, Characterization of alkylphenol components in ginkgo biloba sarcotesta by thermochemolysis-gas chromatography/mass spectrometry in the presence of trimethylsulfonium hydroxide, *Chromatographia.* 75 (2012) 387–395. <https://doi.org/10.1007/s10337-012-2211-y>.
- [238] V. Becerra, J. Odermatt, Interferences in the direct quantification of bisphenol S in paper by means of thermochemolysis, *J. Chromatogr. A.* 1275 (2013) 70–77. <https://doi.org/10.1016/j.chroma.2012.12.034>.
- [239] Y. Ishida, T. Hirota, S. Sato, M. Kamegai, S.K. Kim, S.Y. Park, D.H. Koo, M.S. Shon, G.N. Kim, H.R. Park, S.C. Lee, Discriminative analysis of free and esterified gallic acids in acorn shells by thermochemolysis-gas chromatography/mass spectrometry in the presence of organic alkalis, *J. Anal. Appl. Pyrolysis.* 116 (2015) 114–119. <https://doi.org/10.1016/j.jaap.2015.09.019>.

- [240] Y. Sun, X. Wang, Y. Huang, Z. Pan, L. Wang, Derivatization following hollow-fiber microextraction with tetramethylammonium acetate as a dual-function reagent for the determination of benzoic acid and sorbic acid by GC, *J. Sep. Sci.* 36 (2013) 2268–2276. <https://doi.org/10.1002/jssc.201300239>.
- [241] E. Manzano, L.R. Rodríguez-Simón, N. Navas, R. Checa-Moreno, M. Romero-Gómez, L.F. Capitan-Vallvey, Study of the GC-MS determination of the palmitic-stearic acid ratio for the characterisation of drying oil in painting: La Encarnación by Alonso Cano as a case study, *Talanta*. 84 (2011) 1148–1154. <https://doi.org/10.1016/j.talanta.2011.03.012>.
- [242] E. Jakab, Á. Bora, Z. Sebestyén, J. Borsa, Thermal decomposition of chemically treated cellulosic fibers, *J. Therm. Anal. Calorim.* 132 (2018) 433–443. <https://doi.org/10.1007/s10973-017-6935-7>.
- [243] M. Mizumoto, E. Shimokita, T. Ona, T. Seino, Y. Ishida, H. Ohtani, Rapid and direct characterization of total fatty acids in wood by thermochemolysis-gas chromatography-flame ionization detector/mass spectrometry with tetrabutylammonium hydroxide, *J. Anal. Appl. Pyrolysis*. 87 (2010) 163–167. <https://doi.org/10.1016/j.jaap.2009.11.004>.
- [244] M. Gómez-Brandón, M. Lores, J. Domínguez, A new combination of extraction and derivatization methods that reduces the complexity and preparation time in determining phospholipid fatty acids in solid environmental samples, *Bioresour. Technol.* 101 (2010) 1348–1354. <https://doi.org/10.1016/j.biortech.2009.09.047>.
- [245] C. Biache, A.E. Navarro Frómata, F. Czechowski, Y. Lu, R.P. Philp, Thiosteranes in samples impacted by fecal materials and their potential use as marker of sewage input, *Environ. Pollut.* 196 (2015) 268–275. <https://doi.org/10.1016/j.envpol.2014.10.010>.
- [246] D. Válková, L. Grasset, A. Amblès, Molecular compounds generated by ruthenium tetroxide oxidation and preparative off line thermochemolysis of lignite humic acids from South Moravia: Implications for molecular structure, *Fuel*. 88 (2009) 2113–2121. <https://doi.org/10.1016/j.fuel.2009.01.026>.
- [247] M. Gomes, M. Martins, S. Leath, K. Stelwagen, Direct analysis of fatty acid profile from milk by thermochemolysis – gas chromatography – mass spectrometry, *J. Chromatogr. A*. 1218 (2011) 316–323. <https://doi.org/10.1016/j.chroma.2010.11.011>.
- [248] J. Poerschmann, L. Schultze-Nobre, Rapid screening of phytoremediation effluents by off-line tetramethylammonium hydroxide assisted thermochemolysis, *Sci. Total Environ.* 518–519 (2015) 371–377. <https://doi.org/10.1016/j.scitotenv.2015.02.099>.



- [249] A.M. Tadini, G. Pantano, A.L. de Toffoli, B. Fontaine, R. Spaccini, A. Piccolo, A.B. Moreira, M.C. Bisinoti, Off-line TMAH-GC/MS and NMR characterization of humic substances extracted from river sediments of northwestern São Paulo under different soil uses, *Sci. Total Environ.* 506–507 (2015) 234–240. <https://doi.org/10.1016/j.scitotenv.2014.11.012>.
- [250] X. Zang, J.C. Brown, J.D.H. Van Heemst, A. Palumbo, P.G. Hatcher, Characterization of amino acids and proteinaceous materials using online tetramethylammonium hydroxide (TMAH) thermochemolysis and gas chromatography-mass spectrometry technique, *J. Anal. Appl. Pyrolysis.* 61 (2001) 181–193. [https://doi.org/10.1016/S0165-2370\(01\)00151-6](https://doi.org/10.1016/S0165-2370(01)00151-6).
- [251] J.P. Liu, S.A. Kuehl, A.C. Pierce, J. Williams, N.E. Blair, C. Harris, D.W. Aung, Y.Y. Aye, Fate of Ayeyarwady and Thanlwin Rivers Sediments in the Andaman Sea and Bay of Bengal, *Mar. Geol.* 423 (2020) 106137. <https://doi.org/10.1016/j.margeo.2020.106137>.
- [252] Y. Pan, Y. Liao, Y. Zheng, Effect of biodegradation on the molecular composition and structure of asphaltenes: Clues from quantitative Py-GC and THM-GC, *Org. Geochem.* 86 (2015) 32–44. <https://doi.org/10.1016/j.orggeochem.2015.06.002>.
- [253] J. Veenhoven, S. Saverwyns, M. Van Bommel, F. Lynen, Evaluation of on-line derivatization techniques using TMAH and HMDS for the comprehensive analysis of anacardiaceae thermosetting lacquer polymers using Pyrolysis-GC / MS and deconvolution, (n.d.).
- [254] T. Ohra-Aho, J. Ropponen, T. Tamminen, Thermochemolysis using TMAAc and TMAH reagents as means to differentiate between free acids and esters, in: *J. Anal. Appl. Pyrolysis*, Elsevier B.V., 2013: pp. 31–35. <https://doi.org/10.1016/j.jaap.2012.09.015>.
- [255] S.L. Mason, T.R. Filley, G.D. Abbott, A comparative study of the molecular composition of a grassland soil with adjacent unforested and afforested moorland ecosystems, *Org. Geochem.* 42 (2012) 1519–1528. <https://doi.org/10.1016/j.orggeochem.2010.11.003>.
- [256] A. Andrade-Eiroa, M. Canle, V. Leroy-Cancellieri, V. Cerdà, Solid-phase extraction of organic compounds: A critical review (Part I), *TrAC - Trends Anal. Chem.* 80 (2016) 641–654. <https://doi.org/10.1016/j.trac.2015.08.015>.
- [257] L. Baij, A. Astefanei, J. Hermans, F. Brinkhuis, H. Groenewegen, L. Chassouant, S. Johansson, G. Corthals, C. Tokarski, P. Iedema, K. Keune, Solvent-mediated extraction of fatty acids in bilayer oil paint models: a comparative analysis of solvent application methods, *Herit. Sci.* 7 (2019) 1–8. <https://doi.org/10.1186/s40494-019-0273-y>.
- [258] K. Younes, L. Grasset, Comparison of thermochemolysis and classical chemical degradation

- and extraction methods for the analysis of carbohydrates, lignin and lipids in a peat bog, *J. Anal. Appl. Pyrolysis*. 134 (2018) 61–72. <https://doi.org/10.1016/j.jaap.2018.05.011>.
- [259] O. Bertrand, L. Mansuy-Huault, E. Montargès-Pelletier, P. Faure, B. Losson, J. Argant, P. Ruffaldi, R. Michels, Recent vegetation history from a swampy environment to a pond based on macromolecular organic matter (lignin and fatty acids) and pollen sedimentary records, *Org. Geochem.* 64 (2013) 47–57. <https://doi.org/10.1016/j.orggeochem.2013.09.008>.
- [260] T. Klotzbücher, T.R. Filley, K. Kaiser, K. Kalbitz, A study of lignin degradation in leaf and needle litter using <sup>13</sup>C-labelled tetramethylammonium hydroxide ( TMAH ) thermochemolysis : Comparison with CuO oxidation and van Soest methods, *Org. Geochem.* 42 (2011) 1271–1278. <https://doi.org/10.1016/j.orggeochem.2011.07.007>.
- [261] N.A. Dang, M. Mourão, S. Kuijper, E. Walters, H.G. Janssen, A.H.J. Kolk, Direct detection of *Mycobacterium tuberculosis* in sputum using combined solid phase extraction-gas chromatography-mass spectrometry, *J. Chromatogr. B Anal. Technol. Biomed. Life Sci.* 986–987 (2015) 115–122. <https://doi.org/10.1016/j.jchromb.2015.01.045>.
- [262] D.M. O’Sullivan, S.C. Nicoara, R. Mutetwa, S. Mungofa, O.Y. Lee, D.E. Minnikin, M.W. Bardwell, E.L. Corbett, R. McNerney, G.H. Morgan, Detection of *mycobacterium tuberculosis* in sputum by gas chromatography-mass spectrometry of methyl mycocerosates released by thermochemolysis, *PLoS One*. 7 (2012) e32836. <https://doi.org/10.1371/journal.pone.0032836>.
- [263] Z. Yun, B. He, Z. Wang, T. Wang, G. Jiang, Evaluation of different extraction procedures for determination of organic Mercury species in petroleum by high performance liquid chromatography coupled with cold vapor atomic fluorescence spectrometry, *Talanta*. 106 (2013) 60–65. <https://doi.org/10.1016/j.talanta.2012.12.009>.
- [264] A. Buch, D.P. Glavin, R. Sternberg, C. Szopa, C. Rodier, R. Navarro-González, F. Raulin, M. Cabane, P.R. Mahaffy, A new extraction technique for in situ analyses of amino and carboxylic acids on Mars by gas chromatography mass spectrometry, *Planet. Space Sci.* 54 (2006) 1592–1599. <https://doi.org/10.1016/j.pss.2006.05.041>.
- [265] A. Mojarro, G. Ruvkun, M.T. Zuber, C.E. Carr, Nucleic acid extraction and sequencing from low-biomass synthetic Mars analog soils for in situ life detection, *Astrobiology*. 17 (2017) 747–760. <https://doi.org/10.1089/ast.2016.1535>.
- [266] A. Mojarro, J. Hachey, R. Bailey, M. Brown, R. Doebler, G. Ruvkun, M.T. Zuber, C.E. Carr, Nucleic acid extraction and sequencing from low-biomass synthetic Mars analog soils for in situ life detection, *Astrobiology*. 19 (2019) 1139–1152. <https://doi.org/10.1089/ast.2018.1929>.

- [267] G. Yang, H. Tazoe, M. Yamada, Improved approach for routine monitoring of <sup>129</sup>I activity and <sup>129</sup>I/<sup>127</sup>I atom ratio in environmental samples using TMAH extraction and ICP-MS/MS, *Anal. Chim. Acta.* 1008 (2018) 66–73. <https://doi.org/10.1016/j.aca.2017.12.049>.
- [268] O.S. Humphrey, S.D. Young, E.H. Bailey, N.M.J. Crout, E.L. Ander, M.J. Watts, Iodine soil dynamics and methods of measurement: A review, *Environ. Sci. Process. Impacts.* 20 (2018) 288–310. <https://doi.org/10.1039/c7em00491e>.
- [269] S. Öztan, R.A. Düring, Microwave assisted EDTA extraction - Determination of pseudo total contents of distinct trace elements in solid environmental matrices, *Talanta.* 99 (2012) 594–602. <https://doi.org/10.1016/j.talanta.2012.06.042>.
- [270] Y. He, R. Zhao, L. Yan, Y. Bai, F. Li, The effect of low molecular weight compounds in coal on the formation of light aromatics during coal pyrolysis, *J. Anal. Appl. Pyrolysis.* 123 (2017) 49–55. <https://doi.org/10.1016/j.jaap.2016.12.030>.
- [271] L. Doskočil, V. Enev, L. Grasset, J. Wasserbauer, The characterization of South Moravian lignite in its natural and treated forms using thermal degradation methods, *J. Anal. Appl. Pyrolysis.* 128 (2017) 83–91. <https://doi.org/10.1016/j.jaap.2017.10.022>.
- [272] L. Doskočil, L. Grasset, V. Enev, L. Kalina, M. Pekař, Study of water-extractable fractions from South Moravian lignite, *Environ. Earth Sci.* 73 (2015) 3873–3885. <https://doi.org/10.1007/s12665-014-3671-1>.
- [273] F.Z. El Ouaquodi, A. Meddich, L. Lemée, A. Amblès, M. Hafidi, Assessment of compost-derived humic acids structure from ligno-cellulose waste by TMAH-thermochemolysis, *Waste and Biomass Valorization.* 10 (2019) 2661–2672. <https://doi.org/10.1007/s12649-018-0268-z>.
- [274] A. Andrade-Eiroa, M. Canle, V. Leroy-Cancellieri, V. Cerdà, Solid-phase extraction of organic compounds: A critical review. part ii, *TrAC - Trends Anal. Chem.* 80 (2016) 655–667. <https://doi.org/10.1016/j.trac.2015.08.014>.
- [275] A. Andrade-Eiroa, V. Leroy, P. Dagaut, Y. Bedjanian, Determination of polycyclic aromatic hydrocarbons in kerosene and bio-kerosene soot, *Chemosphere.* 78 (2010) 1342–1349. <https://doi.org/10.1016/j.chemosphere.2010.01.005>.
- [276] N. V. Heuett, C.E. Ramirez, A. Fernandez, P.R. Gardinali, Analysis of drugs of abuse by online SPE-LC high resolution mass spectrometry: Communal assessment of consumption, *Sci. Total Environ.* 511 (2015) 319–330. <https://doi.org/10.1016/j.scitotenv.2014.12.043>.
- [277] X. Zhang, D. Zhu, C. Huang, Y. Sun, Y.I. Lee, Sensitive detection of bisphenol A in complex

- samples by in-column molecularly imprinted solid-phase extraction coupled with capillary electrophoresis, *Microchem. J.* 121 (2015) 1–5. <https://doi.org/10.1016/j.microc.2015.01.012>.
- [278] L. Mariño-Repizo, F. Kero, V. Vandell, A. Senior, M. Isabel Sanz-Ferramola, S. Cerutti, J. Raba, A novel solid phase extraction - Ultra high performance liquid chromatography-tandem mass spectrometry method for the quantification of ochratoxin A in red wines, *Food Chem.* 172 (2015) 663–668. <https://doi.org/10.1016/j.foodchem.2014.09.094>.
- [279] M. Havelcová, I. Sýkorová, K. Mach, Z. Dvořák, Organic geochemistry of fossil resins from the Czech Republic, *Procedia Earth Planet. Sci.* 10 (2014) 303–312. <https://doi.org/10.1016/j.proeps.2014.08.021>.
- [280] B. Allard, S. Derenne, Characterization of soil organic matter using microwave assisted acid and base hydrolysis, *Org. Geochem.* 65 (2013) 103–117. <https://doi.org/10.1016/j.orggeochem.2013.10.009>.
- [281] L. Han, K. Sun, J. Jin, B. Xing, Some concepts of soil organic carbon characteristics and mineral interaction from a review of literature, *Soil Biol. Biochem.* 94 (2016) 107–121. <https://doi.org/10.1016/j.soilbio.2015.11.023>.
- [282] L.H. Lin, M.J. Simpson, Enhanced extractability of cutin- and suberin-derived organic matter with demineralization implies physical protection over chemical recalcitrance in soil, *Org. Geochem.* 97 (2016) 111–121. <https://doi.org/10.1016/j.orggeochem.2016.04.012>.
- [283] M. Gao, Z. Yang, Y. Wang, Y. Bai, F. Li, K. Xie, Impact of calcium on the synergistic effect for the reactivity of coal char gasification in H<sub>2</sub>O/CO<sub>2</sub> mixtures, *Fuel.* 189 (2017) 312–321. <https://doi.org/10.1016/j.fuel.2016.10.100>.
- [284] R. Spaccini, X.Y. Song, V. Cozzolino, A. Piccolo, Molecular evaluation of soil organic matter characteristics in three agricultural soils by improved off-line thermochemolysis: The effect of hydrofluoric acid demineralisation treatment, *Anal. Chim. Acta.* 802 (2013) 46–55. <https://doi.org/10.1016/j.aca.2013.09.031>.
- [285] L. Decq, F. Lynen, M. Schilling, W. Fremout, V. Cattersel, D. Steyaert, C. Indekeu, E. Van Binnebeke, S. Saverwyns, The analysis of European lacquer: optimization of thermochemolysis temperature of natural resins, *Appl. Phys. A Mater. Sci. Process.* 122 (2016) 1–8. <https://doi.org/10.1007/s00339-016-0550-5>.
- [286] S.S. Choi, J.E. Ko, Dimerization reactions of amino acids by pyrolysis, *J. Anal. Appl. Pyrolysis.* 89 (2010) 74–86. <https://doi.org/10.1016/j.jaap.2010.05.009>.

- [287] A. Venema, R.C.A. Boom-Van Geest, In-situ hydrolysis/methylation pyrolysis CGC for the characterization of polyaramides, *J. Microcolumn Sep.* 7 (1995) 337–343.  
<https://doi.org/10.1002/mcs.1220070406>.
- [288] W. Montgomery, E.A. Jaramillo, S.H. Royle, S.P. Kounaves, Di. Schulze-Makuch, M.A. Sephton, Effects of oxygen-containing salts on the detection of organic biomarkers on Mars and in terrestrial analog soils, *Astrobiology.* 19 (2019) 711–721.  
<https://doi.org/10.1089/ast.2018.1888>.
- [289] K. Oba, H. Ohtani, S. Tsuge, Confirmation of the xanthone structure in thermally treated polycarbonates by reactive pyrolysis-gas chromatography / mass spectrometry, *Polym. Degrad. Stab.* 74 (2001) 171–176.
- [290] D. Fabbri, V. Baravelli, G. Chiavari, S. Prati, Profiling fatty acids in vegetable oils by reactive pyrolysis – gas chromatography with dimethyl carbonate and titanium silicate, *J. Chromatogr. A.* 1100 (2005) 218–222. <https://doi.org/10.1016/j.chroma.2005.09.051>.
- [291] L. Wang, Y. Ishida, H. Ohtani, S. Tsuge, Characterization of natural resin shellac by reactive pyrolysis - gas chromatography in the presence of organic alkali, *Anal. Chem.* 71 (1999) 1316–1322.
- [292] J.M. van Mourik, K.G.J. Nierop, D.A.G. Vandenberghe, Radiocarbon and optically stimulated luminescence dating based chronology of a polycyclic driftsand sequence at Weerterbergen (SE Netherlands), *Catena.* 80 (2010) 170–181. <https://doi.org/10.1016/j.catena.2009.11.004>.
- [293] C.E. Stewart, Evaluation of angiosperm and fern contributions to soil organic matter using two methods of pyrolysis-gas chromatography-mass spectrometry, *Plant Soil.* 351 (2012) 31–46.  
<https://doi.org/10.1007/s11104-011-0927-3>.
- [294] J. Templier, F. Miserque, N. Barré, F. Mercier, J.P. Croué, S. Derenne, Is nitrogen functionality responsible for contrasted responses of riverine dissolved organic matter in pyrolysis?, *J. Anal. Appl. Pyrolysis.* 97 (2012) 62–72. <https://doi.org/10.1016/j.jaap.2012.05.002>.
- [295] A. Vidal, K. Quenea, M. Alexis, S. Derenne, Molecular fate of root and shoot litter on incorporation and decomposition in earthworm casts, *Org. Geochem.* 101 (2016) 1–10.  
<https://doi.org/10.1016/j.orggeochem.2016.08.003>.
- [296] P. Barré, K. Quéneá, A. Vidal, L. Cécillon, B.T. Christensen, T. Kätterer, A. Macdonald, L. Petit, A.F. Plante, F. van Oort, C. Chenu, Microbial and plant-derived compounds both contribute to persistent soil organic carbon in temperate soils, *Biogeochemistry.* 140 (2018)

- 81–92. <https://doi.org/10.1007/s10533-018-0475-5>.
- [297] J. Campo, R.J. Stijssiger, E. Nadal-Romero, E.L.H. Cammeraat, The effects of land abandonment and long-term afforestation practices on the organic carbon stock and lignin content of Mediterranean humid mountain soils, *Eur. J. Soil Sci.* 70 (2019) 947–959. <https://doi.org/10.1111/ejss.12799>.
- [298] M. Fischer, B.M. Scholz-Böttcher, Simultaneous trace identification and quantification of common types of microplastics in environmental samples by pyrolysis-gas chromatography-mass spectrometry, *Environ. Sci. Technol.* 51 (2017) 5052–5060. <https://doi.org/10.1021/acs.est.6b06362>.
- [299] F. Ohira, M. Yamamoto, K. Takemura, A. Hayashida, Response of vegetation in central Japan to precession during the last 147,000 years: A lignin record from Lake Biwa core BIW08-B, *Quat. Int.* 349 (2014) 59–67. <https://doi.org/10.1016/j.quaint.2013.10.059>.
- [300] S.K. Dodla, J.J. Wang, R.L. Cook, Molecular composition of humic acids from coastal wetland soils along a salinity gradient, *Soil Sci. Soc. Am. J.* 76 (2012) 1592–1605. <https://doi.org/10.2136/sssaj2011.0346>.
- [301] C. Ferro-Vázquez, J. Kaal, F.J. Santos Arévalo, F. Criado Boado, Molecular fingerprinting of 14 C dated soil organic matter fractions from archaeological settings in NW Spain, *Radiocarbon.* 61 (2019) 101–130. <https://doi.org/10.1017/RDC.2018.62>.
- [302] R.N.T.M. Kabuyah, B.E. van Dongen, A.D. Bewsher, C.H. Robinson, Decomposition of lignin in wheat straw in a sand-dune grassland, *Soil Biol. Biochem.* 45 (2012) 128–131. <https://doi.org/10.1016/j.soilbio.2011.10.014>.
- [303] G.D. Abbott, E.Y. Swain, A.B. Muhammad, K. Allton, L.R. Belyea, C.G. Laing, G.L. Cowie, Effect of water-table fluctuations on the degradation of Sphagnum phenols in surficial peats, *Geochim. Cosmochim. Acta.* 106 (2013) 177–191. <https://doi.org/10.1016/j.gca.2012.12.013>.
- [304] L. Jeanneau, A. Jaffrezic, A.-C. Pierson-Wickmann, G. Gruau, T. Lambert, P. Petitjean, Constraints on the sources and production mechanisms of dissolved organic matter in soils from molecular biomarkers, *Vadose Zo. J.* 13 (2014). <https://doi.org/10.2136/vzj2014.02.0015>.
- [305] H. Guénet, E. Demangeat, M. Davranche, D. Vantelon, A.C. Pierson-Wickmann, E. Jardé, M. Bouhnik-Le Coz, E. Lotfi, A. Dia, J. Jestin, Experimental evidence of REE size fraction redistribution during redox variation in wetland soil, *Sci. Total Environ.* 631–632 (2018) 580–588. <https://doi.org/10.1016/j.scitotenv.2018.03.005>.

- [306] N. Fujisawa, M. Fukushima, M. Yamamoto, H. Iwai, T. Komai, Y. Kawabe, D. Liu, Structural alterations of humic acid fractions in a steel slag-compost fertilizer during fertilization. Analysis by pyrolysis/methylation-gas chromatography/mass spectrometry, *J. Anal. Appl. Pyrolysis*. 95 (2012) 126–133. <https://doi.org/10.1016/j.jaap.2012.01.017>.
- [307] R. Okabe, A. Miura, M. Fukushima, M. Terashima, M. Sasaki, S. Fukuchi, T. Sato, Characterization of an adsorbed humin-like substance on an allophanic soil formed via catalytic polycondensation between catechol and glycine, and its adsorption capability to pentachlorophenol, *Chemosphere*. 83 (2011) 1502–1506. <https://doi.org/10.1016/j.chemosphere.2011.01.053>.
- [308] K. Nagasawa, B. Wang, K. Nishiya, K. Ushijima, Q. Zhu, M. Fukushima, T. Ichijo, Effects of humic acids derived from lignite and cattle manure on antioxidant enzymatic activities of barley root, *J. Environ. Sci. Heal. - Part B Pestic. Food Contam. Agric. Wastes*. 51 (2016) 81–89. <https://doi.org/10.1080/03601234.2015.1080516>.
- [309] M. Fukushima, M. Yamamoto, T. Komai, K. Yamamoto, Studies of structural alterations of humic acids from conifer bark residue during composting by pyrolysis-gas chromatography/mass spectrometry using tetramethylammonium hydroxide (TMAH-py-GC/MS), *J. Anal. Appl. Pyrolysis*. 86 (2009) 200–206. <https://doi.org/10.1016/j.jaap.2009.06.005>.
- [310] L. Grasset, P. Rovira, A. Amblès, TMAH-preparative thermochemolysis for the characterization of organic matter in densimetric fractions of a Mediterranean forest soil, *J. Anal. Appl. Pyrolysis*. 85 (2009) 435–441. <https://doi.org/10.1016/j.jaap.2008.09.004>.
- [311] R. Spaccini, P. Mazzei, A. Squartini, M. Giannattasio, A. Piccolo, Molecular properties of a fermented manure preparation used as field spray in biodynamic agriculture, *Environ. Sci. Pollut. Res.* 19 (2012) 4214–4225. <https://doi.org/10.1007/s11356-012-1022-x>.
- [312] D. Martinez-Balmori, R. Spaccini, N.O. Aguiar, E.H. Novotny, F.L. Olivares, L.P. Canellas, Molecular characteristics of humic acids isolated from vermicomposts and their relationship to bioactivity, *J. Agric. Food Chem.* 62 (2014) 11412–11419. <https://doi.org/10.1021/jf504629c>.
- [313] D. Martinez-Balmori, F.L. Olivares, R. Spaccini, K.P. Aguiar, M.F. Araújo, N.O. Aguiar, F. Guridi, L.P. Canellas, Molecular characteristics of vermicompost and their relationship to preservation of inoculated nitrogen-fixing bacteria, *J. Anal. Appl. Pyrolysis*. 104 (2013) 540–550. <https://doi.org/10.1016/j.jaap.2013.05.015>.
- [314] A. Špaldoňová, J. Frouz, The role of *Armadillidium vulgare* (Isopoda: Oniscidea) in litter

- decomposition and soil organic matter stabilization, *Appl. Soil Ecol.* 83 (2014) 186–192.  
<https://doi.org/10.1016/j.apsoil.2014.04.012>.
- [315] J. Frouz, T. Cajthaml, O. Mudrak, The effect of lignin photodegradation on decomposability of *Calamagrostis epigeios* grass litter, *Biodegradation.* 22 (2011) 1247–1254.  
<https://doi.org/10.1007/s10532-011-9479-8>.
- [316] J.A. Siles, T. Cajthaml, A. Filipova, S. Minerbi, R. Margesin, Altitudinal, seasonal and interannual shifts in microbial communities and chemical composition of soil organic matter in Alpine forest soils, *Soil Biol. Biochem.* 112 (2017) 1–13.  
<https://doi.org/10.1016/j.soilbio.2017.04.014>.
- [317] . Angst, T. Cajthaml, G. Angst, H. . ˇSimackova, J. Brus, J. Frouz, Retention of dead standing plant biomass (marcescence) increases subsequent litter decomposition in the soil organic layer, *Plant Soil.* 418 (2017) 571–579. <https://doi.org/10.1007/s11104-017-3318-6>.
- [318] E.Y. Swain, G.D. Abbott, The effect of redox conditions on sphagnum acid thermochemolysis product distributions in a northern peatland, *J. Anal. Appl. Pyrolysis.* 103 (2013) 2–7.  
<https://doi.org/10.1016/j.jaap.2012.12.022>.
- [319] P. Zhou , G.X.Pan, R . Spaccini & A . Piccolob, Molecular changes in particulate organic matter ( POM ) in a typical Chinese paddy soil under different long-term fertilizer treatments, *Eur. J. Soil Sci.* 61 (2010) 231–242. <https://doi.org/10.1111/j.1365-2389.2009.01223.x>.
- [320] A. Nebbioso, A. Piccolo, Advances in humeomics: Enhanced structural identification of humic molecules after size fractionation of a soil humic acid, *Anal. Chim. Acta.* 720 (2012) 77–90.  
<https://doi.org/10.1016/j.aca.2012.01.027>.
- [321] G. Pascaud, M. Soubrand, L. Lemee, J. Laduranty, A. El-Mufleh, M. Rabiet, E. Joussein, Molecular fingerprint of soil organic matter as an indicator of pedogenesis processes in Technosols, *J. Soils Sediments.* 17 (2017) 340–351. <https://doi.org/10.1007/s11368-016-1523-1>.
- [322] A. Sawicka, A. Burnstock, F.C. Izzo, K. Keune, J.J. Boon, K. Kirsch, K.J. Van Den Berg, An Investigation into the Viability of Removal of Lead Soap Efflorescence from Contemporary Oil Paintings, in: *Issues Contemp. Oil Paint*, 2014: pp. 311–332. <https://doi.org/10.1007/978-3-319-10100-2>.
- [323] H.E. Barden, U. Bergmann, N.P. Edwards, V.M. Egerton, P.L. Manning, S. Perry, A. van Veelen, R.A. Wogelius, B.E. van Dongen, Bacteria or melanosomes? A geochemical analysis



- of micro-bodies on a tadpole from the Oligocene Enspel Formation of Germany, *Palaeobiodiversity and Palaeoenvironments*. 95 (2015) 33–45. <https://doi.org/10.1007/s12549-014-0177-5>.
- [324] D.R.J.C. Olivella M À, Suberin composition from different bark layers of *Quercus suber* L. by Py-GC/MS in the presence of tetramethylammonium Hydroxide (TMAH), *Bioresources*. 6 (2011) 4936–4941.
- [325] H. van Keulen, M. Schilling, AMDIS & EXCEL: A powerful combination for evaluating THM-Py-GC/MS results from European lacquers, *Stud. Conserv.* 64 (2019) S74–S80. <https://doi.org/10.1080/00393630.2019.1594580>.
- [326] G.J.M. Versteegh, P. Blokker, K.A. Bogus, I.C. Harding, J. Lewis, S. Oltmanns, A. Rochon, K.A.F. Zonneveld, Infra red spectroscopy, flash pyrolysis, thermally assisted hydrolysis and methylation (THM) in the presence of tetramethylammonium hydroxide (TMAH) of cultured and sediment-derived *Lingulodinium polyedrum* (Dinoflagellata) cyst walls, *Org. Geochem.* 43 (2012) 92–102. <https://doi.org/10.1016/j.orggeochem.2011.10.007>.
- [327] M. Fukushima, X. Tu, A. Aneksampant, A. Tanaka, Analysis of branched-chain fatty acids in humic substances as indices for compost maturity by pyrolysis–gas chromatography/mass spectrometry with tetramethylammonium hydroxide (TMAH-py–GC/MS), *J. Mater. Cycles Waste Manag.* 20 (2018) 176–184. <https://doi.org/10.1007/s10163-016-0559-z>.
- [328] G.J.M. Versteegh, P. Blokker, K.A. Bogus, I.C. Harding, J. Lewis, S. Oltmanns, A. Rochon, K.A.F. Zonneveld, Infra red spectroscopy , flash pyrolysis , thermally assisted hydrolysis and methylation ( THM ) in the presence of tetramethylammonium hydroxide ( TMAH ) of cultured and sediment-derived *Lingulodinium polyedrum* ( Dinoflagellata ) cys, *Org. Geochem.* 43 (2012) 92–102. <https://doi.org/10.1016/j.orggeochem.2011.10.007>.
- [329] T. Ohra-Aho, P. Niemi, A.M. Aura, M. Orlandi, K. Poutanen, J. Buchert, T. Tamminen, Structure of Brewer’s Spent Grain Lignin and Its Interactions with Gut Microbiota in Vitro, *J. Agric. Food Chem.* 64 (2016) 812–820. <https://doi.org/10.1021/acs.jafc.5b05535>.
- [330] J. Lodowska, D. Wolny, S. Kurkiewicz, L. Węglarz, The pyrolytic profile of lyophilized and deep-frozen compact part of the human bone, *Sci. World J.* (2012). <https://doi.org/10.1100/2012/162406>.
- [331] G. Qi, D. Yue, M. Fukushima, S. Fukuchi, Y. Nie, Enhanced humification by carbonated basic oxygen furnace steel slag - I. Characterization of humic-like acids produced from humic precursors, *Bioresour. Technol.* 104 (2012) 497–502.

<https://doi.org/10.1016/j.biortech.2011.11.021>.

- [332] R. Ploeger, A. Shugar, G.D. Smith, V.J. Chen, Late 19th century accounts of Indian yellow: The analysis of samples from the Royal Botanic Gardens, Kew, Dye. Pigment. 160 (2019) 418–431. <https://doi.org/10.1016/j.dyepig.2018.08.014>.
- [333] B. Chefetz, J. Tarchitzky, A.P. Deshmukh, P.G. Hatcher, Y. Chen, Structural characterization of soil organic matter and humic acids in particle-size fractions of an agricultural soil, Soil Sci. Soc. Am. J. 66 (2002) 129–141. <https://doi.org/10.2136/sssaj2002.1290>.
- [334] S. Wei, V. Pintus, V. Pitthard, M. Schreiner, G. Song, Analytical characterization of lacquer objects excavated from a Chu tomb in China, J. Archaeol. Sci. 38 (2011) 2667–2674. <https://doi.org/10.1016/j.jas.2011.05.026>.
- [335] U. Wongsiriwan, Y. Noda, C. Song, P. Prasassarakich, Y. Yeboah, Lignocellulosic biomass conversion by sequential combination of organic acid and base treatments, Energy and Fuels. 24 (2010) 3232–3238. <https://doi.org/10.1021/ef901553r>.
- [336] D. Pinna, M. Galeotti, A. Rizzo, E. Cantisani, G. Sciutto, M. Zangheri, S. Prati, R. Mazzeo, A. Roda, A follow-up on the analytical study of discolouration of the marble statues of Orsanmichele in Florence, Environ. Sci. Pollut. Res. 24 (2017) 334–352. <https://doi.org/10.1007/s11356-016-7773-z>.
- [337] S. Saverwyns, M. Vermeulen, E. Van Binnebeke, Preliminary Investigation of the Chemical Composition of European Lacquers Using Pyrolysis Gas Chromatography-Mass Spectrometry, E-Preservation Sci. 11 (2014) 64–75.
- [338] X. Hao, M.R. Schilling, X. Wang, H. Khanjian, A. Heginbotham, J. Han, S. Auffret, X. Wu, B. Fang, H. Tong, Use of THM-PY-GC/MS technique to characterize complex, multilayered Chinese lacquer, J. Anal. Appl. Pyrolysis. 140 (2019) 339–348. <https://doi.org/10.1016/j.jaap.2019.04.011>.
- [339] K.I. Kuroda, A. Nakagawa-Izumi, Tetramethylammonium hydroxide (TMAH) thermochemolysis of lignin: Behavior of 4-O-etherified cinnamyl alcohols and aldehydes, J. Agric. Food Chem. 53 (2005) 8859–8865. <https://doi.org/10.1021/jf058085g>.
- [340] M. Morisson, A. Buch, C. Szopa F. Raulin, and M. Stambouli, TMAH thermochemolysis of a Martian regolith simulant: optimization of an analytical method for the detection of trace organic matter by the MOMA-Pyr-GC-MS experiment onboard the ExoMars-2020 Rover, in: Lunar Planet. Sci. XLVIII, 2017. <https://www.hou.usra.edu/meetings/lpsc2017/pdf/1079.pdf>.

- [341] C. Riedo, D. Scalarone, O. Chiantore, Pyrolysis-GC/MS for the identification of macromolecular components in historical recipes, *Anal. Bioanal. Chem.* 401 (2011) 1761–1769. <https://doi.org/10.1007/s00216-011-5142-9>.
- [342] Yustiawati, Y. Kihara, K. Sazawa, H. Kuramitz, M. Kurasaki, T. Saito, T. Hosokawa, M.S. Syawal, L. Wulandari, Hendri I, S. Tanaka, Effects of peat fires on the characteristics of humic acid extracted from peat soil in Central Kalimantan, Indonesia, *Environ. Sci. Pollut. Res.* 22 (2015) 2384–2395. <https://doi.org/10.1007/s11356-014-2929-1>.
- [343] M. Schilling, M. Bouchard, H. Khanjian, T. Learner, A. Phenix, R. Rivenc, Application of chemical and thermal analysis methods for studying cellulose ester plastics, *Acc. Chem. Res.* 43 (2010) 888–896. <https://doi.org/10.1021/ar1000132>.
- [344] C.J. Tsai, C.C. Liu, L.B. Hung, B.S. Pan, TMAH-catalyzed transesterification of EPA and DHA in encapsulated fish oil products, *J. Am. Oil Chem. Soc.* 89 (2012) 9–16. <https://doi.org/10.1007/s11746-011-1880-2>.
- [345] D.T. Mannion, A. Furey, K.N. Kilcawley, Comparison and validation of 2 analytical methods for the determination of free fatty acids in dairy products by gas chromatography with flame ionization detection, *J. Dairy Sci.* 99 (2016) 5047–5063. <https://doi.org/10.3168/jds.2015-10795>.
- [346] H. Kano, T. Okamoto, S. Kitagawa, Y. Iiguni, H. Ohtani, H. Ito, K. Iwai, M. Kuno, A novel analytical pyrolysis device applicable for measurements of less volatile pyrolyzates, *J. Anal. Appl. Pyrolysis.* 113 (2015) 165–173. <https://doi.org/10.1016/j.jaap.2014.12.008>.
- [347] O. Katsibiri, R.F. Howe, Microscopic, mass spectrometric and spectroscopic characterisation of the mordants used for gilding on wall paintings from three post-Byzantine monasteries in Thessalia, Greece, *Microchem. J.* 94 (2010) 83–89. <https://doi.org/10.1016/j.microc.2009.09.006>.
- [348] I.C.A. Sandu, A. Candeias, K.J. van den Berg, E.G. Sandbakken, E.S. Tveit, H. van Keulen, Multi technique and multiscale approaches to the study of ancient and modern art objects on wooden and canvas support, *Phys. Sci. Rev.* 4 (2019) 1–31. <https://doi.org/10.1515/psr-2018-0016>.
- [349] I. Pastorova, K.J. Van Der Berg, J.J. Boon, J.W. Verhoeven, Analysis of oxidised diterpenoid acids using thermally assisted methylation with TMAH, *J. Anal. Appl. Pyrolysis.* 43 (1997) 41–57.

- [350] J. Kaal, O. Lantes-Suárez, A. Martínez Cortizas, B. Prieto, M.P. Prieto Martínez, How useful is pyrolysis-GC/MS for the assessment of molecular properties of organic matter in archaeological pottery matrix? An exploratory case study from north-west Spain, *Archaeometry*. 56 (2014) 187–207. <https://doi.org/10.1111/arcm.12057>.
- [351] C. Granzotto, K. Sutherland, J. Arslanoglu, G.A. Ferguson, Discrimination of Acacia gums by MALDI-TOF MS: applications to micro-samples from works of art, *Microchem. J.* 144 (2019) 229–241. <https://doi.org/10.1016/j.microc.2018.08.058>.
- [352] I.D. Van Der Werf, C.D. Calvano, R. Laviano, A. Simonetti, L. Sabbatini, Multi-technique chemical characterisation of a 12-13th-century painted Crucifix, *Microchem. J.* 106 (2013) 87–94. <https://doi.org/10.1016/j.microc.2012.05.011>.
- [353] C.D. Calvano, I.D. van der Werf, F. Palmisano, L. Sabbatini, Revealing the composition of organic materials in polychrome works of art: the role of mass spectrometry-based techniques, *Anal. Bioanal. Chem.* 408 (2016) 6957–6981. <https://doi.org/10.1007/s00216-016-9862-8>.
- [354] S. Dallongeville, N. Garnier, C. Rolando, C. Tokarski, Proteins in art, archaeology, and paleontology: from detection to identification, *Chem. Rev.* 116 (2016) 2–79. <https://doi.org/10.1021/acs.chemrev.5b00037>.
- [355] X. Yu, C. Liu, Y. Guo, T. Deng, Speciation analysis of trace arsenic, mercury, selenium and antimony in environmental and biological samples based on hyphenated techniques, *Molecules*. 24 (2019) 926. <https://doi.org/10.3390/molecules24050926>.
- [356] Y. and K.K. Matsuzaki, H., Tsuchiya, Y.S., Muramatsu, Y., Maejima, Y., Miyairi, Comparison of Depth Profiles of  $^{129}\text{I}$  and  $^{14}\text{C}$  Concentration in the surface layer of soil collected from northeastern Japan, *Radiocarbon*. 52 (2010) 1487–1497.
- [357] S. Chung, A. Chan, Y. Xiao, V. Lin, Y.Y. Ho, Iodine content in commonly consumed food in Hong Kong and its changes due to cooking, *Food Addit. Contam. Part B Surveill.* 6 (2013) 24–29. <https://doi.org/10.1080/19393210.2012.721011>.
- [358] and S.S.F.A.-K. A. A. Al-Absi, Conversion of Arabian light crude oil to light olefins via catalytic and thermal cracking, *Energy & Fuels*. 32 (2018) 8705–8714. <https://doi.org/10.1021/acs.energyfuels.8b01932>.
- [359] E. Duborská, M. Urík, M. Bujdoš, M. Matulová, Influence of physicochemical properties of various soil types on iodide and iodate sorption, *Chemosphere*. 214 (2019) 168–175. <https://doi.org/10.1016/j.chemosphere.2018.09.041>.

- [360] Z. Huang, X.D. Pan, J.L. Han, P.G. Wu, J. Tang, Y. Tan, Determination of methylmercury in marine fish from coastal areas of Zhejiang, China, *Food Addit. Contam. Part B Surveill.* 5 (2012) 182–187. <https://doi.org/10.1080/19393210.2012.683881>.
- [361] T.S. Peretyazhko, B. Sutter, R. V. Morris, D.G. Agresti, L. Le, D.W. Ming, Fe/Mg smectite formation under acidic conditions on early Mars, *Geochim. Cosmochim. Acta.* 173 (2016) 37–49. <https://doi.org/10.1016/j.gca.2015.10.012>.
- [362] S. Smoleń, W. Sady, Influence of iodine fertilization and soil application of sucrose on the effectiveness of iodine biofortification, yield, nitrogen metabolism and biological quality of spinach, *Acta Sci. Pol. Hortorum Cultus.* 10 (2011) 51–63.
- [363] J.E. Olson, M.L. Adamic, D.C. Snyder, J.L. Brookhart, P.A. Hahn, M.G. Watrous, Independent measurements of <sup>129</sup>I content in environmental reference materials using accelerator and thermal ionization mass spectrometry, *Nucl. Instruments Methods Phys. Res. Sect. B Beam Interact. with Mater. Atoms.* 438 (2019) 84–88. <https://doi.org/10.1016/j.nimb.2018.07.018>.
- [364] E. Duborská, M. Urík, M. Bujdoš, J. Kubová, Aging and Substrate Type Effects on Iodide and Iodate Accumulation by Barley (*Hordeum vulgare* L.), *Water. Air. Soil Pollut.* 227 (2016) 407. <https://doi.org/10.1007/s11270-016-3112-8>.
- [365] K. Gołąbek, K.A. Tarach, K. Góra-Marek, Xylenes transformation over zeolites ZSM-5 ruled by acidic properties, *Spectrochim. Acta - Part A Mol. Biomol. Spectrosc.* 192 (2018) 361–367. <https://doi.org/10.1016/j.saa.2017.11.028>.
- [366] J. V. Hogancamp, B. Sutter, R. V. Morris, P.D. Archer, D.W. Ming, E.B. Rampe, P. Mahaffy, R. Navarro-Gonzalez, Chlorate/Fe-bearing phase mixtures as a possible source of oxygen and chlorine detected by the Sample Analysis at Mars (SAM) Instrument in Gale Crater, Mars, J. *Geophys. Res. Planets.* 123 (2018) 2920–2938. <https://doi.org/10.1029/2018JE005691>.
- [367] C. Feng, Z. Pedrero, P. Li, B. Du, X. Feng, M. Monperrus, E. Tessier, S. Berail, D. Amouroux, Investigation of Hg uptake and transport between paddy soil and rice seeds combining Hg isotopic composition and speciation, *Elem. Sci. Anthr.* 4 (2016) 000087. <https://doi.org/10.12952/journal.elementa.000087>.
- [368] E. Pagliano, B. Campanella, A. D’Ulivo, Z. Mester, Derivatization chemistries for the determination of inorganic anions and structurally related compounds by gas chromatography - A review, *Anal. Chim. Acta.* 1025 (2018) 12–40. <https://doi.org/10.1016/j.aca.2018.03.043>.
- [369] M. Miyamoto, K. Mabuchi, J. Kamada, Y. Hirota, Y. Oumi, N. Nishiyama, S. Uemiya, para-

- Selectivity of silicalite-1 coated MFI type galloaluminosilicate in aromatization of light alkanes, *J. Porous Mater.* 22 (2015) 769–778. <https://doi.org/10.1007/s10934-015-9950-8>.
- [370] A. Khosravanipour Mostafazadeh, O. Solomatnikova, P. Drogui, R. Dayal Tyagi, A review of recent research and developments in fast pyrolysis and bio-oil upgrading, *Biomass Conv. Bioref.* 8 (2018) 739–773. <https://doi.org/10.1007/s13399-018-0320-z>.
- [371] A. Quéro, R. Molinié, D. Mathiron, B. Thiombiano, J.X. Fontaine, D. Brancourt, O. Van Wuytswinkel, E. Petit, H. Demailly, G. Mongelard, S. Pilard, B. Thomasset, F. Mesnard, Metabolite profiling of developing *Camelina sativa* seeds, *Metabolomics*. 12 (2016) 1–14. <https://doi.org/10.1007/s11306-016-1135-1>.
- [372] A.M. Tadini, I.C. Constantino, A. Nuzzo, R. Spaccini, A. Piccolo, A.B. Moreira, M.C. Bisinoti, Characterization of typical aquatic humic substances in areas of sugarcane cultivation in Brazil using tetramethylammonium hydroxide thermochemolysis, *Sci. Total Environ.* 518–519 (2015) 201–208. <https://doi.org/10.1016/j.scitotenv.2015.02.103>.
- [373] S. Farzadnia, R.D. Nimmagadda, C. McRae, A comparative structural study of nitrogen-rich fulvic acids from various Antarctic lakes, *Environ. Chem.* 14 (2017) 502–514. <https://doi.org/10.1071/EN17095>.
- [374] E.V. Abakumov, T. Cajthaml, J. Brus, J. Frouz, Humus accumulation, humification, and humic acid composition in soils of two post-mining chronosequences after coal mining, *J. Soils Sediments*. 13 (2013) 491–500. <https://doi.org/10.1007/s11368-012-0579-9>.
- [375] L. Nieto, J. Jiménez-Barbero, A.T. Martínez, J. Rencoret, A. Gutiérrez, J.C. del Río, White and brown rot decay as two models for biotechnological processing of wood: structural analysis by 2D NMR and analytical pyrolysis, *Oxidative Enzym. as Sustain. Ind. Biocatal.* (2010) 1–6.
- [376] L. Xiao, Y. Li, Y. Liao, H. Ma, J. Wu, Y. Zhang, J. Yao, Bioconversion of lignite humic acid by white-rot fungi and characterization of products, *3 Biotech.* 8 (2018) 258. <https://doi.org/10.1007/s13205-018-1281-4>.
- [377] K.I. Kuroda, T. Ashitani, K. Fujita, Tetramethylammonium hydroxide (TMAH) thermochemolysis of lignin: Formation of (E)-5-formyl-2,3,3',4'-tetramethoxystilbene and its origins, *J. Anal. Appl. Pyrolysis*. 89 (2010) 233–238. <https://doi.org/10.1016/j.jaap.2010.08.008>.
- [378] A. Gomiero, K.B. Øysæd, T. Agustsson, N. van Hoytema, T. van Thiel, F. Grati, First record of characterization, concentration and distribution of microplastics in coastal sediments of an

- urban fjord in south west Norway using a thermal degradation method, *Chemosphere*. 227 (2019) 705–714. <https://doi.org/10.1016/j.chemosphere.2019.04.096>.
- [379] F.C. Izzo, A. Carrieri, G. Bartolozzi, H. van Keulen, I. Lorenzon, E. Balliana, C. Cucci, F. Grazi, M. Piccolo, Elucidating the composition and the state of conservation of nitrocellulose-based animation cells by means of non-invasive and micro-destructive techniques, *J. Cult. Herit.* 35 (2019) 254–262. <https://doi.org/10.1016/j.culher.2018.09.010>.
- [380] S. Chang, K.Y.A. Lin, C. Lu, Efficient adsorptive removal of Tetramethylammonium hydroxide (TMAH) from water using graphene oxide, *Sep. Purif. Technol.* 133 (2014) 99–107. <https://doi.org/10.1016/j.seppur.2014.06.050>.
- [381] M. Collard, B. Teychené, L. Lemée, Comparison of three different wastewater sludge and their respective drying processes: Solar, thermal and reed beds – Impact on organic matter characteristics, *J. Environ. Manage.* 203 (2017) 760–767. <https://doi.org/10.1016/j.jenvman.2016.05.070>.
- [382] S. Aveni, M.B. Failla, A. Gatti, L. Mannina, T. Poli, A Japanned Telescope from Cavour Castle in Santena: Study and Conservation Treatment of an Eighteenth-Century Scientific Instrument, *Stud. Conserv.* 64 (2019) S147–S153. <https://doi.org/10.1080/00393630.2018.1563348>.
- [383] H. Szczepanowska, R. Ploeger, The chemical analysis of Southeast Asian lacquers collected from forests and workshops, *J. Cult. Herit.* 40 (2019) 215–225. <https://doi.org/10.1016/j.culher.2019.05.015>.
- [384] J. Kotulová, D. Starek, M. Havelcová, H. Pálková, Amber and organic matter from the late Oligocene deep-water deposits of the Central Western Carpathians (Orava–Podhale Basin), *Int. J. Coal Geol.* 207 (2019) 96–109. <https://doi.org/10.1016/j.coal.2019.02.006>.
- [385] K. Helwig, É. Forest, A. Turcotte, W. Baker, N.E. Binnie, E. Moffatt, J. Poulin, The formation of calcium fatty acid salts in oil paint: two case studies, in: 2019: pp. 297–311. [https://doi.org/10.1007/978-3-319-90617-1\\_17](https://doi.org/10.1007/978-3-319-90617-1_17).
- [386] M. Kirpluks, E. Vanags, A. Abolins, A. Fridrihsone, U. Cabulis, Chemo-enzymatic oxidation of tall oil fatty acids as a precursor for further polyol production, *J. Clean. Prod.* 215 (2019) 390–398. <https://doi.org/10.1016/j.jclepro.2018.12.323>.
- [387] S. El-Guendouz, B. Lyoussi, J.P. Lourenço, A.M. Rosa da Costa, M.G. Miguel, C. Barrocas Dias, A. Manhita, L. Jordao, I. Nogueira, M.L. Faleiro, Magnetite nanoparticles functionalized with propolis against methicillin resistant strains of *Staphylococcus aureus*, *J. Taiwan Inst.*

- Chem. Eng. 102 (2019) 25–33. <https://doi.org/10.1016/j.jtice.2019.05.018>.
- [388] M.P.C. P. G. Hammer, D. R. Locke, A. S. Burton, Thermal studies of ammonium cyanide reactions: A model for thermal alteration of prebiotic compounds in meteorite parent bodies, in: 2017.
- [389] R.A. Parildar, A.A.B. Ibik, Characterization of tertiary amine and epoxy functional all-acrylic coating system, *Prog. Org. Coatings*. 76 (2013) 955–958. <https://doi.org/10.1016/j.porgcoat.2012.10.019>.
- [390] S. Drouin, M. Boussafir, J.L. Robert, P. Alberic, A. Durand, Carboxylic acid sorption on synthetic clays in sea water: In vitro experiments and implications for organo-clay behaviour under marine conditions, *Org. Geochem*. 41 (2010) 192–199. <https://doi.org/10.1016/j.orggeochem.2009.10.006>.
- [391] J. Zhang, C. Yip, C. Xia, Y. Liang, Evaluation of methane release from coals from the San Juan basin and Powder River basin, *Fuel*. 244 (2019) 388–394. <https://doi.org/10.1016/j.fuel.2019.02.020>.
- [392] S.I. Yamasaki, A. Takeda, T. Watanabe, K. Tagami, S. Uchida, H. Takata, Y. Maejima, N. Kihou, N. Tsuchiya, Bromine and iodine in Japanese soils determined with polarizing energy dispersive X-ray fluorescence spectrometry, *Soil Sci. Plant Nutr*. 61 (2015) 751–760. <https://doi.org/10.1080/00380768.2015.1054773>.
- [393] J. Zhang, K. Anderson, D. Britt, Y. Liang, Sustaining biogenic methane release from Illinois coal in a fermentor for one year, *Fuel*. 227 (2018) 27–34. <https://doi.org/10.1016/j.fuel.2018.04.061>.
- [394] K. Sutherland, Bleached shellac picture varnishes: Characterization and case studies, *J. Inst. Conserv*. 33 (2010) 129–145. <https://doi.org/10.1080/19455224.2010.495242>.
- [395] F. Beckett, A. Holden, G.D. Smith, Seeing the light: Research, conservation and exhibition of a 1980s daylight fluorescent painted leather jacket designed by Sprouse and painted by Castronovo, *J. Am. Inst. Conserv*. 58 (2019) 233–247. <https://doi.org/10.1080/01971360.2019.1614290>.
- [396] D. Rucker, V. Kisand, B. Scholz-Böttcher, T. Kneib, A. Lemke, J. Rullkötter, M. Simon, Differential decomposition of humic acids by marine and estuarine bacterial communities at varying salinities, *Biogeochemistry*. 111 (2012) 331–346. <https://doi.org/10.1007/s10533-011-9653-4>.



- [397] X. Fan, J. Song, Comparative study for separation of atmospheric humic-like substance ( HULIS ) by ENVI-18 , HLB , XAD-8 and DEAE sorbents : Elemental composition , FT-IR , <sup>1</sup> H NMR and off-line thermochemolysis with tetramethylammonium hydroxide ( TMAH ) , *Chemosphere*. 93 (2013) 1710–1719. <https://doi.org/10.1016/j.chemosphere.2013.05.045>.
- [398] X. Fan, S. Wei, M. Zhu, J. Song, P. Peng, Molecular characterization of primary humic-like substances in fine smoke particles by thermochemolysis–gas chromatography–mass spectrometry, *Atmos. Environ.* 180 (2018) 1–10. <https://doi.org/10.1016/j.atmosenv.2018.02.033>.
- [399] Z. Steinmetz, M.P. Kurtz, J.P. Zubrod, A.H. Meyer, M. Elsner, G.E. Schaumann, Biodegradation and photooxidation of phenolic compounds in soil—A compound-specific stable isotope approach, *Chemosphere*. 230 (2019) 210–218. <https://doi.org/10.1016/j.chemosphere.2019.05.030>.
- [400] S.-S. Choi, J. Ko, Analysis of cyclic pyrolysis products formed from amino acid monomer, *J. Chromatogr. A*. 1218 (2011) 8443–8455. <https://doi.org/10.1016/j.chroma.2011.09.055>.
- [401] F. Benlboukht, L. Lemee, S. Amir, A. Ambles, M. Hafidi, Biotransformation of organic matter during composting of solid wastes from traditional tanneries by thermochemolysis coupled with gas chromatography and mass spectrometry, *Ecol. Eng.* 90 (2016) 87–95. <https://doi.org/10.1016/j.ecoleng.2016.01.074>.
- [402] P. kaur, C. Balomajumder, Simultaneous biodegradation of mixture of carbamates by newly isolated *Ascochyta* sp. CBS 237.37, *Ecotoxicol. Environ. Saf.* 169 (2019) 590–599. <https://doi.org/10.1016/j.ecoenv.2018.11.029>.
- [403] J. Waissman, M. Honig, S. Pecker, A. Benyamini, A. Hamo, S. Ilani, Realization of pristine and locally tunable one-dimensional electron systems in carbon nanotubes, *Nat. Nanotechnol.* 8 (2013) 569–574. <https://doi.org/10.1038/nnano.2013.143>.
- [404] R.S. Patkar, M.G. Seelan, V. Ramgopal Rao, A highly sensitive piezoresistive cantilever based sensor platform for detection of macronutrients in soil, *IEEE-NANO 2015 - 15th Int. Conf. Nanotechnol.* (2015) 751–754. <https://doi.org/10.1109/NANO.2015.7388717>.
- [405] M. Xu, T. Bearda, H.S. Radhakrishnan, M. Filipič, I. Gordon, M. Debucquoy, J. Szlufcik, J. Poortmans, Laser assisted patterning of a-Si:H: detailed investigation of laser damage, *Phys. Status Solidi - Rapid Res. Lett.* 11 (2017) 1–5. <https://doi.org/10.1002/pssr.201700125>.
- [406] J. Patočka, A. Krejčová, K. Stojarová, K. Hrdá, M. Pouzar, The ICP-OES method for

- determination of zinc in *Enchytraeus crypticus* and agarose gel from ecotoxicological tests, *Chem. Pap.* 73 (2019) 159–164. <https://doi.org/10.1007/s11696-018-0563-y>.
- [407] G. Karavalakis, G. Anastopoulos, D. Karonis, S. Stournas, Biodiesel production using tetramethyl- and benzyltrimethyl ammonium hydroxides as strong base catalysts, *Fuel Process. Technol.* 91 (2010) 1585–1590. <https://doi.org/10.1016/j.fuproc.2010.06.006>.
- [408] E. Kaschak, B. Knopf, J.H. Petersen, N.H. Bings, H. König, Biotic methylation of mercury by intestinal and sulfate-reducing bacteria and their potential role in mercury accumulation in the tissue of the soil-living *Eisenia foetida*, *Soil Biol. Biochem.* 69 (2014) 202–211. <https://doi.org/10.1016/j.soilbio.2013.11.004>.
- [409] D. Grotto, J. Vicentini, J.P. Friedmann Angeli, E. Francisco Latorraca, P.A. Pontes Monteiro, G.R. Mazzaron Barcelos, S. Somacal, T. Emanuelli, F. Barbosa, Evaluation of protective effects of fish oil against oxidative damage in rats exposed to methylmercury, *Ecotoxicol. Environ. Saf.* 74 (2011) 487–493. <https://doi.org/10.1016/j.ecoenv.2010.10.012>.
- [410] H.D.C. Viégas, J.M.S. Almeida, C.A. Lacerda, J.B. Silva, A.L.B. Marques, E.P. Marques, A rapid and sensitive voltammetric determination of sulphur in biodiesel in samples not treated and treated with TMAH, *Fuel*. 202 (2017) 464–469. <https://doi.org/10.1016/j.fuel.2017.04.048>.
- [411] A. Iveković, G. Dražić, S. Novak, Densification of a SiC-matrix by electrophoretic deposition and polymer infiltration and pyrolysis process, *J. Eur. Ceram. Soc.* 31 (2011) 833–840. <https://doi.org/10.1016/j.jeurceramsoc.2010.11.021>.
- [412] R. Mayén-Mondragón, G. Falk, R. Clasen, Electrophoretic impregnation/deposition complemented with polymeric templating for the fabrication of functionalized-porosity layered-ceramics: A Solid-oxide-fuel-cells approach, *J. Am. Ceram. Soc.* 95 (2012) 593–599. <https://doi.org/10.1111/j.1551-2916.2011.04960.x>.
- [413] Z. Li, B. Wang, S. Ge, L. Yan, Y. Liu, Z. Li, A. Ren, A simultaneous analysis method of polycyclic aromatic hydrocarbons, nicotine, cotinine and metals in human hair, *Environ. Pollut.* 219 (2016) 66–71. <https://doi.org/10.1016/j.envpol.2016.09.045>.
- [414] A.M. Nunes, T.S. Acunha, E.Q. Oreste, F.G. Lepri, M.A. Vieira, A.J. Curtius, A.S. Ribeiro, Determination of Ca, Cu, Fe and Mg in fresh and processed meat treated with tetramethylammonium hydroxide by atomic absorption spectrometry, *J. Braz. Chem. Soc.* 22 (2011) 1850–1857. <https://doi.org/10.1590/S0103-50532011001000004>.
- [415] H.E. Bowley, S.D. Young, E.L. Ander, N.M.J. Crout, M.J. Watts, E.H. Bailey, Iodine

- bioavailability in acidic soils of Northern Ireland, *Geoderma*. 348 (2019) 97–106.  
<https://doi.org/10.1016/j.geoderma.2019.04.020>.
- [416] H. Fujiwara, Observation of radioactive iodine (<sup>131</sup>I, <sup>129</sup>I) in cropland soil after the Fukushima nuclear accident, *Sci. Total Environ.* 566–567 (2016) 1432–1439.  
<https://doi.org/10.1016/j.scitotenv.2016.06.004>.
- [417] V.C. Costa, R.M. Pereira, J.E. Mello, J.R. Brum, R.S. Picoloto, M.F. Mesko, Indirect determination of chlorine and fluorine in eye shadow by ion chromatography after an eco-friendly sample preparation method based on combustion reaction, *Microchem. J.* 150 (2019) 104125. <https://doi.org/10.1016/j.microc.2019.104125>.
- [418] A. Osswald, A. Poszwa, M. Bueno, C. Arnaudguilhem, D. Billet, Y. Thiry, C. Leyval, Contribution of microbial activity to formation of organically bound chlorine during batch incubation of forest soil using <sup>37</sup>Cl as a tracer, *Soil Biol. Biochem.* 100 (2016) 210–217.  
<https://doi.org/10.1016/j.soilbio.2016.06.012>.
- [419] S.C. Sheppard, J.M. Long, B. Sanipelli, Plant/soil concentration ratios for paired field and garden crops, with emphasis on iodine and the role of soil adhesion, *J. Environ. Radioact.* 101 (2010) 1032–1037. <https://doi.org/10.1016/j.jenvrad.2010.08.001>.
- [420] I. Shtangeeva, P. Perämäki, M. Niemelä, E. Kurashov, Y. Krylova, Potential of wheat (*Triticum aestivum* L.) and pea (*Pisum sativum*) for remediation of soils contaminated with bromides and PAHs, *Int. J. Phytoremediation.* 20 (2018) 560–566.  
<https://doi.org/10.1080/15226514.2017.1405375>.
- [421] I. Shtangeeva, M. Niemelä, P. Perämäki, A. Ryumin, S. Timofeev, S. Chukov, G. Kasatkina, Phytoextraction of bromine from contaminated soil, *J. Geochemical Explor.* 174 (2017) 21–28.  
<https://doi.org/10.1016/j.gexplo.2016.03.012>.
- [422] N. Yamaguchi, M. Nakano, R. Takamatsu, H. Tanida, Inorganic iodine incorporation into soil organic matter: Evidence from iodine K-edge X-ray absorption near-edge structure, *J. Environ. Radioact.* 101 (2010) 451–457. <https://doi.org/10.1016/j.jenvrad.2008.06.003>.
- [423] E. Duborská, M. Urík, J. Kubová, Interaction with soil enhances the toxic effect of iodide and iodate on barley (*Hordeum vulgare* L.) compared to artificial culture media during initial growth stage, *Arch. Agron. Soil Sci.* 64 (2018) 46–57.  
<https://doi.org/10.1080/03650340.2017.1328104>.
- [424] K. Tagami, S. Uchida, A. Takeda, S. Yamasaki, Estimation of plant-unavailable iodine

- concentrations in agricultural fields, *Soil Sci. Soc. Am. J.* 74 (2010) 1562–1567.  
<https://doi.org/10.2136/sssaj2009.0423>.
- [425] D. Mani, S.S. Kumar, M.A. Rasheed, D.J. Patil, A.M. Dayal, G.G. Rao, V. Balaram, Soil iodine determination in deccan syncline, india: implications for near surface geochemical hydrocarbon prospecting, *Nat. Resour. Res.* 20 (2011) 75–88. <https://doi.org/10.1007/s11053-010-9134-9>.
- [426] D.B. Kumssa, E.J.M. Joy, S.D. Young, D.W. Odee, E.L. Ander, M.R. Broadley, Variation in the mineral element concentration of *Moringa oleifera* Lam. and *M. stenopetala* (Bak. f.) Cuf.: Role in human nutrition, *PLoS One.* 12 (2017) 1–26.  
<https://doi.org/10.1371/journal.pone.0175503>.
- [427] M. Roulier, M. Bueno, Y. Thiry, F. Coppin, P.O. Redon, I. Le Hécho, F. Pannier, Iodine distribution and cycling in a beech (*Fagus sylvatica*) temperate forest, *Sci. Total Environ.* 645 (2018) 431–440. <https://doi.org/10.1016/j.scitotenv.2018.07.039>.
- [428] S. Smoleń, I. Ledwożyw-Smoleń, W. Sady, Iodine biofortification of spinach by soil fertigation with additional application of humic and fulvic acids, *New Zeal. J. Crop Hortic. Sci.* 45 (2017) 233–250. <https://doi.org/10.1080/01140671.2017.1314307>.
- [429] M. Roulier, F. Coppin, M. Bueno, M. Nicolas, Y. Thiry, C. Della Vedova, L. Février, F. Pannier, I. Le Hécho, Iodine budget in forest soils: Influence of environmental conditions and soil physicochemical properties, *Chemosphere.* 224 (2019) 20–28.  
<https://doi.org/10.1016/j.chemosphere.2019.02.060>.
- [430] S. Uchida, K. Tagami, Iodine transfer from agricultural soils to edible part of crops, *Proc. Radiochem.* 1 (2011) 279–283. <https://doi.org/10.1524/rcpr.2011.0048>.
- [431] S. Smolen, L. Skoczylas, I. Ledwożyw-Smolen, R. Rakoczy, A. Kopec, E. Piktkowska, R. Bieanowska-Kopec, M. Pysz, A. Koronowicz, J. Kapusta-Duch, T. Pawlowski, Iodine and selienium biofortification of lectuce (*Lactuca sativa* L.) by soil fertilization with various compounds of these elements, *Acta Sci. Pol. Cultus.* 15 (2016) 69–91.
- [432] I. Cakmak, C. Prom-u-thai, L.R.G. Guilherme, A. Rashid, K.H. Hora, A. Yazici, E. Savasli, M. Kalayci, Y. Tutus, P. Phuphong, M. Rizwan, F.A.D. Martins, G.S. Dinali, L. Ozturk, Iodine biofortification of wheat, rice and maize through fertilizer strategy, *Plant Soil.* 418 (2017) 319–335. <https://doi.org/10.1007/s11104-017-3295-9>.
- [433] A. Daraoui, R. Michel, M. Gorny, D. Jakob, R. Sachse, H.A. Synal, V. Alfimov, Iodine-129,

- Iodine-127 and Caesium-137 in the environment: Soils from Germany and Chile, *J. Environ. Radioact.* 112 (2012) 8–22. <https://doi.org/10.1016/j.jenvrad.2012.02.011>.
- [434] M.J. Watts, J. O'Reilly, A. Maricelli, A. Coleman, E.L. Ander, N.I. Ward, A snapshot of environmental iodine and selenium in La Pampa and San Juan provinces of Argentina, *J. Geochemical Explor.* 107 (2010) 87–93. <https://doi.org/10.1016/j.gexplo.2009.11.002>.
- [435] G. Yang, J. Hu, H. Tsukada, H. Tazoe, Y. Shao, M. Yamada, Vertical distribution of <sup>129</sup>I and radiocesium in forest soil collected near the Fukushima Daiichi Nuclear Power Plant boundary, *Environ. Pollut.* 250 (2019) 578–585. <https://doi.org/10.1016/j.envpol.2019.04.053>.
- [436] T.H. Hu, L.M. Whang, P.W.G. Liu, Y.C. Hung, H.W. Chen, L. Bin Lin, C.F. Chen, S.K. Chen, S.F. Hsu, W. Shen, R. Fu, R. Hsu, Biological treatment of TMAH (tetra-methyl ammonium hydroxide) in a full-scale TFT-LCD wastewater treatment plant, *Bioresour. Technol.* 113 (2012) 303–310. <https://doi.org/10.1016/j.biortech.2012.02.070>.
- [437] T. Danshita, Y. Miyaoka, N. Matsuura, H. Sumino, T. Yamaguchi, K. Syutsubo, Influence of tetramethylammonium hydroxide (TMAH) on the microbial properties of anaerobic granular sludge acclimated to isopropyl alcohol (IPA) wastewater under psychrophilic conditions, *J. Environ. Sci. Heal. - Part A Toxic/Hazardous Subst. Environ. Eng.* 53 (2018) 1015–1021. <https://doi.org/10.1080/10934529.2018.1471034>.
- [438] L.M. Whang, T.H. Hu, P.W.G. Liu, Y.C. Hung, T. Fukushima, Y.J. Wu, S.H. Chang, Molecular analysis of methanogens involved in methanogenic degradation of tetramethylammonium hydroxide in full-scale bioreactors, *Appl. Microbiol. Biotechnol.* 99 (2015) 1485–1497. <https://doi.org/10.1007/s00253-014-6058-z>.
- [439] A. Duval, M. Lawoko, A review on lignin-based polymeric, micro- and nano-structured materials, *React. Funct. Polym.* 85 (2014) 78–96. <https://doi.org/10.1016/j.reactfunctpolym.2014.09.017>.
- [440] P. Azadi, O.R. Inderwildi, R. Farnood, D.A. King, Liquid fuels, hydrogen and chemicals from lignin: A critical review, *Renew. Sustain. Energy Rev.* 21 (2013) 506–523. <https://doi.org/10.1016/j.rser.2012.12.022>.
- [441] D.C. Waggoner, D.C. Waggoner, Lignin contribution to the global carbon pool : investigating the abiotic modification of lignin by reactive oxygen species, 2017. <https://doi.org/10.25777/74m6-z498>.
- [442] J.S. Schilling, J. Ai, R.A. Blanchette, S.M. Duncan, T.R. Filley, U.W. Tschirner,

- Lignocellulose modifications by brown rot fungi and their effects, as pretreatments, on cellulolysis, *Bioresour. Technol.* 116 (2012) 147–154.  
<https://doi.org/10.1016/j.biortech.2012.04.018>.
- [443] J.A. Ceja-Navarro, U. Karaoz, M. Bill, Z. Hao, R.A. White, A. Arellano, L. Ramanculova, T.R. Filley, T.D. Berry, M.E. Conrad, M. Blackwell, C.D. Nicora, Y.M. Kim, P.N. Reardon, M.S. Lipton, J.N. Adkins, J. Pett-Ridge, E.L. Brodie, Gut anatomical properties and microbial functional assembly promote lignocellulose deconstruction and colony subsistence of a wood-feeding beetle, *Nat. Microbiol.* 4 (2019) 864–875. <https://doi.org/10.1038/s41564-019-0384-y>.
- [444] J. Ke, D.D. Laskar, D. Singh, S. Chen, In situ lignocellulosic unlocking mechanism for carbohydrate hydrolysis in termites : crucial lignin modification, *Biotechnol. Biofuels.* 4 (2011) 17.
- [445] J. Kaal, O. Serrano, K.G.J. Nierop, J. Schellekens, A. Martínez Cortizas, M.Á. Mateo, Molecular composition of plant parts and sediment organic matter in a Mediterranean seagrass (*Posidonia oceanica*) mat, *Aquat. Bot.* 133 (2016) 50–61.  
<https://doi.org/10.1016/j.aquabot.2016.05.009>.
- [446] J. Kaal, O. Serrano, A. Martínez Cortizas, J.A. Baldock, P.S. Lavery, Millennial-scale changes in the molecular composition of *Posidonia australis* seagrass deposits: Implications for Blue Carbon sequestration, *Org. Geochem.* 137 (2019) 103898.  
<https://doi.org/10.1016/j.orggeochem.2019.07.007>.
- [447] L. Lemée, D. Kpogbemabou, L. Pinard, R. Beauchet, J. Laduranty, Biological pretreatment for production of lignocellulosic biofuel, *Bioresour. Technol.* 117 (2012) 234–241.  
<https://doi.org/10.1016/j.biortech.2012.04.056>.
- [448] J. Kaal, O. Serrano, C. José, J. Rencoret, Radically different lignin composition in *Posidonia* species may link to differences in organic carbon sequestration capacity, *Org. Geochem.* 124 (2018) 247–256. <https://doi.org/10.1016/j.orggeochem.2018.07.017>.
- [449] T. Klotzbücher, K. Kaiser, T.R. Filley, K. Kalbitz, Processes controlling the production of aromatic water-soluble organic matter during litter decomposition, *Soil Biol. Biochem.* 67 (2013) 133–139. <https://doi.org/10.1016/j.soilbio.2013.08.003>.
- [450] P.J. Hatton, S. Chatterjee, T.R. Filley, K. Dastmalchi, A.F. Plante, S. Abiven, X. Gao, C.A. Masiello, S.W. Leavitt, K.J. Nadelhoffer, R.E. Stark, J.A. Bird, Tree taxa and pyrolysis temperature interact to control the efficacy of pyrogenic organic matter formation, *Biogeochemistry.* 130 (2016) 103–116. <https://doi.org/10.1007/s10533-016-0245-1>.

- [451] J.S. Watson, W.T. Fraser, M.A. Sephton, Formation of a polyalkyl macromolecule from the hydrolysable component within sporopollenin during heating/pyrolysis experiments with Lycopodium spores, *J. Anal. Appl. Pyrolysis*. 95 (2012) 138–144.  
<https://doi.org/10.1016/j.jaap.2012.01.019>.
- [452] H. Lu, W. Wu, Y. Chen, H. Wang, M. Devare, J.E. Thies, Soil microbial community responses to Bt transgenic rice residue decomposition in a paddy field, *J. Soils Sediments*. 10 (2010) 1598–1605. <https://doi.org/10.1007/s11368-010-0264-9>.
- [453] A.J. Blyth, J.S. Watson, J. Woodhead, J. Hellstrom, Organic compounds preserved in a 2.9million year old stalagmite from the Nullarbor Plain, Australia, *Chem. Geol.* 279 (2010) 101–105. <https://doi.org/10.1016/j.chemgeo.2010.10.006>.
- [454] K.G.J. Nierop, E.N. Speelman, J.W. de Leeuw, G.J. Reichart, The omnipresent water fern *Azolla caroliniana* does not contain lignin, *Org. Geochem.* 42 (2011) 846–850.  
<https://doi.org/10.1016/j.orggeochem.2011.05.001>.
- [455] R.A. Smith, E. Gonzales-Vigil, S.D. Karlen, J.-Y. Park, F. Lu, C. Wilkerson, A.L. Samuels, J. Ralph, S.D. Mansfield, Engineering monolignol p-coumarate conjugates into Poplar and *Arabidopsis* lignins, *Plant Physiol.* 169 (2015) 2992–3001.  
<https://doi.org/10.1104/pp.15.00815>.
- [456] G.D. Abbott, A. Muhammad, L. Belyea, C. Laing, G.L. Cowie, The biogeochemistry of Sphagnum mosses - the effects of substrate source on their phenolic composition, in: 19th World Congr. Soil Sci. Soil Solut. a Chang. World, Brisbane, Australia, 2010: pp. 195–197.
- [457] A.M. Baetsen-Young, J.E. Kaminski, M. Tien, Lignocellulose degrading capabilities of in creeping bentgrass, *Int. Turfgrass Soc. Res. J.* 13 (2017) 145–152.  
<https://doi.org/10.2134/itsrj2016.05.0400>.
- [458] J. Ke, D.D. Laskar, S. Chen, Tetramethylammonium hydroxide (TMAH) thermochemolysis for probing in situ softwood lignin modification in each gut segment of the termite, *J. Agric. Food Chem.* 61 (2013) 1299–1308.
- [459] Q. Chen, M.N. Marshall, S.M. Geib, M. Tien, T.L. Richard, Effects of laccase on lignin depolymerization and enzymatic hydrolysis of ensiled corn stover, *Bioresour. Technol.* 117 (2012) 186–192. <https://doi.org/10.1016/j.biortech.2012.04.085>.
- [460] M. Olivella, C. Bazzicalupi, A. Bianchi, J.C. del R o, N. Fiol, I. Villaescusa, Binding interactions between suberin monomer components and pesticides, *Sci. Total Environ.* 527–

- 528 (2015) 159–164. <https://doi.org/10.1016/j.scitotenv.2015.04.118>.
- [461] J.W. Turner, B.E. Hartman, P.G. Hatcher, Structural characterization of suberan isolated from river birch (*Betula nigra*) bark, *Org. Geochem.* 57 (2013) 41–53. <https://doi.org/10.1016/j.orggeochem.2013.01.004>.
- [462] M.W. Haenel, Recent progress in coal structure research, *Fuel.* 71 (1992) 1211–1223. [https://doi.org/10.1016/0016-2361\(92\)90046-Q](https://doi.org/10.1016/0016-2361(92)90046-Q).
- [463] Y. He, L. Yan, Y.Y. Liu, Y.Y. Liu, Y. Bai, J. Wang, F. Li, Effect of SiO<sub>2</sub> /Al<sub>2</sub>O<sub>3</sub> ratios of HZSM-5 zeolites on the formation of light aromatics during lignite pyrolysis, *Fuel Process. Technol.* 188 (2019) 70–78. <https://doi.org/10.1016/j.fuproc.2019.02.004>.
- [464] L. Yan, Y. Bai, Y. Liu, Y. He, F. Li, Effects of low molecular compounds in coal on the catalytic upgrading of gaseous tar, *Fuel.* 226 (2018) 316–321. <https://doi.org/10.1016/j.fuel.2018.03.191>.
- [465] M. Radke, R.G. Schaefer, D. Leythaeuser, M. Teichmüller, Composition of soluble organic matter in coals: relation to rank and liptinite fluorescence, *Geochim. Cosmochim. Acta.* 44 (1980) 1787–1800. [https://doi.org/10.1016/0016-7037\(80\)90228-8](https://doi.org/10.1016/0016-7037(80)90228-8).
- [466] J. Kong, X.Y. Wei, M.X. Zhao, Z.K. Li, H.L. Yan, Q.X. Zheng, Z.M. Zong, Effects of sequential extraction and thermal dissolution on the structure and composition of Buliangou subbituminous coal, *Fuel Process. Technol.* 148 (2016) 324–331. <https://doi.org/10.1016/j.fuproc.2016.03.014>.
- [467] C. Xia, T. Wiltowski, S. Harpalani, Y. Liang, Coal depolymerization using permanganate under optimal conditions, *Int. J. Coal Geol.* 168 (2016) 214–221. <https://doi.org/10.1016/j.coal.2016.10.011>.
- [468] L. Grasset, Z. Vlčková, J. Kučerík, A. Amblès, A. Grasset, L., Vlčková, Z., Kučerík, J., and Amblès, Characterization of lignin monomers in low rank coal humic acids using the derivatization/reductive cleavage method, *Org. Geochem.* 41 (2010) 905–909. <https://doi.org/10.1016/j.orggeochem.2010.03.016>.
- [469] S. Nasir, T.B. Sarfaraz, T.V. Verheyen, A.L. Chaffee, Structural elucidation of humic acids extracted from Pakistani lignite using spectroscopic and thermal degradative techniques, *Fuel Process. Technol.* 92 (2011) 983–991. <https://doi.org/10.1016/j.fuproc.2010.12.020>.
- [470] M. Stefanova, Molecular indicators of the Oligocene Bobov Dol coal organic matter composition from bitumen analysis and preparative off-line thermochemolysis, *Int. J. Coal*



- Geol. 118 (2013) 1–7. <https://doi.org/10.1016/j.coal.2013.08.001>.
- [471] J. Kaal, W.H. Abdullah, Y. Makeen, K.A. Mustapha, L. Asiwaju, S.G. Sia, G. Almendros, Effects of maturity on the pyrolytic fingerprint of coals from North Borneo, *Int. J. Coal Geol.* 182 (2017) 1–13. <https://doi.org/10.1016/j.coal.2017.09.002>.
- [472] E.E. Igbini, C.C.Z. Mutambanengwe, P.D. Rose, Phyto-bioconversion of hard coal in the *Cynodon dactylon*/coal rhizosphere, *Biotechnol. J.* 5 (2010) 292–303. <https://doi.org/10.1002/biot.200900201>.
- [473] X.M. Ma, R. Lu, T. Miyakoshi, Application of pyrolysis gas chromatography/mass spectrometry in lacquer research: A review, *Polymers (Basel)*. 6 (2014) 132–144. <https://doi.org/10.3390/polym6010132>.
- [474] A. Heginbotham, J. Chang, H. Khanjian, M.R. Schilling, Some observations on the composition of Chinese lacquer, *Stud. Conserv.* 61 (2016) 28–37. <https://doi.org/10.1080/00393630.2016.1230979>.
- [475] R. Takei, R. Lu, T. Miyakoshi, Dimer structures and laccase-catalyzed polymerization mechanism of laccol in fresh *Rhus succedanea* lacquer sap, *Int. J. Polym. Anal. Charact.* 18 (2013) 199–210. <https://doi.org/10.1080/1023666X.2013.755655>.
- [476] R. Oshima, Y. Yamauchi, C. Watanabe, J. Kumantani, Enzymic oxidative coupling of urushiol in sap of the lac tree, *Rhus vernicifera*, *J. Org. Chem.* 50 (1985) 2613–2621. <https://doi.org/10.1021/jo00215a002>.
- [477] F. Modugno, F. Di Gianvincenzo, I. Degano, I.D. van der Werf, I. Bonaduce, K.J. van den Berg, On the influence of relative humidity on the oxidation and hydrolysis of fresh and aged oil paints, *Sci. Rep.* 9 (2019) 5533. <https://doi.org/10.1038/s41598-019-41893-9>.
- [478] N. Niimura, T. Miyakoshi, Structural study of oriental lacquer films during the hardening process, *Talanta*. 70 (2006) 146–152. <https://doi.org/10.1016/j.talanta.2005.12.039>.
- [479] M.J. Petisca, C.R. Matsen, Lisbon as seen from China: Conundrums posed by a set of lacquered nesting tables, *Stud. Conserv.* 64 (2019) S91–S100. <https://doi.org/10.1080/00393630.2018.1564592>.
- [480] O. Katsibiri, R.F. Howe, Characterisation of the transparent surface coatings on post-Byzantine icons using microscopic, mass spectrometric and spectroscopic techniques, *Microchem. J.* 94 (2010) 14–23. <https://doi.org/10.1016/j.microc.2009.08.004>.

- [481] S.Q. Fang, H. Zhang, B.J. Zhang, Y. Zheng, The identification of organic additives in traditional lime mortar, *J. Cult. Herit.* 15 (2014) 144–150. <https://doi.org/10.1016/j.culher.2013.04.001>.
- [482] J. Kumanotani, Urushi (oriental lacquer) - a natural aesthetic durable and future-promising coating, *Prog. Org. Coatings.* 26 (1995) 163–195. [https://doi.org/10.1016/0300-9440\(95\)00559-5](https://doi.org/10.1016/0300-9440(95)00559-5).
- [483] Jessica Burkhart Chasen and Madeline Corona Winterthur/University, The treatment and technical study of Chinese export lacquer at the Winterthur museum, garden & library, 2016.
- [484] A.S. Le Hô, M. Regert, O. Marescot, C. Duhamel, J. Langlois, T. Miyakoshi, C. Genty, M. Sablier, Molecular criteria for discriminating museum Asian lacquerware from different vegetal origins by pyrolysis gas chromatography / mass spectrometry, *Anal. Chim. Acta.* 710 (2012) 9–16. <https://doi.org/10.1016/j.aca.2011.10.024>.
- [485] A.M. Committee, A. No, Analytical pyrolysis in cultural heritage, *Anal. Methods.* 10 (2018) 5463–5467. <https://doi.org/10.1039/c8ay90151a>.
- [486] J. Dorscheid, J. Köhler, M. de Vlam, I. Joosten, H. van Keulen, P. van Duin, Dutch inlaid aventurine decoration: study, analysis, and conservation, *Stud. Conserv.* 3630 (2019) 1–10. <https://doi.org/10.1080/00393630.2018.1563347>.
- [487] L. Decq, Y. Jones, D. Steyaert, V. Cattersel, C. Indekeu, E. Van Binnebeke, W. Fremout, F. Lynen, S. Saverwyns, Black lacquered papier-mâché and turned wooden furniture: unravelling the art history, technology and chemistry of the 19th-century Japanning industry, *Stud. Conserv.* 64 (2019) S31–S44. <https://doi.org/10.1080/00393630.2019.1569361>.
- [488] R. Nakagawa, S. Nakai, T. Miyakoshi, T. Honda, Materials and provenance determination of lacquerware from the Ryukyu Kingdom period by pyrolysis-gas chromatography/mass spectrometry and  $^{87}\text{Sr}/^{86}\text{Sr}$  isotope ratio, *J. Archaeol. Sci. Reports.* 25 (2019) 72–76. <https://doi.org/10.1016/j.jasrep.2019.03.026>.
- [489] C.E. Rogge, K. Lough, Fluorescence fails: the color of UVA-induced visible fluorescence of tintype varnishes does not discriminate between varnish materials, *Top. Photogr. Preserv.* 15 (2013) 239–248.
- [490] L. Decq, E. Abatih, H. Van Keulen, V. Leyman, V. Cattersel, D. Steyaert, E. Van Binnebeke, W. Fremout, S. Saverwyns, F. Lynen, Nontargeted pattern recognition in the search for pyrolysis gas chromatography/mass spectrometry resin markers in historic lacquered objects,

- Anal. Chem. 91 (2019) 7131–7138. <https://doi.org/10.1021/acs.analchem.9b00240>.
- [491] D. Teetaert, M. Boudin, S. Saverwyns, P. Crombé, Food and soot: organic residues on outer pottery surfaces, *Radiocarbon*. 59 (2017) 1609–1621. <https://doi.org/10.1017/RDC.2017.25>.
- [492] D. Cauzzi, G. Chiavari, S. Montalbani, D. Melucci, D. Cam, H. Ling, Spectroscopic and chromatographic studies of sculptural polychromy in the Zhongshan Grottoes (R.P.C.), *J. Cult. Herit.* 14 (2013) 70–75. <https://doi.org/10.1016/j.culher.2012.02.011>.
- [493] C.E. Rogge, The varnished truth: The recipes and reality of tintype coatings, *J. Cult. Herit.* 15 (2014) 57–63. <https://doi.org/10.1016/j.culher.2013.02.002>.
- [494] C. Canevali, P. Gentile, M. Orlandi, F. Modugno, J.J. Lucejko, M.P. Colombini, L. Brambilla, S. Goidanich, C. Riedo, O. Chiantore, P. Baraldi, C. Baraldi, M.C. Gamberini, A multi-analytical approach for the characterization of powders from the Pompeii archaeological site, *Anal. Bioanal. Chem.* 401 (2011) 1801–1814. <https://doi.org/10.1007/s00216-011-5216-8>.
- [495] A. Rizzo, N. Shibayama, D.P. Kirby, A multi-analytical approach for the identification of aloe as a colorant in oil-resin varnishes, *Anal. Bioanal. Chem.* 399 (2011) 3093–3107. <https://doi.org/10.1007/s00216-010-4402-4>.
- [496] A. Le Gac, R. Estrompa, J.C. Frade, S. Pessanha, T.I. Madeira, A. Cardoso, L. Piorro, L. Dias, J. Mirão, A. Candeias, M.L. Carvalho, Multianalytical approach for the authenticity of an eighteenth-century Pascal Taskin harpsichord, *J. Anal. At. Spectrom.* 27 (2012) 626–643. <https://doi.org/10.1039/c2ja10226a>.
- [497] C. Riedo, D. Scalarone, O. Chiantore, Multivariate analysis of pyrolysis-GC/MS data for identification of polysaccharide binding media, *Anal. Methods*. 5 (2013) 4060–4067. <https://doi.org/10.1039/c3ay40474a>.
- [498] V. Pitthard, S. Stanek, M. Griesser, C. Jordan, S. Miklin-Kniefacz, R. Miklin, The technical investigation of an eighteenth-century Chinese imperial carved lacquer screen and its role in developing an appropriate conservation treatment, *Stud. Conserv.* 61 (2016) 97–108. <https://doi.org/10.1080/00393630.2016.1227117>.
- [499] U. Körber, M.R. Schilling, C.B. Dias, L. Dias, Simplified Chinese lacquer techniques and Nanban style decoration on Luso-Asian objects from the late sixteenth or early seventeenth centuries, *Stud. Conserv.* 61 (2016) 68–84. <https://doi.org/10.1080/00393630.2016.1227052>.
- [500] M. Kokkori, M.O. Hubert, N. Balcar, G. Barabant, K. Sutherland, F. Casadio, Gloss paints in late paintings by Francis Picabia: a multi-analytical study, *Appl. Phys. A Mater. Sci. Process.*

- 122 (2016) 1–11. <https://doi.org/10.1007/s00339-015-9532-2>.
- [501] M.A. Yandrisevits, P. Londero, F. Carò, A. Rizzo, C. Cappuccini, Wavelength-dependent absorption and scattering effects on laser cleaning of a corroded iron alloy European scale armor, *Lasers Conserv. Artworks XI*. (2017) 27–45. <https://doi.org/10.12775/3875-4.02>.
- [502] B. Klempan, K. Helwig, F. Colivicchi, Examination and analysis of Etruscan wall paintings at Caere, Italy, *Archaeometry*. 59 (2017) 1082–1094. <https://doi.org/10.1111/arcm.12304>.
- [503] Y. Song, F. Gao, A. Nevin, J. Guo, X. Zhou, S. Wei, Q. Li, A technical study of the materials and manufacturing process used in the Gallery wall paintings from the Jokhang temple, Tibet, *Herit. Sci.* 6 (2018) 1–13. <https://doi.org/10.1186/s40494-018-0182-5>.
- [504] L. Wei, W. Chen, G. Jin, Z. Guo, Y. Wang, B. Kang, N. Wang, A. Gu, Y. Zhang, Y. Lei, Scientific analysis of tie luò, a Qing Dynasty calligraphy artifact in the Palace Museum, Beijing, China, *Herit. Sci.* 6 (2018) 1–14. <https://doi.org/10.1186/s40494-018-0193-2>.
- [505] A.K. Hansen, M.B. Christiansen, J. Sanyova, K.P. Simonsen, Analysis of Poul Gernes' painted folding doors at Herlev Hospital, *Herit. Sci.* 6 (2018) 1–8. <https://doi.org/10.1186/s40494-018-0196-z>.
- [506] J. Park, M.R. Schilling, H. Khanjian, J. Lee, Stratigraphic examination of a Korean lacquered wooden coffin sample by Pyrolysis/GC/MS, *Chromatographia*. 81 (2018) 1685–1694. <https://doi.org/10.1007/s10337-018-3628-8>.
- [507] H. Han, S. Wei, J. Yang, L. Guan, W. Li, Characterization of the residues in Han Dynasty bronze lamps by pyrolysis–gas chromatography–mass spectrometry, *Herit. Sci.* 7 (2019) 1–9. <https://doi.org/10.1186/s40494-019-0279-5>.
- [508] X. Ma, Y. Shi, H. Khanjian, M. Schilling, M. Li, H. Fang, D. Cui, I. Kakoulli, Characterization of early imperial lacquerware from the Luozhuang Han Tomb, China, *Archaeometry*. 59 (2017) 121–132. <https://doi.org/10.1111/arcm.12226>.
- [509] M. Vermeulen, J. Sanyova, K. Janssens, Identification of artificial orpiment in the interior decorations of the Japanese tower in Laeken, Brussels, Belgium, *Herit. Sci.* 3 (2015) 1–9. <https://doi.org/10.1186/s40494-015-0040-7>.
- [510] S. Wei, V. Pintus, M. Schreiner, A comparison study of alkyd resin used in art works by Py-GC/MS and GC/MS: The influence of aging, *J. Anal. Appl. Pyrolysis*. 104 (2013) 441–447. <https://doi.org/10.1016/j.jaap.2013.05.028>.

- [511] E.Z. F. C.Izzo, E. Balliana, F. Pinton, A preliminary study of the composition of commercial oil, acrylic and vinyl paints and their behaviour after accelerated ageing conditions, *Conserv. Sci. Cult. Herit.* 14 (2014) 353–369. <https://doi.org/10.6092/issn.1973-9494/4753>.
- [512] R. Ploeger, O. Chiantore, Characterization and stability issues of artists' alkyd paints, *Smithson. Contrib. to Museum Conserv.* 3 (2012) 89–95. <https://repository.si.edu/bitstream/handle/10088/20494/16.Ploeger.SCMC3.Mecklenburg.Web.pdf?sequence=1>.
- [513] R.L. Cook, T.S. Bianchi, R.D. DeLaune, K.R. Reddy, C.J. Richardson, J.P. Megonigal, Characterization of Wetland Soil Organic Matter, in: 2014: pp. 289–316. <https://doi.org/10.2136/sssabookser10.c15>.
- [514] B.W. Murphy, Impact of soil organic matter on soil properties - A review with emphasis on Australian soils, *Soil Res.* 53 (2015) 605–635. <https://doi.org/10.1071/SR14246>.
- [515] J. Routh, T.S. Bianchi, J.A. Hutchings, P. Kuhry, R.K. Ranjan, Organic carbon characteristics in Swedish forest soil trace post-depositional carbon dynamics, *Eur. J. Soil Sci.* 67 (2016) 492–503. <https://doi.org/10.1111/ejss.12358>.
- [516] D. Elhottová, A. Koubová, M. Šimek, T. Cajthaml, J. Jirout, J. Esperschuetz, M. Schloter, A. Gatteringer, Changes in soil microbial communities as affected by intensive cattle husbandry, *Appl. Soil Ecol.* 58 (2012) 56–65. <https://doi.org/10.1016/j.apsoil.2012.03.009>.
- [517] N. Weiss, J. Kaal, Characterization of labile organic matter in Pleistocene permafrost (NE Siberia), using Thermally assisted Hydrolysis and Methylation (THM-GC-MS), *Soil Biol. Biochem.* 117 (2018) 203–213. <https://doi.org/10.1016/j.soilbio.2017.10.001>.
- [518] C.S. Lee, T.M. Sung, H.S. Kim, C.H. Jeon, Classification of forensic soil evidences by application of THM-PyGC/MS and multivariate analysis, *J. Anal. Appl. Pyrolysis.* 96 (2012) 33–42. <https://doi.org/10.1016/j.jaap.2012.02.017>.
- [519] M. Nakakuni, C. Dairiki, G. Kaur, S. Yamamoto, Stanol to sterol ratios in late Quaternary sediments from southern California: An indicator for continuous variability of the oxygen minimum zone, *Org. Geochem.* 111 (2017) 126–135. <https://doi.org/10.1016/j.orggeochem.2017.06.009>.
- [520] F. Baudin, J.R. Disnar, P. Martinez, B. Dennielou, Distribution of the organic matter in the channel-levees systems of the Congo mud-rich deep-sea fan (West Africa). Implication for deep offshore petroleum source rocks and global carbon cycle, *Mar. Pet. Geol.* 27 (2010) 995–

1010. <https://doi.org/10.1016/j.marpetgeo.2010.02.006>.
- [521] M. Nakakuni, J. Kitano, H. Uemura, S. Yamamoto, Modern sediment records of stanol to sterol ratios in Lake Suigetsu, Japan: An indicator of variable lacustrine redox conditions, *Org. Geochem.* 119 (2018) 59–71. <https://doi.org/10.1016/j.orggeochem.2018.02.004>.
- [522] J.A. Baldock, J. Sanderman, L.M. MacDonald, A. Puccini, B. Hawke, S. Szarvas, J. McGowan, Quantifying the allocation of soil organic carbon to biologically significant fractions, *Soil Res.* 51 (2013) 561–576. <https://doi.org/10.1071/SR12374>.
- [523] M. Thevenot, M.F. Dignac, C. Rumpel, Fate of lignins in soils: A review, *Soil Biol. Biochem.* 42 (2010) 1200–1211. <https://doi.org/10.1016/j.soilbio.2010.03.017>.
- [524] O.O. Sonibare, R.J. Huang, D.E. Jacob, Y. Nie, E. Kleine-Benne, T. Hoffmann, S.F. Foley, Terpenoid composition and chemotaxonomic aspects of Miocene amber from the Koroglu Mountains, Turkey, *J. Anal. Appl. Pyrolysis.* 105 (2014) 100–107. <https://doi.org/10.1016/j.jaap.2013.10.008>.
- [525] C.J. Saunders, M. Gao, R. Jaffé, Environmental assessment of vegetation and hydrological conditions in Everglades freshwater marshes using multiple geochemical proxies, *Aquat. Sci.* 77 (2015) 271–291. <https://doi.org/10.1007/s00027-014-0385-0>.
- [526] D.V. Guimarães, M.I.S. Gonzaga, T.O. da Silva, T.L. da Silva, N. da Silva Dias, M.I.S. Matias, Soil organic matter pools and carbon fractions in soil under different land uses, *Soil Tillage Res.* 126 (2013) 177–182. <https://doi.org/10.1016/j.still.2012.07.010>.
- [527] E.Y. Swain, Molecular characterization of terrestrial organic carbon in some organic-rich soils in the northern latitudes, 2013.
- [528] M. David, N.Y. Musadji, J. Labanowski, R. Sternberg, C. Geffroy-Rodier, Pilot for validation of online pretreatments for analyses of organics by gas chromatography-mass spectrometry: application to space research, *Anal. Chem.* 88 (2016) 5137–5144. <https://doi.org/10.1021/acs.analchem.6b00052>.
- [529] A. Buch, R. Sternberg, C. Szopa, C. Freissinet, C. Garnier, E.J. Bekri, C. Rodier, R. Navarro-González, F. Raulin, M. Cabane, M. Stambouli, D.P. Glavin, P.R. Mahaffy, Development of a gas chromatography compatible Sample Processing System (SPS) for the in-situ analysis of refractory organic matter in martian soil: preliminary results, *Adv. Sp. Res.* 43 (2009) 143–151. <https://doi.org/10.1016/j.asr.2008.05.001>.
- [530] C. Freissinet, D.P. Glavin, A. Buch, C. Szopa, S. Kashyap, H.B. Franz, J.L. Eigenbrode, W.B.

- Brinckerhoff, R. Navarro-González, S. Teinturier, C.A. Malespin, B.D. Prats, P.R. Mahaffy, First in situ wet chemistry experiment on Mars using the SAM instrument: MTBSTFA derivatization on a Martian Mudstone, in: 46th LPSC Lunar Planet. Sci. Conf., 2015: p. 2934. <https://www.hou.usra.edu/meetings/lpsc2015/pdf/2934.pdf>.
- [531] M. Millan, C. Szopa, A. Buch, P. Coll, D.P. Glavin, C. Freissinet, R. Navarro-Gonzalez, P. François, D. Coscia, J.Y. Bonnet, S. Teinturier, M. Cabane, P.R. Mahaffy, In situ analysis of martian regolith with the SAM experiment during the first mars year of the MSL mission: Identification of organic molecules by gas chromatography from laboratory measurements, *Planet. Space Sci.* 129 (2016) 88–102. <https://doi.org/10.1016/j.pss.2016.06.007>.
- [532] D.W. Ming, P.D. Archer, D.P. Glavin, J.L. Eigenbrode, H.B. Franz, B. Sutter, A.E. Brunner, J.C. Stern, C. Freissinet, A.C. Mcadam, P.R. Mahaffy, M. Cabane, P. Coll, J.L. Campbell, S.K. Atreya, P.B. Niles, J.F. Bell, D.L. Bish, W.B. Brinckerhoff, A. Buch, P.G. Conrad, D.J. Des Marais, B.L. Ehlmann, A.G. Fairén, K. Farley, G.J. Flesch, P. Francois, R. Gellert, J.A. Grant, J.P. Grotzinger, S. Gupta, K.E. Herkenhoff, J.A. Hurowitz, L.A. Leshin, K.W. Lewis, S.M. McLennan, K.E. Miller, J. Moersch, R. V. Morris, R. Navarro-González, A.A. Pavlov, G.M. Perrett, I. Pradler, S.W. Squyres, R.E. Summons, A. Steele, E.M. Stolper, D.Y. Sumner, C. Szopa, S. Teinturier, M.G. Trainer, A.H. Treiman, D.T. Vaniman, A.R. Vasavada, C.R. Webster, J.J. Wray, R.A. Yingst, P.D.A. Jr, D.P. Glavin, J.L. Eigenbrode, H.B. Franz, B. Sutter, A.E. Brunner, J.C. Stern, C. Freissinet, A.C. Mcadam, P.R. Mahaffy, M. Cabane, P. Coll, J.L. Campbell, S.K. Atreya, P.B. Niles, J.F.B. Iii, D.L. Bish, W.B. Brinckerhoff, A. Buch, P.G. Conrad, D.J. Des Marais, B.L. Ehlmann, I. Pradler, S.W. Squyres, R.E. Summons, A. Steele, E.M. Stolper, D.Y. Sumner, J. Klein, MSL Science Team, P.D. Archer, D.P. Glavin, J.L. Eigenbrode, H.B. Franz, B. Sutter, A.E. Brunner, J.C. Stern, C. Freissinet, A.C. Mcadam, P.R. Mahaffy, M. Cabane, P. Coll, J.L. Campbell, S.K. Atreya, P.B. Niles, J.F. Bell, D.L. Bish, W.B. Brinckerhoff, A. Buch, P.G. Conrad, D.J. Des Marais, B.L. Ehlmann, A.G. Fairén, K. Farley, G.J. Flesch, P. Francois, R. Gellert, J.A. Grant, J.P. Grotzinger, S. Gupta, K.E. Herkenhoff, J.A. Hurowitz, L.A. Leshin, K.W. Lewis, S.M. McLennan, K.E. Miller, J. Moersch, R. V. Morris, R. Navarro-González, A.A. Pavlov, G.M. Perrett, I. Pradler, S.W. Squyres, R.E. Summons, A. Steele, E.M. Stolper, D.Y. Sumner, C. Szopa, S. Teinturier, M.G. Trainer, A.H. Treiman, D.T. Vaniman, A.R. Vasavada, C.R. Webster, J.J. Wray, R.A. Yingst, Volatile and organic compositions of sedimentary rocks in Yellowknife Bays, Gale Crater, Mars, *Science*. 343 (2014) 1–10. <https://doi.org/10.1126/science.1245267>.
- [533] C. Geffroy-Rodier, L. Grasset, R. Sternberg, A. Buch, A. Amblès, Thermochemolysis in search for organics in extraterrestrial environments, *J. Anal. Appl. Pyrolysis*. 85 (2009) 454–459.

<https://doi.org/10.1016/j.jaap.2008.10.005>.

- [534] J.L. Vago, F. Westall, L.S. Pasteur Instrument Teams, A.J. Coates, R. Jaumann, O. Korablev, V. Ciarletti, I. Mitrofanov, J.-L. Josset, M.C. De Sanctis, J.-P. Bibring, F. Rull, F. Goesmann, H. Steininger, W. Goetz, W. Brinckerhoff, C. Szopa, F. Raulin, F. Westall, H.G.M. Edwards, L.G. Whyte, A.G. Fairén, J.-P. Bibring, J. Bridges, E. Hauber, G.G. Ori, S. Werner, D. Loizeau, R.O. Kuzmin, R.M.E. Williams, J. Flahaut, F. Forget, J.L. Vago, D. Rodionov, O. Korablev, H. Svedhem, E. Sefton-Nash, G. Kminek, L. Lorenzoni, L. Joudrier, V. Mikhailov, A. Zashchirinskiy, S. Alexashkin, F. Calantropio, A. Merlo, P. Poulakis, O. Witasse, O. Bayle, S. Bayón, U. Meierhenrich, J. Carter, J.M. García-Ruiz, P. Baglioni, A. Haldemann, A.J. Ball, A. Debus, R. Lindner, F. Haessig, D. Monteiro, R. Trautner, C. Voland, P. Rebeyre, D. Gouly, F. Didot, S. Durrant, E. Zekri, D. Koschny, A. Toni, G. Visentin, M. Zwick, M. van Winnendael, M. Azkarate, C. Carreau, the ExoMars Project Team, Habitability on early Mars and the search for biosignatures with the ExoMars Rover, *Astrobiology*. 17 (2017) 471–510. <https://doi.org/10.1089/ast.2016.1533>.
- [535] B.M. Scholz-Böttcher, A. Nissenbaum, J. Rullkötter, An 18th century medication “Mumia vera aegyptica” - Fake or authentic?, *Org. Geochem.* 65 (2013) 1–18. <https://doi.org/10.1016/j.orggeochem.2013.09.011>.
- [536] A. Sun, Z. Lai, M. Zhao, L. Mu, X. Hu, Native nanodiscs from blood inhibit pulmonary fibrosis, *Biomaterials*. 192 (2019) 51–61. <https://doi.org/10.1016/j.biomaterials.2018.10.045>.
- [537] R.N. Qureshi, E. Kaal, H.G. Janssen, P.J. Schoenmakers, W.T. Kok, Determination of cholesterol and triglycerides in serum lipoproteins using flow field-flow fractionation coupled to gas chromatography-mass spectrometry, *Anal. Chim. Acta.* 706 (2011) 361–366. <https://doi.org/10.1016/j.aca.2011.04.057>.
- [538] Y. Lu, P.B. Harrington, Classification of bacteria by simultaneous methylation-solid phase microextraction and gas chromatography/mass spectrometry analysis of fatty acid methyl esters, *Anal. Bioanal. Chem.* 397 (2010) 2959–2966. <https://doi.org/10.1007/s00216-010-3840-3>.
- [539] N.A. Dang, A.H.J. Kolk, S. Kuijper, H.G. Janssen, G. Vivo-Truyols, The identification of biomarkers differentiating *Mycobacterium tuberculosis* and non-tuberculous mycobacteria via thermally assisted hydrolysis and methylation gas chromatography-mass spectrometry and chemometrics, *Metabolomics*. 9 (2013) 1274–1285. <https://doi.org/10.1007/s11306-013-0531-z>.



- [540] S.C. Nicoara, D.E. Minnikin, O.C.Y. Lee, D.M. O'Sullivan, R. McNerney, C.T. Pillinger, I.P. Wright, G.H. Morgan, Development and optimization of a gas chromatography/mass spectrometry method for the analysis of thermochemolytic degradation products of phthiocerol dimycocerosate waxes found in *Mycobacterium tuberculosis*, *Rapid Commun. Mass Spectrom.* 27 (2013) 2374–2382. <https://doi.org/10.1002/rcm.6694>.
- [541] E. FID, Determinative Chromatographic Separations, in: *Method 8000C Determ. Chromatogr. Sep.*, 2003. <https://doi.org/10.16309/j.cnki.issn.1007-1776.2003.03.004>.
- [542] S. Nishimura, N. Maie, M. Baba, T. Sudo, T. Sugiura, E. Shima, Changes in the quality of chromophoric dissolved organic matter leached from senescent leaf litter during the early decomposition, *J. Environ. Qual.* 41 (2012) 823–833. <https://doi.org/10.2134/jeq2011.0342>.
- [543] K.P. Mosse, T. Vincent Verheyen, A.J. Cruickshank, A.F. Patti, T.R. Cavagnaro, Thermochemolysis of winery wastewater particulates - Molecular structural implications for water reuse, *J. Anal. Appl. Pyrolysis.* 97 (2012) 164–170. <https://doi.org/10.1016/j.jaap.2012.06.005>.
- [544] F. Orange, J.R. Disnar, P. Gautret, F. Westall, N. Bienvenu, N. Lottier, D. Prieur, Preservation and evolution of organic matter during experimental fossilisation of the hyperthermophilic *Archaea methanocaldococcus jannaschii*, *Orig. Life Evol. Biosph.* 42 (2012) 587–609. <https://doi.org/10.1007/s11084-012-9318-x>.
- [545] I. Deniau, J.R. Disnar, F. Baudin, J.P. Houzay, Characterization of organic matter in the Oligocene (Chattian) turbiditic fine grained deposits, offshore Angola, *Org. Geochem.* 41 (2010) 135–145. <https://doi.org/10.1016/j.orggeochem.2009.11.004>.
- [546] A.W.R. Seddon, M. Jokerud, T. Barth, H.J.B. Birks, L.C. Krüger, V. Vandvik, K.J. Willis, Improved quantification of UV-B absorbing compounds in *Pinus sylvestris* L. pollen grains using an internal standard methodology, *Rev. Palaeobot. Palynol.* 247 (2017) 97–104. <https://doi.org/10.1016/j.revpalbo.2017.08.007>.
- [547] C. Estournel-Pelardy, F. Delarue, L. Grasset, F. Laggoun-Défarge, A. Amblès, Tetramethylammonium hydroxide thermochemolysis for the analysis of cellulose and free carbohydrates in a peat bog, *J. Anal. Appl. Pyrolysis.* 92 (2011) 401–406. <https://doi.org/10.1016/j.jaap.2011.08.004>.
- [548] J. Templier, N. Gallois, S. Derenne, Analytical TMAH pyrolysis of dipeptides: Formation of new complex cyclic compounds related to the presence of the peptide bond, *J. Anal. Appl. Pyrolysis.* 104 (2013) 684–694. <https://doi.org/10.1016/j.jaap.2013.09.017>.

- [549] W.K. Musker, Nitrogen yields. III. Explosive decomposition of tetramethylammonium amide, *J. Org. Chem.* 32 (1967) 3189–3191. <https://doi.org/10.1021/jo01285a055>.
- [550] C.S. Macomber, J.M. Boncella, B.S. Pivovar, J.A. Rau, Decomposition pathways of an alkaline fuel cell membrane material component via evolved gas analysis, *J. Therm. Anal. Calorim.* 93 (2008) 225–229. <https://doi.org/10.1007/s10973-007-8930-x>.
- [551] H. Finkbeiner, Chelation as a driving force in organic reactions.1 A generics synthesis of amino acids by the carboxylation and alkylation of 3-phenylhydantoin, *J. Am. Chem. Soc.* 86 (1964) 961–962. <https://doi.org/10.1021/ja01059a071>.
- [552] S. Chempath, B.R. Einsla, L.R. Pratt, C.S. Macomber, J.M. Boncella, J.A. Rau, B.S. Pivovar, Mechanism of tetraalkylammonium headgroup degradation in alkaline fuel cell membranes, *J. Phys. Chem. C.* 112 (2008) 3179–3182. <https://doi.org/10.1021/jp7115577>.
- [553] A. Surpateanu, G., Catteau, J.P., Karafiloglou, P. and Lablache-Combiere, Structure and reactivity of cycloimmonium ylides, *Tetrahedron.* 32 (1976) 2647–2663.
- [554] S. Chempath, J.M. Boncella, L.R. Pratt, N. Henson, B.S. Pivovar, Density functional theory study of degradation of tetraalkylammonium hydroxides, *J. Phys. Chem. C.* 114 (2010) 11977–11983. <https://doi.org/10.1021/jp9122198>.
- [555] H. Long, B.S. Pivovar, Hydroxide degradation pathways for substituted benzyltrimethyl ammonium: A DFT Study, *J. Phys. Chem. C.* 116 (2012) 9419–9426. <https://doi.org/10.1149/2.0041501eel>.
- [556] C.W. Wang, C. Liang, Oxidative degradation of TMAH solution with UV persulfate activation, *Chem. Eng. J.* 254 (2014) 472–478. <https://doi.org/10.1016/j.cej.2014.05.116>.
- [557] Y. Wang, Z. Zhang, C. Jiang, T. Xu, Electrodialysis process for the recycling and concentrating of tetramethylammonium hydroxide (TMAH) from photoresist developer wastewater, *Ind. Eng. Chem. Res.* 52 (2013) 18356–18361. <https://doi.org/10.1021/ie4023995>.
- [558] Y. He, A. Buch, C. Szopa, A.J. Williams, M. Millan, M. Guzman, C. Freissinet, C. Malespin, D.P. Glavin, J.L. Eigendbrode, D. Coscia, S. Teinturier, Pin lu, M. Cabane, P.R. Mahaffy, The search for organic compounds with TMAH thermochemolysis: From Earth analyses to space exploration experiments, *TrAC - Trends Anal. Chem.* 127 (2020) 1–27. <https://doi.org/10.1016/j.trac.2020.115896>.
- [559] A.J. Williams, K.L. Craft, M. Millan, S.S. Johnson, C.A. Knudson, M. Juarez Rivera, A.C. McAdam, D. Tobler, J.R. Skok, Fatty Acid Preservation in Modern and Relict Hot-Spring

- Deposits in Iceland, with Implications for Organics Detection on Mars, *Astrobiology*. in review (2020) 1–23. <https://doi.org/10.1089/ast.2019.2115>.
- [560] Y. He, A. Buch, C. Szopa, A.J. Williams, C.A. Malespin, D.P. Glavin, C. Freissinet, J.L. Eigenbrode, S. Teinturier, D. Coscia, J. Bonnet, J.C. Stern, F. Stalport, M. Guzman, N. Chaouche-mechidal, P. Lu, R. Navarro-gonzalez, V. Butin, J. El Bekri, S. Johnson, M. Cabane, P.R. Mahaffy, Influence of Calcium Perchlorate on the Search for Organics on Mars with Tetramethylammonium Hydroxide Thermochemolysis, *Astrobiology*. 21 (2021) 1–19. <https://doi.org/10.1089/ast.2020.2252>.
- [561] C. Rodier, C. Laurent, C. Szopa, R. Sternberg, F. Raulin, Chirality and the origin of life: In situ enantiomeric separation for future space missions, *Chirality*. 14 (2002) 527–532. <https://doi.org/10.1002/chir.10090>.
- [562] M.C. Pietrogrande, Enantioselective separation of amino acids as biomarkers indicating life in extraterrestrial environments *Amino Acid Analysis, Anal. Bioanal. Chem.* 405 (2013) 7931–7940. <https://doi.org/10.1007/s00216-013-6915-0>.
- [563] C. Rodier, R. Sternberg, C. Szopa, A. Buch, M. Cabane, F. Raulin, Search for organics in extraterrestrial environments by in situ gas chromatography analysis, *Adv. Sp. Res.* 36 (2005) 195–200. <https://doi.org/10.1016/j.asr.2004.12.072>.
- [564] W. Goetz, W.B. Brinckerhoff, R. Arevalo, C. Freissinet, S. Getty, D.P. Glavin, S. Siljeström, A. Buch, F. Stalport, A. Grubisic, X. Li, V. Pinnick, R. Danell, F.H.W. Van Amerom, F. Goesmann, H. Steininger, N. Grand, F. Raulin, C. Szopa, U. Meierhenrich, J.R. Brucato, MOMA: The challenge to search for organics and biosignatures on Mars, *Int. J. Astrobiol.* 15 (2016) 239–250. <https://doi.org/10.1017/S1473550416000227>.
- [565] T.P. Mawhinney, R.S.R. Robinett, A. Atalay, M.A. Madson, Analysis of amino acids as their tert.-butyldimethylsilyl derivatives by gas-liquid chromatography and mass spectrometry, *J. Chromatogr. A.* 358 (1986) 231–242. [https://doi.org/10.1016/S0021-9673\(01\)90333-4](https://doi.org/10.1016/S0021-9673(01)90333-4).
- [566] M. V Kashutina, S.L. Ioffe, V.A. Tartakovskii, Silylation of Organic Compounds, *Russ. Chem. Rev.* 44 (1975) 733–747. <https://doi.org/10.1070/rc1975v044n09abeh002373>.
- [567] and V.D. Moldoveanu, Serban C., Derivatization Methods in GC and GC/MS, in: *Sample Prep. Appl.*, 2019: pp. 1–33. <https://doi.org/10.5772/32009>.
- [568] C. Malespin, C. Freissinet, D. Glavin, P. Mahaffy, M. Millan, A. Buch, C. Szopa, S. Teinturier, A. Mcadam, R. Williams, C. Malespin, C. Freissinet, D. Glavin, P. Mahaffy, M. Millan, T.

- First, C. Sam, The First Complete SAM Wet Chemistry Experiment on Mars, in: 49th Lunar Planet. Sci. Conf. 2018, Mar 2018, Houston, United States. <hal-01815570>, 2018.
- [569] J.C. Stern, B. Sutter, C. Freissinet, R. Navarro-González, C.P. McKay, P.D. Archer, A. Buch, A.E. Brunner, P. Coll, J.L. Eigenbrode, A.G. Fairen, H.B. Franz, D.P. Glavin, S. Kashyap, A.C. McAdam, D.W. Ming, A. Steele, C. Szopa, J.J. Wray, F.J. Martín-Torres, M.-P. Zorzano, P.G. Conrad, P.R. Mahaffy, Evidence for indigenous nitrogen in sedimentary and aeolian deposits from the Curiosity rover investigations at Gale crater, Mars, *Proc. Natl. Acad. Sci.* 112 (2015) 4245–4250. <https://doi.org/10.1073/pnas.1420932112>.
- [570] J.L. Bishop, H.B. Franz, W. Goetz, D.F. Blake, C. Freissinet, H. Steininger, F. Goesmann, W.B. Brinckerhoff, S. Getty, V.T. Pinnick, P.R. Mahaffy, M.D. Dyar, Coordinated analyses of Antarctic sediments as Mars analog materials using reflectance spectroscopy and current flight-like instruments for CheMin, SAM and MOMA, *Icarus*. 224 (2013) 309–325. <https://doi.org/10.1016/j.icarus.2012.05.014>.
- [571] I. Molnár-Perl, Z.F. Katona, GC-MS of amino acids as their trimethylsilyl/t-butyl dimethylsilyl derivatives: In model solutions III, *Chromatographia*. 51 (2000) 228–236. <https://doi.org/10.1007/bf02492811>.
- [572] K.E. Miller, J.L. Eigenbrode, C. Freissinet, D.P. Glavin, B. Kotrc, P. Francois, R.E. Summons, Potential precursor compounds for chlorohydrocarbons detected in Gale Crater, Mars, by the SAM instrument suite on the Curiosity Rover, *J. Geophys. Res. Planets*. 121 (2016) 296–308. <https://doi.org/10.1002/2015JE004939>.
- [573] K.E. Miller, B. Kotrc, R.E. Summons, I. Belmahdi, A. Buch, J.L. Eigenbrode, C. Freissinet, D.P. Glavin, C. Szopa, M.E.T. Al, Evaluation of the Tenax trap in the Sample Analysis at Mars instrument suite on the Curiosity rover as a potential hydrocarbon source for chlorinated organics detected in Gale Crater, *J. Geophys. Res. Planets*. 120 (2015) 1446–1459. <https://doi.org/10.1002/2015JE004825>.Received.
- [574] E.A.G. Zagatto, F.J. Krug, H. Bergamin F, S.S. Jørgensen, B.F. Reis, Merging zones in flow injection analysis. Part 2. Determination of calcium, magnesium and potassium in plant material by continuous flow injection Atomic Absorption and Flame Emission Spectrometry, *Anal. Chim. Acta*. 104 (1979) 279–284. [https://doi.org/10.1016/S0003-2670\(01\)84009-5](https://doi.org/10.1016/S0003-2670(01)84009-5).
- [575] Z. Špirić, I. Vučković, T. Stafilov, V. Kušan, M. Frontasyeva, Air pollution study in Croatia using moss biomonitoring and ICP-AES and AAS analytical techniques, *Arch. Environ. Contam. Toxicol.* 65 (2013) 33–46. <https://doi.org/10.1007/s00244-013-9884-6>.

- [576] A.O. Fayiga, L.Q. Ma, Using phosphate rock to immobilize metals in soil and increase arsenic uptake by hyperaccumulator *Pteris vittata*, *Sci. Total Environ.* 359 (2006) 17–25. <https://doi.org/10.1016/j.scitotenv.2005.06.001>.
- [577] R. Milačić, J. Štupar, N. Kožuh, J. Korošin, Critical evaluation of three analytical techniques for the determination of chromium(VI) in soil extracts, *Analyst.* 117 (1992) 125–130. <https://doi.org/10.1039/AN9921700125>.
- [578] W.M. Seaman, W.H. McComas, G.A. Allen, Determination of water by Karl Fischer reagent, *Anal. Chem.* 21 (1949) 510–512. <https://doi.org/10.1021/ac60028a016>.
- [579] W. Ewa, S. Piotr, Water determination in bee products using the Karl Fisher titration method, *J. Apic. Sci.* 53 (2009) 49–56.
- [580] G.C. Galletti, R. Piccaglia, Water determination in silages by Karl Fischer titration, *J. Sci. Food Agric.* 43 (1988) 1–7. <https://doi.org/10.1002/jsfa.2740430102>.
- [581] E.A. Burns, R.F. Muraca, Karl Fischer determination of water in ammonium perchlorate with automatic titration apparatus: evaluation of reaction rate parameters and statistical evaluation, *Anal. Chem.* 34 (1962) 848–854. <https://doi.org/10.1021/ac60187a040>.
- [582] P. Bryan, P. Bhaskara, Comparison of standards in the Karl Fischer method for water determination, *Anal. Chim. Acta* 84 (1976) 149–155.
- [583] S.H. Royle, W. Montgomery, S.P. Kounaves, M.A. Sephton, Effect of Hydration State of Martian Perchlorate Salts on Their Decomposition Temperatures During Thermal Extraction, *J. Geophys. Res. Planets.* 122 (2017) 2793–2802. <https://doi.org/10.1002/2017JE005381>.
- [584] A. Shareef, C.J. Parnis, M.J. Angove, J.D. Wells, B.B. Johnson, Suitability of N,O-bis(trimethylsilyl)trifluoroacetamide and N-(tert-butyldimethylsilyl)-N-methyltrifluoroacetamide as derivatization reagents for the determination of the estrogens estrone and 17 $\alpha$ -ethinylestradiol by gas chromatography-mass spectrometry, *J. Chromatogr. A.* 1026 (2004) 295–300. <https://doi.org/10.1016/j.chroma.2003.10.110>.
- [585] M. Millan, C. Szopa, A. Buch, R.E. Summons, R. Navarro-Gonzalez, P. Mahaffy, S.S. Johnson, Influence of Calcium Perchlorate on Organics under SAM-like Pyrolysis Conditions: Constraints on the Nature of Martian Organics, *J. Geophys. Res. Planets.* 125 (2020) e2019JE006359. <https://doi.org/10.1029/2019JE006359>.
- [586] A. Buch, C. Freissinet, C. Szopa, D. Glavin, P. Coll, J. Eigenbrode, R. Navarro-gonzález, J. Stern, A. Buch, C. Freissinet, C. Szopa, D. Glavin, P. Coll, Detection of Organics at Mars :

- How Wet Chemistry Onboard SAM Helps, in: 44th Lunar Planet. Sci. Conf., 2013.
- [587] A. Migdał-Mikuli, J. Hetmańczyk, Thermal behavior of  $[\text{Ca}(\text{H}_2\text{O})_4](\text{ClO}_4)_2$  and  $[\text{Ca}(\text{NH}_3)_6](\text{ClO}_4)_2$ , *J. Therm. Anal. Calorim.* 91 (2008) 529–534.  
<https://doi.org/10.1007/s10973-007-8511-z>.
- [588] D. Angin, Effect of pyrolysis temperature and heating rate on biochar obtained from pyrolysis of safflower seed press cake, *Bioresour. Technol.* 128 (2013) 593–597.  
<https://doi.org/10.1016/j.biortech.2012.10.150>.
- [589] H. Mißbach, H. Steininger, V. Thiel, W. Goetz, Investigating the Effect of Perchlorate on Flight-like Gas Chromatography-Mass Spectrometry as Performed by MOMA on board the ExoMars 2020 Rover, *Astrobiology.* 19 (2019) 1339–1352.  
<https://doi.org/10.1089/ast.2018.1997>.
- [590] L. Remusat, S. Derenne, F. Robert, H. Knicker, New pyrolytic and spectroscopic data on Orgueil and Murchison insoluble organic matter: A different origin than soluble?, *Geochim. Cosmochim. Acta.* 69 (2005) 3919–3932. <https://doi.org/10.1016/j.gca.2005.02.032>.
- [591] S. Derenne, F. Robert, Model of molecular structure of the insoluble organic matter isolated from Murchison meteorite, *Meteorit. Planet. Sci.* 45 (2010) 1461–1475.  
<https://doi.org/10.1111/j.1945-5100.2010.01122.x>.
- [592] M. Komiya, A. Shimoyama, Organic Compounds from Insoluble Organic Matter Isolated from the Murchison Carbonaceous Chondrite by Heating Experiments, *Bull. Chem. Soc. Jpn.* 69 (1996) 53–58. <https://doi.org/10.1246/bcsj.69.53>.
- [593] F. Okumura, K. Mimura, Gradual and stepwise pyrolyses of insoluble organic matter from the Murchison meteorite revealing chemical structure and isotopic distribution, *Geochim. Cosmochim. Acta.* 75 (2011) 7063–7080. <https://doi.org/10.1016/j.gca.2011.09.015>.
- [594] C. Procaccini, J.W. Bozzelli, J.P. Longwell, A.F. Sarofim, K.A. Smith, Formation of chlorinated aromatics by reactions of Cl, Cl<sub>2</sub>, and HCl with benzene in the cool-down zone of a combustor, *Environ. Sci. Technol.* 37 (2003) 1684–1689. <https://doi.org/10.1021/es011432s>.
- [595] G.G. Marvin, L.B. Woolaver, Thermal Decomposition of Perchlorates, *Ind. Eng. Chem. - Anal. Ed.* 17 (1945) 474–476. <https://doi.org/10.1021/i560144a004>.
- [596] A.M. Bruck, B. Sutter, D.W. Ming, P. Mahaffy, Thermal decomposition of calcium perchlorate/iron-mineral mixtures: implication of the evolved oxygen from the rocknest eolian deposit Gale crater, Mars, in: 45th Lunar Planet. Sci. Conf., The Woodlands, TX; United State,

2014. <http://www.enecho.meti.go.jp/about/whitepaper/2017html/2-1-4.html>.
- [597] K.A. Farley, P. Martin, P.D. Archer, S.K. Atreya, P.G. Conrad, J.L. Eigenbrode, A.G. Fairén, H.B. Franz, C. Freissinet, D.P. Glavin, P.R. Mahaffy, C. Malespin, D.W. Ming, R. Navarro-Gonzalez, B. Sutter, Light and variable  $^{37}\text{Cl}/^{35}\text{Cl}$  ratios in rocks from Gale Crater, Mars: Possible signature of perchlorate, *Earth Planet. Sci. Lett.* 438 (2016) 14–24. <https://doi.org/10.1016/j.epsl.2015.12.013>.
- [598] S.P. Kounaves, B.L. Carrier, G.D. O’Neil, S.T. Stroble, M.W. Claire, Evidence of martian perchlorate, chlorate, and nitrate in Mars meteorite EETA79001: Implications for oxidants and organics, *Icarus*. 229 (2014) 206–213. <https://doi.org/10.1016/j.icarus.2013.11.012>.
- [599] K.M. Cannon, B. Sutter, D.W. Ming, W. V. Boynton, R. Quinn, Perchlorate induced low temperature carbonate decomposition in the Mars Phoenix Thermal and Evolved Gas Analyzer (TEGA), *Geophys. Res. Lett.* 39 (2012) 2–6. <https://doi.org/10.1029/2012GL051952>.
- [600] H. Steininger, F. Goesmann, W. Goetz, Influence of magnesium perchlorate on the pyrolysis of organic compounds in Mars analogue soils, *Planet. Space Sci.* 71 (2012) 9–17. <https://doi.org/10.1016/j.pss.2012.06.015>.
- [601] M.A. Sephton, J.M.T. Lewis, J.S. Watson, W. Montgomery, C. Garnier, Perchlorate-induced combustion of organic matter with variable molecular weights: Implications for Mars missions, *Geophys. Res. Lett.* 41 (2014) 7453–7460. <https://doi.org/10.1002/2014GL062109>.
- [602] J.L. Vago, A.J. Coates, R. Jaumann, O. Korablev, V. Ciarletti, I. Mitrofanov, J.-L. Josset, F. Westall, M.C. De Sanctis, J.-P. Bibring, F. Rull, F. Goesmann, W. Brinckerhoff, F. Raulin, E. Sefton-Nash, H. Svedhem, G. Kminek, D. Rodionov, P. Baglioni, The ExoMars Team, Searching for Traces of Life With the ExoMars Rover, in: Cabrol & Grin (Ed.), *From Habitability to Life Mars*, 2018: pp. 309–347. <https://doi.org/10.1016/B978-0-12-809935-3.00011-6>.
- [603] A. V Bridgwater, G.V.C. Peacocke, Fast pyrolysis processes for biomass, *Renew. Sustain. Energy Rev.* 4. 4 (2000) 1–73.
- [604] O. Onay, O. Mete Kockar, Slow, fast and flash pyrolysis of rapeseed, *Renew. Energy*. 28 (2003) 2417–2433. [https://doi.org/10.1016/S0960-1481\(03\)00137-X](https://doi.org/10.1016/S0960-1481(03)00137-X).
- [605] W. He, Z. Liu, Q. Liu, D. Ci, C. Lievens, X. Guo, Behaviors of radical fragments in tar generated from pyrolysis of 4 coals, *Fuel*. 134 (2014) 375–380. <https://doi.org/10.1016/j.fuel.2014.05.064>.

- [606] M. W.k, A Reinvestigation of the Pyrolysis of Tetramethylammonium Hydroxide, *J. Am. Chem. Soc.* 86 (1964) 960–961. <https://doi.org/10.1021/ja01059a070>.
- [607] A. T. Lawson and Norman Collie, The action of heat on the salts of tetramethylammonium, *J. Chem. Soc. Trans.* 53 (1888) 624–636.
- [608] S. Majumdar, K.B. Sloan, N-Alkyl-N-alkyloxycarbonylaminomethyl (NANAOCAM) prodrugs of carboxylic acid containing drugs, *Bioorganic Med. Chem. Lett.* 17 (2007) 1447–1450. <https://doi.org/10.1016/j.bmcl.2006.11.074>.
- [609] V. Subramanian, 1,3,5-Trimethyl-1,3,5-triazacyclohexane, in: L. John Wiley & Sons (Ed.), *Encycl. Reagents Org. Synth.*, Wiley, 2009: pp. 1–2. <https://doi.org/10.1002/047084289X>.
- [610] Y. Ogata, A. Kawasaki, The kinetics of the reaction of formaldehyde with ammonia, *Bull. Chem. Soc. Jpn.* 37 (1964) 514–519. <https://doi.org/10.1246/bcsj.37.514>.
- [611] A. Zeffiro, S. Lazzaroni, D. Merli, A. Profumo, A. Buttafava, N. Serpone, D. Dondi, Formation of hexamethylenetetramine (HMT) from HCHO and NH<sub>3</sub> – relevance to prebiotic Chemistry and B3LYP consideration, *Orig. Life Evol. Biosph.* 46 (2016) 223–231. <https://doi.org/10.1007/s11084-015-9479-5>.
- [612] P. Attri, P. Venkatesu, A. Kumar, Temperature effect on the molecular interactions between ammonium ionic liquids and N, N-dimethylformamide, *J. Phys. Chem. B.* 114 (2010) 13415–13425. <https://doi.org/10.1021/jp108003x>.
- [613] P. Suprana, T. Liaskopoulos, P.G. Tsoungas, G. Varvounis, DMF-catalysed thermal dehydration of aldoximes: A convenient access to functionalized aliphatic and aromatic nitriles, *Synlett.* (2007) 2671–2674. <https://doi.org/10.1055/s-2007-991067>.
- [614] C.L. Yu, C. Wang, M. Frenklach, Chemical kinetics of methyl oxidation by molecular oxygen, *J. Phys. Chem.* 99 (1995) 14377–14387. <https://doi.org/10.1021/j100039a027>.
- [615] T.R. Filley, R.D. Minard, P.G. Hatcher, Tetramethylammonium hydroxide (TMAH) thermochemolysis: Proposed mechanisms based upon the application of <sup>13</sup>C-labeled TMAH to a synthetic model lignin dimer, *Org. Geochem.* 30 (1999) 607–621. [https://doi.org/10.1016/S0146-6380\(99\)00040-6](https://doi.org/10.1016/S0146-6380(99)00040-6).
- [616] K.L. Vieira, M.S. Mubarak, D.G. Peters, Use of Deuterium labeling to assess the roles of tetramethylammonium cation, dimethylformamide, and water as proton donors for electrogenerated tert-butyl carbanions. Evidence for the formation of an ylide (trimethylammonium methyllide), *J. Am. Chem. Soc.* 106 (1984) 5372–5373.



- <https://doi.org/10.1021/ja00330a068>.
- [617] L. Onel, L. Thonger, M.A. Blitz, P.W. Seakins, A.J.C. Bunkan, M. Solimannejad, C.J. Nielsen, Gas-phase reactions of OH with methyl amines in the presence or absence of molecular oxygen. an experimental and theoretical study, *J. Phys. Chem. A.* 117 (2013) 10736–10745. <https://doi.org/10.1021/jp406522z>.
- [618] M.H. Larraufie, G. Maestri, M. Malacria, C. Ollivier, L. Fensterbank, E. Lacte, The cyanamide moiety, synthesis and reactivity, *Synthesis (Stuttg).* 44 (2012) 1279–1292. <https://doi.org/10.1055/s-0031-1289749>.
- [619] C. Anastasi, M.A. Crowe, M.W. Powner, J.D. Sutherland, Direct assembly of nucleoside precursors from two- and three-carbon units, *Angew. Chemie - Int. Ed.* 45 (2006) 6176–6179. <https://doi.org/10.1002/anie.200601267>.
- [620] D. D. Nekrasov, Synthesis and chemical transformations of mono- and disubstituted cyanamides, *Russ. J. Org. Chem.* 40 (2004) 1439–1454. <https://doi.org/10.1007/s11178-005-0030-4>.
- [621] J. Kim, S. Chang, A New Combined Source of “CN” from N,N-Dimethylformamide and Ammonia in the Palladium-Catalyzed Cyanation of Aryl C-H Bonds Jinho, *J. Am. Chem. Soc.* 132 (2010) 10272–10274.
- [622] S. Ding, N. Jiao, Direct Transformation of N , N-Dimethylformamide to -CN : Pd-Catalyzed cyanation od heteroarenes via C-H functionalization, *J. Am. Chem. Soc.* 133 (2011) 12374–12377.
- [623] G. Camino, L. Operti, L. Trossarelli, Mechanism of thermal degradation of urea-formaldehyde polycondensates, *Polym. Degrad. Stab.* 5 (1983) 161–172. [https://doi.org/10.1016/0141-3910\(83\)90007-1](https://doi.org/10.1016/0141-3910(83)90007-1).
- [624] A. Guérinot, S. Reymond, J. Cossy, Ritter reaction: Recent catalytic developments, *European J. Org. Chem.* 2012 (2012) 19–28. <https://doi.org/10.1002/ejoc.201101018>.
- [625] G. Yin, B. Yan, J. Chen, M. Ji, An efficient transformation of methyl ethers and nitriles to amides catalyzed by Iron(III) perchlorate hydrate, *J. Iran. Chem. Soc.* 16 (2019) 1355–1363. <https://doi.org/10.1007/s13738-019-01615-4>.
- [626] M.S. Matheson, E.E. Auer, E.B. Bevilacqua, E.J. Hart, Rate constants in free radical polymerizations. IV. methyl acrylate, *J. Am. Chem. Soc.* 73 (1951) 5395–5400. <https://doi.org/10.1021/ja01155a114>.

- [627] H.C. Hetherington, J.M. Braham, The hydrolysis and polymerization of cyanamide, *J. Am. Chem. Soc.* 45 (1923) 824–829. <https://doi.org/10.1021/ja01656a042>.
- [628] V.G. Wittig, R. , and Polster, Über die Struktur der Stickstoff-ylide, *Justus Liebigs Ann. Chem.* 599 (1956) 1–12.
- [629] W.K. Musker, R.R. Stevens, Nitrogen Ylides . IV . The role of the methyl hydrogen atoms in the decomposition of tetramethylammonium alkoxides, *J. Am. Chem. Soc.* 90 (1968) 3515–3521. <https://doi.org/10.1021/ja01015a040>.
- [630] S. Tsuchiya, M. Seno, On the bond character of N-containing ylides, *J. Org. Chem.* 44 (1979) 2850–2855. <https://doi.org/10.1021/jo01330a007>.
- [631] M.M.B. Marques, Catalytic enantioselective cross-Mannich reaction of aldehydes, *Angew. Chemie - Int. Ed.* 45 (2006) 348–352. <https://doi.org/10.1002/anie.200502630>.
- [632] M. Arend, B. Westermann, N. Risch, Modern variants of Mannich-reaction, *Angew. Chem. Int. Ed.* 37 (1998) 1044–1070. [https://doi.org/10.1002/\(SICI\)1521-3773\(19980504\)37:8<1044::AID-ANIE1044>3.0.CO](https://doi.org/10.1002/(SICI)1521-3773(19980504)37:8<1044::AID-ANIE1044>3.0.CO).
- [633] P.D. Archer, D.W. Ming, B. Sutter, R. V. Morris, B.. C. Clark, P.H. Mahaffy, J.. J. Wray, A.G. Fairen, R. Gellert, A.. S. Yen, D.F. Blake, D.. T. Vaniman, D.P. Glavin, J.L. Eigenbrode, M.G. Trainer, C.P. Mckay, C. Freissinet, Oxychlorine species on Mars: implications from Gale Crater samples, in: *47th Lunar Planet. Sci. Conf.*, 2016: p. 2947.
- [634] B. Sutter, A.C. McAdam, P.R. Mahaffy, D.W. Ming, K.S. Edgett, E.B. Rampe, J.L. Eigenbrode, H.B. Franz, C. Freissinet, J.P. Grotzinger, A. Steele, C.H. House, P.D. Archer, C.A. Malespin, R. Navarro-González, J.C. Stern, J.F. Bell, F.J. Calef, R. Gellert, D.P. Glavin, L.M. Thompson, A.S. Yen, Evolved gas analyses of sedimentary rocks and eolian sediment in Gale Crater, Mars: Results of the Curiosity rover’s sample analysis at Mars instrument from Yellowknife Bay to the Namib Dune, *J. Geophys. Res. Planets.* 122 (2017) 2574–2609. <https://doi.org/10.1002/2016JE005225>.
- [635] A.C. Rustan, C.A. Drevon, Fatty acids: structures and properties, in: L. John Wiley & Sons (Ed.), *Encycl. Life Sci.*, 2005: pp. 1–7. <https://doi.org/10.1038/npg.els.0003894>.
- [636] J. Lee, J.W. Bozzelli, Thermochemical and kinetic analysis of the formyl methyl radical + O<sub>2</sub> reaction system, *J. Phys. Chem. A.* 107 (2003) 3778–3791. <https://doi.org/10.1021/jp030001o>.
- [637] M.A. Sephton, Organic compounds in carbonaceous meteorites, *Nat. Prod. Rep.* 19 (2002) 292–311. <https://doi.org/10.1039/b103775g>.

- [638] R. Hayatsu, Orgueil Meteorite: Organic Nitrogen Contents., *Science* (80-. ). 146 (1964) 1291–3. <https://doi.org/10.1126/science.146.3649.1291>.
- [639] R. Hayatsu, M.H. Studier, A. Oda, K. Fuse, E. Anders, Origin of organic matter in early solar system - II. Nitrogen compounds, *Geochim. Cosmochim. Acta.* 32 (1968) 175–190.
- [640] W. van der Velden, A.W. Schwartz, Search for purines and pyrimidines in the Murchison meteorite, *Geochim. Cosmochim. Acta.* 41 (1977) 961–968. [https://doi.org/10.1016/0016-7037\(77\)90155-7](https://doi.org/10.1016/0016-7037(77)90155-7).
- [641] P.G. Stoks, A.W. Schwartz, Uracil in carbonaceous meteorites, *Nature.* 282 (1979) 709–710. <https://doi.org/10.1038/282709a0>.
- [642] P.G. Stoks, A.W. Schwartz, Nitrogen-heterocyclic compounds in meteorites: significance and mechanisms of formation, *Geochim. Cosmochim. Acta.* 45 (1981) 563–569. [https://doi.org/10.1016/0016-7037\(81\)90189-7](https://doi.org/10.1016/0016-7037(81)90189-7).
- [643] M. a. Sephton, Organic Geochemistry and the Exploration of Mars, *J. Cosmol.* 5 (2010) 1141–1149.
- [644] M.P. Callahan, A.S. Burton, J.E. Elsila, E.M. Baker, K.E. Smith, D.P. Glavin, J.P. Dworkin, A search for amino acids and nucleobases in the Martian meteorite Roberts Massif 04262 using liquid chromatography-mass spectrometry, *Meteorit. Planet. Sci.* 48 (2013) 786–795. <https://doi.org/10.1111/maps.12103>.
- [645] V.A. Basiuk, J. Douda, Pyrolysis of simple amino acids and nucleobases: survivability limits and Implications for extraterrestrial delivery, *Planet. Sp. Sci.* 36. 47 (1999) 577–584. [https://doi.org/10.1016/S0032-0633\(98\)00136-6](https://doi.org/10.1016/S0032-0633(98)00136-6).
- [646] D.P. Glavin, H.J. Cleaves, A. Buch, M. Schubert, A. Aubrey, J.L. Bada, P.R. Mahaffy, Sublimation extraction coupled with gas chromatography-mass spectrometry: A new technique for future in situ analyses of purines and pyrimidines on Mars, *Planet. Space Sci.* 54 (2006) 1584–1591. <https://doi.org/10.1016/j.pss.2005.12.023>.
- [647] C. AbbasHawks, K.J. Voorhees, T.L. Hadfield, In situ methylation of nucleic acids using pyrolysis mass spectrometry, *Rapid Commun. Mass Spectrom.* 10 (1996) 1802–1806. [https://doi.org/10.1002/\(SICI\)1097-0231\(199611\)10:14<1802::AID-RCM761>3.0.CO;2-Y](https://doi.org/10.1002/(SICI)1097-0231(199611)10:14<1802::AID-RCM761>3.0.CO;2-Y).
- [648] S.W. Frazier, K.O. Nowack, K.M. Goins, F.S. Cannon, L.A. Kaplan, P.G. Hatcher, Characterization of organic matter from natural waters using tetramethylammonium hydroxide thermochemolysis GC-MS, *J. Anal. Appl. Pyrolysis.* 70 (2003) 99–128.

[https://doi.org/10.1016/S0165-2370\(02\)00098-0](https://doi.org/10.1016/S0165-2370(02)00098-0).

- [649] M. Le Meur, L. Mansuy-Huault, C. Lorgeoux, A. Bauer, R. Gley, D. Vantelon, E. Montargès-Pelletier, Spatial and temporal variations of particulate organic matter from Moselle River and tributaries: A multimolecular investigation, *Org. Geochem.* 110 (2017) 45–56.  
<https://doi.org/10.1016/j.orggeochem.2017.04.003>.
- [650] D.J. Clifford, D.M. Carson, D.E. McKinney, J.M. Bortiatynski, P.G. Hatcher, A new rapid technique for the characterization of lignin in vascular plants: thermochemolysis with tetramethylammonium hydroxide (TMAH), *Org. Geochem.* 23 (1995) 169–175.  
[https://doi.org/10.1016/0146-6380\(94\)00109-E](https://doi.org/10.1016/0146-6380(94)00109-E).
- [651] A.D. Hendricker, K.J. Voorhees, Amino acid and oligopeptide analysis using Curie-point pyrolysis mass spectrometry with in-situ thermal hydrolysis and methylation: Mechanistic considerations, *J. Anal. Appl. Pyrolysis.* 48 (1998) 17–33. [https://doi.org/10.1016/S0165-2370\(98\)00100-4](https://doi.org/10.1016/S0165-2370(98)00100-4).
- [652] N. Gallois, J. Templier, S. Derenne, Pyrolysis-gas chromatography–mass spectrometry of the 20 protein amino acids in the presence of TMAH, *J. Anal. Appl. Pyrolysis.* 80 (2007) 216–230.  
<https://doi.org/10.1016/j.jaap.2007.02.010>.
- [653] N. Gallois, J. Templier, S. Derenne, Limitations in interpreting TMAH thermochemolysis of natural organic matter via consideration of glycine and alanine derivatives, *Org. Geochem.* 41 (2010) 1338–1340. <https://doi.org/10.1016/j.orggeochem.2010.05.018>.
- [654] C.A. Joll, T. Huynh, A. Heitz, Off-line tetramethylammonium hydroxide thermochemolysis of model compound aliphatic and aromatic carboxylic acids: Decarboxylation of some ortho- and/or para- substituted aromatic carboxylic acids, *J. Anal. Appl. Pyrolysis.* 70 (2003) 151–167. [https://doi.org/10.1016/S0165-2370\(02\)00129-8](https://doi.org/10.1016/S0165-2370(02)00129-8).
- [655] J.C. Del Río, M.A. Olivella, H. Knicker, F.X.C. De Las Heras, Preservation of peptide moieties in three Spanish sulfur-rich Tertiary kerogens, *Org. Geochem.* 35 (2004) 993–999.  
<https://doi.org/10.1016/j.orggeochem.2004.06.002>.
- [656] A. Riboulleau, T. Mongenot, F. Baudin, S. Derenne, C. Largeau, Factors controlling the survival of proteinaceous material in Late Tithonian kerogens (Kashpir Oil Shales, Russia), *Org. Geochem.* 33 (2002) 1127–1130. [https://doi.org/10.1016/S0146-6380\(02\)00081-5](https://doi.org/10.1016/S0146-6380(02)00081-5).
- [657] H. Knicker, J.C.D. Río, P.G. Hatcher, R.D. Minard, Identification of protein remnants in insoluble geopolymers using TMAH thermochemolysis/GC-MS, *Org. Geochem.* 32 (2001)

397–409. [https://doi.org/10.1016/S0146-6380\(00\)00186-8](https://doi.org/10.1016/S0146-6380(00)00186-8).

- [658] P.M. Buch, A., Morisson, M., Szopa, C., Millan, M., Freissinet, C., He, Y., D. Glavin, J.Y. Bonnet, D. Coscia, A.J. Williams, F. Stalport, F. Raulin, M. Stambouli, S. Teinturier, R. Navarro-González, C. Malespin, Optimization of the TMAH thermochemolysis technique for the detection of trace organic matter on Mars by the SAM and MOMA-Pyr-GC-MS experiment., in: 49th LPSC Lunar Planet. Sci. Conf., 2018: pp. 5–6.
- [659] M. Hanus, M. Kabeláč, J. Rejnek, F. Ryjáček, P. Hobza, Correlated ab Initio Study of Nucleic Acid Bases and Their Tautomers in the Gas Phase, in a Microhydrated Environment, and in Aqueous Solution. Part 3. Adenine, *J. Phys. Chem. B.* 108 (2004) 2087–2097. <https://doi.org/10.1021/jp036090m>.
- [660] C. Fonseca Guerra, F.M. Bickelhaupt, S. Sana, F. Wang, Adenine tautomers: Relative stabilities, ionization energies, and mismatch with cytosine, *J. Phys. Chem. A.* 110 (2006) 4012–4020. <https://doi.org/10.1021/jp057275r>.
- [661] H. Kim, D. Ahn, S. Chung, S.K. Kim, S. Lee, Tautomerization of Adenine Facilitated by Water : Computational Study of Microsolvation, 9 (2007) 8007–8012. <https://doi.org/10.1021/jp074229d>.
- [662] M.A. Morsy, A.M. Al-Somali, A. Suwaiyan, Fluorescence of Thymine Tautomers at Room Temperature in Aqueous Solutions, *J. Phys. Chem. B.* 103 (1999) 11205–11210. <https://doi.org/10.1021/jp990858e>.
- [663] M.K. Shukla, J. Leszczynski, Interaction of water molecules with cytosine tautomers: An excited-state quantum chemical investigation, *J. Phys. Chem. A.* 106 (2002) 11338–11346. <https://doi.org/10.1021/jp021317j>.
- [664] Y. Tsuchiya, T. Tamura, M. Fujii, M. Ito, Keto-enol tautomer of uracil and thymine, *J. Phys. Chem.* 92 (1988) 1760–1765. <https://doi.org/10.1021/j100318a013>.
- [665] B.B. Brady, L.A. Peteanu, D.H. Levy, The electronic spectra of the pyrimidine bases uracil and thymine in a supersonic molecular beam, *Chem. Phys. Lett.* 147 (1988) 538–543. [https://doi.org/10.1016/0009-2614\(88\)80264-1](https://doi.org/10.1016/0009-2614(88)80264-1).
- [666] J. Rejnek, M. Hanus, M. Kabeláč, F. Ryjáček, P. Hobza, Correlated ab initio study of nucleic acid bases and their tautomers in the gas phase, in a microhydrated environment and in aqueous solution. Part 4. Uracil and thymine, *Phys. Chem. Chem. Phys.* 7 (2005) 2006–2017. <https://doi.org/10.1039/B501499A>.

- [667] M.K. Shukla, J. Leszczynski, Tautomerism in nucleic acid bases and base pairs: A brief overview, *Wiley Interdiscip. Rev. Comput. Mol. Sci.* 3 (2013) 637–649.  
<https://doi.org/10.1002/wcms.1145>.
- [668] G. Fogarasi, P.G. Szalay, The interaction between cytosine tautomers and water: An MP2 and coupled cluster electron correlation study, *Chem. Phys. Lett.* 356 (2002) 383–390.  
[https://doi.org/10.1016/S0009-2614\(02\)00370-6](https://doi.org/10.1016/S0009-2614(02)00370-6).
- [669] M.N. Manalo, A.C. de Dios, R. Cammi, Solvent Effects on <sup>15</sup>N NMR Shielding of 1,2,4,5-Tetrazine and Isomeric Tetrazoles: Continuous Set Gauge Transformation Calculation Using the Polarizable Continuum Model, *J. Phys. Chem. A.* 104 (2000) 9600–9604.  
<https://doi.org/10.1021/jp001525g>.
- [670] S.A. Trygubenko, T. V. Bogdan, M. Rueda, M. Orozco, F.J. Luque, J. Šponer, P. Slavíček, P. Hobza, Correlated ab initio study of nucleic acid bases and their tautomers in the gas phase, in a microhydrated environment and in aqueous solution : Part 1. Cytosine, *Phys. Chem. Chem. Phys.* 4 (2002) 4192–4203. <https://doi.org/10.1039/B202156K>.
- [671] I.R. Gould, I.H. Hillier, Accurate calculations of the relative energies of the tautomers of cytosine and guanine, *Chem. Phys. Lett.* 161 (1989) 185–187. [https://doi.org/10.1016/0009-2614\(89\)85054-7](https://doi.org/10.1016/0009-2614(89)85054-7).
- [672] G.G. Sheina, S.G. Stepanian, E.D. Radchenko, Y.P. Blagoi, IR spectra of guanine and hypoxanthine isolated molecules, *J. Mol. Struct.* 158 (1987) 275–292.  
[https://doi.org/10.1016/0022-2860\(87\)80024-8](https://doi.org/10.1016/0022-2860(87)80024-8).
- [673] S.M. Szczepaniak K, Matrix isolation infrared studies of nucleic acid constituents: Part 4. Guanine and 9-methylguanine monomers and their keto-enol tautomerism, *J. Mol. Struct.* 156 (1987) 29–42.
- [674] M.S. and W.B.P. Krystyna Szczepaniak, Infrared Studies and the Effect of Ultraviolet Irradiation on the tautomers of 9-methylguanine isolated in an argon matrix, *Chem. Phys. Lett.* 153 (1988) 39–44.
- [675] R. Ramaekers, G. Maes, L. Adamowicz, A. Dkhissi, Matrix-isolation FT-IR study and theoretical calculations of the vibrational, tautomeric and H-bonding properties of hypoxanthine, *J. Mol. Struct.* 560 (2001) 205–221. [https://doi.org/10.1016/S0022-2860\(00\)00733-X](https://doi.org/10.1016/S0022-2860(00)00733-X).
- [676] G. Bazsó, G. Tarczay, G. Fogarasi, P.G. Szalay, Tautomers of cytosine and their excited

- electronic states: a matrix isolation spectroscopic and quantum chemical study., *Phys. Chem. Chem. Phys.* 13 (2011) 6799–807. <https://doi.org/10.1039/c0cp02354j>.
- [677] D.A. Arinbruster, D. Tillman, L.M. Hubbs, Limit of Detection ( LOD )/ Limit of Quantitation ( LOQ ): Comparison of the Empirical and the Statistical Methods Exemplified with GC-MS Assays of Abused Drugs, *Clin. Chem.* 40 (1994) 1233–1238.
- [678] H.Y. Shen, Simultaneous screening and determination eight phthalates in plastic products for food use by sonication-assisted extraction/GC-MS methods, *Talanta*. 66 (2005) 734–739. <https://doi.org/10.1016/j.talanta.2004.12.021>.
- [679] K.G.J. Nierop, T.R. Filley, Simultaneous analysis of tannin and lignin signatures in soils by thermally assisted hydrolysis and methylation using  $^{13}\text{C}$ -labeled TMAH, *J. Anal. Appl. Pyrolysis*. 83 (2008) 227–231. <https://doi.org/10.1016/j.jaap.2008.07.004>.
- [680] F.Q. Yang, J. Guan, S.P. Li, Fast simultaneous determination of 14 nucleosides and nucleobases in cultured *Cordyceps* using ultra-performance liquid chromatography, *Talanta*. 73 (2007) 269–273. <https://doi.org/10.1016/j.talanta.2007.03.034>.
- [681] F.Q. Yang, D.Q. Li, K. Feng, D.J. Hu, S.P. Li, Determination of nucleotides, nucleosides and their transformation products in *Cordyceps* by ion-pairing reversed-phase liquid chromatography-mass spectrometry, *J. Chromatogr. A*. 1217 (2010) 5501–5510. <https://doi.org/10.1016/j.chroma.2010.06.062>.
- [682] A. Biscans, Exploring the emergence of RNA nucleosides and nucleotides on the early earth, *Life*. 8 (2018). <https://doi.org/10.3390/life8040057>.
- [683] U. Pedreira-Segade, J. Hao, A. Razafitianamaharavo, M. Pelletier, V. Marry, S. Le Crom, L.J. Michot, I. Daniel, How do nucleotides adsorb onto clays?, *Life*. 8 (2018) 1–25. <https://doi.org/10.3390/life8040059>.
- [684] Z. Zhang, J. Pawliszyn, Analysis of organic compounds in environmental samples by headspace solid phase microextraction, *J. High Resolut. Chromatogr.* 16 (1993) 689–692. <https://doi.org/10.1002/jhrc.1240161203>.
- [685] V. Lopez-Avila, R. Young, W.F. Beckert, Microwave-Assisted Extraction of Organic Compounds from Standard Reference Soils and Sediments, *Anal. Chem.* 66 (1994) 1097–1106. <https://doi.org/10.1021/ac00079a027>.
- [686] W.R. Edwards, L.H. Reeves, Furfuryl Formate, *J. Am. Chem. Soc.* 64 (1942) 1583–1584. <https://doi.org/10.1021/ja01259a026>.

- [687] J. Alongi, A. Di Blasio, J. Milnes, G. Malucelli, S. Bourbigot, B. Kandola, G. Camino, Thermal degradation of DNA, an all-in-one natural intumescent flame retardant, *Polym. Degrad. Stab.* 113 (2015) 110–118. <https://doi.org/10.1016/j.polyimdegradstab.2014.11.001>.
- [688] L. Zelles, Fatty acid patterns of phospholipids and lipopolysaccharides in the characterisation of microbial communities in soil: A review, *Biol. Fertil. Soils.* 29 (1999) 111–129. <https://doi.org/10.1007/s003740050533>.
- [689] D. Schulze-Makuch, D. Wagner, S.P. Kounaves, K. Mangelsdorf, K.G. Devine, J.P. De Vera, P. Schmitt-Kopplin, H.P. Grossart, V. Parro, M. Kaupenjohann, A. Galy, B. Schneider, A. Airo, J. Frösler, A.F. Davila, F.L. Arens, L. Cáceres, F.S. Cornejo, D. Carrizo, L. Dartnell, J. DiRuggiero, M. Flury, L. Ganzert, M.O. Gessner, P. Grathwohl, L. Guan, J. Heinz, M. Hess, F. Keppler, D. Maus, C.P. McKay, R.U. Meckenstock, W. Montgomery, E.A. Oberlin, A.J. Probst, J.S. Sáenz, T. Sattler, J. Schirmack, M.A. Sephton, M. Schloter, J. Uhl, B. Valenzuela, G. Vestergaard, L. Wörmer, P. Zamorano, Transitory microbial habitat in the hyperarid Atacama Desert, *Proc. Natl. Acad. Sci. U. S. A.* 115 (2018) 2670–2675. <https://doi.org/10.1073/pnas.1714341115>.
- [690] L. Carreto, E. Moore, M.F. Nobre, R. Wait, P.W. Riley, R.J. Sharp, M.S. Da Costa, *Rubrobacter xylophilus* sp. nov., a new thermophilic species isolated from a thermally polluted effluent, *Int. J. Syst. Bacteriol.* 46 (1996) 460–465. <https://doi.org/10.1099/00207713-46-2-460>.
- [691] S. Streif, W.F. Staudinger, W. Marwan, D. Oesterhelt, Flagellar Rotation in the Archaeon *Halobacterium salinarum* Depends on ATP, *J. Mol. Biol.* 384 (2008) 1–8. <https://doi.org/10.1016/j.jmb.2008.08.057>.
- [692] Y. Kinoshita, N. Uchida, D. Nakane, T. Nishizaka, Direct observation of rotation and steps of the archaellum in the swimming halophilic archaeon *Halobacterium salinarum*, *Nat. Microbiol.* 1 (2016) 1–9. <https://doi.org/10.1038/nmicrobiol.2016.148>.
- [693] A.N. Parikh, The role of squalene in the organization of monolayers derived from lipid extracts of *Halobacterium salinarum*, *Langmuir.* 29 (2015) 7922–7930. <https://doi.org/10.1021/la401412t>.The.
- [694] B. Tenchov, E.M. Vescio, G.D. Sprott, M.L. Zeidel, J.C. Mathai, Salt tolerance of archaeal extremely halophilic lipid membranes, *J. Biol. Chem.* 281 (2006) 10016–10023. <https://doi.org/10.1074/jbc.M600369200>.
- [695] C.P.M. Rafael Navarro-González, Fred A. Rainey, Paola Molina, Danielle R. Bagaley, Becky

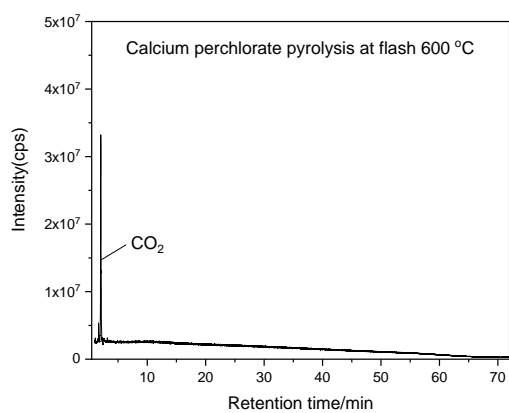


J. Hollen, José de la Rosa, Alanna M. Small, Richard C. Quinn, Frank J. Grunthaner, Luis Cáceres, Benito Gomez-Silva, Mars-Like Soils in the Atacama Desert, Chile, and the Dry Limit of Microbial Life, *Science* (80-. ). 306 (2004) 1289b-1289b.

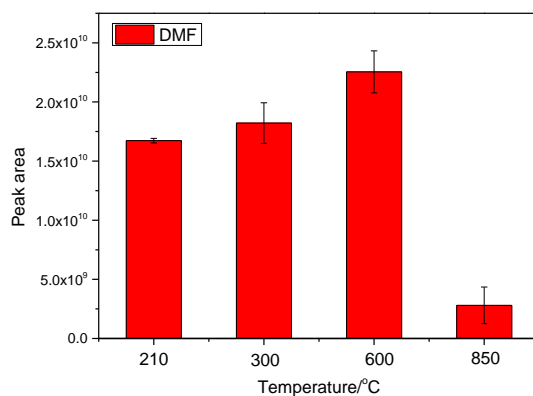
<https://doi.org/10.1126/science.306.5700.1289b>.



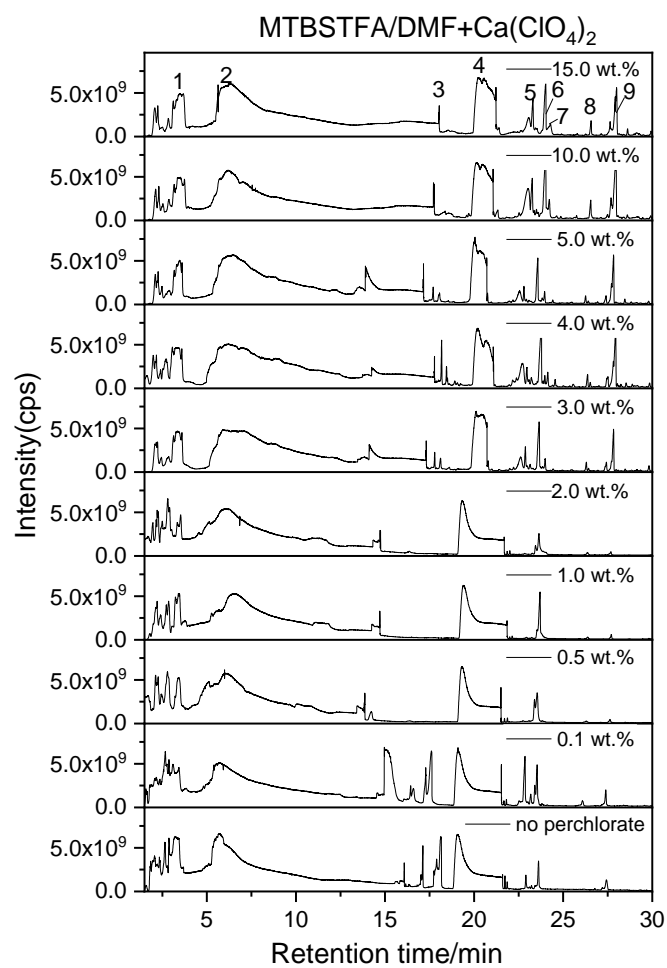
## Appendix



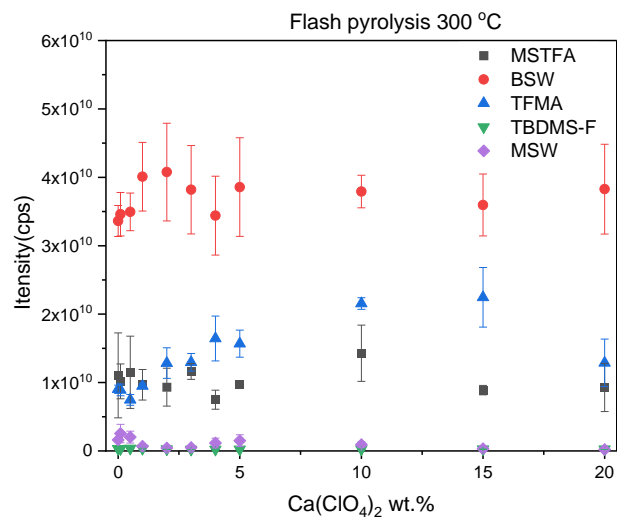
**Figure S2-1:** The chromatogram of the flash pyrolysis at 600 °C of calcium perchlorate.



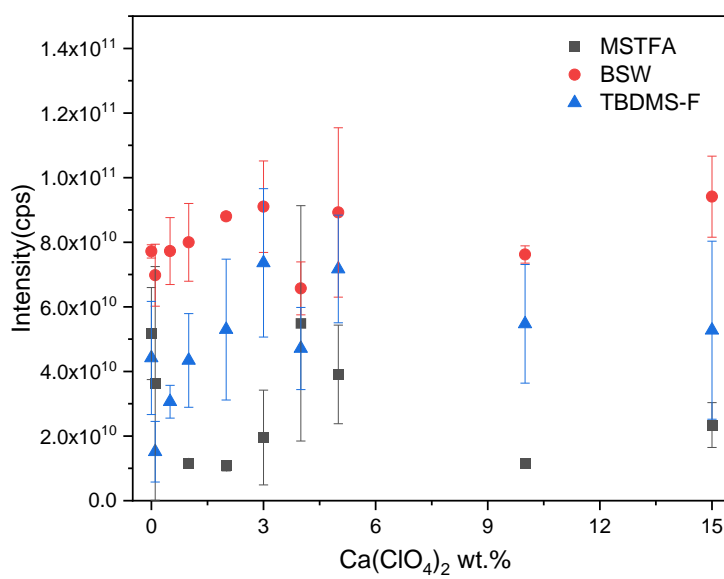
**Figure S2-2:** Influence of the pyrolysis' temperatures on the amount of DMF detected with GC/MS.



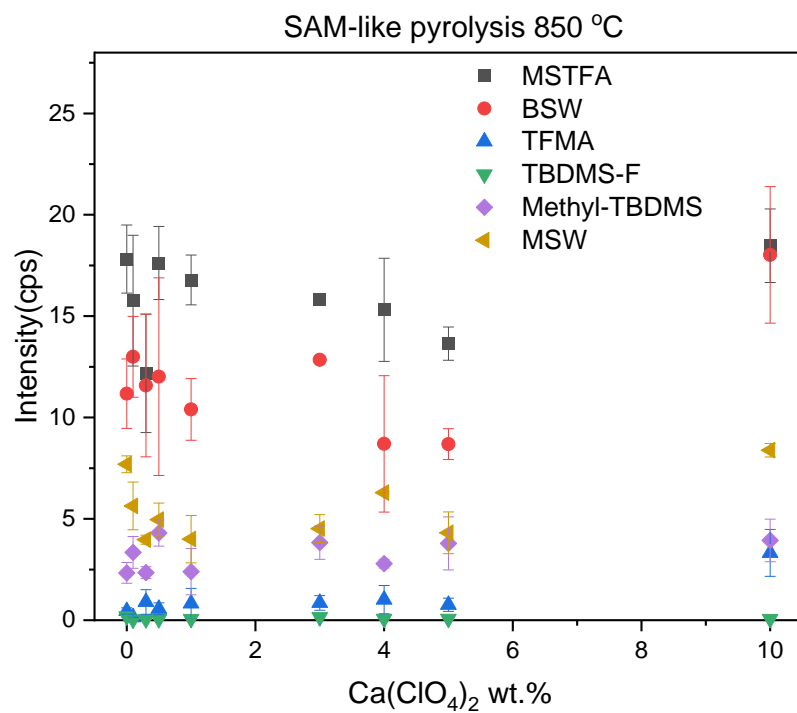
**Figure S2-3:** The chromatograms of MTBSTFA/DMF (4:1) flash pyrolysis without and with calcium perchlorate at 600 °C. Peak attributions : 1: tert-butyldimethylsilyl fluoride; 2: MSW; 3: MSTFA; 4: BSW; 5: Hexamethyl-cyclotrisiloxane; 6: 1,1,3,3-tetramethyl-1,3-bis[(2Z)-pent-2-en-1-yloxy]disiloxane; 7: bis(tert-butyldimethylsilyl)amine; 8:N-(tert-butoxycarbonyl)glycine; 9:Tris(trimethylsilyl)borate.



**Figure S2-4:** The effect of ClO<sub>4</sub><sup>-</sup> on the pyrolysis of MTBSTFA/DMF at 300 °C.



**Figure S2-5:** Effect of calcium perchlorate on the pyrolysis of MTBSTFA/DMF (4:1) at 600 °C.

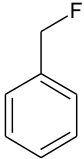
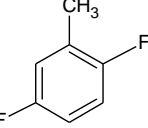
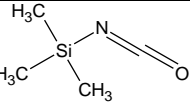
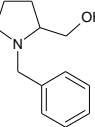
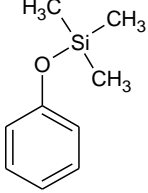
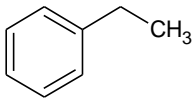
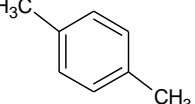
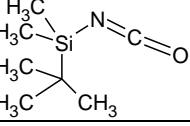
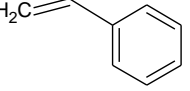
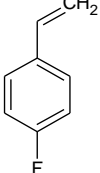
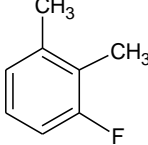


**Figure S2-6:** Influence of the amount of calcium perchlorate on the main chemical products observed when MTBSTFA/DMF (4 :1) pyrolyzing at SAM-like ramp of 850 °C.

**Table S2-1:** The products of MTBSTFA flash pyrolysis at 850 °C (supplement for Table 2).

RT (min)	Masses of fragments* and relative abundance: m/z (%)	Compounds	Structures
1.25	41(100), 56(82), 81(82), 55(33), 53(11)	5-Methyl-1-hexyne	
1.47, 1.53	85(100), 81(86), 80(23), 64(17), 44(16), 47(19), 100(18)	methyltrifluorosilane	
1.61	81(100), 41(71), 44(55), 56(61), 69(66), 45(21), 96(20), 100(17)	Trans-3-Hepten-1-ol	
2.25	158(100), 41(38), 57(32), 81(29), 66(15), 53(15), 130(20), 155(31), 57(32)	2-Naphthol, 5-amino-	
2.34	77(100), 155(77), 103(65), 159(42), 57(14), 66(13), 81(23), 118(20)	[(1E)-3,4-Dimethyl-1-pentenyl](fluoro)dimethylsilane	
2.79	77(100), 56(98), 57(69), 134(51), 151(27), 119(19), 96(16), 41(44), 49(27)	Tert-Butyldimethylfluorodilane	
3.16-3.18	78(100), 77(92), 56(55), 96(29), 51(25), 52(24), 50(21), 57(17), 79(16), 114(13)	Fluorobenzene	
3.40	114(100), 77(71), 58(48), 101(46), 88(25), 47(23), 155(16), 141(11)	1,4-difluoro-Benzene	
3.65	58(100), 69(45), 77(10), 127(33), 146(27), 145(17), 56(13)	Benzene, (trifluoromethyl)-	
3.92	58(58), 69(76), 127(25), 155(32), 181(28), 78(18), 73(16), 233(13)	N-methyltrifluoroacetamide	
4.47	79(100), 52(62), 51(30), 50(23)	Pyridine	
4.83	91(100), 92(77), 65(30), 63(15), 51(12), 7(11)	Toluene	
5.04	155(100), 211(83), 109(46), 81(18), 212(18), 156(19), 127(15)	2-Tributylsilyloxybut-3-yne	

**Table S2-1 (continued)**

RT (min)	Masses of fragments* and relative abundance: m/z (%)	Compounds	Structures
5.13,5.17	109(100),154(68),155(44), 156(29), 83(25), 89(21), 157(15)	Fluoromethyl-benzene	
5.68	127(100)	2,5-difluorotoluene	
6.19	100(100),126(48),70(20),86(12)	Isocyanatotrimethylsilane	
6.42	91(100),160(31),65(11),159(11)	(1-Benzyl-2-pyrrolidiny)methanol	
7.18	151(100),152(18), 73(10)	O-(Trimethyl)phenol	
7.31	91(100),143(26),77(15),106(34),143(26),158(12),65(10),167(11)	Ethylbenzene	
7.76	91(100),106(52),111(23),77(11),51(10)	p-xylene	
8.30	100(100), 101(34), 56(34), 72(31), 157(21), 41(17)	Tert-Butyl-isocyanato-dimethylsilane	
8.67	104(100), 78(73), 103(71), 77(34), 51(30), 91(19), 105(16), 50(13)	styrene	
8.79,8.86, 9.13	122(100),121(39), 96(35),101(36),75(15)	p-fluoro-Styrene	
9.26 ?	109(100),91(58), 64(56),124(43),63(17), 159(14)	2,3-Dimethylfluorobenzene	



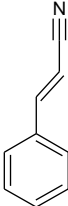
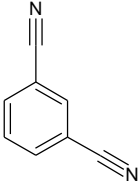
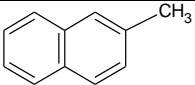
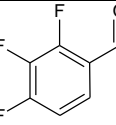
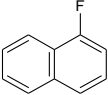
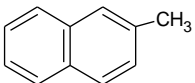
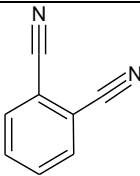
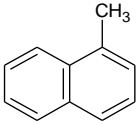
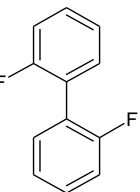
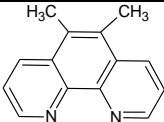
**Table S2-1 (continued)**

RT (min)	Masses of fragments* and relative abundance: m/z (%)	Compounds	Structures
9.90,10.06	122(100),100(34), 100(25), 121(25), 159(23), 101(22), 140(14)	P-fluoron-Styrene	
10.76	77(100),120(67),170(64),143(23)	2,2,2-trifluoro-N-(trimethyl)acetamide	
11.00	139(100),154(30),47(27),91(18),140(16)	2-Hydroxy-5-fluoroacetophenone	
12.10	105(100),211(55),123(37),181(42), 120(32),79(13)	N-benzylvebzamide	
12.33	118(100),117(93), 103(54), 115(35), 78(32), 77(23), 51(13),58(11)	1-methylethenyl-Benzene	
12.58	103(100), 281(82), 77(61), 76(46), 134(42),184(20), 282(20), 50(14) ,121(13),265(13)	Cyano-benzene	
12.82	77(100),134(97),103(87),184(57),73(43),121(10)	N-Methyl-N-(trimethyl)trifluoroacetamide	
13.02, 13.18, 14.39, 14.64	117(100), 121(79), 118(60), 94(34),115(30)	Benzene,2-propenyl-	
13.92	136(100),135(54),133(39),154(27), 155(23), 166(14),131(13)	2-Hydroxy-5-methylbenzaldehyde	
14.08	117(100),105(30),132(52), 115(36), 31(11),120(10)	p-Alytoluene	
15.22	115(100), 116(95), 77(23), 89(17), 117(10),63(14)	1H-Indene	
15.79	133(100),134(81)135(17),107(14)	2-methyl-5-propenyl-,(E)-pyrazine	

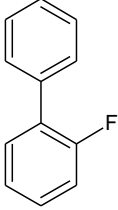
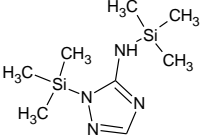
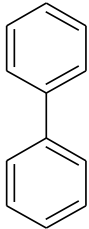
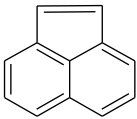
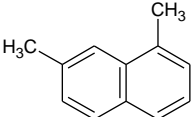
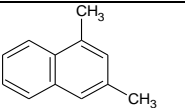
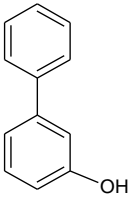
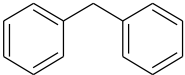
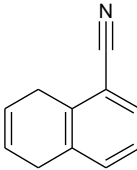
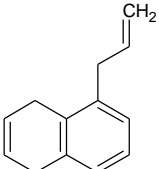
**Table S2-1 (continued)**

RT (min)	Masses of fragments* and relative abundance: m/z (%)	Compounds	Structures
16.09	153(100),125(43),168(33),154(13)	Dimethyl, fluoromethyl,phenylsilane	
16.40,1 7.52,18 .20	117(100),90(60),116(58), 89(34),63(12)	3-methyl-Benzonitrile	
16.97	117(100),132(89),115(49),91(51), 92(27), 131(17), 65(16)	p-Cymene	
17.80	149(100),164(52),47(20),150(14), 123(11)	2-tert-butyl-p-Cresol	
18.53	130(100), 128(46), 129(44), 131(30), 127(20), 115(15), 85(15), 77(12)	1,3-diethenyl-Benzene	
18.88	147(100),73(21),189(22),148(18)	1,3-Ditert-butyl-1,1,3,3-tetramethyldisiloxane	
19.20,2 0.42	133(100), 85(78), 182(65), 73(51),147(33), 117(30),159(47)	Pentamethyl-Disiloxane	
19.65	213(100), 151(75), 166(67),182(48), 197(35), 149(20), 47(20),125(18)	4,4'-isopropylidenedi-phenol	
19.98	117(100) ,90(60), 116(56), 130(41), 115(38), 89(37), 51(15), 63(15), 130(41), 146(13)	Benzyl nitrile(benzyl cyanide)	
20.51	128(100), 127(21), 129(14), 102(14)	Naphthalene	
20.77	130(100), 129(96), 115(54), 128(53), 85(12), 146(30), 229(10)	1,2-dihydro-Naphthalene(Dialin)	
21.13	164(100),85(14), 229(39), 133(14)	m-Fluorobenzotrifluoride	
21.93,2 2.05	128(100), 146(36), 127(18), 129(14), 102(12), 51(10)	1-fluoro-Naphthalene	
22.32	164(100), 229(29), 85(14), 73(7), 144(12)	Salsolinol	

**Table S2-1 (continued)**

RT (min)	Masses of fragments* and relative abundance: m/z (%)	Compounds	Structures
23.56	129(100), 85(81), 207(72), 102(40), 128(37), 159(20), 163(17), 77(22)	Trans-Cinamonitrile	
25.87,26.24,26.61 ?	128(100),129(66), 141(41), 102(41),101(38),142(27),75(22),76(20)	1,3-Dicyanobenzene	
26.89	142(100),141(88), 115(33), 160(30), 159(29),139(13),71(10)	2-methyl-naphthalene	
27.00	159(100),160(86), 133(29)	2,3,4-Trifluorobenzaldehyde	
27.55	141(100), 142(95), 160(87), 115(35), 159(43),139(15)	1-fluorone-naphthalene	
27.97	141(100), 142(75), 115(51), 177(25), 175(20)	2-methylnaphthalene	
28.23	128(100), 210(30), 141(28), 101(28), 75(12)	Phthalonitrile(1,2-Benzenedicarbonitrile)	
28.39 ?	141(100), 142(62), 115(49),128(32), 116(11)	1-methyl-naphthalene	
28.97	190(100), 140(36), 114(33), 189(32), 188(27), 171(22), 191(13)	2,2'-Difluorobiphenyl	
29.35	208(100), 190(85), 193(73), 127(56), 128(47), 189(30), 209(16), 194(15)	1,10-Phenanthroline,5,6-dimethyl-	

**Table S2-1 (continued)**

RT (min)	Masses of fragments* and relative abundance: m/z (%)	Compounds	Structures
29.88	172(100), 171(40), 85(27), 170(25), 172(13), 173(11)	2-Fluoro-1,1'-biphenyl	
30.27,3 1.53	213(100),171(82), 214(20), 172(13), 99(11)	2-trimethylsilyl-3-trimethylsilylamino-1,2,4-triazole	
30.53,3 2.66	154(100),153(43), 152(32), 172(26),76(18), 171(12), 151(10)	Biphenyl	
31.79,3 3.39,34 .64	153(100),154(67), 152(44), 76(21),140(15)	Acenaphthene	
32.10	141(100),156(94), 153(33), 155(20), 115(19),159(10)	1,7-dimethylnaphthalene	
32.28	156(100),141(73), 155(35), 174(31), 159(25), 172(25),77(13)	1,3-dimethylnaphthalene	
32.82,3 2.93	170(100), 85(22), 169(15),172(13)	3-Hydroxybiphenyl	
34.88	168(100), 167(63), 71(41),165(29), 169(15)	Diphenylmethane	
35.30,3 6.50	153(100),126(25)	1-Naphthonitrile	
37.16	168(100),167(43), 153(32), 152(30), 165(20), 115(17)	1-akyl-naphthalene	

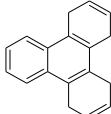
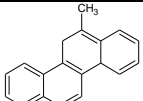
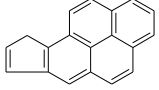
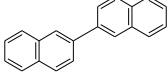
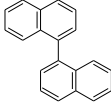
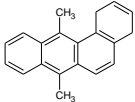
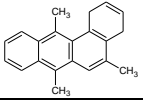
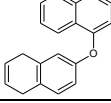
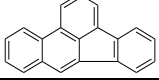
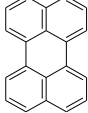
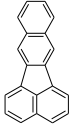
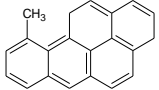
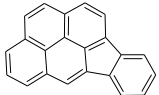
**Table S2-1 (continued)**

RT (min)	Masses of fragments* and relative abundance: m/z (%)	Compounds	Structures
37.93, 38.39,3 8.67,39 .39, 40.28	165(100), 166(61), 82(22),163(18),164(18)	9H-Fluorene	
38.10	183(100), 184(94), 91(15), 92(11)	4,4'-dimethyl-2,2'-bipyridine	
38.80	166(100),197(94), 165(38), 140(33), 139(30),201(10)	1-Naphthaleneacetonitrile	
39.75	166(100), 180(88), 165(66), 167(58), 178(32), 139(16)	4-vinyl-Biphenyl	
40.83	167(100), 166(89), 140(39), 139(16)	9H-Carbazole	
41.06,4 2.92,43 .39	165(100), 166(44), 179(21), 164(17), 82(18)	9-methyl-Fluorene	
43.95	178(100), 176(23), 152(14), 177(12)	Anthracene	
44.43	177(100), 192(33),191(21),150(19),75(12),19 4(12),194(10)	9-Fluorenone oxime	
45.23,4 5.40	196(100), 197(13), 98(12),85(10),170(10)	1-Hydroxyphenazine	
45.90,4 6.23	178(100),176(21), 152(12), 76(14), 196(15), 76(14), 177(13)	phenanthrene	
48.08 ?	222(100), 221(79), 220(20), 192(68), 191(62), 165(39), 197(28), 94(36), 221(27), 222(27), 189(25),77(23)	N-Methyl-9-anthracenemethanamine	
48.43	203(100), 204(84), 202(60), 101(36),201(14),205(14)	1-phenyl-Naphthalene	
48.77	192(100),191(66), 189(30), 190(25), 193(21), 165(19),210(12)	2-Methylantracene	
49.21	210(100),209(71),91(70), 104(42), 94(40), 207(25), 190(20), 211(17)	1H-1,3-Benzimidazol-ol,2-phenyl	

**Table S2-1 (continued)**

RT (min)	Masses of fragments* and relative abundance: m/z (%)	Compounds	Structures
49.69,4 9.88,50 .43,50. 62,	192(100),191(62) ,189(37), 190(24), 193(16), 95(13),210(12)	1-Methylphenanthrene	
50.27	190(100), 189(81), 95(34),187(22)	4H-Cyclopenta[def]phenanthrene	
52.23,5 4.04	204(100), 202(44),203(37),101(21), 205(17), 102(10)	2-phenyl-Naphthalene	
54.92,5 6.44	202(100), 200(22), 101(20), 203(18), 100(14)	Fluranthene	
55.65	202(100),200(23),203(20), 220(15),101(19),88(10)	Pyrene	
56.17	203(100), 202(87), 201(24), 200(21), 101(21), 88(21) ,101(21), 175(11)	9-ethenyl-Anthracene	
57.08,5 7.30,57 .71	203(100),74(52),87(43),176(11),10 1(11),202(15),43(15)	9-Anthronitrile	
58.16,5 8.79,59 .19,59. 29,59.9 3	216(100), 215(95), 213(27), 107 (27), 234(25), 233(23), 217(20)	1-methyl-pyrene	
61.22,6 1.52,62 .04,62. 22,63.7 3	228(100), 94(78), 230(71), 215(65), 113(37), 226(32), 114(31), 22(23), 225(20)	3,4-Benzophenanthrene	
61.73,6 2.86	227(100),226(19), 100(19), 99(14),228(12)	1-Fluorobenzo[a]anthracene	
62.37 ?	227(100),226(40),59(21), 100(18), 244(17), 106(15),121(12)	7-Methyl-3,4-benzophenanthrene	
63.14	226(100),227(93), 113(32),100(26) ,224(24), 225(25), 112(23), 228(16), 200(13)	Benzo[mno]fluoranthene	

**Table S2-1 (continued)**

RT (min)	Masses of fragments* and relative abundance: m/z (%)	Compounds	Structures
63.27,6 3.42	228(100), 226(27), 114(20), 113(18), 229(19),227(12)	Triphenylene	
65.20	242(100), 240(49), 241(62), 239(43), 120(21), 119(30), 120(30), 243(19),107(16)	6-methyckhrysene	
65.50,6 5.71	239(100), 240(97), 119(70), 237(25), 118(19) ,106(16)	9H-cyclopenta[a]pyrene	
66.01	254(100), 152(52), 252(35),126(27), 253(21), 255(20), 106(21)	2,2'-Binaphthyl	
66.18	254(100), 252(37), 240(24), 239(23), 126(23), 121(23), 119(22), 253(19),255(17)	1,1'-Binaphthyl	
66.53	251(100),241(97), 120(90), 239(82), 75(73), 121(58), 253(44),254(45), 112(38), 251(47), 119(35)	Benz[a]anthracene,7,2- dimethyl-	
67.23,6 7.32	270(100),253(24),135(31),134(17), 268(23),271(27)	5,7,12- trimethylbenz(a)anthracene	
67.32	270(100), 135(29), 271(26), 134(21), 268(21), 254(21),112(13)	1-(2-naphthalenyloxy) - Naphthalene	
67.76	252(100), 126(29), 250(28),253(30),113(18)	Benzo[b]fluoranthene	
68.12, 68.88,6 9.19	252(100), 126(62), 113(41), 250(30),125(27),253(15)	Perylene	
68.70	252(100),250(33), 125(28),253(21),113(16)	Benzo[k]fluoranthene	
69.80	266(100), 265(75), 132(40), 131(34),267(27)	10-methylbenzo(a)pyrene	
72.52	276(100), 138(40), 137(30),277(29), 274(23),275(13)	o-Phenylene pyrene	

### Some comments on Chapter 3.3.4:

“Additionally, the concentration of the methyl group (about 86  $\mu\text{mol}$ , calculation can be seen in supplementary materials) used to derivatize the fatty acids is much greater than (in excess) the concentration needed to complete fatty acid methylation (of 16 nmol, calculation can be seen in supplementary materials). Therefore, the calcium perchlorate has no obvious effect on the recovery of the fatty acids.”

The abundance of methyl group for methylation in TMAH is about 86  $\mu\text{mol}$ , as

$$n_{-CH_3} = \frac{V_{TMAH} \times \rho_{TMAH}}{M_{TMAH}} \times 75\% \times 4 \text{ (-CH}_3 \text{ in each TMAH molecule)}$$

$$n_{-CH_3} = 0.866 \text{ g.ml}^{-1} \times 3 \text{ }\mu\text{l} \div 91.15 \text{ g.mol}^{-1} \times 75\% \times 4 = 85.5 \text{ }\mu\text{mol} \approx 86 \text{ }\mu\text{mol};$$

The total amount of fatty acids needed to be methylated should be about 16 nmol, as  $n_{FA} = C_{FA} \times V_{FA} = 0.67 \text{ mmol}^{-1} \times 12 \times 2 \text{ }\mu\text{l} = 16 \text{ nmol}$ .

“The calcium perchlorate used in this study can release  $4 \times 10^{-6}$  mol of  $\text{O}_2$ , the abundance of TMAH is about 4.4 times higher than the amount of  $\text{O}_2$ , and the C abundance is 17.6 times higher than that of  $\text{O}_2$ .”

The abundance of TMAH is about 21.4  $\mu\text{mol}$ , it should be about 4.4 times  $((21.4-4)/4=4.4)$  higher than the amount of  $\text{O}_2$ , and the C abundance is more than 17.6 times higher than that of  $\text{O}_2$ , because there are methanol in the solution, it can also produce methyl when it was heated.

The presence of calcium perchlorate did not show obvious effects on fatty acid recovery (about 11.8 pmol), as  $0.67 \times 10^{-6} \text{ mol.L}^{-1} \times 2.2 \text{ }\mu\text{l} \times 8 \text{ (C}_8 \text{ to C}_{15}) = 11.79 \text{ pmol} \approx 11.8 \text{ pmol}$ , about  $6 \times 10^{-9}$  g.



Table S6-1 *Chroococidiopsis cubana* medium 3N-Bristol

Bristol was made up by blending three previously prepared solutions. The preparation of each solution was done according to the following compositions.

Solution A (for 1L): Stock solution A for medium Bristol.

Compound	Added mass (g)	Concentration(M)
NaNO <sub>3</sub>	75	0.0088
CaCl <sub>2</sub> ×2H <sub>2</sub> O	2.5	1.93×10 <sup>-4</sup>
MgSO <sub>4</sub> ×7H <sub>2</sub> O	7.5	3.045×10 <sup>-4</sup>
FeEDTA	2.0	5.75×10 <sup>-5</sup>

Solution B (for 1L): Stock solution B for medium Bristol.

Compound	Added mass (g)	Concentration(M)
K <sub>2</sub> HPO <sub>4</sub>	7.5	4.3×10 <sup>-4</sup>
KH <sub>2</sub> PO <sub>4</sub>	17.5	0.00128
NaCl	2.0	3.41×10 <sup>-4</sup>

Solution C (for 1L): Stock solution C for medium Bristol.

Compound	Added mass (g)	Concentration(M)
H <sub>3</sub> BO <sub>3</sub>	2.86	4.61×10 <sup>-5</sup>
MnCl <sub>2</sub> ×4H <sub>2</sub> O	1.81	1.20×10 <sup>-5</sup>
ZnSO <sub>4</sub> ×7H <sub>2</sub> O	0.220	1.149×10 <sup>-6</sup>
CuSO <sub>4</sub> ×7H <sub>2</sub> O	0.080	4.221×10 <sup>-7</sup>
MoO <sub>3</sub> 85%	0.036	1.50×10 <sup>-7</sup>
CoSO <sub>4</sub> ×7H <sub>2</sub> O	0.090	4.86×10 <sup>-7</sup>

Note:

- 1) Maintain these three stock solutions in the refrigerator, for obtaining final Bristol Medium.
- 2) For each liter, and 10 ml of solution A; 10mL of solution B; 1 mL of solution C.
- 3) Autoclave the medium.
- 4) Use the medium or keep it for few days.

Table S6-2 *Rubrobacter radiotolerans* medium

Substances	Mass and volume
Trypticase Soy Broth (BBL 11768, Oxoid CM129 or Merck 5459)	30.0 g
Distilled water	1000.0 ml

Autoclave at 121 °C for 15 mins.

Table S6-3 *Halobacterium salinarum* medium

Substances	Mass or volume
Casamino acids	7.5 g
Yeast extract	10.00g
Na <sub>3</sub> -citrate	3.00g
KCl	2.00g
MgSO <sub>4</sub> ×7H <sub>2</sub> O	20.00g
FeSO <sub>4</sub> ×7H <sub>2</sub> O	0.05g
MnSO <sub>4</sub> ×7H <sub>2</sub> O	0.20mg
NaCl	250.00g
Distilled water	1000.0 ml

## Résumer (French)

**Titre :** Application de la dérivation au MTBSTFA/DMF et de la thermochémiolyse au TMAH à la recherche *in situ* de composés organiques martien

**Mots clés :** Bioindice de la vie, Mars, Pyrolysis-GC/MS, thermochémiolyse de TMAH, MTBSTFA/DMF, Perchlorate

**Résumé :** La recherche de biosignatures sur Mars fait parti des sujets scientifiques populaire à la fois dans le grand publique mais également au sein de notre communauté scientifique. Les instruments Mars Organic Molecule Analyzer (MOMA) et Sample Analysis at Mars (SAM) respectivement à bord des rovers Rosalind Franklin (Exomars 2022) et Curiosity (Mars Science Laboratory), sont capables de détecter la matière organique présente en surface et subsurface à des concentrations inférieures au ppb. Afin d'identifier la matière organique, ces deux instruments utilisent la pyrolyse couplée à de la chromatographie gazeuse couplée à la spectrométrie de masse (Pyr-GC/MS). Afin d'analyser la matière organique refractaire les agents de thermochémiolyse, le tétraméthylammonium hydroxyde (TMAH) et de fonctonnalisation, le N-tert-butyldiméthylsilyl-N-méthyltrifluoroacetamide (MTBSTFA) mélangé avec son solvant le N,N-diméthylformamide (DMF) sont utilisés. Cependant, la mise en évidence récente de composés fortement oxydant (perchlorate) à compliqué l'analyse des résultats obtenus par l'expérience SAM. En effet, le MTBSTFA/DMF, en plus de ses sous produits de décomposition peut réagir à haute température avec les perchlorates présents dans le sol martien. Le mélange MTBSTFA/DMF est donc une possible source de carbone correspondant à certains composés organiques qui ont été détectés sur Mars par SAM. Par conséquent, les sous-produits de la dégradation des réactifs avec et sans perchlorates ont été listés et référencés, et des voies possibles de dégradation des réactifs ont été proposées.

La thermochémiolyse au TMAH a récemment été

utilisé à bord de SAM pour analyser un échantillon prélevé à GR. Afin d'aider à l'interprétation de ces nouveaux résultats nous avons utilisé la thermochémiolyse au TMAH pour analyser des composés organiques d'intérêt pur et d'autres contenus dans des échantillons naturels. Parmi les composés organiques testés nous avons inclus des biosignatures telles que les acides deoxyribonucléique (ADN) et ribonucléique (ARN) qui ont certainement été à la base de la formation de la vie sur Terre. Nous les avons étudiées seules et encapsulées dans leur cellule afin de mimer au plus près leurs conditions naturelles. Les températures de thermochémiolyse ont alors été étudiées et optimisées. Les bactéries extrémophiles étudiées dans ce travail comprennent les cyanobactéries (*Chroococcidiopsis cubana*), les actinobactériens (*Rubrobacter radiotolerans*) et l'archée halophile (*Halobacterium salinarum*). Des fragments d'ADN ou d'ARN ont alors été détectés. Parmi eux les dérivés de l'adénine sont les plus faciles et ont la plus grande abondance par rapport aux autres nucléobases. Cependant, les principaux composés détectés dans ces échantillons naturels sont les acides gras tels que le glucopyranoside, l'un des composés détectés majoritairement dans les trois bactéries extrémophiles utilisées. Les résultats ont démontré que la thermochémiolyse au TMAH pouvait être une méthode chimique efficace pour détecter des signatures de vie sur Mars et d'autres planètes lors de futures missions spatiales.

Université Paris-Saclay

Espace Technologique / Immeuble Discovery

Route de l'Orme aux Merisiers RD 128 / 91190 Saint-Aubin, France

## Abstract (English)

**Title:** Search for organic compounds with MTBSTFA/DMF derivatization and TMAH thermochemolysis on Mars

**Keywords:** Life bioindice, Mars, Pyrolysis-GC/MS, TMAH thermochemolysis, MTBSTFA/DMF, Perchlorate

**Abstract:** Searching for life biosignatures on Mars has been a very popular topic in the world. The Mars Organic Molecule Analyzer (MOMA) and Sample Analysis at Mars (SAM) instruments onboard the Exomars 2022 and Mars Science Laboratory rovers, respectively, are capable of organic matter detection and differentiating potentially biogenic from abiotic organics in Martian samples. To identify organics, these instruments both utilize Pyrolysis-Gas Chromatography coupled to Mass Spectrometry (Pyr-GC/MS), and thermochemolysis using the reagent tetramethylammonium hydroxide (TMAH) and derivatization using a mixture of N-tert-butyltrimethylsilyl-N-methyltrifluoroacetamide (MTBSTFA) and N,N-dimethylformamide (DMF). Both thermochemolysis and derivatization help to increase organic volatility of labile and refractory compounds. However, with the detection of chloride-bearing compounds on Mars, MTBSTFA/DMF, which is leaking on SAM, was considered as a possible carbon source of some organics that have been detected on Mars. Therefore, the reagent byproducts following degradation, both in the presence of and the absence of perchlorates, are proposed as a data reference, as well as possible routes of reagent degradation.

In addition to MTBSTFA, TMAH is also used to search for organic compounds that could possibly be bioindicators and biosignatures in Martian samples. Deoxyribonucleic acids (DNA) as an information carrier and ribonucleic acid (RNA) form the basis for life on Earth. However, the optimal experimental conditions for the detection of DNA or RNA fragments and other organic compounds important to Earth life were poorly understood. Therefore, in this thesis, the building blocks of nucleic acids, such as nucleobases, nucleosides, nucleotides, PolyA, and

bacteria were analyzed by Pyrolysis-GC/MS with TMAH thermochemolysis using a SAM-like ramp and flash pyrolysis at different temperatures (from 100 to 600 °C). The methylated nucleobases, ribose, and phosphate were detected at the highest intensities at 200 and 300 °C, respectively. Methylated adenine and adenosine are the main thermochemolysis products of Poly A. In addition, bacteria such as *E. coli* were also analyzed with TMAH thermochemolysis. Results demonstrated that TMAH thermochemolysis is able to characterize the fragments of DNA and RNA even at high temperatures with a limit of detection lower than  $10^4$  cells of *E. coli*.

TMAH thermochemolysis was also applied to analyze the organic compounds from natural samples such as bacterial cells. The important organic compounds of extremophile bacteria have been studied and the thermochemolysis temperatures were optimized. The extremophile bacteria include cyanobacteria (*Chroococcidiopsis cubana*), anctinobacteria (*Rubrobacter radiotolerans*), and halophilic Archaea (*Halobacterium salinarum*). DNA or RNA fragments could be detected, with Adenine-derivatives being the easiest to detect and with the highest abundance compared with other nucleobases. However, the main compounds and the most detectable organic compounds from these natural samples are fatty acids. Glucopyranoside is one of the most important target compounds from the three extremophile bacteria used herein. Results demonstrated that TMAH thermochemolysis could be an efficient chemical method to detect life signatures on other planets for future missions.

Université Paris-Saclay

Espace Technologique / Immeuble Discovery

Route de l'Orme aux Merisiers RD 128 / 91190 Saint-Aubin, France